UNIVERSIDADE DA BEIRA INTERIOR
Faculdade de Engenharia

Twin Impinging Jets Inline with a Low-Velocity Crossflow

Diana Filipa da Conceição Vieira

Thesis in fulfilment of the requirements for the degree of PhD in
Aeronautical Engineering
(3rd cycle of studies)

Supervisor: Prof. Doutor Jorge Manuel Martins Barata

Covilhã, January 2017

Dedication

To my parents, who throughout my academic career have encouraged and supported me at all times and are constantly on my side and never letting me give up this project.

The entire rest of my family, who was always by my side.

And last but not least, the person to whom my heart belongs, for the strength, affection, dedication, attention, companionship, patience and many other feelings, without which this winding path would have been much harder.

"What we anticipate seldom occurs; the least we expect generally happens"

Benjamin Disraeli

Acknowledgements

First of all, I am thankful for the financial support provided by the Foundation for Science and Technology, through the PhD grant under the QREN - POPH program - Type 4.1 - Advanced Training, subsidized by the European Social Fund and national MEC funds, contract SFRH / BD / 86434/2012.

I want to thank my advisor, Professor Jorge Manuel Martins Barata, for his dedication, encouragement, knowledge, availability and help.

At the same time, I want to thank all the teachers that I had the opportunity to meet throughout my academic life and that somehow helped me to get here and instilled in me all their knowledge. In a special way, I wish to thank Professor André Resende Rodrigues da Silva, his availability shown throughout this work. Without their help none of this would have been possible.

I also want to thank the lab technician Mr. Rui Paulo for the help provided during the experimental work.

I want to thank Fabio Guilherme dos Santos Marques de Oliveira and his family for their friendship, affection, companionship, encouragement, dedication, strength, patience and heart given during this phase of my academic career. They never let me to give up, always pushing me to fight for my goals and especially for making me a more rational and humane person.

Last but not least, I thank my family, especially my parents for all the support on this study cycle, all the encouragement, love, dedication, patience and strength that they gave me so that this project was finalized.

Diana Vieira

Covilhã, 2016

Resumo

Durante a fase em que uma aeronave de descolagem rápida/vertical e aterragem vertical paira no ar, um campo de escoamento tridimensional é criado entre o escoamento dos jatos de elevação, a superfície inferior da aeronave e o solo. O escoamento em torno da aeronave durante a fase de transição de voo pairado para voo convencional é de particular importância. Essa fase é dominada pelos fenómenos provocados pela interação dos jatos de elevação com o escoamento cruzado, devido ao aparecimento de um escoamento complexo na parte inferior da aeronave. Os jatos de parede, criados devido ao impacto de cada um dos jatos de elevação no solo, convergem para a linha de estagnação, formando um escoamento ascendente, como um "repuxo", que interage com a aeronave. Por vezes, este escoamento ascendente fornece benefícios contribuindo para os efeitos de elevação da aeronave. No entanto, e na maior parte dos casos, o escoamento ascendente resultante produz características indesejáveis para este tipo de aeronave, entre elas a ingestão de gases quentes nas tubeiras de admissão, aumentos de pressão, temperatura e ruído, mudanças das forças de elevação, perdas de elevação e aumento de temperatura na fuselagem. A interação do jato de parede, resultante do impacto dos jatos de elevação no solo, com o escoamento livre leva à formação de vórtice de parede a montante do jato incidente. A forma do vórtice de solo resultante é fortemente afetada pelas condições do campo de escoamento e, devido ao escoamento ascendente, o efeito induzido de suckdown tende a ser reduzido.

Passadas três décadas, as características do campo de escoamento associado a este tipo de aeronave tem sido exaustivamente estudada. Mas devido à grande complexidade das novas configurações das aeronaves VSTOL juntamente com requisitos muito rigorosos é de máxima importância a continuação da investigação deste tipo de escoamentos. Com o contínuo desenvolvimento das aeronaves VSTOL e a crescente dependência de técnicas de design computacional, é imperativo o melhoramento do conhecimento da aerodinâmica inerente à aeronave, mais propriamente aos jatos de elevação, quando esta opera com efeito de solo.

Este trabalho é assim dedicado à continuação do trabalho experimental iniciado no decurso da tese de mestrado, ou seja, a análise detalhada do complexo campo de escoamento originado por dois jatos circulares de ar turbulentos em linha com um escoamento cruzado de baixa velocidade, incidentes numa superfície plana perpendicular ao eixo geométrico do bocal de saída do jato. As condições de saída do jato são mudadas no decurso do trabalho, de modo a entender o comportamento do campo de escoamento. De forma a completar a análise experimental e validar os seus resultados é também efetuado um estudo numérico detalhado, mantendo-se todas as condições que foram utilizadas no estudo experimental.

Os resultados numéricos validam os resultados obtidos experimentalmente e revelam que a deflexão do segundo jato é devida às influências concorrentes da esteira, da camada de

corte, do jato de parede a montante resultante do primeiro jato e do escoamento cruzado. A deflexão do primeiro jato e a localização do centro do vórtice de parede é dependente da razão de velocidades entre a saída do jato e da alteração da altura de impacto e o escoamento cruzado. Através da alteração da velocidade de saída do segundo jato é possível verificar a sua rápida deflexão, nunca tocando diretamente no solo, ou seja, o jato a jusante é arrastado pelo jato a montante (primeiro jato) e não pelo escoamento cruzado, como seria de esperar. Através da alteração da altura de impacto é possível observar a ausência de escoamento ascendente na região entre jatos de impacto, como era esperado. Nesta região inesperadamente é observada a formação de um segundo vórtice de solo, algo ainda não reportado na literatura.

Palavras-chave

VSTOL, Jatos de impacto através de escoamento cruzado, efeito de solo, Validação numérica, Vórtice de parede.

Abstract

Vertical/short take-off and landing aircrafts at their hovering phase of flight create a three dimensional flowfield between lift jet streams, the airframe surface and the ground. The flowfield surrounding the aircraft during transition from hover to wing borne flight is of particular importance. During the transitional flight phase, the jets in crossflow phenomenon represent the most relevant configuration due to the complex flowfield that is created beneath the aircraft. The wall jets created by the impingement on the ground of the individual turbulent jet flow meet at a stagnation line and form an upwards flowing "fountain" that interacts with the airframe. Sometimes the fountain can provide a beneficial lift – generating ground cushion. Although, in most of the cases the fountain flow created generates a variety of undesirable characteristics, such as, hot gas ingestion, pressure, thermal and acoustic loads, change of the lift forces, lifting losses and the fuselage skin raise. The wall jet created by the jets impingement on the ground interacting with the free stream, results in a formation of a ground vortex far upstream of the impingement jet. This resulting ground vortex shape is strongly affected and the corresponding induced suckdown effect tends to be reduced by the upload produced by the fountain.

During the past three decades, the flowfield characteristics associated with this type of aircraft have been studied extensively. However, the complexity of the new VSTOL configurations with the very stringent requirements demands more investigation. The continued development of a VSTOL aircraft with an increasing reliance on computational design techniques is dependent on a better understanding of aerodynamics of the lift jets of an aircraft in ground effect.

This work is dedicated to the continuation of the experimental study began during the master's thesis, i.e., a detailed analysis of the complex flowfield of two in-line turbulent circular air jets with a low velocity crossflow impinging on a flat surface perpendicular to the geometrical jet nozzle axis. The jets exit conditions are changed along the study to provide a better understanding of the flowfield. To complete this analysis and in order to validate the experimental results a detailed numerical study is also presented, where all the features of the experimental flow are maintained.

The numerical results extend the experimental study, revealing that the deflection of the rear jet is due to the competing influences of the wake, the shear layer, the downstream wall jet of the first jet and the crossflow. The first jet deflection and the location of the ground vortex depend on the velocity ratio between the jet exit and the crossflow as well as the impingement height used. Through the rear jet velocity change, it is possible to verify the quick deflection of the second jet, never reaching the ground directly, i.e., the downstream jet is entrained by the upstream jet and not by the crossflow itself. Through the impingement

height change, it is possible to observe the absence of upwash fountain formation in the region between the impingement jets, as it was expected. In this region, it is unexpectedly observed the formation of a second ground vortex, something not yet reported in the literature.

Keywords

VSTOL, Impinging jets through a crossflow, Ground effect, CFD Validation, Ground Vortex.

Index

List of Figures

List of Tables

List of Acronyms

ASM	Anisotropic Equation Model
CTOL	Conventional Take-Off and Landing
DNS	*Direct Numerical Simulation*
HGI	*Hot Gas Ingestion*
LDA	Laser Doppler anemometry
LDV	Laser Doppler velocimetry
LES	*Large Eddy Simulation*
LRIP	*Low Rate Initial Production*
LRM	*Low Reynolds number Model*
NPR	*Nozzle Pressure Ratio*
RNG	*Renormalization Group Method*
RSM	*Reynolds Stress Equation Model*
UK	*United Kingdom*
USAF	United States Air Force
USAAF	United States Academy Air Force
USMC	United States Marine Corps
USS	United States Ship
VSTOL	Vertical/Short take-off and landing
VTOL	vertical take-off and landing

Nomenclature

A_w, A_n, A_e, A_s	cell faces areas
b'	source term to the pressure correction
C_μ, $C_{\varepsilon 1}$, $C_{\varepsilon 2}$	turbulence model constants
CD1	represents $C_{\varepsilon 1}$ in the computational program
CD2	represents $C_{\varepsilon 2}$ in the computational program
CM	represents C_μ in the computational program
D	diameter of the jet
EPSX	grid expansion coefficient in x direction
EPSY	grid expansion coefficient in y direction
EPSZ	grid expansion coefficient in z direction
EWALL	wall turbulent kinetic energy dissipation
f_D	Doppler frequency
f_{neg}	negative frequency
f_{pos}	positive frequency
f_0	focal length of focusing lens
f_{shift}	shift frequency
g_i	gravity acceleration
H	impinging height
IMAX	maximum points number in the y direction
JMAX	maximum points number in the z direction
k	turbulent kinetic energy
k_{in}	jet turbulent kinetic energy for the initial conditions
K	velocimeter transfer constant
KMAX	maximum points number in the x direction
L	Interjet spacing in the crossflow direction
L/D	dimensionless interject spacing in the crossflow direction

NS	represents the highest number of points in the grid for the three directions
NSKIP	Maximum number of interactions on the computational program
NXYZ	total number of points in the grid
NX	number of points of the grid at x direction
NY	number of points of the grid at y direction
NZ	number of points of the grid at z direction
p'	pressure correction
PKE	Prandtl numbers in the *k* and ε equations
PR	Prandtl number
R	radius of cylindrical coordinates
Re	Reynolds number
RHOREF	air density at T=20ºC
R_p	absolute residual at point P
S	Beam spacing
S	distance between the jets axis in the direction normal to the crossflow
S/D	dimensionless interject spacing on the experimental results
STOL	Short take- off and landing
S_φ	source term
S_p	source in cell P
$\overline{u_0}$	velocity outside the boundary layer
$\bar{u}$	mean velocity of the boundary layer
u^+	boundary layer dimensionless velocity
u_j	instantaneous velocity component in direction x_j
u_k	instantaneous velocity component in direction x_k
U_i	instantaneous velocity component in direction x_i
u_w, u_n, u_e, u_s	horizontal velocity at the faces
U_{neg}	negative horizontal velocity
U_{pos}	positive horizontal velocity
U_w, U_n, U_e, U_s	horizontal velocity at the cell centers
v_w, v_n, v_e, v_s	vertical velocity at the faces
V	vertical velocity, $\bar{V} + v'$ ou $(V_{mean} + V')$
VJ1	first jet vertical velocity at the computational program
VJ2	second jet vertical velocity at the computational program
V_r	velocity ratio, V_j/U_0
V_w, V_n, V_e, V_s	vertical velocity at the cell centers
W	transverse velocity, $\bar{W} + w'.(W_{mean} + W')$
WAIR	air molar mass
X	horizontal coordinate
XTOT	computational domain length in x direction (corresponding to half of the test section width)
Y	vertical coordinate
Y	height away the wall
y^+	dimensionless wall distance

YHOLE	vertical location of the impinging jets
YTOT	computational domain length in y direction (equal to the impingement height)
Z	transverse coordinate
ZHOLE	location of the center of the first impinging jet
ZHOLE1	location of the center of the first impinging jet at the computational program
ZHOLE2	location of the center of the second impinging jet at the computational program
ZTOT	distance between the centers of the two impinging jets

Greek symbols

Γ_h	diffusion coefficient of h
Γ_ϕ	diffusion coefficient of ϕ
Γ_ϕ	transport coefficient
ε	turbulent kinetic energy dissipation
ε_{in}	jet turbulent kinetic energy dissipation for the initial conditions
μ_T	turbulent viscosity
μ_τ	friction velocity
ρ	density
σ_k, σ_ε	turbulent Prandtl/ Schmidt number
ϕ	variable in general conservation equation
Φ	turbulent kinetic energy production term
ν	cinematic viscosity
λ	wave length
θ	calculated half angle of beam intersection
τ	shear stress
τ_w	wall shear stress
δ	total depth of the boundary layer
κ	von Karman constant

Subscriptions

J	exit jet value
J1	exit first jet value
J2	exit second jet value
o	crossflow value

Chapter 1

Introduction

To start this work, nothing better than to raise the question, **"What is a VSTOL aircraft?"**. In some words we could say that the VSTOL aircraft is considered one of the aviation's hopes and future and its importance could be perceived from its name. "VSTOL" stands for Vertical / Short Take Off and Landing. The VSTOL aircraft is an intermediate version between the conventional aircraft and the helicopter, however this type of aircraft by incorporating both the ability to take-off and land vertically as the helicopter, the ability to cruise, fly with high ranges, speeds comparable with those of conventional aircraft or even higher, and moderate payloads makes it suitable for applications that none of the other systems can carry out alone. They differ from the helicopter since they assume a more favourable aerodynamic figure together taking advantage of the wings, which both allow increased speed and range. This type of aircraft can assume different types of operation, such as, military, cargo transfer, ambulance, rescue operations. The first concept of the VSTOL aircraft has emerged in the early 1950's, and as a novelty and innovation it captured a lot of attention and research effort. Several configurations with different propulsion, lift, and aerodynamic systems were built in the whole world, but only one of them went through operation and had success. However, this plane with the latest version called AV-8B due to its big engine could not be adapted to supersonic flight, and a new world program to develop a new VSTOL airplane started in the early 80's (Figure 1).

Figure 1 VSTOL aircrafts: Left: Harrier AV-8B; Right: Yakolev_YAK-141

But first it is important to know how born this concept of aircraft and what is its evolution over the last 50 years.

1.1 VSTOL Aircraft History

1.1.1 The VSTOL Idea

The idea to create a VSTOL aircraft was born as an attempt to solve some technical limitation existing on the conventional aircraft flight. So the design and configuration of the VSTOL aircrafts depended of the conventional flight problems resolution. Nevertheless, this task was not easy to achieve due to the complexity of integrating in the aircraft a propulsion system that offers up the lift force required to make the aircraft landing vertically and hover near the ground.

Looking around us in the nature, it is possible to establish a parallelism with the propulsion system required to the VSTOL aircraft operation. Birds depend mostly on their wings to lift and fly, but in the nature there are some species where their legs are responsible for the most of the vertical thrust when they want to fly. So in nature it is possible to see the two fundamental concepts for the operation of any aircraft, the propulsion and lift concepts. When the birds use their legs to start their fly, the third Newton law is applied (figure 2). The third law states that for every action (force) in nature there is an equal and opposite reaction. In other words, if the bird exerts a force at the site where it is the take off, then this site also exerts an equal and opposite force on bird legs. Notice that the forces are exerted on different objects.

Looking now to the aircraft case, the principle of action and reaction is very important. The third Newton law explains the lift generation of an aerofoil. According to this law, the production of a propulsive force generates a reaction: the aircraft movement (Figure 2). The engine produces thrust through action and reaction. The engine produces hot exhaust gases which flow out from the back of the engine. In reaction, a thrusting force is produced in the opposite direction.

In the VSTOL aircraft case, the most important requisite is the thrust produced by the engine to be higher than the aircraft weight at the take-off moment. The engine capable to produce such thrust was the turbofan engine, but despite the reaction engine concept have appeared through the invention of the eolipila by Heron of Alexandria in the 1st century BC, only with the end of the Second World War it was open the reaction engine era.

Stage 1

Stage 2

Stage 3

Stage 4

Stage 5

Figure 2: Preparing bird fly stages[1]

[1] http://www.huffingtonpost.com/2014/02/05/slow-motion-animal-gifs_n_4720541.html

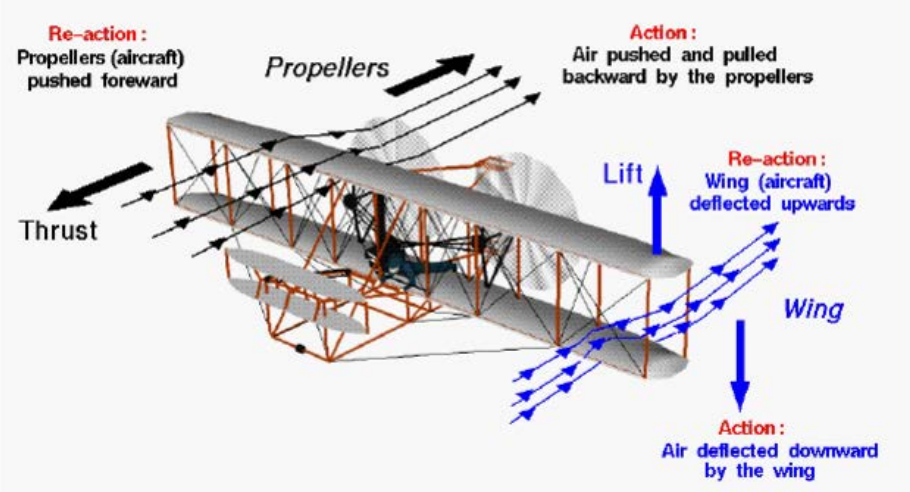

Figure 3: Third Newton Law applied to an aircraft[2]

When the Second World War ended, several lessons have been seized and new ideas have been emerging looking at the destruction the war had caused. On these new ideas was the development of an aircraft capable of take-off or landing from spaces that were not runways or in small places. The need for an aircraft with such characteristics came from the fear of a new war where a possible attack would destroy runways, aircrafts or the military installations. With the development of this aircraft type it would be possible to respond effectively to an attack of this nature.

1.1.2 Development and conception of the idea

In 50's decade was developed the first British fixed-wing vertical take-off and landing (VTOL) aircraft, the Short S.C.1 aircraft. This aircraft was designed to meet a Ministry of Supply request for a vertical take-off research aircraft issued in September 1953. The ministry request was accepted and two aircraft were construed, the XG900 and the XG905 (figure 4), to meet Specification ER.143D dated 15 October 1954.

The first European VTOL aircraft was a single-seat low wing tailless delta wing aircraft of approximately 3,629 Kg all-up weight (max. 3,493 Kg for vertical flight). It was powered by four vertically mounted (figure 5), lightweight Rolls-Royce RB108 lift engines providing a total vertical thrust of 3,900 Kg and one RB108 cruise engine in the rear to provide thrust for forward flight. The lift engines were mounted vertically in side-by-side pairs in a central bay so that their resultant thrust line passed close to the centre of gravity of the aircraft. These pairs of engines could be swivelled about transverse axes; they were therefore able to produce vectored thrust for acceleration/deceleration along the aircraft's longitudinal axis.

[2] http://wright.nasa.gov/airplane/newton3.html

Bleeds from the four lift engines (using approximately 10% of the intake air mass/thrust) powered variable nose, tail and wing tip jets providing pitch, roll and yaw control at low speeds, when there was insufficient airflow over the control surfaces for conventional control.

The Short SC 1 was constructed at Short's Belfast factory in Northern Ireland. The first conventional take-off and landing (CTOL) flight was made on 2 April 1957. One year later the second prototype made the first tethered vertical flight on 26 May 1958. On 25th October of the same year it was made the first free vertical flight. The first in-flight transition was made on 6 April 1960. During the experimental flights the high aircraft height and the practically unknown type flow produced by the four incident jets raised serious aerodynamic problems, turning the aircraft unavailable for this type of flight.[3]

At the same time in California, an experimental vertical take-off and landing (VTOL) aircraft was developed by the USAF (United State Air Force) to test the validity of an aircraft that could take off vertically, achieve horizontal flight and land vertically under turbojet power, the Ryan X-13 Vertijet (figure 6). Just after the Second World War the Navy had been studying the feasibility of submarine-based aircraft, and from 1947 to 1951, Ryan conducted a series of tethered flight tests with unmanned VTOL aircraft. Based on that project, in 1953, the company was awarded a USAAF (United States Army Air Forces) contract to develop two prototypes of a full-size, manned VTOL aircraft.

Figure 4: XG905 aircraft[4]

[3] https://en.wikipedia.org/wiki/Short_SC.1

[4] Jean-Christophe Carbonel. Short SC.1, Le premier VTOL européen. Airprofils n°7, ISBN 978-2-919231-05-8.

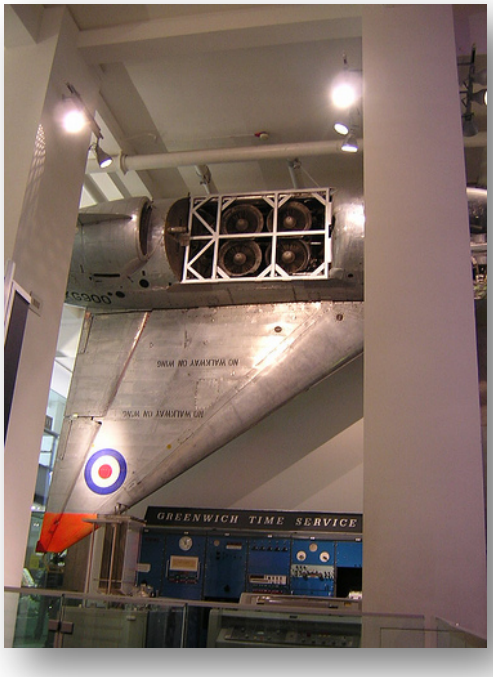

Figure 5: The four lift jets[5]

The chubby dimensions of the Ryan X-13 Vertijet meant it was not the most beautiful aircraft the world had ever seen. It compact dimensions were necessary to keep the weight to a minimum. There was just enough room within the aircraft's fuselage for a single seat cockpit, and a 10,000 lbf (45kN) Rolls-Royce Avon turbojet engine. The wings were mounted at the very peak of the fuselage, and they had a pronounced Delta-wing shape. The high position of the wings was intended to improve stability in horizontal flight.

Between 1955 and 1958, the Air Force tested two X-13 vertical take-off fighter demonstrators in response to an emerging demand for aircraft that could operate independently of nuclear-vulnerable airfield infrastructure. The lightweight designs took off and landed in a vertical orientation from a mobile launch and recovery platform, eliminating the excess weight of landing gear. This approach proved to be impractical from the pilot's perspective and the aircraft lacked the performance to be an adequate interceptor. While the Vertijet was an improvement over the other so-called "tail sitters" like the Convair POGO (an experiment in vertical take-off and landing designed, constructed, and tested by Lockheed and Convair in 1951), its operational profile has since been regarded as a technological dead-end for vertical take-off and landing aircraft.[6]

[5] http://www.symscape.com/blog/science-museum-vertical-takeoff-landing
[6] http://www.militaryfactory.com/aircraft/detail.asp?aircraft_id=780

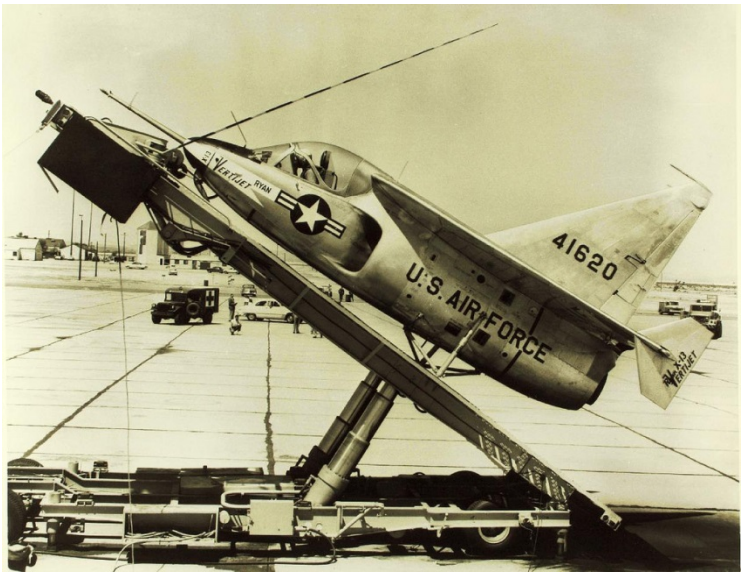

Figure 6: Ryan X-13 Vertijet[7]

In the 1960s and early 70s, Germany planned three different VTOL planes. One used the F-104 startfighter (figure 7) as a base for research for a V/STOL aircraft. Although two models (X1 and X2) were built, the project was cancelled due to high costs and political problems as well as changed needs in the Luftwaffe and NATO. The EWR VJ 101C (figure 8) did perform free VTOL take-offs and landings, as well as test flights beyond Mach 1 in the mid- and late 60's. The others were the VFW-Fokker VAK 191B light fighter and reconnaissance plane, and the Dornier. d31 (troop) transport.[8]

Figure 7: F-104 Starfighter[9]

[7] https://www.flickr.com/photos/sdasmarchives/6335531684

[8] http://airandspace.si.edu/collections/artifact.cfm?object=nasm_A19600018000

[9] http://fas.org/nuke/guide/usa/airdef/f-104.htm

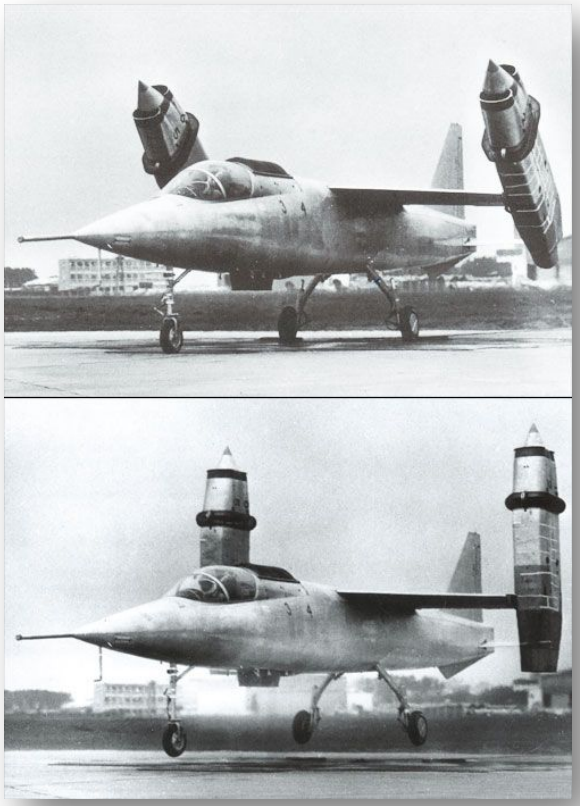

Figure 8: EWR VJ 101C experimental German jet fighter VTOL tilt jet aircraft[10]

The EWR-VJ 101 was similar in appearance to the Bell XF-109 (figure 9), both with rotating engines in nacelles at the wingtips. In addition to the wingtip engines, two further lift jets were installed in the fuselage to supplement the main engines in hovering flight. In total the aircraft had six Rolls Royce engines.

Figure 9: Bell XF-109[11]

[10] https://www.pinterest.com/pin/257408934923528364/

[11] http://combatace.com/topic/63319-bell-xf-109/

The VAK 191B (figure 11) was produced by the German company Vereinigte Flugtechnische Werke (VFW) a company formed by Focke-Wulf and Weser-Flugzeugbau. Propulsion (figure 10) was provided by a Rolls-Royce/MAN Turbo RB.193-12 vectored thrust engine for both lift (force) and cruise (aeronautics) which was augmented by two Rolls-Royce vertical lift engines. There was produced three VAK 191B aircraft (figure 11). The first hovering flight was made in Bremen on 20 September 1971 and the first transition from vertical flight to horizontal and vice versa was achieved on 26 October 1972 in Munich[12].

The Dornier Do 31 (figure 12) was designed to meet a NATO specification (NBMR-4) for a tactical support aircraft for the EWR VJ 101 VTOL strike aircraft designed under the NATO contract of BMR-3. Due to the high costs, technical problems and a change of requirement the project was cancelled in 1970. Three prototypes were constructed, E1, E2 and E3. Initial designs incorporated a Bristol Pegasus vectored-thrust turbofan in each of the two inboard nacelles and four Rolls-Royce RB162 lift engines in each of the outer nacelles E1 was powered only by the Pegasus engines, and was designed to test horizontal flight. E2 was a static test airframe, and did not fly. E3 had both Pegasus and RB162 lift engines installed, and was designed to test the vertical flight mode. The first prototype (E1) first flew on 10 February 1967 with just the two Pegasus engines. The third prototype (E3) flew in July 1967 with all ten engines fitted. The first hovering flight took place on 22 November 1967. Full forward and backward transitions were made in December 1967[13].

Figure 10: Rotating nozzle detail[14]

[12] https://en.wikipedia.org/wiki/VFW_VAK_191B

[13] https://en.wikipedia.org/wiki/Dornier_Do_31

[14]https://en.wikipedia.org/wiki/VFW_VAK_191B#/media/File:Aircraft_engine_VAK191B_hover_swing_nozzles_LH_2.jpg

Figure 11: The VFW-Fokker VAK-191B[15]

Figure 12: Dornier Do 31[16]

All the aircrafts presented had problems during the take-off and on the transition to the convectional flight, can be regarded during these flight stages as a dead weight, which strongly limits the payload and autonomy.

[15] http://www.anigrand.com/AA2119_VAK-191.htm

[16] http://www.diseno-art.com/news_content/2013/10/strange-vehicles-dornier-do-31-vtol-jet-transport/

1.1.3 Harrier/ AV-8B generation – the way for the success

The idea of using the same engine for vertical and horizontal flight by altering the path of the thrust led to the Bristol Siddeley Pegasus engine. This engine is able to direct thrust downwards which can then be swivelled to power a jet aircraft forward. This was developed side by side with an airframe, the Hawker P.1127 (figure 13), which became subsequently the Kestrel and then entered production as the Hawker Siddeley Harrier, though the supersonic Hawker Siddeley P.1154 was cancelled in 1965[17].

The Hawker P.1127 made its first hover on 21 October 1960 on tethers, but this was not considered to be beneficial to feel out the aircraft response, so the first untethered hover was made less than a month later, on 19 November 1960. First conventional flight was made on 7 July 1961 and first double transition on 12 September 1961. Control power was low about all axes, which, combined with suck-down and limited height control power, resulted in a high pilot workload in hover. Hot gas ingestion was overcome with a low forward speed in take-off and landing. This problem is transversal for all the VSTOL aircrafts[18].

Figure 13: Hawker P.1127 Kestrel[19]

[17] https://info.aiaa.org/tac/AASG/VASTC/VSTOL%20History/Prop_Hover_FwdFlight.aspx
[18] https://sites.google.com/site/mechvtol/vtol-history
[19] http://www.portierramaryaire.com/fichas/harrier_1.php

It can justifiably be said that the Harrier is Britain's greatest post-war aviation success. However, it had originally been the RAF's intention to introduce a far more formidable 'jump-jet' to the front line - the Hawker Siddeley P.1154 (figure 14). The cancellation of this project in February 1965 was a huge blow to the prospects of the British aircraft industry, with long-term consequences. The opportunity to provide the world's first supersonic V/STOL fighter was lost.

Figure 14: Hawker P.1154 RN Osprey/Sea Harrier[20]

The French in competition with the Hawker P.1154 had developed a version of the Dassault Mirage III (figure 15) capable of attaining Mach 1. The Dassault Mirage IIIV achieved transition from vertical to horizontal flight in March 1966, reaching Mach 1.3 in level flight a short time later. The Mirage IIIV model followed the Dassault Mirage III and featured eight small vertical lift jets straddling the main engine. The design was in response to a NATO specification for a VTOL strike fighter.

Dassault modified the first Mirage III prototype as the Balzac V to serve as an interim VTOL testbed. The Dassault Mirage IIIV had eight Rolls-Royce RB.108 lift engines and an un-reheated Bristol Orpheus BOr 3 as the main engine. The Balzac began tethered hovering on 12 October 1962 and achieved the first free hover some days later. The first accelerating transition from vertical take-off to horizontal flight took place on its 17th sortie on March 18, 1963.

The Yakovlev Yak-38 (figure 16) was the Soviet Navy's VTOL aircraft for their light carriers, cargo ships, and capital ships. It was developed from the Yakovlev Yak-36 experimental aircraft. Attempting to fulfil the same role as did the British Aerospace Harrier VTOL (Vertical

[20] http://www.gengriz.co.uk/just%20like%20the%20real%20thing.htm

Take-Off and Landing), the YAK-38 seems to have been limited in design in some respects to prevent it from reaching its operating apex. The main thrust vectoring turbojet was held at rear of the fuselage and complimented by two smaller lift-jets mounted forward. These lift-jets were mounted specifically to produce the downward flow of thrust, allowing the system to achieve vertical take-offs from Soviet carriers. The first of the Yak-38 prototypes flew in early 1971[21].

Figure 15 Dassault Mirage III:[22]

Before the Soviet Union collapsed, a supersonic VTOL aircraft was developed as the Yak-38's successor, the Yak-141, which never went into production.

Designed in the late 1970s as an Anglo-American development of the British Hawker Siddeley Harrier, it was born the AV-8B Harrier II, the first operational V/STOL aircraft. The project that eventually led to the AV-8B's creation started in the early 1970s as a cooperative effort between the United States and United Kingdom (UK), aimed at addressing the operational inadequacies of the first-generation Harrier (Hawker P.1127). Early efforts centred on a powerful revamped Rolls-Royce Pegasus engine to dramatically improve the capabilities of the Harrier. Due to budgetary constraints, the United Kingdom abandoned the project in 1975. With development costs estimated to be around €375-416 million (1974 tax rates), the United States (McDonnell Douglas) was unwilling to fund development by itself, and ended the project later that year. McDonnell Douglas modified two AV-8As with new wings, revised intakes, redesigned exhaust nozzles, and other aerodynamic changes; the modified forward fuselage and cockpit found on all subsequent aircraft were not incorporated on these

[21] http://www.militaryfactory.com/aircraft/detail.asp?aircraft_id=189

[22] https://en.wikipedia.org/wiki/Dassault_Mirage_IIIV#/media/File:Dassault_Mirage_IIIV.jpg

prototypes. Designated YAV-8B, the first converted aircraft flew on 9 November 1978, performing three vertical take-offs and hovered for seven minutes. Flight testing of these modified AV-8s continued into 1979. Between 1978 and 1980, the McDonnel Douglas and United States Navy repeatedly attempted to terminate the AV-8B program.

Figure 16: Yakovlev Yak-38 (Forger) Vertical Take Off and Landing (VTOL) Carrier-Borne Strike Fighter[23]

In August 1981, the program received a boost when British Aerospace (BAe) and McDonnell Douglas signed a Memorandum of Understanding, marking the UK's re-entry into the program. Through this cooperation four full-scale development aircraft were constructed. The first of these used mainly for testing performance and handling qualities, made its maiden flight on 5 November 1981. The second and third full scale development aircraft, which introduced wing leading-edge root extensions and revised engine intakes, first flew in April the following year and the fourth aircraft followed in January 1984[24].

Since the 1980s the aircraft is powered by a version of the Pegasus, which gives the aircraft its V/STOL ability, but the engine that equipped the more recent aircrafts it was upgraded over several years. Today the Harrier AV-8B II is a fixed-wing vertical/short take-off and landing (V/STOL) aircraft. Its ability to take off vertically makes it one of the most manoeuvrable combat aircraft in service. It can zoom out of the range of enemy fire extremely quickly[25].

[23] http://www.militaryfactory.com/imageviewer/ac/pic-detail.asp?aircraft_id=189&sCurrentPic=pic1
[24] https://en.wikipedia.org/wiki/McDonnell_Douglas_AV-8B_Harrier_II/
[25] http://www.boeing.com/history/products/av-8-harrier-ii.page

Figure 17: Harrier AV-8B hovering[26]

1.1.4 Joint Strike Fighter – F35-B – The Future of the VSTOL aviation

The Joint Strike Fighter program was initiated and designed to replace some fighter aircrafts, namely the F-16, A-10/A-18 and the AV-8B tactical fighter and attack aircraft. To keep the down costs of the development, production and operation, a common design was plane in three variants that share 80 percent of their parts. The three variants are the F-35A (a conventional take-off and landing aircraft), the F-35B (the short take –off and vertical landing aircraft) and the F-35C (Catapult Assisted Take-Off but Arrested Recovery aircraft)[27].

The JSF development contract was signed on 16 November 1996. In 1997, Lockheed Martin was selected as one of two companies to participate in the Joint Strike Fighter concept demonstration phase. In October 2001, the Lockheed Martin X-35 (figure 18) was chosen as the winner of the competition and teamed with Northrop Grumman and BAE Systems to begin production[28]. The X-35 design was considered to have less risk and more growth potential. The designation of the new fighter as "F-35" is out-of-sequence with standard United States Department of Defence aircraft numbering.

[26] http://www.marines.com/operating-forces/equipment/aircraft/av-8b-harrier-2#purpose
[27] https://en.wikipedia.org/wiki/Lockheed_Martin_F-35_Lightning_II
[28] https://www.f35.com/about/history

The first production F-35A (figure 19) rolled out of the assembly in Fort Worth, Texas, in February of 2006. Later that year, the stealthy F-35 Joint Strike Fighter, in development by the United States and eight other countries, was named the "Lightning II," in homage to two earlier fighters.

In December of 2006, the F-35 completed its first flight. Over the next few years, flight and ground test articles of all three variants rolled off the production line and began collecting test points. More specifically the development of the F-35B in November 2003 (figure 20). The maiden flight of the first F-35B prototype took place in June 2008. The low rate initial production (LRIP) contract for six F-35B STOVL aircraft was placed in July 2008. The second prototype achieved its first flight in February 2009.

Figure 18: X-35 aircraft[29]

The F-35B accomplished its hover capability during a flight test that took place at Naval Air Station Patuxent River in March 2010. It accomplished supersonic speeds in June 2010. The shipboard testing of the aircraft on the flight deck of the USS Wasp (LHD-1) aircraft carrier was completed in October 2011. The first two F-35Bs were delivered to the USMC in January 2012. The assembly of the UK's first production F-35B aircraft, designated BK-1, was completed in November 2011. The maiden flight of the BK-1 took place in April 2012[30]. In 2012, the F-35 ramped up with 30 aircraft deliveries and increased testing operations across the United States. The program reached several milestones in weapons separation testing, angle of attack testing, aerial refuelling training, and surpassed more than 5,000 flight hours with more than 2,100 recorded flights in that year.

[29] http://www.superrune.com/gallery/x35.php

[30] http://www.naval-technology.com/projects/f-35b-lightning-ii-joint-strike-fighter-stovl-variant/

In terms of propulsion, the Pratt & Whitney F135 and the General Electric/Rolls Royce F136 power the F-35 models. Both engines use common parts and it may be interchangeable. Present in VSTOL version to able the lift system, the General Electric/Rolls Royce F136 is an additional motor developed and produced by the Rolls-Royce. The Pratt & Whitney F-135 is an evolution of the successful F-119 that drives the F-22 Raptor (but is not enabled for super cruise, as the F-119). The Pratt & Whitney F135 engine with Rolls-Royce Lift System, including roll posts, and rear vectoring nozzle for the F-35B. The Lift System (figure 22) is composed of a lift fan that generates a column of air that produces the nearly 20,000 pounds of lift power also providing cooling for down drafting air compared to previous STOL offering, along with an equivalent amount of thrust from the "Three Bearing Swivel Module" (3BSM), drive shaft connecting the lift fan to the power plant while working in conjunction with the Three Bearing Swivel Model and two roll posts (wing-mounted thrust nozzles for roll control). The 3BSM is a thrust vectoring nozzle which allows the main engine exhaust to be deflected downward at the tail of the aircraft. The air-flow through the fan is controlled via variable inlet guide vanes. The lift fan is near the front of the aircraft and delivers a counterbalancing thrust using two counter-rotating hollow-bladed titanium blisks (a bladed disk achieved by super-plastic forming of the blades and linear friction welding to the blisk (a turbomachine component comprising both rotor disk and blades) hub. It is powered by the engine's low-pressure (LP- 2 stages) turbine via a drive shaft and gearbox. Roll control during slow flight is achieved by diverting unheated engine bypass air through wing-mounted thrust nozzles called Roll Posts. The lift system was successfully demonstrated during a flight test of the X-35B during the summer of 2001.

Figure 19: Joint Strike Fighter F-35A[31]

[31] https://www.flickr.com/photos/lockheedmartin/8680029233/in/album-72157628445024825/

Figure 20: Joint Strike Fighter F-35B[32]

Figure 21: Joint Strike Fighter F-35C Arrestment Landing[33]

[32] https://www.flickr.com/photos/lockheedmartin/9547198105/in/album-72157625859980836/
[33] https://www.flickr.com/photos/lockheedmartin/14120789370/in/album-72157626318767009/

Figure 22: The Pratt & Whitney F135 engine with Rolls-Royce Lift System, including roll posts, and rear vectoring nozzle for the F-35B[34].

1.2 General considerations

When a VSTOL aircraft operates there are three different stages during the flight, being all different, with its own flow characteristics and with different kind of problems associated. A VSTOL flight comprises the **hover phase**, the **transition to forward flight phase** and the **forward flight operation** (figure 23). The hover phase is the most complex phase during the flight and can be further divided into two more phases because the flowfield associated in each phase is completely different. So, the hover phase can be subdivided into out-of-ground-operation and hover in the vicinity of the ground.

The forward flight operation involves aerodynamic and propulsion problems, while the transition to the forward flight adds to these problems the necessity for the integration, via suitable control, of the aerodynamic and the propulsion systems on the aircraft. The hover out-of-ground stage is principally affected by the propulsion system and its ability to provide the necessary thrust that carries the aircraft enough distance above the ground before transition to forward operation. The hover in ground vicinity involves a complex flow field with several phenomena resulting in a considerable reduction of lift generated by the jets. This reduction in the lift can reach at a height-to-jet-diameter ratio of two up to 60% of the presumable jet thrust. This loss on the jet thrust may compromise significantly the aircraft's

[34] https://en.wikipedia.org/wiki/Rolls-Royce_LiftSystem#/media/File:Engine_of_F-35.jpg

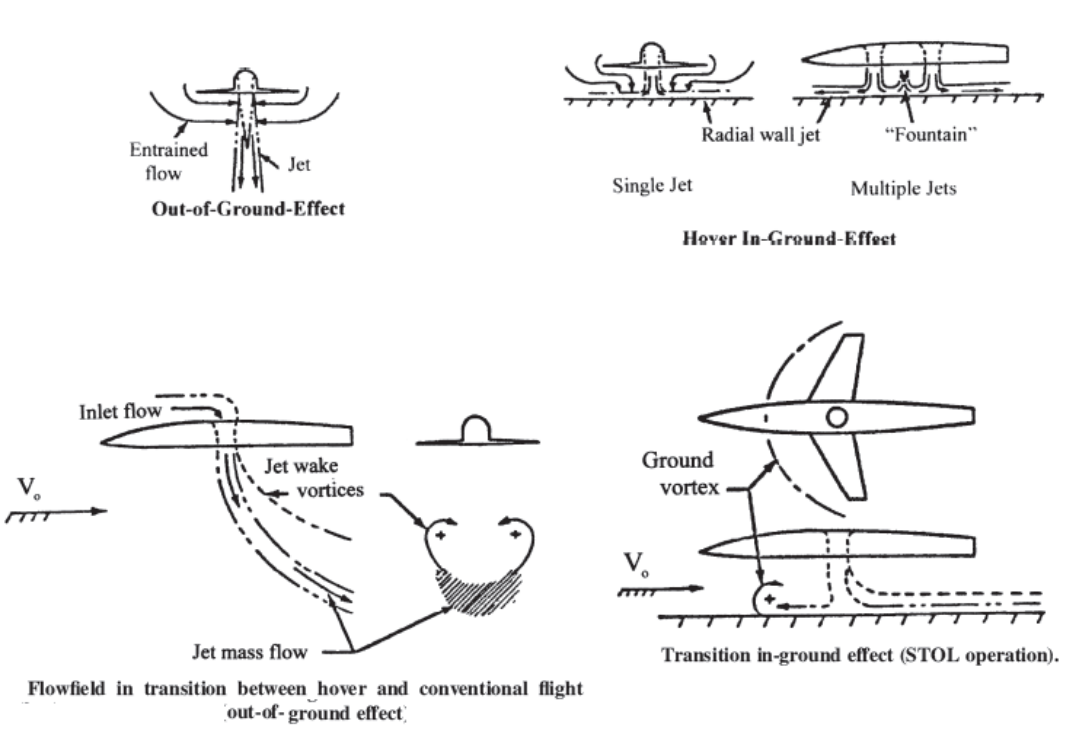

Figure 23: Various operational flow fields associated with the VSTOL aircraft[35].

capabilities as well as its objective. Another problem that occurs in the hover out of ground stage is the hot gas ingestion. This ingestion of exhaust gases by the engine has a considerable number of consequences. The first consequence is the reduction of the overall pressure rise, reducing the engine thrust. The second effect is the increase of the turbine inlet temperature. The greater the temperature rise as a result of ingestion, the greater the power needed to maintain thrust. This can only be accommodated up to the point where either the maximum rotor speed limit or the maximum turbine inlet temperature is reached. The HGI, Hot Gas Ingestion is a phenomenon that can develop very quickly, with the temperature of the air entering the inlets fluctuating as a function of height and time, and it can be a limiting factor in determining the maximum landing mass of the aircraft at the highest operating temperatures required by the operator. The flow mechanisms leading to hot gas ingestion can be broken into three categories: far field, crossflow and near field (figure 24).

[35] Kuhn R. E, Margason R. J, Curtis P. (2006). Jet-induced Effects: The Aerodynamics of Jet- and Fan-powered V/STOL Aircraft in Hover and Transition. Volume 217. Chapter 1. Frank K. Lu, Editor-in-chief. Published by the American Institute of Aeronautics, Inc. 1801 Alexander Bell Drive, Reston, Virginia 20191-4344.

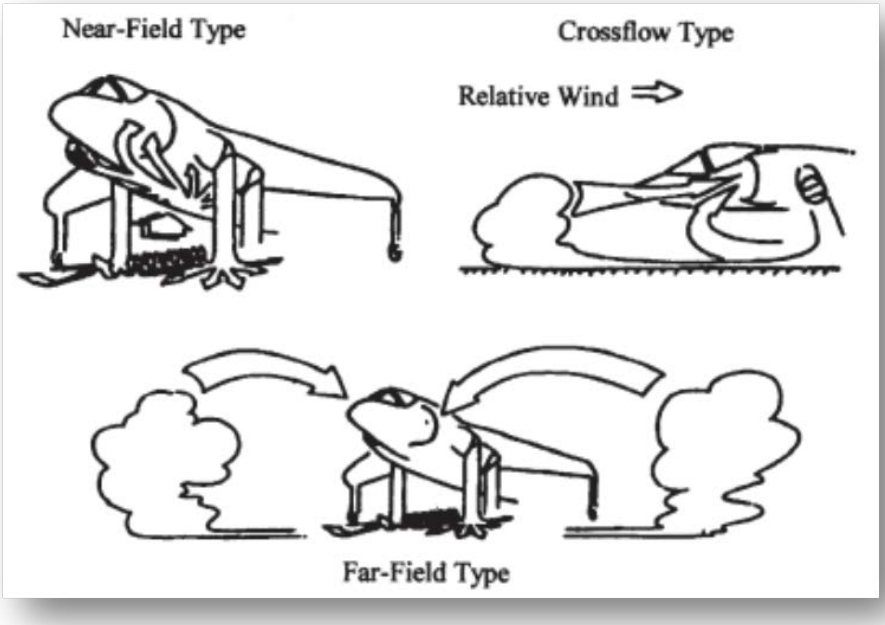

Figure 24: Flowfield that can lead to hot -gas ingestion[36]

The first mechanism results from the forward away initially movement of the ground sheet wall jet due to the aircraft movement. This happened because the hot gases after some distance lose their momentum, rising and separating from the ground. The portion of the hot gases that separate from the ground mixes with the surrounding air and backs again to the intake. The second mechanism is a consequence of the instability of the jet and the fountain flows. The entrainment action into the flow leads to discrete vortices which can detach from the main jet. The latter mechanism, near field ingestion is usually the most serious and occurs when fountain flows find their ways to the aircraft inlet, being that when exists multiple impinging jets, its impact on the ground plane create a fan shape up wash fountain beneath the aircraft. When the fountain impinges on the underside of the fuselage, flowing from the fuselage to the intake, the engine may sucks the flow to the intake, creating severe temperature distortion to the intake, since, these gases are much hotter than those from the far field ingestion.

1.3 Flowfield on hover in ground effect

The hover at the vicinity of the ground involves several complex fluid flow phenomena's, resulting in a considerable reduction of the lift produced by the jets. At this moment, the reduction of the lift can reaches up to 60% of the supposable jet thrust at low impingement

[36] Kuhn R., Margason R. J., Curtis P. (2006). Jet Induced Effects: The aerodynamics of Jet and Fan Powered V/STOL Aircraft in Hover and Transition. Volume 217. Chapter 5. Frank K. Lu, Editor-in-Chief. Published by the American Institute of Aeronautics and Astronautics, Inc. 1801 Alexander Bell Drive, Reston, Virginia 20191-4344.

heights. The huge jet thrust loss difficult the aircraft to accomplish the mission for which it was projected by the reduction of its capabilities.

During hover in ground vicinity the flow field can be generally divided into several zones. Figure 25 shows all of these zones. The interaction of the lift jets, identified by number 1, with the ground and the airframe surface, identified by number 2, results in the formation of a wall jet that can be described as a deflected flow turning into a high-speed flow parallel the ground plane, identified by number 3 (inner wall jet region) and 4 (outer wall jet region). The collision of the encountering wall jets, one from each jet, results in the formation of the fountain flow (identified by number 5), and a stagnation line between the two jets. Above the rising flow resulting from the collision of the two wall jets, the fountain upwash flow begins and develops (identified by number 6). It is a fan-shaped flow directed upwards. The fountain spreads as it moves further upwards with relatively higher spreading rates than those of the main jets. The fountain flow continues to rise until it hits the under surface of the aircraft fuselage.

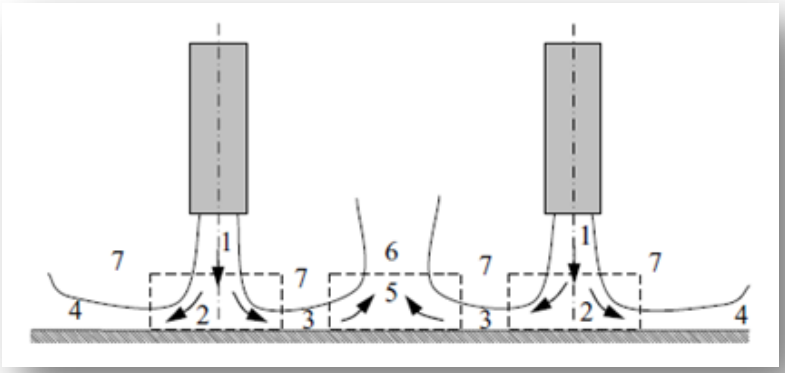

Figure 25: Different region on the flow field when the VSTOL aircraft operates in ground vicinity[37]

This zone is called the fountain impingement region. The fountain impingement continues to exist but with higher momentum for heights of the aircraft above the ground from four to five times the diameter of the jets. This fountain impingement causes a spreading flow below the aircraft surface. Sometimes it is called upper wall jet region. However, at relatively high distances to the ground, the flow lacks the characteristics of a jet. Laterally the shear layers accompanying the high-speed flows of the main jet, wall jet, and spreading flow below the aircraft, the flow is entrained in the viscous entrainment region. Below the aircraft, this entrainment accelerates nearby fluid, which results in a considerable decrease of pressure,

[37] Kate R. P., Das P. K., Chakraborty S. (2007). An experimental investigation on the interaction of hydraulic jumps formed by two normal impinging circular liquid jets. Journal of Fluid Mechanical. 590: 355-380.

causing what is called “suck-down” effect underneath the airframe. The flow field that includes the fountain flow also generated vortex like flows between the upward fountain and the downward flowing jets. This vortex like flows are characterized by induced high suction pressure between the jets and fountain, higher than would be induced by the wall jets alone, being responsible for the lift losses. This lift loss is about 4% when hovering out of ground effect. On the other hand, in ground proximity, when suck-down effect is combined with the entertainment around the wall jet, very low negative pressures are induced that produce the high lift loss mentioned earlier. After the jets impinge on the ground, the generated wall jets continue to flow on the ground plane. The wall jet facing the free stream extends to a certain distance depending on some factors such as, the jet strength, and the boundary layer thickness on the ground plane, if any, due to any freestream motion. Finally, the ground vortex separates in what is called, ground wall jet separation zone. The recirculation of the separated wall jet takes place above the separation zone and at the lower surface of the aircraft. This recalculated flow moves further towards the engine inlets causing what are known as hot gas ingestion mentioned in the above text. This recirculation is amplified upon the introduction of free stream or crossflow.

1.4 Motivation

The study of turbulent jets impinging on a flat surface through a low velocity crossflow is imperative when the aircraft in study is the VSTOL type, and the objective of the study is to understand what happens beneath in this type of aircraft when landing or hovering. This type of turbulent jets that impinge on a flat surface with the presence of a low velocity crossflow are also found in another applications, such as, cooling of the turbines blades, dispersion of pollutants into the atmosphere through a chimney, discharge of liquid waste for rivers and injection of air into the dilution zone of the combustion chamber of the gas turbine. As mentioned before the objective of this study is focused in the V/STOL applications, being the Lockheed Martin F-35 Lightning II the focused aircraft. This aircraft is a family of single seat, single engine, and fifth generation multirole fighter under development to execute ground attack, reconnaissance and air defence missions with secrecy capability. There are three main models of F-35: a conventional take-off and landing variant represented by the F-35A, a short take-off and vertical landing variant represented by the F-35B, and a carrier based variant represented by the F-35C. This family of aircrafts follows the line established by the experimental aircraft developed for the Joint Strike Fighter program, the X-35, to replace the United States military F-16, A-10, F/A-18 and AV-8B tactical fighter aircraft.

The F-35 seems to be smaller, single engine sibling of the twin engine Lockheed Martin F-22 Raptor, and actually drew elements from it. With respect to the exhaust duct design, it was inspired by the General Dynamics Model 200 design (figure 26), that it was proposed for a 1972 supersonic VTOL fighter requirement for the Sea Control Ship. Since the 1960s, several

experimental designs have been study and developed, but unsuccessfully as the Rockwell XFV-12, being the F-35B the first STOVL stealth fighter operational supersonically.

This study is focused in a specific aircraft, the F-35B. The F-35B is the first aircraft capable of combining the benefits of stealth technology with the benefits of STOVL capabilities. This combination of benefits allows F-35B to land and take off from virtually any surface on the planet, such as, moving naval ships, roads or unprepared rough airfields, making this aircraft unique among any aircraft in history. The propulsion system incorporates the lift fan system, that it is positioned just aft of the cockpit, being that put into action when the pilot sets the aircraft into vertical flight mode for either take off, hover or landing flight actions.

Figure 26: General Dynamics 200[38]

Thus, when the aircraft is in one of this situations, the lift fan works in conjunction with the positional aft thruster duct (figure 27) that itself is positioned at a downwards angle deliver upwards thrust when it is in vertical position (figures 28 and 29). In this case, a lift fan operates as a counter balance for the power delivered through the rear jet exhaust. Also acts as supplying cooler air into the hot jet wash that it was generated by the engine nozzle. The lift fan is powered via a drive shaft from the front of the engine and it is seen in operation when a pair of dorsal and ventral doors is opened. There are other panels just aft of the lift fan that are also opened to afford the necessary mass flow to the auxiliary engine. To control the balance and the rolling, F-35B use the twin roll post, and like the Harrier's vertical flight puffer jets, the twin roll posts work through its ducted wings and fuselage points.

[38] https://www.flickr.com/photos/sdasmarchives/8126230168/

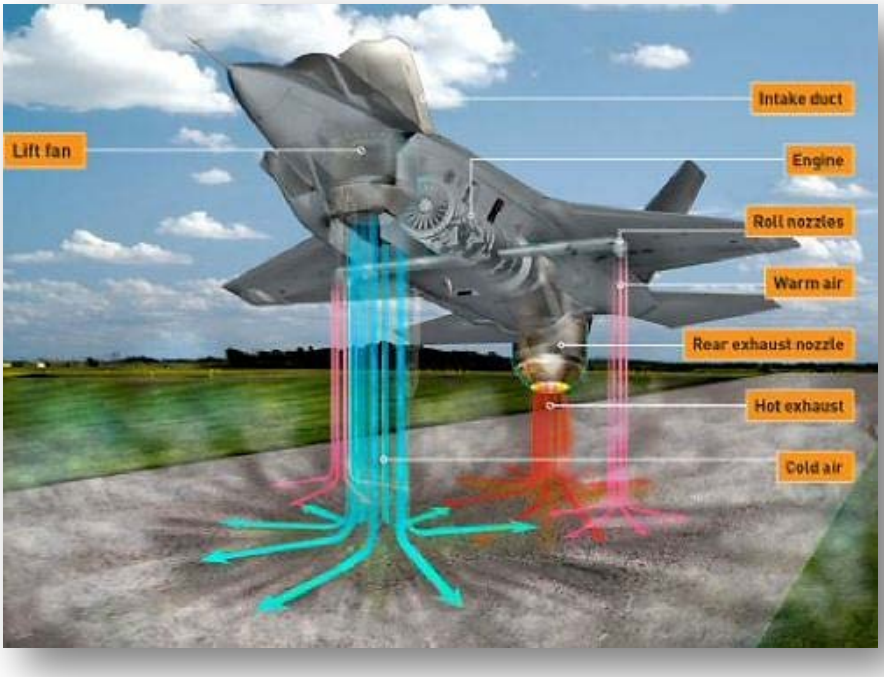

Figure 27: F-35's thrust vectoring nozzle and lift fan[39]

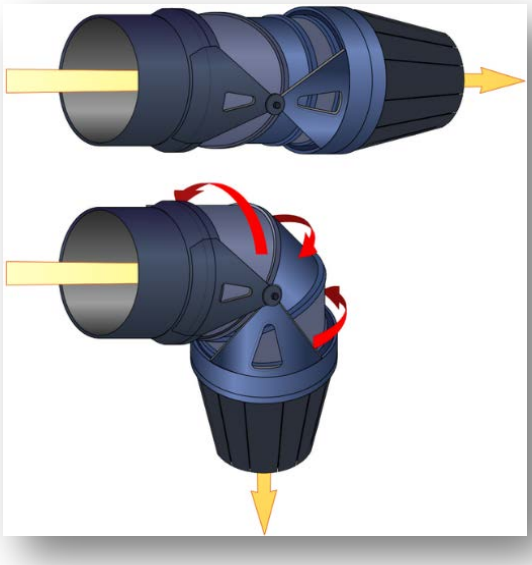

Figure 28: Thrust vectoring nozzle of the F135-PW-600 STOVL variant[40].

[39] http://www.rense.com/1.imagesH/f2.jpg

[40]http://en.wikipedia.org/wiki/Pratt_%26_Whitney_F135#mediaviewer/File:Jet_engine_F135%28STOVL_variant%29%27s_thrust_vectoring_nozzle_N.PNG

Figure 29: Thrust Vectoring in the real F-35B aircraft[41]

Regarding the operation of this aircraft, the F-35 completed its first flight in December of 2006. In the next few years, flight and ground test articles for all the variants of the F-35 rolled off the production line and began collecting test points. In February of 2011, the first production F-35 conducted its first flight with deliveries of the aircraft beginning that very same year. The complexity of this VSTOL aircraft configuration together with the very stringent requirements has required an enormous amount of R&D in last decade. On 12th May 2012 the 200th test flight of the F-35B (BF-3) (figure 30) measurement of stresses on the aircraft during supersonic manoeuvres was done. Also during this year, the F-35 ramped up with 30 aircraft deliveries and increased testing operations across the United States. As the F-35 Lightning II program progresses, more bases around the United States are flying the aircraft. At test sites, the Integrated Training Centre and the first operational base, the U.S. Air Force, Navy and Marine Corps as well as international partners are experiencing the 5th Generation capability of the F-35. In addition to the military bases, F-35's also flies from Lockheed Martin's shared runway with NAS Fort Worth JRB in Texas.

Aerodynamically, the landing phase or near the ground hovering phase, creates a complex three dimensional flow field between the jet streams, the airframe surface and the ground on this type of aircraft (figure 31). When ground effect occurs, the lift force on the aircraft changes, cause hot gas re ingestion into the engine intake and due to the fountain upwash and ground flows the fuselage skin temperature raises. The unsteadiness of the flow and raise of the temperature cause several problems in the engine performance, such as, compressor surge or even stall and thrust reduction. In respect to the intake ingestion phenomenon, it is

[41] An image taken from the video at the following website: https://www.youtube.com/watch?v=iRgcC9eqEJg&ab_channel=cywolf32

very complex and can be associated with the design and operational parameters, such as, jet configuration, head wind velocity, jet impingement height or intake configuration.

Figure 30: F-35B aircraft[42]

During a landing or hover the impingement of each downward-directed jet on the ground results in the formation of a wall jet which flows radially from the impinging point along the ground surface. The interaction of this wall jet with the free stream results in the formation of a ground vortex far upstream of the impinging jet (figure 32). This flow field transports exhaust gases away from the ground and up toward the intake region. The level and intensity of the ingestion resulting from this mechanism depends critically on the forward velocity. If there are two or more adjacent jets, the resulting wall jets meet, and a fan-shaped upwash, or "fountain", is normally formed between the jets (figure 33). The fountain upwash flow depending on its strength and direction affects the forces and moments induced in the aircraft when operating in ground effect. The resulting ground vortex shape is strongly affected and the corresponding induced suckdown effect tends to be reduced by the upload produced by the fountain. In the last thirty or forty years, this type of complex flow fields have been studied extensively, but improve the knowledge are ever required because the aircraft design have been changed since its first design, and the some problems were solved but others were not. There can also occur a phenomena related to the lateral flow resulting in a changing of the application point and the direction of the lift force which difficult the aircraft control when landing or hover.

[42] http://www.revistaoperacional.com.br/wp-content/uploads/2014/07/F-35B-Yuma.jpg

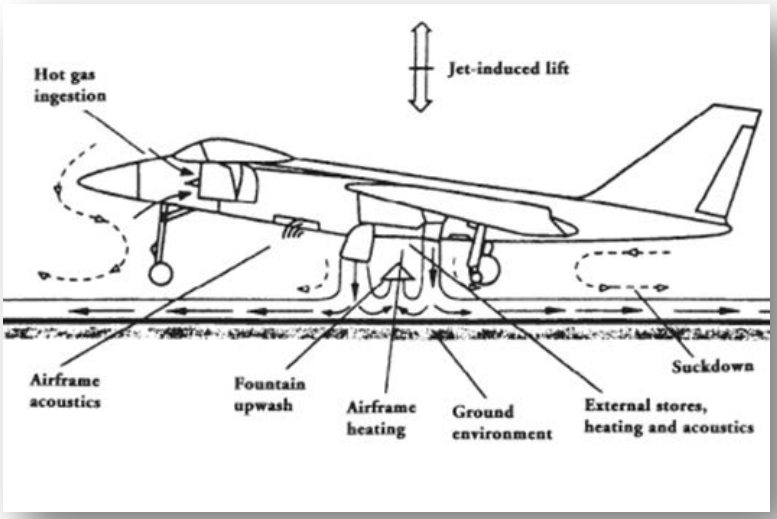

Figure 31: Flow field around STOVL aircraft in hover showing how two vertical lift-producing jets interact and affect the flow around the aircraft[43].

In the present study the flow field is confined, thus being able to reproduce the situation described in figure 32.

Figure 32: Representation of the ground vortex flow phenomena adapted to the JSF F-35 Variant B[44]

[43] Kuhn R., Margason R. J., Curtis P. (2006). Jet Induced Effects: The aerodynamics of Jet and Fan Powered V/STOL Aircraft in Hover and Transition. Volume 217. Chapter 1. Frank K. Lu, Editor-in-Chief. Published by the American Institute of Aeronautics and Astronautics, Inc. 1801 Alexander Bell Drive, Reston, Virginia 20191-4344.

[44] Barata J. M. M., Durão S. D. G., Santos P. J. C. T., Silva A. R. R (2010). Turbulent Energy Budgets of a Ground Vortex Flow. *Proceedings of the 15th International Symposium on Applications of Laser Techniques to Fluid Mechanics*, Lisbon, Portugal, 05-08 July 2010.

The experimental study of this type of flows with one or multiple jets impinging on a flat surface through a low velocity crossflow has proved major improvements over the last 20 years with respect to turbulence models and numerical methods to quantify the curvature of the flow, recirculation zones, high turbulence intensity zones and the formation of a ground vortex[45] (figure 33).

For the next generation of VSTOL aircrafts F-35 no relevant studies can be found, because the impinging jets are aligned with the crossflow and this geometry has not yet been considered. Therefore, most of the published work reported so far has only peripheral relevance to the F35-B/JSF ground effect problem. In the literature can be found several numerical and experimental studies either performed with different motivations corresponding to different jet geometry and velocity ratios between the jet and the crossflow. An appreciation of the flow fields under and around a jet V/STOL aircraft is necessary to understand the aerodynamics effects of the jet flow as well as the empirical and CFD methods used for estimating them. A literature review was performed and grouped into four major groups according to the type of study performed, being the first group related to the experimental studies for a single impingement jet, the second group to the experimental studies for a multiple impingement jets, the third group to the numerical studies and the fourth and last group to the joint of the experimental and numerical studies.

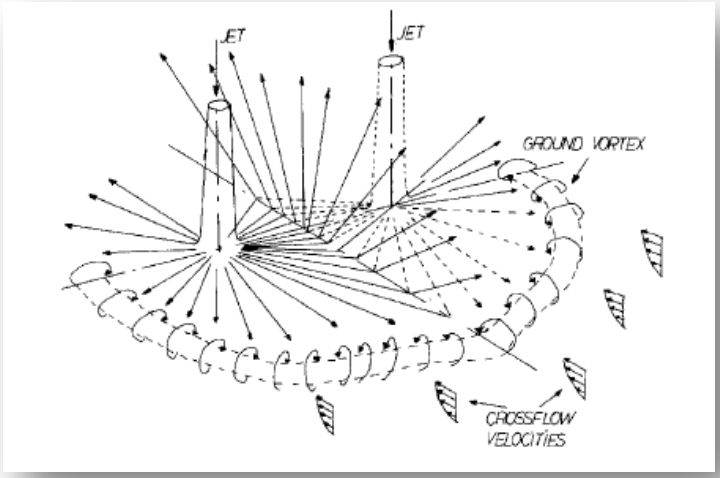

Figure 33: Fountain flow and Ground vortex created by twin impinging jets[46]

[45] The word "ground vortex "is used to refer to a rotating flow with incidence on the surface where the jet stream lines exhibit a circular pattern.

[46] Jorge M. M. Barata (1996), "Ground vortex Formation with Twin Impinging Jets", International Powered Lift Conference Jupiter, Florida November 18-20, 1996.

1.5 Literature Review

1.5.1 Experimental Studies

The interaction of a jet or multiple jets with the presence of a crossflow has been over the years the subject of several experimental studies aiming to uncover and understand the various phenomena associated to this type of flow due to the complexity of the flow under study. The studies were carried out for different reasons, corresponding to different techniques, either as a display of measurements parameters. Below, the tables are condensing information about experimental work.

1.5.1.1 Single jets

Table 1 shows all the experimental works concerning to the study of one impinging jet and is mostly related to the unconfined crossflow, velocity ratios between jet and crossflow less than 73 and relatively low impingement heights, being these works of great interest for the study of the phenomena that occurred in VSTOL aircrafts. Firstly it is important to explain how a single impinging jet affects the aircraft performance. As already mentioned in hover out of ground effect the jet or fan streams entrain air, inducing suction pressures on the lower surface of the aircraft causing a small download or lift loss. But close to the ground, the download can be considerably larger. With a single jet configuration, the impinging jet flows radially outwards from the impingement point, and the entrainment area is greatly increased, causing an increase in download, which varies inversely with the height of the aircraft above the ground. Bradshaw and Love (1959) studied the flow of a turbulent jet on a flat plate (e.g. figure 34), concluding that the experimental results resembled to an ideal wall jet that stretched for two to three diameters from the impact point, being registered large pressure gradients on the centre of the flow.

Stoy and Bem - Haim (1973) showed important result for VSTOL aircraft applications, by considering the impact for relatively small impingement height, H/D equal 3, but only were able to verify that the jet impact point of the jet for confined changes spatially with the crossflow, since the measurements were insufficient to show in more detail the nature of the flow. Furthermore, this study had no special interest as far as VSTOL is concerned, since the velocity ratios used are very small. Crabb, Durão and Whitelaw (1981) present laser anemometry measurements for the upstream region characterized by large intensities of turbulence in the downstream region and measurements were made for velocity ratios the 1.15 and 2.3 through hot-wire anemometry. These authors observed the anisotropy of the flow in the upstream region and concluded that the zero turbulent kinetic energy gradients and mean velocity was not in agreement with the zeros of shear stresses. These observations led to the conclusion that the study for small velocity ratios is important as they allow the knowledge of the general characteristics of a jet flow through crossflow. However, this study

does not provide sufficient knowledge to the turbulent quantities to allow us to understand, assess and develop the capacities of the turbulence data models. Andreopoulos and Rodi (1984) studied the flow of an air jet through an unconfined crossflow through hot wire anemometry, but their study is of little value for VSTOL applications, because the velocity ratios studied were very small. Landret and Adrian (1990) used water as the working fluid for the study of a circular impingement jet on a flat plate, for low impingement height and low velocity. Through the use of PIV they obtained instantaneous velocity fields that allowed clear identification of different generating vortices phases, as well as its location and trajectory after the impact. It was also detected interaction between vortices and wall jet flow boundary layer.

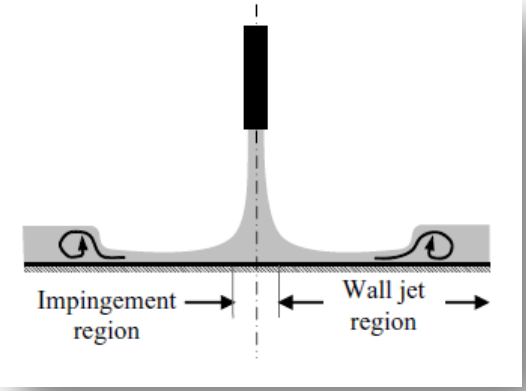

Figure 34: Schematic of a normal impinging jet on a flat plate or ground[47].

Barata, Durão and Heitor (1991a) focused their work in the study of the turbulent energy budgets in the impinging zone through the impingement of a turbulent jet on a flat plate with the presence a low velocity cross stream (figure 35). The shear layer surrounding the jets was a region of intense velocity fluctuations with maximum values located in the region of highest mean velocity gradients. In the impingement and stagnation zones associated with the formation of the ground vortex, were noted large effects of flow distortion in the turbulence structure.

The analysis of the authors to the terms in the conservation equation of turbulent kinetic energy attributed this flow behaviour to the interaction between normal stresses and normal strains. Also it was verified that along the impinging jet the production by shear stress was the largest term in the outer edge of the jet and likely to be balanced by turbulent dissipation. Along the centre of the jet, the most important term was the advection or convection term, which was related to the spread of the jet, presenting a loss of turbulent

[47] Kate, R. P., Das, P., K. and Chakraborty, Suman, "An experimental investigation on the interaction of hydraulic jumps formed by two normal impinging circular liquid jets", *J. Fluid Mech.* (2007), *vol.* 590, *pp.* 355-380.

energy. As the jet approached the flat plate the turbulence production, was higher than the turbulence production by the shear stress along the impinging jet.

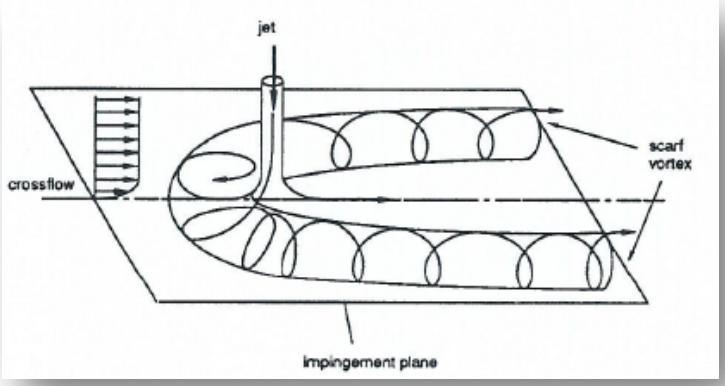

Figure 35: Sketch of floe development for a jet impinging on a flat surface through a low velocity crossflow[48]

This turbulent energy gain can explain the large distortion of the flow in the impingement zone. To finish their analysis, the authors verified that the radial wall jet deceleration was associated with an increase in the advection term, resulting in a turbulence kinetic energy gain. On the case of the recirculation flows, like the ground vortex, the approach to the stagnation point was characterized by a rapid increased in the turbulent kinetic energy production due to the interaction of the normal stresses with the normal strains.

Dennis and Margason (1993) used a pressure transducer modules and Schliren Photography to study the flow of a subsonic jet through a cross-flow on a flat plate for several velocity ratios. The results obtained by the authors showed that for higher velocity ratios the pressure distribution on the surface of the jet is a result of the overlapping effect of changing the shape of the jet velocity and the acceleration of the flow in the wall jet shear layer. Kuhlman and Cavage (1994) used the LDV technique and through a pitot static probe and micro manometer to study an impinging jet with a presence of a crossflow. The data obtained by visualization techniques were confirmed by the LDV results. For low velocity ratios the results were consistent with the results obtained by other authors. However, increasing the velocity ratio, the authors confirmed that the location and the impingement point of the jet was swept to downstream, being the ground vortex narrower in this situation, although it is observed an increase in the entrainment levels and a reduction in aircraft lift losses in the ground vortex region. Knowles and Myszko (1994) carried out flow visualization and obtained profiles for mean and turbulent velocities for the flow of a turbulent jet impinging on a

[48] Barata J. M. M., Durão D. F. G., Heitor M. V. (1991a). Turbulent Energy Budgets in Impinging Zones. Proceedings of Eight Symposium on Turbulent Shear Flows, Munich, Germany, 9-11 September, 1991.

stationary plate. This study was performed by hot wire anemometry and using the Pitot tube to measure the velocity profiles. The authors concluded that the impinging height is related to the increase in the velocity peak and thickness of the wall jet. Through the results of the turbulent velocity profiles, they concluded that the intensity turbulent peak in the jet remains constant whatever the impinging height. Knowles and Saddington (1996) underwent a series of studies of a generic model of a lift jet characteristic of a STOVL aircraft in transition in an open wind tunnel. This study allowed the authors to draw some important conclusions about the suckdown effect present on the aircraft wing. They also verified that the jet in the direction of the flow generates less lift losses to low U_{∞}. Nishino, Samada, Kasuya and Torii (1996) through technical PTV obtained results for the velocity distribution and turbulent stresses for a vertical axisymmetric jet on a flat plate. The results revealed that the turbulent normal stress in the axial direction has a major contribution to the increase in static pressure near the wall, occurring also an excess of radial turbulent intensity. Zhang and Collins (1997) decided to study an inclined rectangular jet through the boundary layer using laser anemometry Doppler and oil flow visualization. Through visualization and velocity profiles obtained for these two authors it was found that the vortex produces momentum transfer detected in the flow direction and in the transverse direction. This study was marked by the fact that the maximum vorticity is at the bottom centre of the vortex.

Nakabe, Inaoka, Al and Suzuki (1997) studied a jet flow through a confined crossflow through particle tracking velocimetry. These authors observed that the generation of vortices effectively improves the heat transfer. Lee, Chung and Kim (1997) set out to study a circular jet impinging on a curved surface in order to obtain data on the mean velocity and turbulent Nusselt number profiles. The results obtained concluded that the Nusselt number increases in stagnation point due to the increased curvature of the surface, once it has been detected acceleration to the stagnation point of sharpest curvature surface. Finally, it was also shown a strong dependence of the Nusselt number with the Reynolds number. Fitzgerald and Garimella (1998), using Laser Doppler Velocimetry technique studied the flow of a fluid jet impinging on a flat plate. The results obtained by the authors showed that increasing the diameter of the impinging jet, resulting in the decrease in the radial velocity peak, but increased turbulent peak levels. The increase of the impinging height showed the decrease in magnitude of the radial velocities and turbulent peaks. Webster and Longmire (1997) obtained important results in the study of the flow of an inclined water jet. The authors concluded that the inclination of the jet nozzle caused a profound change in the flow, breaking the jet axisymmetric. The increase of the jet inclination caused the increase in radial diffusion, enhanced mixing and entrainment in the jet flow. Guillard, Fritzon, Revstedt, Tragardh, Aldén and Funchs (1998) conducted a study of a turbulent water jet impinging orthogonally on a flat plate. Since the working fluid was water the technique used in the study was the planar laser-induced fluorescence technique. The results obtained by the authors showed relatively to the free jets mixing an improvement in the deflection zone and

the outer edge of the jet, due to increased diffusion in the radial direction. Parson and Han (1998) conducted a study of the rotation effect of an impinging jet using a scan valve unit. Through their study concluded that the pressure and mass flux distributions were virtually the same whether it is considered rotating jet or not. Knowles and Myszko (1998) conducted a study of a jet impinging on a flat plate. The results obtained by the authors on the mean, and turbulent shear stress confirmed the axisymmetric of the flow and the self-similarity of the mean velocity profiles. The impingement height showed affects the growth of the wall jet, being the thickness of the jet lower to the higher impingement height. Nakabe, Suzuki, Inaoka, Higashio Acton and Chen (1998) chose the study of the flow of an inclined water jet with the presence of crossflow using Laser Doppler Velocimetry and Thermochromic liquid crystal. The purpose of their study consists mainly in the study of the distribution of the Nusselt number and velocity distribution. As a result of their study the authors found that the supply flow to the region of upwash near the surface caused a peak on the Nusselt number distribution. Regarding the vorticity high values of the velocity fluctuation component were checked. Barata (1998) studied the flow of a jet through crossflow using laser anemometry for high velocity ratios, presenting results for the trajectory of the jet in the vertical plane of symmetry, characteristic region for the formation of a vortex upstream associated with a low pressures region due to the interaction of the jet with the crossflow. The results obtained by the author showed the inability of the visualization method used to correctly reproduce the crossflow acceleration on the vortex region. Behrouzi and McGuirk (2000) presented a study of the flow of a combined system of a jet intake with and without crossflow. The study was conducted through particle image velocimetry and aimed to get results of visualization and instantaneous velocity fields. By employing this technique, the results obtained allowed the provision of velocity composed of a highly complex flow fields such as intake / jet impact allowing the analysis of the dynamics of vortex structures. Zhang (2000) studied the flow of a back inclined rectangular jet through the presence of the boundary layer using the same technique and using the same parameters used in their 1996 study. This time was to analyse the kinetic energy and produce turbulence in such a way forming a database for validation of numerical models for this type of flow characteristic for complex features such as turbulent kinetic energy distribution of the normal stresses and primary shear stresses. Fleischer, Kramer and Goldstein (2001) analysed the flow of a circular jet impinging on a convex surface to different impingement heights. The technique used by the authors in order to obtain the visualization of the structure that makes up the flow of the impingement jet was the smoke wire. Through the results of the two types of vortex breaks were detected and it was still possible to conclude that the relative curvature strongly influenced the angle of separation of the vortex. Lawson, Eyles and Knowles (2002) studied the flow of a circular jet impinging on a moving plate with the presence of a crossflow. The results obtained by the particle image velocimetry technique were compared with those obtained using laser Doppler anemometry. The authors concluded from the data analysis that the PIV technique is sufficient capacity to capture most of the features of the transient flow of the ground vortex, also making some

recommendations as to the spectral energy for future work. Camussi, Guj and Stella (2002) conducted a study of the flow of a water jet with the presence of crossflow at low Reynolds numbers. The velocity field and the vorticity were obtained by using the visualization through PIV and LIF. Regarding the results, the authors concluded that the main vortical system formed by the interaction of the jet with the crossflow and by the jet distortion and expansion by the increase distance from the outlet nozzle of the jet are at all similar to the results observed for Reynolds numbers higher than those used in this study. Barata and Durão (2004) studied the flow of a jet through a cross flow using laser anemometry for high velocity ratios, introducing measured jet trajectories and mean velocity in the vertical plane of symmetry. Barata and Durão (2004) showed that for velocity ratios sufficiently high and small impingement heights, two different flow regimes were identified. One is characterized by the contact between the ground vortex and the impinging jet, while another is detached upstream the impinging zone. They also found that the acceleration of crossflow on the "ground vortex" is directly related to the jet exit velocity. Barata and Durão (2005) studied the flow of a wall jet through the boundary layer at low velocity ratios using Laser Doppler velocimetry. The authors noted the deflection angle of the jet upon collision with the boundary layer and the anisotropic turbulence levels were recorded, and registered major distorting effects of the flow near the stagnation point. Barata, Castro and Silvestre (2005) studied the same flow presented by the authors cited above, but using laser anemometry for measurements of the jet trajectory, mean and turbulent velocities and shear stresses.

The results show the existence of a small recirculation zone located upstream of the separation point not reported before. San and Shiao (2006) studied a flow of a hot jet incident on a flat surface without crossflow through thermal imaging liquid crystal and thermocouples for temperature. This study shows the distribution of heat transfer as a function of Reynolds number and the impingement height. The data revealed that the Nusselt number at the stagnation point increase with the Reynolds number, thereby promoting greater heat transfer while the increased of the impingement height deteriorates the heat transfer due to recirculating flow before the jet reaches the surface. This type of studies for H/D less than 6 are important to understand the phenomena that occur for VSTOL applications. Said, Stefanini, Bournot, Darreau and Caminat (2006) performed the visualization of the flow of an inclined jet impinging with the presence of a crossflow. The authors concluded that the slope of the jet enables the control of the jet penetration and growth. It was also found that the development of the flow was strongly dependent on the initial conditions imposed on the flow. Lakhamraju, Murugappan, Coppness and Gutmark (2007) conducted a study of the effect of the variation of density and velocity ratio in a circular jet with the presence of crossflow. This study showed that the influence of the velocity ratio on the jet penetration is more significant when compared with the influence of density. For low density there is a strong vorticity in the side of the crossflow, increasing the production of turbulence with rapid mixing. Barata, Ribeiro, Santos and Silva (2009a)

returned to study the flow of a wall jet with the presence of a crossflow, as reported by Barata et al. (2000, 2004, and 2005) but for different velocity ratios. Throughout this study, the authors were able to verify the existence of small vorticity structures downstream of the separation point that were not found in their earlier works. Fan Jing-yu, Zhang Yan and Wang Dao-zeng (2009) studied the flow of circular water jet through the crossflow using the PIV technique measurements for velocity fields and the LIF visualization technique to visualize the flow field and vortical structure. With this study it was found that for the same value of H / D ratio of the reduction gear led to the jet to be deflected downstream by the crossflow at the same time of the collision on the wall. Langer, Fleck and Wilson (2010) studied a flow of an elliptical jet through a cross flow through the induced fluorescence technique for low crossflow velocities. The results regarding the elliptical trajectories show that the jet behaves similarly to the circular jet flow containing three regions, consistent with the experimental data with the analytical Briggs model. Barata, Durão, Santos and Silva (2010) studied the flow of a wall jet colliding with a boundary layer using Laser Doppler Anemometry and for a velocity ratio equals to 2. Detailed measurements of the turbulent kinetic energy are presented, revealing that the shear layer around the jets is characterized by a region of intense velocity fluctuations and the jet collision with the boundary layer wall area there is gain of the local energy by convection. Wang, Sundén, Borg and Abrahamsson (2011) conducted a study of an impingement jet with the end on quarter arc through a crossflow in order to verify the heat transfer by convection flow. They used the technique of thermal thermography liquid, concluding that the presence of the rib at the edge significantly alter the pattern of heat transfer from the impingement jet for this improved lower velocity ratio. In the case of higher velocity ratio was observed its uniformity due to the presence of the rib. Recently Hassan, Assoum, Sobolik, Vetel, Aberd-Merain, Garon and Sakout (2012) studied through polagraphic method and Particle Image Velocimetry the flow of an impingement jet on a flat plate. This study allowed the authors to find that there are high turbulent intensity in the free jet region and the impingement region. Furthermore they concluded that increasing the Reynolds number significantly affects the stress variation in the boundary layer. In order to explore the convective heat transfer of an impinging jet in a crossflow Li Guoneng, Zheng Youqu, Hu Guilin and Zhang Zhiguo,(2014) reports a study where the enhancement factor was found to increase with the jet-to-crossflow mass ratio and the Reynolds number, but decrease with the jet diameter. The presence of a crossflow was observed to degrade the heat transfer performance.

Authors	Experiment	Technique	Results	Comments
Bradshaw, Love(1959)	Flow of a turbulent circular jet impinging normally on a flat surface D= 25.4 mm V_{jet}= 41.1525 m/s H/D= 18	Velocity – Diamond-section yawmeter e round pitot tube Static pressure- disc static probe Wall tension– flat pitot tube	Magnitude and velocity direction Static pressure Wall tension	Through the results, the authors concluded that the flow studied experimentally was a good approximation to an ideal wall jet extending for more than two or three diameters from the impact point of the jet. However close to the centre, this region characterized for large pressure gradients.
Stoy, Bem-Haim (1973)	Air jet through a confined crossflow Re = 70000 V_j/U_0 = 2,5 e 7,7 H/D = 3.05	Pitot tube(data in an input card for 8 computational programs)	Jet trajectory Jet impingement point Potential core region length	The impingement point of the confined jet changes spatially with the crossflow
Crabb, Durão, Whitelaw (1981)	Circular air jet through a unconfined crossflow V_j/U_0 = 1,15 e 2,3 D = 25,4 mm	LDA Hot hire	U, V, W, U'^2,V'^2,W'^2,U'V', V'W', U'W' in symmetry plane	There is a pair of vortices in the downstream area of the jet exit. In the upstream region the turbulent structure of the flow is characterized by a substantial anisotropy. In the downstream region there is a tendency of the flow to be isotropic although significant variations occur, especially in the wake region.

Table 1: Summary of experimental work on the flow of a jet through a crossflow

					The zeros of the turbulent kinetic energy gradients and mean velocity are not in agreement with the zeros of shear stresses.
Andreopoulos, Rodi (1984)	Air circular jet flows through an unconfined crossflow. V_j/U_0 = 0,5, 1 e 2 Re = 20500, 41000 e 82000 D= 0,05 m	Hot hire	U, V, W, $U'_2, V'_2, W'_2, U'V', V'W', U'W'$ in symmetry plane		For small velocity ratios, i.e. 0.5, it appears that the deflection of the jet occurs instantaneously after its exit. The wake formed behind the jet increases in size when V_j/U_0 increases. When the boundary layer is approaching the jet generates a counter rotating horseshoe vortex shaped. The turbulent kinetic energy and shear stress u'v' can be described by a model of turbulent viscosity.
Landreth, Adrian (1990)	Circular water impingement jet on a flat surface. D=26.9 mm H/D=4 V_j= 244±2 mm/s R_e= 6564	PIV	Instantaneous velocity fields		The set of measurements made allows us to clearly identify the different stages of the generation of vortices and their interaction near the wall jet flow boundary layer, including flow separation from the wall. The corresponding vorticity maps revealed vortexes on the shear jet layer and their trajectories after the impact

Table 1: (Continuation)

					The deformation rate tension maps revealed structures that occur simultaneously with those shown by the maps of vorticity.
Barata, Durão, Heitor (1991a)	Study of the budgets of turbulent kinetic energy in the vicinity of the stagnation zone created by the impingement of a turbulent jet on a flat plate through a low velocity cross stream. V_j/U_0= 30 H/D=5 Re_j= 60,000 V_j= 3 m/s U_0= 0.1 m/s	LDV		Turbulent kinetic energy contours Mean and turbulent velocity profiles	The results showed the formation of a fairly thin radial wall jet, giving rise to a ground vortex wrapped around the jet due to the interaction of the upstream radial wall jet with the cross stream. The shear stress and shear strain signs were consistent with the gradient diffusion hypothesis. In the impingement zone and stagnation zone this was not verified due to large effects of flow distortion on the turbulence structure parameters that determine the empirical constants in engineering models of turbulence.
Dennis, Margason (1993)	Perpendicular subsonic jet on a flat surface through a subsonic crossflow. $4<V_r$ (effective velocity ratios)<12 M_j(jet Mach number at exit)=0.94	Pressure modules transducers. Schlirien photography		Visualization Pressure distribution	This study has shown that for the higher effective velocity ratio studied the pressure distribution on the surface near the edge of jet can be qualitatively viewed as a superposition of the effect of changes in velocity due to blockage of the flow by the shape of the jet, and the acceleration by entrainment of flow in the jet wall shear layer.

Table 1: (Continuation)

Kuhlman, Cavage (1994)	A jet impinging on a flat surface through a low velocity crossflow. Three different diameters for the standard configuration – 0.95, 1.27 e 2.54 cm Annular configuration – 1.27 cm $V_{\infty max}$ (maximum crossflow velocity)=76 m/s V_j= 91.4 m/s Re_j= $5.4x10^4$, $7.2x10^4$ e $1.43x10^5$ $V\infty/V_j$ (crossflow-to-jet velocity ratio)= 0.075, 0.1, 0.11, 0.125, 0.14, 0.15, 0.18 H/D= 3, 5.5, 7	LDV Pitot static probe and micro manometer	Visualization Velocity profiles Turbulent intensity	The results showed that changing the size of the standard jet nozzle and fixing all other parameters, the effect on the ground vortex size was very small, at least for $V\infty / V_j \geq 0{:}15$. Speaking further on the size and shape of the vortex ground and jet impact point, the results confirmed the conclusions obtained by other authors. However increasing the velocity ratio, they confirmed that the location and the impingement point of the jet was swept to downstream, being the ground vortex narrower in this situation. For the annular jet has been found that the increase in the velocity ratio reduces the size of the ground vortex region around 30-50% compared to a standard jet. Despite this decrease is observed an increase in the entrainment levels and a reduction on the aircraft lift losses. The LDV results were consistent with the visualization results, indicating high levels of turbulence in the central line and downstream of the impact point on the ground vortex region.

Table 1: (Continuation)

Myszko, Knowles (1994)	Circular turbulent jet impinging on a stationary plate. D= 12.70 mm H/D= 10 NPR= 1.05-4.0	Static pitot tube - Velocities Hotwire anemometry - Turbulence	Visualization Wall jet mean velocity profiles Turbulence intensity profiles	Through the study conducted, the authors concluded that there are effects on flow field related to the impinging height, providing its growth, the increase in velocity peak, thickness of the wall jet and the increase in the flow momentum. However, the increase of NPR, caused the decrease of the thickness of the wall jet. With respect to the turbulence intensity levels after the jet impingement was observed that the intensity peak in the turbulent wall jet remains constant with the different impinging height. However, the turbulent intensities for the free jet within the impact region increased due to a large deterioration of itself.
Saddington, Knowles (1996)	Several experimental studies in an open wind tunnel with a generic model of a VSTOL aircraft lift jet on transition phase. Θ=60º NPR= 2.0, 3.0, 4.0 Jet position: central flow direction, against of the flow direction.	Static pressure plugs	Cp	Through the work developed by the authors it was possible to conclude that for not obstructed admissions with the jet on, there are lift losses on the wing due to the suck-down effect, depending on the jet position and NPR. It was found that the jet in the flow direction generates less lift losses to low V_∞, the opposite situation occurs for the positioning of the jet in the opposite direction of the flow.

Table 1: (Continuation)

Saddington, Knowles (1996)	V_∞ (crossflow velocity) = 10, 20 e 30 m/s H= 1.5 m			For Admissions Suction type and the jet off, there is obtained an elevation gain on the wing, and it is greater for low V_∞. Finally, with the admission of the jet suction and blowing, this appears as the creator of the downward velocity of admission flow that probably reduced the enhancing effect on the elevation component.
Nishino, Samada, Kasuya, Torii (1996)	The flow of an axisymmetric water jet impinging vertically on a flat plate. Re=13000 D=40mm H/D=5.86	PTV	Mean velocity distribution Turbulent stresses Triple correlation of the velocity fluctuations	The results show that the turbulent normal stress in the axial direction has a significant contribution to the increase in static pressure near the wall, being this region characterized by a reduced axial turbulent intensity. It has been shown that the negative turbulent kinetic energy production occurred in the region near the wall, where there was excessive radial turbulent intensity.
Zhang, Collins (1997)	Inclined rectangular jet through a boundary layer. U_∞ (freestream velocity)=20.2 m/s $E_{equivalente}$ (Equivalent hydrodynamic diameter)=14 mm Iα (pitch angles)= 30°, 45° e 60° β (skew angle)=45°	LDA Oil flow visualization	Visualization Velocity profiles Vorticity contours	The results showed that the vortex produces transfer of momentum in both directions, flow and transverse direction. Distributions of secondary vorticity in the near wall area and the downstream side were also observed. A salient feature of the flow in the study was the fact that the maximum vorticity position be located under the centre of the vortex, for angles of 30 ° and 45 °

Table 1: (Continuation)

	λ (velocity ratio) = 1.0, 2.0			inclination and for the lower velocity ratio.
Nakabe, Inaoka, Al, Suzuki (1997)	Flow of a circular jet through a confined crossflow. D = 10 mm H/D = 4 Jet vortex generator D = 6mm Φ (skew angle)=90 ° Θ (pitch angle)= 45 ° Re = 40000 H/D = 5	PTV	Nusselt number distribution Heat transfer	Experiments have shown that the heat transfer was enhanced around the origin, depending on the velocity jet. The generation of vortices effectively improves the heat transfer from the inner surface of the fixed blades of a gas turbine.
Lee, Chung, Kim (1997)	An impinging circular jet on a curved surface 11000<Re <50000 2<L/d (nozzle to surface distance)<10 0.034<d/D (dimensionless surface curvature)<0.089	Thermochromic liquid crystal	Velocity profiles Turbulent intensity profiles Nusselt number	It was found that the potential core region extends to regions from 3.1 to 4.2 jet diameters for the Reynolds numbers studied. The Nusselt number at the stagnation point increases with the increase of the surface curvature due to the acceleration of the stagnation point for the more pronounced curvature of the surface. The heat transfer is less pronounced on the curved surface than in the wall jet region

Table 1: (Continuation)

				comparing the stagnation point region. The mean Nusselt number on the curved surface is well connected with all parameters and shows a strong dependence on the Reynolds number.
Fitzgerald, Garimella (1998)	Confined Liquid jet impinging on a flat surface D= 6.35 e 3.18 mm H/D= 2, 3, 4 R_e= 8500, 13000, 23000	LDV	Radial velocity profiles - u/V_j Turbulent intensity profiles - u_{rms}/V_j	The maximum velocity and maximum levels of turbulence in the wall jet zone occur very close to the impact surface. With the increase of H / D was found to reduce the magnitude of the radial velocity, as well as a reduction in the peak intensity of the turbulent flow field. Increasing the diameter of the jet results in a decrease of the radial velocity peak, but increased turbulent peak levels
Webster, Longmire (1997)	Study of a water circular jet with nozzles slope length between 0° e 45°. V_j= 304 mm/s Re_D= 9000 D= 30 mm Lengths of slope= D/4 (14°), D/2 (26°), 3D/4 (37°) e D (45°) St_D (strouhal number)= 0.25, 0.5,	PIV	Axial velocity profiles Instantaneous vorticity fields Velocity fields Visualization	The results found that the slope of the nozzle has fundamentally altered the flow field, breaking the jet axisymmetric. The radial growth increased slightly on the spontaneous flow in particular for ψ = 0. The artificially thrust flow amplified the asymmetry of the radial diffusion effects. The radial diffusion increased with the nozzle inclination angle and decreased with the Strouhal number increase. Thus, the results obtained and the

Table 1: (Continuation)

	0.75 e 1.0			combination of nozzle geometry and artificial buoyancy of the flow appears to be an effective means of increasing the mixing and entrainment of the jet. The results show a vorticity structure consisting on inclined continuous vortex rings for all conditions tested.
Parsons, Han (1998)	Study of the rotation effect of a cooling impinging jet through a set of a circular jets inline. D= 1.59mm T_j (jet temperature)=27 °C H/D=4 S/D=5.0 5000<Re <10000 0<Ro (average jet rotation number)<0.0028 Pr (prandtl number)=0.72	Inclined manometer Scanivalve unit	Nusselt number Pressure and mass flux distribution	The results showed that for a determined Re jet, the pressure and mass flux distributions are virtually the same whether or not there is rotation. For non-rotating conditions, the impact plate on Nu increases with Re jet and having the same tendency to studies conducted by other researchers. For the conditions of rotation of the Nu on the impingement plate decreases by about 20% due to the collision of the jets being affected by the rotating secondary flows induced by buoyancy and centrifugal forces.
Guillard, Fritzon, Revstedt, Tragardh, Aldén, Fuchs (1998)	Flow study of a turbulent confined water jet flowing orthogonally on a flat Wall Re=11000 D=33 mm	Planar Laser-Induced Fluorescence technique	Radial concentration fluctuations Concentrations correlations functions and point	It has been found to improve of the mixing in the deflection zone and in the jet outer edge relatively to the found on the free jet. This fact may be explained by the deceleration of the fluid in this region, increasing the diffusion in the radial

Table 1: (Continuation)

	D=33 mm H/D=4.8		concentrations probability densities Mean concentrations structure in the centre plane of the jet	direction.
Knowles, Kirkham (1998)	Flow of a free coaxial jet (normal and inverted profiles) on a flat plate D_i (inner diameter)= 12.7 mm D_o (outside diameter) = 13.7 mm NPR_i= 1.3, 1.8, 2.2 NPR_o= 1.3, 1.8, 2.2, 3.0 H/D_i= 2, 4, 10	Static pitot tubes - Record the properties of the free jet at various distances from the exit plane of the jet.	Velocity profiles of the free jet and normalized and non-normalized Wall jet Velocity fluctuations on the central line Maximum velocity decay Free jet and Wall jet growth	The results showed that the profiles inverted in case the inner subsonic jet (velocity jet greater inside relative to outside) disclose axis acceleration caused by the entrainment jet inside to the outside, depending on the degree of NPR_o acceleration. The maximum velocity and the decay rate are increased by increasing the NPRO. The increase of NPRI leads to decreased growth rate and decay rate. It was found that for distances greater than 25Di the wall jets exhibit self-similarity and this is not affected by changes in NPRI, NPRO and H / Di. As regards the wall jet growth rate, the increase in H / Di involves the reduction of thickness. However for H / Di equals 4 is increased it. Finally, through this study it was confirmed the inside jet pressurization.

Table 1 (Continuation)

Nakabe, Suzuki, Inaoka, Higashio, Acton, Chen (1998)	Inclined circular water impinging jet through a crossflow Θ (skew angle) =90° Φ (pitch angle) =45° D=6mm H/D=5 Re_c (crossflow Reynolds) =5000 1500<Re_j (jet Reynolds) <3500 V_r (V_j/U_0)=3, 5, 7	Laser Doppler Velocimetry Thermochromic liquid crystal	Nusselt number distribution Velocity distribution No dimensional RMS intensity distribution	The peak for the Nusselt number appears in Z / d = 4-5 position being caused by the supply of fluid to the upwash region near the surface of the target plate. In the region of the longitudinal vortices and / or impinging jet high values of RMS velocity fluctuation component are found.
Barata (1998)	Flow of a simple jet with a presence of a crossflow. Re = 60000 V_j=3 m/s V_j/U_0= 30 H/D = 5	LDA	Trajectories	The results show the inability of 2-D visualization method to illustrate the crossflow acceleration on the upstream vortex associated with regions of low pressure
Behrouzi, McGuirk (2000)	Study of the flow of a combined system of an admission jet with or without presence of a crossflow. D_j= 12.4 mm D_{intake}=3D_j H/D_j= 7 H_{ntake}/D_J= 9.5 V_j= 2.66 m/s R= 18, 24, 35	PIV	Visualization Instantaneous velocity profiles Instantaneous velocity fields	The results showed that the method was successful employed in providing quantitative measurements of the velocity fields in a complex flow field of an inlet / jet impingement. The images captured with this technique were used to illustrate the analysis of the dynamics of instantaneous vortex structures.

Table 1: (Continuation)

Zhang (2000)	Flow of an inclined rectangular jet through a boundary layer U_∞=20 m/s Re= 3800 $E_{equivalente}$ Equivalent hydrodynamic diameter)=14 mm A (jet pitch angle)= 30° 0°<B (jet skew angle)<135° λ (velocity ratio) = 1.0	LDA	Turbulent kinetic energy Turbulence production Velocity contours vectors	The study provided a database for the validation of numerical models of an inclined rectangular jet through a boundary layer. When properly organized, the rectangular jet is capable of producing a strong vortex to control the flow of a circular jet with the same mass flow rate. Both the turbulent kinetic energy, normal stress and the primary shear stress distribution suggest complex flow characteristics, particularly in areas around the centre of the vortex and between the vortex and the wall.
Fleischer, Kramer, Goldstein (2001)	Flow of a circular impingement jet on a convex surface. 0.18<d/D<0.38 1<H/d<4	Smoke – wire technique	Visualization of the flow jet structure	The only parameter that shows a strong effect on the separation vortex angle is the relative curvature. This study also identified two types of vortex breaks: the breakdown of the vortex melting before impact and breakage due to flow separation at the surface.
Eyles, Lawson, Knowles (2002)	Circular impingement jet on a plate with movement through a crossflow. Comparison with the LDA results. 2<NPR (nozzle pressure ratio)<4	PIV LDA	Visualization PIV vector instantaneous map PIV average time vector map	The results showed that for PIV the ground vortex is more sensitive to changes in the crossflow velocity V_∞ and less sensitive to changes at the impingement height. Analysis of additional data in the case of

Table 1: (Continuation)

	3<H/d_n (nozzle height to diameter ratio)<10 12.5<d_n (nozzle diameter)<25.4 V_∞ (crossflow velocity)=10, 15, 20 m/s		Central vortex position Instantaneous position of the central vortex position Spectral distribution	LDA spectrum, taken from the core of the vortex showed that most of the spectral energy is present to about 30 Hz This result indicates that, therefore, the present system with a rate PIV 15 Hz frames has sufficient to capture most of the transient characteristics of the ground vortex flow capacity. However, the authors recommend that for further studies, the PIV operate with a minimum of 60 Hz to ensure that most of the characteristics of unstable ground vortex flow are captured.
Camussi, Guj, Stella (2002)	Flow of a water circular jet with the presence of a crossflow for low Reynolds numbers. 1.5<R (velocity ratio)<4.5	PIV LIF	Visualization Velocity profiles Vorticity	Holistically, the results showed that the main vortical system formed by the interaction of the jet with the crossflow is at all similar to that observed for higher Reynolds numbers. Quantitative analysis showed the authors that the axis of the jet is distorted and expanded the greater distance to the outlet nozzle of the jet, and these results consistent with those outlet nozzle of the jet, and these results consistent with those recorded for higher values of Re .

Table 1: (Continuation)

				For velocity ratios less than 3, longitudinal vorticity was dominated by wake-like structures that carried vorticity of opposite sign compared to those formed in free jets. For velocity ratios higher than 3 jet-like structures are dominant.
			Trajectories Mean velocity on the vertical plane of symmetry	The results show that the distance from the collision zone is related to the shear stress signal according to the turbulent viscous hypothesis. The lower height of the ground vortex to higher rates of velocity is compensated for by increased resistance of the vortex. For sufficiently high $U_j/U0$ and H / D small, two regions are observed: a region of the incidents and the ground vortex upstream of the jet and the crossflow. The acceleration of the crossflow on the ground vortex is directly related to the velocity of the jet.
		LDA		
	Study oh the flow of a circular jet with the presence of a crossflow. D = 20 mm H/D = 3, 5 V_j = 3, 4.2 e 6 m/s U_0 = 0.1, 0.093, 0.082 m/s V_j/U_0 = 30, 45 e 73			
Barata e Durão (2004)				

Table 1: (Continuation)

Lawson, Eyles, Knowles (2004)	An impingement jet on a plate with movement. 2.3<NPR (nozzle pressure ratio)< 3.7 3<H/D<10 D= 12.7 mm $10<V_{\infty}<20$ m/s $19<V_e^{-1}<38$	LDA PIV	Vector maps Vortex centre position Spectral distribution	The results showed that the ground vortex formed by the impact of a jet on a moving surface is more sensitive to changes in the crossflow velocity and nozzle pressure ratio when compared to the changes experienced by the change at the impingement height. It was also observed even through the PIV instantaneous results that the ground vortex demonstrates fluctuations by chaotic *rms* movements. Finally, the results obtained by both PIV such as LDA showed that most of the spectral energy of the ground vortex flows to values greater than 30 Hz
Barata, Durão (2005)	Flow of a Wall jet through a boundary layer. U_0 =3.48 m/s U_j =6 m/s U_j/U_0 = 1.7	LDV	Mean velocity Turbulent velocity Shear stresses $u'v'$	Upon a jet collision with the boundary layer, the jet is strongly deflected backwards at an angle of 36 degrees with the surface. The turbulence is anisotropic. In the region of the deflected upward flow, the sign of the shear stress is consistent with the sign of the shear pressures according to the viscous turbulent circumstances. In the region where the boundary layer starts to be deflected upwards due to

Table 1: (Continuation)

					the influence of the small ground vortex, and near the stagnation point, large flow distortion effects on the structure of turbulence are expected.
Barata, Castro, Silvestre ,Durão (2005)	Flow of a Wall jet through a boundary layer. U_0=3,48 m/s U_j=6 m/s	LDA	Trajectories Mean velocities *U'V'*		Only in the upward deflected region the shear stress signal is related to the shear pressure in accordance with the hypothesis of turbulent viscosity. The results show that the turbulent flow structure of the highly curved is subject to distortion. The results reveal the existence of even a small recirculation zone located upstream of the separation point. The results reveal the existence of even a small recirculation zone located upstream of the separation point.
San, Shiao (2006)	A circular impingement jet on a hot flat surface without presence of a crossflow D = 1.5, 3, 6 e 9 mm 10000<Re <30000 1 <H/D > 6 q (constant surface heat flux) =1000 W/m^2	Temperature: thermocouple Liquid crystal thermal image	Nusselt number distribution Nusselt number on stagnation point		The data show that the Nusselt number increases with the Reynolds number. The increase of W / D and L / D promotes the decrease of the Nusselt number at the stagnation point, but the increase in the Nusselt number on the stagnation point increases with the increase of Re. The increase of H / D greater distance allows

Table 1: (Continuation)

	4.17 <W/D (width-to-jet diameter ratio)< 41.7 5.5 <L/D < 166.7			mixing with recirculated stream before the stream reaches the surface, deteriorating heat transfer.
Said, Stefanini, Bournot, Darreau, Caminat (2006)	An inclined impingement jet through a crossflow $2.7x10^4<Re_F$ (wind tunnel flow Reynolds number)$<2.2x10^5$ $1.1x10^3<Re$ (jet Reynolds number)$<6x10^6$ A (jet discharge angle) =60° d=10 mm 0<h<7 cm	PIV	Flow visualization Kelvin-Helmholtz structure development	Through this study it was possible to conclude that the inclination of the jet is an important parameter in controlling the development of structures in the flow, as the penetration and growth of the jet. Various types of structures in the flow were observed as counter rotating pair's vortex and vortices and instabilities in the boundary layer of the Kelvin-Helmholtz. It was found that this flow is strongly dependent on initial conditions and Re. Thus for high Re it was verified high gradients near the wall for all the velocity ratios checked.
Lakhamraju, Murugappan, Coppness, Gutmark (2007)	Study of the effect of the density variation and velocity ratio on a circular jet trough a crossflow U_0=50 m/s T=24°C±1°C D=4.83 mm	PIV	Reynolds stresses Turbulent kinetic energy Jet Propagation rate Mean velocity decay on central line Jet trajectory and jet penetration	The study revealed that although the jet penetration is proportional to the velocity ratio and density, the influence of the velocity ratio is dominant. In low-density jets, rapid breakdown and poor penetration resulted in a strong vorticity in the crossflow side of the core jet. It was found that the transverse Reynolds stresses and the turbulent kinetic energy are greater for lower ratios of density due to

Table 1: (Continuation

					increased production of turbulence with rapid mixing near the jet exit.
Barata, Ribeiro, Santos, Silva (2009a)	Study the flow of a Wall jet through a boundary layer U_j=13.7 m/s U_0=6.9 m/s V_R (U_j/U_0) =0.5	LDV	Mean velocity Turbulent velocity Vorticity		This study revealed the presence of small vortexes located downstream of the separation point has not yet reported in previous studies
Fan Jing-yu, Zhang Yan, Wang Dao-zeng (2009)	A circular water impingement jet through a boundary layer D=5 mm H/D= 10 e 20 U_j= 1,2 m/s U_j/U_0= 8, 12, 20 Re_j (jet Reynolds number)= 6000 Re_c (crossflow Reynolds number)= 3000 to 15000	LIF Flow Visualization PIV measurement	Visualization of the flow field and vortical structure Velocity fields		It was found that the fluid entrainment into the jet body is associated with the characteristics of the shear layer between the jet and the surrounding fluid, and with the vortices formed by the wall. Through visualization was possible to conclude that H / D = 20, due to the rather weak impact wall, there is the formation of a vortex at very low amount that does not persist for a long time, and downstream check the effect of wall friction In the case of H / D = 10 there is the formation of a vortex amount of the stagnation point for any of the velocity ratios studied. With the decrease in the velocity ratio, it was observed that the collision with the jet wall has become oblique and not perpendicular as it was observed for higher velocity ratios.

Table 1: (Continuation)

Langer, Fleck, Wilson (2010)	Study of the flow of an elliptical jet through a crossflow 0.041 ≤ V_∞ (crossflow velocity) ≤ 0.081 m/s $2x10^4$< Re< $4x10^4$ V= 0.47, 0.78, 1.10 m/s h (step height)= 2.54, 3.81, 5.08 cm H= 5d, 9d,15d	PLIF	Trajectories	The experimental data were compared with the analytical Briggs model. Similarity with the flow of a circular jet, also the elliptical profile contains 3 regions.
Barata, Durão, Santos, Silva (2010)	The flow of a Wall jet through a boundary layer. U_j= 13,7 m/s U_0 = 6.9 m/s U_j/U_0= 2	LDA	Turbulent kinetic energy	The results revealed that turbulent kinetic energy in the collision zone of the wall jet with the boundary layer there is a local energy gain by convection. The authors concluded that the shear layer around the jet is a region of intense velocity fluctuations. Production of turbulent kinetic energy tends to be balanced by the loss of diffusion and dissipation. The small contribution of the convective term in the production of turbulent kinetic energy is less than the output due to normal and shear stresses. The results indicate that the turbulence modelling of this flow may require suitable treatment for the production of normal stresses, which is important for the production of normal stresses, which

Table 1: (Continuation)

					is important for the collision zone due to normal and shear stresses.
Wang, Sundén, Borg, Abrahamsson (2011)	An impingement jet with the end on quarter arc through a crossflow 80000<$Re_{crossflow}$<160000 20000<Re_{jet}<8000 1.0<V_r (velocity ratio)<2.8 d (internal diameter)=22.5 mm D (outer diameter) =25mm	LCT – liquid crystal thermography		Nusselt number Maximum Nusselt number Nusselt number contour Re effect on the stagnation point position Velocity ratio effect on the Nusselt number distribution	In general, the presence of the rib significantly alters the pattern of heat transfer from the jet incident. In all cases tested, the variation of the Nusselt number by changing the stagnation point presents a bell shape, which indicates that the region of enhanced heat transfer expands more as the use of the rib. In particular, the presence of the rib has a more pronounced effect on improving the heat transfer to the lower velocity ratios. For higher velocity ratios the presence of the rib makes the rate of heat transfer more uniform, and at the same time, it appears that the effect of impingement jet tends to be weaker.
Hassan, Assoum, Sobolik, Vétel, Abed-Meraim, Garon, Sakout (2012)	A circular jet impinging on a flat plate Re = 1260, 2450 D=7.8 mm L/D=2.08	Polagraphic method – boundary layer stress PIV – velocity fields		Mena velocity on the flow direction Normal shear stresses Friction coefficients on the surface Vortex Dynamics visualization Energy spectrum	Intensity turbulent high values were verified on the free jet region and on the impingement region where the azimuthal vortices are developed, being the maximum value of the turbulence intensity correspondent to the region of impact of the transverse structures The distribution of the mean friction coefficient on the surface shows a peak in the region where the primary structures of long range collide with the wall. It was found that when Re increased, so the vortices with large or small frequency variation affecting the tension in the boundary layer.

Table 1: (Continuation)

	Li Guoneng, Zheng Youqu, Hu Guilin, Zhang Zhiguo (2014)	A jet in crossflow impinging on a rectangular flat plate. D= 2-4 mm Jet-to-crossflow mass ratio=2%-8% Re_d= 1434-5735 H/d= 9.813-19.625	HTCC: high temperature co fired ceramic	Heat transfer enhancement factor Average surface temperature Radiation heat flux	The cross-correlations for the boundary layer stresses confirm the importance of the different vortical structures on the stress boundary layer distribution. The results show that the heat transfer enhancement factor increase with the jet-to-crossflow mass ratio and the Reynolds number when the other parameters remains constant. In the case of the jet diameter it is observed a decrease on the enhancement factor, being the jet diameter carefully optimized in order to obtain better heat transfer performance. In respect to the presence of a crossflow, it degrades the heat performance by 13.6%, which is caused by the blockage effect of the crossflow. The impinging jets are found to be capable of enhancing the heat transfer process. The vortices created in a JICF system move downstream and help to improve the heat transfer process.

Table 1: (Continuation)

1.5.1.2 Multiple jets

For VSTOL applications the flow field created by multiple impingement jets on a plate with the presence of a crossflow it is of utmost importance, due to the formation of a fountain upwash flow (figure 36).

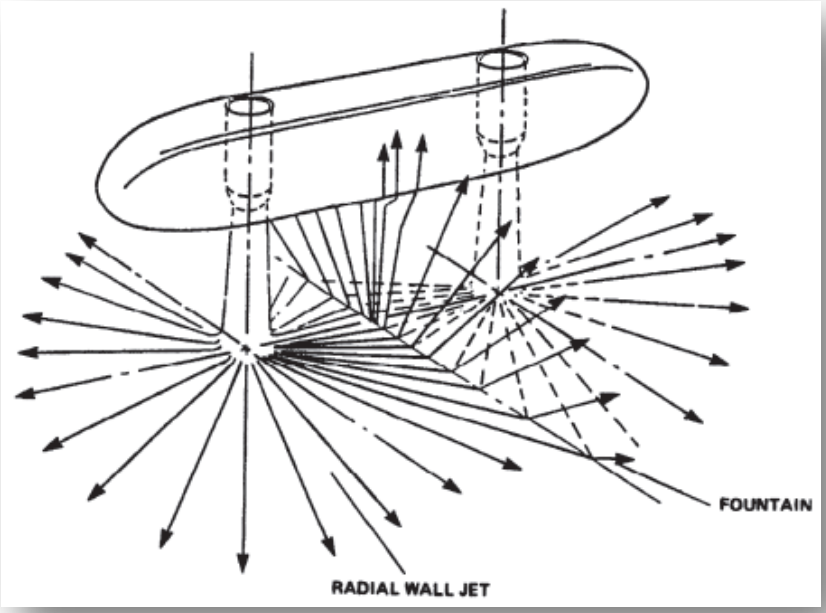

Figure 36: Fountain flow generated between two impinging jets[49]

With multiples jets, an upflow or fountain upwash is created by the collision of the wall jets, that flowing outwards from the impingement points of the adjacent jets, meet. This fountain flow produces a lifting force where it impinges on the lower surface of the VSTOL aircraft, partially offsetting the download created by the entrainment action of the wall jet flow on the ground. The direction and strength of this fountain flow is strongly dependent on the parent jets strength and orientation assuming a uniform ground surface. The fountain flow is known to involve complex flow structures.

This fountain flow is of remarkable importance concerning the overall lift power provided by the impinging jets. When the jets impinge on the ground, they entrain ambient air with them. When this happens below the VSTOL aircraft surface the suck down phenomenon may take place. This suckdown effect of the ambient air around the impinging jets results in a great lift loss. The fountain flow helps in the reduction of this lift loss by generating a positive lift. If instead of two jets, there are three or more jets, three or more stagnation lines appears,

[49] Kuhn R., Margason R., Curtis P., Jet Induced Effects: The Aerodynamics of jet and Fan Powered V/STOL Aircraft in Hover and Transition, AIAA book, Volume 217, Chapter 1.

and where they intersect the fountain is reinforced, and thus stronger than for two jets and depending on the jet spacing, can produce a net lift gain close to the ground. The strength of the fountain and the height at which it is established are, to the first order, inversely proportional to the distance between the jet nozzles.

In transition between hover and the horizontal flight, the case of study, the lifting jet, or fan is swept rearward by the interaction with the freestream or crossflow, being the jet flow rolled up into a pair of vortices. These vortices, along with the entrainment action and blockage effect of the jet, induce suction pressures behind and beside the jet and positive pressures ahead of the jet.

Figure 37: F-35B in transition flight from hover to horizontal flight[50]

Table 2 shows experimental works concerning the study of multiple impinging jets with or without the presence of a crossflow, confined or unconfined, for different velocities ratio, impingement height and experimental techniques.

Kamotani and Greber (1974) proceeded to the flow study of turbulent circular jets with and without heating in the presence of crossflow. The techniques used by the authors to get results were the hot wire probe and iron-constantan thermocouple. Through the velocity profile on the centre line of the turbulent jets and the temperature profile the authors concluded that the jet velocity and its temperature are dynamically related, being the temperature dependent on the density ratio. Later, Jenkins Jr. and Hill (1977) studied the flow of two axisymmetric subsonic impingement jets with the presence of low velocity crossflow. In this study were used different impingement heights, as well as different

[50] Pedro José da Costa Teixeira Santos (2009). Vorticity, Kinetic Energy and Momentum Analysis of the Collision Zone Between a Plane Wall Jet and a Crossflow. Master Thesis in Aeronautics Engineering.

spacing's between the jets. From the results the authors concluded that the spacing between impingement jets and the geometry of the fuselage are extremely important in the forces that govern the aircraft hovering. For smaller spacing than 2.8 was not checked any instabilities, although produced less favourable instability forces. Saripalli (1983) dedicated his work to the visualization of multiple impingement jets in aqueous media for different spacing between the jets, through the application of tracers with a fluorescent dye. Their observations revealed vertical regions and stagnation lines in the flow circulation region, and when the moments of both jets were equals the ascending source was vertical and centred between the two jets. In the case when the mass flows of the unequal-sized jet were equal, the fountain was inclined towards the larger jet and mixed with it. Schetz, Jakubowski and Aoyagi (1984) set out to study the flow of one or two jets aligned side by side and the configuration of the jets in line with the presence of cross-flow. This study was done for several velocity ratios, spacing between impingement jets and angles measured from the horizontal. This study focused on obtaining pressure distribution results in the impact surface of the jets. The results obtained for the aligned jets found to the protection of the rear jet by the first jet. Increasing the velocity ratio caused the location of the centre of the effective normal force moves it forward. Increasing the spacing between jets reduces the interaction between the jets. Moving on to the alignment setting side by side jets the authors found that the flow was characterized by two effects. Due to channelling of the flow between the jets noted that the flow velocity was increased between jets, due to the increase of the crossflow block there was an increase in the free area flow of the side jets. Barata, Durão and Heitor (1988a), Barata, Durão and Heitor (1989a) and Barata, Durão and Heitor (1992a) made studies for multiple impingement jets on a flat plate through a low velocity (figure 38) and for a velocity ratio equal to 30 and an impingement height equal to 5. The experimental results to the mean and turbulent velocity were obtained through laser Doppler velocimeter. The results revealed a large penetration of the impingement jets, exhibiting a similar pattern for the two and three jets configuration. When the impinging jets touched the plate a fairly thin wall jets were formed. The collision of the consecutive wall jets with the cross stream gave rise to a fountain upwash flow (figure 39), which when interacted with the cross stream originating a complex vertical structure wrapped around the impinging jets. The turbulence part of the studies revealed that shear layer that surrounding the jets, the impingement region and the fountain upwash flow zones were characterized by an intense velocity fluctuations, producing higher flow distortions effects. Through these studies the authors concluded that it was necessary a complex numerical analysis of the flow turbulent structure in the three zones aforementioned using a modelled transport equations in order to correctly calculate the turbulent levels of the impingement and fountain flows.

Knowles and Bray (1993) studied the flow of one or two jets impinging on a fixed or moving plate. The visualization and the pressure profiles in the ground plane revealed that there is a

relationship between the distance of penetration, the separation distance and the position of the core of the vortex, allowing clearly quantifying the jet penetration in the ground plane.

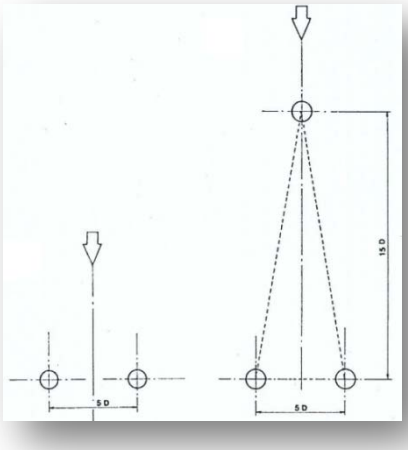

Figure 38: Geometrical arrangement of the jets. Left: two jets configuration. Right: three jets configuration.[51]

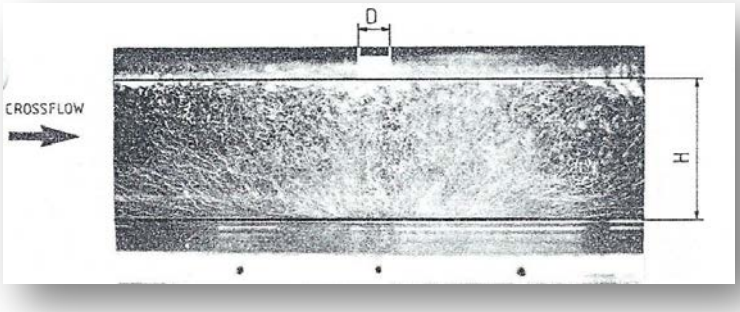

Figure 39: Visualization of the fountain upwash flow in the vertical plane of symmetry for twin jets configuration.[52]

They also verified that the increase of the velocity ratio, impingement height and nozzle pressure ratio increases the penetration of the jet as would be expected, but it decreases when the ground plane is moving, largely due to the reduction of the deficit of the momentum of the crossflow and the consequent increase in the tension of the jet shear layer and the pressure profiles in the ground plane revealed that there is a relationship between the distance of penetration, the separation distance and the position of the core of the

[51] Barata, J.M.M., Durão, D.F.G., e Heitor, M.V. (1988b). Laser-Doppler Measurements of Multiple Impinging Jets through a Crossflow. Proceedings of 4th International Symposium on Applications of Laser Anemometry to Fluid Mechanics, Lisbon, 11-14 July, 1988.

[52] Barata, J.M.M., Durão, D.F.G., Heitor, M.V. (1992a). Velocity Characteristics of Multiple Impinging Jets through a Crossflow. Journal of Fluids Engineering. 114: 231-239.

vortex, allowing clearly to quantify the jet penetration in the ground plane. They also verified that the increase of the velocity ratio, impingement height and nozzle pressure ratio increases the penetration of the jet as would be expected, but it decreases when the ground plane is moving, largely due to the reduction of the deficit of the momentum of the crossflow and the consequent increase in the tension of the jet shear layer. Fernandes, Sobiesiak and Pollard (1996) through Laser Doppler Anemometry, wire smoke and laser-sheet visualization studied two configurations of impingement jets with the presence of confined crossflow and get the flow visualization. The authors were able to conclude that the confinement of the flow causes less bend in the jet, and the velocity profiles exhibit a slower decay rate of the over velocity than that observed studies without confinement. They also verified that the flow confinement limits the counter rotating vortices growth. In the case of two impingement jets a lower curvature of the flow was verified than that registered for a single jet and the formation a pair of vortices in opposite direction upstream of the impact region. Barata (1998) studied a flow of two or three water jets impinging on a flat surface through low velocity crossflow by the same technique used in the previous study with a velocity ratio equal to 30. This study allowed the analysis of the reasons for the prediction failure of the turbulent structure of the impact zone and the location of the "ground vortex". Carcasci (1999) studied the impingement of jets on a flat surface with or without the presence of crossflow. This author has used two different techniques to get results of this study. When the author used the smoke technique the spacing between jets and impingement height were kept constant, but for the oil and pigment technique the author has changed the two above mentioned parameters. Using these two techniques the author observed that for smaller impingement height and high Reynolds number, the ring vortex around the centre line influenced the heat transfer coefficient around the stagnation point in the impact surface. Through each impinging jet was resulted a main vortex, and when they interacted with each other were generated in the space between the main vortexes and the flat plate two vortexes, called lower adverse vortexes. In the plate where the holes were situated a second series of vortexes appeared, called upper adverse vortexes. To finish the study, the author incorporated the crossflow presence and concluded that only the upper adverse vortexes were influenced by the crossflow, being dragged by it.

Failla, Liburdy and Bishop (1999) performed a study of a circular impingement jets on a flat plate with finned surfaces on the presence of crossflow. The study was conducted by thermocouples in order to calculate the Nusselt number and consequently the heat transfer coefficient. The authors concluded that the balance to ensure a higher heat transfer depends on the characteristic length of ribs of the channel. Baydar (1999) studied the flow of one and two jets impinging on a flat plate without the presence of crossflow through the hot wire anemometer. In this study, the authors achieved the velocity profiles and the impact pressure distribution plate in case of one and two impingement jets. As expected by earlier results obtained in this study the impact jet is sensitive to change of the impingement height, and

when the jet feel the wall jet occurs a deceleration, being subsequently deflected. For the case of twin jets, the author noted that the second stagnation point was located in the centre of the jets. On the study of the impingement height effect, the results showed that for H/D less than 2 the sub atmospheric region was located at the impact plate being stronger with Re increase and H/D decrease. Bernard, Brizzi and Bousgarbiès (2000) studied the flow impingement jets on a flat plate using argon laser. The results were reflected in the flow visualization and the pressure coefficient distribution. Through the pressure coefficient distribution they found that its maximum coincided with the impact centre, while the minimum corresponds to the projection of the centre of the vortex. Comparing the visualization results with the results of the pressure coefficient distribution on the wall, led the authors to establish a correlation between the presences of individual streamlines on the impact wall and pressure distribution in it. Counter rotation vortexes pair upstream of the impact region was observed. Behrouzi and McGuirk (2000) conducted a research work that consisted in the study of 3 different cases. The first reported the case of twin water jets with and without the presence of crossflow. In case 2 the study reported the flow of twin jets with introduction of intake geometry, but without flow admission through the crossflow. Finally, the third case was the same structure as the second case, but intake flow through the crossflow. All case studies were performed by laser Doppler velocimetry technique for obtaining mean velocities and turbulent flow structure. The authors could conclude that the mean and turbulent velocity profiles are essentially independent of the crossflow magnitude or the presence of the engine admission. In the study cases where the crossflow presence was felt there was a 10% increase in the turbulence in the mixing region. As a final note the authors found that the results confirmed the flow behaviour for the impingement height and velocity ratio selected were typical of re ingestion flow fields known. Brizzi, Bernard, Bousgarbiés, Dorignac and Vullierme (2000) dedicated to the study of multiple jets impinging on a plate considering the constant heat flux density. The visualization results and flow fields were obtained by two methods of visualization and LDA respectively. The authors showed a cellular aspect of the impact plate flow in the presence of detachment and reattachment lines in the frontal areas. Saddington and Knowles (2000) studied the flow of co-annular jets impinging on a flat plate. They used two settings to obtain results, with a pitot probe and the other with three weight cells. The authors were able to conclude that the annular jet had a good axisymmetric, with identical results to those obtained by Knowles and Kirkham (1998) with respect to the decay rate and the acceleration of the inverted core profile. Turning to the effect of the suckdown force found that for subsonic flow, the results are highly dependent of NPR, while for supersonic flow, the results indicate that the normal jet profile has low percentages of suckdown. Nakabe, Fornalik, Eschenbacher, Yamamoto, Ohta and Suzuki (2001) studied the flow of two jets inclined 45º with in-line and staggered configuration in the presence of crossflow. The work was intended to get the results of flow visualization, Nusselt number and axial velocity profile. Through the visualization was

possible to observe the longitudinal vortices formation by the inclination of the jets, being the vortex number dependent of the jets configuration. Regarding the Nusselt number the authors found that upstream of the jets is higher than that recorded downstream to the in-line jets configuration. For the staggered jets the situation was reversed. Kolár, Takao, Todoroki, Savory, Okamoto and Toy (2003) through hot wire anemometry technique decided to study the vorticity associated to twin jets in crossflow for two different schemes. Through the results the authors showed that the distribution and intensity of vorticity, the vortex strength and transverse penetration ability were strongly affected by the geometrical parameters of the different schemes used. Geers, Tummers and Hanjalic (2004) studied the flow of one or two jets incident on a surface without crossflow for lower impingement heights by Particle Image Velocimetry and Laser Doppler Anemometry, obtaining measurements for the mean velocities and turbulent stresses. The present results led the authors to conclude that the turbulence stresses field was strongly anisotropic. Later, Dano, Liburdy and Kanokjanuvijit (2005) studied the flow of circular and ellipsoidal arrays jet through crossflow for a velocity ratio equal to 30 and through the Particle Digital Image Velocimetry. Measurements of mean velocity, Nusselt number and flow coefficient were obtained. The results of this study showed that the ellipsoidal jet is the profile that most affects the wall region influenced by the interactions of the crossflow, showing an increase in flow coefficient that was more sensitive to variations on the impingement height. The ellipsoidal profile is the one with higher vorticity levels near the stagnation point. With the H/D and Reynolds number increase the Nusselt number decrease for all the jet configurations presented. In terms of sensivity to the study parameters (like H/D, Re) the cusped ellipse jet configuration was the one that showed the higher sensitivity with the impingement height variation. Kanikjaruvijit and Martinez-botas (2005) studied the distribution of the Nusselt number on a flow with multiple circular jets impinging on a concave plate with the presence of crossflow in different schemes and impingement heights. From the results, the authors found that the heat transfer was higher on the downstream side of the concavity relatively to the upstream side. For smaller impingement heights, the impact of the jets on the surface caused recirculation inside the concavities, being possible to conclude that the hemispherical geometry on the plate is more efficient in terms of pressure loss, production and economy when compared with the elliptical plate geometry. Kelman, Greenhalg and Whiteman (2006) studied the flow of micro-jets through confined turbulent cross flow by Laser Anemometry. The conclusions drawn from this study are important in gas turbine applications, since they are characterized by small diameter jets and low Reynolds number.

Dano and Liburdy (2007) studied the flow of no circular impingement jets in the presence of semi-confined crossflow to obtain the instantaneous velocity fields. This study revealed that non-circular jets at 0º produce more kinetic energy, therefore increasing the turbulent kinetic energy when compared with the jet guidance to 90º. Although the modal energy distributions for the circular and non-circular jets are similar, non-circular jets had an increase in the

number of vortices. Yin, Zhang and Lin (2007) aimed to study the mean velocity profiles, turbulent energy and shear stresses of the flow of two circular jets varying the jets velocity and the spacing between them. The study allowed the authors certify that the velocity profiles and turbulent energy are symmetrical for various Reynolds numbers and spacing between jets. With respect to interference between the jets has been found that increased with the decrease in the Reynolds number, or by increasing the spacing between jets. To end the length of two jets mixing could be increased by the decrease on the spacing between jets by or increasing the Reynolds number. Kolár and Savory (2007) did a brief survey of some studies of twin jets in a crossflow. The results showed that the tandem configuration is the one that had more rapid mixing and greater penetration into the crossflow. In respect to transverse penetration ability and vortex strength were subject to the nozzle arrangement. In the two schemes it was shown some dominant vortical structures and counter rotating vortexes, being this type of structures responsible by the convective entrainment. Kate, Das and Chakraborty (2007) studied the spreading flow due to the normal impingement of two closely spaced liquid jets. This work allowed to the authors observed different hydraulic jump (the flow of the thin film) interactions by varying the spacing between the jets and their relative strength. Saddington, Knowles and Cabrita (2008) through Particle Image Velocimetry and Laser Doppler Velocimetry studied the flow of twin jets impinging on a flat plate. The study was done to various impingement heights and spacing between jets. The results showed that the mean vertical velocity was independent of the impingement height and pressure ratio. The maximum vertical velocity location of the source decreased with the increase of the impingement height. Gutmark, Ibrahim and Murugappan (2008) dedicated to the study of circular and no circular subsonic jets in the presence of crossflow. The study of these authors aimed to represent the streamlines corresponding to this type of flow. As the main conclusion of this study the authors found that each of the geometries produced a reverse flow region, and for the geometry of low aspect ratio the reverse flow region had lesser magnitude relative to other geometries. Saddington, Cabrita and Knowles (2009) studied the flow of circular jets with in or out tapered configuration. During their work, the authors did vary the jets impingement height, the jet nozzle inclination angle and the pressure ratio. The authors conclude that the inclusion of tapered nozzles did not significantly alter the momentum flux distribution when compared with normal nozzle configuration. Ozmen (2011) studied the confined flow of two jets incident on a surface without crossflow by hot wire anemometry technique. The results showed that the size and location of the vortices are affected by the jet height and the ratio between the length and the diameter of the jet (L/D) and the pressure distribution on the surface was independent of Re but dependent of H/D and L/D. The jet height is one of the factors relevant to the VSTOL, being rarely considered the crossflow effect that causes the deflection of the impingement jets on the plate, the upwash flow and the formation of recirculation zones upstream of the impact point characterized by vorticity. Caliskan and Bakaya (2012) through infrared thermal imaging studied the heat

transfer and the flow field associated to a circular jet array that impinging on smooth surfaces and V-shaped –ribs surfaces for different Reynolds numbers and jet to plate spaces. The authors observed that for low impingement heights the production of turbulent kinetic energy was higher in the case of V shaped-rib surfaces. In respect to the heat transfer, the V shaped ribs surfaces showed the higher Nusselt number, being the location of the peaks and the minima influenced by the crossflow velocities. On the stagnation points the Nusselt number decreased with the impingement height increase. Recently Barata (2013) summarizes thirty years of impinging jets through a low crossflow work. The studies were conducted for different Re, velocity ratios, impingement heights and for different spatial configurations of the impinging jets. The results were flow visualization, mean and turbulent velocity profiles through LDA, and show a great penetration of jets and the ascending fountain that is formed during the collision of the radial wall jets and deflected by the interaction with the crossflow (figures 40 to 42).

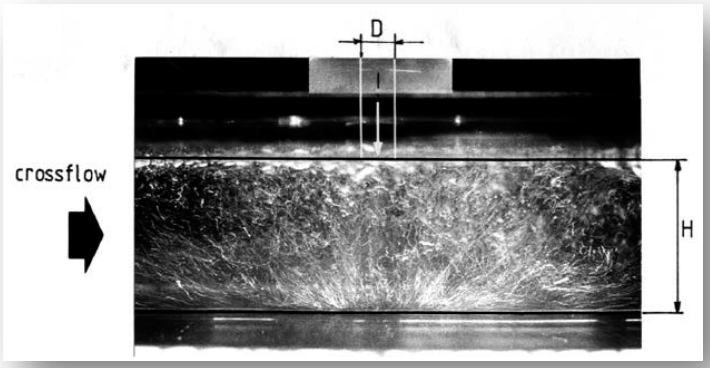

Figure 40: Flow visualization of the fountain upwash flows in the vertical plane of symmetry for twin jets side-by-side.[53]

For the tandem configuration jets the author presents 3 types of standard flow. In this configuration, the first jet has a large penetration being deflected by the presence of the crossflow when impacting on plate giving rise to a ground vortex due to the collision with the radial wall with the crossflow that wraps round the impact point. The second jet, practically didn't felt the crossflow influence because it was protected the crossflow influence by the first jet. To finish the experimental works there are two recently studies about this thematic. First, Mehryar, Giovannini (2014) through PIV technique studied the cooling effect of nine confined jets arranged in square in line array, showing a twisted symmetry pattern of the flow field and the heat transfer on the impact plate when the impingement height equal to the jets centre spacing. It was also shown that the central jets attracted the peripheral jets and a repulsion of the peripheral jets caused by the central wall jet.

[53] Barata, J.M.M (2013). Multiple Jet/Wall/Cross-Wind Interaction Relevant to VSTOL Ground Effects. *Proceedings of the 2013 International Powered Lift Conference*, Los Angeles, California, August 12-14 2013. AIAA paper 2013-4380.

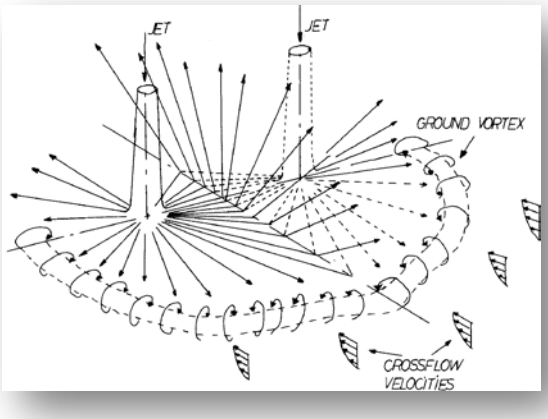

Figure 41: Fountain flow and ground vortex generated by twin impinging jets side-by-side[54].

Second and to finish, Li, Zheng, Hu, Zhang (2014) dedicated their work to the study of the impinging jet in a crossflow to explore the convection heat transfer used high temperature co-fired ceramic. Several parameters were varying during the study leading the authors to conclude that the enhancement factor was to increase with the jet to crossflow mass ratio and the Re, but decreased with the jet diameter. The presence of a crossflow was observed to degrade the heat transfer performance.

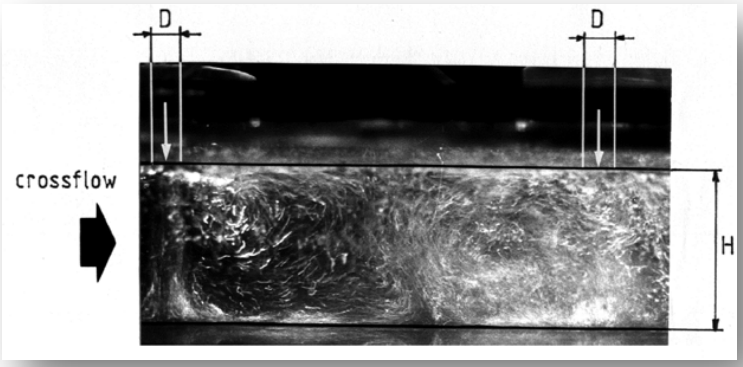

Figure 42: Flow visualization of the fountain upwash flows in the vertical plane of symmetry for the three jets configuration[55].

[54] Barata, J.M.M (2013). Multiple Jet/Wall/Cross-Wind Interaction Relevant to VSTOL Ground Effects. *Proceedings of the 2013 International Powered Lift Conference*, Los Angeles, California, August 12-14 2013. AIAA paper 2013-4380.

[55] Barata, J.M.M (2013). Multiple Jet/Wall/Cross-Wind Interaction Relevant to VSTOL Ground Effects. *Proceedings of the 2013 International Powered Lift Conference*, Los Angeles, California, August 12-14 2013. AIAA paper 2013-4380.

Authors	Experiment	Technique	Results	Comments
Kamotani, Greber (1974)	The study of turbulent circular jets with and without heating through a crossflow.	Hot wire probe Iron-constantan thermocouple	Velocity profile on central line Temperature profile on the central line	Through the results, the authors concluded that the jet velocity and temperature correspondent trajectories are mainly determined by the dynamic relation, being the temperature dependent of the density ratio.
Jenkins, Hill Jr.(1977)	Study of two axisymmetric subsonic impinging jets thorough a low velocity crossflow Vj= 91.4 m/s D= 5.08 cm 2<H/D <8 2<S/D <8	Sting balance – to measure the interference of the ground forces on the aircraft model and bi-dimensional models. Kiel Probe e static probe – to measure the upwash flowfield properties X-Y recorder – to measure pressure and forces	Velocity profiles Pressure profiles Effect of the jets centre spacing on the stagnation maximum pressure line Maximum pressure variation on the ground Impinging height effects Dynamic pressure decay	The results showed that the resultant forces in ground effect when a VSTOL aircraft hovering can be very sensitive to the spacing between the jets and the geometry of the fuselage of the aircraft. It was observed that the interference forces increased as the spacing between jets is decreased, reaching a maximum between 3 <S / D <4. Instabilities were found in the flow with and without an upwash in the flow model using an S around three diameters at low impact altitudes. Spacing between jets below 2.8 were free of this instability, but produced less favourable interference forces

Table 2: Summary of experimental work on the flow of a multiple jet through a crossflow

Saripalli (1983)	Study of multiple impinging jets flowing on an aqueous medium H/D= 4 S/D= 12, 6, 4.1 m_{j2}/m_{j1} (jet momenta ratio)= 1, 0.419 e 0.25 Re= 23780	Visualization method through tracers on an aqueous medium with illumination by a sheet of light fluorescent sodium fluorescent ink	Visualization	This work allowed the author to clearly define all flow phenomena observing the ascending flow. It was still possible to view vortical regions and stagnation lines in the recirculation region. Finally the author concluded that when the momentum of the two jets was equal the upwash flow was vertical and centred. However, when the mass flows of the unequal-sized jet were equal, the fountain was inclined towards the larger jet and mixed with it.
Schetz, Jakubowski, Aoyagi (1984)	Flow study of one or two impinging jets (side-to-side and line configuration) through crossflow R= 3-8 V_∞ (crossflow velocity)= 14.5 - 35.8 m/s θ =90, 75, 105 ° D= 4.92 cm S/D= 2- 6	Scanivalves	Surface pressure distribution Isobaric maps of ΔC_p	The results obtained by the authors showed that in the case of aligned jets the interaction between them resulted in rear jet protection by the first jet. However increasing R there was an increase in the surface area affected by the jets and the change of the location of the centre of the effective normal force to the front. With regard to the spacing between jets, its increase significantly decreased the interaction between jets. Turning to the results obtained for the nozzles placed side by side it was found that the flow was characterized by two effects: significantly higher flow velocity of the jet due to channelling of the flow between the nozzles and increased

Table 2: (Continuation)

					nozzle blockage and increased of the crossflow blocking and the flow spread to the sides, resulting in an increase in the flow velocity in the lateral areas of free jets.
Barata, Durão, Heitor (1988a)	Study of two and three impingement jets against a wall through a low velocity crossflow. V_j/U_0=30 Re_j= 105,000 H/D= 5 D= 20 mm	LDV	Visualization Mean and turbulent velocities		The results for the two configurations revealed similar pattern in the case of the large penetration of the impinging jets. In the case of three jets the fountain flow was extended by the interaction with the third radial wall jet. The fountain flow zone was dominated by strong curvature effects and intense velocity fluctuations.
Barata, Durão, Heitor (1989a)	Study of a single, two and three impingement jets on a wall through a low velocity crossflow. V_j= 3.0 and 5.1 m/s Re_j= 60,000 and 105,000 H/D= 5 D= 20 mm V_j/U_0=30 S/D= 5	LDV Visualization: air bubbles or fluorescent dye	Mean and turbulent velocity visualization		All the configurations shown a large penetration of the impinging jets and in the multiple jets configurations a fountain upwash flow was formed and deflected by the crossflow. The shear stress surrounding the jets, the impingement region and the fountain upwash flow zones were dominated by strong curvature effects.

Table 2: (Continuation)

Barata, Durão, Heitor (1992a)	The Study of the flowfield resulting from the impingement of two or three jets on a Wall through a low velocity cross stream. V_j= 5.1 m/s Re_j= 105,000 H/D= 5 D= 20 mm V_j/U_0=30 S/D= 5	LDV	Mean and turbulent velocity Visualization	As showed in Barata, Durão, Heitor (1989a), the two study configurations giving rise to a fountain upwash flow formation by the collision of the consecutive wall jets. In the case of three impingement jets the fountain upwash flow was extended due the interaction of the third wall jet. The turbulence velocity analysis suggested that the calculation for these complex impinging flows must be found modelled by transport equations.
Knowles, Bray (1993)	Flow of one or two incident jets on a plate with/without movement 2<H/D <10 1.05<p_{rn} (nozzle pressure ratio)<4 0.013<V_e (crossflow-to-jet velocity ratio)<0.1 -5°< vector angle<10° V_∞ (crossflow velocity)=42 m/s	Standoff probe	Pressure profiles on the ground plane Flow visualization	Through study it was confirmed that there is a constant relationship between the distances of penetration, the separation distance and the position of the core of the vortex, thus any one of these can be used to quantify the penetration into the ground. The penetration of the jets increases with the effective velocity ratios , nozzle height, nozzle pressure ratio and vectoring nozzles and decreases when the surface moves due to the reduction of the deficit at the time of cross-flow and an increase in tension of the jet shear layer.

Table 2: (Continuation)

Fernandes, Sobiesiak, Pollard (1996)	Study of two configurations (a single jet and two opposed jets with different momentum flux ratios) through confined crossflow D=19.3 mm L/D=55 Re_D (jet Reynolds number)=19100, 31200 $Re_{crossflow}$=9300, 9400, 9500 $U_{crossflow}$=2.43 m/s J (jet to crossflow momentum flux ratio,)= 60, 155	LDA Smoke-wire Laser-sheet visualization	Mean velocity profiles Turbulence intensity profiles Flow Visualization	Through this study we observed that the flow confinement has a significant effect on its development, identified several regions in the jet flow and the lesser curvature of the jet when confined. It was observed a poor transport in the confined jet, apart from the maximum deformation region being due to the fact that the walls confining the growth of vortices in opposite directions. The flow of two opposite jets is characterized by a progressive melting of the jets in the far field, after which the flow resembles that of single jet propagation. The lesser curvature of respect to the situation jets with only one jet was observed, then seeing their collision in the centre of the test section. The flow is characterized by a pair of vortices in opposite directions, which are formed upstream of the impact region.
Barata (1998)	Flow study of two or three circular water jets impinging on a flat plate through low velocity crossflow. D = 20 mm H/D = 5	LDV	Mean velocities Turbulence intensity	It was identified the formation of an irrelevant wall jet which gave rise to a vortex ground around the jet impact resulting from the radial jet interaction with crossflow. The results confirm that the impact zone is characterized by considerable deviation in the conventional

Table 2: (Continuation)

	Re = 60000 V_j= 3 m/s V_j/U_0= 30	Flow of impingement jets on a flat surface with and without crossflow presence Smoke technique: D=20mm L/D=6 Z/D=2 Oil and pigment technique: L/D= 6, 12 Z/D= 2, 4, 8	Oil and pigment, smoke and thermotropic liquid crystal	Visualization	Through the work we observed that the ring vortex that turns the centre line is generated by the interaction of the free jet with neighbouring flow. It was observed that for small distance between the surfaces and elevated Re, the ring vortex that turn the centre line influenced the high heat transfer coefficient around the stagnation point on the flat surface. When the crossflow was present in the activity, the "lower adverse vortexes" were not particularly affected, while the "upper adverse vortexes" were dragged by the crossflow. To complete it was found that in the situation described above the ring vortexes were influenced by crossflow.	dimensionless values of the turbulence model. The analysis explains the reasons for the failure of the turbulence model to predict the structure of the impact zone and the location of the ground vortex
	Carcasci (1999)					

Table 2: (Continuation)

Failla, Bishop, Liburdy (1999)	Flow study of circular jets impinging on a plate with finned surfaces through crossflow. D= 1.6 mm 1<H/D<7 S/D=4 590<Re_{dH} (Reynolds number based on hydraulic diameter and channel velocity)<1900 1550<Re_d (Reynolds number based on jet diameter and exit velocity) <4620	Thermocouple	Nusselt number Heat transfer coefficient	It was found from the results obtained in terms of total flow capacity that there is a balance between the impact and flow rates of the channel to achieve a higher heat transfer. The appropriate balance thus depends on the characteristic length of the channel formed by the finned surfaces, and small finned surfaces are the best to increase the jet Reynolds and decrease channel Reynolds for a determinate energy flow. If we have large finned surfaces then we have the reverse situation.
Baydar (1999)	Flow study of a single and two impinging jets on a flat surface 300<Re <10000 0.5<H/D <4 V_j <30 m/s L= 4 mm D= 4 mm	Manometer Hot wire anemometry	Velocity profiles Pressure distribution	Analysing the results, the authors concluded that the impact of jet is sensitive when the impingement height was changed. The presence of the impact plate was sensed by the wall jet causing the deceleration, starting the jet to be deflected around one of the plate diameter. In the case of twin jets, the second stagnation point occurs in the centre of the two jets. To impingement heights below 2, a sub atmospheric region occur in the impact plate for the two cases studied, making it stronger with increasing Re and the impact height decreased.

Table 2: (Continuation)

Bernard, Brizzi, Bousgarbiès (2000)	Flow study of circular jets impinging on a flat surface D=10 mm Re_j (jet Reynolds number)=12600	Argon Laser	Flow Visualization Pressure coefficient distribution	The main maximum of Cp profiles corresponds to the impact centre, the second maximum corresponds to the line of rehabilitation and the minimum corresponds to the projection of the centre of the vortex. Thus, the results of the comparison and visualization of pressure distribution in the wall allow the establishment of connections between the individual streamlines in the presence of the wall and the impact pressure distribution on the wall. It was observed the generation of a counter rotating vortex pair, being the latter located at z / d = 0 for any value of Vr. The increase in heat transfer can be achieved to the greatest extent region, increasing for any value of Vr.
Behrouzi, McGuirk (2000)	Case 1: Flow of twin water jets with and without crossflow. Case 2: Flow of twin water jets with admission geometry introduction, without admission flow through the crossflow Case 3: Flow of twin water jets with admission geometry	LDV	Mean velocities Turbulent structure	Through the study of the three test cases the authors found that the mean velocity profiles and turbulent velocity profiles are both essentially independent of the magnitude of crossflow or intake presence or your own suction flow. It was also found that the introduction of crossflow creates over 10% turbulence in the mixing flow region.

Table 2: (Continuation)

	introduction and with admission flow through the crossflow D_j=12.4 mm H/D_j=7 R (velocity ratio) = 35, 24, 18 Re= 400000 V_j=2.66 m/s 0.076<W_c (crossflow velocity)<0.15 m/s			Finally the results confirmed that the flow behaviour for the impingement height and velocity ratio selected were typical of re ingestion flow fields known.
	Saddington, Knowles (2000)	Flow study of co-annular jets impinging on a flat plate D= 50.28 mm d_a (annular stream nozzle inner diameter)= 35.81 mm d_c (core stream nozzle diameter)= 35.33 mm	Configuration 1: Pitot probe Configuration 2: three weight cells	Pressure profiles Jet induced suckdown	The results showed that the co- annular jets have well axisymmetric. The results were similar to the observations made by Knowles and Kirkham, with respect to the decay rate and acceleration of the core in some cases of the inverted profile, so the results of Knowles and Kirkham apply equally well for the co-annular jets in the present study jets. With regard to the results of suckdown force, we can conclude that for the subsonic core flow the results are largely independent of NPR as to flow with supersonic core, the results indicate that co annular jet normal profile has a low percentage of suckdown for h / D <5.

Table 2: (Continuation)

Brizzi, Bernard, Bousgarbiés, Dorignac, Vullierme (2000)	Flow study of multiple impingement jets on a plate with constant heat density flow D= 10 mm S/D= 4 H/D= 2 Re_j= 12600 T_{placa}= 70ºC	Visualization: Coating calcium carbonate particles suspended in oil Laser light sheet with seeding in the flow Measurements: LDA Thermography by infrared	Visualization Wall streamlines Flow field	The results revealed a cellular aspect of the flow in the impingement plate and the presence of detachment and reattachment lines of the flow in the frontal zones between different cells observed. One goal of the authors was in the present study show the importance of the crossflow induction effect on the cooling efficiency.
Nakabe, Fornalik, Eschenbacher, Yamamoto, Ohta, Suzuki (2001)	Flow of two inclined jets in line and staggered arrangements with crossflow Re = 5000 H/D=3.5 VR=5 Pitch angle = ± 45º Skew angle = ± 90º In line jets crossflow jets: S/D = 10 d = 6 mm Staggered jets: D= 6	Thermochromic liquid crystal Fluorescence dyes PIV	Flow visualization Nusselt number Axial velocity profile	The authors observed the formation of longitudinal vortices as a result of the impingement jets inclination, and the number of vortices depends on the jets spatial configuration. The peak of the Nusselt number is higher upstream than that observed downstream in the case of both jets are in-line. If the jets are staggered, the situation is opposite to that mentioned above. It was also found that the interaction between the jets is dependent on its spatial configuration, being the vortical structure and the heat transfer area affected by this fact.

Table 2: (Continuation)

	S/D=10 Transverse distance between the jet centres = 5D			
kolár, Takao, Todoroki, Savory, Okamoto, Toy (2003)	Study of twin jets in crossflow with two different jets scheme (tandem and side by side) S/D=5 R (velocity ratio) =8 D=13.5 mm U_J=25.0 m/s Re_J=2.24x104 U_C=3.125 m/s	Hot wire anemometry	Vorticity distribution Turbulent vorticity transport	The authors found that the vorticity distribution, vortex strength, transverse penetration ability and intensity of vorticity transport are strongly dependent function of the geometrical parameters, such as, nozzle centre to centre separation distance, angle between nozzle centre to centre connection line and crossflow direction.
Geers, Tummers, Hanjalic (2004)	Flow of single or two circular impingement jets on a surface without crossflow For a single jet: H/D = 2 D = 36 mm	PIV LDA	Mean velocities Turbulent tensions	The turbulent stress field is characterized by a strong anisotropy.

Table 2: (Continuation)

)	Re_j= 2.3x10^4 V_j = 9,6 m/s For two jets: H/D = 4 D = 13 mm Re_j= 18.3x10^3				
Dano, Liburdy, Kanokjanuviji t (2005)	Flow of circular and ellipsoidal jet arrays through cross-flow. 8500 < Re < 15900 2< H/D < 4 Dc= 1.27x10^{-3} mm De= 1.138x10^{-3} mm Θ = 0° e 90 ° D_H (hydraulic diameter of the circular orifice)= 1.27x10^{-3} mm D_e (hydraulic diameter of the cusped ellipse orifice)= 1.138x10^{-3} mm Θ (cusped ellipse nozzle orientation) = 0° e 90 °	DPIV Flow visualization	C_D Mean velocity Nusselt number	The results show that the ellipsoidal jet compared with the circular jet affects more the wall region influenced by the interactions of the crossflow. With the decrease of H / D there is a rapid decline of C_D in the flow direction. Increased V_j/U_0 along the downstream direction to the crossflow, C_D decreases. The ellipsoidal profiles showed an increase in C_D compared with circular profiles and they were more sensitive to H / D. For high Re the vorticity decreased near the surface. The ellipsoidal profile at 0 ° was the case that had higher levels of vorticity near the stagnation point. The circular profile produced the greatest heat transfer. With the H/D and Reynolds number increase the Nusselt number decrease. The cusped ellipse jet showed a higher sensitivity to H/D.

Table 2: (Continuation)

					In the case of the impact surface being isothermal ellipsoidal geometry (0 °) behaves similarly to a circular geometry. If the surface is uniform the ellipsoidal geometry (0º) has a higher Nusselt number.
Kanokjaruvijit , Martinez-botas (2005)	Flow of several circular jets on a concave plate through different crossflow schemes Re = 11500 D=10mm H/D= 2, 4, 8	Transient wide band liquid crystal method		Nusselt number distribution	Through the study it was observed that heat transfer on the downstream side was larger than the upstream side concavity. In the case of H/D = 2, the impact of the jets in the concave plate caused a marked recirculation inside the concavities, and the heat transfer aggravated compared with a flat plate. Finally it was possible to prove that the spherical geometry on the plate in terms of pressure losses production and economy is more efficient than the elliptical configuration on the plate.
Kelman, Greenhalgh, Whiteman (2006)	Flow study of micro jets through turbulent confined crossflow	LDA		Mena velocity Jet Flow concentration	The jet fluid is a mixture of methane and acetone. Increased the turbulence in the crossflow will tend to break the vortex structure surrounding the jet.

Table 2: (Continuation)

Dano, Liburdy (2007)	Flow of circular and no circular jets through semi confined crossflow 8500<Re <15900 S/D=6.25 H/D=4 $D_{circular}$=1.27x10^{-3} $D_{not-circular}$= 1.138x10^{-3} 0 <Vr <0.19	DPIV POD Vortex detection algorithm	Instantaneous velocity flowfield	The study revealed that the non-circular jets (0 °) exhibit a higher kinetic energy generation, thus corresponding to an increase in turbulent kinetic energy, especially when compared with the same jet with orientation of 90°. It is also detected an increased on the vortices number as compared with the circular jet, although the modal power distributions are similar.
Yin, Zhang, Lin (2007)	Flow of two circular jets D=44mm 1.5<B <1.89 10 m/s<V_j< 25 m/s 3.33x10^4 <Re <8.33x10^4	Movable X-hot wire probe	Mean velocity profiles Turbulent energy Shear stresses	In the flow direction, the twin jets are clearly separated near the jet outlet nozzle. Outside this region, the two jets interact, blending as if they were just a jet. As for the velocity and turbulent energy profiles are quite symmetrical in relation to the centre line of the two jets for various Re and spacing's between the jets. Interference between the jets is increased when the Re decreases, but if we speak of the spacing between jets the existing situation is contrary. The mixing length of the two jets can be increased by reducing B, or increasing Re.

Table 2: (Continuation)

Kolár, Savory (2007)	A brief survey of the study of twin jets in crossflow	Hot wire anemometry PLIF	Vorticity	A brief survey of the recent studies of twin jets in crossflow by the present authors is carried out. The tandem configuration show more rapid mixing and greater penetration into the crossflow than side by side configuration. It was also shown hoe the transverse penetration ability and vortex strength in terms of circulation are subject to the nozzle arrangement. All cases of TJICF la qualitatively to the some dominant vortical structure, CVP being responsible by convective entrainment.
Kate, Das, Chakraborty (2007)	Study of two normal impinging liquid jets S/D=7.69, 11,15.4 H/D=9.23, 10, 14.4, 16.9 Q (volume flow rate)=1.0x10^{-5}m^{3}s^{-1}, 1.25x10^{-5}m^{3}s^{-1}, 3.33x10^{-5}m^{3}s^{-1}, 4.12x10^{-5}m^{3}s^{-1}, 8.33x10^{-5}m^{3}s^{-1}		Visualization	The results showed that the spreading flow due to the normal impingement of two closely spaced liquid jets depending on the spacing between the two jets and their relative strength, different kinds of hydraulic jump interactions were possible, resulting in a variety of flow pattern.
Saddington, Knowles, Cabrita (2008)	Flow study of twin impingement jets on a flat plate. 1.05<NPR (nozzle pressure ratio) <4 2<H/D <10 3<S/D <7	PIV LDV	Flow visualization Velocity flowfields Decay rate Energy spectrum	The study carried out showed that the source mean vertical velocity was consistent throughout the test performed and therefore independent of the jet impingement height and pressure ratio. The local maximum vertical velocity of the source decreased with the increase of the

Table 2: (Continuation)

	D=12.7 mm				jet impingement height. Regarding the decrease rate was observed which is dependent on jet pressure ratio.
Gutmark, Ibrahim, Murugappan (2008)	Flow of subsonic circular and no circular jets through crossflow. V_∞ (mainstream velocity)=12.5 m/s T_∞ (flow temperature)=21°C V_j/V_∞=3.8 e 8	PIV	Streamlines representation		The crossflow turbulent boundary layer is affected by the incident jet. There is its deceleration by the jet presence. It was found that the triangular geometry aligned in the direction flow shown to induce spanwise spillage on the edges of the nozzle
Saddington, Knowles, Cabrita (2009)	Flow study of circular jets with in or out tapered configuration D = 12.7 mm S /D= 7 H/D = 2.4 a 8.4 α (nozzle splay angle) = ± 15° NPR (nozzle pressure ratio)= 1.05 a 4	PIV	Quantify and analyse the jet tapered effect on: Impingement jet Flow field characteristics Fountain dissemination and deterioration Flow momentum ratio		For the present study it was shown that at low NPR observed a good correlation between the product of the moment jet transported to the fountain region formation and the lateral spacing of the jet stagnation points, as well as the relation of the vertical velocity fountain peaks. For under expanded pressure relations stagnation points, as well as the relation of the vertical velocity fountain peaks. For under expanded pressure relations there was a correlation, however, there was more scatter in the data. The rate of deterioration of the maximum vertical velocity at the fountain showed a

Table 2: (Continuation)

				strong dependence on NPR. With this study it was found that the inclusion of tapered nozzles did not significantly alter the fountain flow momentum rate distribution when compared to the equivalent parallel configuration.
Ozmen (2011)	Confined flow of two circular impingement jets on a surface without crossflow presence. Re = 30000, 40000 e 50000 H/D = 0,5, 1, 2 e 4 L/D = 0,5, 1 e 2 D = 25 mm	TSI – IFA – 100 hot wire anemometer Smoke-wire	Pressure distribution. Mean velocity. Turbulence intensity.	There is a relation between the sub atmospheric and heat transfer coefficient peak regions for the low values of H / D. The size and location of the vortices are affected by the relation of H / D and L / D. The pressure distribution on both impact and containment surfaces are independent of the Reynolds number, but depend on the H / D and L / D.
Caliskan, Bakaya (2012)	Study of the flow field and heat transfer of a circular jet array impinging on smooth surfaces and surfaces with V-shaped ribs. H/D= 3 and 12 Re= 2000, 6000 and 10000	Infrared thermal imaging	Velocity vector distribution Axial velocity distribution Axial *rms* velocity distribution Reynolds stress distribution	The results showed that for low jet to plate spacing the production of turbulence kinetic energy is higher for V-SR surfaces. The Nusselt number is higher for the V-SR surface. The location of the peaks the minim were influenced by the crossflow velocities. The Nusselt numbers at the stagnation points decrease with the H/D increase.

Table 2: (Continuation)

			Radial velocity distribution Nusselt number distribution	.
Barata (2013)	Flow study of turbulent circular jets on a impingement plate perpendicular to the jet geometric axis with the presence of a low velocity crossflow 43000<Re <105000 7.5<V_r (velocity ratio) <90 5<H/D <20 S/D=5 L/D=6	LDA Visualization	Mean and turbulent velocity profiles Fluctuation velocity Visualization	The results obtained by the author showed a significant penetration of the impingement jets and the upwash fountain formed by the collision of the radial wall jets and deflected by the cross low. In the case of Tandem position of impact jets were observed 3 types of flow standard. The results showed a significant penetration of the first jet, which is deflected by the crossflow and on the impact moment on the plate gave rise to a ground vortex due to the collision with the radial with the crossflow, winding itself around the impact point. The second jet is not affected by crossflow because this is protected by the first jet.
Mehryar, Giovannini (2014)	Study of the cooling effect of nine confined jets arranged in square in line array D= 3 mm S/D= 2	PIV	Temperature field Contours of iso-Nusselt number Velocity vector field Vorticity field	The results showed a twisted symmetry pattern of the flow field and heat transfer on the impingement plate when the confined ratio equal to jet to jet spacing ratio and showed two different effects between the central jet and the neighbouring jet, being the first effect the attraction of peripheral jets by the central

Table 2: (Continuation)

	1<H/D<4	Study of an impinging jet in a crossflow. Jet to crossflow mass ratio,X= 2%-8% Re= 1434-5735 D= 2-4 mm	HTTC (high temperature co-fired ceramic)	Radiation heat flux Temperature Nusselt number	jet and the second effect was the repulsion of the peripheral jets by the wall jet of the central jet
					The authors found that the enhancement factor was found to increase with the jet to crossflow mass ratio and the Reynolds number, but decreased with the jet diameter. The presence of a crossflow was observed to degrade the heat performance in respect to the effect of impinging jet to the target surface only.
	Li, Zheng, Hu, Zhang (2014)				

Table 2: (Continuation)

1.5.2 Numerical Studies

Patankar, Basu and Alpay (1977) demonstrated the possibility of calculating a jet through unconfined crossflow by the method of finite differences, hybrid scheme and *"k- ε"* turbulence model, getting a reasonable agreement between the numerical results and the experimental results of other authors, because discrepancies appearing in some regions which can be attributed to the low density of the mesh used. Adler and Baron (1979) used numerical methods in that it was necessary to use a function that characterized the air entrainment rate at rest by the jet from experimental data of other authors characterizing the trajectory of the jet. Rodi and Srivatsa (1980) used in the numerical calculation the finite difference method to calculate a flow of an air jet through crossflow for small velocity ratios. The numerical results were in agreement with the experimental exception to the velocity ratio equal to 0.3 where some discrepancies appeared which not assess the accuracy of the method used uncompressible form, getting a reasonable agreement between the numerical results and the experimental results of various authors on the most features. The results showed that the flow can be represented by a series of vortex rings emitted by the jet fountain, and for high velocity ratios the initial vorticity rings were distorted in a pair of vortices in the apparent horizontal line. Rizk and Menon (1988) performed by LES the numerical study of the flow of two impingement jets in line, which showed that the mesh selected for the simulation was insufficient to resolve the smallest details of this type of flow. When compared with experimental data of the same nature, these numerical results are consistent quantitatively and qualitatively. Barata, Durão and McGuirk (1989b) demonstrated the possibility of calculating the flow of a circular water impinging jet through a confined low velocity crossflow for velocity ratios of 30 using a finite difference method, hybrid scheme and turbulence model "*k-ε*". The numerical results were similar to those obtained experimentally, although in some regions there was a disparity that were due to the insufficient mesh nodes used and the turbulence method "*k-ε*" not correctly predicted the pressure distribution in the impact zone. In the same year, Barata and Durão (1989c) developed a numerically which the purpose was the development and validation of a computational method to analysis the flow characteristics of a single and multiple jets impinging on a flat surface through the influence of a low velocity cross stream. The turbulent model chosen was the standard "k-ε" turbulence model and the numerical results were compared with the ones obtained by Barata et al. (1987). The numerical results showed a good agreement with the Barata et al. (1987), but in the fountain upwash flow region the maximum vertical velocity values were under predicted. The author's confirmed the advantages of the QUICK differencing scheme over the hybrid scheme in respect the less computational resources needed by the QUICK scheme for the same accuracy level. Ince and Leschziner (1990) carried out the simulation of two types of flow comparing their results with those obtained previously by other authors. The computer simulation was performed using Reynolds stress transport closure model and the "*k-ε*" eddy-viscosity model. The results obtained by the authors have shown that by using the second

moment closure model the approximation to the experimental results were higher than that for other computational model also used in this study. Savory, Toy, McGuirk and Sakellariou (1990) from the "*k*-*ε*" turbulent method demonstrated the numerical calculation of a flow of a circular jet in crossflow through small velocity ratios (4 to 8) and concluded that the previsions given by the numerical method showed significant differences in strength, size and location of the counter rotating vortexes due to numerical errors. Zhang (1994) directed their study to the power loss in VSTOL aircraft due to the impact of vertical jet on the ground. For this study they used the "*k*-*ε*" model showing the results for low impingement height the existence of a vortex beneath the plate and thereby induce a significant pressure drop on the lower surface of the plate, thus creating a favourable gradient of pressure to delay imminent separation flow on the edge of the plate. On the case of significant impingement heights, the field induced flow between the ground and the plate is dominated by induced jet entrainment and by the separation on the edge of the plate, resulting in the formation of recirculation close to the edge of the plate. Leschziner and Ince (1995) compared their numerical simulation with experimental data of Saripalli (1987), Abbot and White (1989), Barata et al. (1992a) but could not draw strong conclusions from their work since emerged instability, hampering comparisons with experimental data. Knowles (1996) studied the modelling of the flow of impingement jets on the basis of the Rodi and Malin corrections. The author used a finite volume model PHOENICS finite volume code and "*k*-*ε*" turbulent model by varying the jet nozzle pressure ratio to get the velocity profiles, decay of axial velocity and the wall jet growth for each study case. The results revealed that the increase of the nozzle pressure ratio tended to reduce the decay rate of the jet velocity, while increasing the intensity of the turbulent jet promoting rapid mixing. It was found that increasing the impingement height increased the thickness of the wall jet. However, it was also found that the "*k*-*ε*" model oversized the growth rate of the free jet, but underestimates the wall jet growth. Tchavdarov (1997) used the Chorin's random vortex method for the study of the flow of an impingement jet first on a flat surface and then on a surface with a shallow cavern of sharp edges. With the results obtained by the author its simulation showed that for the case of flat impact surface results were in agreement with experimental evidence, being observed in non-sticky region tertiary vortices resulting from primary vortices. In the case of the impact surface with a shallow cavern of sharp edges there was a strong push from the main vortex at the time with the collision with the cave together with a strong eruption of the boundary layer, forming a secondary vortex which merged with the principal. Voke and Gao (1998) through large eddy simulation study implemented the of rectangular water jets flow on a flat surface. All parameters were kept constant during the simulation of temperature and mean and turbulent velocity fields. Through this simulation the authors were able to largely reproduce the physical behaviour of a real jet. Turbulent fluctuations were observed in the flow jet region caused by instabilities. Soong, Tzeng and Hsieh (1998) used a numerical model of Navier-Stokes equations for incompressible laminar flow in order to study the effect of confinement on a flow with twin impingement jets. With this simulation the authors found

that the instabilities and the bifurcation phenomenon on the flow and had also referenced by other authors in experimental field were associated with the effects of changing the parameters, such as, Re, S/H and S/D. Yang and Shyu (1998) studied the flow of a multiple impingement jets located on a confined inclined surface. Their goal was to study the Nusselt number implementing the simulation through the "*k*-*ε*" standard model and "*k*-*ε*" low Reynolds model. The simulation results showed that the inclination of the jets significantly influenced the distribution of the Nusselt number at an impact area, and the increase of the jets slope decreased the maximum local Nusselt. Yang and Hao (1999) through the implementation of "*k*-*ε*" model studied the flow of a three turbulent jets with and without moving surface. The objective of this study was to measure the coefficient of friction on the surface and the Nusselt number. After the flow simulation the authors found that the interference effects were largely due by the increasing proximity of the jets and increased the impingement height. For the wall jets was observed that they were becoming increasingly important within the flow when the spacing between jets and the impingement height had the minimum value assumed by the authors and the jet velocity assumed its maximum value. Behrouzi and McGuirk (1999) as a means of validation of experimental results obtained by Laser Doppler Velocimetry simulated with the turbulence model "*k*-*ε*" and Quick scheme two of the three case studies in Behrouzi and McGuirk (2000). The simulation results showed that the velocity fields were consistent with those obtained experimentally. However, with regard to the prediction of turbulent fluctuations in the inlet region and in the region of ground vortex penetration, the results obtained were dominated by turbulence production errors, thus being unsatisfactory. Yan, Street and Ferziger (1999) performed a simulation study of a normal jet flow in a crossflow with LES. The results of this simulation were compared with the experimental results obtained by the aforementioned authors and their comparison revealed discrepancies in the results due to differences in the Re used and the internal flow conditions of the simulation. However, the computer simulation revealed several new structures in the flow at a location nearby the jet. Chuang and Nieh (2000) studied the flow of a rectangular configuration turbulent jets incident on a flat plate for low impingement heights through its simulation by Jones Launder "*k*-*ε*" turbulence model. The results of the axial velocities showed good agreement with the experimental results obtain by Barata *et al.* (1991b). The results revealed that the depth of the transverse axis has a strong influence on the recirculation zone, the distribution of pressure of the lower and upper plates, and on the lift of the flow, i.e., on the fountain upwash height. They also observed that recirculation zones were close to the main jet nozzles and gradually spread over the ground surface when further up the upper plate. Behrouzi (2000) through changes on the version of the finite volume with the pressure correction based in the code used by Barata et al. (1991b) conducted a study of twin jets incidents on a flat plate. This study was performed for different impingement heights and the centre spacing of the jets in order to obtain results for trajectories, velocity profiles, decay of the maximum velocity and flow rate growth. The

author concluded that the numerical results of velocity fields were in agreement with the results obtained experimentally by Saripalli (1987) through LDV. As for the fountain region, the agreement with the experimental results was not achieved, largely due to errors produced by the numerical model in predicting the vortical region. Chiriac and Ortega (2002) studied the flow of a jet incident in an isothermal surface. The numerical study was carried out by approximation by finite differences. By visualizing the flow numerically was possible to prove the complexity of the flow, oscillating between the stable and unstable, and all the proposed parameters for study reached its peak in the stagnation point of the neighbourhood. They also observed the heat transfer improved by decreasing the dependence of the Nusselt number with the Reynolds number on the unstable regime. In the case of stable flow, it was found that the stagnation Nusselt number was directly proportional to the Reynolds number, although depending on the magnitude of the velocity. Aldabbagh and Sezai (2002) used three-dimensional Navier Stokes and energy equations for incompressible flows in the simulation of a flow of multiple square configuration jets impinging on a heated surface. During the simulation, the Reynolds number, the impingement height and the spacing between jets were changed. The results showed that the flow field was quite complex, characterized by the vortex formation around the jets and upwash flow. The change in impingement height influenced the size and location of the vortex and the distribution of the Nusselt number. As for changing the spacing between the centres of the jets, it did not have effect on the magnitude of the maximum Nusselt number as expected. Souris, Liakos, Founti, Palyvos and Markatos (2002) using LRM, RSM and ASM demonstrated numerically the flow collision of an axisymmetric air jet on a flat plate with an impinging height equal to 10. Looking at the numerical results obtained by the three, the ASM results were closer to the experimental data, including the rate of the velocity decay, predicting both methods an excessive thickness the free jet region. Aldabbagh and Sezai (2002) studied the flow and the heat characteristics of impinging laminar square twin jets through the 3D Navier Stokes equations in a steady case. The results of its work demonstrated that the flow field and the heat transfer characteristics were strongly affected by the impinging height changing. Tsubokura, Kobayashi and Taniguchi and Jones (2003) using DNS and LES simulated a circular impinging jet and a planar impinging on a flat. The objective of the study was the instant preview of the eddy-type structure and the study of instantaneous scaling distribution and vorticity. The results showed that close to the stagnation point of the eddy structures for the planar jet was well organized while for the circular jet the situation was reversed. In the case of the planar jet, the higher Reynolds number enhanced the development of the jet, and the vortexes were therefore much distorted, since they were disturbed by the surrounding turbulence. Panday, Sankaran and Murman (2003) simulated the flow of an impingement jet on a plate with the presence of low velocity crossflow using OVERFLOW code with an unsteady low- Mach number preconditioner. The OVERFLOW code is a compressible Navier-Stokes code that uses the Chimera overset grid approach for simulating complex-body configurations. The OVERFLOW code used by the authors was the OVERFLOW 2.2 that could operate in two-dimensional or

axisymmetric mode, used structured overset grid system. The results obtained by the authors were possible to prove that the OVERFLOW 2.2 code has shown itself capable of simulating highly complex flows despite the unstable behaviour in question. How to numerical results were compared with experimental results of another author, showing good agreement between both. It was further observed that increasing the crossflow velocity caused the vortex height decrease. The contrary moved the ground vortex separation point for further of the impingement jets. Wegner, Huai and Sadiki (2004) based on the work done by Andreopoulos (1983) and Andreopoulos and Rodi (1984) performed the numerical study of the effect of the jet slope relative to the direction of the cross flow in a flow and mixing phenomenon flow using LES. With the results obtained by varying the jet discharge angle from the point of view of engineering, the flow injection through a jet with an opposite direction to the direction of the crossflow was beneficial. Souris, Liakos and Founti (2004) studied the performance of two equation turbulence models to numerical modelling the jet impingement cooling onto a semi-circular concave surface. In all cases both models predicted the trend of the experimental data quite accurately, but under predicted measurements because of the calculations of smaller mean and fluctuating velocity values in both the free jet and wall jet regions. Yang and Wang (2005) studied numerically the flow of an inclined jets impinging on a heated surface through the crossflow, validating the theoretical method used by them from experimental data available in the literature. Gaby and Kaminski (2005) conducted a flow study of an arrangement of jets impinging on a sloping surface with the crossflow presence. The models used by the authors for this simulation were the standard "k-ε" and the Yang-Shih models. The results obtained by the authors showed that "k-ε" model was able to model the turbulence for high values of Reynolds numbers, but is not advised for near-wall region due to viscous effects. In the case of Yang Shih model was suitable for low Reynolds numbers, although this method during the simulation had overestimated the Nusselt number peak.

Fan, Zhang and Wang (2006) conducted the study of the large scale vortical structures produced by an impinging density jet in a shallow crossflow using RNG turbulence model. The results of the characteristics scales of the upstream vortex showed distinguished three-dimensionality and the corresponding longitudinal and lateral scales increased with the water depths and velocity ratios increase, while the vertical scales increased with the velocity ratios increase and slightly vary with the water depths. The scarf vortex for small velocity ratios showed an important role to the distinct lateral high concentration at the lateral edge between the bottom layer wall jet and the ambient crossflow, which was dominated by the scarf vortex in the near field. Worth and Yang (2006) studied the flow of a single jet in crossflow in order to validate and evaluate the performance of the RSM turbulence model, and the results were compared with experimental results from Barata *et al* (1992b), with other numerical results of the "k-ε" model and the LES. The results showed that the RSM model while bringing some improvements, it was even an inadequate method for predicting the flow field of this type of flow. Fan, Zhang and Wang (2007) through LES studied the three

dimensional vortical structure for an impinging transverse jet in the near region to reproduce the skewed jet shear layer close to the jet nozzle and the scarf vortex in the near wall zone. The results showed good agreement with the experimental observations with different vortical modes in the skewed jet shear layer close to the jet nozzle depending upon the velocity ratio used. In the scarf vortex case it wrapped around the impinging jet in the near wall zone showed distinct asymmetry with regard to its bilateral spiral legs within the near region. Aldabbagh and Mohamad (2007) simulated the flow of 5 rectangular jets aligned with the crossflow using three-dimensional Navier-Stokes and the energy equation for uncompressible flows. The study was conducted for different velocity ratios as well as for different values of spacing between the centre of the impact jets and impingement heights. The results indicated that increasing the impingement height reducing the number of jets incident on the plate, thus reducing the number of peaks in the variation of the Nusselt number. It was also found that increasing the impingement height decreased substantially the magnitude of the local Nusselt number. However, it was found that the decrease of the velocity ratio caused an increase in the Nusselt number on the downstream direction of the flow. Bevilacqua, Margason and Gaharan (2007) aimed to formalize a theory for the lift loss of the incident jet through computer simulation using the "*k-ε*" turbulence model. In order to validate their theory the results were compared with experimental data of various authors. From the results obtained the authors were able to conclude that the solutions for the jet through the experimental data were validated by the turbulence model used in respect of the potential length of the jet cone and jet entrainment flow field. However, the sensitivity mesh study and the turbulence revealed that the mesh size influenced the results obtained when the turbulence intensity was 10% lower of the mean velocity. Li, Page and McGuirk (2007) through LES studied two sets of multiple impingement jets taking to compare the experimental study of Barata *et al.* (1991b) and Behrouzi and McGuirk (2000). This comparative study allowed the authors to assess the sensitivity of LES when applied to a multiple jet flow with the actual geometry of the aircraft. The results were in agreement with the experimental results obtained previously, being LES a tool capable of simulating such flows. The study was also carried out between the inlet jets, and the results revealed that the increase in inlet temperature was about 50% of the jet temperature due to hot gas ingestion phenomenon such as in VSTOL aircraft when they operated close to the ground. Fernández, Elicer-Cortés, Valencia, Pavageau and Gupta (2007) through three different numerical models studied the flow of two jets impact on a flat surface with partial recirculation and no recirculation. Analysing the results, it's were not good enough on the authors perspective, because of the simplicity of turbulence models employed, the inaccuracy of numerical predictions was acceptable in view of the low computational costs required during the simulation. Page and McGuirk (2009) conducted the study of the flow in the Harrier AV-8B / GR-7 aircraft at the time of landing (figure 43), using LES (figure 44).

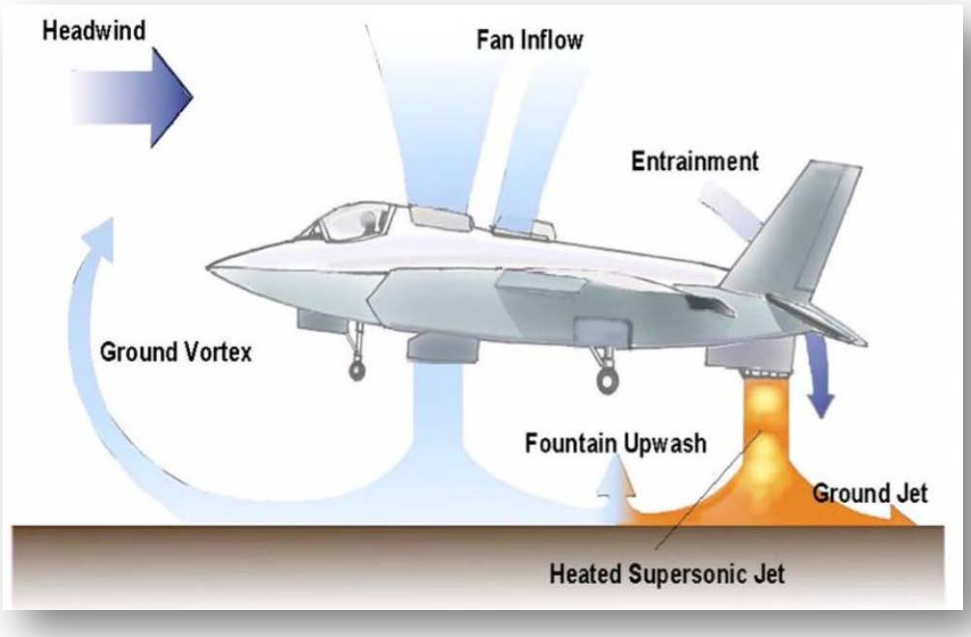

Figure 43: STOVL aircraft ground effect aerodynamics[56].

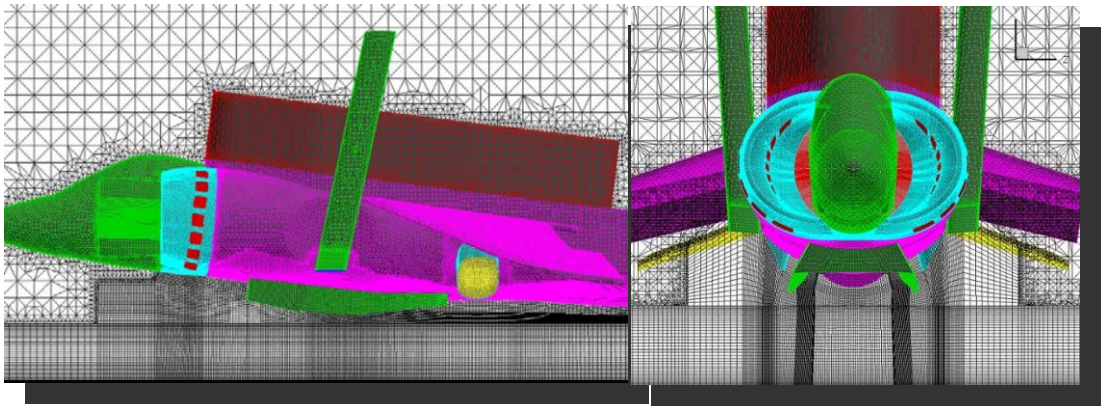

Figure 44: Mesh for scale model Harrier used in the study performed by Page and McGuirk (2009)[57].

The results obtained by the authors point out the success of the numerical implementation of the LES for this type of flow at the time of landing, revealing an extremely useful tool in shaping the intake phenomenon of hot gases in this type of aircraft. Relevant events were detected in instantaneous flow field, including unstable turbulent structures that affect the behaviour of the ascending fountain, being responsible for the admission of hot gases.

Miao, Wu and Chen (2009) from the "*k-ε*" turbulent method numerically demonstrated the flow of multiple cooling jets confined by crossflow with different orientations, and the hybrid

[56] Page G.J., McGuirk J.J (2009). Large Eddy Simulation of a complete Harrier aircraft in ground effect. *The Aeronautical Journal*. **113(1140)**: 99-106.

[57] Page G.J., McGuirk J.J (2009). Large Eddy Simulation of a complete Harrier aircraft in ground effect. *The Aeronautical Journal*. **113(1140)**: 99-106.

orientation which created the lower pressure drop than in cases of parallel and opposed orientation. Xiao et al (2011) by using the numerical simulation of "*k*-*ε*" turbulence model studied the flow of multiple jets on tandem configuration with the presence of crossflow. This study was performed for different velocity ratios thus allowing the study of various parameters. Analysing the results, the authors found that the trajectories of the rear jets were less deflected compared with the first jet. Looking then at the flow field was possible to conclude that the single jet and the jet of the first group showed a similar development, and the adjacent jets could be divided into two parts. Recently Ostheimer and Yang (2012) using RANS with a RSM approach conducted the study of twin jets positioned side by side with the presence of a crossflow. The results obtained by the authors were clear with regard to the efficiency of the computational model used, mainly to the velocity profiles results, which were very close to the experimental results. However comparing the "*k*-*ε*" model, the RSM showed no superiority in the simulation. Regarding the simulation time, the authors concluded that the RANS proved to be faster than the LES, and as to the estimated quantities turbulent, the model used proved ineffective when compared with this. To conclude the analysis of numerical work Yang (2014) compared his numerical study of twin jets in a crossflow with the experimental work of Barata *et al.* (1991b) through URANS approach with a RSM. The results obtained by the authors demonstrated clearly that the URANS approach was superior to the SRANS approach but still the predictions of Reynolds stress were not accurate enough.

Authors	Experience	Model	Results	Comments
Patankar, Basu, Alpay (1977)	Comparison of the numerical simulation with experimental data of several authors: Flow of an air jet through unconfined crossflow $2 < V_j/U_0 < 10$	Finite differences method Hybrid scheme "*k-ε*" turbulent model	Velocity profiles Trajectories	Numerical Method obtained with a normal grid with 2250 points. The centreline of the jet curves faster for smaller V_j/U_0 values. The agreement between the numerical results and the experimental results is reasonable, because in some regions appear discrepancies that can be attributed to low density of the grid used in the finite difference method.
Adler, Baron (1979)	Kamotani and Greber experiences (1972) flow study of fair through unconfined crossflow.	Integral method	Trajectories	One of the problems observed is the applicability of the present assumptions with respect to the entrainment rate and the cross-sectional shape may not be acceptable. To this solution is necessary to employ a function that characterizes the air entrainment rate at rest by jet.
Rodi, Srivatsa (1980)	Flow of an air jet through crossflow. V_j/U_0 =0,1 e 3	Finite differences method	Total pressure	The results obtained are similar to that obtained experimentally to $V_j/U_0 = 0.1$. For $V_j/U_0 = 3$ there are discrepancies between the results and the experimental data due to the use of viscosity model / turbulent diffusivity.

Table 3: Summary of numerical work on the flow of a single or multiple jets through a crossflow

Sykes, Lewellen, Parker (1986)	Comparison through numerical simulation with experimental data of several authors V_j/U_0 = 2,4 e 8	Navier Stokes Equations (incompressible)	Trajectories U, V, W, U'2, V'2, W'2, U'V', V'W', U'W' on the symmetry plane	The agreement between the numerical results and the experimental data is reasonable on the most features. For large values of V_j/U_0 the initial vorticity rings are distorted in an apparent pair of vortices in the horizontal line. For values of $V_j/U_0 \leq 4$ the vertical vorticity component in the fountain is important. The flow may be represented by a series of vortex rings emitted by the jet fountain
Rizk, Menon (1988)	Numerical study of the two in line impingement jets S/D= 3 Re=1000 H/D=1.5 e 3.0	LES	Vorticity contours Velocity profiles Trajectories Velocity vectors	The results obtained by the authors showed that the mesh used during for the simulation was insufficient to resolve small details of this type of flow. However, the study showed qualitatively and quantitatively that the numerical results agree with experimental observations
Barata, Durão, McGuirk (1989b)	Flow study of a circular water jet through confined low velocity crossflow. V_j/U_0 <10 H/D = 5 Re = 60000	Finite Differences method *k–ε* turbulent model Hybrid scheme Quick	Mean velocity Trajectories Shear stress	Numerical calculations made with a mesh of 69360 points and 8670 points The numerical results are similar to those obtained experimentally, although in some regions there is a disparity that are due to insufficient mesh points used.

Table 3: (Continuation)

	V_j = 3 m/s U_0 = 0.1 m/s				The distribution of shear stresses in the impact zone was not predicted correctly by the "*k-ε* " turbulence model.
Barata, Durão (1989c)	Study of a single and multiple impingement jets configuration on a flat plate through the influence of a low velocity crossflow. D= 20 mm H/D= 5 Re_j= 60,000 V_j= 3 m/s U_0= 0.1 m/s V_j/U_0= 30	Standard "*k-ε*" turbulence model	Mean and turbulent velocity		The numerical results were compared with the experimental results presented by Barata *et al.* (1987). The results obtained showed a good agreement with the experiments, although the maximum values of the vertical velocity in the fountain upwash region were under predicted. The results showed the advantages of QUICK differencing scheme over the hybrid scheme.
Ince, Leschziner (1990)	This study consists of two types of flow simulation, and comparison with experimental studies by other authors - Study of a free jet with the presence of strong crossflow - Study of an impingement jet with the presence of crossflow	Reynolds stress transport closure model "*k-ε*" eddy- viscosity model	Velocity vectors Pressure coefficient Velocity fields Velocity profiles		This study aimed to a computational study of two study cases that had been experimentally studied by other authors. Through the results the authors were able to prove that the second moment closure model was superior in terms of approximation with the experimental results when compared to the eddy viscosity model.

Table 3: (Continuation)

Savory, Toy, McGuirk, Sakellariou (1990)	Flow study of a circular jet through crossflow V_j/U_0 =4, 6 e 8 U_0 = 12 m/s D = 28,5 mm Re = 23×10^4	K-ε turbulent model	U, V, W	The predictions showed significant discrepancies in strength, size and location of counter rotating vortex, probably due to errors on the turbulence model.
Zhang, Ing (1994)	Numerical study of the lift loss effect due to the impact of a vertical jet on a wall M_j (jet exit Mach number)= 0.71 V_j= 240 m/s 0.15<η (no dimensional ground height)<0.8 D (jet diameter)= 50 mm D (baffle plate diameter)= 500 mm ρ_j (jet density)= 1.262 P_r (pressure ratio)= 1.4	"*k-ε*" turbulence model	Velocity fields Turbulent kinetic energy fields Pressure distribution Wall friction coefficient Lift losses predictions	After this study, the authors verified the existence of a vortex under the plate for η <0:25, thus inducing a significant pressure drop on the lower surface of the baffle plate near the edge, and creates a favourable pressure gradient to delay. For η> 0:25, the flow field induced between the ground and the baffle plate is dominated by the jet-induced entrainment and separation on the edge of the plate, which results in a edge of the plate, which results in a recirculating region forming near the edge on the jet side of the plate, the extent of which increases with the ground height. The study was conducted for three types of plate edges. Therefore, the authors concluded that the chamfered edge induces the strongest separation at the edge of the plate, and subsequently the highest pressure loss on the lower surface. In contrast the rounded edge

Table 3: (Continuation)

				induced the weakest separation. Through the computational model used the authors concluded that the differential Reynolds stress model offered better results than the model used by them.
Leschziner, Ince (1995)	Comparison of the numerical simulation with the Saripalli(1987), Abbot e White(1989), Barata *et al.*(1992a) experimental results 2.7 < H/D < 4.5 Saripalli experimental work (1987)– Flow of two compressible impingement jets on a flat surface without crossflow presence 2.7 < H/D < 4.5 V_j/U_0 =30	Application of a finite volume code Quick "*k-ε*" turbulent model	Trajectories U, V, W, $U'_2, V'_2, W'_2, U'V'$, V'W', U'W' on symmetry plane	For numerical calculations were used mesh points with 88660, 380000 and 1431106 points respectively for each of the reported experiments. Appeared some instability, hampering comparisons with experimental data.
Knowles (1996)	Study of the modelling of impingement jets using Rodi and Malin corrections: Study of a free jet and an impingement jet. 1.05<pr_n (nozzle pressure ratio)<3 1%<Tu_i (nozzle exit turbulence intensities)<15%	PHOENICS – finite volume commercial code "*k-ε*" turbulence model	Velocity profiles Axial velocity decay Wall jet growth	The results revealed that the increase of the nozzle pressure ratio tends to reduce the velocity decay rate in line with the jet. The turbulent intensity increase in the jet output promoted the rapid mixing and hence the decay of the free jet. Increasing the nozzle height was found to increase the thickness of the wall jet at a one determinate radius. The decay rate, however, did not seem to be affected,

Table 3: (Continuation)

				being the main influence the increase in initial wall thickness jet. It was found that the "*k-ε*" model under scales the growth rate of the free jet and sub scales the growth rate of the radial wall jet. Finally it was concluded that the wall jet prediction was seen to be strongly dependent of the free jet calculation.
			Mean axial velocity profiles Turbulent velocity profiles Visualization of the impingement jet region	The conducted study revealed that the results of the flat surface are in agreement with experimental evidences. Were observed in no-viscous region tertiary vortices resulting from the primary vortices. Regarding the study of the collision of a jet a surface with a shallow cavern of sharp edges was observed, a strong main vortex impetus, while it collided with the front line of the cave, while at the same time, a strong eruption of the boundary layer immediately downstream of the front line, formed a secondary vortex which merged with the main vortex.
		Chorin's random vortex method		
	Flow of an impingement jet on a flat surface as well as on a surface with a shallow cavern of sharp edges H/D=6 Re=23000			
	Tchavdarov (1997)			

Table 3: (Continuation)

Voke, Gao (1997)	Flow of a rectangular water jet on a flat plate H (half width of channel)=36 mm Pr (Prandtl number)=6.95 Thermal diffusion=0.19 mm^2/s R_{emean} (mean flow Reynolds number)=6500 Pe_{mean} (mean flow Peclet number)=45175	LES – Large eddy simulation	Temperatures Mean and turbulent velocity fields	Through this study it was found that this numerical simulation widely reproduces the physical behaviour of a real jet. Analysing the fluctuation velocities was found that in the jet flow region, there were instabilities which produced turbulent fluctuations. As early as around the edges of recirculation regions were not clearly demonstrated evidence of the production of turbulent fluctuations.
Soong, Tzeng, Hsieh (1998)	Numerical study of the confinement effect on the flow of twin impingement jets. 5<S/D<10 0.1<S/H<0.9 83.33<L/D<1500 5<Re<200	Navier – Stokes Equation for uncompressible and laminar flow	Trajectories Spectral diagrams Flow maps	Through computer simulation of this flow, the authors concluded that the instabilities and the bifurcation phenomenon observed in the flow were associated with the effects of changing some parameters, such as, Re, S / H and S / D. According to the confinement effects of the sidewall, the flow can be classified as strong or weak in terms of confinement. In general, the interaction between the jets.dominated the flow mechanism and the jets have a greater degree of freedom, in particular in the transverse direction. A flow with low confinement tends to be asymmetric but was in steady state. While in the presence of strong confinement, the wall jet interaction dominated the flow, whereby the oscillation motion is in the transverse direction and, ultimately, the

Table 3: (Continuation)

					instability o the flow could be effectively suppressed. With this stabilizing effect, the non-periodic oscillation and chaotic behaviour may be delayed.
Yang, Shyu (1998)	Flow study of multiple impinging jets localized on a confined inclined surface $0° \leq \theta$ (inclination angle of confinement surface)$\leq 15°$ $11000 \leq Re \leq 21000$	"*k-ε*" standard model Re "*k-ε*" low Re model	Nusselt number		The results of the study showed that the surface inclination angle has a significant effect on the local Nusselt distribution on the impact plate. It was also found that the increase of the inclination of the plate lowers the maximum local Nu, whereas the value of the local Nu increases on the downstream direction.
Yang, Hao (1999)	Flow of three turbulent jets with and without movement surface R_e= 11000, 22000, 44000 P/W (dimensionless pitch)= 5, 3, 2 H/W (dimensionless nozzle to surface space)= 6,8 U_s/V_j (dimensionless velocity ratio)=0.05, 0.025	"*k-ε*" turbulence model	Friction coefficient on the surface Nusselt number		After the numerical study, the authors concluded that the interference effects were intensified when the jets were closest; the separation of the jets exit was small and when the impact surface of the jets was relatively large. Through the study was also possible verified that the wall jets are becoming increasingly important when the spacing between jets and the distance of impact were small and the jet velocity was increased.

Table 3: (Continuation)

Behrouzi, McGuirk (1999)	Study of the flowfield associated with a generic twin jet plus intake model operating under ingestion flow conditions. (based on the experiments did by Behrouzi and McGuirk (1999) R= 24, ∞ Re= 40000 D= 12.5 mm H/D= 7	*"k-ε"* turbulence model First and second order of QUICK	Velocity fields Men and turbulent velocity profiles	The results showed that the velocity fields in the flow region were mostly consistent with the experimental results. As for the previsions for the turbulent fluctuations, especially in the inlet region and the ground vortex penetration region were unsatisfactory, due to the errors production in the form of velocity profiles and turbulence levels by the admission.
Yuan, Street, Ferziger (1999)	Flow study of a normal jet on a crossflow R= 2.0 e 3.3 Re= 1050 e 2100	LES	Mean velocities Reynolds stresses Turbulent kinetic energy	The computational results were compared with the experimental results presented by the authors cited. However found discrepancies between the simulation results and experimental results, being these attributed to differences of jet Reynolds number and internal conditions of the flow. Several new structures were observed in the flow near the jet, as spanwise rollers, hanging vortices, counter rotating vortices and upright vortices.
Chuang, Nieh (2000)	Flow study of rectangular turbulent impingement jets on a flat plate without crossflow interference S/D=5	*"k-ε"* Jones-Launder turbulent model		The results showed that the depth of the y-axis has a strong influence on the recirculation zone, the pressure distributions of the upper and lower plates and the flow elevation.

Table 3: (Continuation)

	H/D=3 Re=105000 V_j=16.212 m/s			The recirculation zones were close to the main jet nozzles, which gradually spread over the impact surface when this is above the upper plate.
Behrouzi (2000)	Flow study of twin impingement jets on a flat plate H/D_j= 3 e 5.5 S/D_j= 9 e 14	Two equations of the do "*k-ε*" turbulent model	Trajectories Velocity profiles Maximum velocity decay Flow growth	The study conducted revealed that the predictions for the obtained velocity fields are mostly in accordance with the LDV results obtained experimentally. Regarding the outlook for the fountain region, these proved to be very distant from the experimental results due to the many mistakes made by the turbulence model "*k-ε*" in predicting the vortical region.
Chiriac, Ortega (2002)	Flow of an impingement jet on a isothermal plate 250<Re <750 L/W=25 H/W=5 Pr=0.72 V_j= 0.2-0.6 m/s	Approximation by numerical finite differences	Wall pressure Friction Heat transfer coefficient	The visualization of the numerical simulations showed the complexity of the stable as unstable flow field. All parameters studied reached a peak in the stagnation point of the neighbourhood were as expected. The impact of the dependence of the Nusselt number with the Re was reduced in the unstable regime because the heat transfer is improved by non-linear unstable mechanisms. In contrast to the stable cases, the

Table 3: (Continuation)

					stagnation Nusselt number is directly proportional to the Reynolds number of the jet, depending mainly on the magnitude of the velocity.
Aldabbagh, Sezai (2002)	Flow of multiple square jets on a hot flat plate. X_n/D and Y_n/D (dimensionless jet –jet spacing in x and y direction)=4, 5, 6 $0,25<L_z/D$ (dimensionless length surface in z direction)<9 Re=100, 200, 300, 400, 500 Pr (prandtl number)=0,71	Navier Stokes tridimensional equations Energy equation for uncompressible flows	Nusselt number Velocity fields Flow fields		The results showed very complex flow field with the formation of a peripheral vortex around each jet and the fountain upwash flow on the collision point of the jets. The size and location of any peripheral vortex depend on the impact of jet-plate spacing. The Nusselt number is higher away from the impact zone than for higher jet impact-plate spacing due to the wall jet velocity is high. Finally, the heat transfer is strongly affected by the spacing jet- impact plate, where, however, the magnitude of the maximum Nusselt number is not affected by the spacing between jets.
Souris, Liakos, Founti, Palyvos, Markatos (2002)	Flow collision of an axisymmetric air jet with a flat plate V_j= 90,15 m/s H/D= 10 D = 12,7 mm Re = 90×10^3	LRM RSM ASM	Velocity profiles		The results obtained by ASM were closer to the experimental data. In the free jet region both models used predict an excessive thickness for the jet. The decay rate of the velocity peak was much larger than the experimentally recorded for both turbulence models. In the case of the ASM velocity decay rate adjusted itself better to the experimentally data obtained. recorded

Table 3: (Continuation)

	Re = 90×10^3			for both turbulence models. In the case of the ASM velocity decay rate adjusted itself better to the experimentally data obtained.
Aldabbagh, Sezai (2002)	Investigation of the flow and heat transfer characteristics of an impinging laminar square twin jets 0.25<H/D<5 S/D= 4, 6, 8 Re=100, 300, 500 Pr= 0.71	3D Navier Stokes equations Energy equations in a steady state	Stream trace Velocity profiles Nusselt number	The results showed that the flow field on a heated plate was strongly affected by the H/D distance, being that for very small distances no upwash fountain flow were detected, but foe such nozzle to plate distances the wall jet filled the whole between the plates with no vortex motion around the twin jets.
Tsubokura, Kobayashi, Taniguchi, Jones (2003)	Flow study of a circular/planar jet impinging on an impact plate R_{eDNS}=2000 R_{eLES}=6000 H/D=10	DNS LES	Instantaneous scalar visualization of the eddy type structures	Through the study it has been found that the development or transition of both jets (planar, circular) was similar on the direction where the roll-up vortices appeared, near the nozzle showing instability and the development of the upstream flow and the growth of a counter rotation vortices pair. Eddy structures near the stagnation point were different for planar jet and circular jet. In the planar jet showed organized structures, such as twin vortices in opposite directions in the transverse jet direction. In contrast, no organization defined in the structures in the stagnation

Table 3: (Continuation)

				region was found for the circular jet. In the case of the planar jet, the development of the jet was increased to the highest Re case. Because of this, the individual vortices in the stagnation region was greatly distorted and disturbed by the surrounding turbulence.
Panday, Murman, Sankaran (2003)	Flow of an impingement jet on a plate with the presence of a low velocity crossflow V_j= 45.72 m/s V_∞(freestream velocity)=4.572 m/s Re= 80000	OVERFLOW	Mean velocity vectors Visualization streak lines instantaneous videos Eddy viscosity Graphic of the impingement height relation and separation point location in function of the crossflow velocity	Through this work it was concluded that the OVERFLOW was able to simulate highly complex flow fields using a step of commensurate time with unstable flow behaviour under study. The results of numerical simulation were compared with experimental results from another author, having obtained a good agreement between the results. To conclude, the author observed that increasing the crossflow velocity caused the decrease of the vortex height. Already reduced the velocity of the cross flow moved the ground vortex separation point for further away from the impact jet.
Wegner, Huai, Sadiki (2004)	Flow study of the jet inclination effect relatively to the crossflow direction on a flow and the flow mixture phenomenon. Study based on the work developed by Andreopoulos (1993) and	LES	Mean velocity profiles Turbulent kinetic energy Men mixture fraction	Through the results the authors were able to prove once again the LES's ability in predicting flows of this type. By varying the angle of the jet discharge has been found that this influences the characteristics of the secondary flow which in turn affected

Table 3: (Continuation)

)	Andreopoulos e Rodi (1994) R=0.5 D=50 mm U_{jet} (jet exit velocity)= 6.95 m/s U_{cf} (crossflow velocity)= 13.9 m/s Rj_{et}= 20500 A (angle between the jet and the oncoming angle)= 60°, 90° e 120°		Fluctuations	the flow mixture process. With this work the authors showed that from an engineering point of view there were benefits in the flow injection through a jet with opposite direction to the direction of the crossflow
	Souris, Liakos, Founti (2004)	Jet impingement onto a semi-circular concave surface. D= 150 mm Re= 1780, 2960, 4740 H/B= 4.6, 10	"*k-ε*" model vs Reynolds stress model	Axial mean velocity Velocity fluctuations Mean velocity Nusselt number	The results showed for both models, discrepancies between experiments and predictions increase, as the H/B was decreased from 10 to 4 nozzle slot jet widths. The variation of the Reynolds number had no significant influence on the predictions. Accurate prediction of the wall boundary layer characteristics improved calculations with both models, away from the stagnation point and in the circumferential direction. The maximum heat transfer occurred at the highest Reynolds number, attributed to turbulent augmentation.

Table 3: (Continuation)

Yang, Wang (2005)	Flow of inclined jets impinging on a surface through crossflow D = 6 mm H/D = 5 Re = 5000 V_j/U_0 =3, 5 e 7 T_{in} (inlet temperature of crossflow and the inclined jet respectively) = 30 e 40 °C 340 ≤ q_w (heat flux)≤ 1000 w/m^2	Finite differences method K-ε turbulence model Simple	Nusselt number distribution Turbulent kinetic energy Trajectories	The theoretical model is validated by comparing its predictions with experimental data available in the literature. A mesh base with 106,080 points was used. A pair of counter rotating vortices is clearly identified with an anti-clockwise regardless of the Vj/U0 value The maximum value of the Nusselt number is found around Z / D = 4.
El - Gabry, Kaminski (2005)	Flow of an inclined impingement jet array on a flat plate through crossflow. Θ (jet angle)=30°, 60° e 90° 10000<Re <35000 Pressure ratio=1.17	standard "*k-ε*" model Yang-Shih model	Nusselt number Turbulent kinetic energy Mean Nusselt number	The result showed that the standard "*k-ε*" model is a model for turbulent high Reynolds values, and was best able to model turbulent core flow regions and did not apply very near the wall, where viscous effects were dominant. The models of low Reynolds number can be integrated with the wall, thereby eliminating the need for a special treatment. The Yang-Shih model, though it over predicted peak Nusselt numbers (more so than the standard k-e model), was more effective in predicting heat transfer between jets.
Fan, Wang, Zhang (2006)	Flow study of an impinging density jet in a shallow crossflow. D= 0.005 m R (velocity ratio) = U_j/U_0= 7.79, 15.9	RNG turbulence model	Velocity vector diagram Pressure distributions	The characteristics scales of the upstream vortex showed distinguished three-dimensionality and the corresponding longitudinal and lateral scales increased with the increasing water depths and velocity ratios, while the vertical scales increased with the increasing water depths and velocity

Table 3: (Continuation)

	ρ_j (jet exit density)=1170 kg/m3 Fr_d (jet Froude number)= 10.21			ratios, while the vertical scales increased with the increasing velocity ratios and slightly vary with the water depths. The scarf vortex structure in the near fields plays an important role in the lateral concentration distributions.
Worth, Yang, (2006)	Flow of multiple confined refrigerated jets through crossflow with different orientations Re=60000 D= 0.02 m D = 5 mm U_0= 0.1 m/s V_j= 3 m/s	RANS approximated with RSM	Mean velocity profiles Normal stresses Mean shear stress	RSM model showed improvements in relation to the K-ε model, with respect to the prediction of the vortex ground length and provide the ability to predict the anisotropy of the flow field. This method proved it's ineffective in relation to the form and location of the vortex. Through this study it was concluded that the RSM model despite showing improvements in some aspects, it was still an inadequate method for the study of this type of flow for only provide a rough approximation and inadequate for this flow field.
Fan, Zhang, Wang (2007)	Flow study of a circular water jet through low velocity confined crossflow D=5mm H/D=10 V_J/U0=8,12 e 20	LES – Large-Eddy Simulation Uncompressible Navier Stokes equations	Mean velocity profiles RMS velocity profiles Flowfield with Streamlines	The computational results reproduced a shear layer distortion which originated vortices near the jet nozzle and a scarf type vortex near the same region mentioned above, being the results consistent with the experimental results. Different vorticity modes have been identified in the region mentioned above

Table 3: (Continuation)

	Aldabbagh, Mohamad (2007)	Flow study of five rectangular jets aligned with the crossflow Xn/B (jet to jet spacing)=4 2<z/B (jet to plate spacing)<20 R (velocity ratio)= 0.5, 1.0, 2.5, 5 7.5, 10 Re=200 Pr (Prandtl number)=0.71	Tridimensional Navier Stokes Equations Energy equation for uncompressible flows	Nusselt number Flow visualization on z-x plane	For a velocity ratio higher than 5 and the same spacing between the jets and the plate were observed 2 horseshoe vortex types. For R = 2.5, the increase in the spacing between the nozzles and the plate caused a decrease in the number of jets impinging on the plate and the decrease in the number of peaks in the variation of the local Nusselt number. The magnitude of the local Nusselt number decreased with increased of the spacing between the jet and the plate, although it was not affected by the number of combined jets. However, for the same spacing between the nozzles and the plate and velocity ratio value, the increased number of incidents jets increased the plate heat.
					being its shape depends of the velocity ratio used, varying the shape of the vortex to axisymmetric for helical according to the velocity ratio used. Near the impact zone, the spiral vortex edges exhibit symmetries. It was found that the drag concerning to the crossflow was influenced by the vortex near the wall.

Table 3: (Continuation)

					Finally, for even spacing between jets, the local maximum Nusselt number increased in the downstream direction with the decrease of the velocity ratio.
Bevilacqua, Margason, Gaharan (2007)	Theory formalization for the lift jet loss in VSTOL aircrafts, through the computational simulation and comparison with the experimental results	"*k-ε*" turbulence model	Static pressure distribution Jet axial velocity Jet vertical velocity Lift loss		Through the study it was concluded that solutions to the jet given by the experimental data is valid for the potential length of the jet cone and jet entrainment flow field through the use of "*k-ε* "t urbulence model. Study sensitivity and turbulence mesh showed that the mesh size affects the result when the turbulence intensity was 10% lower than the mean velocity.
Li, Page, McGuirk (2007)	Study of two configurations of multiple impinging jets considering the experimental study of Barata *et al.* (1991b) and Behrouzi and McGuirk (2000)	LES	Velocity magnitude contours Mean velocities Normal stresses Upwash flow energy spectrum Computational visualization		Through this work the authors sought to assess the LES sensitivity when applied to a flow with multiple jets incidents with the actual aircraft geometry. Computational results showed agreement with the experimental results, and the authors concluded that applying the LES was quite feasible to this flow type. In the study case with admission between the jets, the authors estimated that the increase in inlet temperature was about 50% of the jet temperature due to hot gas ingestion phenomenon such as in VSTOL

Table 3: (Continuation)

				aircraft when they operate near the ground of the jet temperature due to hot gas ingestion phenomenon such as in VSTOL aircraft when they operate near the ground
			Mean velocities Turbulent kinetic energy fields	Through the work the authors concluded that the models used underestimated the jet expansion rate and overestimated the mean velocity in the impact region. The main differences between the numerical results and the experimental results used for comparison and evaluation were found in the impact region. The observed discrepancies can be attributed to underlying formulations and eddy viscosity modelling, Reynolds stresses, and the use of wall functions. The "*k-ε*" reliable model showed the closest results to the experimental data, and the "*k-ω*" standard model had the worst performance for all investigated settings. Although the comparison between the results and the data is not good enough, because of the simplicity of turbulence models employed, the inaccuracy of numerical predictions was acceptable in view of the relevant low computational costs and its target applications.
		"*k-ε*" standard model "*k-ε*" realizable model "*k-ω*" standard model		
	Numerical flow study of two impingement jets on a flat surface with partial recirculation and non-recirculation H/e (jet operation ratio)= 10 Re= 6000 e 14000			
	Fernández, Elicer-Cortés, Valencia, Pavageau, Gupta (2007)			

Table 3: (Continuation)

Page, McGuirk (2009)	Flow study of the Harrier AV-8B/GR-7 aircraft on the landing moment $T_{rear\ jet}$ (rear jet temperature)=700 K $NPR_{rear\ jet}$ (nozzle pressure ratio)=2.0 $T_{front\ jet}$ (jet temperature)=350 K $NPR_{front\ jet}$ (nozzle pressure ratio)=2.5 U_{∞} (freestream velocity)= 6 m/s $Re_{front\ jet}$ =80000000 $Re_{rear\ jet}$ =7000000	LES	Vertical velocity profiles Instantaneous contours of Mach number Stagnation temperature instantaneous contours instantaneous pressure field	The results obtained by the authors can conclude that the LES successfully represented the flow of a VSTOL aircraft at the landing time. Important phenomena were also observed in the instantaneous flow, particularly unstable turbulent structures that affected the fountain flow behaviour. As for the structure used at the bottom of the aircraft, it showed some control over the upward flow, being the phenomenon responsible for the possible entry of hot gas for admission intake. Finally the authors praised the LES as a promising tool to model the ingestion of hot gases in VSTOL aircraft.
Miao, Wu, Chen (2009)	Flow study of multiple confined cooling jets through crossflow with different orientations $2440 \leq R_e \leq 1464$ H/D = 1,3 e 6 D = 5 mm	K-ε turbulent model	Nusselt number Trajectories	With the jet Reynolds number increasing the heat transfer was improved. The hybrid orientation of the crossflow created less pressure drop when compared with the parallel and opposite orientation cases. The local and mean Nusselt numbers were higher in the case of hybrid orientation. For the same Nusselt number with H / D = 3, the configuration of all jets in line provided better cooling than the case where the nozzles were staggered.

Table 3: (Continuation)

Xiao et al. (2011)	Flow study of multiple impinging jets in tandem configuration through crossflow R= 2.38, 4.67, 8.83, 17.88 D=0.01 m S/D=5	K-ε model	Jet trajectory Velocity deterioration Velocity fields Turbulent kinetic energy	The trajectories of a single jet were slightly larger than those recorded for the first jet of the group to the same R, and the differences decrease with the decreasing of R. The trajectories of rear jets were less deflected when compared with the deflection of the first jet. Flow fields for a single jet and the first jet group showed a similar development near the flow, and the region between two adjacent jets could be divided into two parts. The turbulent kinetic energy associated to a single jet and the first jet of the group showed similar distributions, as well as the three rear jets.
Ostheimer, Yang (2012)	Study of twin jet side to side positioned with the crossflow presence Re= 105,000 R (velocity ratio) = 30 S/D= 5 D= 20 mm	RANS with RSM approach	Velocity vectors Velocity profiles Fluctuations Shear stresses	From the study it could be concluded that the RANS model with RMS approach was efficient for the simulation of this type of flow, with respect to the velocity profiles, since the profiles were very similar to those obtained experimentally. However, comparing with the "*k-ε*" model, the RMS showed no superiority in the simulation. Regarding the simulation time, the authors concluded that the RANS proved faster than the LES. As for the prediction of turbulent quantities,

Table 3: (Continuation)

				the model used proved ineffective when compared with LES.
Yang (2014)	Twin jets in a crossflow - Comparison with the experimental work of Barata *et al.* (1991b). Re= 105,000 V_r (velocity ratio) = 30 S/D= 5 D=0.02 m H/D= 5	URANS approach with a RSM	Velocity vectors Mean horizontal velocity Shear stress Fluctuations	Through the obtained results the author concluded that both SRANs and the URANS performed well overall as far as the mean flow field, showing good trend of the experimental results as well as good accuracy, with slightly better predictions by the URANS approach. The SRANS approach performed very poorly in terms of Reynolds stress predictions. Because the URANS approach indicated the better results in all the flow characteristics studied, this is a strongly indication that for the flow case with large-scale unsteady flow features the URANS approach is definitely better than the SRANS approach. The URANS approach only failed to predict Reynolds stresses. Even though the URANS approach may able to capture some large-scale unsteady flow motion, it cannot capture turbulence well.

Table 3: (Continuation)

1.5.3 Numerical and Experimental Studies

In the late 80's began to appear the first studies that encompassed experimental and numerical techniques in the same work of impinging jets through a crossflow. This type of study has been important for the numerical simulation development of trajectories and turbulence structures by experimental data obtained in the same study. Table 4 contains the more relevant experimental and numerical studies that have been performed.

Barata (1989d)[58] presented a most comprehensive study of single and multiple impinging jets through a low velocity crossflow relevant to VSTOL. The experiments were obtained with Laser Doppler Velocimetry for velocity ratios between the jet and the crossflow from 30 to 73 and impinging distances of 3, 4 and 5. The numerical study included the comparison of higher order numerical schemes to evaluate the convection terms in a three-dimensional configuration for the very first time. This author also performed a detailed analysis of the momentum equations terms and turbulence energy budgets. This study had been partially published in Barata *et al.* (1986a), Barata *et al.* (1986b) Barata *et al.* (1987), Barata *et al.* (1988a), Barata *et al.* (1988b) Barata *et al.* (1988c), Barata *et al.* (1989b), and more detailed analysis of the results were published in the early 90´s in several conference and journal papers such as Barata *et al.* (1989c), Barata *et al.* (1991b), Barata *et al.* (1992a), Barata *et al.* (1992b), Barata *et al.* (1993a), Barata *et al.* (1993b) or Barata (1996a), Barata (1996b) among others.

Barata, Durão and Heitor (1986a), Barata, Durão and Firmino (1986b), Barata, Durão, Heitor and McGuirk (1987, 1988b, 1988c, 1991b and 1992b) made studies for a single or multiple confined impingement jets using a plate at the exit of the jets for jet to crossflow velocity ratios between 25 and 73, to analyse and compare experimental and numerical results. In the case of the experimental studies it was used the laser Doppler velocimeter to measure the characteristic mean and turbulent velocity field. These experimental results were obtained for different impingement heights and Reynolds number (based on the exit jet conditions). The experimental results revealed a large penetration of the impingement jets, which exhibit a pattern similar for the single and twin jets configurations. From the configurations with more than one impingement jet, the authors observed the fountain upwash flow formation by the deflection of the radial wall jets by the crossflow. The numerical calculations represented the gross features of the flow through the grid independence of the single or multiple impinging jets flows, with QUICK scheme and "k-ε" turbulence model. The results obtained numerically revealed that the method to predict the turbulent structure of the impingement zone and fountain flow failed, not being these zone represented by the turbulent viscosity

[58] Barata, J.M.M. "Estudo Numérico e Experimental de Jactos Incidentes Sobre Placas Planas Através de um Escoamento Cruzado". PhD Thesis (in Portuguese). Universidade Técnica de Lisboa, Instituto Superior Técnico, 1989.

hypothesis. In the ground vortex region the authors observed that the numerical results could be influenced by the failure of the notion of the wall at the separation point, since the flow was no longer controlled by the wall shear stress. Bray and Knowles (1992) studied a flow of a jet through crossflow gathering all the data available in a set of unified statements. In their study found that the vortex penetration increases with V_j/U_0, and the numerical modelling simulates the main characteristics of the "ground vortex". Knowles, Bray, Bailey and Curtis (1992) dedicated their work to study one or two confined jets incident on a moving surface with the presence of crossflow. With the results of this study the authors concluded that for the ground vortex phenomenon, the relation between the distance of penetration, separation and the core of the vortex was kept constant, and the penetration of the vortex decreased when the impact plate moves by reducing the power deficit and the subsequent increase in the wall jet shear stress. As regards the impingement height was found that for the case of two jets increased the vortex penetration could be associated with the two jets merger. Barata, Durão, Heitor and McGuirk (1993a) simulated the turbulence structure near and far of the impact region through the data obtained by experimental techniques of laser anemometry, using these data for the numerical simulation through Navier Stokes equations. The results obtained by the authors revealed that the turbulent structure of the flow was affected by flow distortion at the impinging zone, which results in an unconventional behaviour of the dimensionless structure parameters that determined the empirical constants in engineering models of turbulence. Barata (1993b) studied a flow of multiple circular jets through low velocity cross-flow, checking that the studied showed a flow pattern similar to that which occurs for a single jet, although the numerical method to confirm the failure in predicting the levels of turbulence in upwash flow or fountain (figure 45). This type of study was very important for VSTOL applications since the jet height was small and the velocity ratio equal to 30. Three years later, Barata (1996a) through Laser Doppler Velocimetry studied the flowfield created by two-axisymmetric impingement jets on ground plane with the presence of low velocity cross stream. The results obtained experimentally and numerically showed the formation of a fountain upwash through the collision of the radial wall jets deflected by the cross stream (figure 46). The numerical visualization allowed to understand physically the complex three dimensional nature of the ground vortex (figure 47) and the upwash flows. In the same year Barata (1996b) performed an experimental and numerical study of the main characteristics of the vortex and upwash flows generated by multiples water jets in a cross stream. The experimental and numerical results showed good agreements in terms of the mean velocity in the most important zones of the flowfield, the impact jets region and the upwash flow. In the case of the turbulent velocity, the results showed that the shear stress signal was consistent with the shear signal in the hypothetical diffusion gradients direction with the exception of the stagnation zones associated with the ground vortex formation, because it was a region with intense diffusion gradients.

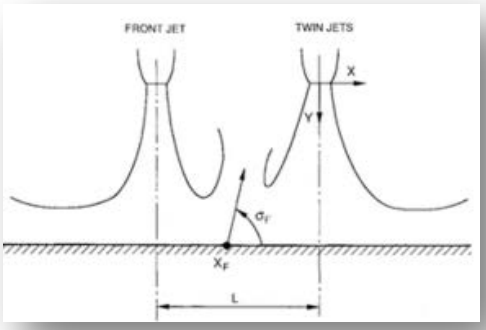

Figure 45: Schematic of fountain flow. (X_F represents the fountain origin and σ_F represents the jet inclination angle)[59].

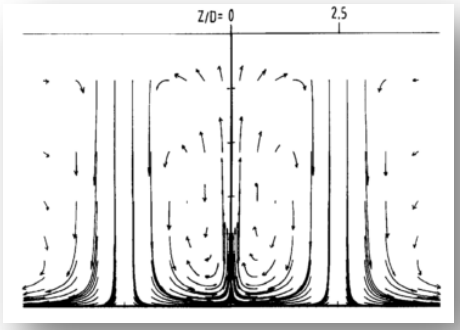

Figure 46: Fountain upwash flow formation in the middle of the impingement jets.[60]

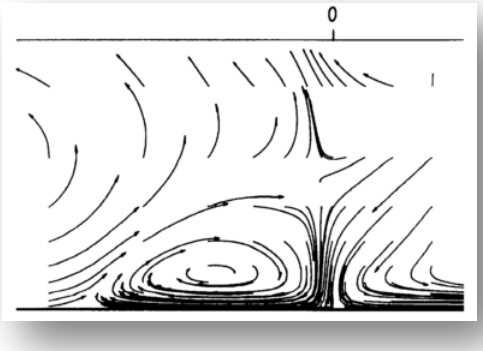

Figure 47: Ground vortex formation in the upstream side of the first impinging jet.[61]

[59] Barata J. M. M. (1993b). Fountain Flows Produced by Multijet Impingement on a Ground Plane. Journal of Aircraft. 30(1): 50-56.

[60] Barata, J.M.M. (1996a). Ground Vortex Formation with Twin Impinging Jets. *Proceedings of the International Powered Lift Conference*, Jupiter, Florida, 18-20 Nov., 1996. Paper SAE 962257.

[61] Barata, J.M.M. (1996a). Ground Vortex Formation with Twin Impinging Jets. *Proceedings of the International Powered Lift Conference*, Jupiter, Florida, 18-20 Nov., 1996. Paper SAE 962257.

Behrouzi and McGuirk (1998) dedicated to the study of twin water impingement with the presence of crossflow to an impact height and spacing jets equal. The technique chosen by these authors was Laser Doppler Velocimetry to obtain the turbulent fields and mean velocities. The author found that on the upwash flow region the turbulence level was high, and high turbulence production rates were observed. To complement their work the authors simulated the flow using the "k-ε" turbulent model, showing that it is quite appropriate to predict the mean flowfield. Knowles and Davies (1999) conducted an experimental and numerical study for the flow of a turbulent circular jet, isothermal impinging on a flat surface in motion. The experimental part of the work was completed using static pitot tubes, while the numeric part was done using the PHOENICS commercial code with the Lam-Bremhorst low Reynolds number turbulence mode. Through this work, the authors confirmed a strong asymmetry between the sides of advance and retreat of the impact zones. The computer simulation predicted the heat transfer performance, and the effects of the surface velocity on the mean heat transfer rate for circular jets had no interest for the study. In 2002, Alvi, Ladd and Bower (2002) obtained experimentally and numerically results for the moderately under expanded supersonic jet impinging on a surface. Although the case of study in this thesis to be for subsonic jets, this work developed by this authors is important because the goal of their work was to develop a better understanding of the impinging jet flowfield, which is of significant interest because of its presence in STOVL aircraft during hover as well as in other aerospace related and industrial applications. The study of these authors reveals that the models used in the computational study captured the significant features of the complex flow. Both experimental and computational results revealed the presence of the impingement zone stagnation bubble, characterized by low velocity recirculating flow. The authors concluded that the ability to measure and predict accurately the impinging behaviour is critical near the ground plate due to the regions with high mean shear, thermal loads or unsteady pressure, contributing these facts to the problem of ground erosion in STOVL applications. Later, Baydar and Ozmen (2005) studied a flow of a circular jet incident on a surface without crossflow, being the numerical simulation performed only for impingement heights below 0.1, because the high importance to understand what the effects of this type of flow for such small jet heights. It was concluded that there existed a linkage among the sub atmospheric region, turbulence intensity and heat transfer coefficients. The numerical results obtained using the standard "k–ε" turbulence model was in agreement with the experimental results except for the nozzle-to-plate spacing less than one. Abdel-Fattah (2007), using finite volume methods and experimental technique to study the flow of two confined circular air jets on a plate, for different impingement heights and different jet angles of incidence. It was concluded that the stagnation primary point moved away in the radial main flow direction by increasing the jet angle. This shift became stronger by increasing the nozzle to nozzle centreline spacing. A secondary stagnation point was detected between the two jets. The value of the pressure at this point decreased by decreasing Reynolds number and increasing the jet angle. The sub atmospheric region occurred on the impingement plate. It

increased strongly by increasing Reynolds number and decreased as the jet angle and a nozzle to plate spacing increased. The spreading of the jet decreased by increasing the nozzle to plate space. The intensity of the recirculation zone between the two jets decreased by the increasing of the impingement height and the jet angle. The increase of turbulence kinetic energy occurred within high gradient velocity. Salewski, Stankovic and Fuchs (2007) have their contribution in the field by studying coherent structures and mixing in the flow field of a jet in crossflow. The experimental part and visualization was performed with PIV and LIF, while the numerical simulation was done by LES. The numerical results showed that the distribution of a passive scalar in a cross-sectional plane could be single- or double-peaked, depending on the nozzle shape and orientation. A proper orthogonal decomposition of the transverse velocity indicated that coherent structures might be responsible for this phenomenon. The nozzles which had a single-peaked distribution had stronger modes in transverse direction, and the global mixing performance was superior. It was further demonstrated that the flow field contains large regions in which a passive scalar was transported up the mean gradient (counter-gradient transport) which implies failure of the gradient diffusion hypothesis. Koseoglu and Baskaya (2009) studied the flow of a jet through confined crossflow to different impingement heights. The results obtained by the authors showed that buoyancy induced natural convection might have opposing or assisting influence on local heat transfer at different locations of the target plate. It has also been shown that especially at low jet inlet velocities the average heat transfer coefficient at the highest modified Grashof number, where the natural convection is effective, was higher than the value corresponding to the lowest Grashof number at which buoyancy effects were negligible, by as much as 37%. Radhouane, Bournot, Said, and Mhiri Palec (2009) through Navier Stokes equations and velocimetry technique of particle images for different initial inclination angles, concluded that for higher initial slope value the jet tend to straighten favoring vertical expansion instead of the longitudinal and determining the presence of a system with four main vortex. More recently, Wae-hayee, Tekasakul, Eiamsa-ard and Nuntadusit (2014) studied the effect of crossflow velocity on flow and heat transfer characteristics on impinging jet in the case of low impingement heights. The results obtained by the authors showed that the Nusselt number peak shifts downstream and the Nusselt peak increased with the increasing crossflow velocity.

Authors	Experience	Technique/Model	Results	Comments
Barata, Durão, Heitor (1986a)	The study of an axisymmetric jet in ground effect through a confined crossflow D= 20mm H/D= 5 Re_j= 60,000 V_j= 3 m/s V_j/U_0= 25	Experimental: LDV and fluorescent dye (visualization technique) Numerical: "*k-ε* " turbulence model	Mean and fluctuating velocity	The gross features of the mean flow field are well predicted, but important local differences occur between measurements and calculations of the mean and turbulent fields, due to numerical and turbulence model errors. The experiments have shown a large penetration of the jet through the crossflow and the jet was slightly bent and gave rise to a recirculation zone upstream of the jet. The numerical results showed intense velocity fluctuations in the shear layer surrounding the jet, and the shear stress and the shear strain signs were consistent with the mean flow direction. The numerical results were extended to cover a large set of flow conditions.
Barata, Durão, Firmino (1986b)	Study of a perpendicular jet impinging on a plate. D= 14 mm H/D= 12 Re_j= 42,500	Experimental: LDV, Smoke visualization Numerical: "*k-ε*" turbulence model	Visualization Pressure distribution	The numerical results revealed to be in acceptable agreement with the experimental results in the impinging jet and wall jet regions. The wall jet region was characterized by high turbulence intensities. In the case of velocity distribution in the same region, the results showed a distribution similar to a Gaussian distribution.

Table 4: Summary of experimental and numerical joint work for one or more impingement jets

Barata, Durão, Heitor, McGuirk (1987)	Study of the impingement of a single axisymmetric jet against a wall after penetrating a confined cross flowing stream. Rej = 60,000, 84,000, 120,000 $30<V_j/U_0<73$ H/D=5 D= 20 mm U0= 0.1, 0.09, 0.08 m/s	Experimental: LDV Numerical: K-ε turbulence model	Mean and turbulent velocities	Through the experiments for different V_j/U_0 the authors observed that the deflection of the impinging jet by the crossflow is attenuated by the increase of V_j/U_0. The impinging jet deflection terminated in a scarf vortex which increased in size and strength with the V_j/U_0 increase. In the case of the turbulent structure the results showed its independence from the velocity ratio studied. The numerical study showed the importance of the grid refinement to reduce the numerical errors. The use of the high order QUICK scheme improves considerably the numerical results. The shear stresses in the impingement zone were not predicted correctly, not being this zone represented by the turbulent viscosity hypothesis.
Barata, Durão, Heitor, McGuirk (1988b)	Numerical and experimental study of a single axisymmetric jet through a cross flowing stream. D= 20 mm Re_j= 60,000 V_j/U_0= 30 m/s H/D= 5 V_j= 3 m/s	Experimental: LDV Numerical: K-ε turbulence model	Mean and turbulent contours velocities	The experimental results allowed to validate the numerical results. The shear layer that surrounding the jets and the impinging zone were characterized by intense fluctuations where its maximum values were coincident with the highest mean velocity gradients. Taking into account the gradient of diffusion hypothesis the shear stress distribution was consistent with that of the shear strain.

Table 4: (Continuation)

Barata, Durão, Heitor and McGuirk (1988c)	Flow study of a single and twin jets against a wall through a low velocity crossflow. D= 20 mm Re_j= 60,000 and 105,000 V_j/U_0= 30 m/s V_j= 3.0 m/s and 5.1 m/s	Experimental: Visualization with air bubbles or fluorescent dye and LDV Numerical: K-ε turbulence model	Visualization Mean and turbulent velocity profiles	For the two configurations (single and twin jets) it was shown a large penetration of the impinging jets. In the twin jets case a fountain upwash flow was formed by the deflection of the radial wall jets by the crossflow. The shear layer of the fountain, impingement region and impingement jets zones were characterized by intense velocity fluctuations. The numerical model failed to predicted the turbulent structure in the impingement region and fountain flow because the inapplicability of the turbulent viscosity hypothesis.
Barata, Durão, Heitor, McGuirk (1991b)	Flow of one or two circular impingement jets on a flat surface through low velocity crossflow H/D = 5 V_j/U_0 =30 R_e = 6000 e 10500 V_j = 3 e 5.1 m/s	"*k- ε*" turbulence model QUICK	Mean velocity Turbulent velocity	The experimental results were used to validate the numerical calculations. The surrounding shear layer of the jets, the region of impact and the fountains are areas with intense velocity fluctuations. The method to determining turbulent structure of the impact areas and fountain flow failure due to the inability of eddy viscosity hypothesis
Barata, Durão, Heitor, McGuirk (1992b)	Study of the flowfield resulting from a single impingement jet on a wall after penetrating a confined cross-flowing stream.	Experimental: LDV Numerical: standard "*k-ε*" turbulence model	Mean and Turbulent velocity	The experimental results allowed an evaluation of the numerical calculations accuracy. The results showed that the deflection of the impingement jet by the crossflow increase with the velocity ratio decrease.

Table 4: (Continuation)

	Re_j= 60,000, 84,000, 120,000 H/D=5 D= 20 mm V_j= 3, 4.2, 6 m/s U_0= 0.100, 0.093, 0.082 m/s V_j/U_0= 30, 45, 73			The scarf vortex resulting from the interaction of the upstream wall jet with the crossflow with the velocity ratio increase moved to upstream and increased in size. The turbulent structure if the flow seemed to be independent of the velocity ratio used.
Bray, Knowles (1992)	Work that brings together all the data available in a set of unified statements. Flow of a single jet through crossflow	Experimental Numerical: -Navier Stokes equations	Velocity Static pressure distribution	In numerical modelling was used a mesh with 32256 points and 36864 points. The vortex penetration increased with Vj / V0. A better correlation of the data was obtained when the effective velocity ratio used was based on the square root of the dynamic pressure, responsible for the compressibility. With the numerical modelling, had been shown to be possible to simulate the main features of a ground vortex.
Knowles, Bray, Bailey, Curtis (1992)	Flow of a single or two (side by side configuration) confined impingement jets on a moving surface through crossflow d_n (nozzle diameter)= 25.4 mm h/ d_n (dimensionless impingement height)= 2, 4, 8	Experimental: Five-hole probe Pitot rake Pitot-static tube Numerical: PHOENICS "*k-ε*" turbulence model	Experimental: Likeness of the wall jet and ground vortex. Vortex penetration Effect of the impact moving surface on the	From the results obtained it was found that with respect to the ground vortex was shown to constant-relation between the penetration distance, the separation distance and the position of the core of the vortex. Taking into account the different parameters they could conclude that: The penetration increased with velocity ratio.

Table 4: (Continuation)

			separation distance Vectoring effect, impingement height and nozzle pressure ratio on the separation distance Numerical: velocity vector on the plate C_p distribution on the plate	However, if the impact surface had movement the penetration decreased due to the reduction of the power deficit or due to the increase in the wall jet shear stress. When increased the impingement height, in the case of twin jets, there was penetration and might be associated with the merger of the jets. It has been found that the penetration increased with the nozzle pressure ratio even go into shock. Vectoring nozzles forward relatively to the geometric point of impact increased the jets penetration. In the contrary case, the result was a reduction of approximately 20%.in the penetration
Barata, Durão, Heitor, McGuirk (1993a)	Flow of a turbulent circular impingement jet through low velocity crossflow D = 20 mm H/D = 5 $V_j/U_0 = 30$ $R_e = 6x10^4$	Experimental – LDA Numerical – a solution of the finite difference form of the fully three- dimensional Reynolds-averaged Navier-Stokes equations, incorporating the turbulence viscosity concept.	Mean and turbulent velocity profiles Flowfield visualization	By combining experimental and numerical tasks was possible through the turbulent viscosity model simulate the turbulence structure near and far from the impact. In the numerical solution were used a mesh 8670 points and 69360 points. The results, which had relevance to flows found beneath VSTOL aircraft in ground effect, showed the presence of a complex 3-D scarf vortex formed around the impinging jet. The turbulent structure of the flow was affected by flow distortion at the impinging zone, which results in an unconventional behaviour of the dimensionless structure parameters that determine the empirical

Table 4: (Continuation)

					constants in engineering models of turbulence. The relative magnitude of the terms involved in the transport equations for the turbulent stresses was quantified from the experimental data in order to assess the importance of these effects and showed the extent to which the turbulent structure of the impingement zone was affected by extra rates of strain
	Barata (1993b)	Flow of multiple circular jets through low velocity crossflow D = 20 mm H/D = 5 V_j/U_0 =30 U_0 =0,17 m/s	Experimental: - LDA Numerical: -K-ε turbulence model	Trajectories Mean velocity profiles Turbulent kinetic energy	The numerical method was obtained with a mesh with a 22382 points and 86112 points for 2 and 3 jets respectively. The results of the study showed a flow pattern similar to that which occurs for a single jet, comprising a potential-length region and an impact region with the jets deflection. There were large areas of low pressure. Also it was observed that the numerical method failure to prediction the turbulence levels in the upwash fountain.
	Barata (1996a)	Flow of axisymmetric twin jets through low velocity crossflow H/D = 5 D = 20 mm Re_j= 1.05x10^5 V_e (crossflow to jet velocity ratio)= 0.033 m/s V_j= 5.1 m/s	LDV	Mean velocities Turbulent velocities	In areas where it is not possible to obtain numerical data, details of the flow are displayed numerically using Navier-Stokes equations in the form of finite difference, incorporating the concept of turbulent viscosity.

Table 4: (Continuation)

Barata (1996b)	Flow study of multiple water jets through low velocity crossflow R_{ej} = 60000 e 105000 V_j/U_0 = 30 m/s H/D = 5 D = 20 mm	Numerical: solution of the finite difference form of the three-dimensional Reynolds averaged Navier-Stokes equations, incorporating the turbulence viscosity concept Experimental: LDV	Trajectories Mean velocity profiles Numerical visualization	The mean velocity profiles showed good agreement with the experimental data on the impact jets and upwash flows. The shear stress signal was consistent with the shear signal in the hypothetical diffusion gradients direction with the exception of the stagnation zones associated with the ground vortex formation.
Behrouzi, McGuirk (1998)	Flow study of twin jets through crossflow H/D=13 S/D=13 D=15 mm V_j=2.5 m/s Re_j (jet Reynolds number)=37100 Re (crossflow Reynolds number)=41000	LDV	Mean and turbulent velocity fields	It was found that the upward flow zone is characterized by strong turbulence and it is a region where the production of normal stresses is quite evident. The K-ε model was well suited to predict the experimental results.

Table 4: (Continuation)

Knowles, Davies (1999)	Flow study of a turbulent circular and isothermal jet impinging on a flat surface with movement D= 12.70 mm Vg= 10 m/s Vn= 90 m/s H/D= 4, 8, 10 NPR= 1.05 Re= $9x10^4$	Experimental: static pitot tubes Numerical: PHOENICS Lam-Bremhorst low Reynolds number turbulence model	Velocity profiles Radial variation of Wall jet momentum flux Nusselt number distribution Velocity profile	The results confirmed a strong asymmetry between the sides of advance and retreat of the impact zones. On the centre line of retreat (where the wall jet and the impact surface were moved in the same direction) the wall jet was found to be extremely thin. Through computer simulation, it was possible to predict the heat transfer performance for this type of configuration, being verified that the effects of the surface velocity on the mean heat transfer rate for circular jets had no interest for the study.
Alvi, Ladd, Bower (2002)	The study of a moderately under expanded axisymmetric supersonic jet issuing from a converging nozzle impinging on a ground plane. D (nozzle exit diameter) =25.4 mm D (lift plane diameter)=10d NPR (nozzle pressure ratio)=5 T (normal jet stagnation temperature)= 20°C h/d = 3 Molecular Prandtl= 0.72	Experimental**:** PIV Numerical: Wind program One-equation Spalart-Allmaras model SST – two equations shear stress transport model Spalart-Allmaras model with the correction for stream line curvature and system rotation	Experimental: Flow visualization Surface-pressure distribution Velocity fields Numerical: Surface-pressure distribution Velocity fields	On this study the detailed experimental results were used to verify the accuracy of, and served as benchmark for, the computational methods. The computational results from SARC and SST were nearly identical. Both models were able to capture the significant features of the complex flow and were good agreement with the experimental data. The SST turbulence models have proven to be robust and efficient to produce good results in the aerospace industry. Both experiments and computational results revealed the presence of the stagnation bubble, at a level resolution not seen before.

Table 4: (Continuation)

	Turbulent Prandtl= 0.9	(SARC)		
Baydar, Ozmen (2005)	Flow of a circular jet impinging on a surface with the crossflow presence Re = 30000, 40000 e 50000 D = 25 mm 0.2 < H/D < 6	Experimental - TSI – IFA – 100 hot wire anemometer Numerical: –K-ε turbulence model	Mean velocity profiles Turbulence intensity Pressure distribution.	The numerical results were in agreement with the experimental results, except for the results obtained for the impingement height less than 1. The numerical study was used to H / D <0.1. The pressure distributions over the impact surface was independent of the Reynolds number, but strongly dependent of the H / D.
Abel-Fattah (2007)	Two dimensional impinging circular twin-jet flow with no-cross flow D = 10 mm 3 <H/D <12 L/D = 3,5 e 8 $0^o \leq \theta \leq 20^o$ $9.5 \times 10^4 \leq R_e \leq 22.4 \times 10^4$	Experimental: digital thermometer, pressure gauge Numerical: – Finite volume method	Pressure distribution Velocity profiles	The results obtained by the authors showed a sub atmospheric region created with jets of higher Reynolds number and at lower nozzle to plate spacing. By increasing jet Reynolds number the pressure increased in the above atmospheric region, and the sub atmospheric region became stronger. As the jet angle increased, the pressure decreased and its maximum value, at the primary stagnation point shifts in radial direction and this shift changes in shorter distances by increasing the nozzle to nozzle spacing. The difference between the pressure at secondary stagnation point and the primary stagnation point decreased by increasing the nozzle to plate spacing and by decreasing jet Reynolds number.

Table 4: (Continuation)

				The recirculation zone between twin jets became wider by increasing the jet angle, l/d and h/d. The increment of jet spreading decreased by increasing the nozzle to plate spacing h/d. The turbulent kinetic energy increased within each vortex region, and this increment decreased by increasing of jet angle and/or the nozzle to plate spacing.
			Energy spectrum Scalar spatial distribution Mixture parameters Turbulence	Single or double peaked in cross-sectional planes, depending on nozzle shape and orientation. Proper orthogonal decomposition of the velocity fields revealed that this phenomenon may be related to the occurrence of large-scale coherent structures: Single-peaked distributions occurred in cases in which the first eigen mode had a large corresponding eigenvalue. The nozzles with single- peaked distribution, i.e. the elliptic nozzle with high aspect ratio and the blunt square nozzle, had superior mixing performance. Furthermore, it was shown that regions of counter-gradient transport were contained in the flowfield.
		LES PIV LIF		
	Study of the nozzle shape effect in a water jet flows with the crossflow presence L/D= 20 Re= 10000 R (velocity ratio)= 4 T (water temperature)= 20°C Bulk velocity =0.1 m/s			
	Salewski, Stankovic, Fuchs (2007)			

Table 4: (Continuation)

Koseoglu, Baskaya (2009)	Flow of a jet through confined crossflow H/D = 2,4, 6, 8 e 12 250≤ R_e ≤ 5000	Numerical: finite volume equation discretization Experimental: LDA	Nusselt number Heat transfer	Through the results it had been determined that buoyancy induced natural convection might have opposing or assisting influence on local heat transfer at different locations of the target plate. It had also been shown that especially at low jet inlet velocities the average heat transfer coefficient at the highest modified Grashof number, where the natural convection was effective, was higher than the value corresponding to the lowest Grashof number at which buoyancy effects were negligible, by as much as 37%.
Radhouane, Bournot, Said, Mhiri, Palec (2009)	Flowfield study resulting from the interaction of twin inclined elliptic jets with an oncoming crossflow D = 10 mm α (Injection angle with reference to the free stream)= 30°, 45°, 60° e 90° U_∞ (crossflow velocity)= 2.5 m/s	Experimental: PIV Numerical: Navier-Stokes equations with the finite volume method and the Reynolds stress model (RSM) second-order turbulent model	Trajectories Mean velocity flowfield Shear stress flowfield	The results revealed the presence of a complex resulting flowfield. This complexity was expressed by the establishment of an elaborated vortical system composed of four main vortices: the horseshoe vortices, the upright vortices, the shear layer vortices and the counter rotating vortex pair. Increasing the initial emission angle provided the jets with a higher impulse to expand deeper vertically in the environing flow which resulted in a further vertical mixing. Decreasing the initial inclination factor, on the contrary, allowed rather a span wise expanding since the jets were rapidly deflected by the oncoming crossflow; which promoted the trapping of the jets' flow close to the injection The authors also examined the impact of the initial inclination on the shear stress

Table 4: (Continuation)

	Wae-hayee, Tekasakul, Eiamsa-ard, Nuntadusit (2014)	Study of the effect of crossflow velocity on a flow and heat transfer characteristics of an impingement air jet on a plate. H/D= 2 V_R (velocity ratio)= 3, 5, 7	Experimental: thermochromics liquid crystal sheet, image processing method, oil film technique Numerical: shear stress transport "k-ω" turbulent model	Nusselt number distribution Temperature distribution Flow pattern visualization Velocity vectors and contours Turbulence kinetic energy contours	The results obtained by the authors showed that the impingement region shifted downstream as crossflow velocity was increased, coinciding with the shifting of the high Nusselt number area. When the crossflow velocity was increased, the upstream impingement region was contracted while the downstream one was extended, resulting in the rapid decrease of Nusselt number in the upstream and increase of Nusselt number in the downstream It was also shown that the Nusselt number peak in impingement region increased with increasing crossflow velocity.
					components and could show that the straightest were the jets, the highest were the shear stresses. This could be justified by the fact that the straightest jets were provided with a stronger ''impulse'' that engenders a more ''violent'' interaction with the mainstream and then resulted in stronger vortices and consequently in a better mixing which it was not a good idea in case of contaminated jets.

Table 4: (Continuation)

1.6 Thesis Contribution

Impingement jets penetrating on a crossflow with a relatively low velocity give rise to a flow interaction highly turbulent. When the jets touch the ground, it results in a formation of a wall jet which flows radially from the impinging point along the ground surface, being rapidly deflected by the crossflow. The wall jet deflection is particularly significant or intense as larger is the ratio between the jet velocity and the crossflow velocity, fundamentally due to the pressure field in this region. On the downstream region of the wall jet is notorious the gradual dilution of the wall jet deflection essentially due to the momentum equalization associated to the vorticity. At the moment that the jet starts to bend due to its interaction with the crossflow there is a deformation in its cross section, spreading laterally and curving on the initial jet direction, assuming the characteristic shape of a kidney (Figure 48), often described in the literature by many authors.

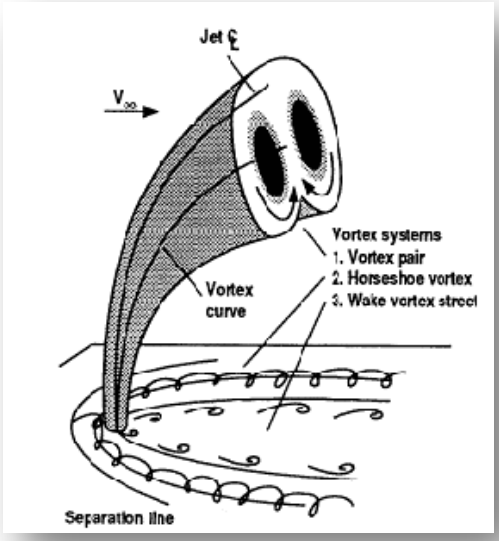

Figure 48: The three vortex systems associated with the Jet in a Cross Flow[62]

This cross-structure development results in the formation of a pair of counter-rotating vortices due to the lateral displacement of the crossflow for entraining and its lower pressure zones. In addition to the roll up of the jet into a vortex pair there is a turbulent region in the wake of the jet and a horseshoe vortex looped around the jet in the exit plane. Typically, this vorticity structure is intense, long lasting and is responsible for the pressure field induced in the plane of the jet impact and downstream of the jet impact area. The purpose of this thesis is to reproduce in the most realistic way possible what happens in the future F-35 VSTOL aircraft, through the detailed analysis of the complex flow field beneath two impinging jets

[62] Margason, R. J., 1993, 'Fifty Years of Jet in Cross Flow Research', AGARD meeting on 'Computational and Experimental Assessment of Jets in Cross Flow', April 1993.

aligned with the crossflow. This analysis was composed by an experimental part and a numerical part, through a physical and mathematical model that allows to characterize the behaviour of the occurring phenomena's on this type of aircrafts and providing a quantitative and a qualitative picture of the flow. Both the experimental and the numerical parts of the characterization of the flow field were done for different velocity ratios in order to find out how the velocity ratio variation influences the presence or development of the above described phenomena's and the flow behaviour. The numerical analysis is of most importance for this work because not only validates the computational method using the results obtained experimentally, but also allows a better analysis and visualization of the flow to detect some structures that experimentally are not possible to see and allow the extension of the experimental results for velocity ratio beyond the experimental conditions.

So far, a large part if not all the jet configuration studied experimentally or numerically are characteristic by the impingement jets positioned perpendicular to the direction of the crossflow propagation. The present study is a piece of a most comprehensive experimental and numerical study on inline impinging jet flows in ground effect. The main focus of the numerical study is to extend the experimental study for velocity ratios and impingement heights beyond the limits of the experimental installation.

This thesis is dedicated to a configuration that has not been considered so far in the published literature, but is the most relevant for the simulation of the aerodynamics ground effects of the future VSTOL aircraft generation.

The present work shows that due to the downstream wall jet flowing radially from the impact point, the second jet does not reach the ground for a combination of the highest impingement height (H/D=20.1) with $V_j/U_0 \leq 43.8$. This is a most important result for the F-35 aircraft operating in ground vicinity, and is the major novelty not yet reported before. Three different types of flow regimes were identified. The regime with strong impingement on ground and with a formation of a ground vortex is the most relevant for the situation of a VSTOL aircraft operating in ground vicinity. The numerical results extend the experimental studies in terms of flow analysis and initial conditions, and prove that the deflection of the rear jet is due to the competing influences the wake, the shear layer, the downstream wall jet of the first jet and the crossflow.

1.7 Thesis Contents

This work is organized into six chapters. The first chapter is the introduction, which is dived into six sections. On the first section the different flight phases on this type of aircraft are explained, as well as its characteristics and the different problems that affect the aircraft performance on each flight phase. Since the objective of this thesis is the study of twin

impinging jets/crossflow interactions relevant to the F-35 VSTOL aircraft ground effects the second section aim is to explain what happens when the VSTOL aircraft operates in the vicinity of the ground. At this phase the complex flowfield is divided in several zones, with the formation of different structures. On the third section the motivation of this work is described with a brief explanation of the aircraft family, the type of propulsion used, its capabilities and the aerodynamic phenomena that happens in the different flight phases. The literature review is presented in the next section, particularly aiming to identify the most significant contributions, either experimentally or numerically, which contributed to achieving the current state of knowledge in this area. This analysis also allows to justify some adopted options and assumptions in order to achieve the main objective of this thesis. On the fifth section are identified the main contribution of this work. The present section describes the thesis content.

On the second chapter is described the experimental method as well as the experimental rig. The experimental method description includes the Laser Doppler Anemometry principles, the signal characterization, the errors estimation on the measurements and the results precision. It also exists a section dedicated to the explanation of the seeding system used to obtain the results.

In the third section the experimental results obtained with flow visualization and measurements with the LDA system are presented. It is also described the calibration process.

In the fourth chapter the mathematical model used in the numerical simulation is presented, with the description of the governing equations, the differential equations coefficients and the turbulent model constants.

The fifth chapter is dedicated to the numerical results that allow a better understanding of the flow behaviour and that are validated against the experimental results obtained with LDA.

The last chapter contains the main conclusions of this study and some suggestions for future work.

Chapter 2

Experimental method

The experimental method selected for this work is the LDA or Laser Doppler Anemometry. The LDA systems are increasingly used in science and industry enabling a clear understanding of fluid mechanics. The laser Doppler anemometry (LDA), also known as a laser Doppler velocimetry (LDV) is a non-intrusive technique for turbulence measurement in gas, liquid, and mixing fluids, flames, rotating machinery, in combustion, channels, chemically reacting flows, wave tanks, wind or water tunnels, in biomedical applications, atmosphere, oceanography and in a wide spectrum of scientific and industrial research where conventional techniques perform poorly.

The principal idea behind the LDA system is to measure the velocity of little particles transported by a flow using the Doppler effect of the light scattered by them. As the particles are small enough to follow the flow, their velocities are assumed to be that of the stream. The LDA system measures the local instantaneous velocities, which is treated statistically in terms of the mean velocity as well as the turbulent quantities, which correspond to the root mean square, flatness and skewness of the distribution. The measurements are important to assist product design in order to improve aerodynamics, efficiency and safety.

2.1 Experimental Setup

The wind tunnel facility designed and constructed for this study is schematically shown in figure 49. A 15KW fan drive a maximum flow of 3000m^3/h through the wind tunnel boundary layer with a 300x302mm outlet section.

The test section is made of Perspex, a transparent and rigid thermoplastic that is widely used due to its optical properties. Its specific name is polymethylmethacrylate (PMMA). The interior dimensions of the test section are those corresponding to the wind tunnel exit, and its length is approximately 1080 mm (figure 50).

The test section has the twin jets mounted vertically on the top wall with the axes contained in the vertical plane of symmetry parallel to the crossflow. The inner diameter, D, of each jet unit is 15mm. The origin of the horizontal, X, and the vertical Y coordinates are taken at the midpoint between the centres of the exit nozzles. The X coordinate is positive in the crossflow direction and Y is positive in the upward vertical direction (see figure 51). The impingement height, H, is 20.1D and the spacing between the centres, S, is 6D.

Figure 49: Wind tunnel exit Section: front view and lateral view

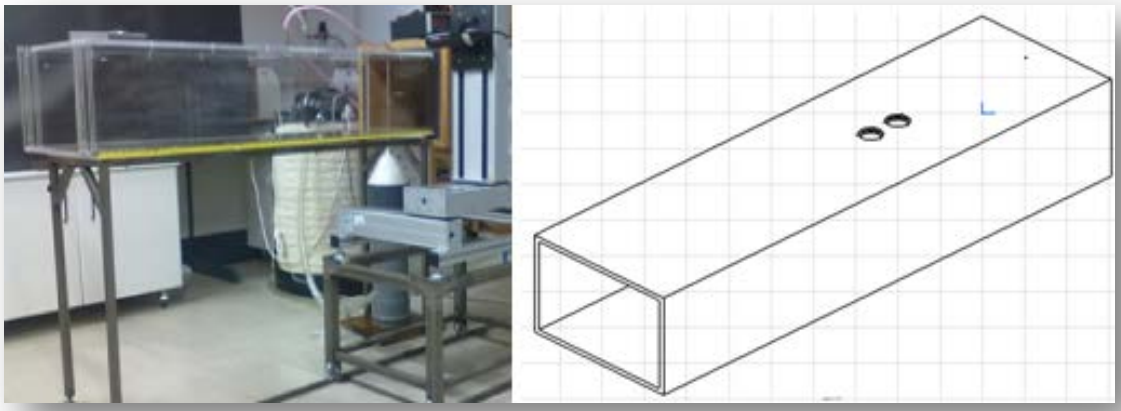

Figure 50: Test section

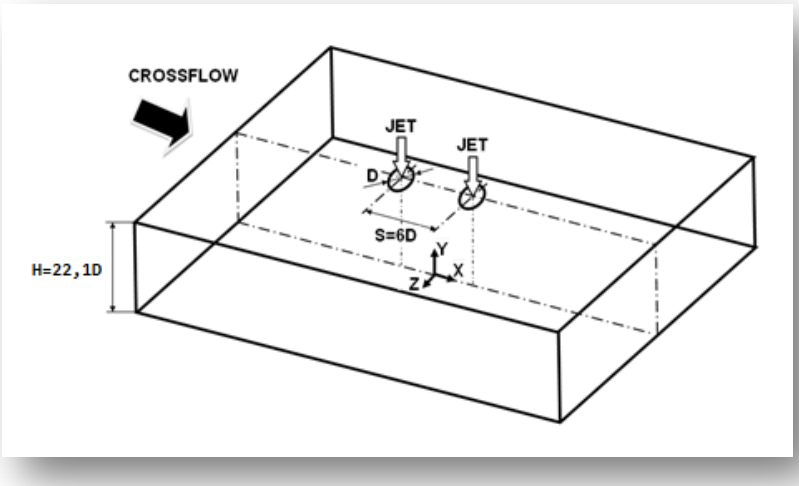

Figure 51: Geometrical arrangement of the jets in the test section

The jet units are inserted in caps (figure 52) which fit on the top wall of the test section. Below are shown in detail all the geometric parameters of the caps where the nozzles are inserted. The caps are also made of Perspex and bolted to the test section through 3 bolts, spaced 120 degrees. In this work were used caps with equal jet diameters but in the in the future measurements may be made with different diameters or with only one jet by using a cap which has no hole. The compressed air hoses are snapped to the caps through accessories for this special purpose, which have been previously screwed on the caps (figure 53).

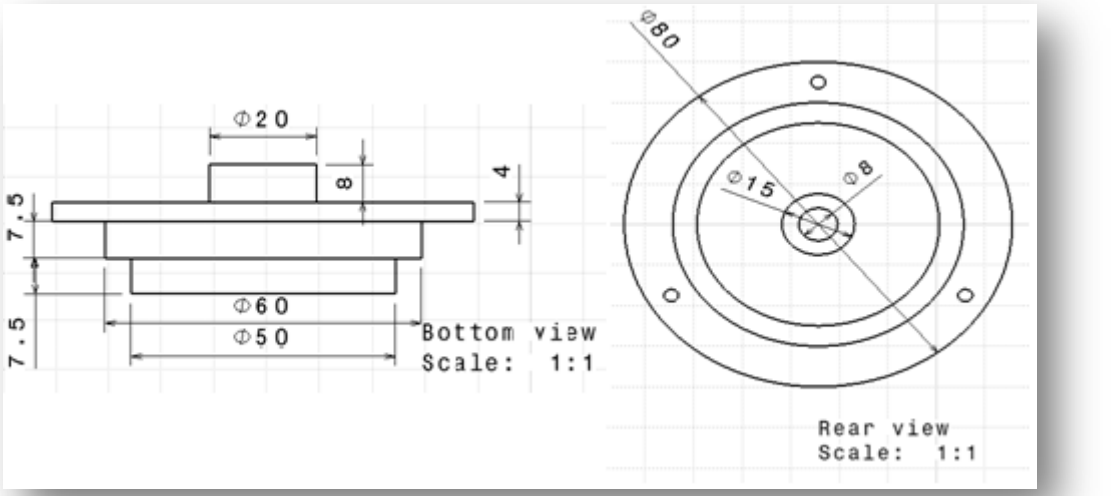

Figure 52: Geometric parameters of the impingement jets caps

Compressed air hoses fitting in the cap

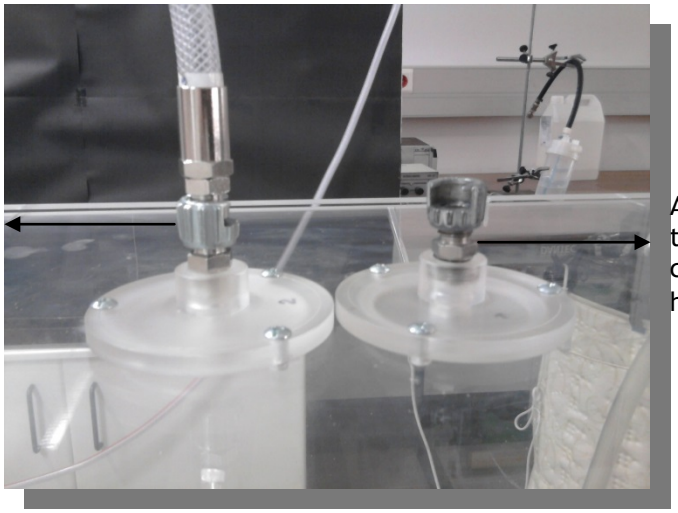

Accessory to fit the compressed air hoses

Figure 53: Representation of the assembly of the caps on the test section and the compressed air hoses fitting.

2.2 Seeding system

In this work, the velocity field was measured with a LDA system using air as working fluid. Therefore, the fluid was seeded with particles in suspension sufficiently small to follow the flow. For this purpose, it was used a JEM-Techno Fog smoke generator and a cyclone, an additional mechanism which its function is the injection of seeding in the impinging jets (figures 50 to 52). The machine generates smoke using a suitable liquid JEM. The smoke generated was expelled with the aid of compressor air with a pressure value of 1 bar that was sent via a conduit to the cyclone.

In the cyclone (figure 54) the smoke is accelerated and sent spiralling to a conical contraction. The smoke is then sent to a thin tube called “comb” (figure 55) that is placed in the vertical plane of symmetry of the test section. This tube was perforated to allow the seeding at different heights.

It is necessary to use low seeding concentrations to avoid the interaction between different particles and measurement problems due to the presence of more than one particle inside the ellipsoid control volume.

Figure 54: Cyclone connected to the smoke generator

Figure 55: Perforated tube that allows the seeding insemination into the test section

The smoke generator has a LED "ready" (figure 56 - left) which is activated when the operating temperature is reached. There is also a timer control to set the pulse repetition rate. The pulse duration is fixed and only the frequency can be changed. When combined with the output level control, this provides a simple manner to set the mist constant level. Pressing the fog switch (at any time since the LED "ready" is lit), makes it possible to obtain a constant fog level production. The LED "Heat" is on when power is being supplied to the heat

exchanger. When the maximum temperature is reached, the LED is off. The "Output Level Control" is rotated clockwise to increase the smoke output level.

Figure 56: Smoke generator: remote control (left); smoke-generating machine (middle); liquid used (right).

For the visualization studies it was used the timer value of 3. The smoke button was pressed in order to maintain a strong and continuous seeding flow injection to allow adequate illumination for a photograph. The tracer used is a monopropylene with demineralized water manufactured by the same smoking machine manufacturer.

The seeding system was efficient for the crossflow measurements. However, for large jet velocities there was not sufficient entrainment of the crossflow fluid and the data rate in the jet region was almost impossible, since only a few bursts were validated. The jets had a velocity 22.5 times greater than the crossflow velocity, thus acting like a solid cylinder with almost no intermittency to allow the entrainment of low velocity fluid from the crossflow that was carrying the seeding. To fix this problem we had to find a solution that was effective and did not disturb the jet flow at the nozzle exit. The best solution found was a seeding insemination system used before by Meireles (2009). This system (figure 57[63]) consists of a pressurized container with a small air ejector on the inside, whose function is to generate small droplets of seeding liquid. Initially, the spray was inspired by a doctor vaporizer, but it could not allow high pressures required. The system under consideration consists in a reservoir and two metal pipes (figure 57a). The two pipes are close on the top with a 1 mm hole, working these pipes one inside of the other (figure 57b). The inner pipe is connected to the air system and its function it is not to let the liquid inside the reservoir go to the compressed air system (figure 57c). The outer pipe (figure 57d) works free just overlay on the first one. The two pipes together allow the liquid to fill the small space between the pipes,

[63] Meireles, M. S. Pedro, Experimental Study of twin air impinging jets, Master Thesis , 2008/2009

being the vibration on the second pipe that will bubbled the liquid inside of the reservoir. With this system is possible to seeding the twin jets to the inside of the test section.

The mixture used (70% glycerol + 30% water) was the same that was used by Meireles (2009). The combination of the reservoir pressure (low pressure 2 bar) and the ejector pressure (about 1.2 bars) allows the formation of a "fog" formed by droplets of the liquid mixture. The outlet of the tank was forked so that it can be out the same amount of "fog" for both jets.

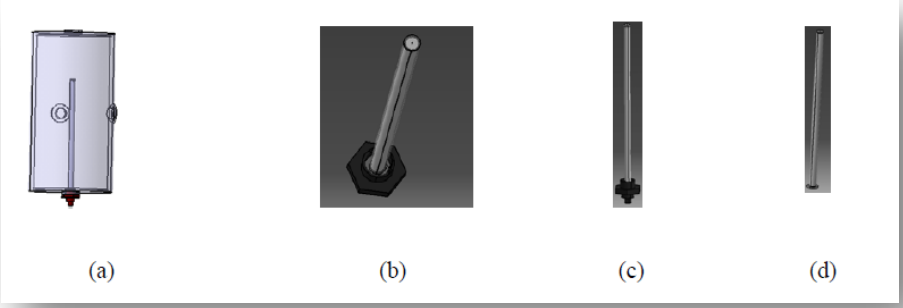

Figure 57: Views of the vaporizer system: (a) complete vaporizer system, (b) two pipes of the vaporizer, (c) inner pipe, (d) outer.[64]

Figure 58: Seeding setup: a, vaporized pressure control manometer; b, pressure inlet for the reservoir; c, pressure inlet for the air ejector; d, vaporized input; e, inlet reservoir pressure control manometer; f, reservoir.

[64] Meireles, M. S. Pedro, Experimental Study of twin air impinging jets, Master Thesis , 2008/2009

For the flow visualization it was found that seeding insemination by this method had not the desired effect. The droplets of the mixture glycerine + water condensate in the tubes as well as in impact surface of the test section, requiring many interruptions to clean the solid surfaces. Additionally, it was also verified the existence of drops in the nozzle fluid itself which would change the actual area of the nozzle, resulting in erroneous measurements of the flow under consideration.

So, another way to inseminate seeding into the impinging jets was investigated. Following the previous experience, the attempt to create seeding through vaporization of a mixture was out of the question, because the tubes length between the seeding generator and the impinging jets exit would allow the condensation to occur. There were many ideas that have emerged but there was always something that would made it inapplicable to the present be viable for the study case. One of the alternatives that emerged was the seeding insemination directly from the smoking machine through needles just before the exit section of the impinging jet. However, this option could not be adopted since the pressure difference between the fluid inside the tube and the seeding needle was too large.

Since the pressures differential across the flow that feeds the jets (from the compressor) and the seeding (from the smoking machine) was large, the only solution to adopt would be to seek a way of lowering the pressure of a part of the jets to the seeding insemination pressure but maintaining the total pressure of each jet. The resulting system is shown in figure 59.

The system adopted for the seeding insemination is a closed system, so that in this way it is ensured that all the flow from the compressor at a certain pressure enters into the test section without disruption of the jet velocity.

To vaporize the liquid used for the seeding it was necessary to increase its temperature above a certain level. Consulting the specifications of the liquid seeding used in the machine (“Dj regular fluid”) it was found that the melting point is <20.1ºC and the boiling point is 101.6ºC. Thus, it was possible the using of induction plates to heat the seeding liquid in a container that is resistant to the heat emanating from the induction plate, but also resistant to pressures up to two bar (the pressure of the main flow coming to the compressor).

The laboratory bottle GL45 clear 10000 ml, DURAN pressure plus, were chosen because thanks to a modified geometry, the bottle has a guaranteed pressure-resistance and consequently offers optimum safety both for user and content (vacuum or pressure resistance guaranteed from -1 bar to +1.5 bars). The Duran laboratory glass bottles allow a diverse connection system enabling safe transfer of liquid media within a closed and sterile system. From the various options that were offered the most suitable for the system would be the Screw cap GL 45, 2-ports GL 14. Below it is shown the bottle and the cap used in the system.

Each element and their fittings are shown in detail in figure 60. The bottles and accessories are shown in figure 61, and the screw cap assembly in figure 62. Figure 63 shows the final assembly of the bottle in the seeding system.

Figure 59: New seeding setup: 1, connection of the second jet compressed air tube with the installation; 2, connection of the first jet compressed air tube with the installation; 3, hot plate; 4, laboratory bottle GL45 clear 10000 ml, DURAN pressure plus with seeding inside; 5, pressure regulator; 6, manometer; 7, pipe carrying the diverted flow through the manometer; 8, pipe transporting the seeding and diverted air from the bottle to the main flow; 9, valve to control the pressure drop required to allow the seeding suction into the main flow; 10, seeding and diverted air entering into the main flow.

Point 1 and 2

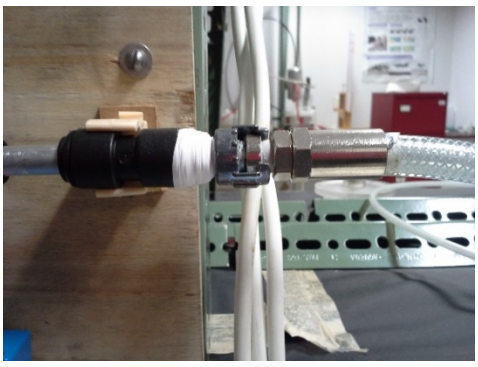

Point 5

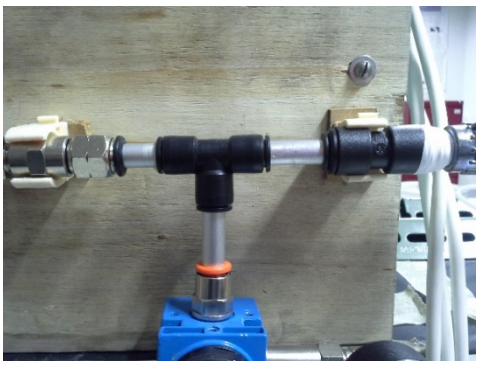

Figure 60: Details of the seeding system.

Point 6

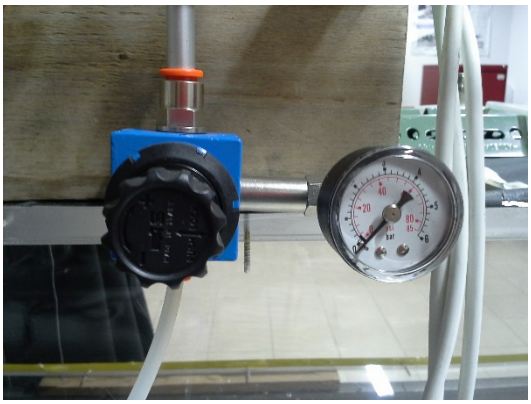

Point 7

Point 8

Point 9

Point 10

Connection to the jets caps

Figure 60 (cont'd): Details of the seeding system.

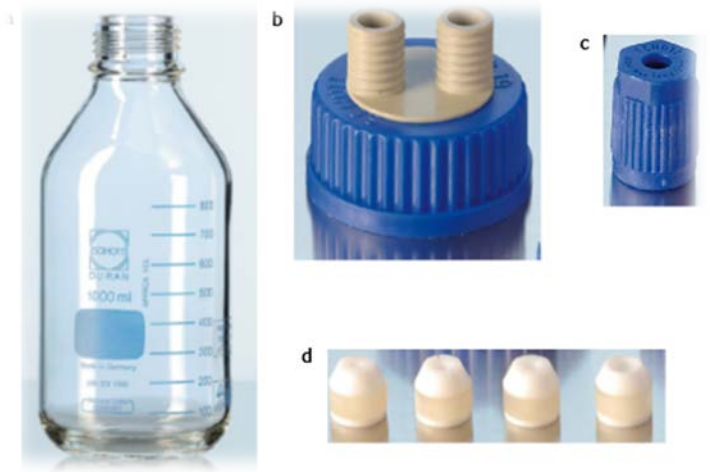

Figure 61: Pressure bottle and accessories: a, DURAN pressure plus bottle GL45 clear 10000 ml; b, Duran screw cap GL45 PP 2 Port GL14; c, Duran screw cap GL14 for hose connection; d, Duran Insert for Screw Cap GL14 3.2mm and 6.0 mm[65].

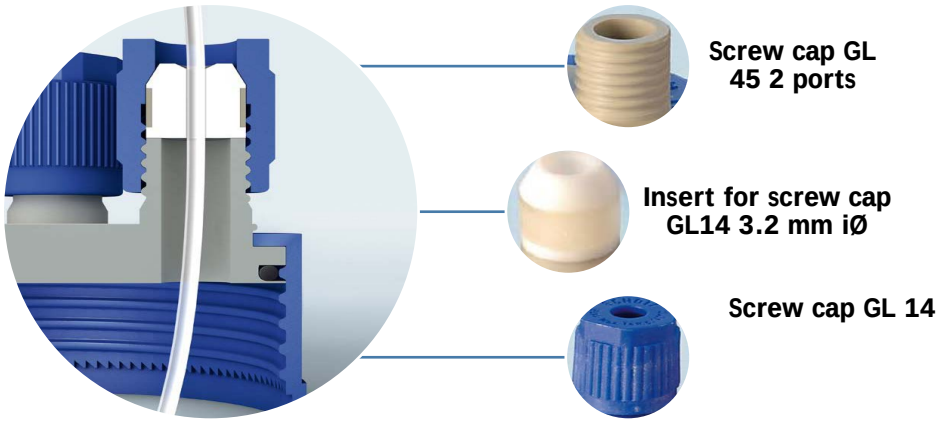

Figure 62: Screw cap assembly[66]

To produce extremely small seeding particles forming the fog, the heating plates have to be connected at maximum power for about 20 minutes before any measurements for the seeding to heat up to about 100ºC. When inside the bottle the fog formation becomes visible, the remainder of the system can be connected so as to inject seeding on the impinging jets. To explain the operation method of the system, it will be used the numbering presented in figure 60. So, the first step is to regulate the air that comes directly from the compressor to each jet to 2 bar (Point 1 and 2). The pressure in the pipe flow coming from point 1 through the point 5 is controlled with the pressure regulator represented by the point 6 which diverts part of the main flow to point 7.

[65]http://www.durangroup.com/uploads/tx_fedownloads/DURAN_Laboratory_glass_bottles_and_accessories_A5_E.pdf.

[66]http://www.durangroup.com/uploads/tx_fedownloads/DURAN_Laboratory_glass_bottles_and_accessories_A5_E.pdf.

Figure 63: Final bottle assembly: a, pipe that transports the seeding particles that it are inside the bottle to the main flow; b, pipe that carries the diverted flow of the main flow by the manometer working as a bubbler.

This flow that is taken from the main flow goes directly to the bottle where will act as a bubble trap which will increase the production of very small particles of seeding. On point 9 a valve is placed to allow the control the amount of flow that passes to point 10. Without the existence of this valve it would be impossible to inject seeding in the main flow, because the pressure of the main flow is larger. Thus through a compromise between the valve opening and the pressure regulator it is possible to create a pressure differential that allows the seeding injection of the impinging jets. After point 10 the flow goes directly to the test section.

2.3 Laser Doppler Anemometry

As noted above the experimental technique used to obtain the results was Laser Doppler Anemometry (LDA). So it becomes necessary to know a little more about this technique in order to understand its method of operation, as well as the possibility of interpreting the results and possible errors that may occur during the operation. Thus it is imperative to focus on its main technical features, its evolution over the years, its principles, and the errors inherent in the use of this type of system.

The LDA technique is a widely accepted tool for fluid dynamic investigations in gases and liquids and has been used successfully for more than three decades. It is a well-established technique that gives information about the mean and turbulent flow velocities. It is a non-

intrusive technique, and its directional sensitivity makes it very suitable for applications with reversing flow regions, chemically reacting or high-temperature media and rotating machinery, where physical sensors are difficult or impossible to use. The Laser Doppler Anemometry offers unique advantages in comparison with other experimental techniques[67], such as:

Non-contact optical measurement

LDA probes the flow with focused laser beams and can determine the velocity without disturbing the flow in the measuring volume. The only necessary conditions are a transparent medium with a suitable concentration of tracer particles (or seeding) and optical access to the flow through windows, or via a submerged optical probe.

No calibration – no drift.

The laser anemometer has a unique intrinsic response to fluid velocity–absolute linearity. The measurement is based on the stability and linearity of optical electromagnetic waves, which can be considered unaffected by other physical parameters such as temperature and pressure.

Well-defined directional response.

The quantity measured by LDA is the projection of the velocity vector on the measuring direction defined by the optical system.

High spatial and temporal resolution.

The optics of the laser anemometer are able to produce a very small measuring volume and thus providing good spatial resolution and allowing local measurement of velocity. The small measuring volume combine with fast signal processing electronics also permits high bandwidth, time-resolved measurements of fluctuating velocities, providing excellent temporal resolution.

Multi-component and multi-directional measurements.

Combinations of laser anemometer systems with component separation based on colour, polarization or frequency shift allow one, two or three-component LDA systems to be put together based on common optical modules. Optoacoustic frequency shift allows the measurement of reversing flow velocities.

This technique also presents some limitations such as the cost of the equipment. The flow must be seeded with particles if none naturally exist, it is a single point measurement technique and sometimes can be difficult to collect data very near walls.

[67] Jensen K. D. (2004). Flow Measurements. Journal of the Brazilian Society of Mechanical Science and Engineering. XXVI(4): 400:419.

A variant of this optical technique (LDA reference beam) without proper calibration has been first reported by Yeh and Cummins (1964)[68]. Presently, two collimated beams of monochromatic and coherent laser light are used. These two beams are usually obtained by splitting a single beam, thus ensuring consistency between them, and are made to intersect at the focal point of a laser beam, where they interfere and generate a measurement volume that can be modelled with a series of straight parallel fringes. A sensor is then aligned with the flow such that the fringes are perpendicular to the direction of flow. The small seeding particles are entrained in the flow in order to follow the flow and to disperse the light when they travel through the control volume.

Once the seeding particles pass through the fringe, they produce a burst of light which is collected by a photodetector. By measuring the Doppler frequency of the scattered light, it is possible to calculate the particle velocity that corresponds to the flow velocity. The adequate use of this technique allows a very high precision, as well as high spatial resolution due to small size of the measurement volume (figure 64).

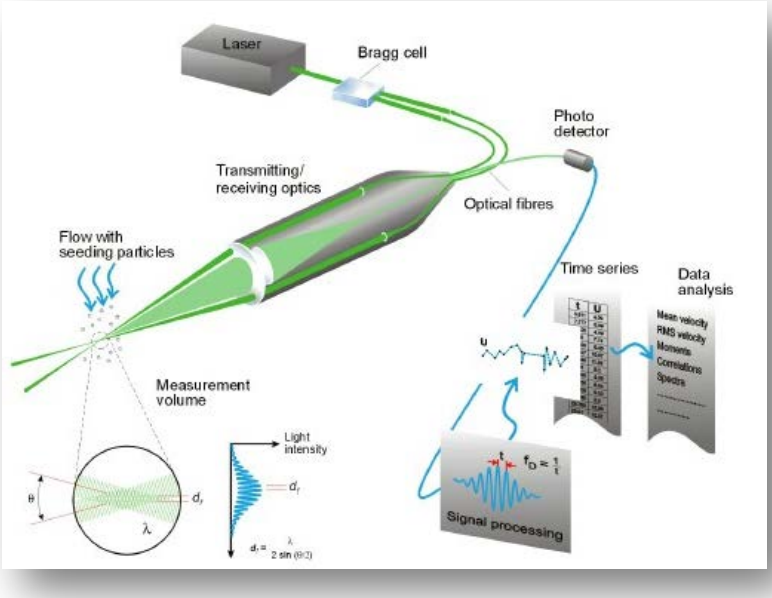

Figure 64: Laser Doppler Anemometry principle.[69]

2.3.1 LDA Principles

The basic configuration of an LDA (figure 65) consists of:

- ✓ A continuous wave laser;

[68] Yeh Y., Cummins H. Z. (1964). Localized Fluid Flow Measurements with a He-Ne Laser Spectrometer. *Applied Physics Letters*. **4 (10)**: 176-178.

[69] http://www.dantecdynamics.com/measurement-principles-of-lda

- ✓ Transmitting optics, including a beam splitter and a focusing lens;
- ✓ Receiving optics, comprising a focusing lens, an interference filter and a photodetector;
- ✓ A signal conditioner and a signal processor.

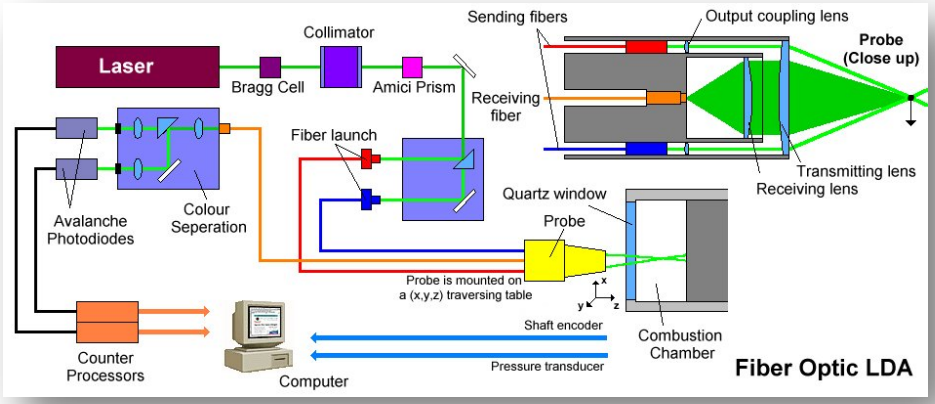

Figure 65: LDA Scheme[70]

2.3.1.1 Laser Beam

The special properties of the laser gas, making it so well suited for the measurement of many mechanical properties, are the spatial a temporal coherence. The intensity along all cross section of the laser beam has a Gaussian distribution (figure 66), where the width of the beam is defined by the edge intensity, being $1/e^2$=13% of the core intensity. At one point the cross section gets its smallest value, being the laser beam uniquely described by the size and position of this so-called beam waist.

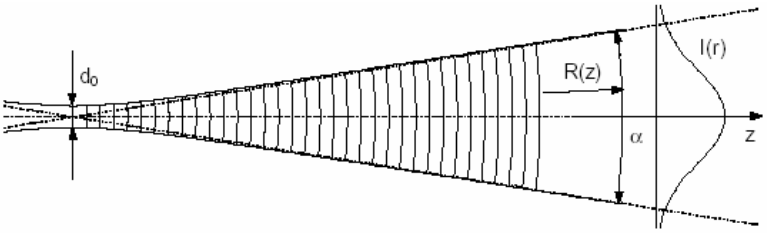

Figure 66: Laser Beam with Gaussian intensity distribution[71]

$$\textbf{Beam divergence } \alpha = \frac{4\lambda}{\pi d_0} \qquad (2.1)$$

where λ represent the wavelength and d_0 the beam waist

[70] http://www.eng.warwick.ac.uk/oel/courses/engine/ic036.htm

[71] Jensen K. D. (2004). Flow Measurements. Journal of the Brazilian Society of Mechanical Science and Engineering. XXVI(4): 400:419.

$$\boldsymbol{Beam\ diameter\ d(z)} = d_0\sqrt{1+\left(\frac{4\lambda z}{\pi {d_0}^2}\right)^2}\ \alpha z\ for\ z \to \infty \tag{2.2}$$

$$\boldsymbol{Beam\ diameter\ d(z)} = d_0\sqrt{1+\left(\frac{4\lambda z}{\pi {d_0}^2}\right)^2}\ \alpha z\ for\ z \to \infty \tag{2.3}$$

$$\boldsymbol{Wave\ front\ Radius\ R(z)} = z\left[1+\left(\frac{\pi {d_0}^2}{4\lambda z}\right)^2\right]\begin{cases}\infty\ for\ z \to 0\\ z\ for\ z \to \infty\end{cases} \tag{2.4}$$

Visually the laser beam appears to be straight and of constant thickness. It is important however to refer, that is not the case, since the measurements should take place in the beam waist to get the optimal performance of the LDA equipment. This is due to the wave front being straight on the beam waist and curve elsewhere. Taking into account the equation for the wave front radius, its approaches infinity for z approaching zero, meaning that the wave fronts are approximately straight in the immediate vicinity of the beam waist. This simplifies the calculations and allows the applications of the theory of the planes waves.

2.3.1.2 Bragg Cell

On this system the Bragg cell is often used together with a beam splitter. It is a glass crystal with a vibrating piezo crystal attached. The vibration generates acoustical waves acting like an optical grid and modulates the frequency of the laser beam.

The objective is to solve the problem of directional ambiguity, and a glass slab (Bragg cell, figure 67) is introduced into the path of the laser beams. On one side thereof, an electromechanical transducer driven by an oscillator produces an acoustic wave propagating through the slab generating a periodic pattern of high and low density movement. The opposite side of the slab is shaped to minimize reflection of the acoustic wave and is connected to a material that absorbs sound energy. The incident light beam reaches a series of wave fronts traveling acting as a thick diffraction grating. The interference of light scattered by each acoustic wave front causes a maximum intensity to be issued in several directions. By adjusting the acoustic signal strength and the θ_B angle of the Bragg cell, the intensity balance between the direct beam and first-order diffraction can be adjusted. The Bragg cell change adds a fixed frequency f0 for the diffracted beam. Since the particle velocity does not introduce a negative frequency deviation f_0 numerically greater than the Bragg cell will ensure a positive Doppler frequency f_D. This frequency change will thus allow the measurement of speed without directional ambiguity. Up measurable maximum velocity is limited only by the photo-multiplier and the response time constraints of electronic signals followed. In short, with the frequency offset to a beam relative to each other, the

interference fringes appear to move in the offset frequency and a “negative” frequency shift velocity (lower than the shift frequency) can be distinguished. In the probe, the parallel exit beams from the fibres are focused by a lens to intersect in the probe volume.

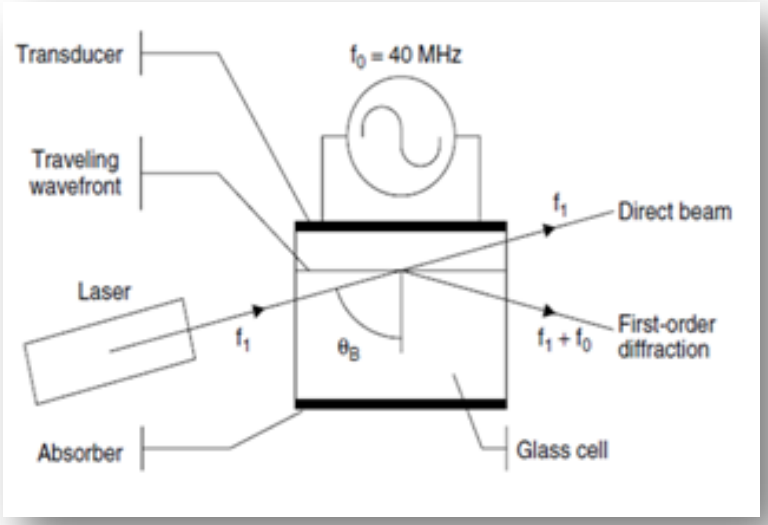

Figure 67: Bragg Cell principle[72]

2.3.2 The Probe Volume

The probe volume is typically a few millimetres long (figure 68). Since the distribution of light intensity across the beam diameter is Gaussian, the volume where the two beams intersect is an ellipsoid. The light intensity is modulated due to interference between the laser beams. This produces parallel planes of high light intensity, the so called fringes. The fringe distance d_f is defined by the wavelength of the laser light and the angle between the beams.

Each particle passage scatters light proportional to the local light intensity. Flow velocity information comes from light scattered by tiny "seeding" particles carried in the fluid as they move through the probe volume. The scattered light contains a Doppler shift, the Doppler frequency f_D, which is proportional to the velocity component perpendicular to the bisector of the two laser beams, which corresponds to the x axis shown in the probe volume. The scattered light is collected by a receiver lens and focused on a photo-detector. An interference filter mounted before the photo-detector passes only the required wavelength to the photo-detector. This removes noise from ambient light and from other wavelengths. Figure 69 shows schematically this process of velocity measurement.

[72] Blondel, D. 2010. Laser Doppler Anemometry. Handbook of Combustion. 2:7:189–217.

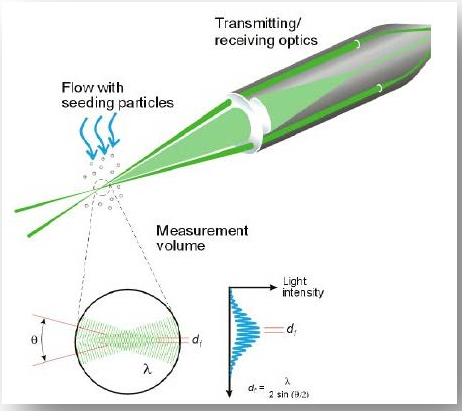

Figure 68: The probe volume[73]

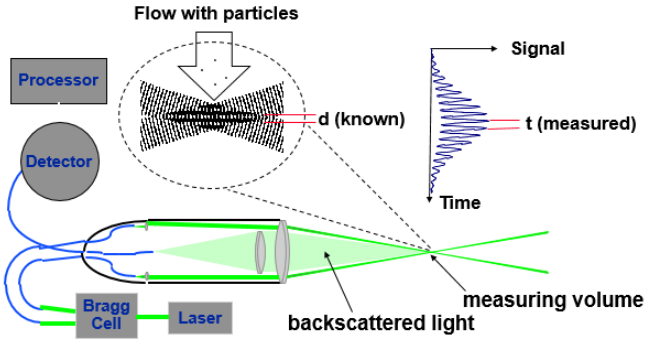

Figure 69: Velocity measurement[74].

2.3.3 Signal Processing

The photo-detector converts the fluctuating light intensity to an electrical signal, the Doppler burst, which is sinusoidal with a Gaussian envelope due to the intensity profile of the laser beams (figure 70).

The Doppler bursts are filtered and amplified in the signal processor, which determines f_D for each particle, often by frequency analysis[75] using the robust Fast Fourier Transform algorithm Dimotakis,1976)[76]. The fringe spacing, d_f provides information about the distance travelled by

[73] http://www.dantecdynamics.com/measurement-principles-of-lda

[74] http://www.dantecdynamics.com/measurement-principles-of-lda

[75] The burst frequency can also be determined using other methods such as counting the number of times that a filtered signal crosses the x-axis (Frequency Counters), but in the present study digital filtering and a FFT method were used.

[76] Dimotakis P. E. (1976). Single scattering particle laser Doppler measurements of turbulence. Proceedings of the AGARD Conference – Applications of non-intrusive instrumentation in Fluid Flow Research. 193.

the particle (figure 71). The Doppler frequency f_D provides information about the time:

$$t = 1/f_D \tag{2.5}$$

Since velocity equals distance divided by time, the expression for velocity thus becomes:

$$V = d_f . f_D . \tag{2.6}$$

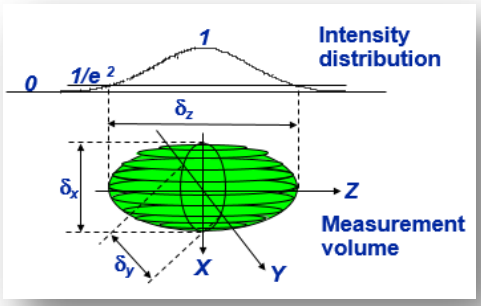

Figure 70: Measurement of the ellipsoid volume with a Gaussian intensity in 3 dimensions[77]

2.3.3.1 The fringe model

When two coherent laser beams intersect, they will interfere in the volume of the intersection. If the beams intersect in their beam waists, the wave fronts are approximately planes, and the interference will produce parallel planes of light and darkness.

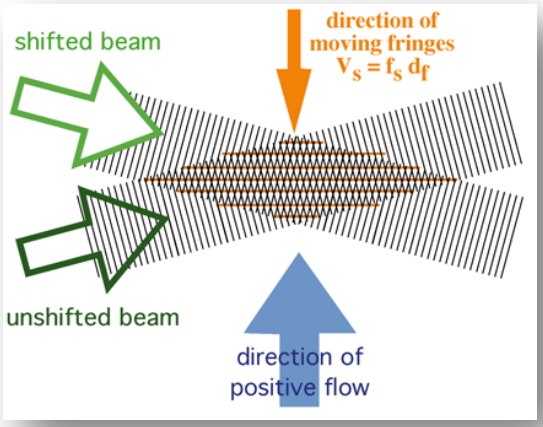

Figure 71: Fringes at the point of intersection of two coherent beams[78]

[77] http://www.dantecdynamics.com/measurement-principles-of-lda

[78] http://web.mit.edu/fluids-modules/www/exper_techniques/LDA.text.pdf

The interference planes are known as fringes, and the distance δ_f (or d_f) between them depends on the wavelength and the angle between the incident beams.

$$\delta_f = \frac{\lambda}{2sin(\theta/2)} \tag{2.7}$$

The fringes are oriented normal to the x-axis, so the intensity of the light reflected from a particle moving through the measuring volume will vary with a frequency proportional to the x-component, u_x, of the particle velocity.

$$f_D = \frac{u_x}{\delta_f} = \frac{2\sin(\theta/2)}{\lambda} u_x \tag{2.8}$$

If the two laser beam do not intersect at them beam waists, the wave fronts will be curved rather than plane, and as a result the fringe spacing will not be constant but depend on the position within the intersection volume. In this case the Doppler frequency will also depend on the particle position, and as such it will no longer directly proportional to the particle velocity, hence resulting in a velocity bias.

2.3.3.2 Measuring volume

The measurements take place in the intersection between the two incident focused laser beams, and the measuring volume is defined as the volume within which modulation depth is higher than e^{-2} times the peak core value. Due to the Gaussian distribution in the beam the measuring volume is an ellipsoid (see figure 70).

The length of the LDA measurement is:

length: $$\delta_z = \frac{4F\lambda}{\pi E D_L sin(\theta/_2)} \tag{2.9}$$

The width of the LDA measurement is:

width: $$\delta_y = \frac{4F\lambda}{\pi E D_L} \tag{2.10}$$

The height of the LDA measurement is:

height: $$\delta_x = \frac{4F\lambda}{\pi E D_L cos(\theta/_2)} \tag{2.11}$$

where: F is the lens' focal length, E is the beam expansion and D_L is the initial beam thickness (e^{-2}). (see table 5)

For a He-Ne laser the dimensions of the measuring control volume are given in the next paragraphs.

length: $$\delta_z = \frac{4 \times 400 \times 10^{-3} \times 633 \times 10^{-9}}{\pi \times 1 \times 1.35 \times 10^{-3} sin\left(2.78º \times 2/2\right)} = 40.084 \times 10^{-4} m$$

width: $$\delta_y = \frac{4 \times 400 \times 10^{-3} \times 633 \times 10^{-9}}{\pi \times 1 \times 1.35 \times 10^{-3}} = 2.007 \times 10^{-4} m$$

height: $$\delta_x = \frac{4 \times 400 \times 10^{-3} \times 633 \times 10^{-9}}{\pi \times 1 \times 1.35 \times 10^{-3} \cos\left(2.78º \times 2/2\right)} = 2.008 \times 10^{-4} m$$

For Diode laser:

length: $$\delta_z = \frac{4 \times 400 \times 10^{-3} \times 532 \times 10^{-9}}{\pi \times 1 \times 1.35 \times 10^{-3} sin\left(2.8º \times 2/2\right)} = 48.884 \times 10^{-4} m$$

width: $$\delta_y = \frac{4 \times 400 \times 10^{-3} \times 532 \times 10^{-9}}{\pi \times 1 \times 1.35 \times 10^{-3}} = 2.388 \times 10^{-4} m$$

height: $$\delta_x = \frac{4 \times 400 \times 10^{-3} \times 532 \times 10^{-9}}{\pi \times 1 \times 1.35 \times 10^{-3} \cos\left(2.8^o \times 2/2\right)} = 2.389 \times 10^{-4} m$$

2.3.4 Determination of the sign of the flow direction

The frequency shift produced by the Bragg cell makes the fringe pattern to move at a constant velocity which corresponds to the frequency shift. Particles which are not moving will generate a signal of the shift frequency f_{shift}. The velocities U_{pos} and U_{neg} will generate signal frequencies f_{pos} and f_{neg}, respectively (see figure 72). In general, the velocity is obtained from the frequency of the scattered light minus the frequency shift. The LDA

systems without frequency shift cannot distinguish between positive and negative flow direction or measure zero velocities.

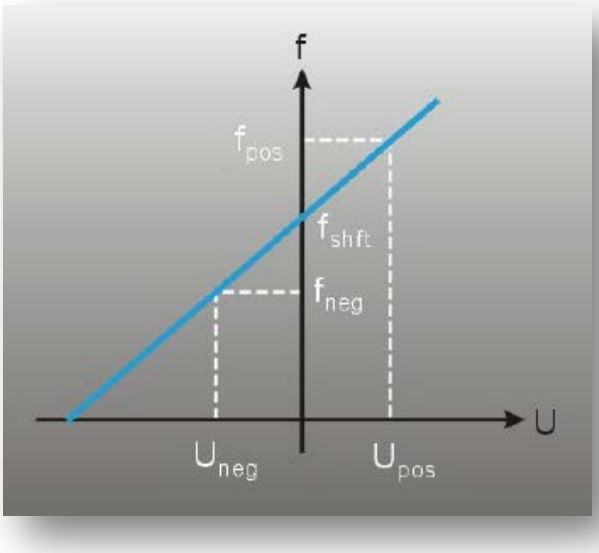

Figure 72: Doppler frequency to velocity transfer function for a frequency shifted LDA system.[79]

2.3.5 Signal Characteristics

The main objective of the LDA system user is to create an environment in which the measurement results can be obtained with minimal effort and cost. The main result of a LDA measurement is a current pulse from the photodetector, the frequency of which contains information related to the velocity to be measured and also contains the noise that can be obtained from various sources such as photo-detecting secondary electronic noise, thermal noise preamplifier circuit, optical noise, scattered light from outside the measurement volume, or impurities accumulated dirt, scratches on the walls of the test section, the ambient light, various particles , unwanted reflections, such as windows, lenses, mirrors. The number of simultaneous seeding particles in the measuring volume is very important to signal quality, and the performance of the signal processor. The figure below shows the filtered signal which is actually the input signal to the signal processor. The DC portion, which was removed by high- pass filter is known as the Doppler pedestal, and is often used as a trigger signal that starts from a sampling timing signal (figure 73).

The envelope of the modulated current Doppler reflects the Gaussian intensity distribution in the measurement volume. If the particles are present in more than simultaneously measuring volume, it is a multi-particle signal. The current detection is the sum of the power of each individual particle bursts within the illuminated region.

[79] http://www.dantecdynamics.com/measurement-principles-of-lda.

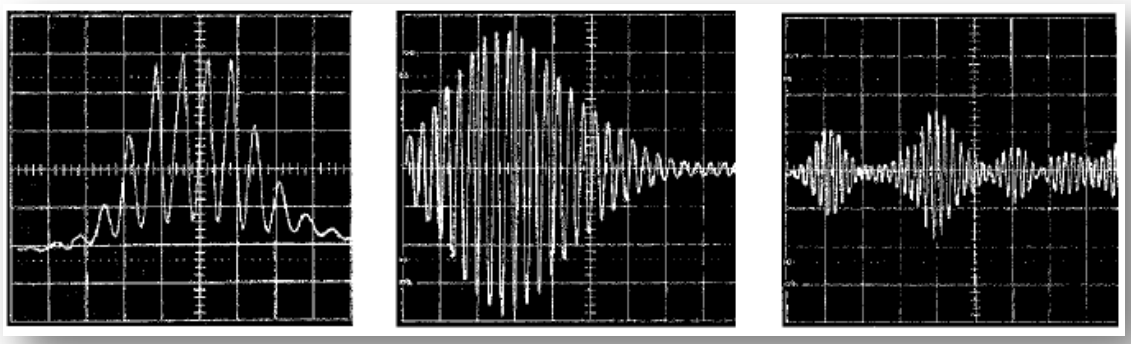

Figure 73: Typical Doppler burst of a particle or multiple particles: Left - Doppler Burst; Middle - Filtered and triggered Doppler burst; right - multiple particles[80].

2.3.6 LDA measurement errors estimation

As shown in figure 70, the main axis δz is much greater than δx and δy, due to the ellipsoid shape of the measuring volume. This makes widespread LDA retro sensitive to velocity gradients in the measuring volume. For a small dimensional measuring volume being traversed by marker particles a tight control on the size of the marker particles must exist. To LDA measure the velocity of particles suspended in the stream, they must be small enough to accurately control the flow and large enough to scatter enough light to detect the Doppler frequency. This limitation of particle size in order to be able to effectively disperse the laser light means that the particle diameter should be at least the same size as the laser light wavelength. Although LDA technique has many advantages over methods such as hot wire and hot film Anemometry, the resulting action may contain some specific errors of this technique, such as hardware errors, velocity bias, bias fringe and marginal distortion effects.

2.3.6.1 Fringes Bias

It is the source of errors associated with the direction of propagation of particles in the measuring volume, known as fringe bias and it was mindfully analysed by (Durão et al., 1980). Under a fixed relationship between signal and noise (S / N), the Doppler burst synchronization signal is dependent on the signal level above the background noise level and the minimum number of fringes shown in burst signal. The maximum number of fringes within the burst can often be achieved when the trajectory of the centre of the particles in the measuring volume intersects perpendicularly to the fringes. However, when the measurement volume is located near wall locations and regions of flow recirculation, the particles could travel to the parallel fringes in the measurement volume and no Doppler burst is produced. This will cause a reduction in the data rate and is a source of error for the particle velocity statistics.

[80] http://faculty.ksu.edu.sa/azzeer/Documents/534%20PHYS/LN7_LDA_s.pdf

2.3.6.2 Marginal distortion effects

The figure 74 illustrates four types of fringe distortion reported in the literature. The first three types (figure 74 a, b, c) were observed by (Zhang, 2010)[81]. The first type (figure 74a) takes place when the tangential velocity of the flow in a circular tube is measured without matching refractive index fluid. The second type (figure 74b) is considered simply as a matter of improper optical layout. The third type (figure 74c) associated with astigmatism due to the refractions of the laser beam and illustrates the movement of all four focal points of the two laser beams (A, B) from the measurement volume. This type of fringe distortion shown in (figure 74d) causes interferences in the fringe pattern.

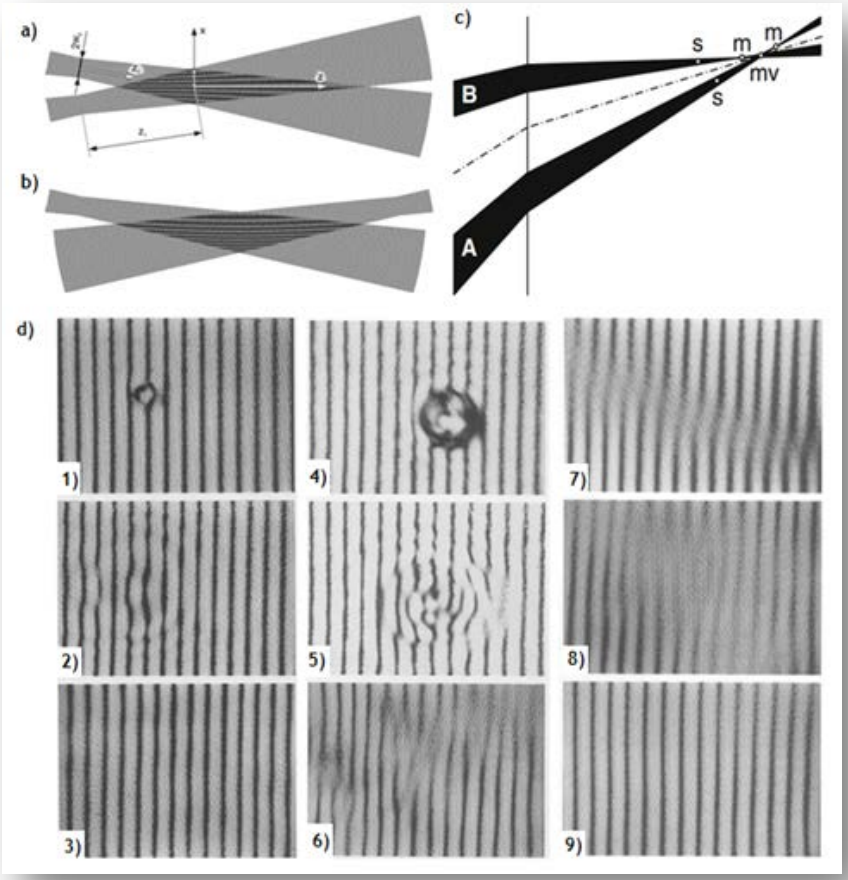

Figure 74: Different types of fringe distortion[82]

It is important to calculate the refraction angle associated to the beam passing through the test section made of Perspex. But first it is important to know what the refraction phenomenon is. Refraction is the change in direction of propagation of a wave due to a

[81] Zhang Z. (2010). *LDA Application Methods, Laser Doppler Anemometry Fluid Dynamics*. 1st edition, Springer-Verlag Berlin Heidelberg. e-ISBN 978-3-642-13514-9.

[82] Zhang, Z. (2010). *LDA Application Methods, Laser Doppler Anemometry Fluid Dynamics*. 1st edition, Springer-Verlag Berlin Heidelberg e-ISBN 978-3-642-13514-9.

change in its transmission medium. This phenomenon can be explained through the conservation of energy and conservation of momentum. Due to change the medium, the phase velocity of the wave is changed but its frequency remains constant. The refraction light is the most commonly observed phenomenon, but any type of the wave can refract when it interacts with a medium. The law that describes the refraction is the Snell's law, which states that for a given pair of media and a wave with a single frequency, the ratio of the sines of the angle incidence θ_1 and angle of refraction θ_2 is equivalent to the opposite ratio of the indices of refraction:

$$\frac{\sin\theta_1}{\sin\theta_2} = \frac{n_2}{n_1} \tag{2.12}$$

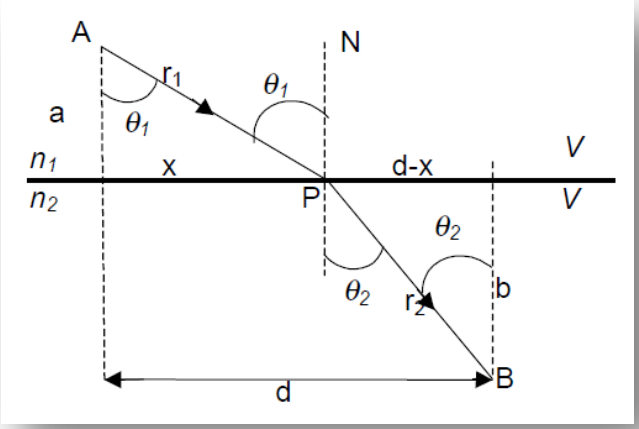

Figure 75: Refraction of light to pass through two transparent distinct material means.[83]

For the Perspex refractive index equal to 1.495, the air refractive index equal 1 and θ_1 (Calculated half-angle of beam intersection, see table 5) , refraction θ_2 is calculated as follows:

$$\theta_2 = \sin^{-1}\left(\frac{\sin\theta_1}{n_2}\right) \tag{2.13}$$

As shown in table 5 the two lasers used have almost the same values of θ, giving a value of θ_1 equal to 2.8°. So, the value of θ_2 is equal to:

$$\theta_2 = \sin^{-1}\left(\frac{\sin 2.78^o}{1{,}495}\right) \rightarrow \theta_2 = 1{,}872^o \tag{2.14}$$

[83] Apostila teórica – Óptica Técnica I – Faculdade de Tecnologia de São Paulo. Lilia Coronato Courrol and André de Oliveira Preto.

Knowing now what the refractive angle is possible to calculate which is the error Δz that refraction causes on the volume control positioning.

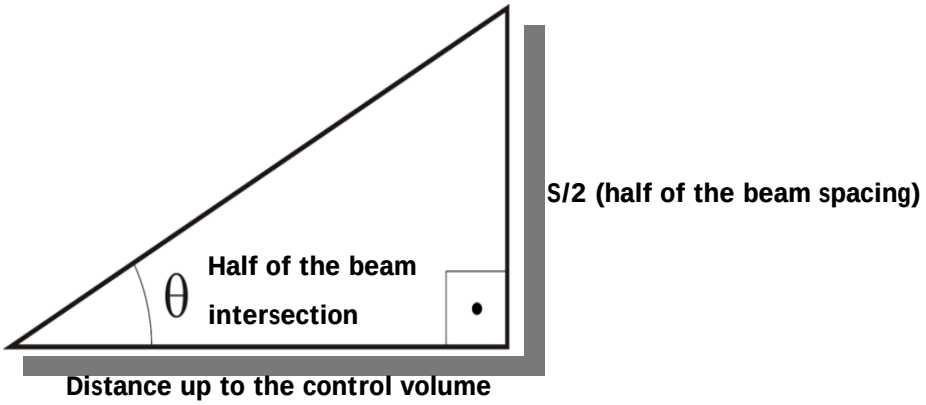

Applying the Pythagoras theorem, without refraction:

$$z_{without\ refraction} = \frac{S/2}{\tan 2.8^o} \rightarrow z_{without\ refraction} = 0.3974\ m \tag{2.15}$$

With refraction

$$z_{with\ refraction} = \frac{S/2}{\tan 1.87^o} \rightarrow z_{with\ refraction} = 0.5953\ m \tag{2.16}$$

$$\Delta z = z_{with\ refraction} - z_{without\ refraction} = 0.1979\ m \tag{2.17}$$

As it was known in advance that this refractive effect would move the control volume position, during the preparation of the experimental activity this question was taking into account and the control volume was correctly positioned in the symmetry plane of the test section by the adjust of the LDA laser positioning through the transverse unit where it was installed. So this question does not represent a source of error to the measurement process.

In sub section 2.3.3.2 it was described how to calculate the control volume dimension. Looking at the equations that described the measures of the volume control (length and height), they are dependent of beam angle intersection, θ. So, the refraction of the beams also influences the dimension of the control volume. The new dimensions of the control volume are given in the next page.

For the He-Ne laser:

length: $$\delta_{z(refracted)} = \frac{4 \times 400 \times 10^{-3} \times 633 \times 10^{-9}}{\pi \times 1 \times 1.35 \times 10^{-3} sin\left(1.87º \times 2/_2\right)} = 61.504 \times 10^{-4} m$$

width: $$\delta_{y(refracted)} = \frac{4 \times 400 \times 10^{-3} \times 633 \times 10^{-9}}{\pi \times 1 \times 1.35 \times 10^{-3}} = 2.007 \times 10^{-4} m$$

height: $$\delta_{x(refracted)} = \frac{4 \times 400 \times 10^{-3} \times 633 \times 10^{-9}}{\pi \times 1 \times 1.35 \times 10^{-3} \cos\left(1.87º \times 2/_2\right)} = 2.008 \times 10^{-4} m$$

For the Diode laser:

length: $$\delta_{z(refracted)} = \frac{4 \times 400 \times 10^{-3} \times 532 \times 10^{-9}}{\pi \times 1 \times 1.35 \times 10^{-3} sin\left(1.87º \times 2/_2\right)} = 73.180 \times 10^{-4} m$$

width: $$\delta_{y(refractd)} = \frac{4 \times 400 \times 10^{-3} \times 532 \times 10^{-9}}{\pi \times 1 \times 1.35 \times 10^{-3}} = 2.388 \times 10^{-4} m$$

height: $$\delta_{x(refracted)} = \frac{4 \times 400 \times 10^{-3} \times 532 \times 10^{-9}}{\pi \times 1 \times 1.35 \times 10^{-3} \cos\left(1.87º \times 2/_2\right)} = 2.389 \times 10^{-4} m$$

Compared this results with those obtained in section 2.3.3.2 for the case without refraction, it can be concluded that the refraction effect only have effect on the length of the control volume, making it longer.

$$\Delta\delta_{z(He-Ne\ laser)} = \delta_{z(refracted)} - \delta_z = 61.504 \times 10^{-4} - 40.084 \times 10^{-4} = 21.420 \times 10^{-4} m$$

$$Error = \frac{21.420 \times 10^{-4}}{61.504 \times 10^{-4}} \times 100 = 34.8\%$$

$$\Delta\delta_{z(Diode\ laser)} = \delta_{z(refracted)} - \delta_z = 73.180 \times 10^{-4} - 48.884 \times 10^{-4} = 24.296 \times 10^{-4} m$$

$$Error = \frac{24.296 \times 10^{-4}}{73.180 \times 10^{-4}} \times 100 = 33.2\%$$

The results show that for the two colour laser beams, the refraction effect increases the control volume length by approximately 30%. With the volume control increase there is an increase of the noise in the laser anemometer measurement through the current pulse that comes from the photodetector. This current contains the frequency information relating to the velocity to be measured. The primary source of noise is the photo detection shot noise, which is a fundamental property of the detection process. The interaction between the optical field and the photo-sensitive material is a quantum process, which unavoidably impresses a certain amount of fluctuation on the mean photocurrent. In addiction there is mean photocurrent and shot noise from undesired light reaching the photodetector. A laser anemometer is most advantageous operated under such circumstances that the shot noise in the signal is the predominant noise source. This shot noise limited the performance can be obtained by proper selection of laser power, seeding particle size and optical parameters. In addition, noise should be minimized by selecting only the minimum bandwidth needed for measuring the desired velocity range by setting low-pass and high-pass filters in the signal processor input.

For the quality signal and the performance of the signal processor it is very important the number of seeding particles present simultaneously in the measuring volume. As it seen before the refraction effect increased the measuring volume. This means that a higher number of seeding particles passes through the measuring volume, increasing the noise on the signal. If on average much less than one particle is present in the volume, we speak of a burst type Doppler signal. A typical Doppler burst signal is shown in the figure 76. The figure shows the filtered signal which is actually input to the signal processor. Through the high pass filtered remove the DC-part also known as the Doppler Pedestal, and it is often used as a trigger-signal, which starts sampling of an assumed burst-signal. The envelope of the Doppler modulated current reflects the Gaussian intensity distribution in the measuring volume.

If more particles are present in the measuring volume simultaneously, it is a multi-particle signal. The detector current is the sum of the current bursts from each individual particle within the illuminated region. Since the particles are located randomly in space, the individual current contributions are added with random phases, and the resulting Doppler signal envelope and phase will fluctuate.

Although the size of the measuring volume has been increased by the Perspex refractive effect, by adjusting the LDA signal properties it was possible to calibrate the signal.

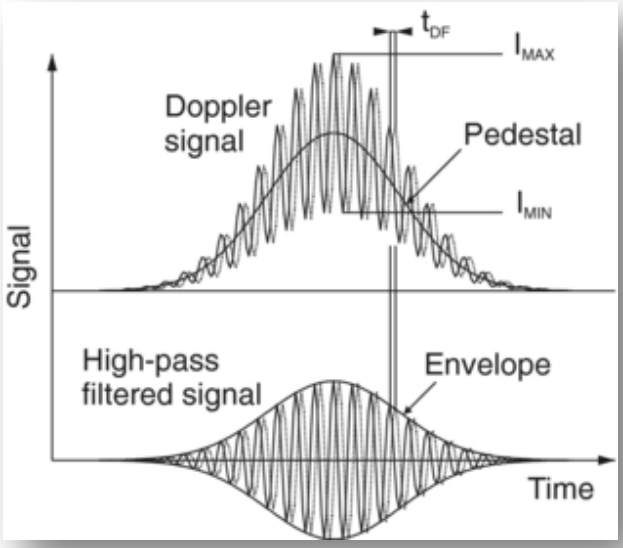

Figure 76: Doppler signal obtained by two close detectors[84].

2.3.7 LDA characteristics

The velocity field was measured with a two-colour (two-component) Laser-Doppler velocimetry (Dantec Flowlite 2D), which comprised a 10mW He-Ne and a 25mW diode-pumped frequency doubled Nd:YAG lasers, sensitivity to the flow direction provided by frequency shifting from a Bragg cell at f_0=40MHz, a transmission and backward-scattered light collection focal lens of 400mm. The half-angle between the beams was 2.8° and the calculated dimensions of the axis of the measuring ellipsoid volume at the e^{-2} intensity locations were 135x6.54x6.53μm and 112x5.46x5.45μm respectively (see Table 5 for details). The horizontal and vertical mean and turbulent velocities were determined by a two-velocity channel Dantec BSA F60 processor. The transmitting and collecting optics is mounted on a three-dimensional traversing unit, allowing the positioning of the centre of the control volume within ±0.1mm (figure 77).

Errors incurred in the measurement of velocity by displacement and distortion of the measuring volume due to refraction on the duct walls and change in the refractive index were found to be negligibly small and within the accuracy of the measuring equipment (see LDA signal calibration on section 3.1.4). Non-turbulent Doppler broadening errors due to gradients of mean velocity across the measuring volume may affect essentially the variance of the velocity fluctuations, but for the present experimental conditions are of the order of $10^{-4}V_j^2$ and, therefore, sufficiently small for their effect to be neglected. The largest statistical (random) errors derived from populations of, at least, 10000 velocity values were of 0.5 and

[84] Calvo Garcia J., Santolaya J. L., Garcia I., Aisa L. (2012). A framework about flow measurements by LDA – PDA as a spatio-temporal average: application to data post-processing. Measurement Science and Technology. 23 (17pp). doi:10.1088/0957-0233/23/5/055202

	He-Ne laser	Diode Laser
- Wave length, λ [nm]	633	532
- Focal length of focusing lens, f [mm]	400	400
- Beam diameter at e-2 intensity [mm]	1.35	1.35
- Beam spacing, s [mm]	38.87	39.13
-Calculated half-angle of beam intersection, θ	2.78°	2.8°
- Fringe spacing, d_f [μm]	6.53	5.45
-Velocimeter transfer constant, K [MHz/ms^{-1}]	0.153	0.183

Table 5: Principal characteristics of the 2D Laser-Doppler velocimeter

Figure 77: Data acquisition system (left) and Optical and transverse unit (right).

3%, respectively for the mean and the variance values, according to the analysis recommended by (Melling and Whitelaw, 1975)[85] for a 95% confidence interval.

No corrections were made for sampling bias, but no correlations were found between Doppler frequencies and time interval between consecutive bursts even in the zones of the flow characterized by the lowest particle arrival rates, suggesting that those effects are unimportant for the present flow conditions. Systematic errors incurred in the measurements of Reynolds shear stresses can arise from lack of accuracy in the orientation angle on the normal to the anemometer fringe pattern, as shown by (Baker, 1980)[86], and can be particularly large in the vicinity of the zones characterized by zero shear stress: for the present experimental conditions the largest errors are expected to be smaller than -2.5%.

[85] Melling A., Whitelaw J.H. (1975). Turbulent Flow in a Rectangular Duct. *Journal of Fluid Mechanics*. **78**: 285-315.

[86] Baker O.J. (1980). The Turbulent Horseshoe Vortex. Journal of Wind Engineering and Industrial Aerodynamics. 6 (1-2): 9-23.

Chapter 3

Experimental Results

This chapter presents the flow visualization and the LDA measurements.

The first subchapter describes the calibration of the experimental set-up. The second subchapter presents the main results of the flow visualization studies. Finally, the mean and turbulent velocity measurements for all of the velocity ratios are presented.

3.1 Calibration

The pressure, velocity and direction determination are essential to the flow studies. Most of the flows are turbulent, with enhanced rates of transport of heat and mass. Turbulence is responsible by most of the friction loss, translated into pressure losses on fluid systems. In this section all the calibrations carried out on the experimental set up will be presented.

According to the International Bureau of Weights and Measures, calibration is defined as the operation that, under specified conditions establishes a relation between the quantify values with measurement uncertainties provided by measurement standards and corresponding indications with associated measurement uncertainties of the calibrated instrument, using the information to establish a relation for obtaining a measurement result from an indication. The calibration process before the beginning of the experimental study avoids some errors. The nature of these errors is quite varied, and may be due adjustments in the frequency of the vector drive which feeds the crossflow, the pressure imposed on the input of system that powers the impingement jets as well as the calibration signal that LDA system receives at each particle measurement. Each device used in the experimental activity plays an important role in the definition of the experimental conditions (crossflow velocity, jets velocity, velocity ratio, pressure, temperature and others.). The wind tunnel is fed by an axial fan controlled by a vector drive, allowing the continuous variation of the crossflow velocity, with a smaller turbulence intensity. So, the crossflow velocity is the result of the frequency imposed in the vector drive. In the experimental installation where this work has been done, the axial fan is installed on the outside of the laboratory. The weather conditions (temperature, humidity, pressure) are not constant every day, and this is a question to take into account during the experimental activity. At this point it is important to differentiate the control variables calibration and the instrument calibration. The calibration in the control variables affected directly the constant values of the variables imposed to the experimental work, i.e. helps to define the initial conditions of the experiments (impinging jets velocity,

crossflow velocity). On the other hand, the calibration measurement instruments are used to maintain instrument accuracy, avoiding some errors in the results during the experimental activity and providing the best performance of the system.

The calibration of this experimental facility was essentially focused on four fundamental points:

- Crossflow calibration
- Impinging jets calibration
- Seeding calibration for the visualization
- LDA signal calibration

3.1.1 Crossflow calibration

It should be pointed out that the wind tunnel calibration was carried out without the presence of the impinging jets, and with a wind tunnel fan operational frequency of 30 Hz. The velocity of the wind tunnel was fixed through the frequency controller to 30 Hz (figure 78).

The crossflow velocity for the imposed frequency was higher than the required crossflow velocities for the three different velocity ratio studied. In this case the crossflow velocity calibration was essential.

Figure 78: Wind tunnel control variation

The crossflow calibration consisted mainly on the guillotines adjustment to control the air passage from the compressor to the wind tunnel (figure 79). The crossflow and the seeding were feed with the flow produced by a single fan. So, two separate guillotines were needed, and the corresponding flows were dependent on its position as well as on the working point of the compressor which was set using the control variation. Since the correct position of the guillotine in order to obtain the required velocity ratio was unknown, the mean crossflow velocity was measured for several positions of the guillotines.

In the test A, the guillotine 1 was completely closed, and the opening of the guillotine 2 was decreased (figure 80) . In test B the guillotine 2 was fully opened, and the opening of the

guillotine 1 was increased. Finally, in test C the guillotine 1 was fully opened, and the opening of the guillotine 2 was decreased

Figure 79: Guillotine illustration

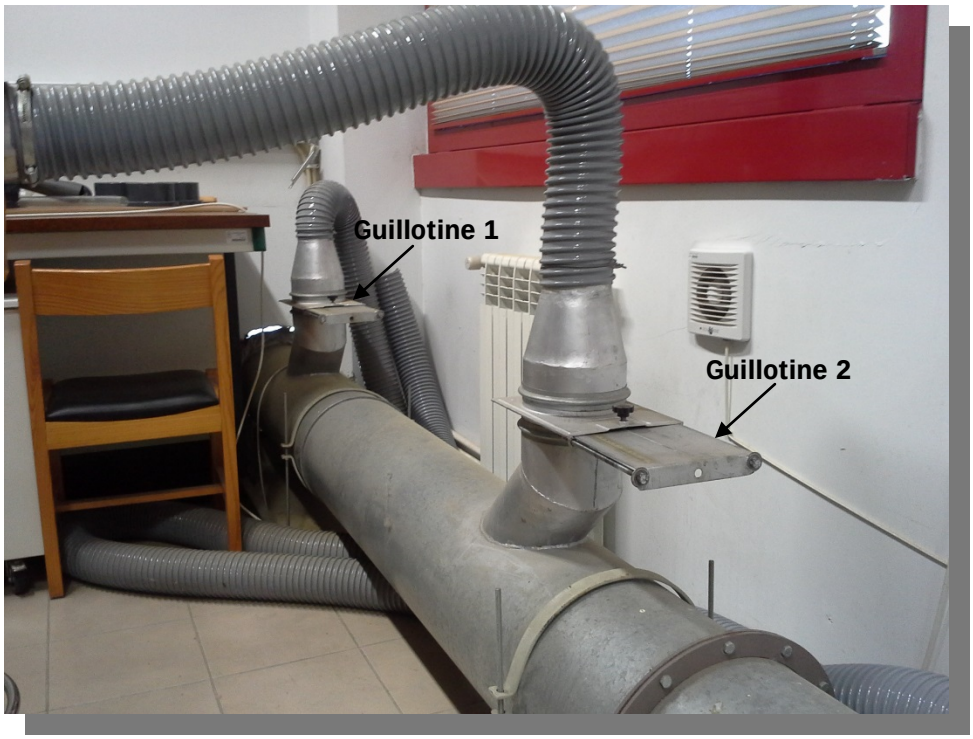

Figure 80: Location of guillotines 1 and 2 on the experimental setup.

The results of tests A and B revealed that the changes on the crossflow velocity were very small (figure 81). In the case of test C, the opening variation of the guillotine 2, keeping the guillotine 1 fully opened, allows a good control of the crossflow velocity.

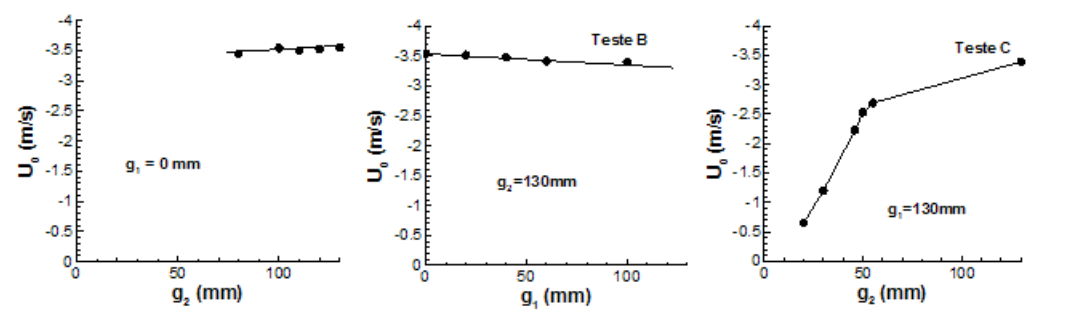

Figure 81: Graphics of the guillotine position study: test A-left, test B-centre, test C-right.

3.1.2 Impinging jets calibration

The impinging jets calibration was performed with a constant crossflow velocity corresponding to a reading value of 0.63 mm of H_2O in the micromanometer. The present micromanometer (Furness Controls FC012) is a sensitive instrument that can measure very small pressure differences in the range of ±199.9Pa with an error less than ±0.5%.

The jets were supplied with air from a compressor. Each jet unit had a separate pipe and pressure control valve. The calibration was performed with the laser anemometer measuring the mean vertical velocity at the centre of the jet. The results obtained are shown in figure 82. This figure shows that up to a pressure of approximately 5 bars in the pressure control valve, the impinging jet velocity increases linearly with the pressure. For pressures above 5 bars it was found a hysteresis cycle, indicating the possibility of the presence of a shock wave inside the jet unit.

Through this calibration it was stipulated that the guillotine 1 position would be 130 mm and the guillotine 2 position would be 32 mm corresponding to a crossflow velocity of U_0=1.067m/s. To obtain the desired velocity ratio V_j/U_0, the jet exit velocity, V_j, was set using the pressure control valves. Changing the crossflow velocities with guillotine 2 more different combinations could be set.

As already mentioned before, it was quite difficult to seed the flow at the potential core region of each jet, and a new seeding apparatus with a deposit was designed. Since there had been a change in the experimental rig, it was re-calibrated. First, the jets were calibrated again. Since the nozzles were now fed by the deposit, its pressure was used for calibration purposes. As the deposit had also inside the sprayer, the pressure imposed to the sprayer was taken into account as well, in order to produce the seeding. The jets pressure on the exit of the deposit was a result of the imposed sprayer pressure and the inside deposit pressure.

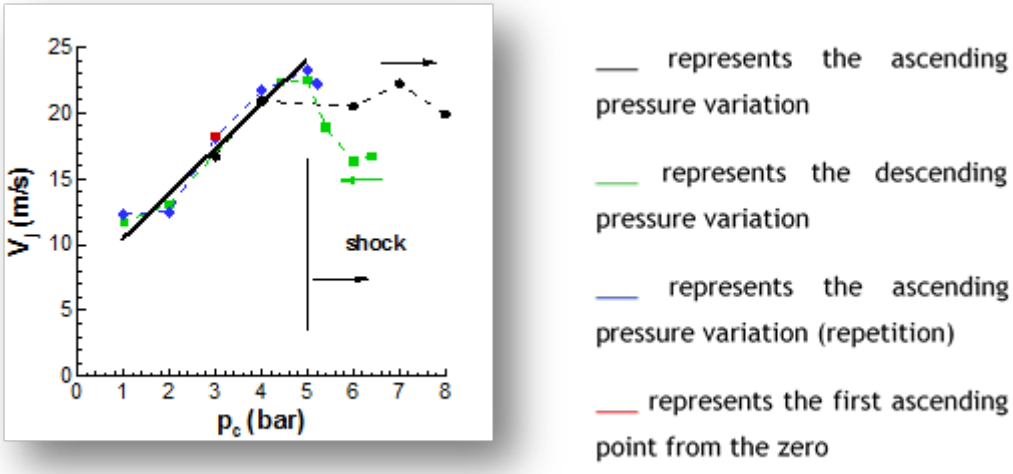

Figure 82: Impinging jets calibration

Figure 83: Micro manometer used in the crossflow calibration

It must also be added some pressure drop arising from the tubes that connect the deposit to the test section and the links between the deposit output and the hoses of the both impinging jets. The recalibration of the jets was made analogously to the previous calibration, beginning with the measurement of the impinging jet velocity at the point in the centre of the jet and near of the impinging jet exit. The pressures imposed to the sprayer (inside of the tank) were always greater than 0.4 bar of pressure imposed into the deposit inside. This extra pressure in the sprayer was necessary to avoid the rise of the sprayer mixture and beginning to leak out of the deposit through tube that provided the pressure for the inside of the deposit. Thus, the pressure chosen for the deposit inlet was 2 bar and 2.4 bar for the sprayer. Taking into account the calibration performed for the nozzles, the velocity of the impinging jet at the test section entrance for this pressure range would be approximately V_j = 36 m/s. Taking this jet velocity value into account it was carried out the crossflow calibration for the three different velocity ratios, adjusting position of the guillotine 1 and 2. Again, it was concluded that the easier way to control the crossflow velocity would be to fully open the

guillotine 1 and varying the opening of the guillotine 2. To monitor the crossflow velocity at the exit of the wind tunnel a micro manometer was used. This device allowed us to know through a pitot tube at each moment the dynamic fluid flow pressure that it was expressed by the difference between the stagnation pressure and the static pressure (H) in H_20 mm.

From the Bernoulli equation of fluid mechanics:

$$P_T = P_0 + \frac{1}{2}\rho {U_0}^2 \tag{3.1}$$

$$U_0 = \sqrt{\frac{2(P_T - P_0)}{\rho}} \tag{3.2}$$

As these expressions depend of the fluid density, the position of the guillotine 2 was verified every day (the weather conditions, like temperature, pressure, humidity, were different every day) to ensure that the crossflow velocity was the correct to the velocity ratio used. The ambient pressure and temperature of the laboratory were obtained through an analogical manometer present in the room.

The static pressure can be obtained through a tube in the coaxial direction with lateral holes perpendicular to the flow (Prandtl tube, figure 84).

Through the calibration graph it was easily identifiable which positions the guillotine 2 had to be set to obtain the velocity ratios required. The final results are presented in the table 6.

Velocity ratio [V_j/U_0]	Guillotine 2 position [mm]	Guillotine 1 position[mm]	Crossflow velocity [m/s]
22.5	41.5	130	1.6
33.7	32		1.067
43.8	27.3		0.8

Table 6: Crossflow calibration results

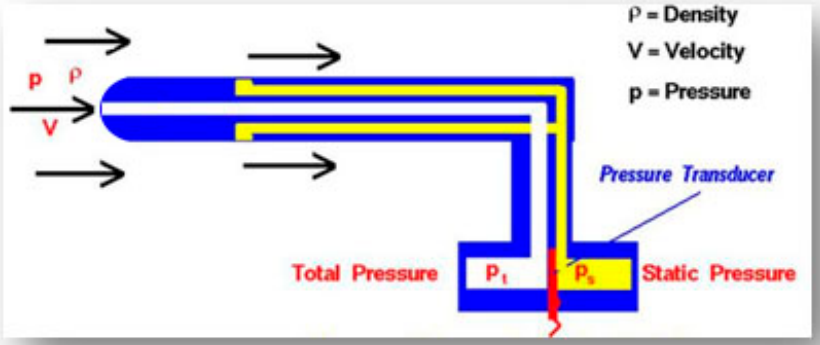

Figure 84: Prandtl tube schematic drawing[87].

The jet exit velocity profiles were measured in the vertical plane of symmetry without the presence of the crossflow (figure 85). The profile included 22 points, more concentrated near the jets and at the outside of the impinging jets with the laser LDA inclined half-angle of the beam intersection (2.8º) to allow the measurements near the jet exit plane. The results showed similar profiles for both jets exhibiting a good symmetry and the difference between the maximum values was less than 1.5%. The profile is approximately parabolic as expected due to the design of the nozzle with a small variation of area from the feeding pipe.

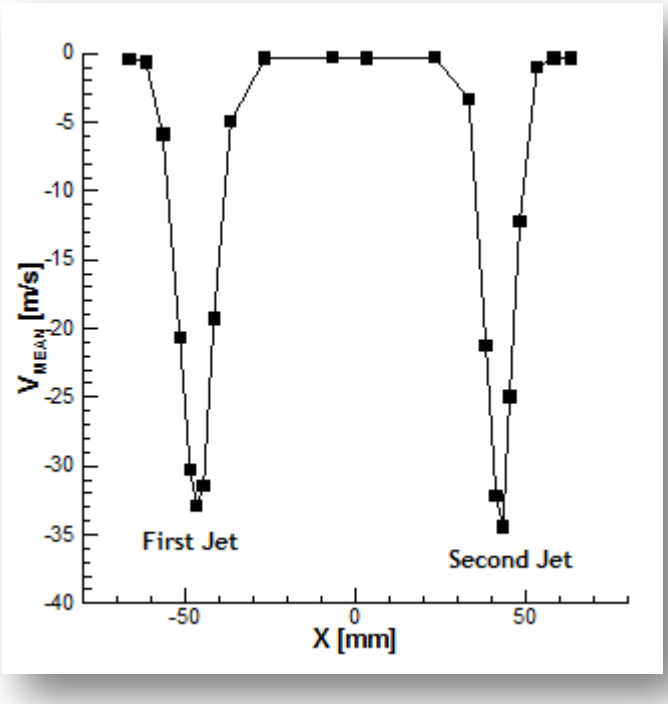

Figure 85: Jet exit profiles

[87] Adapted from https://www.grc.nasa.gov/www/k-12/airplane/pitot.html

During the flow visualization it was found that seeding insemination was insufficient. It was noticeable the droplets condensation of the mixture glycerine + water in the tubes as well as in impact surface, and that sometimes stop the experimental procedure for cleaning the test section. It was also verified the existence of drops in the nozzle fluid itself which would give wrong results in the flow measurement. To correct this situation it was installed the solution described in the chapter 2 on the section 2.2. This installation was calibrated so as to adjust the imposed pressure for each jet, and the opening of the control pressure valves.

3.1.3 Seeding calibration

The seeding system was presented and described in chapter 2 on the section 2.2 (Seeding System). The calibration of the system was performed experiencing several positions of the tap that induces a pressure drop to allow the seeding suction to the main flow (position 10 in the figure 60). The pressure that comes from the compressor was always kept constant during all the calibration process, equals to 2 bars. The power level of the heat plates was also calibrated, and it was found that the better power level to obtain the intended results was the maximum power level. It is important to note that as this is a method where the seeding has to be heated in order to produce fog, it is important that the seeding system turns on 20 minutes before starting the experimental activity.

3.1.4 LDA operation

The Doppler signal processors have the essential task of estimating the frequency of oscillation of the Doppler signal. Achieving this goal is always hampered by the presence of noise in the Doppler signal (as referred in sub section 2.3.6.2 – Marginal distortion effects) , which comes from different sources of noise, such as laser modulation noise, the difference in the optical path of the incoming laser beams, the distortion of the front stage marker particles on the input beam, distortion of the laser beams in the measuring volume due to tracer particle, the noise photo-current amplification or noise in electronic filters and amplifiers of the processor. The accuracy of the result depends on these measurement conditions, signal quality, the care taken by the user, etc. Because of this, as a Doppler burst signal is determined by the properties of shape, size and particle surface, as well as the alignment of the optical system and the actual path that the particle takes as it passes through the measuring volume. To do the measurements a good Doppler burst is required. According to the instructions in the installation guide and user BSA Flow Software, the validation rate is a good indicator of a good Doppler burst. These instructions were used to obtain a good data rate and validation adjusting the high voltage settings and the gain register settings in the length range and gain properties.

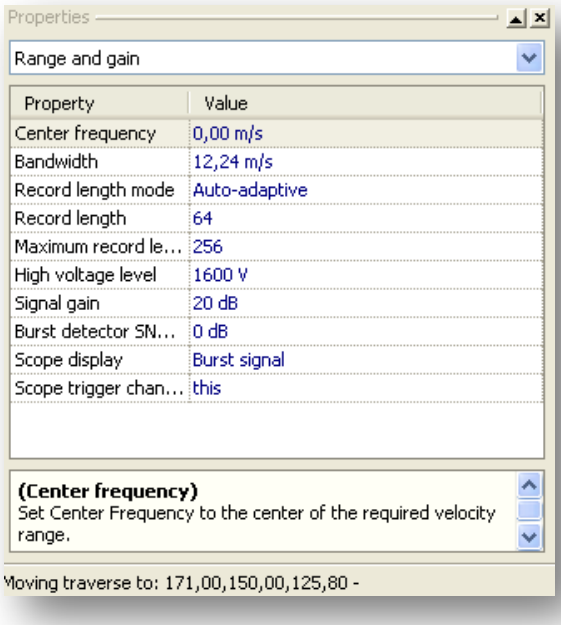

Figure 86: LDA signal settings and properties of the range and gain

Figure 86 shows an example of the calibration result of a burst (figure 87), following the Dantec Flow Lite User Guide recommendations.

Figure 88 exemplify the process used to eliminate the noise of the burst, due to the increase of the measuring volume provoked by the refractive effect of the Perspex. Due to the turbulent nature of the flow under investigation, with zones of very low velocity where the seeding particles were scarcer, sometimes during the experimental work it was necessary to adjust the range and gain signal properties in order to extract the most correct results.

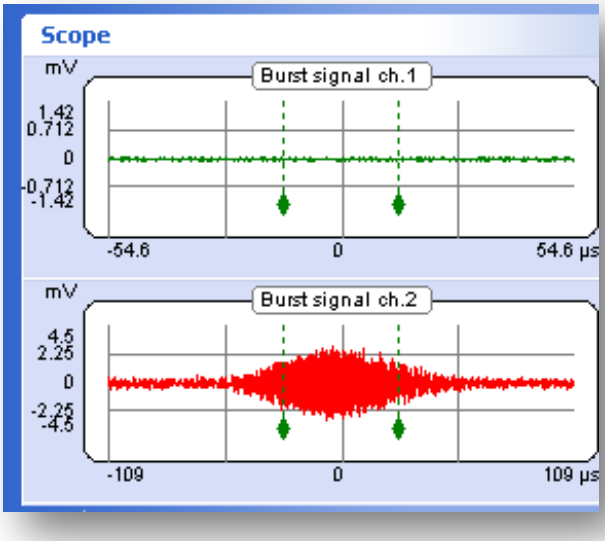

Figure 87: Doppler burst signal calibration.

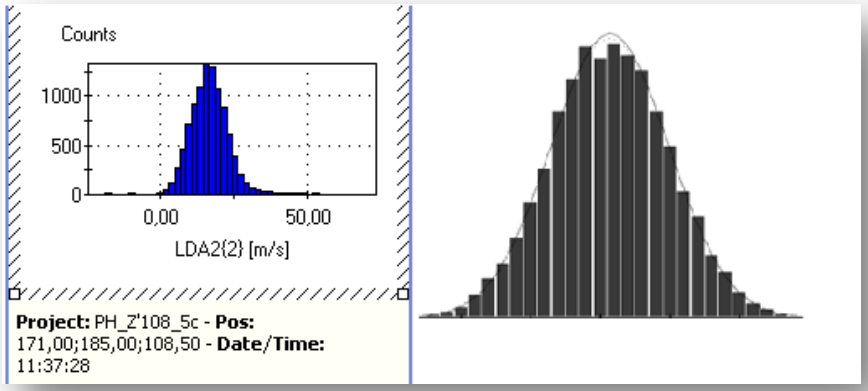

Figure 88: Gaussian distribution (PDF) of a jet flow measured by the method LDA: (left) PDF obtained in the present work by the BSA Flow Lite; (right) theoretical free jet PDF.

All noise speeds that appeared out of this "bell-shaped" have been removed for a more thorough presentation of the velocity results. In this work, all the measurements were made with similar light conditions. The particles marker emission (seeding) was maintained constant.

Each time the measurements had to be restarted, the last two previously measured points were repeated in order to compare the results and check if the entire installation was in the ideal conditions for continuing the measurements. Every time the measurement process suffered some disturbance, this measurement was repeated at the point in question with at least 10,000 samples. Several times it was used as repetitive (continuous) acquisition mode to set-up the output BSA properties without data acquisition. The main parameters for optimizing the BSA property settings are validation and data rate. The validation was always high, often close to 100% and the data rate was good at a few points, with 10,000 samples in less than 120 s. Elsewhere, for lack of marker particles in the flow, the data rate was low and the 5000 samples were used instead. The LDA Laser lens was cleaned every 20 hours of use with a suitable product and a cloth provided by the LDA system manufacturer.

The use of 10,000 samples per measured point allows a statistical result with a maximum relative error for a 95% confidence interval of approximately 0.5% at medium speed and 1.4% in the turbulent intensity according to Yanta and Smith (1978)[88].

The measurements presented in this chapter were partially presented at Vieira (2012), and were extended to conditions beyond the limits of the experimental rig by means of a computational investigation that will be presented in chapter 4.

[88] Yanta W.J., Smith R.A. (1978). Measurements of Turbulent Transport Properties with a Laser-Doppler Velocimeter. *Proceeding of the 11th Aerospace Sciences Meeting*, Washington. AIAA Paper 73-0169

3.2 Visualization

Flow visualization was performed using digital direct photography to guide the choice of the measurement locations and to provide a qualitative picture of the flow. The longitudinal plane of symmetry was illuminated with a sheet of light. This sheet was used to illuminate any cross section that has been seeded with particles. The laser light was dispersed by the seeding particles, and dark images were observed where there was an absence of seeding particles. The photos were taken perpendicular to the vertical plane of symmetry with the camera installed in a tripod to eliminate the vibrations in the photos. The camera used to obtain the images was the Canon 600D (figure 89). This camera has a CMOS APS-C sensor with 18 megapixels that captures images packed with detail and clarity. The ISO range of 100-6400, extendable to ISO 12800, allowed photographing manually and with high quality in low light, without flash. At the heart of the Canon EOS 600D is a 14-bit DIGIC 4 image processor that provided an exceptional colour reproduction, smooth colour gradation and strictly control the noise. The nine AF points, including one central cross-type sensor, spread across the frame for fast, accurate focusing, even with off-centre subjects. The iFCL 63-zone metering always ensures precise exposures. The lens used in the camera was the Canon EF-S 18-55mm f/3.5-5.6 IS II, a zoom lens compact and versatile. The EF-S 18-55mm f / 3.5-5.6 IS II is a standard zoom lens ideal for general applications. The four points Image Stabilizer provides great performance in low light.

Figure 89: Camera used to obtain the visualization images[89].

To create the sheet light it were used 2 different mechanisms simultaneously: a set of three LED high-powered spotlights in the top of the test section (figure 90) and two He-Ne lasers (figure 91).

In the case of the three led spotlight, the entire top of the test section was coated with black paper, with the exception of a strip of about 1 cm in the centre which was coated with

[89]http://www.canon.pt/support/consumer_products/products/cameras/digital_slr/eos_600d.aspx?type=drivers&language=&os=WINDOWS%207%20(64-bit)

"cellophane" red paper, so as to pass the spotlights light and so create the sheet of light in the plane of symmetry.

The lower frequency laser was used to reinforce the sheet light created by the procedure described above and recommended by (Véret C., 1985)[90] and (Porcar et al. 1983)[91]. The beam of light from the two lasers is directed to a cylindrical lens to create a thin sheet of laser light.

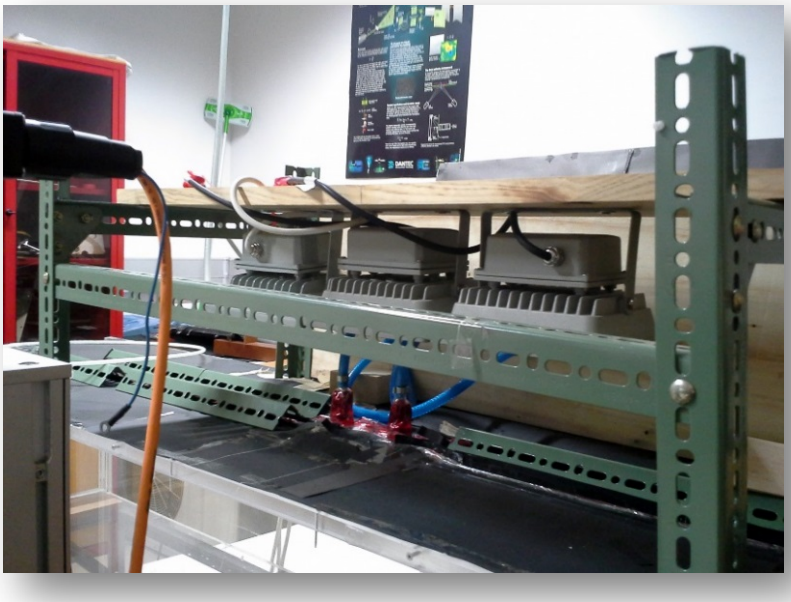

Figure 90: A set of three spotlights.

For the flow studied, the results have shown a pattern similar to that of a single impinging jet (figure 93). Figures 94 to 95 identify the flow development along the vertical plane of symmetry, i.e. Z=0 for the three different velocity ratio studied. Each jet has an initial potential-core jet region, where the flow characteristics are identical to those of a free jet, and near the horizontal plate the impingement region, characterized by considerable deflection of the first jet. This behaviour occurs because in this study H / D >> 1, then the presence of the impact plate has a more reduced interference. The most intense zone of the flowfield is the free jet region. As the jet widening will begin to feel the presence of the impact surface so that the flow is characterized by a significant deflection of the jet.

As the jet approaches to the impact surface (figure 93), the axial velocity decreases rapidly with the increasing of the static pressure and in the presence of a stagnation point on the

[90] Véret C. (1985). Flow Visualization by Light Sheet. *In Flow Visualization III* (W. –J. Yang, ed.), 106-112. Hemisphere, Washington, D. C.

[91] Porcar R., Prenel J. –P., Diemunsch, Hamelin P. (1983). Visualizations by means of Coherent Light Sheets; Applications to Various Flows. Flow Visualization III (W. –J. Yang, ed.). 123-127.

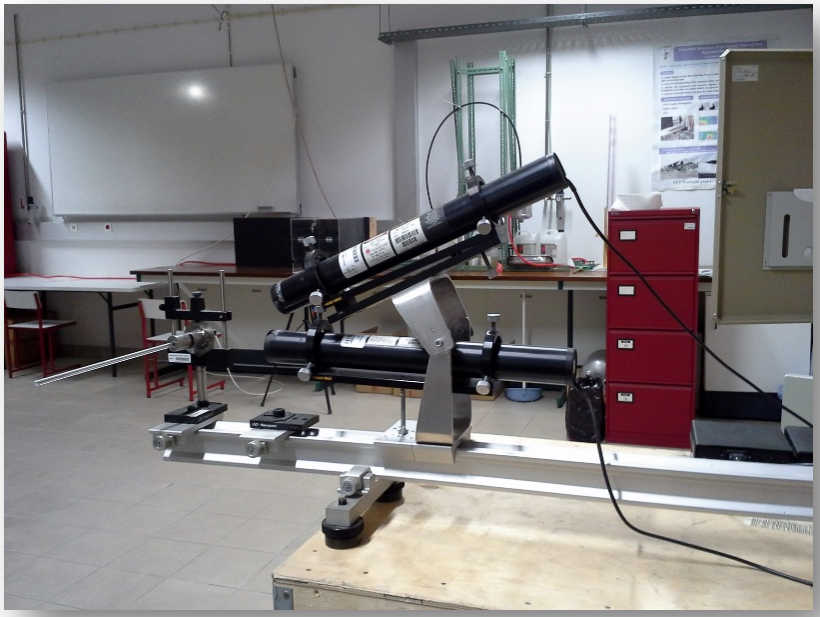

Figure 91: Low frequency lasers (He-Ne).

Figure 92: The sheet of light created by the two mechanisms during the visualization.

surface. Then the jet is deflected radially outward along the impact surface, where the flow is temporarily accelerated due to the local favourable pressure gradient. The upstream wall jet interacts with the crossflow and creates a ground vortex along the impact surface, which involves both impact jets. As a result, two counter rotating vortices in the flow direction develop side by side of the impact zone forming a ground vortex. The nature of the ground vortex is similar to the familiar horseshoe structure generated by the deflection of the boundary layer by a solid obstacle, but is different from the pair of vortex known to exist in a curved jet in the cross flow off the ground. As it will be shown below there is no evidence of a ground vortex corresponding to the downstream impact jet for the experimental conditions.

However, this visualization results give an indication that the upstream impact jet and the corresponding ground vortex and the crossflow are blocking and provoking an alteration of the flow pattern.

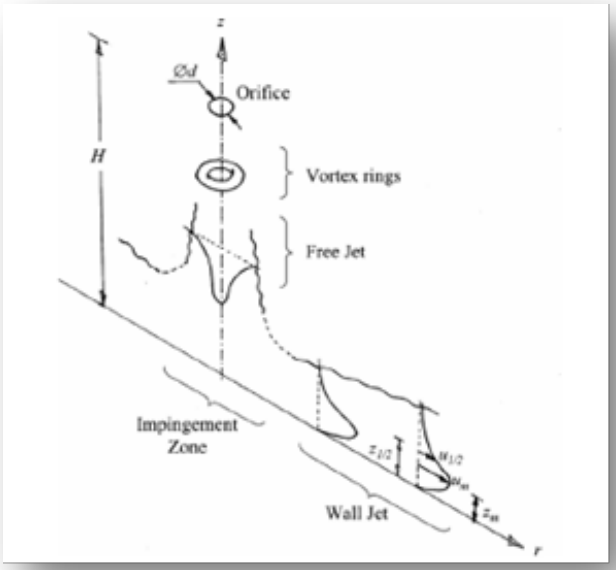

Figure 93: Schematic illustration of the evolution of the flow due to the normal impact of a jet[92]

For the three different velocity ratios each jet has an initial potential-core jet region, where the flow characteristics are identical to those of a free jet, and near the horizontal plate the impingement region, characterized by considerable deflection of the first jet. Analysing figures 94 to 96, it is clear that the deflection of the first increases with the velocity ratio. In the case of the rear jet deflection, for all the velocity ratios we can verify that its deflection is quite small when compared with the first jet deflection because the first jet protects the rear jet from the influence of the crossflow. Figure 94 shows clearly that the second jet did not impact on the ground. As the crossflow velocity was so intense, when the first impinging jet was deflected, the first impinging jet deflected flow eventually catch up the flow from the second impinging jet. In figures 94 c) and 94 d) at half of the impinging height the two jets merged into one single jet flow. But what happens in the reality is the catch up of the second impinging jet by the first jet without the fusion of the two jets flows. When the first jet touches the ground the second jet flows above of the wall jet resulting from the first jet. For this velocity ratio the ground vortex localized upstream of the first impinging jet was not captured during the visualization, despite it seemed to exist from naked eye observation under an oblique position on the test section. Unfortunately in the perpendicular direction to the plane of symmetry, this phenomenon was not captured by the lens of the camera.

[92] Gopi K., Kamran M. (2010). An experimental study of a radial wall jet formed by the normal impingement of a round synthetic jet. *European Journal of Mechanics B/Fluids*. **29(4)**: 269-277.

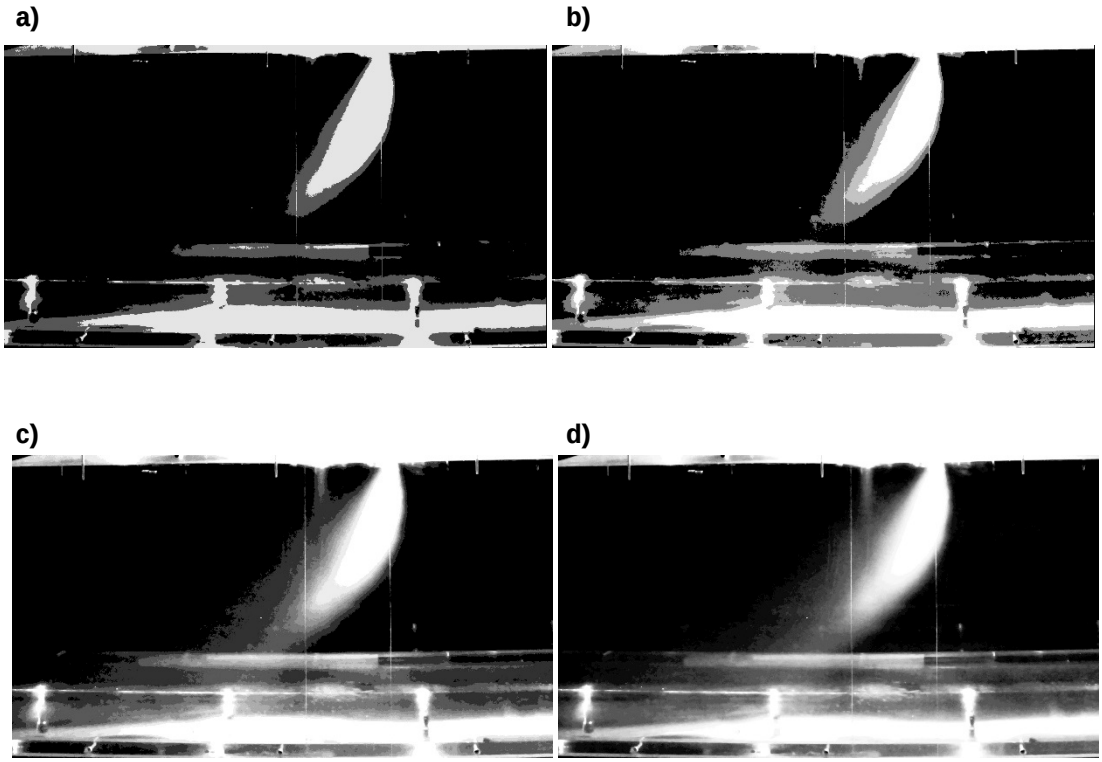

Figure 94: Visualization of the twin jet flow in the vertical plane of symmetry in different phases of the flow development for V_j/U_0=22.5, Re_j=4.3x10^4, H/D=20.1, and S/D=6.

The nature of each ground vortex is similar to the horseshoe structure known to be generated by the deflection of a boundary layer by a solid obstacle (Andreopoulos J. and Rodi W., 1984)[93], but is different from the vortex pair known to exist in a "bent-over" jet in a crossflow far from the ground (Baker, 1980)[94]. Figure 93 allows the identification of all the flow types mentioned before. The upright vortices or ground vortex are generated by the interaction of the wall boundary layer with the jet flow, being for low Re_j only unsteady structures. In the of the horseshoe vortex are formed upstream of the jet and close to the wall. The Counter rotating vortices pair is originated as an effect of the bending of the jet itself. The Counter rotating vortices determine the dominant features of the velocity and vorticity fields, being responsible mainly for mixing, and for mass, momentum and heat transfer (Kamotani and Greber, 1974)[95]. In figures 95 and 96 the deflection of the first jet is practically the same and the second jet also does not touch the ground. The second jet also seems to be catches up by the first jet but for a vertical location closest to the ground. From figures 95 c) and 96 d) is not clear if the second jet touches or not the ground and if it does not touches the ground, the second jet is dragged with the wall jet resulting from the first jet

[93] Andreopoulos, J., Rodi, W. (1984). Experimental Investigation of Jets in a Crossflow. *Journal of Fluid Mechanics*. 138: 93-127.

[94] Baker O.J. (1980). The Turbulent Horseshoe Vortex. *Journal of Wind Engineering and Industrial Aerodynamics*. 6 (1-2): 9-23.

[95] Kamotani Y., Greber I. (1974). Experiments on Confined Turbulent Jets in a Crossflow. *NASA CR-2392*.

to downstream as in the lower velocity ratio case. This question will be addressed again within the numerical simulation chapter (see chapter 5). The ground vortex formation cannot be visualized in the figure 95 for the intermediate velocity ratio, as for the case of the lower velocity ratio. Figure 96 c) shows a notorious a drop in the rear jet potential core region that it has not been reported in literature. The ground vortex resulting from the interaction of the upstream wall jet with the crossflow could not be clearly identified for this velocity ratio.

In the figure 96 e) it is possible see a little ground vortex and the wall jet corresponding to the upstream impinging jet which is almost parallel the ground plate and exhibit a behaviour similar to that of a radial wall jet where the upstream effects of interaction due to impingement are no longer important. The same figure also shows that the crossflow is

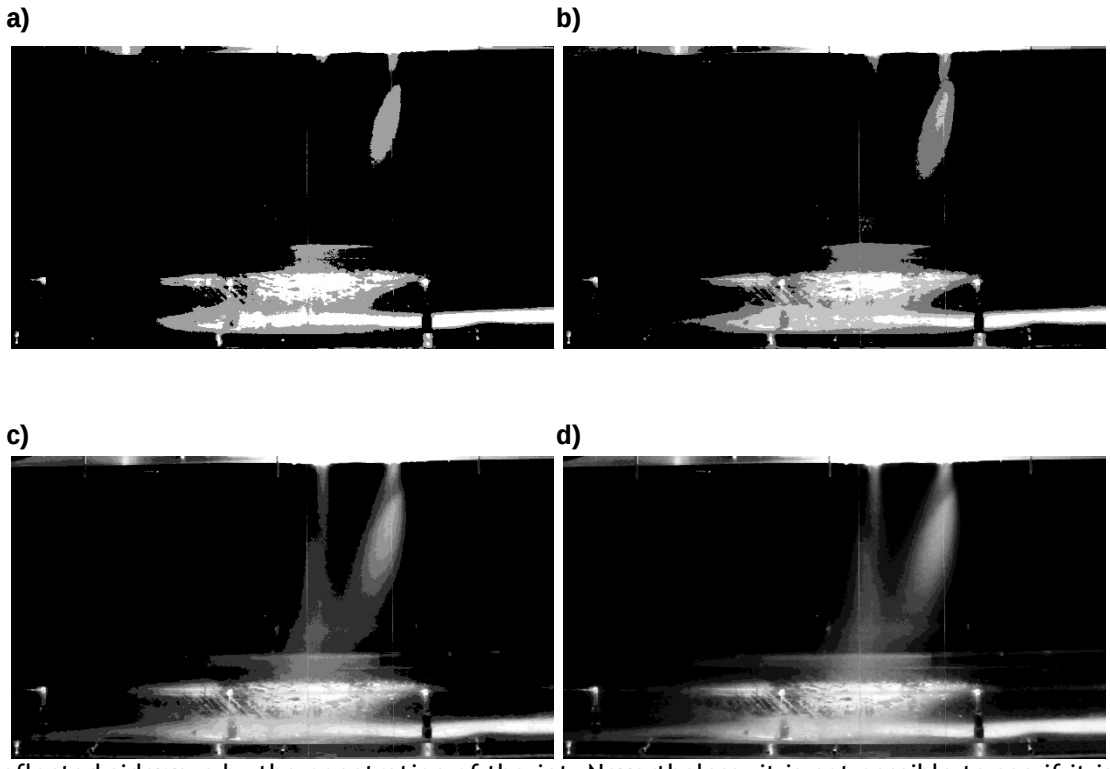

deflected sideways by the penetration of the jet. Nevertheless, it is not possible to see if it is

Figure 95: Visualization of the twin jet flow in the vertical plane of symmetry in different phases of the flow development for V_j/U_0=33.7, Re_j=4.3x10^4, H/D=20.1, and S/D=6.

formed a recirculation region just downstream of the discharge, away from the ground plate, and it is not possible to confirm the formation of a horseshoe vortex. If the jets were positioned side by side in front of the crossflow two ground vortexes would appear as well as a fountain flow in the vertical plane of symmetry due to the collision of the two individual

radial wall jets (Barata, 1996a)[96], (Kotansky, 1981)[97], (Saripalli, 1983)[98], (Siclari *et al.*, 1976[99]). No evidence of a ground vortex corresponding to the downstream impinging jet could

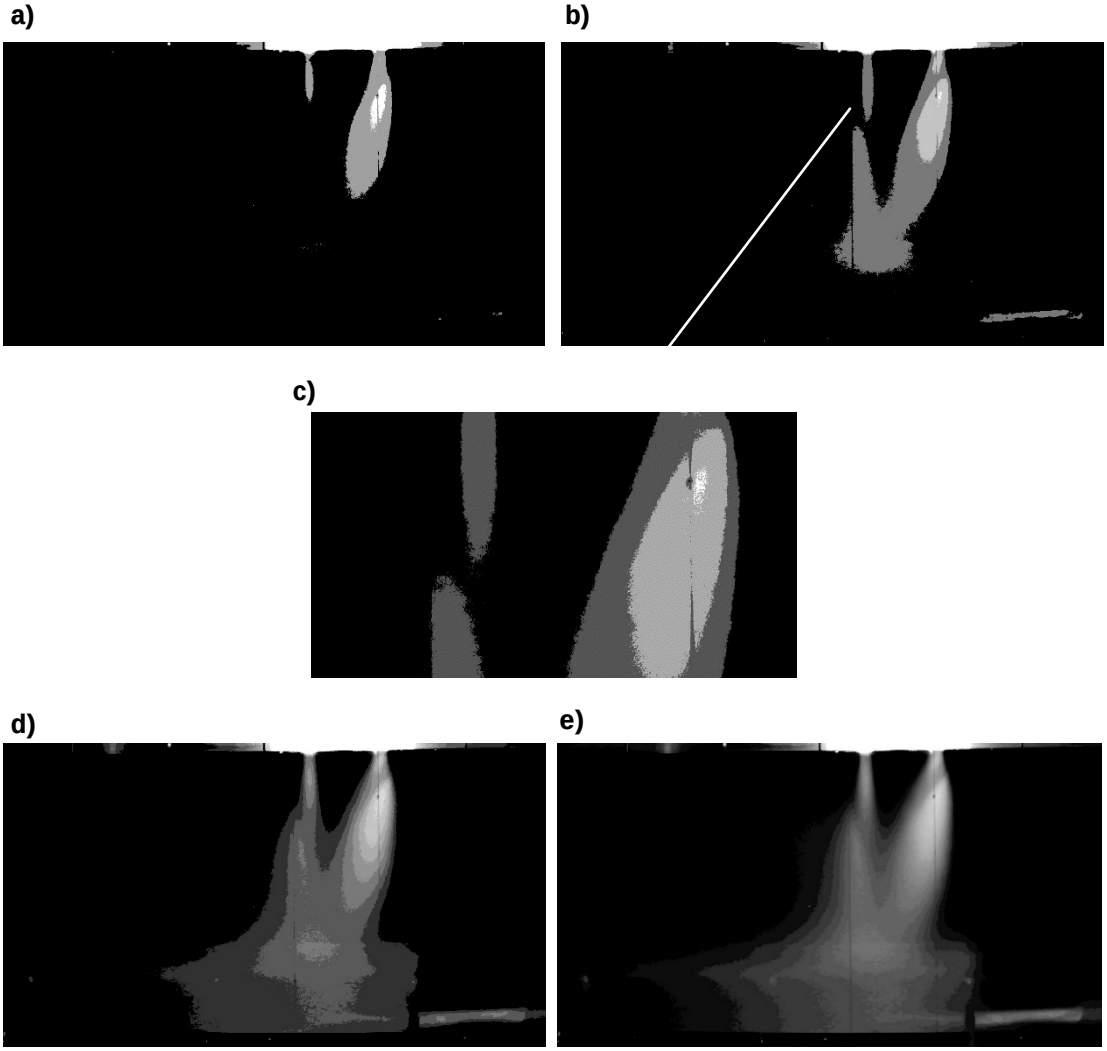

Figure 96: Visualization of the twin jet flow in the vertical plane of symmetry in different phases of the flow development for V_j/U_0=43.8, Re_j=4.3x10^4, H/D=20.1, and S/D=6.

be confirmed for all the velocity ratios studied, which is an indication that the upstream impinging jet and its ground vortex are blocking the crossflow and provoking an alteration to the flow pattern. Also, in the present experimental study no fountain flow was detected for the conditions tested.

[96] Barata, J.M.M. (1996a). Ground Vortex Formation with Twin Impinging Jets. *Proceedings of the International Powered Lift Conference*, Jupiter, Florida, 18-20 Nov., 1996. Paper SAE 962257.

[97] Kotansky D.R. (1981). The Modelling and Prediction of Multiple VTOL Aircraft Flow Fields in Ground Effect. *AGARD CP-308*, Paper 16.

[98] Saripalli K. R. (1983). Visualization of Multijet Impingement Flow. *AIAA Journal*. 21: 483-484.

[99] Siclari M.J., Migdal D., Luzzi T.W. Jr., Barche J., Palcza J.L. (1976). Development of Theoretical Models of Jet-Induced Effects on V/STOL Aircraft. *Journal of Aircraft*. 13(12):.938-944.

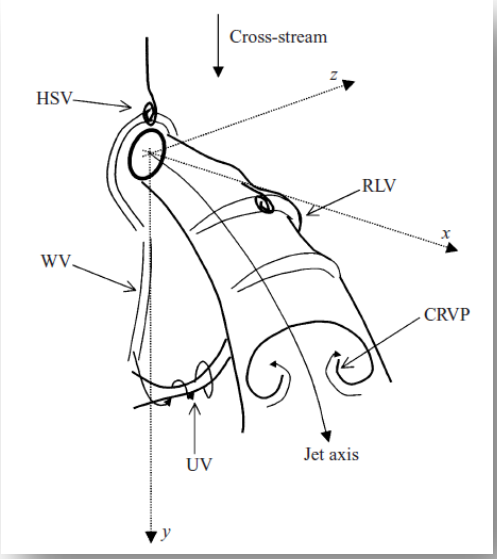

Figure 97: A schematic diagram of the main vortical structures formed in a jet.[100]

3.3 Velocity measurements

The experimental work included measurements of the mean and turbulent velocity fields, including Reynolds shear stress in vertical planes parallel to the plane of symmetry for different velocity ratios between the jet and the crossflow (V_j/U_0=22.5, 33.7 and 43.8).

Figure 98 shows vertical profiles of the mean horizontal velocity component, $\overline{U}$, along the vertical plane of symmetry (Z=0) for velocity ratios of 22.5, 33.7 and 43.8. The results indicate that for V_j/U_0=22.5, the profiles corresponding to X/D = −6.33, −5.0 and −3.67 exhibit high velocity gradients in the region of 0 mm < Y < 30 mm, and for Y > 30mm the horizontal velocity is substantially uniform. For the other two velocity ratios the corresponding profiles present negative values of mean horizontal velocity in the region Y < 30mm, disclosing the presence of a ground vortex resulting from the collision between the wall jet and the crossflow. The profile at X/D = −2.93 exposes the location of the stagnation point upstream the ground vortex resulting from the first impinging jet. This profile and those further upstream exhibit negative values close to the ground, indicating the presence of a wall jet, and revealing the deflection of the first jet by the crossflow. The effect of the velocity ratio on the deflection of the upstream jet can be inferred from figure 98 that reveals that the location of the ground vortex moves upstream when the velocity ratio increases. Far away from the ground the positive values of the horizontal velocity component reach twice the value of the crossflow velocity, suggesting that no upstream wall jet resulting from the rear

[100] Camussi R., Guj G., Stella A. (2002). Experimental Study of a jet in crossflow at very low Reynolds number. *Journal of Fluids Mechanical*. 454: 113-144.

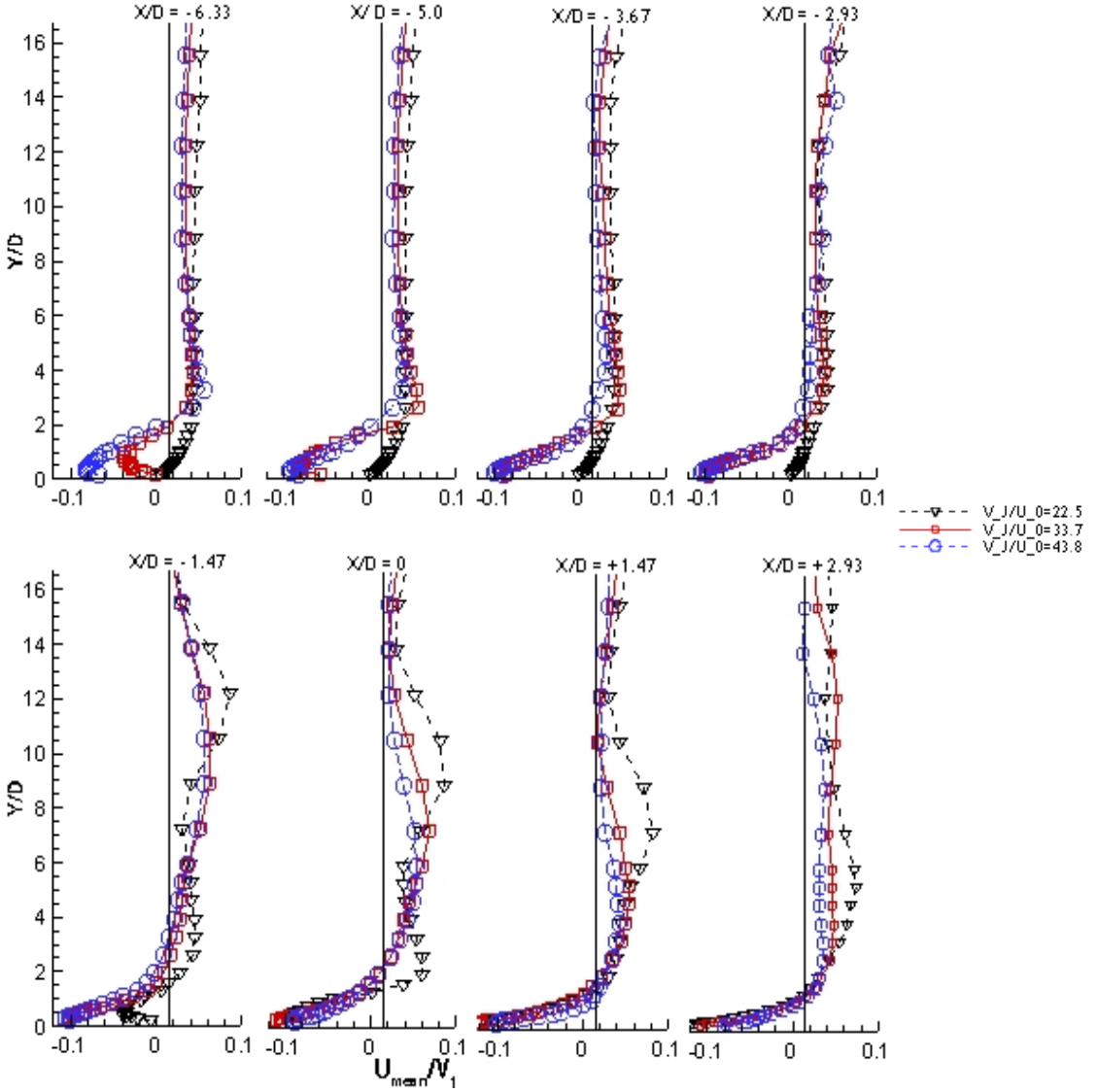

Figure 98: Vertical profiles of the mean horizontal velocity component along the vertical of symmetry for the three different velocity ratios studied. Re_j=4.3x10^4, V_j/U_0=22.5, 33.7 e 43.8, H/D=20.1, e S/D=6.

jet exists, but the complete jet is deflected by the crossflow. This result is consistent with the conclusion of Barata (1996b)[101] that found for a single impinging jet that the ground vortex blocks the passage of the confined crossflow increasing the velocity of the crossflow. This is a most relevant result because a different pressure distribution in the under surface of a VSTOL aircraft may occur when it operates near ground with front wind or small forward movement, and may result in under pressures causing a suction down force and changing the pitching moment.

Figure 99 shows vertical profiles of the mean vertical velocity component, $\overline{v}$, along the

[101] Barata, J.M.M. (1996b). Fountain Flows Produced by Multiple Impinging Jets in a Crossflow. *AIAA Journal.* **34(12)**: 2523-2530 and e AIAA Journal on Disc, Vol. 2, No.1, 1996.

vertical plane of symmetry (Z=0).

The first profile at X/D=−6.33 shows positive values of the mean vertical velocity component for all the velocity ratios studied, and for V_j/U_0 = 33.7 there is an increase at Y/D <2, which is not identified for the other velocity ratios. The next profile shows a large influence of the velocity ratio on the vertical velocity component.

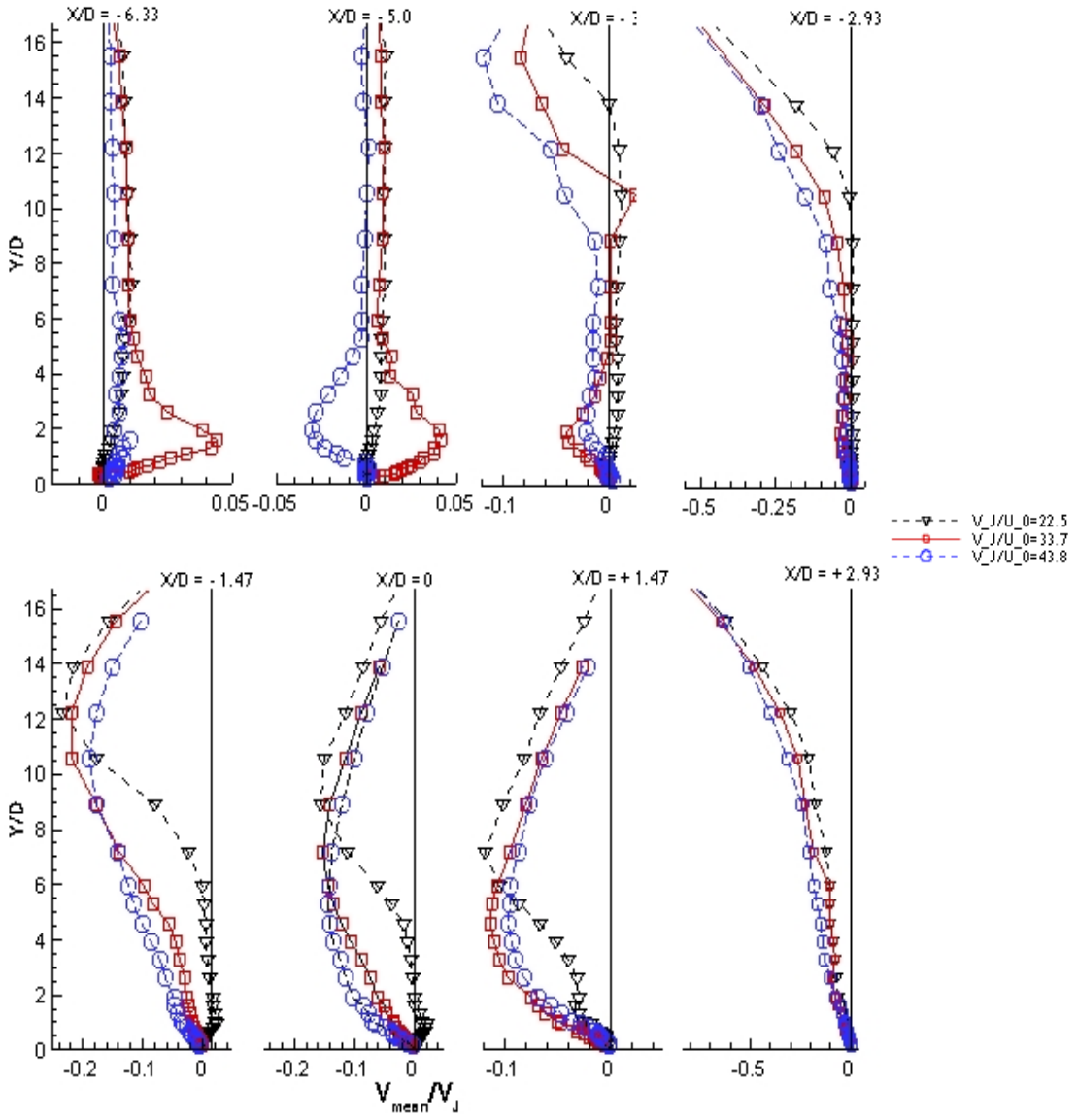

Figure 99: Vertical profiles of the mean vertical velocity component along the vertical of symmetry for the three different velocity ratios studied. Re_j=4.3x10^4, V_j/U_0=22.5, 33.7 e 43.8, H/D=20.1, e S/D=6.

For an intermediate velocity ratio only positive values of the mean vertical velocity exist, with the largest values for Y/D<4 due to a slight acceleration of the flow which passes over the ground vortex. For a higher velocity ratio, the profile at the same location shows negative values of the mean vertical velocity that correspond to a location inside the ground vortex.

The first jet is clearly identified at X/D = −2.93 for all the velocity ratios, through the negative values of vertical velocity close to the top wall, namely for Y/D>12. For X/D= −1.47 and 0 the presence of the first jet it is also noticeable, by the negative values of the vertical velocity, which are more pronounced at V_J / U_0 = 33.7 and 43.8. Finally the second jet it is identified in the profile at X/D = 2.93, that shows values of the mean vertical velocity component greater than those shown in the first jet. This means that there is no wall jet localized upstream of the rear jet, as mentioned before in the analysis of the vertical profile of the mean horizontal velocity component, and the rear jet is completely deflected by the crossflow.

Figure 100 presents vertical profiles located along the test section to the horizontal rms velocity for the three speed ratios studied. The profiles are not much affected by the velocity ratio, and a slight difference lies in the corresponding profiles X/D = -1.47 and 0, where the lower velocity ratio presents a normal horizontal stress lower than the registered for the other two velocity ratios.

Figure 101 presents vertical profiles located along the vertical plane of symmetry of the test section for the vertical rms velocity for the three velocity ratios studied. The first two profiles (X/D=-6.33 and -5.0) show fluctuations peaks in the vertical velocity component for the higher velocity ratios in the region close to the impact plate, due to the proximity of these profiles with the location of the vortex ground for each velocity ratio. Further downstream the fluctuation peaks in the vertical velocity component are clearly identified at 10 <Y/D< 13.33 for all of the velocity ratios. This result was expected, since this region is characterized by high velocity gradients. When the velocity ratio increases (V_j/U_0= 33.7 and 43.8) the results exhibit even higher fluctuation peaks.

Figure 102 show horizontal profiles of the horizontal, $\overline{U}$ mean velocity components for all the velocity ratios studied, and quantify the development of the impinging jets, and confirm the above description of the flow (vertical profiles, figures 98 and 99). In addition, these profiles show that the centre of the first jet is moving in the crossflow direction. For V_j / U_0 = 22.5 the centre of the first jet moves from X/D = −2.87 at Y/H =0.92 to X/D = +0.7 at Y/H= 0.50, corresponding to a deflection angle of 21.9º. For the higher velocity ratios, the jet deflection is smaller, corresponding to an angle of 14.42º for V_j/U_0 = 33.7 and 12.66º for V_J / U_0 = 43.8. The rear jet is less deflected than the first jet due to the alignment with the first jet and the corresponding wake. In this case, the centre of the rear jet is nearly coincident with the geometrical axis of the exit, and for V_j / U_0 = 22.5 and 33.7 it is located in X/D = +4 for Y/H = 0.5, corresponding to a deflection angle of 12.3º. For the other velocity ratio (V_j / U_0 = 43.8), the deflection observed is slightly smaller, of the order of 8.2º.

The horizontal profiles of the mean vertical velocity component (figure 103) exhibit only positive values from the top wall (Y/H= 1) to the middle of the impinging height (Y/H=0.5)

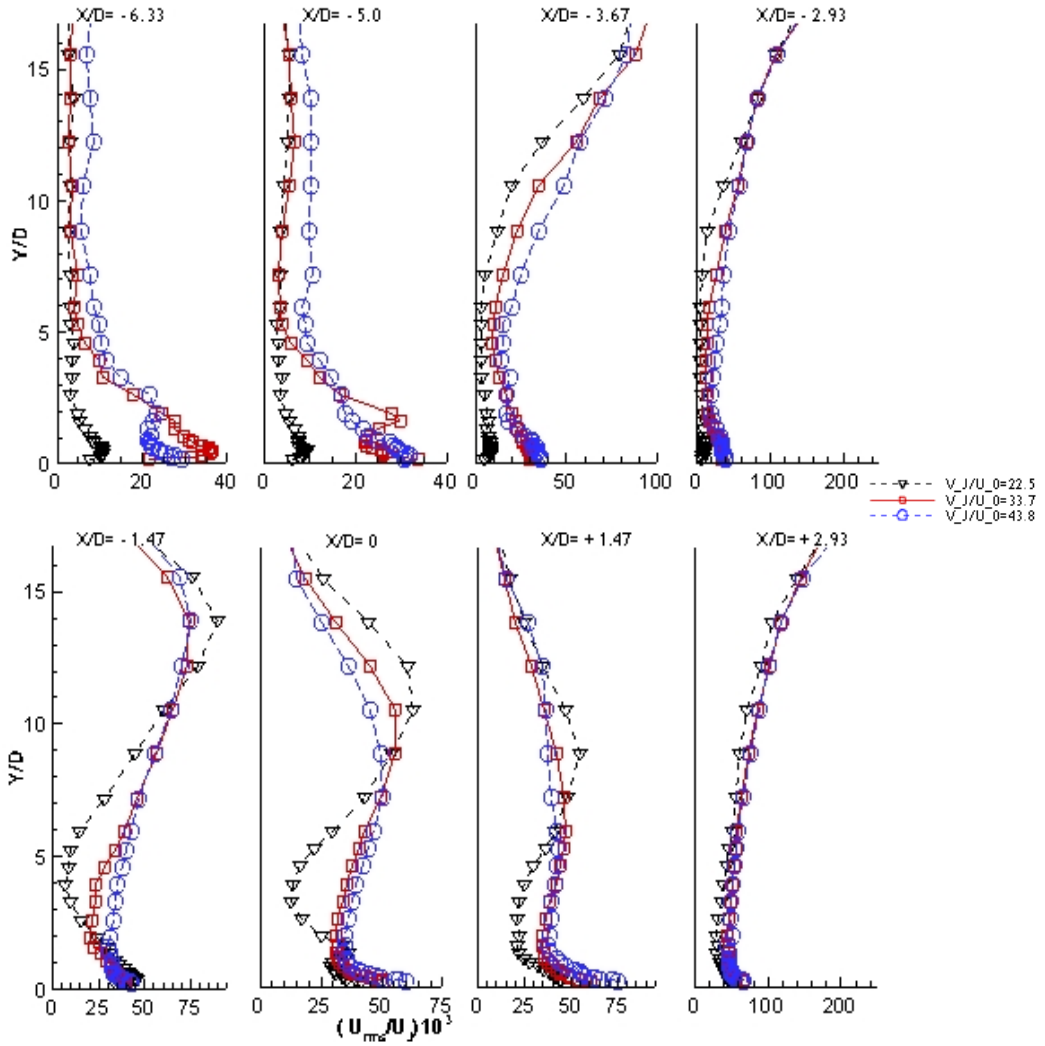

Figure 100: Vertical profiles of horizontal rms velocity along the vertical of symmetry for the three different velocity ratios studied. Re_j=4.3x10^4, V_j/U_0=22.5, 33.7 and 43.8, H/D=20.1, and S/D=6.

for all the velocity ratios studied. This confirms the conclusions drawn from the vertical velocity profiles and discussed above. The asymmetry of the flow can be confirmed from the horizontal profiles of the mean vertical velocity component with higher peaks up to 10% of the vertical velocity in the upstream side (X/D < 3.33). Also it is also possible to ascertain that for all the velocity ratios the horizontal profiles are very similar, showing only a small difference near the centre of the jets for the mean vertical velocity. However, based on the maximum of the mean vertical velocity component the deflection angle of the rear jet is only 4.8º approximately for all the velocity ratios. Thus, this result confirms the initial hypothesis that the alignment of the jets with the crossflow would create a special flow pattern. The wall jet resulting from the first jet flows under the rear jet, and the upstream ground vortex is only interacting with the rear jet induced flow away from the vertical plane of symmetry.

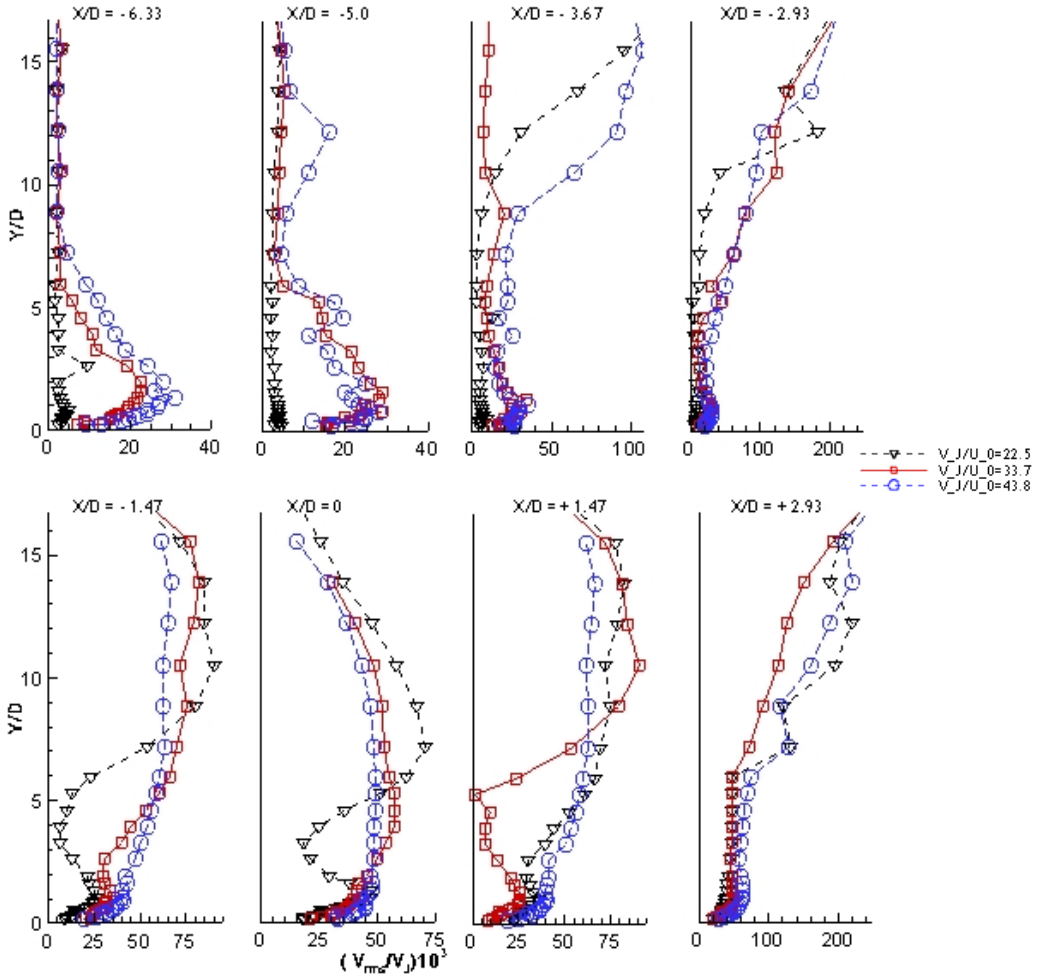

Figure 101: Vertical profiles of vertical rms velocity along the vertical of symmetry for the three different velocity ratios studied. Re_j=4.3x10^4, V_j/U_0=22.5, 33.7 e 43.8, H/D=20.1, and S/D=6.

Figures 104 and 105 shows horizontal profiles of the rms values of the normal stresses, $\overline{u'^2}$ and $\overline{v'^2}$, and quantifies the effect of the velocity ratio. The profiles show results that are somewhat surprising at first sight, because it seems that it is not possible to identify completely the shear layer surrounding the impinging jets. The horizontal profiles of the normal stresses show small peaks in the in the upstream side of the first jet (X/D < 3) for all the velocity ratios. In the downstream side of the first impinging jet others peaks are observed, mainly in the region close to X/D = 0 in Y/H = 0.83 and 0.75, which are more evident for the lower velocity ratio. For Y/H = 0.66 and 0.58, the peaks are practically unrecognizable for V_j/U_0 = 22.5 and 33.7, but for the highest velocity ratio this peaks are very clear, with a maximum value of u_{rms}/V_j = 5.481x10^2 at Y/H = 0.66. Downstream of the rear jet the shear layer surrounding the jet cannot be clearly identified for the lower velocity ratio. For the other velocity ratios, the three profiles under the downstream jet exit of the impinging jets show some enhanced values localized downstream of the rear jet, that need further investigation.

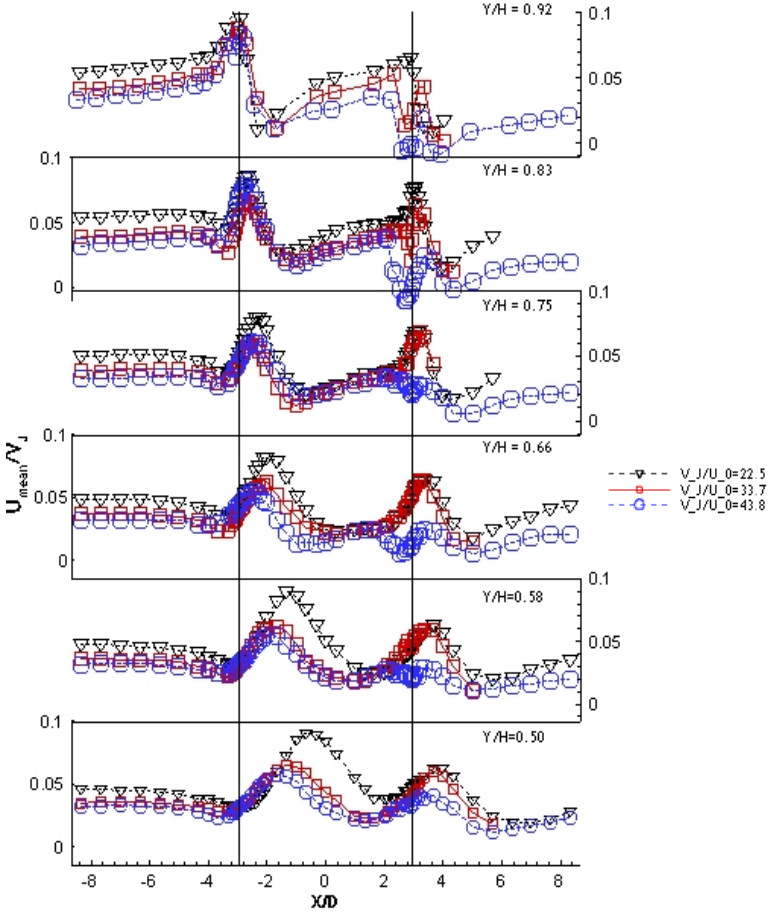

Figure 102: Horizontal profiles of the mean horizontal velocity characteristics along the longitudinal (symmetry) plane crossing the centre of the twin jets: Re_j=4.3x10^4, V_j/U_0=22.5, 33.7 e 43.8, H/D=20.1, and S/D=6.

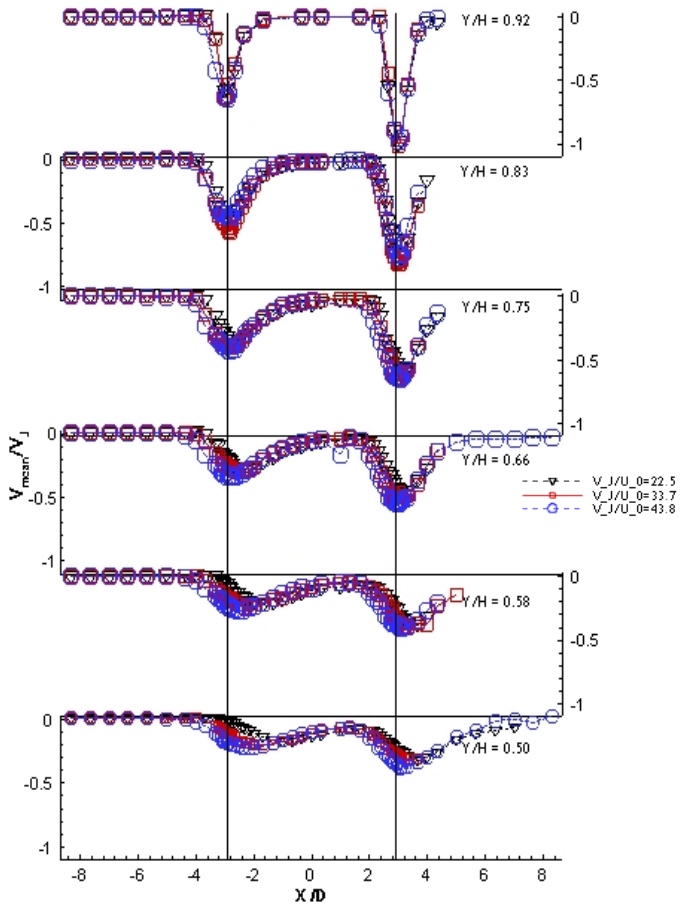

Figure 103: Horizontal profiles of the mean vertical velocity characteristics along the longitudinal (symmetry) plane crossing the centre of the twin jets. Re_j=4.3x10^4, V_j/U_0=22.5, 33.7 e 43.8, H/D=20.1, and S/D=6.

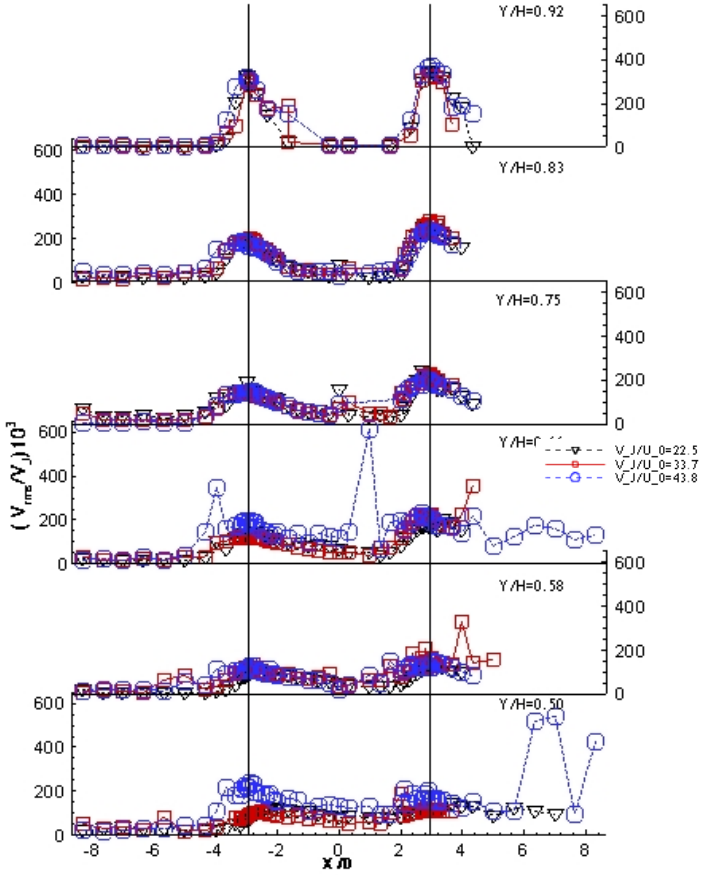

Figure 104: Horizontal profiles of the mean vertical turbulent velocity characteristics along the longitudinal (symmetry) plane crossing the centre of the twin jets. Re_j=4.3x10^4, V_j/U_0=22.5, 33.7 e 43.8, H/D=20.1, and S/D=6.

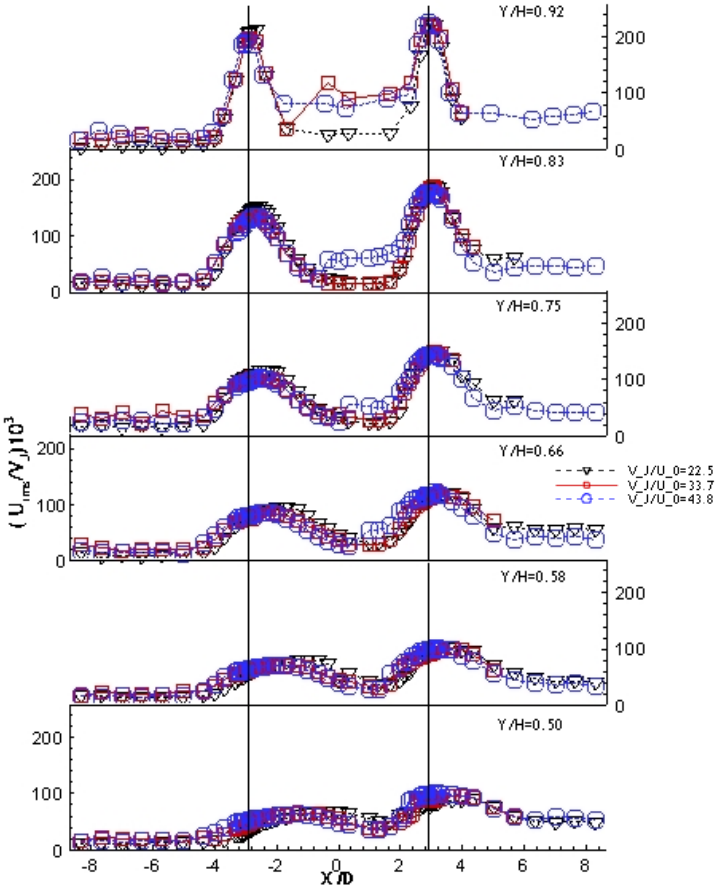

Figure 105: Horizontal profiles of the mean horizontal turbulent velocity characteristics along the longitudinal (symmetry) plane crossing the centre of the twin jets. Re_j=4.3x10^4, V_j/U_0=22.5, 33.7 e 43.8, H/D=20.1, and S/D=6.

3.4 Summary

The contents of the present chapter were partially presented at (Vieira, 2012)[102], (Vieira *et al.*, 2013)[103] and (Vieira *et al.*, 2014)[104]. The results show a large penetration of the first (upstream) jet, which is deflected by the crossflow and impinges on the ground, giving rise to a ground vortex due to the collision of the radial wall and the crossflow that wraps around the impinging point like a scarf. The first jet deflection and the location of the ground vortex depend on the velocity ratio used. For higher velocity ratios, the deflection of the first jet is smaller and further upstream is located the ground vortex centre. The rear jet it is not so affected by the crossflow in terms of deflection for all velocity ratios because it is protected by the upstream jet, but due to the downstream wall jet that flows radially from the impinging point the rear jet does not reach the ground. Also due to the confinement and the ground vortex, the crossflow is blocked and accelerates in the upper part and also contributes to an enhanced mixing of each secondary flow. As consequence, no upstream wall jet or ground vortex resulting from the second (downstream) jet was detected. The effect of the rear jet impinging on the downstream wall jet resulting from the first jet had not been reported so far and requires further investigation. The results show a large penetration of the first (upstream) jet, which is deflected by the crossflow and impinges on the ground giving rise to a ground vortex due to the collision of the radial wall and the crossflow that wraps around the impinging point like a scarf.

[102] Vieira D. F. C. (2012). *Turbulent Structure of the Impact of a Ground Vortex Flow*. Master Thesis in Aeronautical Engineering. University of Beira Interior, Covilhã, 110 pp.

[103] Vieira D.F.C., Silva A.R.R., Carvalho P.S.D., Neves F.M.S.P., Barata, J.M.M. (2013). Numerical and Experimental Study of Two Impinging Jets in a Row through a Crossflow. Proceedings of the 51th AIAA Aerospace Science Meeting Including the New Horizons Forum and Aerospace Exposition, Grapevine (Dallas/Ft. Worth Region), Texas, 7-10 Jan. 2013. AIAA Paper 2013-0806.

[104] Vieira D.F.C, Durão D.F.G., Neves F.M.S.P., Silva A.R.R., Barata J.M.M. (2014). Laser Doppler Measurements of Twin Impinging Jets in Tandem through a Crossflow. *Proceeding of the 17th International Symposium on Applications of Laser Techniques to Fluid Mechanics*, Lisbon, Portugal, 07-10 July 2014.

Chapter 4

Computational Method

4.1 Introduction

In Aeronautics, as in others an area of application of fluids mechanics, the flow of practical relevance is nearly always turbulent. This means that the fluid motion is unsteady, three dimensional and highly random, but not in the Gaussian sense, because in turbulence flows the velocity of the fluid at a point is continuously undergoing changes in both magnitude and direction. So, the turbulent flow is very complex, and the turbulent motion together with the associated heat and mass transfer phenomena associated to this type of flows extremely difficult to describe and predict theoretical or numerically.

The prediction of the turbulent flows is possible through the solution of the fluid dynamic fundamental equations, i.e., the Continuity and the Navier Stokes equations. Until some years ago the dependence on Information Technologies (IT) computing resources was a major constraint on physics-mathematical modelling of such turbulent flows, because the storage capacity and speed of the computers was still not sufficient to allow a solution for any practically relevant turbulent flow. But today the computational resources are much bigger and the use of turbulence models and large eddy simulation has enabled the prediction of many real flows. Nevertheless, the ultimate goal will be the direct solution of the fundamental equations which is only possible in some geometrical and physical simplified cases, and even so demanding important computing resources that are only available to the major research groups and countries.

But what is the definition of a turbulence model? A turbulence model can be described as an analytical procedure to close the system of fundamental mean flow equations, where additional variables related to fluctuating quantities did emerge during the Reynolds averaging process. The turbulence models are based on hypotheses about turbulent processes and require empirical input in the form of constants or functions. The turbulence models do not simulate the details of the turbulent motion but only the effect of turbulence on the mean flow behaviour (i.e. describes the fluctuating variables in terms of the mean variables). The turbulent transport processes are strongly problem dependent due to, for example, the geometrical conditions, viscous, swirl effects, vorticity and buoyancy. The turbulence models

can only give an approximate description, and with a particular set of empirical constants, the turbulence model is valid only for a certain type of flow. The most universal turbulence model is not necessarily the most suitable one for a particular flow problem. In practical applications, the ease and economy of the computational resource when using a model are important, and in the most cases the universal models are usually more complex and thus require more computing time.

4.2 Governing equations

In this section the equations which govern the distribution of the mean flow quantities are presented in its transient form to avoid loss of generality, but in the present work only steady flow predictions will be presented[105]. The origins of these equations are the conservation law for mass, momentum, thermal energy and species concentration (e.g. Wilcox, 1993).

4.2.1 Mass Conservation: Continuity equation

The continuity equation represents the mass conservation principle applied to an infinitesimal control volume. Its mathematical expression is represented by the following equation:

$$\frac{\partial \rho}{\partial t} + \frac{\partial (\rho u_i)}{\partial x_i} = 0 \tag{4.1}$$

Where ρ is the specific mass, t is the time, u_i is the instantaneous velocity component in direction x_i.

4.2.2 Momentum conservation: Navier-Stokes equations

The Navier Stokes equations relate the variation rate of the three components of momentum with the applied forces according to each direction. The equation to the momentum quantity transport, for the *i* generic direction, is represented by:

$$\frac{\partial (\rho u_i)}{\partial t} + \frac{\partial}{\partial x_j}\left(\rho u_j u_i\right) = -\frac{\partial p}{\partial x_i} + \frac{\partial}{\partial x_j}\left[\mu\left(\frac{\partial u_i}{\partial x_j} + \frac{\partial u_j}{\partial x_i} - \frac{2}{3}\frac{\partial u_k}{\partial x_k}\delta_{ij}\right)\right] \tag{4.2}$$

Where t is the time, u_i is the instantaneous velocity component in direction x_i, u_j is the instantaneous velocity component in direction x_j, u_k is the instantaneous velocity component in direction x_k, p is the pressure and δ_{ij} is the Kronecker delta tensor.

[105] As reported by Barata, Ribeiro, Santos, and Silva (2009b) and Silva, Durão, Barata, Santos, Ribeiro (2009), non-stationary behavior can only occur for short jet impingement jets in a crossflow for relatively low jet-to-crossflow velocity ratios (less than 5).

4.2.3 Energy conservation equation

The energy conservation equation is obtained through the energy balance applied to an infinitesimal volume control, considering the fluid like a perfect gas and neglecting the terms corresponding to the viscous dissipation.

$$\frac{\partial(\rho h)}{\partial t} + \frac{\partial}{\partial x_j}\left(\rho u_j h\right) = \frac{\partial}{\partial x_j}\left(\Gamma_h \frac{\partial_h}{\partial_{x_j}}\right) \tag{4.3}$$

Where h is the specific enthalpy and Γ_h is the h diffusion coefficient obtain by the quotient between the fluid thermal conductivity and the specific heat to a constant pressure.

4.2.4 Reynolds-averaging

The turbulent flows are highly irregular, transient and tridimensional, and the equations presented before does not have analytic solution. So to obtain numerical solutions the space and the time have to be discretized. However, due to the small length scales and the time that characterize the turbulent flows, this process lead to large computational memory as well as calculation time requirements. However, most of the engineering problems only require the knowledge of the mean temporal turbulence effects. So, it was used a statistical approximation suggest by Osborne Reynolds, which consists of the decomposition of the instantaneous value of any dependent variable, on the sum of the respective mean value with the value of the fluctuation of the mean value. This approximation is represented by the following expression:

$$\phi = \bar{\phi} + \phi' \tag{4.4}$$

with the mean value defined by:

$$\bar{\phi} = \frac{1}{\Delta t}\int_{t}^{t+\Delta t} \phi(\tau) d\tau \tag{4.5}$$

where τ is the shear stress.

The mean flow equations are obtained by replacing the instantaneous value of the dependent variable for the decomposition Reynolds and integrating in order to time the resulting equations.

Continuity equation

$$\frac{\partial \bar{\rho}}{\partial t} + \frac{\partial(\bar{\rho}\bar{u_i})}{\partial x_i} \tag{4.6}$$

Momentum conservation

$$\frac{\partial(\bar{\rho}\overline{u_i})}{\partial t}+\frac{\partial}{\partial x_j}\left(\rho\overline{u_j}\overline{u_i}\right)=-\frac{\partial\bar{p}}{\partial x_i}+\frac{\partial}{\partial x_j}\left[\mu\left(\frac{\partial\overline{u_i}}{\partial x_j}+\frac{\partial\overline{u_j}}{\partial x_i}-\frac{2}{3}\frac{\partial\overline{u_k}}{\partial x_k}\delta_{ij}\right)\right]+\frac{\partial}{\partial x_j}\left(-\rho\overline{u_i u_j}\right)+\bar{\rho}g_i \quad \textbf{(4.7)}$$

Where g_i represents the gravity acceleration.

Scalar variable

$$\frac{\partial(\bar{\rho}\bar{\phi})}{\partial t}+\frac{\partial}{\partial x_j}\left(\rho\overline{u_j}\bar{\phi}\right)=\frac{\partial}{\partial x_j}\left(\Gamma_\phi\frac{\partial\bar{\phi}}{\partial x_j}\right)+\frac{\partial}{\partial x_j}\left(-\rho\overline{u'_j\phi'}\right) \quad (4.8)$$

Where Γ_ϕ represents the diffusion coefficient of ϕ.

On the equation 4.7 $-\rho\overline{u_i u_j}$ represents the Reynolds stress that involves crossed-fluctuations of the velocity field. On the equation 4.8 $-\rho\overline{u'_j\phi'}$ represents the turbulent scalar fluxes that are obtained by the product of the velocity component fluctuation with the scalar fluctuation. The determination of expressions of these unknowns in terms of the mean quantities will close the system of equations, and called turbulence modelling.

In the present study the turbulence model used is the "*k-ε*" turbulence model that had already been used by other authors in flow configurations relevant to V/STOL (e.g. Barata, 1989d[106]). The present computational code PACEJ is a highly modified version of the PACE code, that was firstly developed by Barata (1989d)[107]. This numerical simulation program is a result of an extensive work along several years with the objective to elaborate a program that could represent a variety of different flow cases using high numerical accuracy. So that this program could properly simulate the present study case were made some changes, notably with regard to boundary conditions and graphical representation of the results.

4.3 Turbulence modelling

The mathematical model used in the numerical simulation is based on the solution of the continuity and momentum equations. A Reynolds-Averaged Navier Stokes (RANS) formulation was adopted with the "*k-ε*" turbulence model to represent the turbulent stresses. The "*k-ε*" turbulence model belongs to the two equations models class. The model transport equations are solved for two turbulence quantities, *k* and *ε*. This model is based on the turbulent viscosity concept introduced by Boussinesq (1887). The turbulent viscosity is calculated by the Prandtl-Kolmogorov relation, taking into account that the turbulent characteristic velocity and the

[106] Barata, J.M.M. (1989d) "Estudo Numérico e Experimental de Jactos Incidentes Sobre Placas Planas Através de um Escoamento Cruzado". PhD Thesis (in Portuguese). Universidade Técnica de Lisboa, Instituto Superior Técnico, 1989.

[107] *idem*

dissipative length scale is defined through the turbulent kinetic energy and the turbulent kinetic energy dissipation.

$$\mu_t = c_\mu \bar{\rho} \frac{k^2}{\varepsilon} \tag{4.9}$$

where c_μ represents a model constant with the value of 0.09. The values of k and ε are determined by the respective transport equations.

This turbulence model is the most widely used, and is incorporated in most commercial CFD codes. The exact transport equations of k and ε are determined from the Navier-Stokes equations. In the case of the k transport equation it is used the Reynolds tension transport equation by the contraction of i and j indexes. In the case of the ε equation there are some terms of the equation that need to be modelled (Jones and Launder, 1972).

The turbulent kinetic energy transport equation is represented by:

$$\frac{\partial \bar{\rho} k}{\partial t} + \frac{\partial}{\partial x_j}\left(\overline{\rho u_j} k\right) = \frac{\partial}{\partial x_j}\left(\Gamma_k \frac{\partial k}{\partial x_j}\right) + G_k - \bar{\rho}\varepsilon \tag{4.10}$$

where

$$\Gamma_k = \frac{\mu_t}{\sigma_k} \tag{4.11}$$

μ_t represents the turbulent viscosity and σ_k is a model constant, and

$$\mathrm{G}_k = \mu_t \frac{\partial \overline{\mu_\imath}}{\partial x_j}\left(\frac{\partial \overline{\mu_\imath}}{\partial x_j} + \frac{\partial \overline{\mu_\jmath}}{\partial x_i}\right) \tag{4.12}$$

The transport equation of the turbulent kinetic energy dissipation rate is represented by:

$$\frac{\partial \bar{\rho} \varepsilon}{\partial t} + \frac{\partial}{\partial x_j}\left(\overline{\rho u_j} \varepsilon\right) = \frac{\partial}{\partial x_j}\left(\Gamma_\varepsilon \frac{\partial \varepsilon}{\partial x_j}\right) + c_{\varepsilon 1} G_k \frac{\varepsilon}{k} - c_{\varepsilon 2} \bar{\rho} \frac{\varepsilon^2}{k} \tag{4.13}$$

where

$$\Gamma_\varepsilon = \frac{\mu_t}{\sigma_\varepsilon} \tag{4.14}$$

μ_t represents the turbulent viscosity and $\sigma_\varepsilon$is a model constant.

The following equation represents the governing equations written in a general form that was used in the numerical simulation.

$$\frac{\partial}{\partial x}(\rho u\phi)+\frac{1}{r}\frac{\partial}{\partial r}(r\rho v\phi)=\frac{\partial}{\partial x}\left(\Gamma_\phi\frac{\partial\phi}{\partial x}\right)+\frac{1}{r}\frac{\partial}{\partial r}\left(r\Gamma_\phi\frac{\partial\phi}{\partial r}\right)+S_\phi \tag{4.15}$$

where the property ϕ represents the velocity, turbulent kinetic energy or dissipation while S_ϕ and $\Gamma_\phi$assume different values related with ϕ as described in table 7.

The turbulent diffusion terms are approximated by two equations from "*k-ε*" turbulent model where the Reynolds stress is related with shear strain by:

$$\rho\overline{u'_\iota u'_J}=-\mu_T\left(\frac{\partial U_i}{\partial x_j}+\frac{\partial U_j}{\partial x_{ij}}\right)+\frac{2}{3}\delta_{ij}\rho k \tag{4.16}$$

where μ_T represent turbulent viscosity.

The turbulent kinetic energy production is expressed by:

$$\Phi=\mu_T\left\{2\left[\left(\frac{\partial U}{\partial x}\right)^2+\left(\frac{\partial V}{\partial r}\right)^2+\left(\frac{V}{r}\right)^2\right]+\left[\frac{\partial U}{\partial r}+\frac{\partial V}{\partial x}\right]^2\right\} \tag{4.17}$$

ϕ	Γ_ϕ	S_ϕ
1	0	0
U	μ_T	$-\frac{\partial p}{\partial x}+\frac{\partial}{\partial x}\left(\mu_T\frac{\partial U}{\partial x}\right)+\frac{1}{r}\frac{\partial}{\partial r}\left(r\mu_T\frac{\partial V}{\partial x}\right)$
V	μ_T	$-\frac{\partial p}{\partial r}+\frac{\partial}{\partial x}\left(\mu_T\frac{\partial U}{\partial r}\right)+\frac{1}{r}\frac{\partial}{\partial r}\left(r\mu_T\frac{\partial V}{\partial r}\right)-2\mu_T\frac{V}{r^2}$
k	μ_T/σ_k	$\Phi-\rho\varepsilon$
ε	μ_T/σ_ε	$C_{\varepsilon1}\Phi\frac{\varepsilon}{k}-C_{\varepsilon2}\rho\frac{\varepsilon^2}{k}$

Table 7: Differential equations coefficients

The turbulent model constants that allow good agreement with experimental results for several types of flows are summarized in table 8.

C_μ	$C_{\varepsilon 1}$	$C_{\varepsilon 2}$	σ_k	σ_ε
0.09	1.44	1.92	1.0	1.3

Table 8: Turbulent model constants

4.4 Boundary Conditions

The computational study of the turbulent flow includes the solution of the continuity equation (4.6), momentum conservation equation (4.7), turbulent kinetic energy transport equation (4.10) and transport equation of the turbulent kinetic energy dissipation rate equation (4.13) in the computational domain considered. The equations have an elliptic form, so it is required the imposition of boundary conditions for all variables in all the borders of the solution domain. The computational domain corresponds to the experimental conditions and has 201 mm of transversal length, 1080 mm of longitudinal length, 402 mm of height where the inner diameter of the jets D is 15 mm, the spacing between jets are S = 6D and the height of impact, H is 20.1 D. To simulate numerically this flow it was necessary to define boundary conditions to reproduce exactly the experimentally situation. As shown in figure 106, the computational domain have 3 walls, namely the north wall with two consecutive impinging jets, the south wall that represents the impact wall in the experiments and the ground in the real situation, and the lateral wall that gives the confinement of the flow. The computational domain has also a plane of symmetry that allows simulating only half of the domain reducing the time of simulation and the costs. The crossflow enters the domain in the x axis direction. The jets flow vertically and may impinge on the south wall depending on the velocity ratio used.

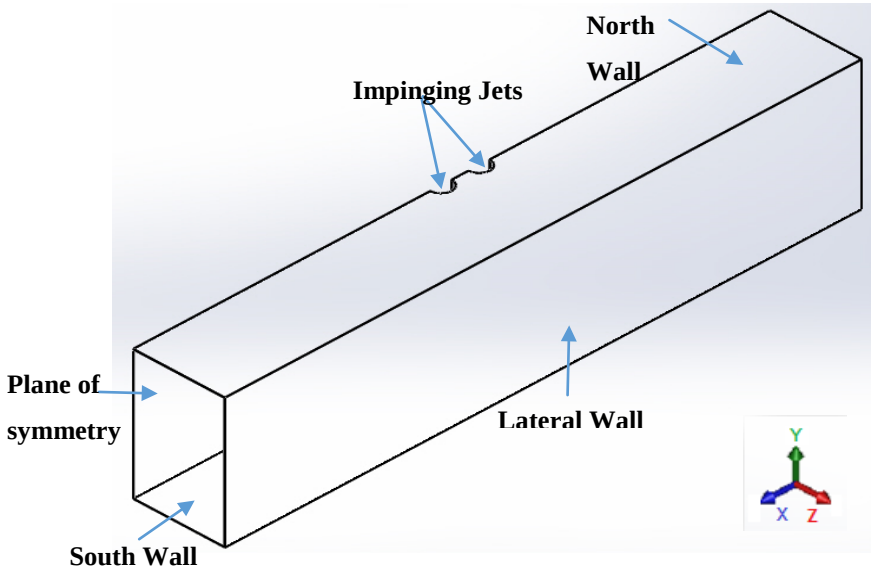

Figure 106: Computational domain used in the numerical simulation

The proximity to a solid boundary or wall influences the flow field because constrains to the physic variables is imposed. On the wall proximity the velocity approaches to zero due to the no slip condition and if the flow is no adiabatic there are energy exchanges between the fluid and the boundary. If there is not energy exchanges by radiation, the thermal conditions of the walls are locally influenced and the energy exchanges can be implemented by temperature gradients close to the walls. The turbulence characteristics quantities are also influenced due to the decrease of the possibilities of the velocity field fluctuations. In the present study case no exchanges of energy were considered.

Close to a wall the flow behaves like a unidimensional Couette flow, being the flow individualized in three distinct zones due to it different behaviour in each zone. The zone close to the wall can be individualized in:

- **Viscous sublayer**: It is the region closer to the wall and its name is due to the prevailing viscous effects.
- **Transition region or Turbulent boundary layer**: It is the region where the flow is completely turbulent
- **Inertia sublayer**: It is the region where the shear stress is assumed constant

4.4.1 Viscous sublayer: Law of the wall

In a turbulent flow, a very thin region next to a wall, typically only 1% of the boundary layer thickness, where turbulent mixing is impeded and transport occurs partly or, if the limit as the wall is approached, entirely by viscous diffusion. Considering a little pressure gradient in a referential with the x axis oriented on the friction flow direction and the y axis on the normal direction to the wall, the friction velocity in this region is traduced by the following expression (Wilcox, 1993):

$$u^+ = y^+ \tag{4.18}$$

where u^+ represents the dimensionless velocity and y^+ represents the dimensionless wall distance.

$$u^+ = \frac{\bar{u}}{u_\tau}, \text{ where } u_\tau \text{is the friction velocity} \tag{4.19}$$

$$u_\tau = \sqrt{\frac{\tau_w}{\bar{\rho}}}, \text{ where } \tau_w \text{ is the shear stress wall} \tag{4.20}$$

$$y^+ = \frac{\bar{\rho} u_\tau y}{\mu}$$, where $u_\tau$is the friction velocity (4.21)

The viscous sublayer is generally defined by the relation $0 \leq y^+ \leq 5$.

4.4.2 Turbulent boundary layer

Outside the viscous sublayer, we can neglect viscosity. Thus the only dimensional parameters that enter in the problem are the turbulent velocity scale or friction velocity u_τ, the total depth of the boundary layer δ, and the height y away from the wall. We can express this dependence as:

$$\bar{u} = u_\tau g\left(\frac{y}{\delta}\right) \tag{4.22}$$

The mean velocity depends on an additional external parameter, the velocity outside the boundary layer $\overline{u_0}$. We know that for $\frac{y}{\delta}$ tends to ∞, we have $\bar{u}$ tends to $\overline{u_0}$.

Integrate from $y \to \infty$ in toward the boundary to obtain $\bar{u}$,

$$\int_y^\infty \frac{d\bar{u}}{dy'}\, dy' \tag{4.23}$$

$$\frac{u_\tau}{\delta}\int_y^\infty g\left(\frac{y'}{\delta}\right) dy' \tag{4.24}$$

$$\bar{u}(y) - \overline{u_0} = u_\tau F\left(\frac{y}{\delta}\right) \tag{4.25}$$

This is a similarity solution for$\bar{u}^+$, which assumes that as the boundary layer changes size, or for different boundary layers $\bar{u}^+$ has the same form. This similarity solution is only valid outside of the viscous boundary layer, and cannot satisfy the boundary condition $\bar{u} = 0$ at the wall.

4.4.3 Inertial sublayer: logarithmic layer

Thus far we have two different laws for $\bar{u}^+$. One applies close to the wall in the viscous sublayer and satisfies the no-slip condition $\bar{u} = 0$. The other applies further away from the wall and is not guaranteed to satisfy the no-slip boundary condition at the wall; actually it turns out that away from the wall $u_\tau \ll \overline{u_0}$ and thus $\bar{u} - \overline{u_0} \approx -\overline{u_0}$. This indicates that a viscous sublayer with very steep gradients is required in order to satisfy the boundary conditions. Of course the

velocity doesn't suddenly jump from one scaling behavior to another. There is a transition region. In this transition region we expect both the law of the wall and the velocity defect law to apply. In these conditions the velocity distribution is represented by the following empiric relation:

$$u^+ = \frac{1}{\kappa}\log(Ey^+) \tag{4.26}$$

where κ is the Von Karman constant (universal value of 0.41) and E represents a parameter that depends of the wall roughness.

The turbulent quantities and the characteristics parameters of the wall laws are defined relatively to the local equilibrium hypothesis on the inertia sublayer. Assuming that in this region the turbulent kinetic energy production rate is equals to the dissipative rate:

$$\bar{\rho}\varepsilon = \mu_t\left(\frac{\partial\bar{u}}{\partial y}\right)^2 \tag{4.27}$$

where ε is the turbulent kinetic energy dissipation rate

Through the turbulent viscous definition we can obtain the equilibrium relation

$$u_\tau = c_\mu^{1/4}k^{1/2} \tag{4.28}$$

The calculation expression of the wall law dimensionless distance can be obtained introducing the previous result on the equation (4.21):

$$y^+ = \frac{\bar{\rho}yc_\mu^{1/4}k^{1/2}}{\mu} \tag{4.29}$$

Through the expressions (4.27) and (4.28) it is possible to define the equations to the logarithmic velocity profile of the inertial sublayer. The equation (4.30) represents the kinetic energy dissipation rate close to the walls used to defined boundary conditions of the transport energy equation:

$$\varepsilon = \frac{c_\mu^{3/4}k^{3/2}}{\kappa y}, \tag{4.30}$$

The equation (4.31) represents the shear tension used to defined boundary conditions of movement quantity equation on the wall proximity:

$$\tau_w = \frac{\kappa \bar{\rho} c_\mu^{1/4} k^{1/2}}{\log(E y^+)}, \tag{4.31}$$

To introduce the boundary conditions of the turbulent kinetic energy transport equation, the source terms of this equation are evaluated assuming a ε profile, traduced by the following equation:

$$\varepsilon = \frac{c_\mu^{3/4} k^{3/2}}{u_\tau} \frac{\partial u}{\partial y} \tag{4.32}$$

4.5 Numerical and computational procedures

A computational solution of the differential equations that represent the flow behaviour is possible through the use of appropriated numerical methods. Numerical equations are obtained in a discretized medium to represent the partial differential equations of the continuum where the universal laws do apply. The computational models face some difficulties related to the strong equations interdependence and difficulties related to the numerical models capacity to preserve the correct representation of the physical phenomena, thus ensuring the numerical stabilization of the model. In complex problems with turbulent flows, the models that have revealed computational robustness and versatility to handle with this kind of restrictions are based on the finite volume method. In this formulation the solution domain is subdivided into a finite number of small control volumes or cells by a grid.

The grid (figure 107) defines the boundaries of the control volumes while the computational node lies at the centre of the control volume. The advantage of finite volume methods is that the integral conservation is satisfied exactly over the control volume.

The net flux through the control volume boundary is the sum of integrals over the four control volume faces or six faces in the tridimensional case. The control volumes do not overlap. The value of the integrand is not available at the control volume faces and is determined by interpolation.

The discretized equations are obtained integrating the flow equations on the control volume defined by the domain discretization. In each volume control are defined a mesh node, in which it is intend to know the flow proprieties value. The central point of the volume control is called P and the point's correspondents to the neighbours' volume control are called N, S, E and W.

The n, s, e and w points are placed on the control volume surfaces and the intersection of the lines connecting two consecutive nodes. These indexes are also used to identify the control surface components.

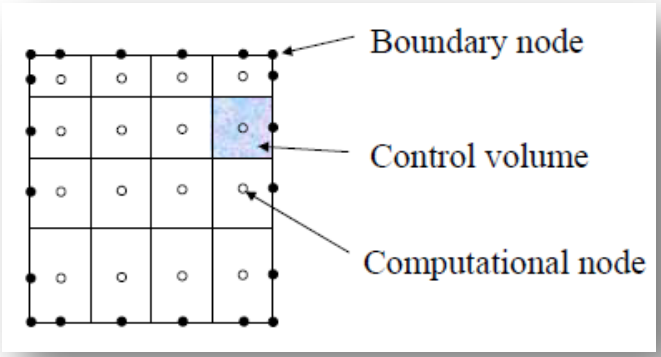

Figure 107: Grid Representation with the different elements[108]

To discretize the variable of an equation we can discretize linearly the equation that can be solved iteratively for all cells in the domain. This is the general approach used to solving partial differential equations used in computational fluid dynamics and it is done for all the conserved variables.

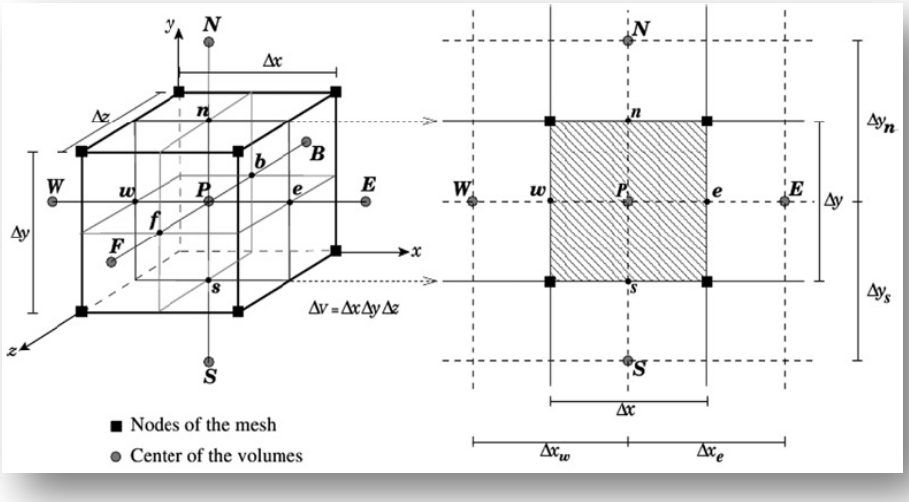

Figure 108: Control Volume representation. The black squares represents the nodes commonly used in finite difference methods, the circles represent the centre of the volumes and are labelled with uppercase letters meanwhile the faces are labelled using lowercase letters[109]**.**

[108] Lecture 5 - Solution Methods Applied Computational Fluid Dynamics, Instructor: André Bakker

[109] http://www.scielo.org.mx/scielo.php?pid=S0016-71692014000100005&script=sci_arttext

Taking the example of the conservation equation for a variable called Φ, the steps to take into account are:

1. **The integration of conservation equation in each cell (see figure 109).**
   Where:

   A_w, A_n, A_e and A_s represent the areas of the faces.

   c_w, c_n, c_e and c_s represent the concentrations at the faces.

   C_W, C_N, C_E and C_S represent the concentrations at the cell centres.

   u_w, u_n, u_e, u_s, v_w, v_n, v_e, vs represent the velocities at the faces.

   U_W, U_N, U_E, U_S, V_W, V_N, V_E, V_S represent the velocities at the cell centres.

   S_P represents de source in cell P.

   D represents the diffusion coefficient.

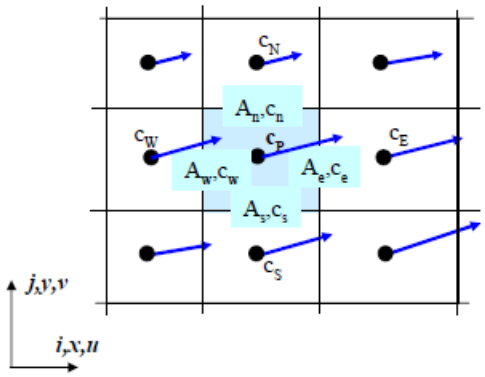

Figure 109: Control volume notation[110]

2. **Calculation of the face values in terms of cell centred values.**

The values at the faces need to be determined from interpolation from the values at the cell centres. The simplest way to determine the values at the faces is by using first order upwind differencing. In this case, it is assumed that the value at the face is equal to the value in the centre of the cell upstream of the face. The resulted equation can be rearranged to provide an expression for the calculated variable value at the centre of cell P as a function of the values of this variable in the surrounding cells, the flow field, and the grid.

[110] Lecture 5 - Solution Methods Applied Computational Fluid Dynamics, Instructor: André Bakker

3. Collection of like terms

$$a_P\phi_P = a_W\phi_W + a_S\phi_S + a_E\phi_E + a_N\phi_N + b$$
$$= \sum_{nb} a_{nb}\phi_{nb} + b \tag{4.33}$$

where nb refers to the neighbouring cells.

The coefficients a_{nb} and b will be different for every cell in the domain at every iteration.

The variable value on the field can be calculated by recalculating ϕ_P from this equation iteratively for all cells in the domain.

4.5.1 Relaxation

At each iteration, it is found a new value for variable ϕ in the cell P can be calculated from that equation. The relaxation is commonly applied in the following form:

$$\phi_P^{new,used} = \phi_P^{old} + URF\left(\phi_P^{new,predicted} - \phi_P^{old}\right) \tag{4.34}$$

Where URF represents the relaxation factor. When URF < 1 the numerical simulation is in under relaxation and this may slow down the convergence speed but in the other hand increase the stability of the calculation, i.e. the possibility of divergence or oscillations in the solutions are decreased. If URF = 1 corresponds to a situation of no relaxation and one uses the variable predicted value. Lastly if URF > 1 the numerical simulation is in over relaxation and this situation is only acceptable sometimes to accelerate the convergence but will decrease the calculation stability and therefore should be avoided.

In most of the numerical simulation cases the under relaxation factors are used because they suppress oscillations of the intermediate solution that result from the numerical errors. While the under relaxation factors are too small, the convergence is significantly slowed down and sometimes it takes the user to think that the solution converged when in the reality that is not what happens. Because of this situation it is always recommended the use of an under relaxation factors that are as high as possible, to ensure the non-occurrence of oscillation or divergence.

If the solution is converged but the pressure residual is still relatively high, the factors for pressure and momentum can be lowered to refine the solution.

4.5.2 Convergence

The iterative process is repeated until the change in the variable from one iteration to the next becomes so small that the solution can be considered and called converged. At convergence all discrete conservation equations are obeyed in all cells up to specific tolerance. Another fact is that the solutions no longer changes much with additional iterations, and were obtained balances for mass, momentum, energy and scalar properties.

The errors that occurred during the integration of conservation equation are called residuals, and measure the imbalance and the absolute residual at point P can be defined through the following expression:

$$R_P = \left| a_P \phi_P - \sum_{nb} a_{nb} \phi_{nb} - b \right| \tag{4.35}$$

Usually the residuals are scaled relatively to the local value of the property ϕ in order to obtain the relative error:

$$R_P = \frac{|a_P \phi_P - \sum_{nb} a_{nb} \phi_{nb} - b|}{\sum_{all\ cells} a_P \phi_P} \tag{4.36}$$

The residuals can also be normalized by dividing the maximum residual that was found at any time during the iterative process.

The overall residual in the computational domain can be express by:

$$R^{\phi} = \frac{\sum_{all\ cells} |a_P \phi_P - \sum_{nb} a_{nb} \phi_{nb} - b|}{\sum_{all\ cells} a_P \phi_P} \tag{4.37}$$

The numerical simulation is commonly considered converged, when the scaled residuals are on the order of $1x10^{-3}$ to $1x10^{-4}$ or less. But determining when the scaled residual values attain those values can be difficult. In order to facilitate this task it is common to monitor the residuals. The residuals monitoring it is important because sometimes the residuals have met the specified convergence criterion but are still decreasing and the solution may not yet be converged. On the other hand if the residuals never meet the convergence criterion, but are no longer changing and other solution monitors do not change either, the solution is converged and there is a problem with the normalization of the residuals. In the present case of study the residuals were also monitored graphically together with the global mass conservation (figure 110).

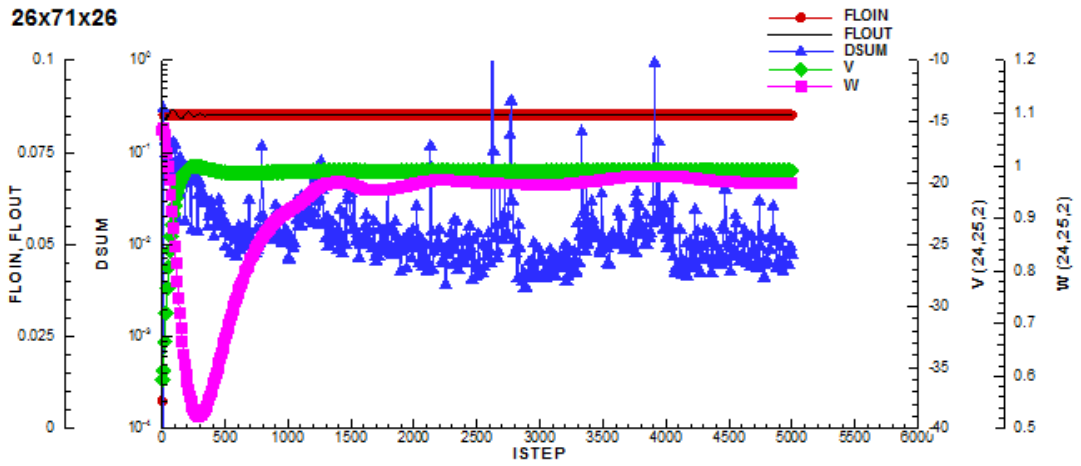

Figure 110: Example of residual monitored in this study: First jet residual monitored

4.5.3 Numerical schemes

The face values of ϕ variable and $\partial\phi / \partial x$ are found by making assumptions about the variation of ϕ between the cell centers. This is done with numerical schemes. There are several different numerical schemes, namely the first-order upwind scheme, the central differencing scheme, the power law scheme, the second-order upwind scheme and the QUICK scheme of Leonard (1979)[111]. For this numerical study only the QUICK scheme and the upwind scheme were used.

4.5.3.1 First order upwind Scheme

The first order upwind scheme (figure 111) is the simplest numerical scheme used. In this method it is assumed that the value of ϕ at the face is the same as the cell centered values in the cell localized upstream of the face. The advantages of this method are its ease implementation and stability. The negative point is the fact that this method is very diffusive, and tends to smear out the gradients verified in the flowfield.

4.5.3.2 Second order upwind Scheme

On the second order upwind scheme (figure 112) the value of ϕ is determined from the cell values in the two cells localized upstream of the face. This method is more accurate than the first order upwind scheme, although in the regions with strong gradients, it is possible that in the face values are outside of the range of the cell values. So, in these cases it is necessary to apply limiters to the predicted face values. This scheme is very popular because it is a combination of accuracy and stability.

[111] Leonard, B.P. "A Stable and Accurate Convective Modelling Procedure Based on Quadratic Upstream Interpolation", *Computer Methods in Applied Mechanics and Engineering, Vol. 19, No. 1, 1979, pp. 59-98.*

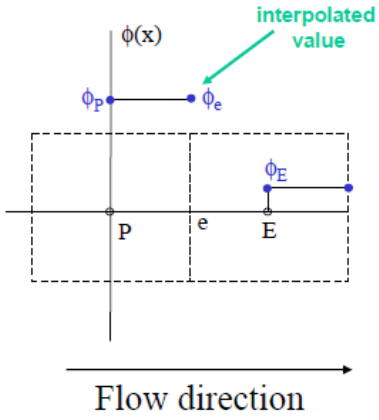

Figure 111: First order upwind scheme illustration[112]

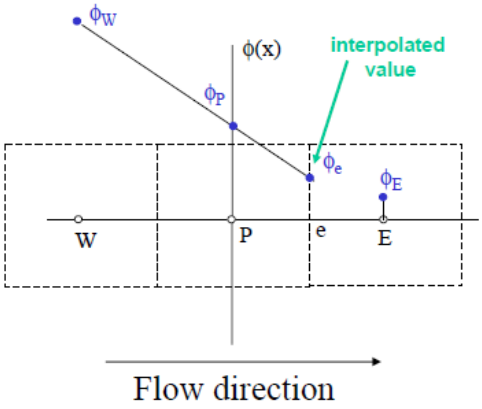

Figure 112: Second order upwind scheme illustration [113]

4.5.3.3 Quick Scheme

The QUICK stands for **Q**uadratic **u**pwind **i**nterpolation for **c**onvective **k**inetics (figure 113). In this scheme a quadratic curve is fitted through two upstream nodes and one downstream node. With this method, the QUICK scheme is a very accurate scheme, but during the interpolation overshoots and undershoots may occur in regions with strong gradients. This problem can bring stability problems in the calculations and allow unphysical values of the variables such as negative values of the turbulent kinetic energy.

Each of the schemes previously presented assume some shape of the function ϕ. The Taylor series polynomials can approximate this function. The Taylor series polynomials can be express by the following expression:

$$\phi(x_e) = \phi(x_P) + \frac{\phi'(x_P)}{1!}(x_e - x_P) + \frac{\phi'(x_P)}{2!}(x_e - x_P)^2 + \cdots + \frac{\phi^n(x_P)}{n!}(x_e - x_P)^n \qquad (4.38)$$

[112] Lecture 5 - Solution Methods Applied Computational Fluid Dynamics, Instructor: André Bakker
[113] *idem*

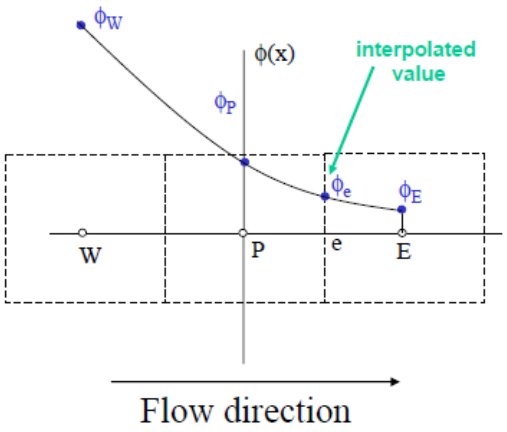

Figure 113: QUICK scheme illustration [114]

In the case of the first order upwind scheme only it is used the constant all the remaining terms are ignored. This scheme is therefore considered first order accurate. The second order upwind scheme does include the first order derivate, but ignores the second order derivate. So this scheme is considered second order accurate. Lastly, the QUICK scheme does take the second order derivative into account, but ignores the third order derivative. So this scheme can be considered third order accurate.

As expected the higher order schemes will be more accurate, but on the other hand they will be less stable and will increase computational time.

The use of QUICK has already been proven to be quite efficient for the strong jet impingement through a crossflow problem (see Barata et al, 1989[115]) and is used in the present study with PACEJ[116].

4.5.3.4 Properties of numerical schemes

All the numerical schemes must have some properties, such as, conservativeness, boundedness and transportiveness. The conservativeness property regards to the global conservation of the fluid property, which must be ensured. In the boundedness property the values predicted by the scheme should be within realistic bounds. For the linear problems without sources, those would be the maximum and the minimum boundary values. The fluid flow is nonlinear and the values in the domain may be outside the range of the boundary values. In the transportiveness propriety the diffusion works in all directions but convection only in the flow direction. The numerical schemes should capable to recognize the direction of the flow and the way that it affects the strength of convection versus diffusion.

[114] Lecture 5 - Solution Methods Applied Computational Fluid Dynamics, Instructor: André Bakker

[115] Barata, J.M.M., Durão, D.F.G. and McGuirk, J.J., "Numerical Study of Single Impinging Jets Through a Crossflow". Journal of Aircraft, Vol.26, No.11, Nov 1989, pp.1002-1008.

[116] The original computer code PACE included only the hybrid scheme.

4.5.3.5 Pressure

For the pressure the convection-diffusion equations cannot be solved, although for the others all variables such equations are available. The gradients in the pressure appears in the momentum equations, thus the pressure field needs to be calculated in order to be able to solve these equations. If the flow is compressible the density can be obtained from the continuity equation, the temperature follows from the enthalpy equation and the pressure can be then calculated from an equation of state. However, if the flow is incompressible the density is constant and not linked to the pressure.

The solution of the Navier-Stokes equations is then complicated by the lack of an independent equation for the pressure.

As mentioned previously the pressure appears in all of the three momentum equations. But the velocity field also has to satisfy the continuity equation. So, even though there is no explicit equation for the pressure, since there are four variables the set of equations needs the same number equations to be closed.

The so called pressure-velocity coupling algorithms are used to derive equations for the pressure from the momentum equations and the continuity equations. From existing algorithms the most popular is the semi-implicit method for pressure–linked equations, or SIMPLE. In this algorithm an algebraic equation for the pressure correction p' is derived, in a form similar to the equations derived for the convection diffusion equations.

$$a_P p' = \sum_{nb} a_{nb} p' + b' \tag{4.39}$$

At each iteration, the pressure field is updated by applying the pressure correction. The source term b' is the continuity imbalance. The other coefficients depend on the mesh used and the flow field.

This method to calculate the pressure it is based on the premise that a fluid flows from regions with high pressure to low pressure. The algorithm is iterative. The basic steps are as follows:

1) Start with an initial guessed pressure field;
2) Look at a cell;
3) If continuity is not satisfied because there is more mass flowing into that cell than out of the cell, the pressure in that cell compared to the neighbouring cells must be too low;
4) Thus the pressure in that cell must be increased relative to the neighbouring cells;
5) The reverse is true for cells where more mass flows out than in;

6) Repeat this process iteratively for all cells;

The important issue is to find a good equation for the pressure correction as a function of mass imbalance.

4.5.4 Mesh generation

A mesh or grid is a discretization of a geometric domain into small simple shapes, such as triangles or quadrilaterals in two dimensions and tetrahedral or hexahedra in three dimensions. Meshes are essential in the numerical solution of partial differential equations arising in physical simulation. It is important that the grid or mesh reproduces the best possible way the computational domain of the numerical simulation. In this numerical simulation the objective is to reproduce integrally the experimental work done, and then to extend the analysis to regions where measurements could not be obtained and to make a parametric study. The grid used in this simulation could not be uniform because it would have to be refined in the areas of the greatest gradients, as the region of the impact jets and the region near the impact wall. In an initial phase it was important to define how many points were within each jet as well as how many points were close to the impact surface. To reproduce the experimental conditions the grid would have to be symmetrical relative to the center of the nozzles, which means that for this point, the number of points at the left and at the right sides should be equal.

The computational domain corresponds to the experimental conditions having 201 mm of transversal length, 1080 mm of longitudinal length, and 402 mm of height. The inner diameter of the jets D was 15 mm, the spacing between jets were S = 6D and the height of impact, H was 20.1 D. With this elements and requirements it was created a FORTRAN routine called GRID to generate a grid that adapts to the flow studied. Several tests were done and three meshes were selected as candidates to do the grid independence tests. The meshes chosen were 17X53X17, 26X71X26 and 34X89X34. Then these three different meshes were used as an input file to the FORTRAN program PACEJ. PACEJ is a FORTRAN program that is subdivided in different routines that together allow the numerical reproduction of the study done experimentally. The program PACEJ consists of the main program, the INIT (is related to the declaration of variables), the PROPS (is related to the calculation of the properties such as density and viscosity), the PROBSP (where the boundary conditions are imposed), COEFF (matrix coefficients assembly using QUICK differencing) and SOLVER (which solves the set of equations for all variables depending on the imposed boundary conditions) and six other subroutines.

The results obtained for the different meshes were condensed graphically and are shown in the Figure 114 for the horizontal profiles of the mean horizontal component. According to Barata et

al. (1989)[117] the most difficult region to simulate for short jet impingement flows through a crossflow is the impingement region, namely the turbulent quantities and the mean horizontal velocity component. So, the profiles of Figure 114 correspond to this region for Y/D≥10 and -8<X/D<+8 and show similar results for all the different meshes. Therefore, in situations like this, where all of the meshes presented similar, the better choice is an intermediate mesh. In the present study the grid chosen was 26X71X26, with a totally of 47,996 points, which in conjunction with the higher order QUICK differencing scheme allows good agreement with the experiments for this type of flows with coarser meshes (e.g. Barata et al., 1989)[118]. It should be

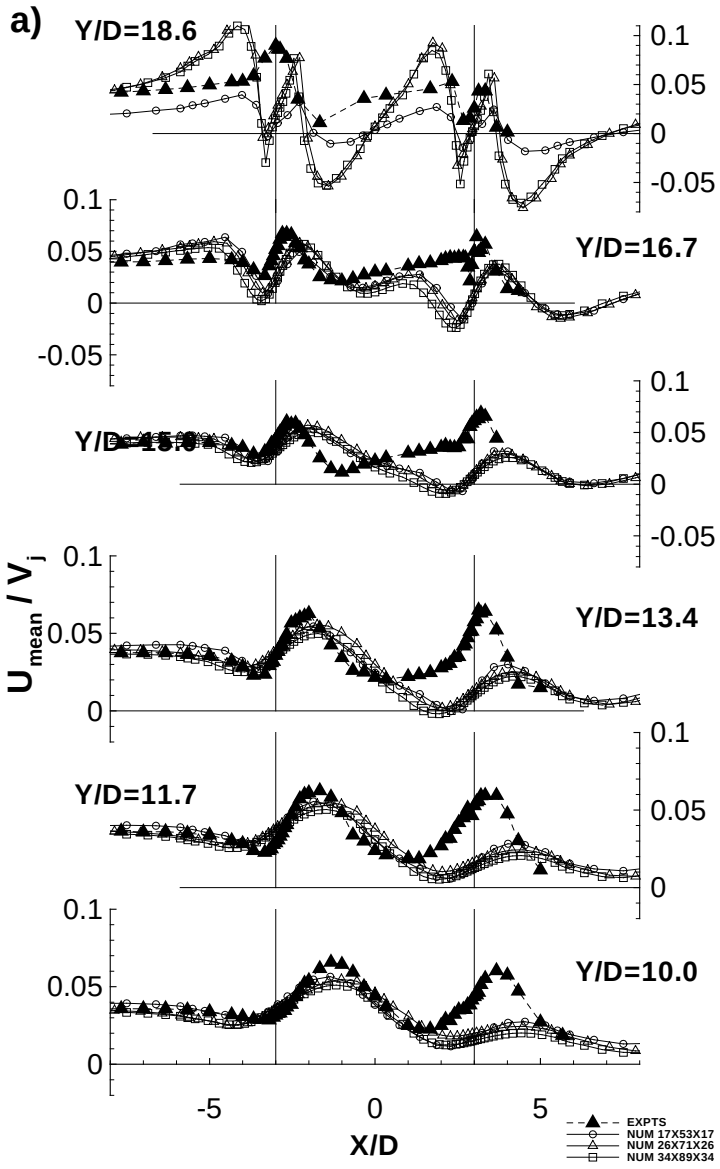

Figure 114: Horizontal profiles of the mean horizontal velocity component. Grid independence verification

[117] Barata J. M. M., Durão D. F. G., McGuirk J. J. (1989b). Numerical Study of Single Impinging Jet through a Crossflow. *Journal of Aircraft*. **26(1)**: 1002-1008.

[118] Idem.

pointed out that in spite of the difficulties to predict the turbulent structure of the impinging zone, the corresponding effect on the simulation of the mean flow field is not too significant, as shown by Barata et al. (1989)[119], because the flow is dominated by large pressure gradients.

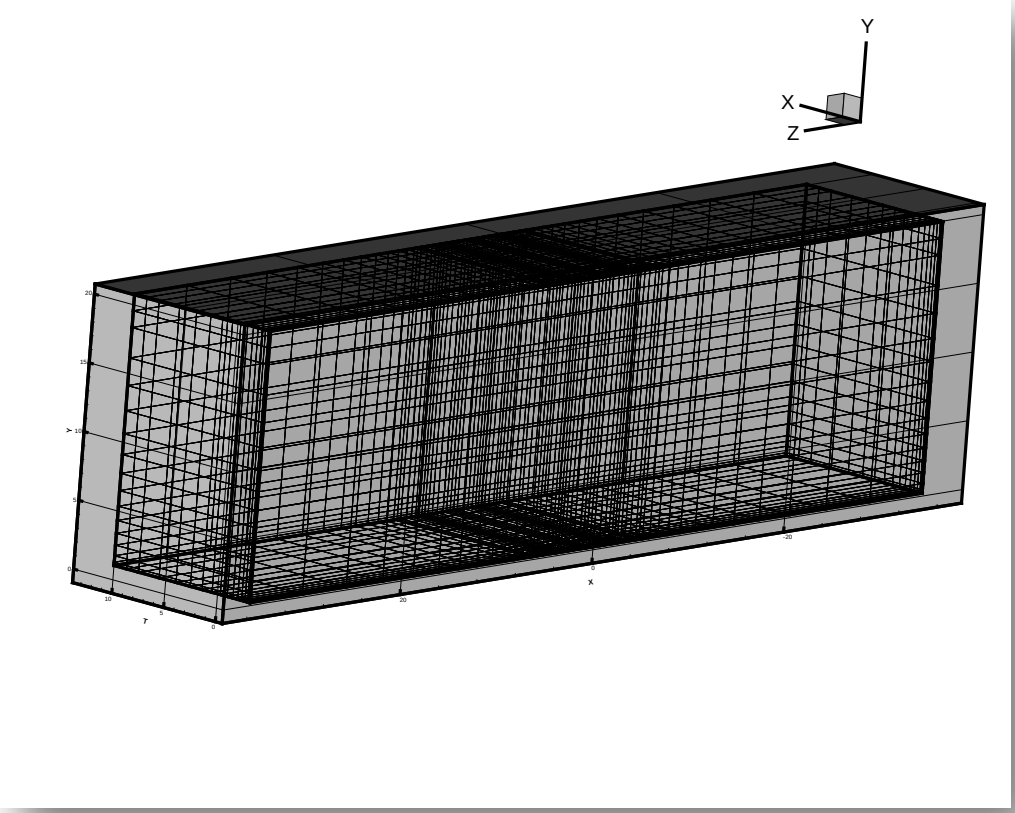

Figure 115: Grid representation on the computational domain

Variable	Value
YTOT	0.302 m
ZTOT	0.09 m
ZHOLE	0.045 m
XTOT	0.201 m
EPSX	1.15
EPSY	1.2
EPSZ	1.2

Table 9: Values used to defined the grid used in the numerical simulation

[119] idem.

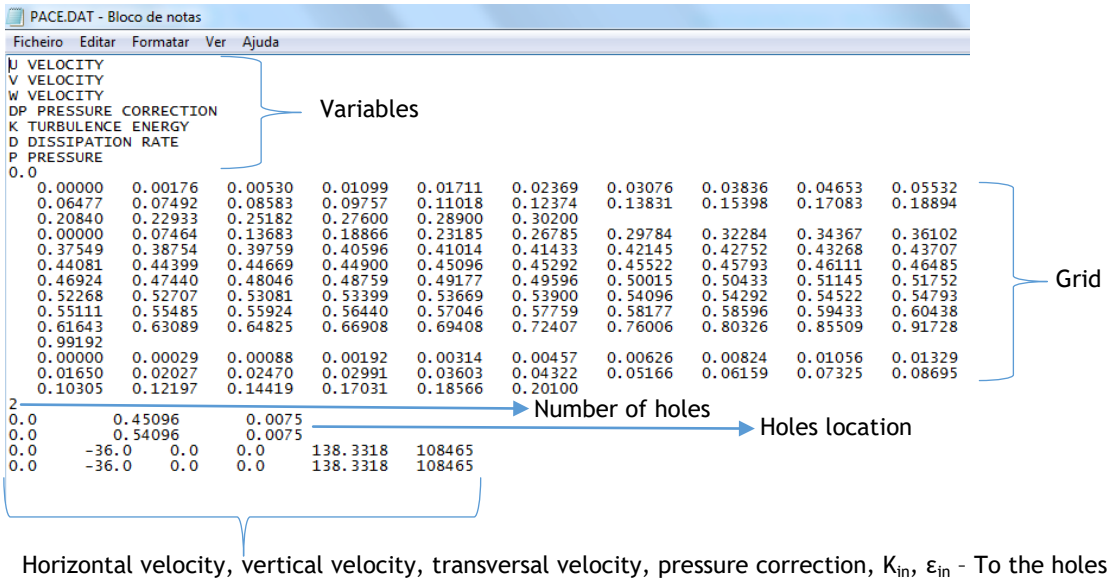

Figure 116: Input file to PACEJ program

4.6 Summary

This chapter presents the computational method employed in the calculations performed to extend the experimental study.

The numeric solution to the turbulent flow studied requires an approximate solution of the discretized algebraic equation system, which is constituted by the continuation equation (Eq. 4.6), momentum conservation equation (Eq. 4.7), turbulent kinetic energy transport equation (Eq. 4.10) and transport equation of the turbulent kinetic energy dissipation rate, on the solution domain. The different boundary layers presented in the solution domain were also specified in the sub-section 4.4. In the next sub section, it was explained the domain discretization through the finite volume method. The finite volume method uses the integral conservation equation applied to a control volume which subdivides the solution domain. The variables value at the faces of the control volume are determined by interpolation. Each time a convergent solution is obtained, the accuracy of the result obtained is a result of the approximation method of convective and diffusive flows on the faces of the finite control volume, and it is quantified through the errors analyse by the truncation developing Taylors series for each approximation method. Three different numerical schemes were presented: the first and second upwind schemes and the QUICK scheme. The upwind schemes (first and second order) attempt to discretize hyperbolic partial differential equations by using differencing based in the direction determined by the sign of the characteristic velocities. The QUICK scheme use a quadratic function passing through two bracketing or surrounding nodes and one

node on the upstream side must be used. The second order central difference is used for the diffusion term and for the convection term the scheme is third order accurate in space and first order accurate in time. Compared the described schemes it was possible to understand how each numerical scheme discretized the equations that provide the domain solution. The QUICK scheme proved to be more accurate that the upwind schemes, because in the QUICK scheme the false diffusion errors are minimized. Also in this chapter was presented the different boundary conditions used to reproduce integrally the experimental situation. To finish the chapter, it was addressed the question of meshing as well as the grid independence process in order to find the appropriate grid for the best reproduction scenario for the study situation.

Chapter 5

Numerical Results

5.1 Introduction

This chapter presents the numerical results that were used to extend the experimental results to velocity ratios beyond the experimental conditions, and to better understand the flowfield, namely the downstream side and the region close to the impact wall. In the downstream side of the working volume the experimental results were not easily obtained because of the jet velocity did not allow the seeding particles to entrain the flow. Close to the impact wall some difficulties to obtain experimental results were also felt due to the seeding particles absence and the deposition of some seeding drops on the impact wall.

5.2 Test conditions

The results presented in this chapter were obtained numerically. The grid and the mathematical model used have been described in detail in chapter 5. The geometry used in the numerical study was the same used in the experimental case. The numerical simulation was a reproduction of the experimental study presented in chapter 3 and partially reported in Vieira, 2012[120]. The results presented in this chapter correspond to the operating conditions shown in table 10.

5.3 Discussion

5.3.1 Measured flowfield simulation

Figures 117 to 119 show the measured mean vertical velocity component (V_{mean}) distribution along the vertical plane of symmetry (i.e. Z=0) together with calculated streamtraces. The velocity ratios presented are the same used in the experimental study. For all the velocity ratios the collision of the upstream wall jet with the crossflow is clearly registered. Meanwhile, the ground vortex is also identified for all velocity ratios, but its centre moves

[120] Vieira D. F. C. (2012). *Turbulent Structure of the Impact of a Ground Vortex Flow*. Master Thesis in Aeronautical Engineering. University of Beira Interior, Covilhã, 110 pp.

NX	26	JMAX	NZ
NY	26	**KMAX**	NX
NZ	71	**NMAX**	6
NS	71	**L**	25
NXYZ	47996	**M**	70
PR	7X0.1	**N**	25
RHOREF	1.2 kg/m^3	**NF**	6
CP	1005 kJ/kg.K	**ITEST**	1
GASCON	8314,3 J/kmol.K	**KLIC**	1
WAIR	28,85 g mol^{-1}	**KRAD**	1
AK	0.433	**D**	0.015 m
CD1	1.44	**VJ1**	36 m/s
CD2	1.92	**VJ2**	36 m/s
CM	0.09	**PUV**	$1x10^6$
EWALL	4.82	**PKE**	$1x10^6$
ISKIP	1	**ZHOLE1**	0,495 m
JSKIP	1	**ZHOLE2**	0,585 m
KSKIP	34	**YHOLE**	0,0075 m
NSKIP	10000	$\mathbf{k_{in}}$	138,3318 m^2/s^4
IMAX	NY	ε_{in}	108,435 m^2/s^6

Table 10: Summary of the constant values used during the computational simulation.

upstream when the velocity ratio increases. The centre of the ground vortex is located at X/D=-4, -7 and -8 for velocity ratios V_j/U_0 of 22.5, 33.7 and 43.8, respectively. The red regions indicate positive values of the mean vertical velocity component exist due to a slight acceleration of the flow which passes over the ground vortex. The second jet seems to be

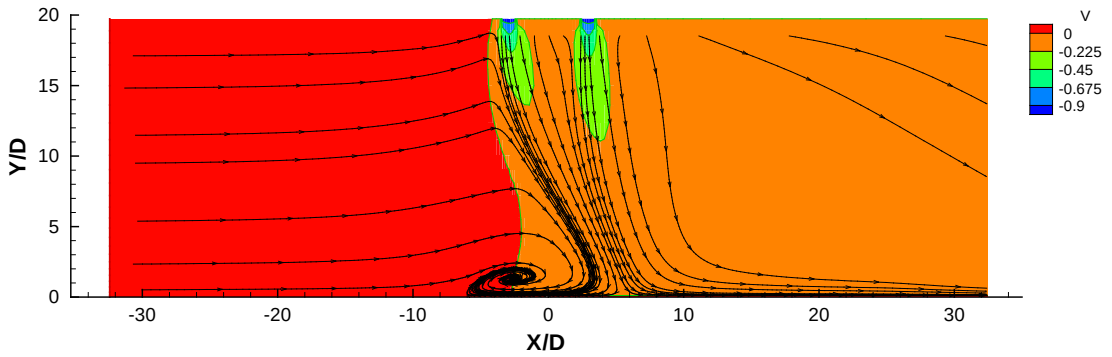

Figure 117: Calculated stream traces and mean vertical velocity component distribution along the vertical plane of symmetry (i.e. Z=0) for V_j/U_0=22.5, Re_j=43,000, H/D=20.1, and L/D=6.

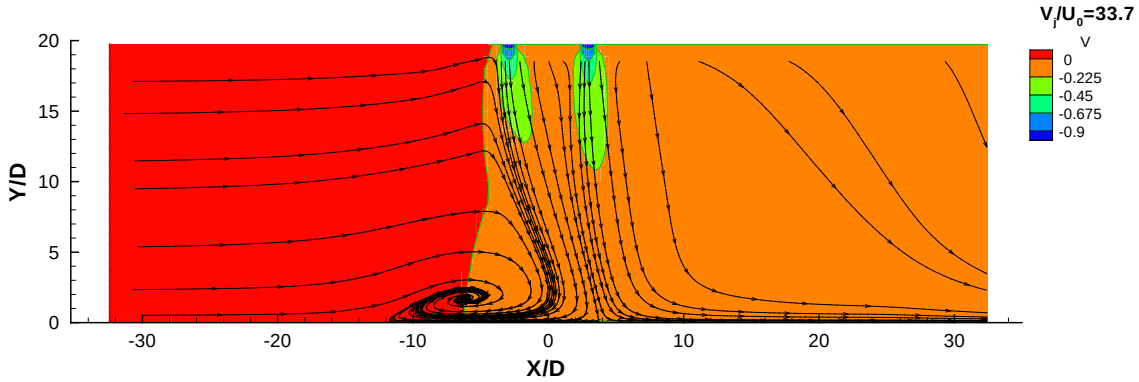

Figure 118: Calculated stream traces and mean vertical velocity component distribution along the vertical plane of symmetry (i.e. Z=0) for V_j/U_0=33.7, Re_j=43,000, H/D=20.1, and L/D=6.

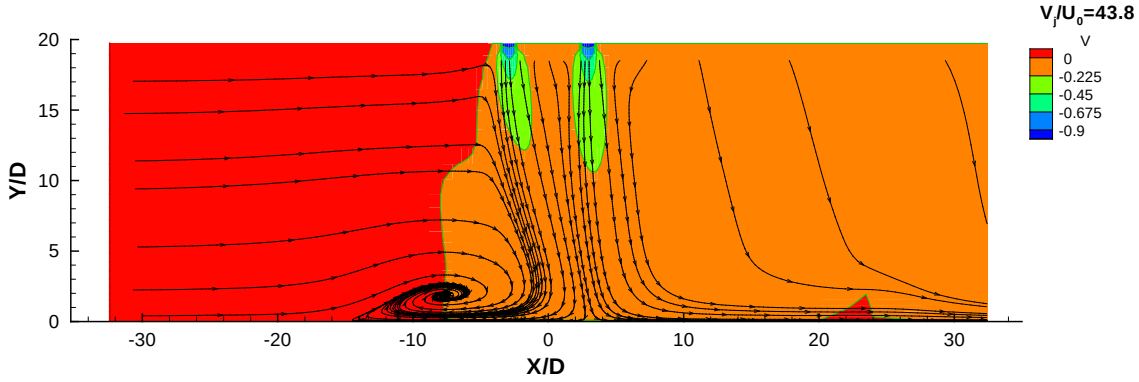

Figure 119: Calculated stream traces and mean vertical velocity component distribution along the vertical plane of symmetry (i.e. Z=0) for V_j/U_0=43.8, Re_j=43,000, H/D=20.1, and L/D=6.

completely deflected by the crossflow for the three different velocity ratios, and no ground vortex is formed. Another result is the decrease of the first jet deflection with the velocity

ratio by the same reason that was mentioned before to the change of the ground vortex centre location.

Figures 120 to 122 show the corresponding mean vertical velocity component (V_{mean}) distributions along the vertical plane of symmetry (i.e. Z=0) obtained experimentally. The resolution of the experimental results is not so complete due to difficulties in obtaining validated results downstream of the second jet. This causes major difficulties to obtain the velocity vectors and streamtraces near the impinging zone where the curvature of the flow is more accentuated. Nevertheless, the numerical and experimental flowfields exhibit similar patterns for all the velocity ratios. The ground vortex could be captured, and the change of its location and size with the velocity ratio agrees with the experimental observations, but some quantitative differences can be observed as shown in table 11.

The centre of the ground vortex is moving upstream and its strength increases with the velocity ratio. These tendencies are also observed experimentally except for the higher velocity ratio that has ground vortex strength smaller by one diameter.

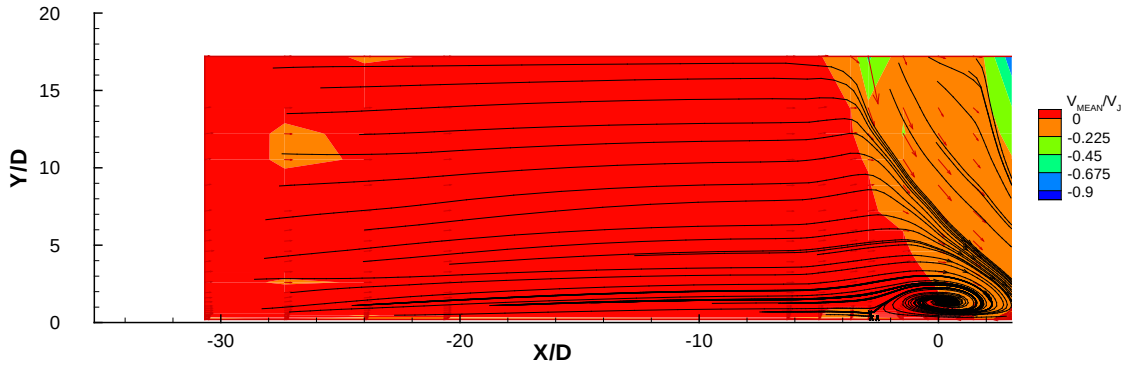

Figure 120: Mean vertical velocity component distribution along the vertical plane of symmetry (i.e. Z=0) obtained experimentally for V_j/U_0=22.5, Re_j=43,000, H/D=20.1, and L/D=6.

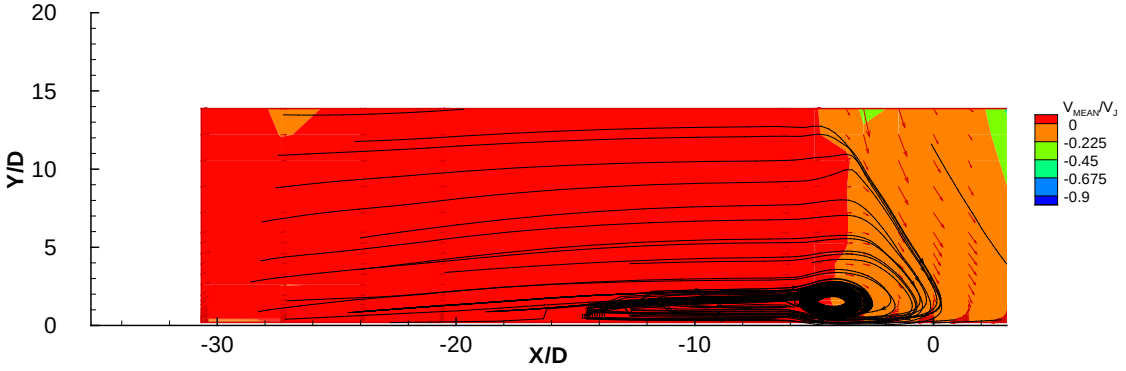

Figure 121: Mean vertical velocity component distribution along the vertical plane of symmetry (i.e. Z=0) obtained experimentally for V_j/U_0=33.7, Re_j=43,000, H/D=20.1, and L/D=6.

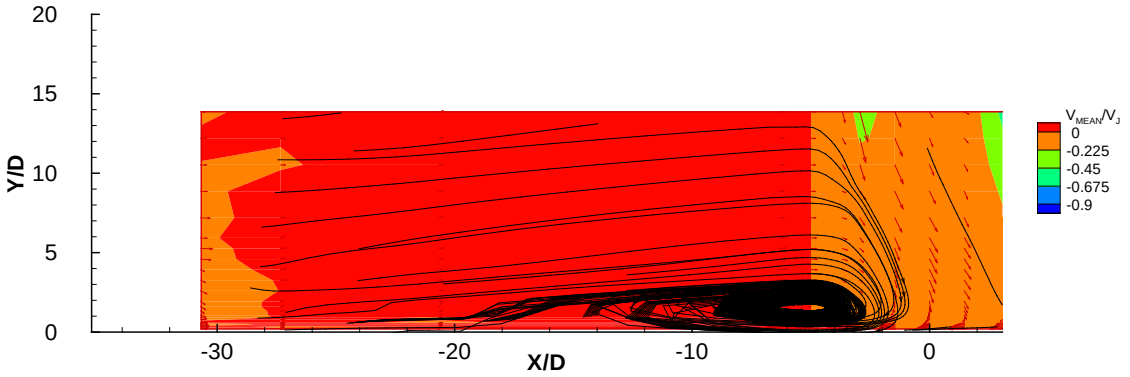

Figure 122: Mean vertical velocity component distribution along the vertical plane of symmetry (i.e. Z=0) obtained experimentally for V_j/U_0=43.8, Re_j=43,000, H/D=20.1, and L/D=6.

For the ground vortex width, the same behaviour of the ground vortex strength is registered both on the numerical and experimental case. This change in the ground vortex dimension is due to the decrease of the crossflow velocity (increase of the velocity ratio), allowing the growth of the ground vortex.

	Numeric			Experimental		
Velocity ratio	Ground vortex center position	Ground vortex strength	Ground vortex width	Ground vortex center position	Ground vortex strength	Ground vortex width
22.5	X/D=-4	X= 10D	Y= 2D	X/D=0.5	X= 6D	Y= 2D
33.7	X/D=-7	X= 11D	Y= 2.5D	X/D=-5	X= 14D	Y= 3D
43.8	X/D=-8	X= 14D	Y= 3D	X/D=-5.5	X= 13D	Y= 4.5D

Table 11: Summary of the ground vortex dimensions.

5.3.2 Numerical flowfields extension

The numerical analysis of this flow allowed extending the experimental results to velocity ratios beyond of the experimental conditions and to better understanding the flowfield behaviour with the velocity ratio increase. In the next figures are presented the results for velocity ratios between 7.5 and 90.

The results show that even for the smallest velocity ratios of V_j/U_0=7.5 and 15 (figures 123 and 124) the jets do not mix, but remain together in two layers. For the figure 123 it is possible to identify a flow regime that it is characterized by the absence of jets impact on the wall and the ground vortex formation. For V_j/U_0=15 (figure 124) the downstream jet does

not reach directly the ground, but it impinges on the wall jet resulting from the first jet which is moving downstream. For this velocity ratio it is possible to identify another flow regime also characterized by the absence of ground vortex formation like the lower velocity ratio. The two different flow regimes are identified by figures 123 and 124, and correspond to the transition between hover and conventional flight. For the two higher velocity ratios (figures 125 and 126) the ground vortex is always present, but its size and location changes. It moves upstream with V_j/U_0 when compared with the results obtained to $V_j/U_0 \leq 43.8$ (figures 117 to 119). For V_j/U_0 = 60.0 and 90.0 another flow regime is identified, which is the most important for a V/STOL aircraft operating in ground vicinity due to the strong jets impingement on the ground with the formation of a ground vortex. In this flow regime the streams from the lifting jets, or fans, are swept back by the freestream and rolled up into vortex pairs. These vortices, along with the entrainment action and blockage effect of the jets, induce suction pressures on the bottom of the configuration beside and behind the jets

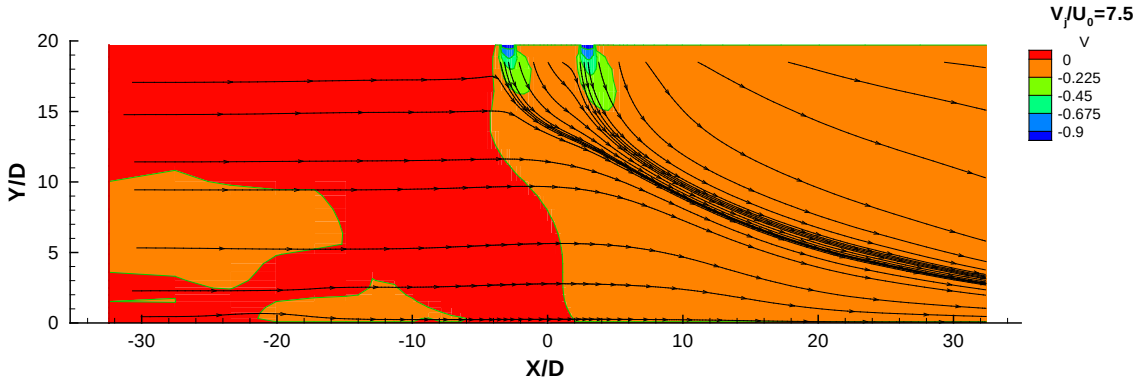

Figure 123: Mean vertical velocity component distribution along the vertical plane of symmetry (i.e. Z=0) obtained experimentally for V_j/U_0=7.5, Re_j=43,000, H/D=20.1, and L/D=6.

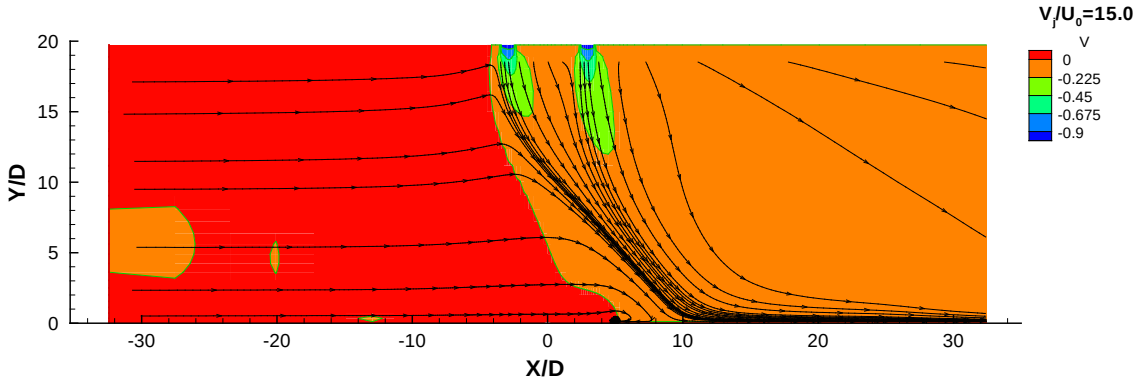

Figure 124: Mean vertical velocity component distribution along the vertical plane of symmetry (i.e. Z=0) obtained experimentally for V_j/U_0=15.0, Re_j=43,000, H/D=20.1, and L/D=6.

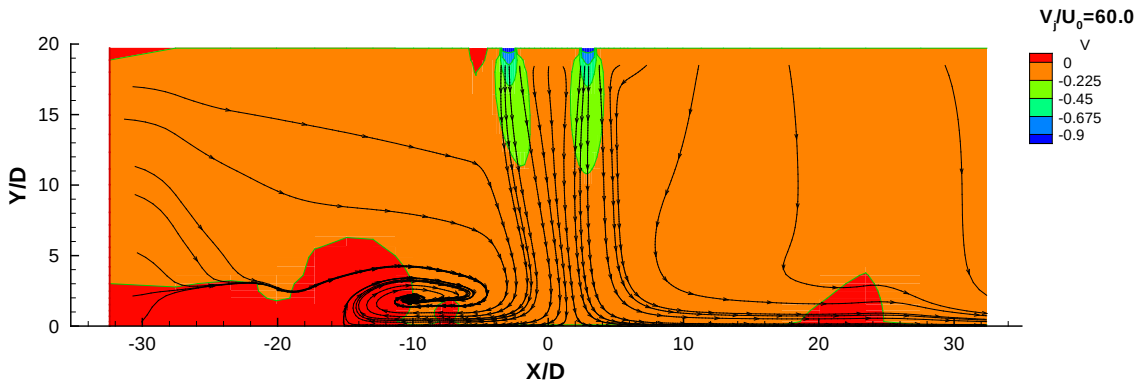

Figure 125: Mean vertical velocity component distribution along the vertical plane of symmetry (i.e. Z=0) obtained experimentally for V_j/U_0=60.0, Re_j=43,000, H/D=20.1, and L/D=6.

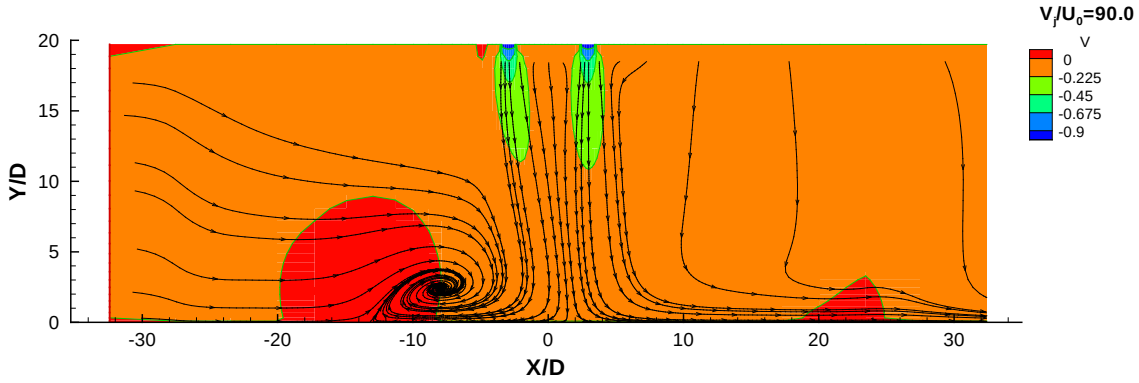

Figure 126: Mean vertical velocity component distribution along the vertical plane of symmetry (i.e. Z=0) obtained experimentally for V_j/U_0=90.0, Re_j=43,000, H/D=20.1, and L/D=6.

and a smaller region of positive pressures ahead of the jet. The induced negative pressures can produce lift losses and pitching moments, although these effects are dependent of the velocity ratio used. Through the analysis of the figures for velocity ratios greater than 22.5, it is not possible to see clearly what happens with the second (rear) jet. It might be impinging on the ground (and then all the flow from the first jet should surround the rear impinging point) or impinging on the wall jet resulting from the first jet (the second jet would become parallel to the ground plane and merge with the wall jet resulting from the first impinging jet) or eventually it deflected completely by the crossflow (similar to the last option but a grounded mixing layer would result instead). So, one major issue in the present flow configuration is the possible deflection of the rear jet by the crossflow without occurring direct impact on the ground. Another possibility (not yet demonstrated) is the impact of the second jet with the first deflected jet or its downstream wall (depending on the velocity ratio). None of the figures presented below it is sufficiently conclusive about this hypothesis, nor about the blending of the two structures further downstream.

5.3.2.1 Second jet behaviour study

In order to better understand this type of flow, and in particular that happened with the rear jet and downstream of the impinging jets, a meticulous numerical study simulation was performed for V_j/U_0=22.5 by varying the velocity of the second jet, V_{j2} , from, 5.4 m/s up to 26.72 m/s. The velocity of the first jet was kept constant to preserve the location of the centre of the ground vortex. The results are shown in figures 127 to 130 for the initial conditions summarized in table 12.

V_{j1}= 36 m/s, U_0= 1.6 m/s, V_{j1}/U_0= 22.5, K_{inj2}= 138.3318 m^2/s^4, ε_{inj2}= 108435 m^2/s^6				
V_{j2} [m/s]	V_{j2}/U_0	$(V_{j1}/U_0)/(V_{j2}/U_0)$	k_{inj2} [m^2/s^4]	ε_{inj2}[m^2/s^6]
26.72	16.7	1.35	76.2064	44350
13.5	8.43	2.67	19.4530	5720
8.99	5.62	4.00	8.6404	1693
5.4	3.37	6.67	3.1105	365.7

Table 12: Summary of the jet velocities used on the wall jet study (V_{J1}/U_0=22.5)

The values of k_{in} and ε_{in} are dependent on the velocity of the impinging jets, and were obtained through the following expressions:

$$k_{in} = \frac{1}{2}\left(\overline{u'^2} + \overline{v'^2} + \overline{w'^2}\right) \quad (5.1)$$

$$\varepsilon_{in} = \frac{k^{3/2}}{D} \quad (5.2)$$

The results are similar when the second jet velocity ratio, V_{j2}/U_0, is varied from 3.37 up to 16.7, and the most significant changes on the flow were observed to $V_{j2}/U_0 \leq$ 8.43.

Figures 127 to 130 show that decreasing the velocity of the second jet in relation to the first jet, the wall jet of the second jet is always above the wall jet formed by the interaction of the first impinging jet with the crossflow, heading the flow to downstream. Decreasing the second jet velocity, the ground vortex size decreases. As far as the location of the ground vortex centre is concerned, decreasing the second jet velocity pushes the ground vortex centre in the downstream direction.

It is also possible to conclude that the fluid of the crossflow is entrained by the first jet and consequently part of it is goes to the scarf vortex inside. Figure 131 shows the static pressure distribution near the impinging wall for V_j/U_0=8.43 that exhibits a negative flow region which

is associated with the ground vortex. In the centre, the largest pressures occur (red colour) identifying a single stagnation zone corresponding to the first (upstream) jet.

As shown by the blue streamtraces of figure 132, then the fluid of the scarf vortex rises and passes over the wall jets. The remaining fluid that is not entrained by the scarf vortex circumvents the incidents jets passing over the scarf vortex and later joins the wall jet resulting from the rear jet (purple streamtraces). These results lead to the conclusion that the second jet reinforces the first jet in terms of strength, since as greater the second jet velocity is as further upstream is located the ground vortex centre. If the first jet velocity and the crossflow velocity are constant, the size and ground vortex centre location changes can only be originated by the change of the second jet velocity. However, the second jet strengthens the first one and allows more fluid to be entrained by the ground vortex changing its size.

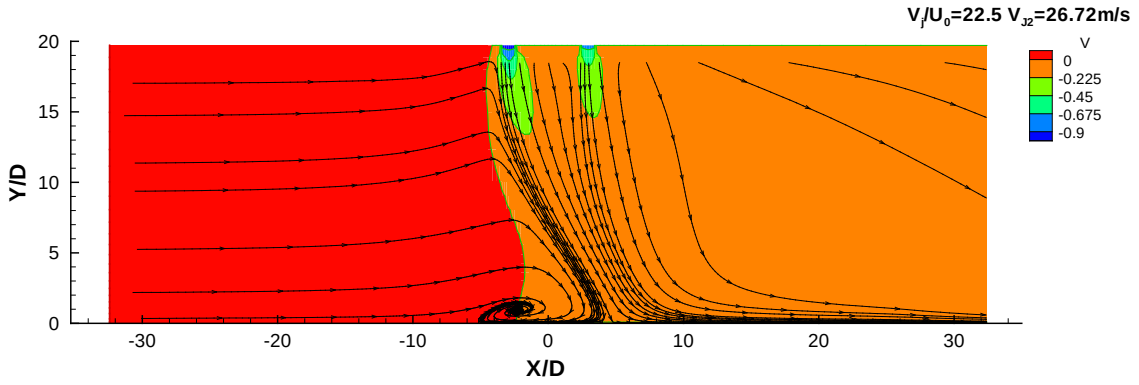

Figure 127: Calculated stream traces and mean vertical velocity component distribution along the vertical plane of symmetry (i.e. Z=0) for V_{j2}/U_0=16.7, H/D=20.1, and L/D=6.

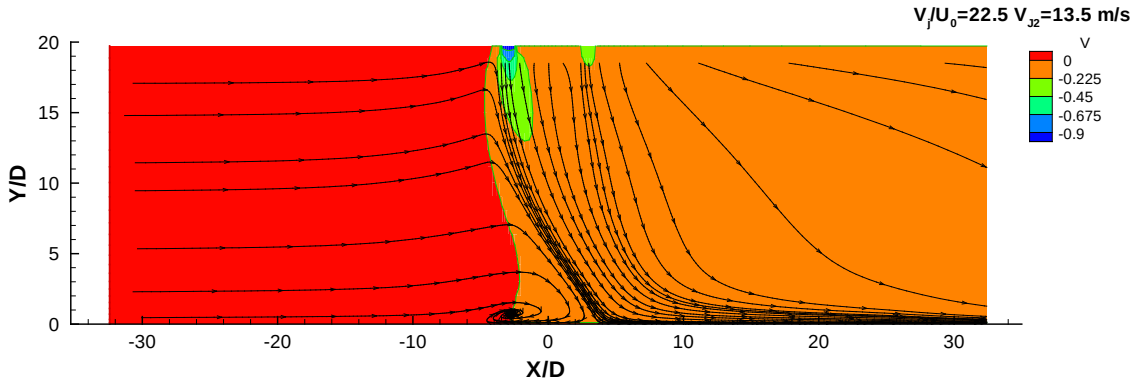

Figure 128: Calculated stream traces and mean vertical velocity component distribution along the vertical plane of symmetry (i.e. Z=0) for V_{j2}/U_0=8.43, H/D=20.1, and L/D=6.

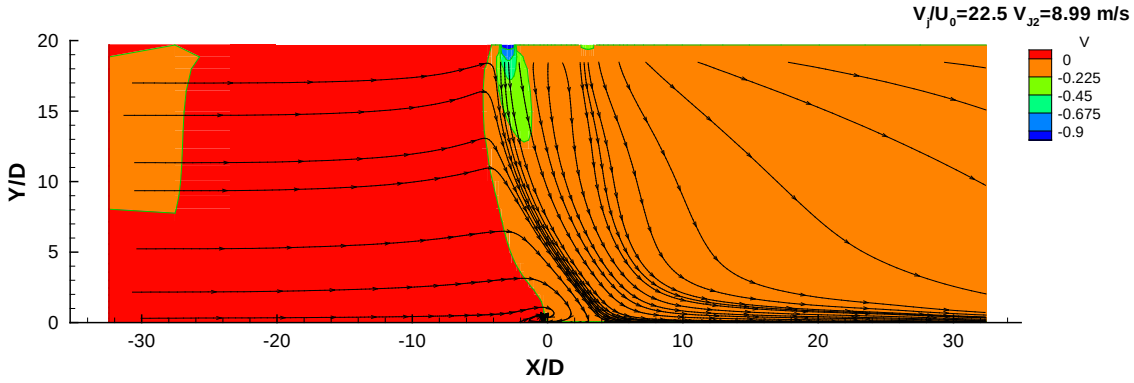

Figure 129: Calculated stream traces and mean vertical velocity component distribution along the vertical plane of symmetry (i.e. Z=0) for V_{j2}/U_0=5.62, H/D=20.1 and L/D=6.

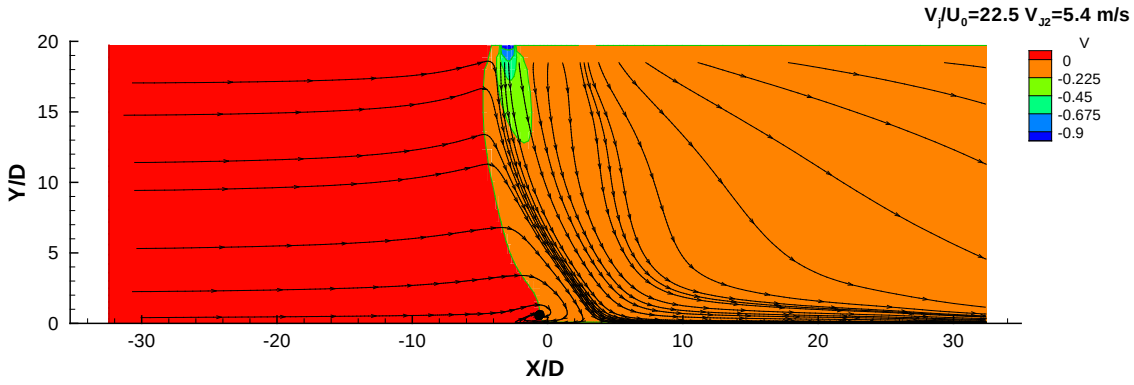

Figure 130: Calculated stream traces and mean vertical velocity component distribution along the vertical plane of symmetry (i.e. Z=0) for V_{j2}/U_0=3.37, H/D=20.1 and L/D=6.

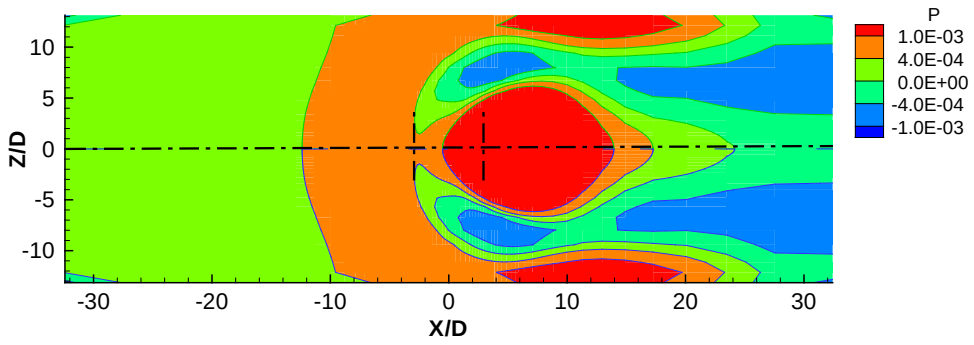

Figure 131: Pressure distribution along the field close to the ground (i.e. Y≈0) for V_{j2}/U_0=8.43, H/D=20.1, and L/D=6 (values nondimensionalized by $1/2\rho V_{j1}^2$).

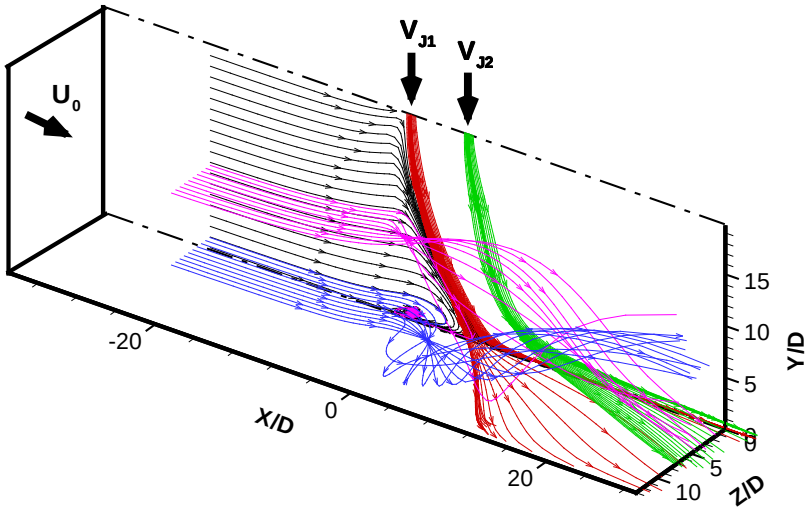

Figure 132: Tridimensional flow interaction visualization. V_{j2}/U_0=8.43, H/D=20.1, and L/D=6.

To confirm this results it was also made a similar numerical analysis for another velocity ratio (V_j/U_0=33.7), and the test conditions are summarized in table 13.

V_{j1}= 36 m/s, U_0= 1.068 m/s, V_{j1}/U_0= 33.7, k_{inj2}= 138.3318 m^2/s^4, ε_{inj2}= 108435 m^2/s^6				
V_{j2} [m/s]	V_{j2}/U_0	$(V_{j1}/U_0)/(V_{j2}/U_0)$	K_{inj2} [m^2/s^4]	ε_{inj2}[m^2/s^6]
27	25.28	1.33	77.8120	45759
18	16.9	2.00	34.5831	13558
9	8.43	4.00	8.6458	1695
6.0	5.62	6.00	3.8426	502.2
3.6	3.34	10.0	1.3833	108.5

Table 13: Summary of the jet velocities used on the wall jet study for V_{j1}/U_0=33.7.

As far as the location and size of the ground vortex is concerned, the results show that for 8.43 ≤ V_{j2}/U_0≤ 25.28 the size of the ground vortex decreases when the second jet velocity increases. For V_{j2}/U_0< 8.43 (figures 136 and 137) the size of the ground vortex begins to decrease when the second jet velocity decreases. For 8.43 ≤ V_{j2}/U_0≤ 25.28 (figures 133 to 135) the ground vortex centre moves slightly upstream. For V_{j2}/U_0 = 8.43 (figure 135) the ground vortex centre location is located at the farthest upstream position. For second jet exit velocities lower that 9 m/s the centre of the ground vortex moves downstream.

Comparing these results with those obtained for the smaller velocity ratio, the same behaviour relatively to the ground vortex occurs for lower second jet velocities (V_{j2}/U_0< 8.43). Also, with this velocity ratio (V_j/U_0=33.7) the second jet still reinforces the first jet in

terms of strength. Since the first jet velocity is always kept constant for all the velocity ratios, a smaller crossflow velocity increases the velocity ratio. So, if the crossflow velocity for this case (V_j/U_0=33.7) is lower, it is expected that the effects of the second jet velocity reduction in the first jet strength will be felt for second jet velocities lower those observed for V_j/U_0=22.5. As the crossflow velocity is lowered the gradual reduction of the second jet velocity is practically not felt, allowing the increase of the ground vortex size and the location of the ground vortex centre to move further upstream. When V_{j2}/U_0< 8.43 the crossflow effect is relatively more important than the effect of the second jet in the first jet strength and the size of the ground vortex decreases and its centre moves further downstream.

Figures 138 and 139 show similar patterns to happened for V_{j1}/U_0=22.5 (figures 131 and 132). It is possible to conclude that the fluid of the crossflow is entrained by the first jet and consequently goes to the scarf vortex inside. However, part of the first jet wall jet seems to be pulled by the scarf vortex, but does not mix with it, and flows over the scarf vortex but then immediately follows the rear jet that is more deflected and stays farther away from the ground up to X/D=26. This figure shows that the second jet seems to interact on the crossflow fluid that is not entrained into the scarf vortex, which is drawn by the same fluid to downstream, where later they merge into a very complex flow structure. This can be confirmed from the static pressure distribution near the ground plane (figure 138) that show relatively small suction zones side-by-side the stagnation zone, and a larger one on farther upstream at -8<X/D<0. It should be pointed out that the same velocity ratio of V_{j2}/U_0=8.43 is now obtained when using a smaller crossflow velocity (1.068 m/s instead of 1.6m/s), and this makes the ground vortex and the wall jet resulting from the upstream impinging jet relatively stronger.

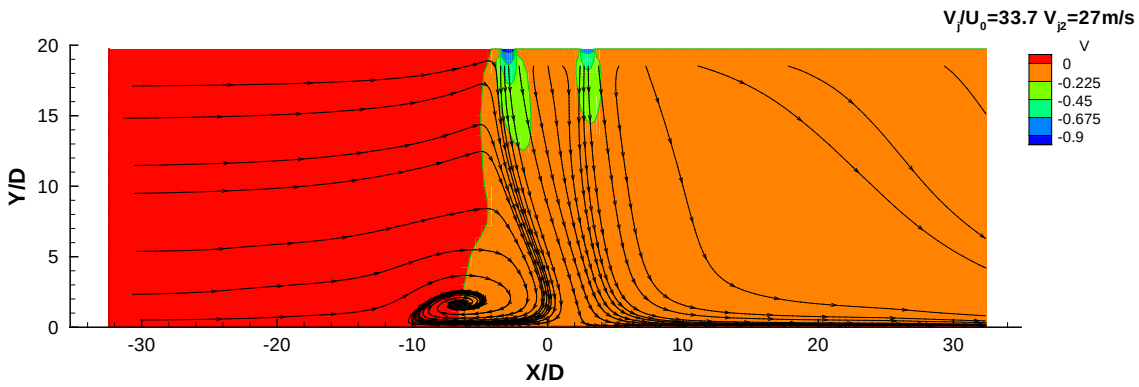

Figure 133: Calculated stream traces and mean vertical velocity component distribution along the vertical plane of symmetry (i.e. Z=0) for V_{j2}/U_0=25.28, H/D=20.1, and L/D=6.

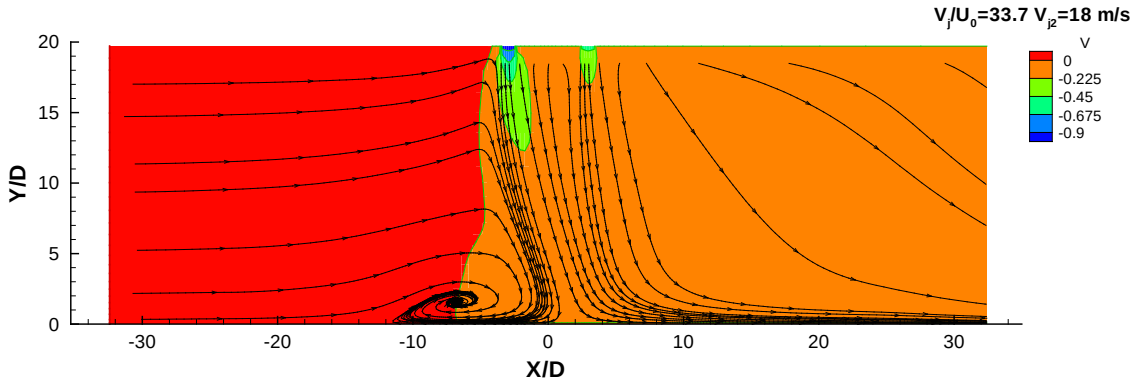

Figure 134: Calculated stream traces and mean vertical velocity component distribution along the vertical plane of symmetry (i.e. Z=0) for V_{j2}/U_0=16.9, H/D=20.1, and L/D=6.

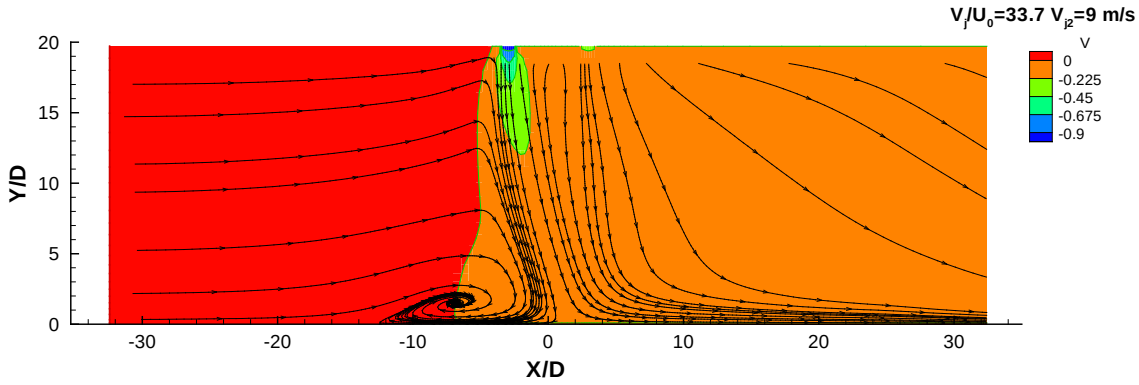

Figure 135: Calculated stream traces and mean vertical velocity component distribution along the vertical plane of symmetry (i.e. Z=0) for V_{j2}/U_0=8.43, H/D=20.1, and L/D=6.

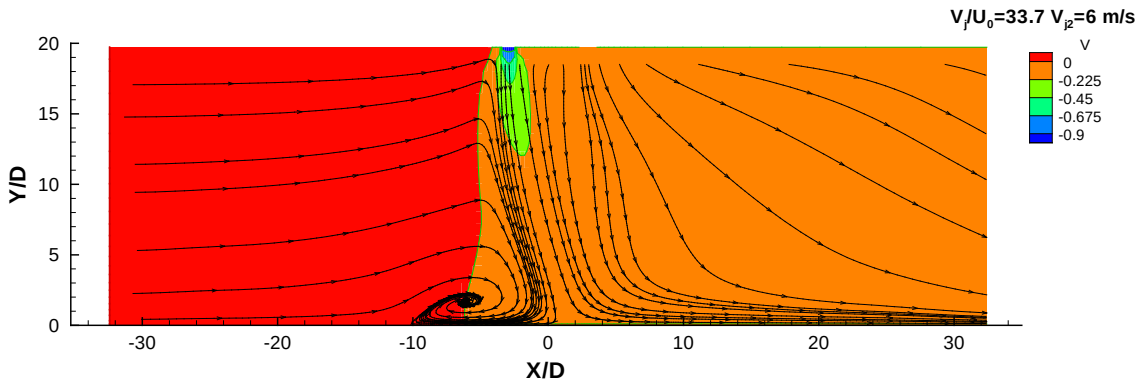

Figure 136: Calculated stream traces and mean vertical velocity component distribution along the vertical plane of symmetry (i.e. Z=0) for V_{j2}/U_0=5.62, H/D=20.1, and L/D=6.

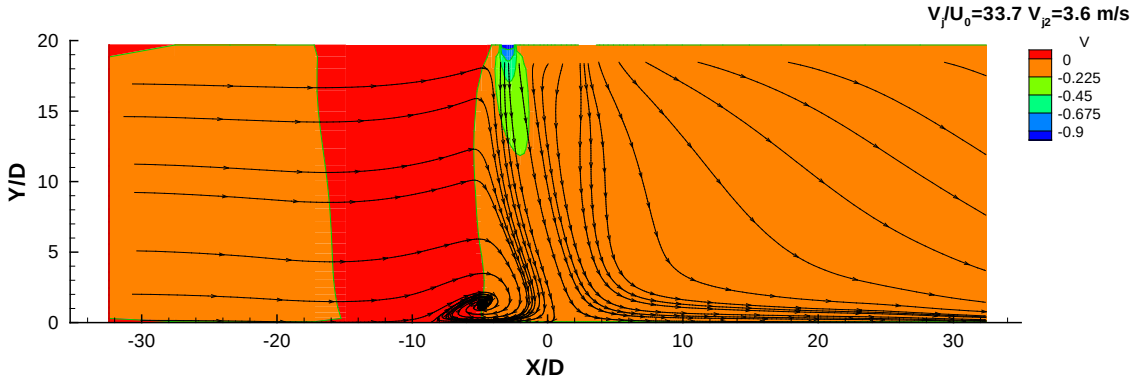

Figure 137: Calculated stream traces and mean vertical velocity component distribution along the vertical plane of symmetry (i.e. Z=0) for V_{j2}/U_0=3.34, H/D=20.1, and L/D=6.

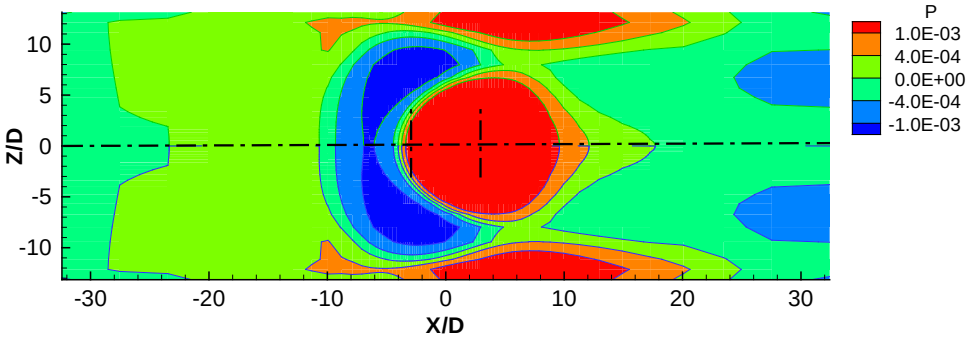

Figure 138: Pressure distribution along the field close to the ground (i.e. Y≈0) for V_{j2}/U_0=8.43, H/D=20.1, and L/D=6 (values nondimensionalized by $1/2\rho V_{j1}^2$).

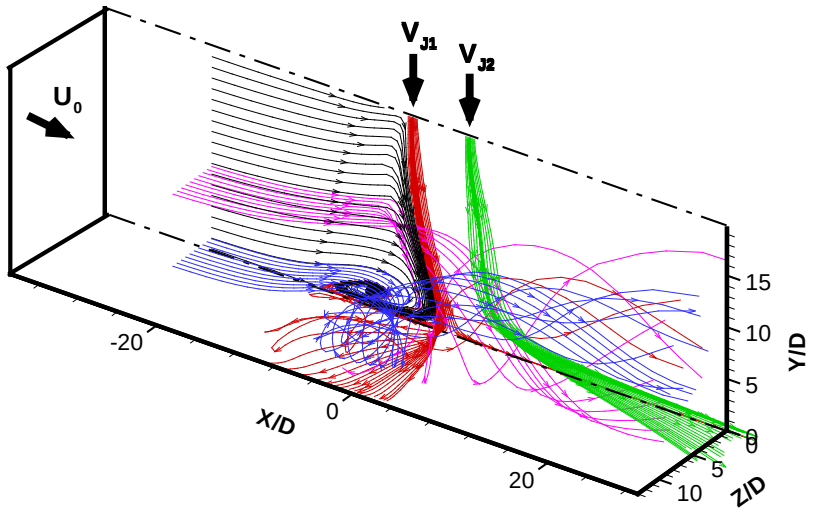

Figure 139: Tridimensional flow interaction visualization for V_{j2}/U_0=8.43, H/D=20.1 and L/D=6.

5.3.2.2 Impinging jets cross section analysis

The numerical analysis presented in previous section showed that the second jet does not impinge on the ground directly and may not originate a ground vortex, depending on the relative exit momentum. To investigate in more detail this aspect, it is important to know what happens in the vertical planes perpendicular to the crossflow (Y-Z plane) and how the jets interact with each other. Additionally, it is also interesting to investigate the possible existence of a kidney shape of the cross section of the jets. Figures 140 to 143 shows isolines of the mean horizontal velocity component U_{mean} obtained in vertical planes perpendicular to the crossflow at X/D = 0.0, 4.9, 9.8 and 19.6 for the lower velocity ratio (V_{j1}/U_0=22.5).

For all the second jet velocities tests, and for X/D = 0, i.e. in the middle between the axis of the jets exit, the kidney shape can be clearly identified for the first jet. The second jet it is not yet visible, because its exit is located further downstream.

At X/D = 4.9, the second jet can be identified by the dark blue area corresponding to velocities larger than $0.03V_{j1}$, that reveals the slight deflection of the second jet inside the wake of the first impinging jet. The kidney shape of the cross section of the first jet is still present, but it is widening rapidly due to the additional influence of the second impinging jet. It should be pointed out that the second impinging jet and first jet do not mix and are separated by lower values of the velocity component in the crossflow direction identified by the light blue area. Additionally, no streamtraces from the second jet are captured by the deflected upstream jet, revealing that a complete mixing between the two jets has not yet occurred. However, from this location downstream (in the crossflow direction) the second impinging jet will suffer two opposing effects: first the fact that is developing in the wake of the first impinging jet will contribute to its less deflection, and secondly since it is impinging in a flow moving in the crossflow direction with a higher velocity it will be forced to deflect. This novel flow configuration that occurs before the first jet reaching the ground is schematically represented in Figure 144, and can be described as a "*kidney shape jet capturing and trying to swallow the second jet in tandem*". To our knowledge this is the very first time that such a phenomenon was detected, and therefore is one major contributions and novelties of the present work.

So, the final behaviour of the second jet can be described as the flow of a jet through a zero or small upstream crossflow (corresponding to the wake of the first jet), impinging on a horizontal jet with a kidney cross section flowing in the crossflow direction with a higher velocity.

In the next downstream location, at X/D = 9.8, the red area identifies a region with relatively large positive values of the velocity component U_{mean} (in the crossflow direction), which is an

indication that the first jet touched the ground. The rear jet impacts on this wall jet resulting from the first jet, and is quickly deflected, but does not reach the ground.

For X/D= 14.7 the kidney shape of the first jet begins to fusion with the second jet, indicating that the merger between the wall jet resulting from the first jet and the second jet took place briefly.

For X/D = 19.6 and 29.4, the entire cross section is occupied by two vortical structures rotating in opposite directions, revealing that the two parallel jets flowing in the crossflow direction finally merge and flows on a unique flow to downstream.

Figures 140 to 143 show the influence of second jet velocities and reveal that there are some modifications on the flowfield behaviour. Starting with the first location, i.e. X/D= 0, where the kidney shape of the cross section of the first jet is identified, it shows that the decrease of the second jet velocity alters the size and vertical position of this structure. The size increases of about 1D in the height and 1.5D in the width of the kidney shape of the cross section of the first jet, when the second jet exit velocity decreases The vertical location of the kidney shape base is repositioned to about 1D down, when the second jet exit velocity decreases.

In the next downstream location, X/D=4.9, the second jet velocity cause alterations on the size of the kidney shape. For all the velocities studied the kidney shape of the cross section of the first jet is widening at this location due to the additional influence of the second jet presence, when the second jet exit velocity decreases.

So, its influence on the kidney shape is smaller. Therefore, the widening of the kidney shape of the first jet decreases with the second jet velocity about 3D. Also, the height of the kidney shape is amended, decreasing about 0.5D with the second jet velocity decreased.

In the previous plane, X/D=0, the vertical position of the kidney shape was also affected by the second jet velocity decrease. For X/D=4.9 this effect is also observed lowering the kidney shape base position about 2D with the second jet velocity decrease.

In the next downstream locations, the behaviour of the flow is practically not affected with the changes in the second jet velocity.

5.3.2.3 Impingement height effect

To investigate further the nature of the novel flow pattern described in the previous sections, it was decided to study also the influence of the impingement height. This numerical study aims to compare the new numerical results with the ones obtained early, to find out how the nozzle impingement height influence the ground vortex location, size and interaction with the

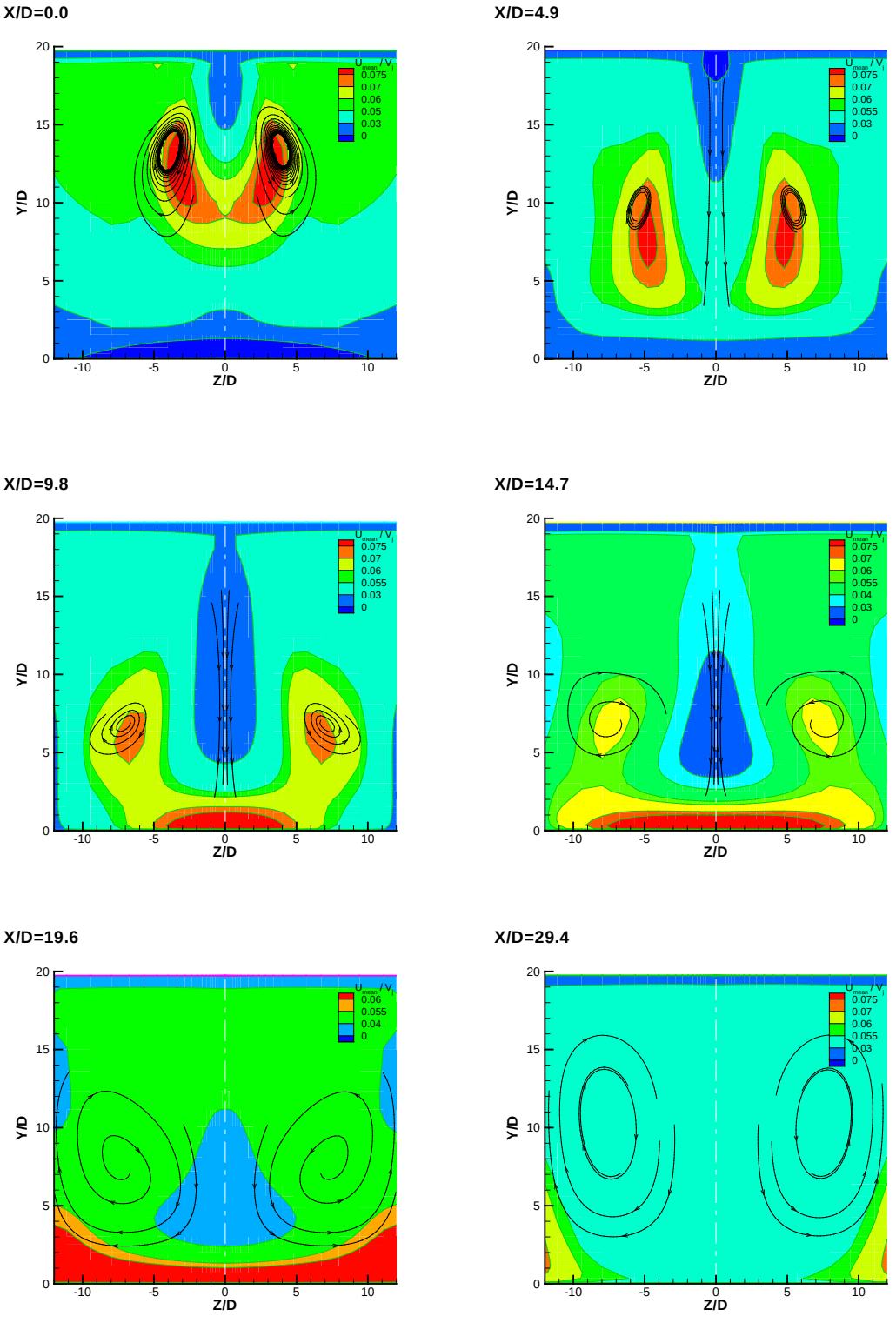

Figure 140: Mean velocity component (U_{mean}/V_j) in a vertical plane perpendicular to crossflow for Re_{j1}=43,000, V_{j2} = 26.72 m/s, Re_{j2} =31,915, V_{j1}/U_0= 22.5 H/D=20.1, V_{j2}/U_0=16.7, $(V_{j1}/U_0)/(V_{j2}U_0)$ = 1.35 and L/D=6.

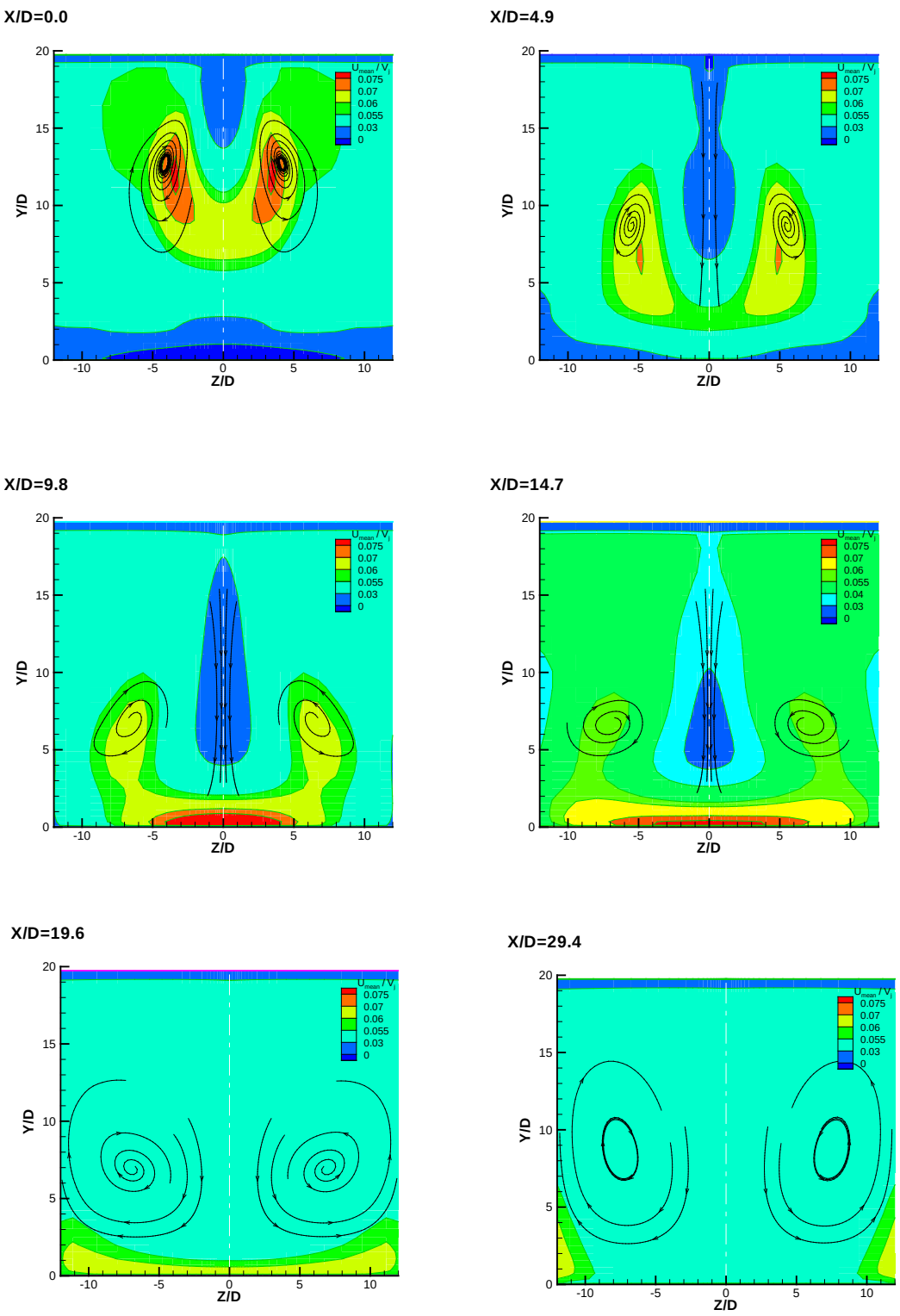

Figure 141: Mean velocity component (U_{mean}/V_j) in a vertical plane perpendicular to crossflow. (Re_{j1}=43,000, V_{j2} = 13.5 m/s, Re_{j2} =16,125, V_{j1}/U_0= 22.5 H/D=20.1, $V_{j2}/_{U0}$=8.43, $(V_{j1}/U_0)/(V_{j2}/U_0)$ = 2.67 and L/D=6.

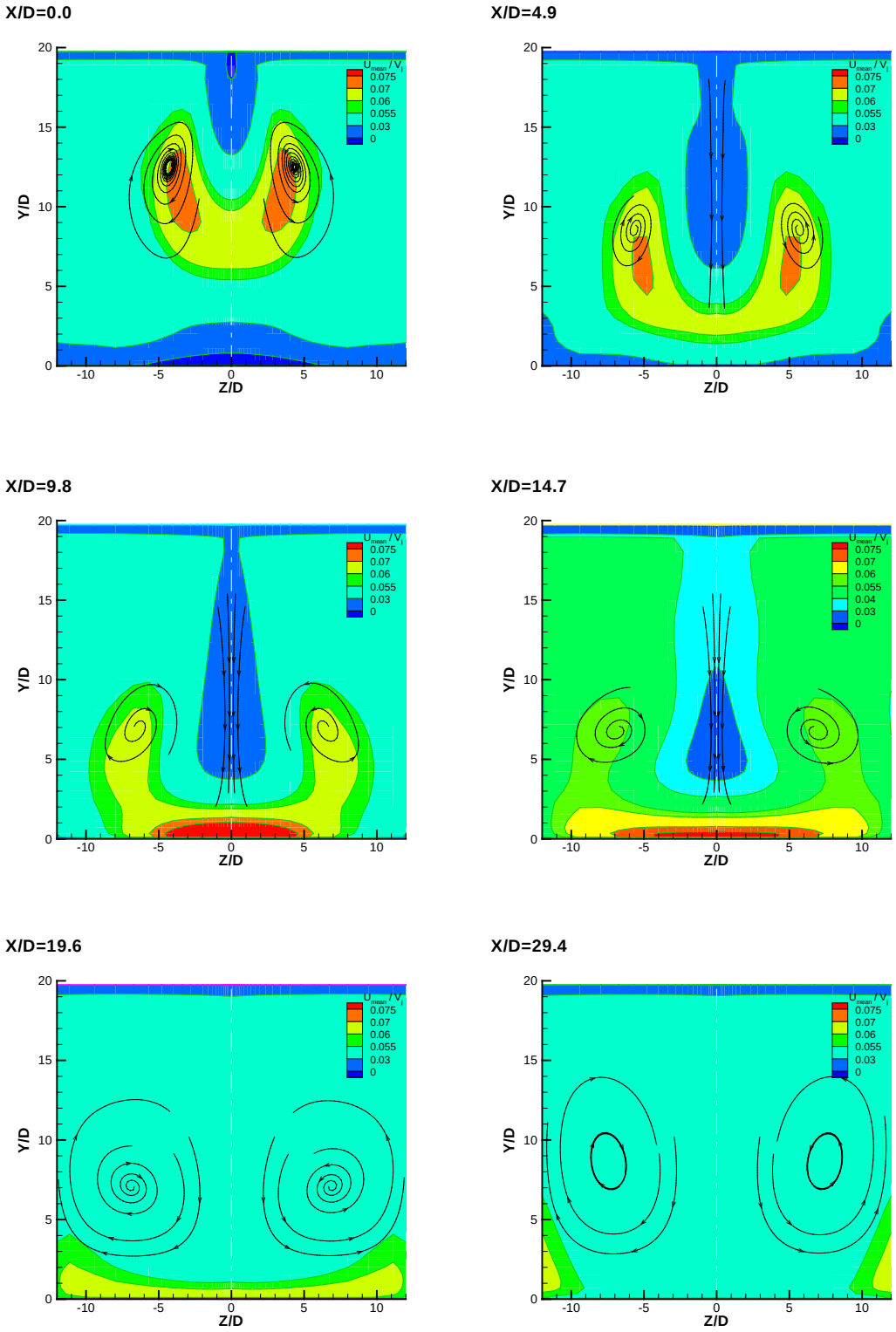

Figure 142: Mean velocity component (U_{mean}/V_j) in a vertical plane perpendicular to crossflow for Re_{j1}=43,000, V_{j2} = 8.99 m/s, Re_{j2} =10,738,V_{j1}/U_0= 22.5 H/D=20.1, V_{j2}/U_0=8.43, $(V_{j1}/U_0)/(V_{j2}/U_0)$ = 5.62 and L/D=6.

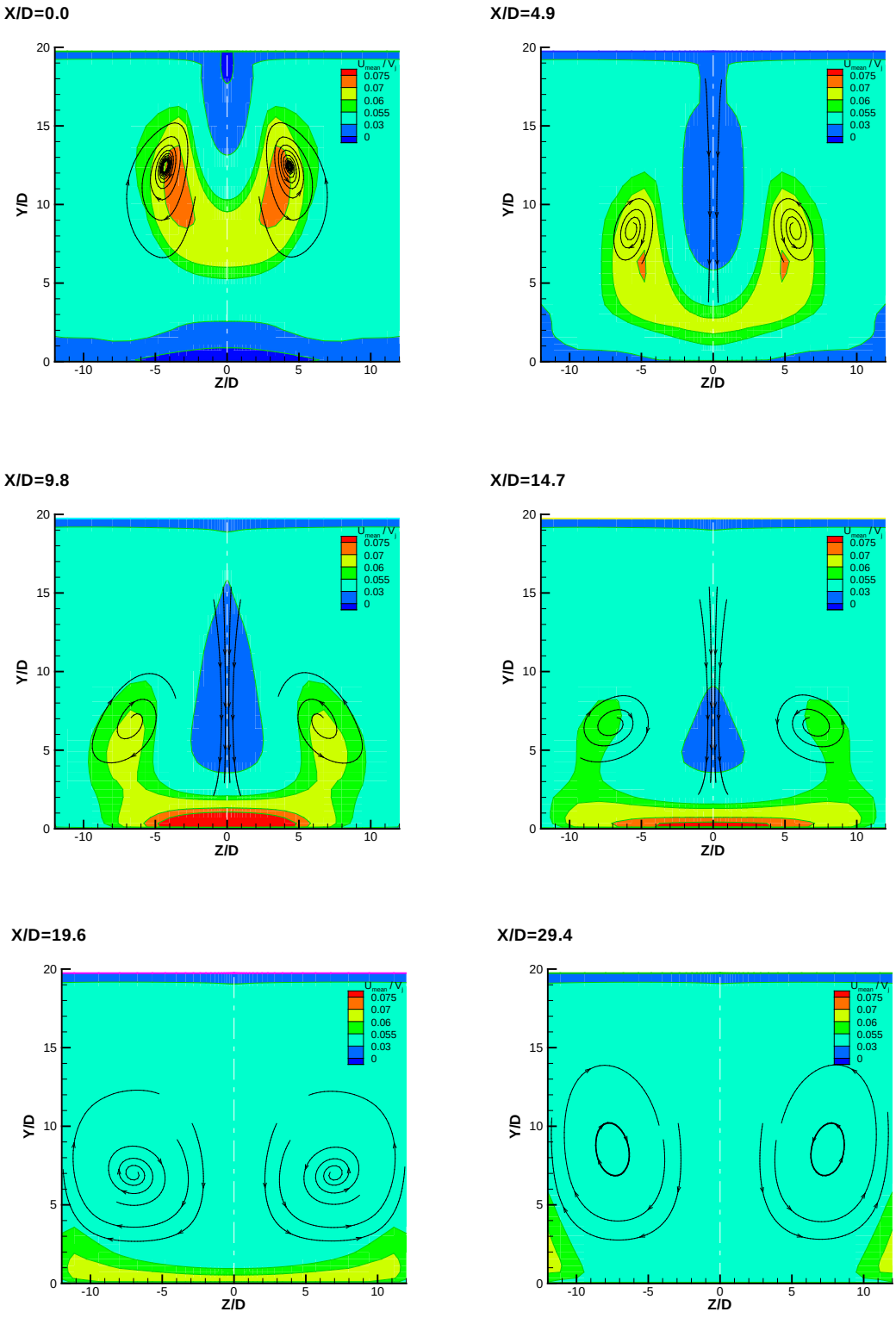

Figure 143: Mean velocity component (U_{mean}/V_j) in a vertical plane perpendicular to crossflow for Re_{j1}=43,000, V_{j2} = 5.4 m/s, Re_{j2} =6,450, V_{j1}/U_0= 22.5, H/D=20.1, V_{j2}/U_0=3.34, $(V_{j1}/U_0)/(V_{j2}/U_0)$ = 6.67 and L/D=6.

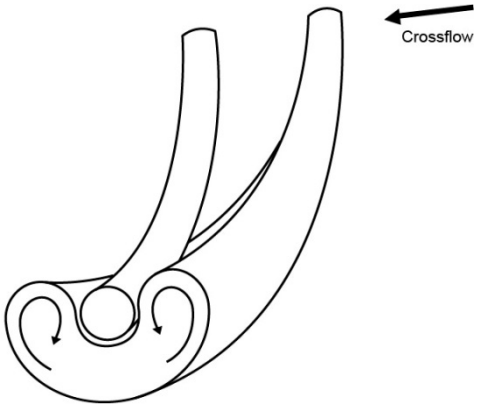

Figure 144: Illustration of the kidney shape of the cross section of the first jet before reaching the ground, capturing and trying to swallow the second (downstream) jet in tandem which remains almost circular.

surrounding flow. It was also intended to find out if there is formation of the fountain upwash flow, something that has not happened for the experimental and numerical study done earlier. The Reynolds number used are based on the jet conditions of 43,000 to 105,000, a jet crossflow velocity of 7.5 to 90, an interject spacing of S= 6D and L=6D. The selected new impingement heights are H/D= 15, 10, 5 and 3.

5.3.2.3.1 Mean flow field

5.3.2.3.1.1 H/D= 15

For H/D=15 and V_j/U_0=7.5 the flow patterns are similar to those observed for H/D=20.1 (figure 145).For the smallest velocity ratio the jets do not mix, but remain together in two layers flowing downstream. For this velocity ratio it is possible to identify a flow regime that it is characterized by the absence of jets impact on the wall and the ground vortex formation.

For the remaining velocity ratios (V_j/U_0=15, 22.5, 33.7, 43.8 and 60) some changes on the formation of a ground vortex can be observed. With the increase of the velocity ratio, the ground vortex becomes larger (in terms of width) and its centre moves upstream. In the case of this impinging height the second jet seems to impinge directly on the ground and then all the flow from the first jet should surround the rear impinging point and converge to downstream. For this range of velocity ratios another flow regime is identified, which the most important for a V/STOL aircraft is operating in ground vicinity due to the strong jet impingement on the ground with the formation of a ground vortex.

Close to the ground in the region between the two jets it is possible to identify an interaction between the upstream and downstream wall jets resulting from each impinging jet that could

undergo to an upwash or a ground vortex, but unfortunately the figures are not conclusive enough.

V_j/U_0=7.5

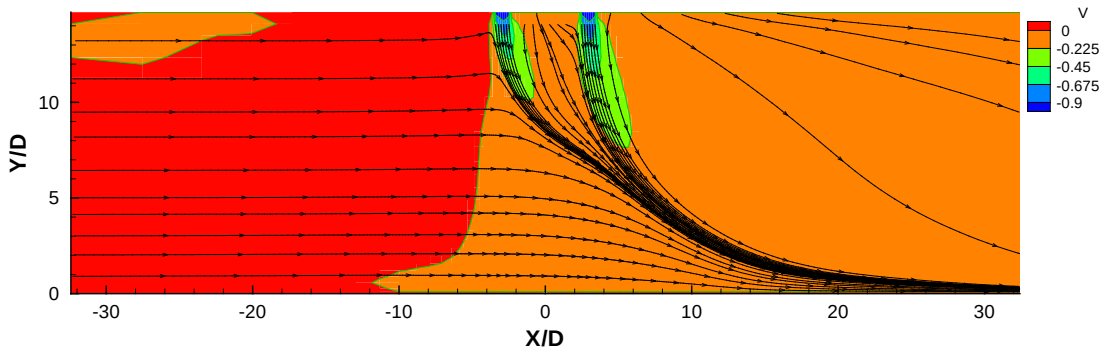

Figure 145: Predicted mean vertical velocity component distribution along the vertical plane of symmetry (i.e. Z=0) for V_j/U_0=7.5, Re_j=43,000, H/D=15 and L/D=6.

V_j/U_0=15

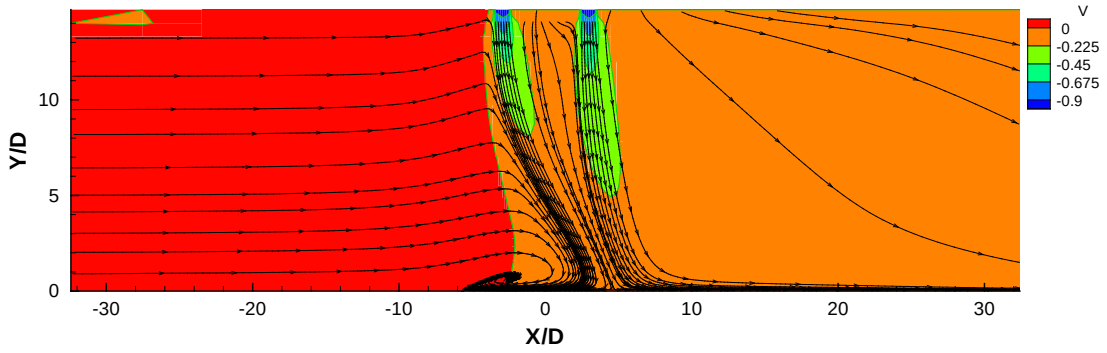

Figure 146: Predicted mean vertical velocity component distribution along the vertical plane of symmetry (i.e. Z=0) for V_j/U_0=15, Re_j=43,000, H/D=15 and L/D=6.

V_j/U_0=22.5

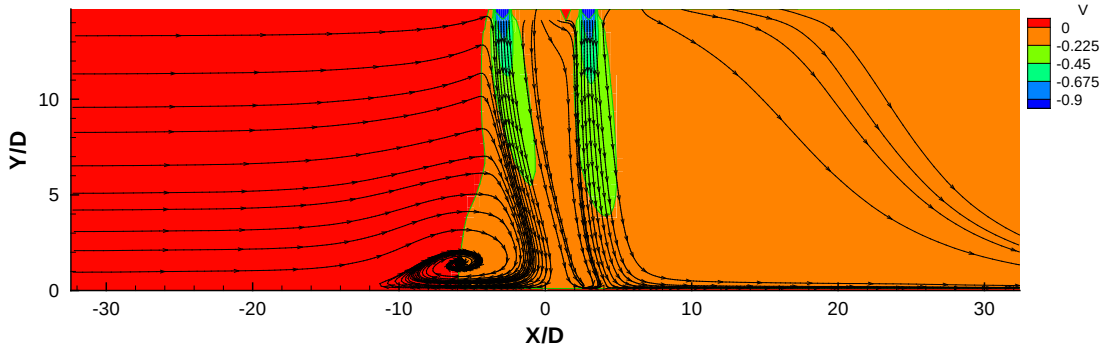

Figure 147: Predicted mean vertical velocity component distribution along the vertical plane of symmetry (i.e. Z=0) for V_j/U_0=22.5, Re_j=43,000, H/D=15 and L/D=6.

V_j/U_0=33.7

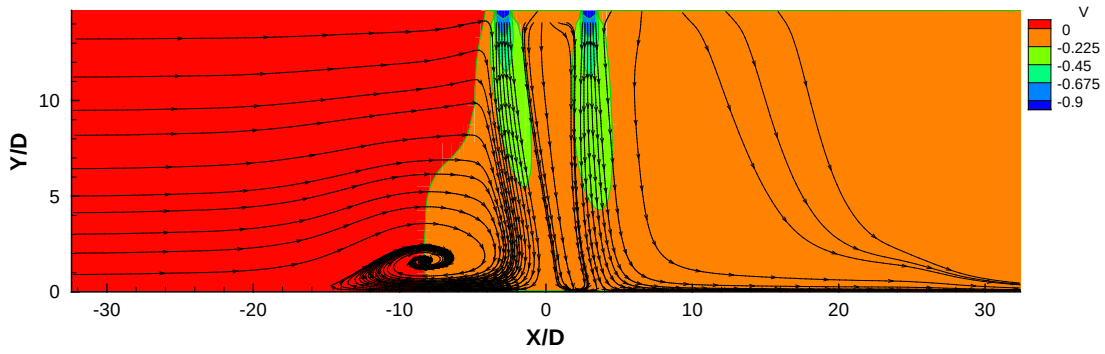

Figure 148: Predicted mean vertical velocity component distribution along the vertical plane of symmetry (i.e. Z=0) for V_j/U_0=33.7, Re_j=43,000, H/D=15 and L/D=6.

V_j/U_0=43.8

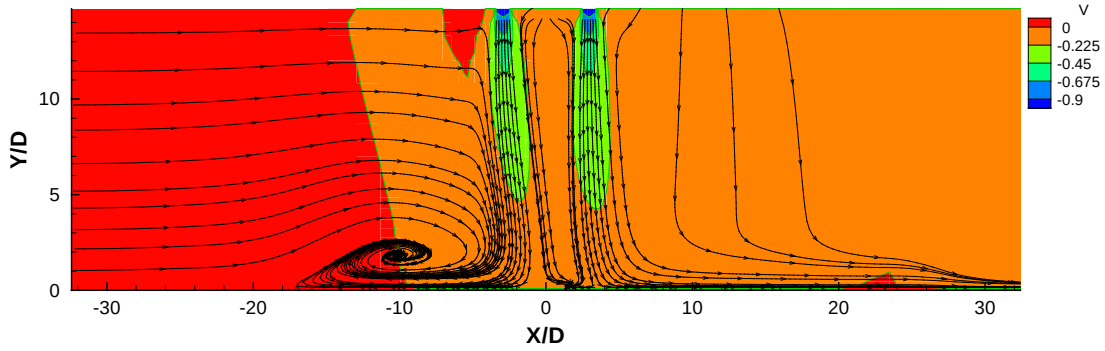

Figure 149: Predicted mean vertical velocity component distribution along the vertical plane of symmetry (i.e. Z=0) for V_j/U_0=43.8, Re_j=43,000, H/D=15 and L/D=6.

V_j/U_0=60

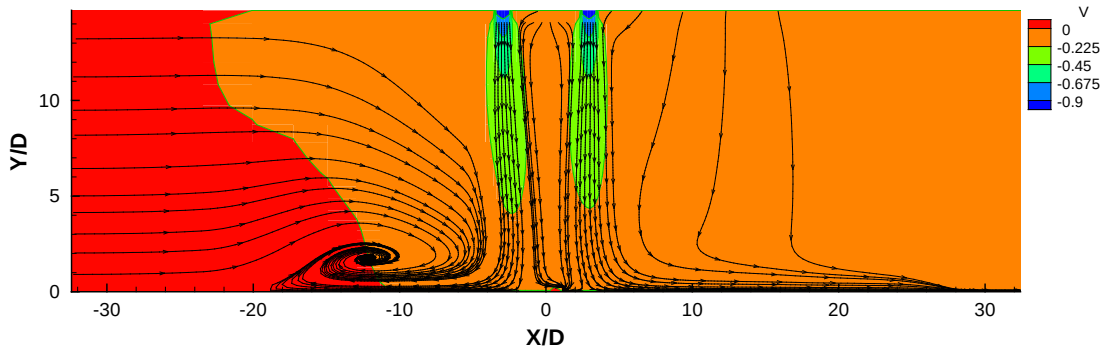

Figure 150: Predicted mean vertical velocity component distribution along the vertical plane of symmetry (i.e. Z=0) for V_j/U_0=60, Re_j=43,000, H/D=15 and L/D=6.

V_j/U_0=90

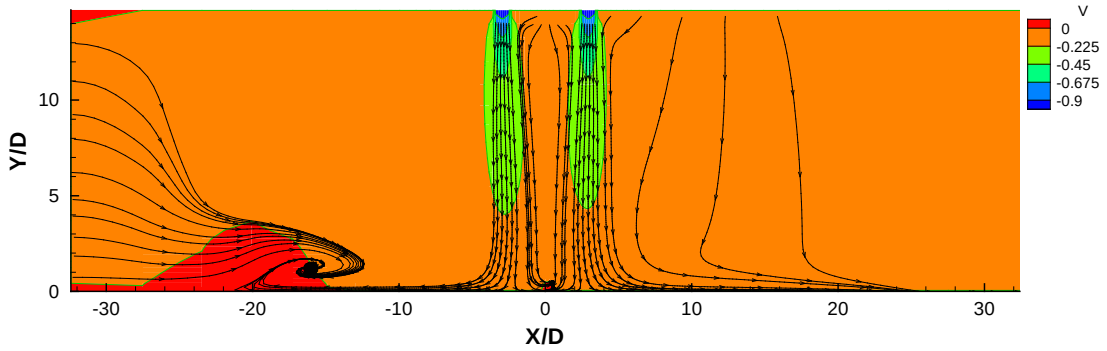

Figure 151: Predicted mean vertical velocity component distribution along the vertical plane of symmetry (i.e. Z=0) for V_j/U_0=90, Re_j=43,000, H/D=15 and L/D=6.

5.3.2.3.1.2 H/D= 10

For H/D=10 and V_j/U_0=7.5 (figure 152) the jets still do not mix and remain together in two layers flowing downstream. For these conditions the second jet continues to impinge on the wall jet of the first jet, flowing in the downstream direction.

For $V_j/U_0 \geq 15$ a ground vortex is formed with its centre located further upstream and the ground vortex size increasing with the velocity ratio. Figures 153 to 158 illustrate the formation of a little recirculation in the region between the two impingement jets, not yet reported before in the permanent literature. The interaction of the impinging jets with the ground results in the formation of a wall jet, that can be described as a deflected flow turning into a high-speed flow parallel to the ground plane (inner wall jet region and outer wall jet region). In the collision of the encountering inner wall jets, one from each jet, the inner wall jet from the first jet is captured by the inner wall jet of the second jet, resulting in the formation of a recirculation that seems to be a ground vortex. Similar to what occurs with the ground vortex formed upstream, this little flow structure moves upstream with the velocity increase, approaching X/D=0. With the increase of the velocity ratio, the crossflow velocity decrease, so the first jet deflection is also lower, and allows this little vortex to go closer and closer to the first jet (see enlarged images 152b) to 156b)).

For the present impingement height and velocity ratio combinations no fountain flow can be observed.

V_j/U_0=7.5

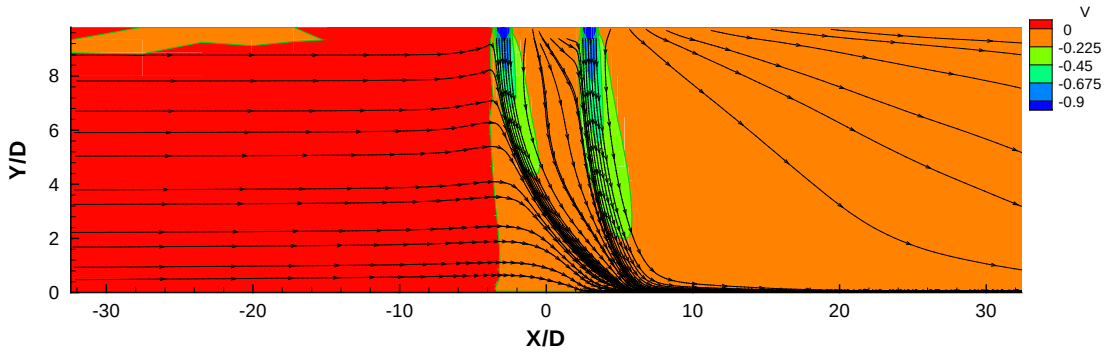

Figure 152: Predicted mean vertical velocity component distribution along the vertical plane of symmetry (i.e. Z=0) for V_j/U_0=7.5, Re_j=43,000, H/D=10 and L/D=6.

V_j/U_0=15

a)

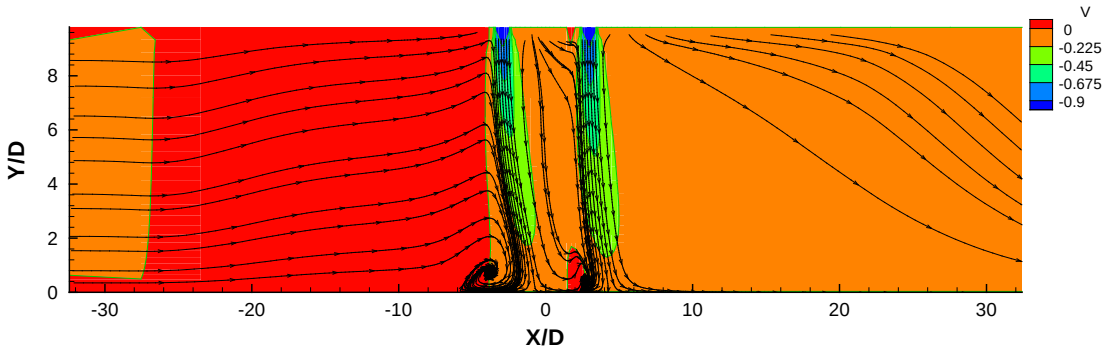

b)

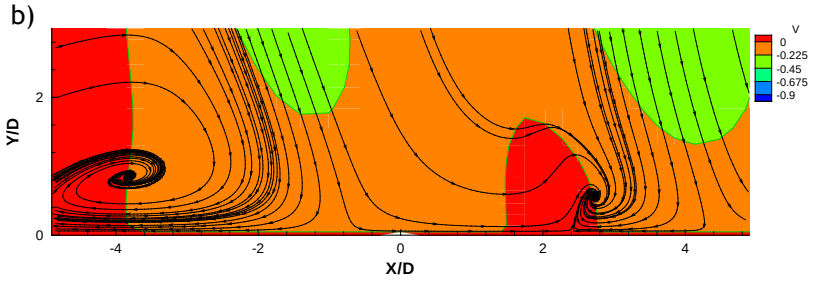

Figure 153: a) Predicted mean vertical velocity component distribution along the vertical plane of symmetry (i.e. Z=0) for V_j/U_0=15, Re_j=43,000, H/D=10 and L/D=6) b) Enlarged image of the region between the two impinging jets.

V_j/U_0=22.5

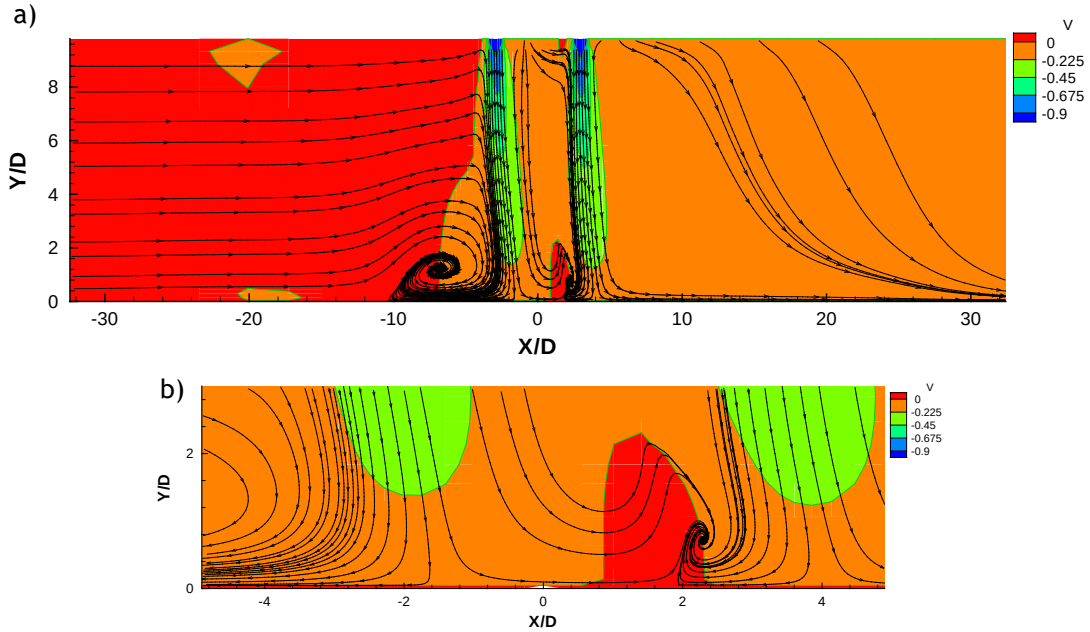

Figure 154: a) Predicted mean vertical velocity component distribution along the vertical plane of symmetry (i.e. Z=0) for V_j/U_0=22.5, Re_j=43,000, H/D=10 and L/D=6. b) Enlarged image of the region between the two impinging jets.

V_j/U_0=33.7

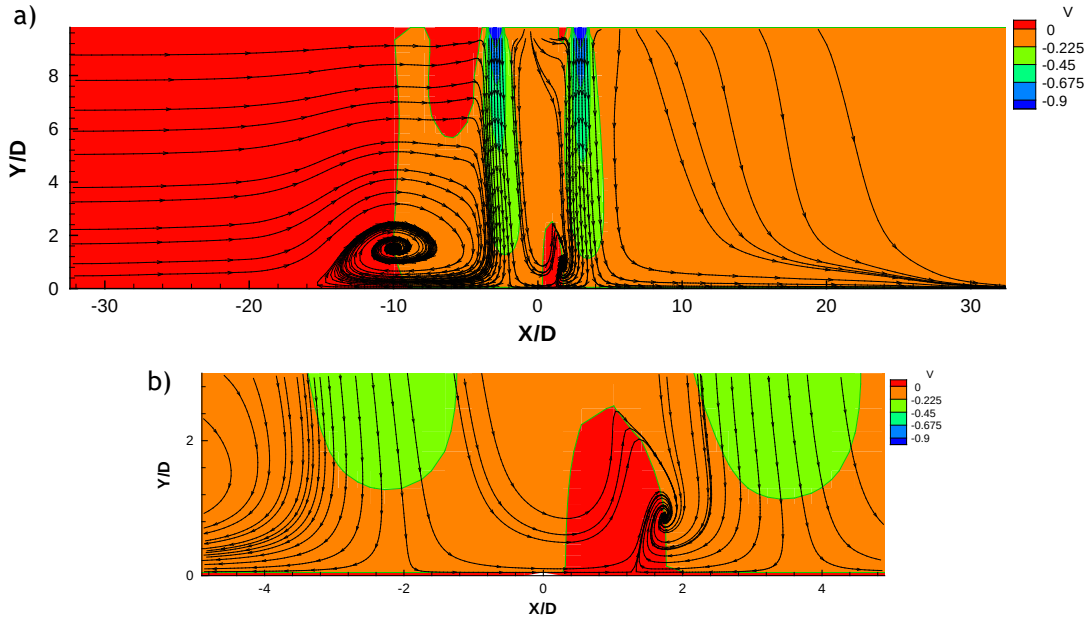

Figure 155: a) Predicted mean vertical velocity component distribution along the vertical plane of symmetry (i.e. Z=0) for V_j/U_0=33.7, Re_j=43,000, H/D=10 and L/D=6. b) Enlarged image of the region between the two impinging jets.

V_j/U_0=43.8

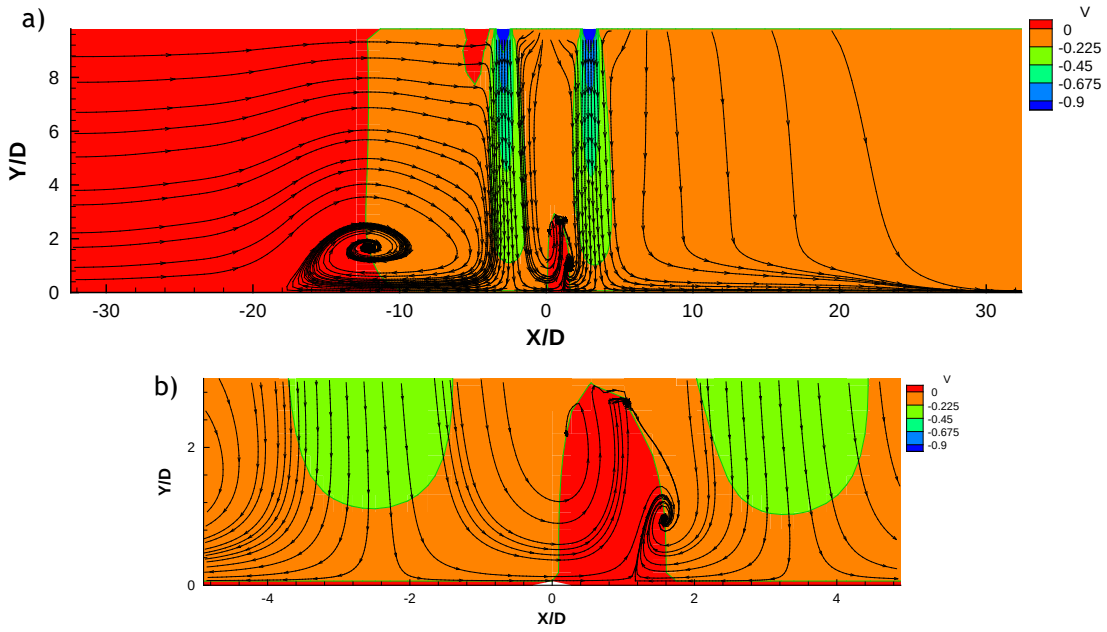

Figure 156: a) Predicted mean vertical velocity component distribution along the vertical plane of symmetry (i.e. Z=0) for V_j/U_0=43.8, Re_j=43,000, H/D=10 and L/D=6. b) Enlarged image of the region between the two impinging jets.

V_j/U_0=60

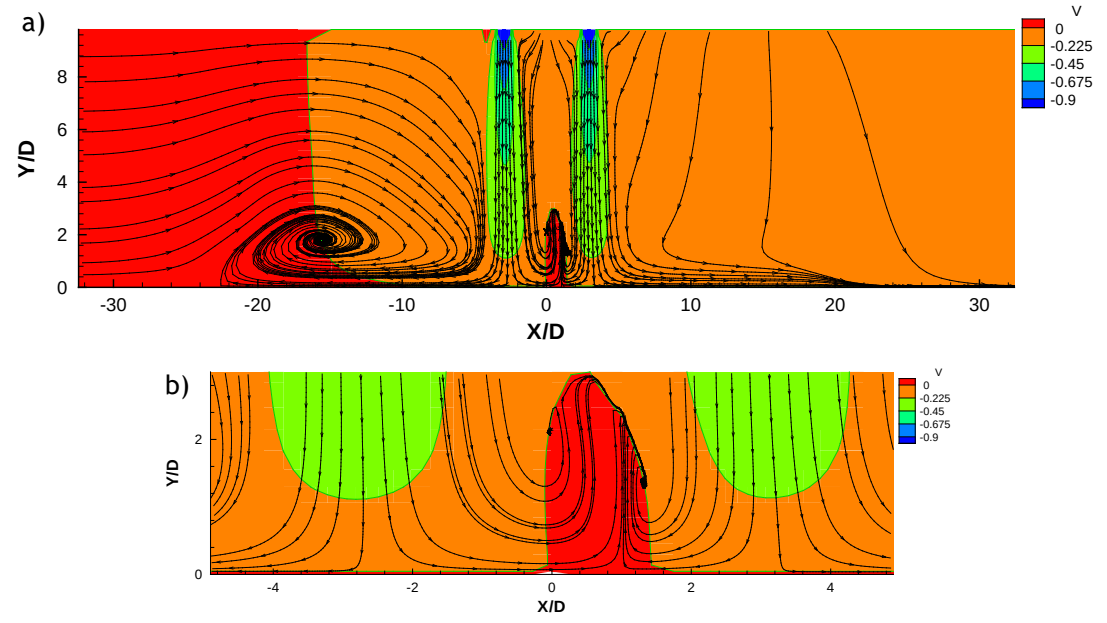

Figure 157: a) Predicted mean vertical velocity component distribution along the vertical plane of symmetry (i.e. Z=0) obtained experimentally for V_j/U_0=60, Re_j=43,000, H/D=10, and L/D=6. b) Enlarged image of the region between the two impinging jets.

V_j/U_0=90

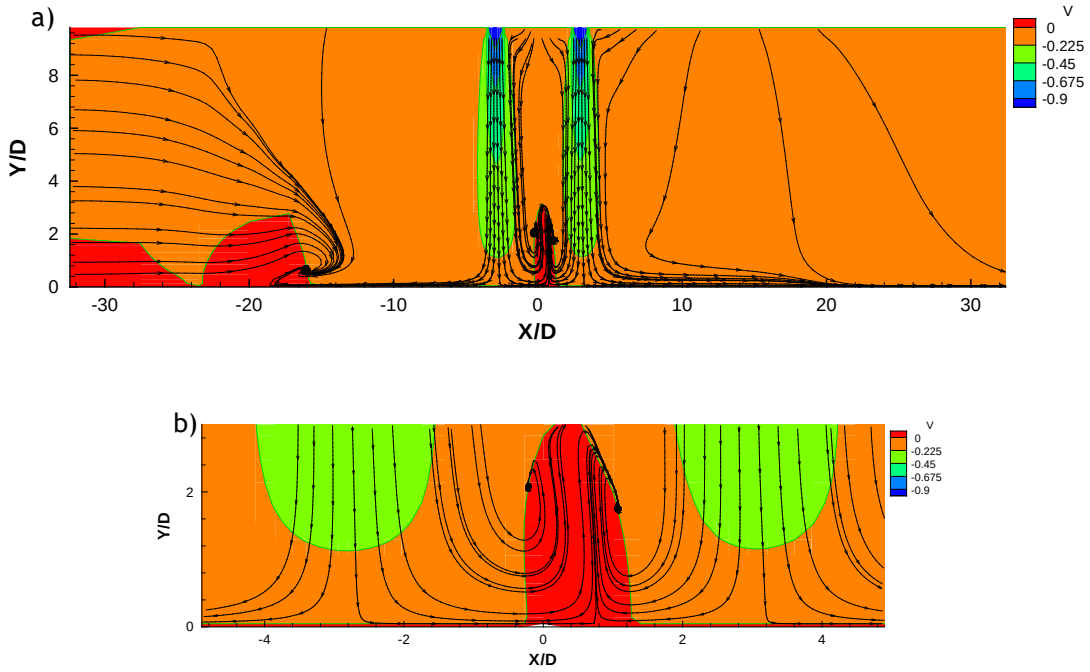

Figure 158: a) Predicted mean vertical velocity component distribution along the vertical plane of symmetry (i.e. Z=0) obtained experimentally for V_j/U_0=90, Re_j=43,000, H/D=10 and L/D=6. b) Enlarged image of the region between the two impinging jets.

For the two higher velocity ratios (V_j/U_0= 60 and 90), in the region between the jets, it is possible to observe the formation of not only one but two counter-rotating recirculation. These configurations show at the vertical plane of symmetry three vortical structures. Two are rotation clockwise and result from the collision of two opposing flows: the upstream wall jet of the first impinging jet against the crossflow and downstream wall jet of the first jet against the upstream wall jet of the rear jet. The third one results from the downstream wall jet of the first impinging jet that is partially blocked by the second ground vortex, and is rotating anti-clockwise. This is another novelty not yet reported before. The enlarged view of figures 157 and 158 show the formation of those vortical structures, one near the second jet and other next of the first jet, with opposite directions of rotation.

In the present study, these are the first test cases in which the second jet impinges directly on the ground, heading the flow to downstream where it will merge in a single flow with the flow resulting from the first jet that is not being entrained by the ground vortex flow.

5.3.2.3.1.3 H/D= 5

In the case of this impinging height, all the velocity ratios tested show the formation of a ground vortex, both downstream of the first impinging jet and the region between the two impinging jets. Unlike the two impingement heights previously analysed and taking as terms of

V_j/U_0=7.5

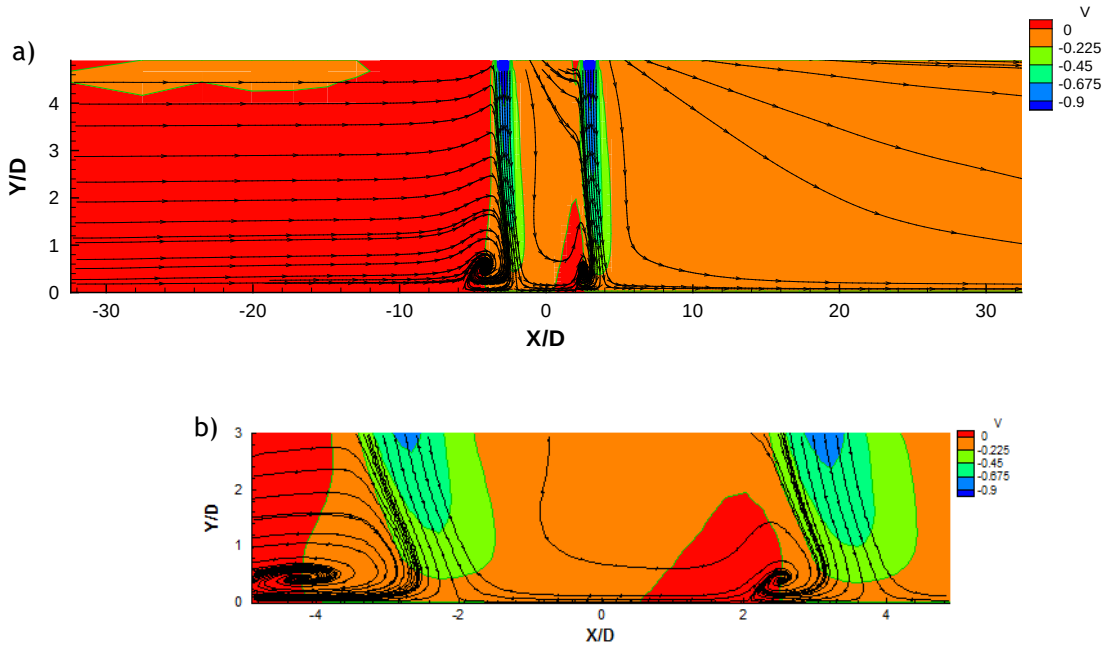

Figure 159: a) Predicted mean vertical velocity component distribution along the vertical plane of symmetry (i.e. Z=0) for V_j/U_0=7.5, Re_j=43,000, H/D=5 and L/D=6. b) Enlarged image of the region between the two impinging jets.

V_j/U_0=15

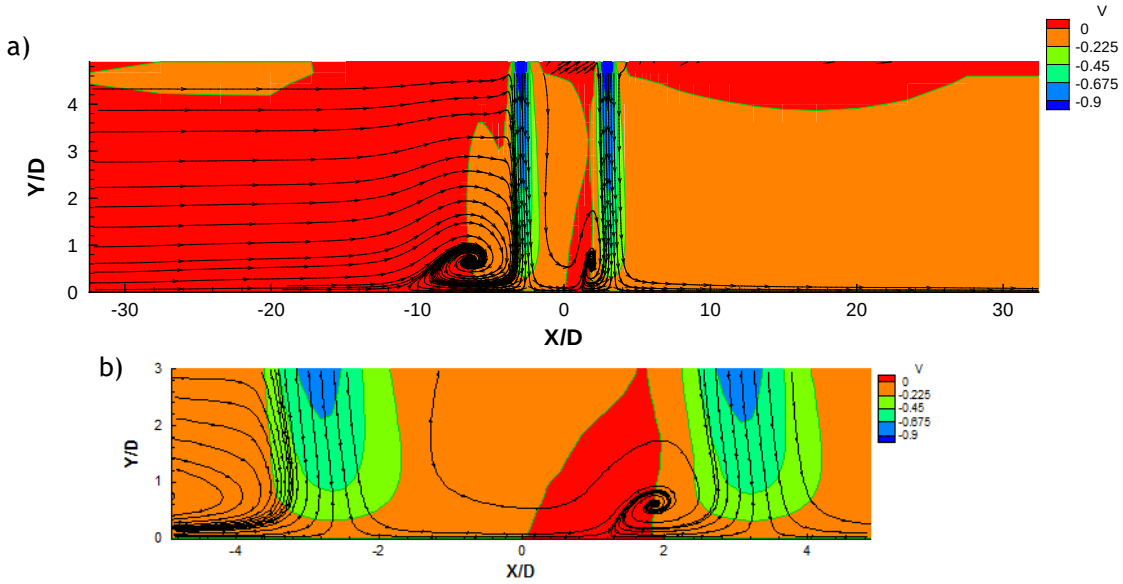

Figure 160: a) Predicted mean vertical velocity component distribution along the vertical plane of symmetry (i.e. Z=0) for V_j/U_0=15, Re_j=43,000, H/D=5, and L/D=6. b) Enlarged image of the region between the two impinging jets.

V_j/U_0=22.5

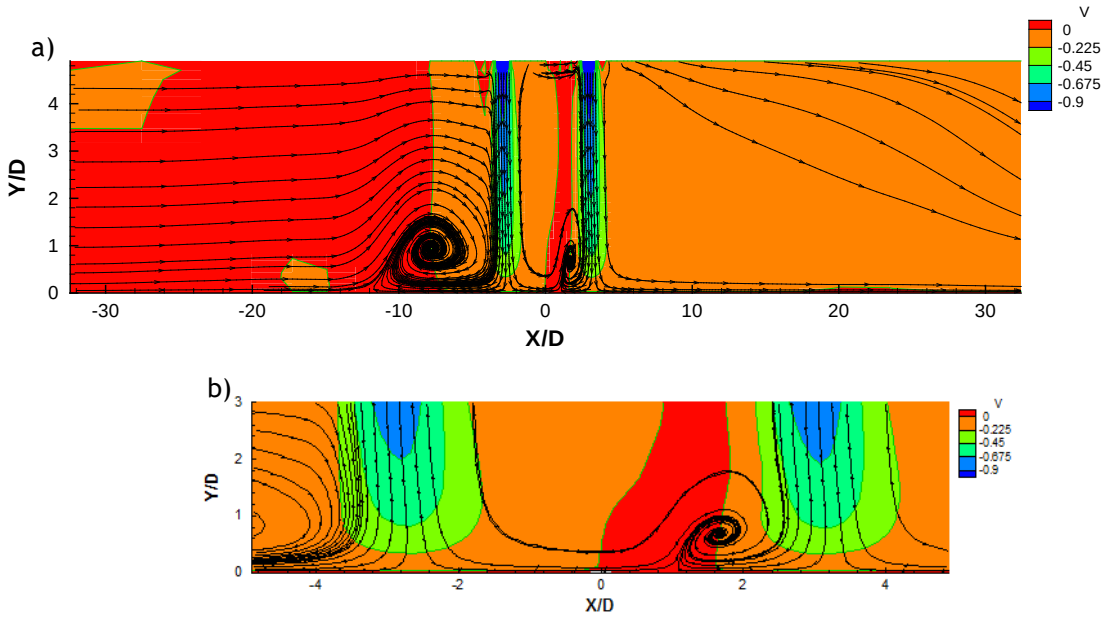

Figure 161: Predicted mean vertical velocity component distribution along the vertical plane of symmetry (i.e. Z=0) for V_j/U_0=22.5, Re_j=43,000, H/D=5 and L/D=6. b) Enlarged image of the region between the two impinging jets.

V_j/U_0=33.7

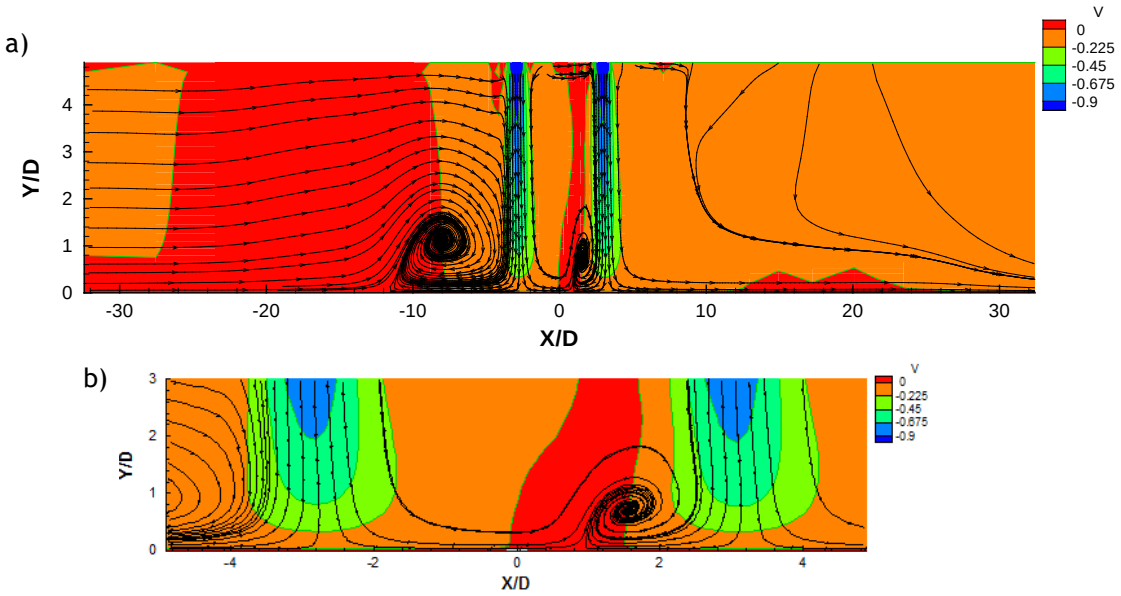

Figure 162: Mean vertical velocity component distribution along the vertical plane of symmetry (i.e. Z=0) obtained experimentally for V_j/U_0=33.7, Re_j=43,000, H/D=5 and L/D=6. b) Enlarged image of the region between the two impinging jets.

V_j/U_0=43.8

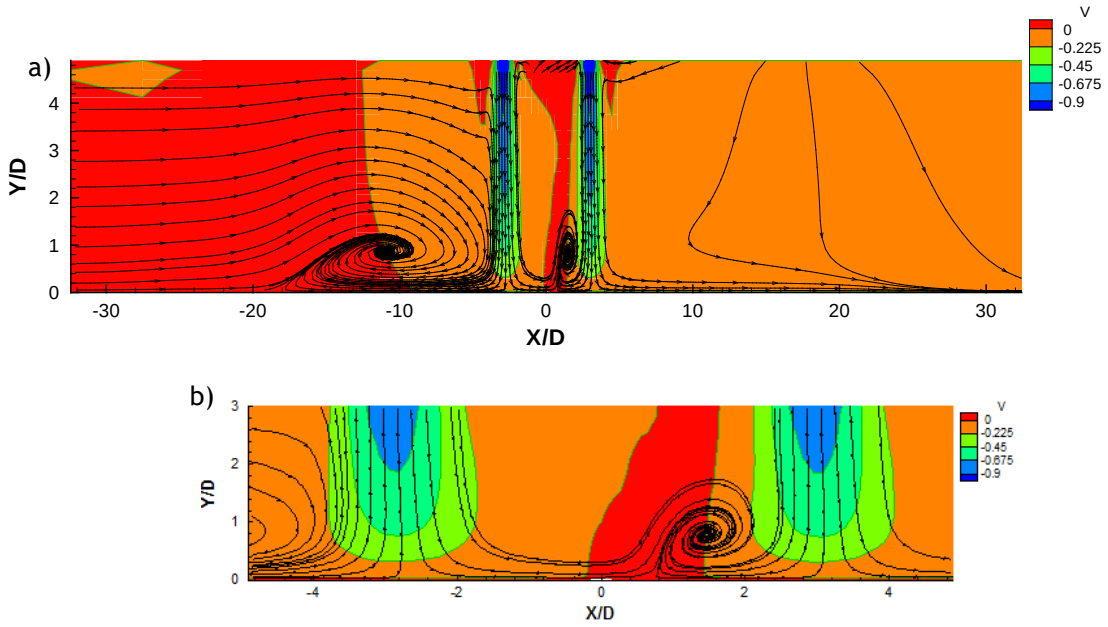

Figure 163: a) Predicted mean vertical velocity component distribution along the vertical plane of symmetry (i.e. Z=0) for V_j/U_0=43.8, Re_j=43,000, H/D=5 and L/D=6. b) Enlarged image of the region between the two impinging jets.

V_j/U_0=60

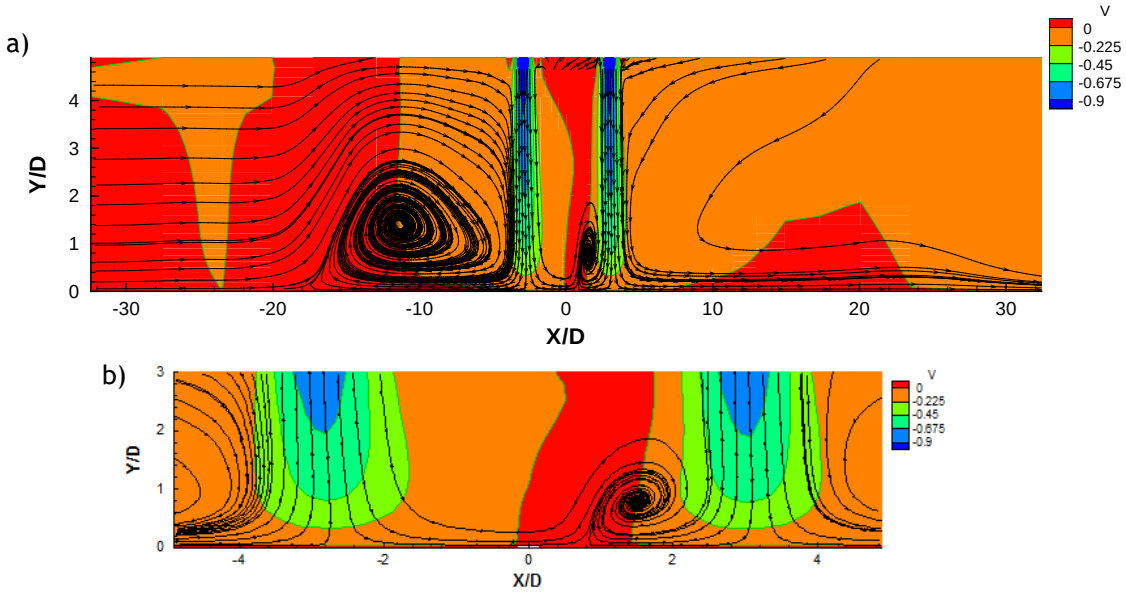

Figure 164: a) Predicted mean vertical velocity component distribution along the vertical plane of symmetry (i.e. Z=0) obtained experimentally for V_j/U_0=60, Re_j=43,000, H/D=5 and L/D=6. b) Enlarged image of the region between the two impinging jets.

V_j/U_0=90

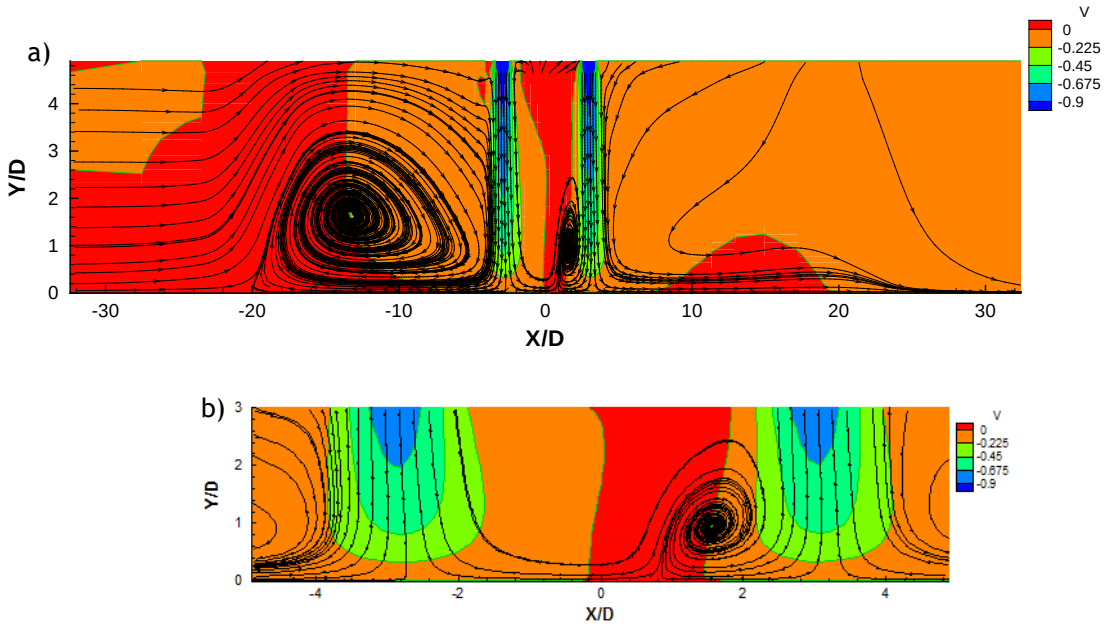

Figure 165: a) Predicted mean vertical velocity component distribution along the vertical plane of symmetry (i.e. Z=0) for V_j/U_0=90, Re_j=43,000, H/D=5 and L/D=6. b) Enlarged image of the region between the two impinging jets.

comparison the smaller velocity ratio, it is possible to see that for small impingement heights, which one the most relevant for the situation of short take-off or landing, the first jet impinges on the ground with a considerably high strength. In this situation the strength of the impact can almost counteract entirely the deflection caused by crossflow on the first jet.

The resulting structures for this impinging height are similar to those described for the impinging height H/D=10. However, it should be emphasized that the increase of the velocity ratio to 60 and 90 leads to an increase of the width of the ground vortex located between the impact jets. For both higher velocity ratios, more than 50% of the flow area downstream of the first jet is occupied by the ground vortex, revealing that with the decrease of the impingement height, the jets impinge strongly on the ground.

5.3.2.3.1.4 H/D= 3

The flowfield for this impingement height exhibits for all the velocity ratios studied ($7.5<V_j/U_0<90$) two ground vortexes corresponding to each impinging jet. The downstream ground vortex becomes bigger and wider with the velocity ratio increase and the centre is moving to downstream. For the higher velocity ratio, the height of the downstream ground vortex is similar to the impingement height, revealing a high blockage effect. The flow patterns are shown in figures 166 to 172 and are similar to those obtained for H/D=5 with enhanced characteristics.

V_j/U_0=7.5

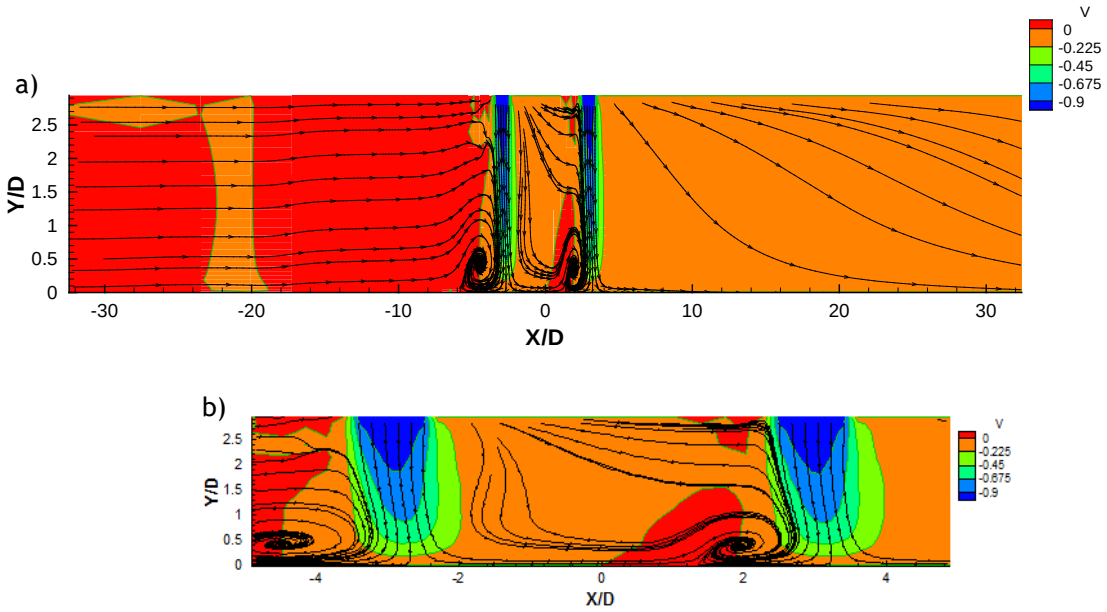

Figure 166: a) Predicted mean vertical velocity component distribution along the vertical plane of symmetry (i.e. Z=0) for V_j/U_0=7.5, Re_j=43,000, H/D=3 and L/D=6. b) Enlarged image of the region between the two impinging jets.

V_j/U_0=15

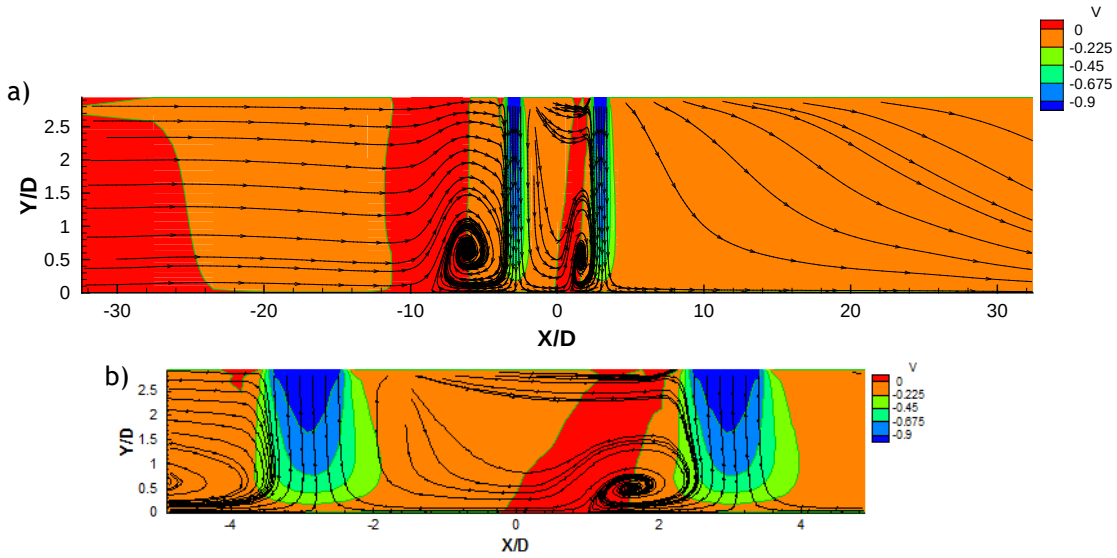

Figure 167: a) Mean vertical velocity component distribution along the vertical plane of symmetry (i.e. Z=0) obtained experimentally for V_j/U_0=15, Re_j=43,000, H/D=3 and L/D=6. b) Enlarged image of the region between the two impinging jets.

V_j/U_0=22.5

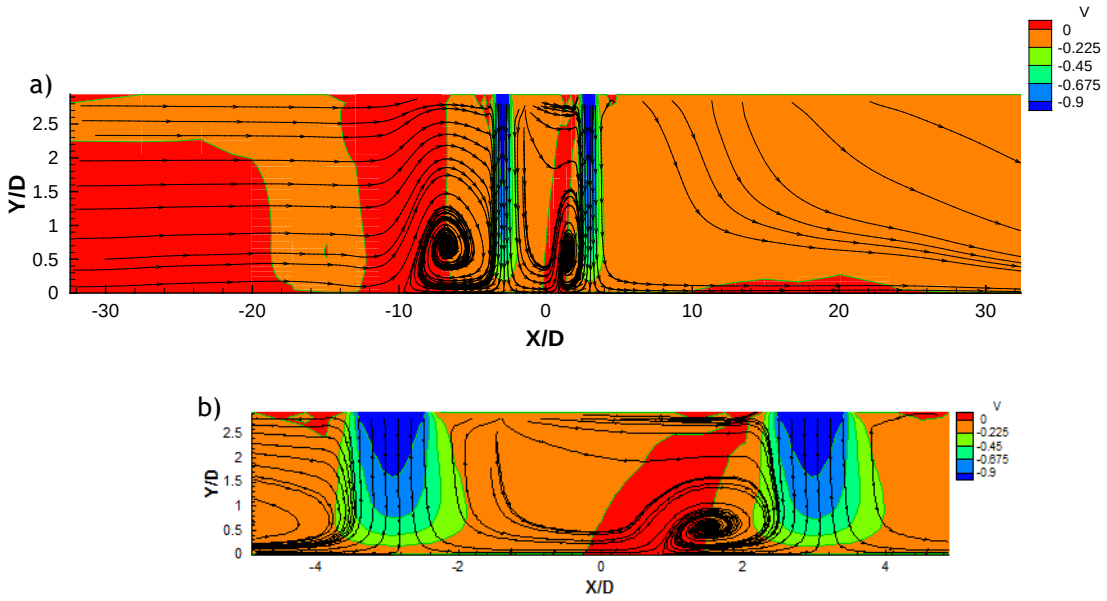

Figure 168: a) Mean vertical velocity component distribution along the vertical plane of symmetry (i.e. Z=0) obtained experimentally for V_j/U_0=22.5, Re_j=43,000, H/D=3 and L/D=6. b) Enlarged image of the region between the two impinging jets.

V_j/U_0=33.7

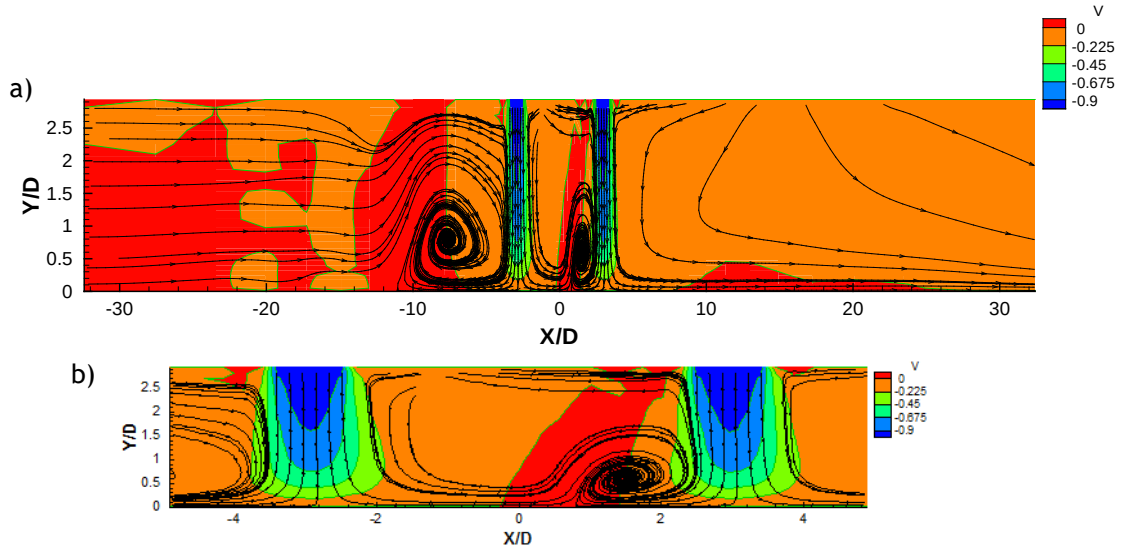

Figure 169: a) Mean vertical velocity component distribution along the vertical plane of symmetry (i.e. Z=0) obtained experimentally for V_j/U_0=33.7, Re_j=43,000, H/D=3 and L/D=6. b) Enlarged image of the region between the two impinging jets.

V_j/U_0=43.8

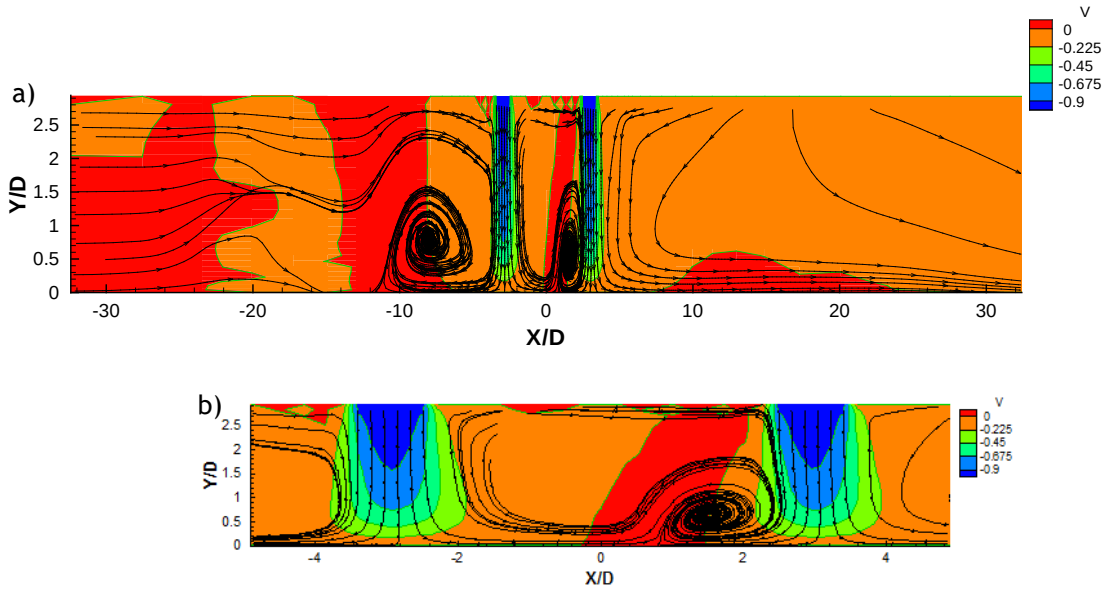

Figure 170: a) Predicted mean vertical velocity component distribution along the vertical plane of symmetry (i.e. Z=0) for V_j/U_0=43.8, Re_j=43,000, H/D=3 and L/D=6. b) Enlarged image of the region between the two impinging jets.

V_j/U_0=60

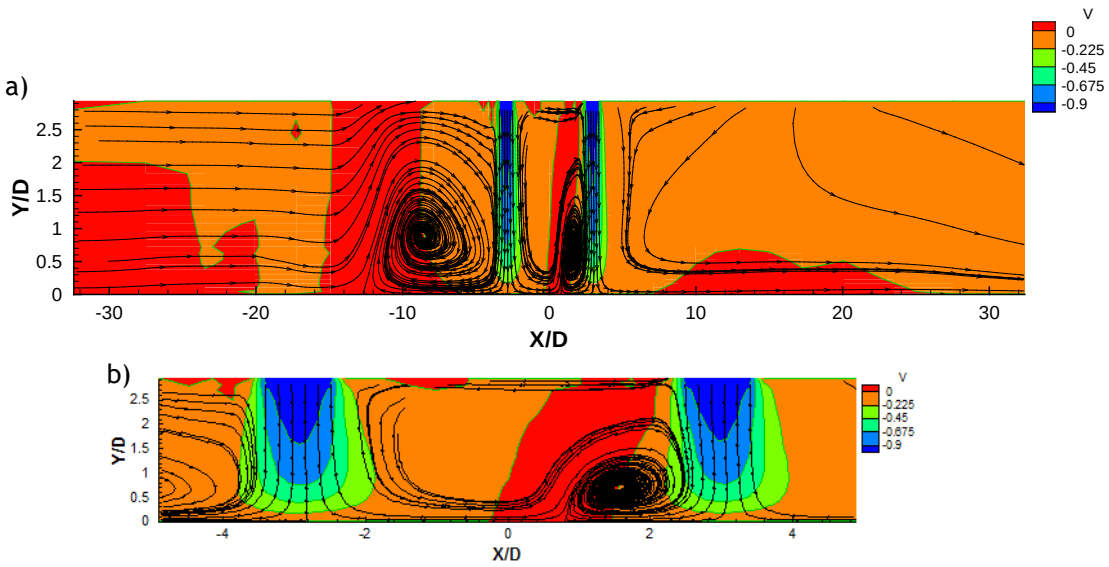

Figure 171: a) Predicted mean vertical velocity component distribution along the vertical plane of symmetry (i.e. Z=0) for V_j/U_0=60, Re_j=43,000, H/D=3 and L/D=6. b) Enlarged image of the region between the two impinging jets.

V_j/U_0=90

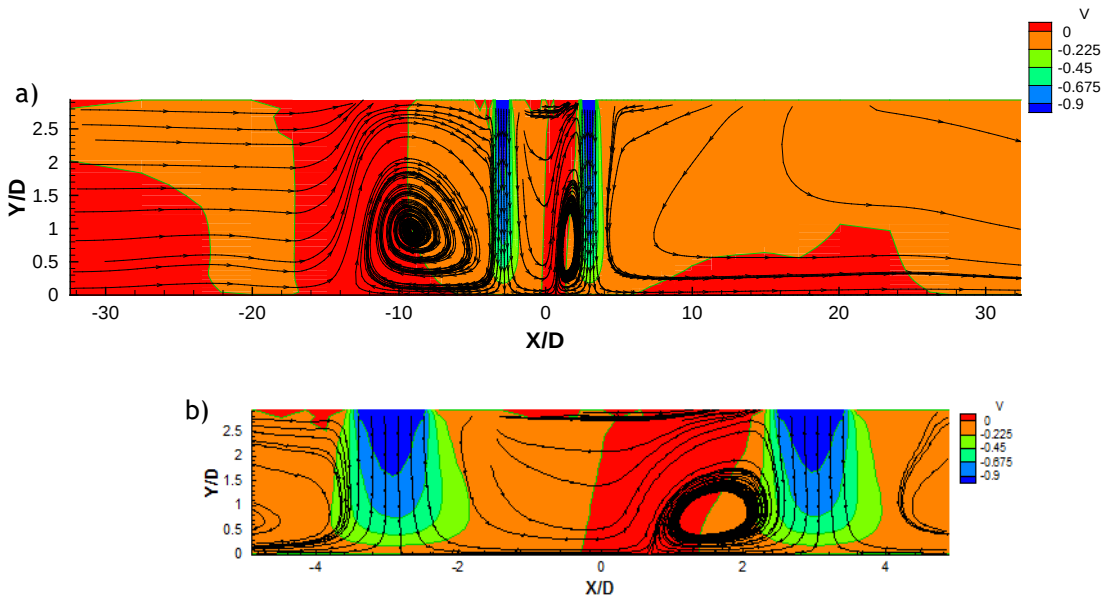

Figure 172: a) Predicted mean vertical velocity component distribution along the vertical plane of symmetry (i.e. Z=0) for V_j/U_0=90, Re_j=43,000, H/D=3 and L/D=6. b) Enlarged image of the region between the two impinging jets.

5.3.2.3.1.5 Summary

Tables 14 and 15 summarize the effect of the velocity ratio and impingement height on the flow pattern, and in particular the ground vortex.

When two ground vortexes are observed their strengths decrease when the impingement height decreases for the same velocity ratio. Only an exception for the downstream ground vortex was observed for V_j/U_0=60, because there is an increase on the ground vortex strength for H/D=10.

Concerning to the ground vortex centre position for V_j/U_0= 7.5 and 15, the position of the ground vortex centre moves upstream when the impingement height decreases. In the case of V_j/U_0= 22.5 the same behaviour is registered for H/D>3. For V_j/U_0=33.7, the ground vortex centre position moves upstream for H/D>5, while for H/D≤5 its position remaining constant.

For the remaining velocity ratios and H/D>5 the same behaviour described above is registered, and for H/D≤5 the centre of the ground vortex moves in reverse, i.e., in the upstream direction.

With regard to the ground vortex height, it is observed that with the impingement height decrease, the percentage of impingement height occupied by the ground vortex increases.

	Upstream ground vortex			Ground vortex between the jets		
Velocity ratio	Ground vortex centre position	Ground vortex strength	Ground vortex height	Ground vortex centre position	Ground vortex strength	Ground vortex height
H/D=15						
7.5	Not applicable			Not applicable		
15	X =-2.5D	X=9D	Y=1.25D	Not Applicable		
22.5	X=-6D	X=11D	Y=5D			
33.7	X=-8.5D	X=13D	Y=5D			
43.8	X=-10.5D	X=15D	Y=5.5D			
60	X=-12D	X=15D	Y=6.5D			
90						
H/D=10						
7.5	Not applicable			Not applicable		
15	X=-4D	X=4D	Y=2D	X=2.7D	X=0.8D	Y=0.7D
22.5	X=-6.5D	X=8D	Y=3.3D	X=2.3D	X=0.6D	Y=1D
33.7	X=-10D	X=12D	Y=4D	X=1.75D	X=0.6D	Y=1.25D
43.8	X=-12D	X=14D	Y=4.3D	X=1.6D	X=0.8D	Y=1.4D
60	X=-15.5D	X=17D	Y=5D	X=1.3D	X=1D	Y=1.8D
90						
H/D=5						
7.5	X/D=-4.2D	X=3D	Y=1D	X=2.5D	X=0.9D	Y=1.4D
15	X=-6.5D	X=7D	Y=1.5D	X=1.9D	X=1.3D	Y=1.7D
22.5	X=-8D	X=7.5D	Y=2.3D	X=1.65D	X=1.4D	Y=1.8D
33.7	X=-8D	X=8D	Y=3D	X=1.55D	X=1.6D	Y=1.8D
43.8	X=-11D	X=14D	Y=3D	X=1.45D	X=1.6D	Y=1.8D
60	X=11.5D	X=13D	Y=4D	X=1.45D	X=1.8D	Y=1.9D
90	X=13.25D	X=16D	Y=4.5D	X=1.55D	X=1.9D	Y=2.4D
H/D=3						
7.5	X=-4.5D	X=2.6D	Y=1.4D	X=1.9D	X=1.2D	Y=1.1D
15	X=-6D	X=5D	Y=2D	X=1.6D	X=1.5D	Y=1.55D
22.5	X=-6.8D	X=6D	Y=2D	X=1.5D	X=1.8D	Y=1.65D
33.7	X=-8.5D	X=7.5D	Y=2.5D	X=1.45D	X=2D	Y=1.75D
43.8	X=-8D	X=7D	Y=2.6D	X=1.5D	X=2D	Y=1.85D
60	X=-8.5D	X=9D	Y=2.8D	X=1.55D	X=2.1D	Y=2.1D
90	X=-9D	X=9D	Y=2.95D	X=1.55D	X=2.1D	Y=2.6D

Table 14: Summary of ground vortex characteristics.

In short, when the impingement height decreases and for the same velocity ratio, there is an increase of the area occupied by the first ground vortex upstream of the first impinging jet.

Velocity ratio	Ground vortex height	Percentage of impingement height occupied by the ground vortex	Ground vortex height	Percentage of impingement height occupied by the ground vortex
H/D=15				
7.5	Not Applicable		Not Applicable	
15	Y=1.25D	8.33%		
22.5	Y=5D	33.33%		
33.7	Y=5D	33.33%		
43.8	Y=5.5D	36.67%		
60	Y=6.5D	43.33%		
90				
H/D=10				
7.5	Not Applicable			
15	Y=2D	20,00%	Y=0,7D	7,00%
22.5	Y=3,3D	33,00%	Y=1D	10%
33.7	Y=4D	40,00%	Y=1,25D	12,50%
43.8	Y=4,3D	43,00%	Y=1,4D	14,00%
60	Y=5D	50%	Y=1,8D	18,00%
90				
H/D=5				
7.5	Y=1D	20.00%	Y=1.4D	28.00%
15	Y=1.5D	30.00%	Y=1.7D	34.00%
22.5	Y=2.3D	46.00%	Y=1.8D	36.00%
33.7	Y=3D	60.00%	Y=1.8D	36.00%
43.8	Y=3D	60.00%	Y=1.8D	36.00%
60	Y=4D	80.00%	Y=1.9D	38.00%
90	Y=4.5D	90.00%	Y=2.4D	48.00%
H/D=3				
7.5	Y=1.4D	46.67%	Y=1.1D	36.67%
15	Y=2D	66.67%	Y=1.55D	51.67%
22.5	Y=2D	66.67%	Y=1.65D	55.00%
33.7	Y=2.5D	83.33%	Y=1.75D	58.33%
43.8	Y=2.6D	86.67%	Y=1.85D	61.67%
60	Y=2.8D	93.33%	Y=2.1D	70.00%
90	Y=2.95D	98.33%	Y=2.6D	86.67%

Table 15: Ground vortex heights.

As far as the ground vortex formed between the jets is concerned, for $7.5 \leq V_j/U_0 \leq 43.8$ the ground vortex centre moves in the first jet direction when the impingement height decreases.

In the case of the remaining velocity ratios, the ground vortex centre moves in the direction of the second jet (downstream) when the impingement height decreases.

Finally, the ground vortex strength increases when the impingement height decreases for all the velocity ratios.

Similarly with the downstream ground vortex, the impingement height decreases and the percentage of impingement height occupied by the ground vortex increases for the same velocity ratio. The bigger percentages of the impingement height occupied by the ground vortexes for different velocity ratios and impingement heights are registered for a combination of the higher velocity ratios and lower impingement heights that corresponds to the situation where the jets impinge on the ground more strongly.

5.3.2.3.2 Impinging jets cross section

This subsection presents the vertical planes perpendicular to the crossflow (Y-Z planes) in order to describe how the jets interact with each other and the possible existence of a kidney shape of the cross section of the jets for different velocity ratios and impingement heights.

The figures show isolines of the mean horizontal velocity component U_{mean} obtained in vertical planes perpendicular to the crossflow for X/D = 0.0, 4.9, 9.8 and 19.6. Complementarily and in order to be better understood the flow development along the flow field, three-dimensional figures are presented for V_J/U_0= 15, 33.7, 60 and H/D= 15, 10, 5 and 3.

5.3.2.3.2.1 H/D= 15

At X/D=0.0 (in the middle between the axis of the jets exit), the kidney shape previously identified for other velocity ratios and impingement heights is observed clearly (figure 173). For X/D=4.9, it is possible to observe the presence of the second impingement jet. Unlike what was observed before, for this combination of velocity ratio and impingement height the second jet impacts directly on the ground, as shown by the streamtraces of the second jet are captured by the first jet. Thus, there is mixing of the wall jet at this location. Due to the presence of the second jet, the kidney shape of the first jet it is widening rapidly.

For X/D=9.8 it is registered the first jet impingement on the ground, identified by the red area that represents a region with large positive values of the horizontal velocity component. Figure 174 confirms the observations of the previous paragraphs and two regions of high static pressure (red colour) are observed corresponding to the impingement regions of the two jets. The “cold” coloured regions correspond to low pressures and are associated with core of the ground vortex.

Analysing figures 175 and 176, the crossflow fluid is entrained by the first jet and it is captured by the scarf vortex. The scarf vortex rises and passes over the wall jets resulting from both jets. For X/D > 14.7 the entire cross section is occupied by two large vortical structures rotating in opposite directions over the rear jet wall jet, revealing that all the different types of flow flowing in the crossflow direction above described finally merge.

V_j/U_0= 15

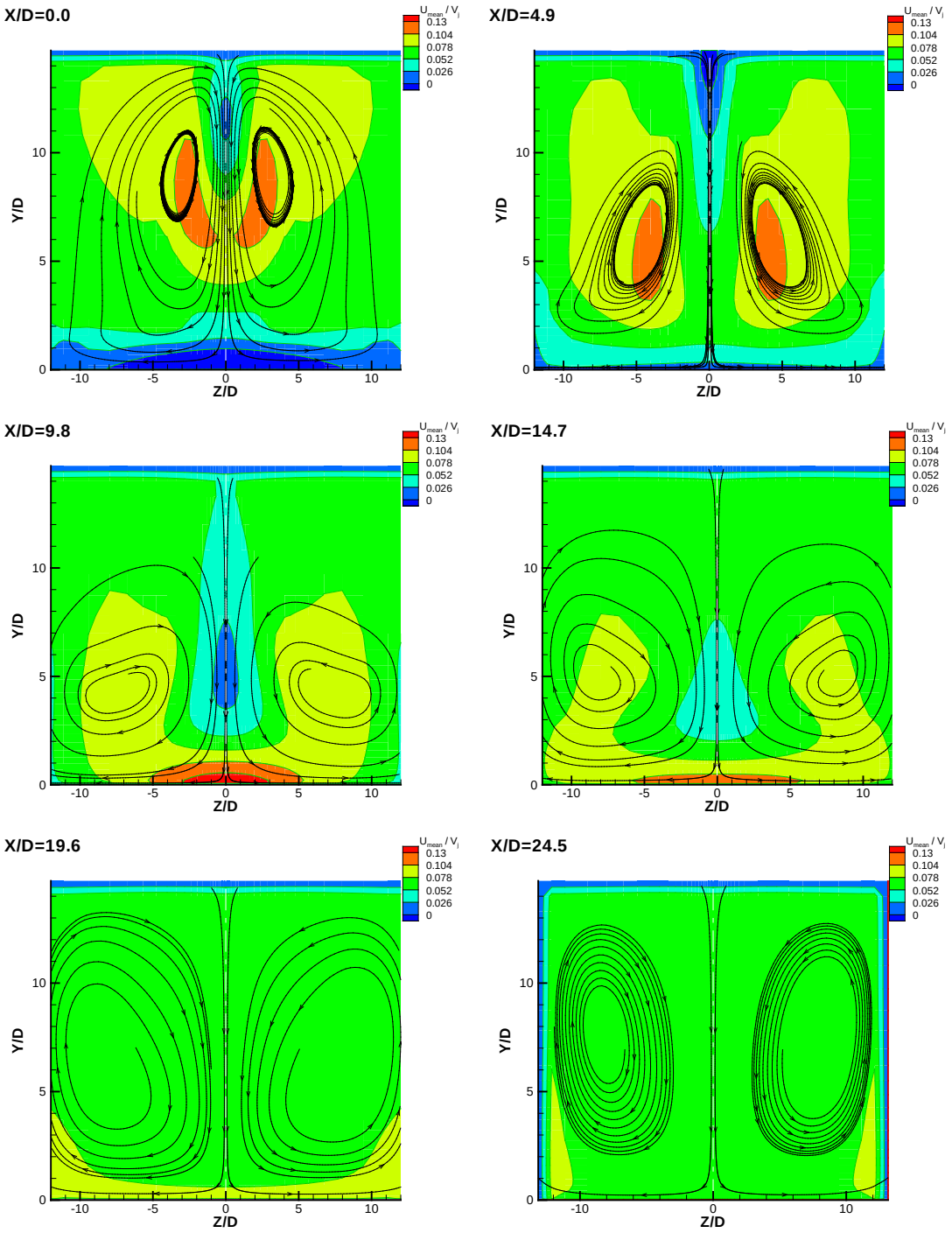

Figure 173: Mean velocity component (U_{mean}/V_j) in a vertical plane perpendicular to crossflow. (Re_j=43,000, V_j/U_0= 15, H/D=15 and L/D=6.

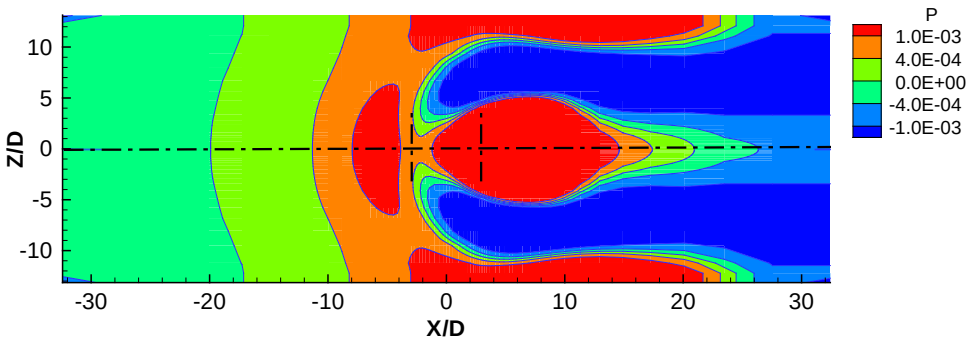

Figure 174: Pressure distribution along the field close to the ground (i.e. Y≈0) for V_j/U_0=15, H/D=15 and L/D=6 (values nondimensionalized by $1/2\rho V_{j1}^2$).

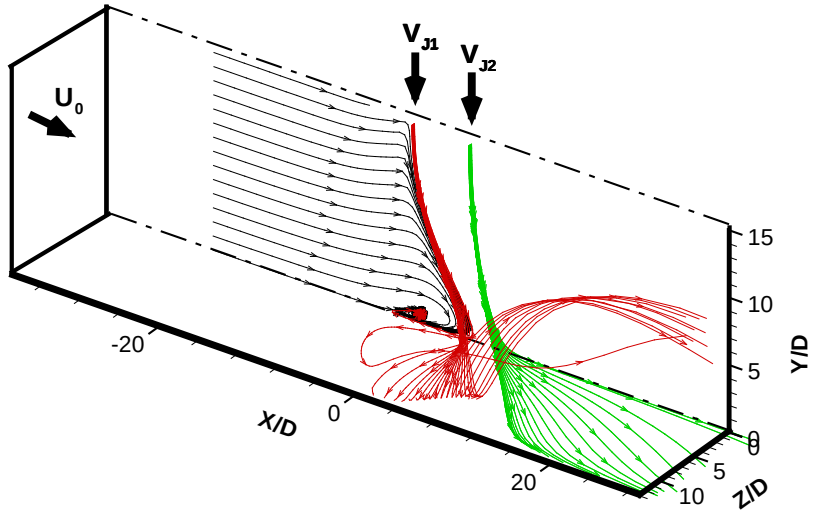

Figure 175: Tridimensional illustration of the jets flow for Re_j=43,000, V_j/U_0= 15, H/D=15 and L/D=6.

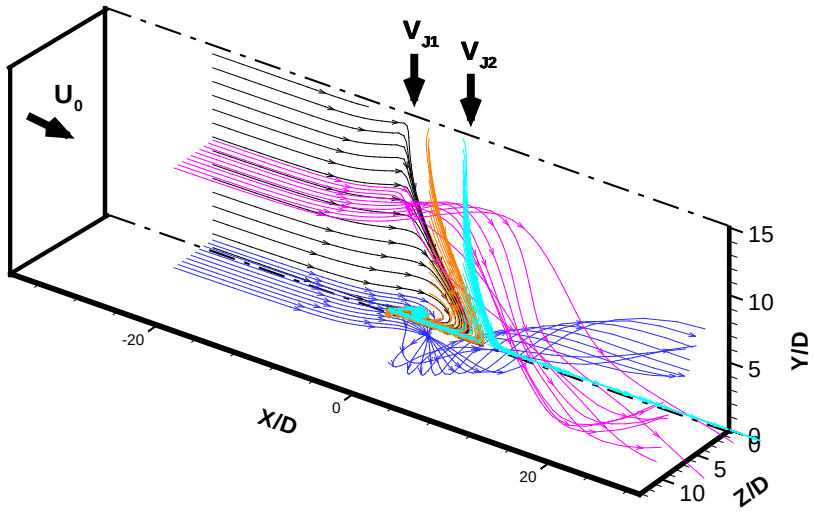

Figure 176: Tridimensional illustration of the jets and scarf vortex flow for Re_j=43,000, V_j/U_0= 15, H/D=15 and L/D=6.

V_j/U_0= 33.7

For this velocity ratio and X/D=0 is not possible to identify the kidney shape of the first jet. When the first jet touches the ground a radial wall jet is formed that when interact with the crossflow forming a ground vortex. The location of the stagnation point due to the first jet is not captured by any of the vertical planes perpendicular to the crossflow presented in the figure 177, because it occurred for X/D< 0. This fact reveals that the influence of the

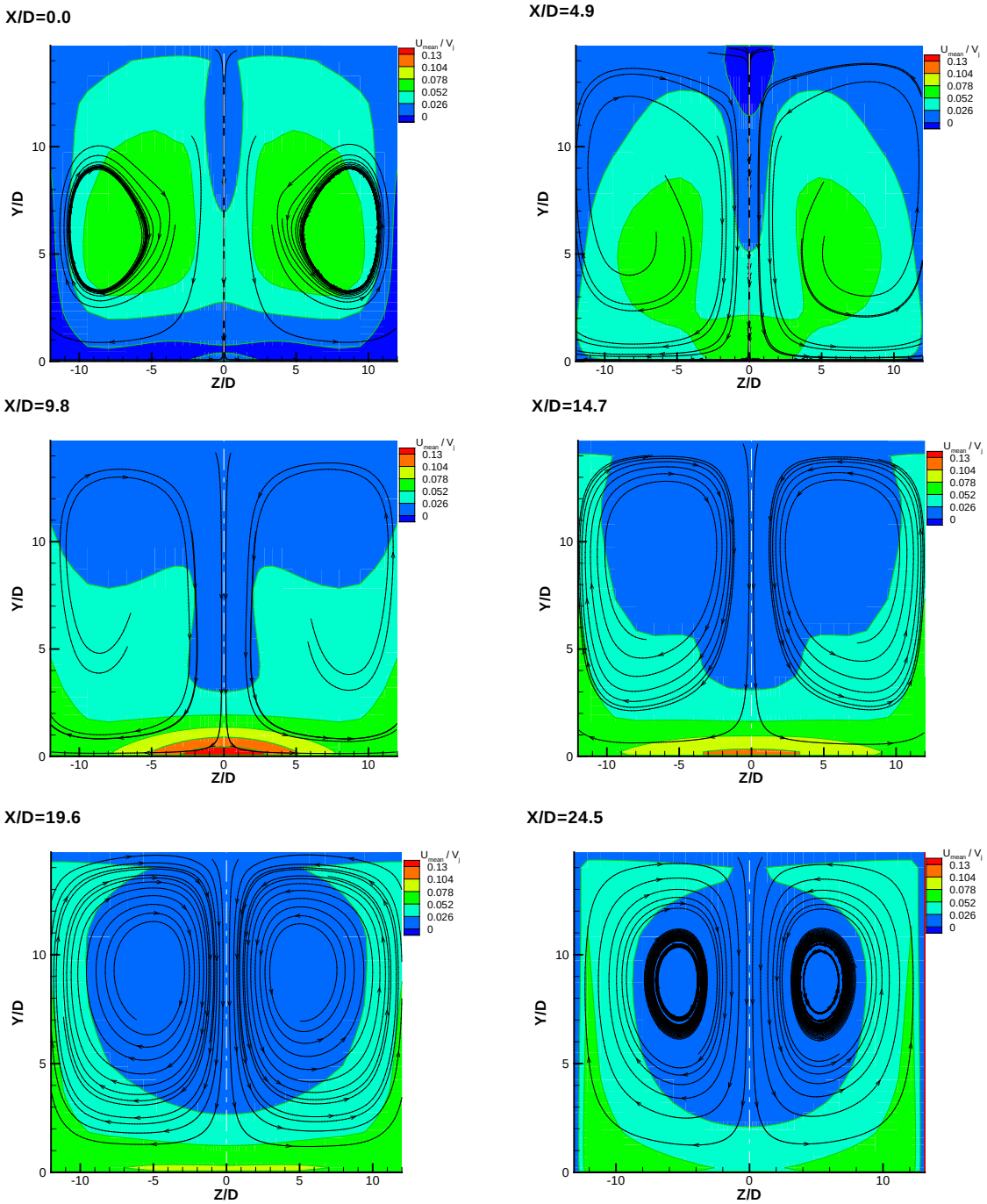

Figure 177: Mean velocity component (U_{mean}/V_j) in a vertical plane perpendicular to crossflow for Re_j=43,000, V_j/U_0= 33.7, H/D=15 and L/D=6.

crossflow in the first jet deflection tends to disappear with the decrease of the impingement height. For X/D=9.8 it is noticed that the second jet touched the ground, identified by the red area in the figure, corresponding to a large values of the horizontal velocity component. The static pressure distribution near the impingement plane (figure 178) also confirms this, but for this velocity ratio only a broader impinging zone due to both jets can be detected.

Analysing now the upstream region of the flow part of the crossflow and first jet fluid gives rise to the scarf vortex. The scarf vortex entrains more fluid and raises passing above the wall jets (figures 179 and 180). Part of the crossflow flow fluid that is not entrained by the scarf vortex passes around the first jet. On the second jet location the flow descends steeply, but near the radial wall jet of the second jet it goes back up, flowing downstream together with the scarf vortex over the second jet radial wall jet (see figure X/D=14.7). For X/D>14.7 the second jet radial wall jet mixes with the remaining flow and two vortical structures rotating in opposite directions flowing in the crossflow direction arise.

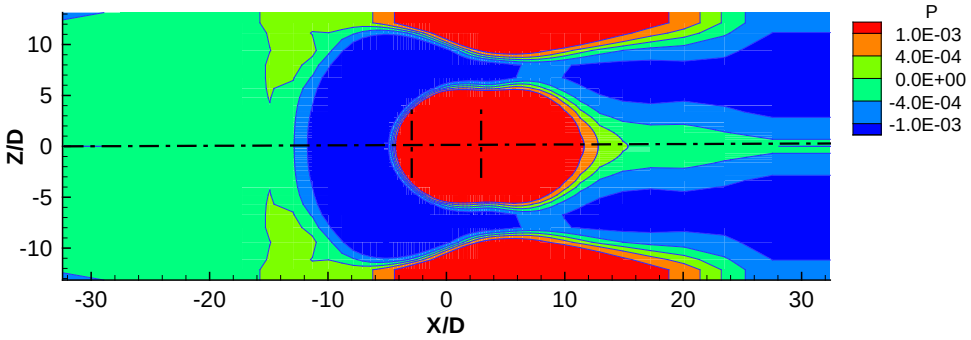

Figure 178: Pressure distribution along the field close to the ground (i.e. Y≈0) for V_j/U_0=33.7, H/D=15, and L/D=6 (values nondimensionalized by $1/2\rho V_{j1}^2$).

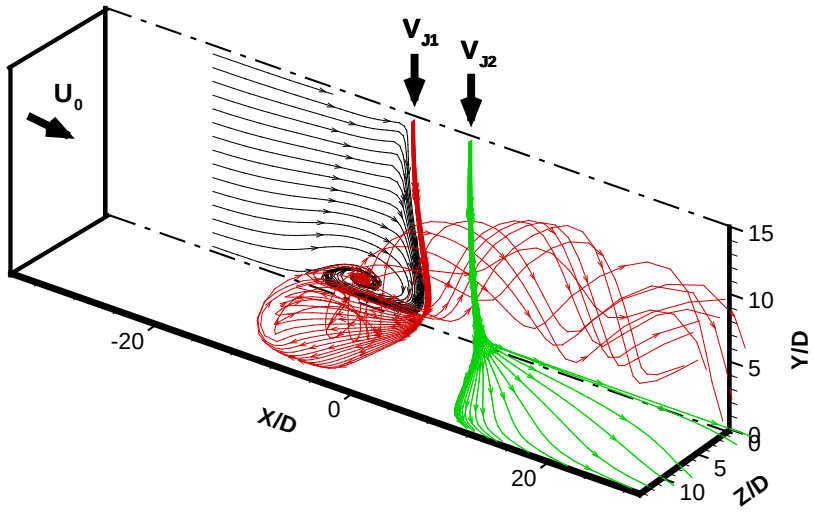

Figure 179: Tridimensional illustration of the jets flow for Re_j=43,000, V_j/U_0= 33.7, H/D=15 and L/D=6.

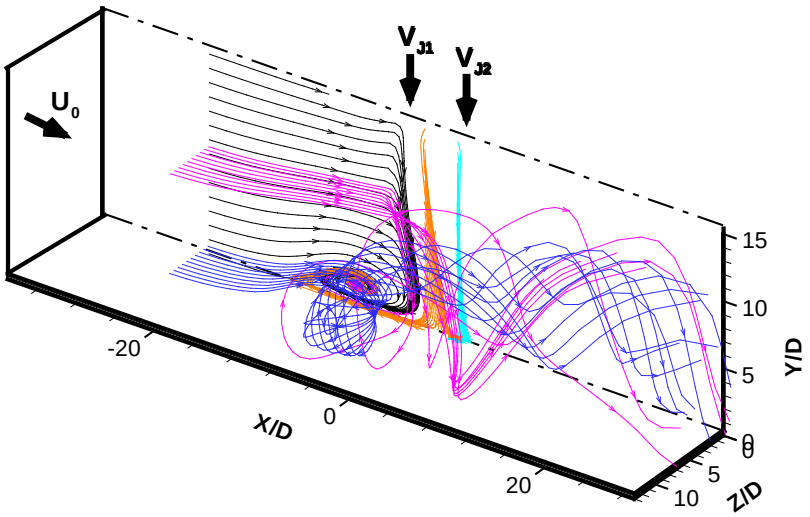

Figure 180: Tridimensional illustration of the jets and scarf vortex flow for Re_j=43,000, V_j/U_0= 33.7, H/D=15 and L/D=6.

V_j/U_0= 60

Figure 181 and in particular the X/D=0.0 and 4.9 planes, show near zero values of the mean horizontal velocity component, indicating that the first jet touched the ground for X/D<0 for this velocity ratio. These profiles show close to the ground (Y/D <2) the wall jet resulting from the first jet after impinging on the ground and which is flowing in the crossflow direction. The second jet touched the ground, forming a radial wall jet that can be observed for X/D=9.8 by the red area with relative large values of the mean horizontal velocity component.

Analysing now figures 182 to 184 they show part of the crossflow fluid is entrained by the scarf vortex. The remaining part of the crossflow fluid due to the rotational effect of the scarf vortex and the first jet radial wall interaction, rises and meander clockwise the scarf vortex and the first jet. Due to the lateral confinement imposed by the lateral walls the scarf vortex fluid rises and originates a large vortical structure flowing downstream together with the part of the crossflow fluid that is not entrained by the first jet, above the second jet radial wall jet. Also due to the lateral confinement, part of the first jet radial wall jet rises, passing over the scarf vortex and in the region between the jets goes down and comes back up and outline the second jet. Then follow the second jet flow direction to the ground and passes through the second jet radial wall jet what makes it rise again and flows to downstream directly.

For X/D ≥ 14.7 all the flows described above merged in a single flow flowing to downstream and the entire cross section is occupied by two vortical structures rotating in opposite directions. This behaviour is confirmed by the static pressure distribution (figure 182) which is less pronounced near the impinging jets.

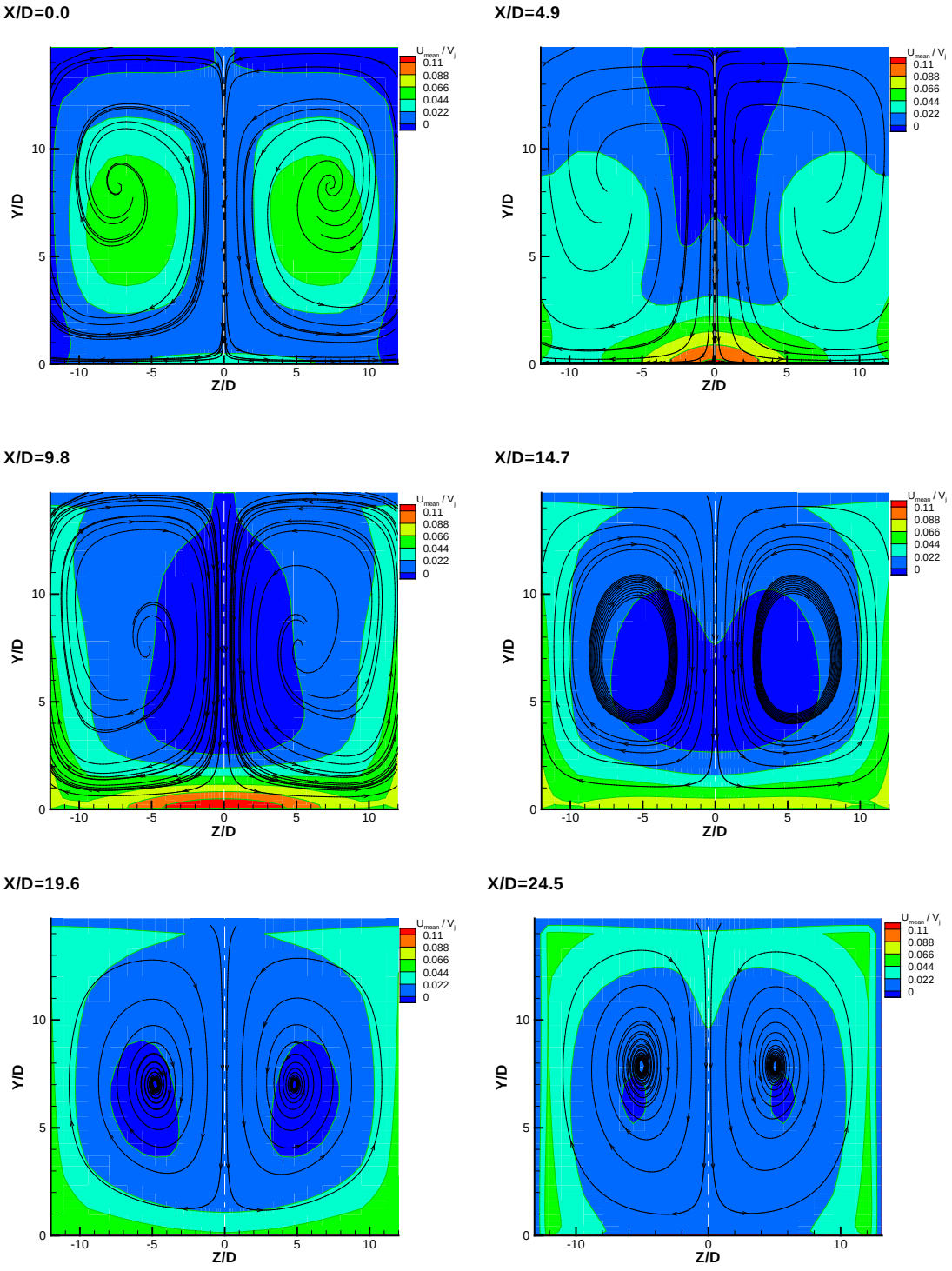

Figure 181: Mean velocity component (U_{mean}/V_j) in a vertical plane perpendicular to crossflow for Re_j=43,000, V_j/U_0= 60, H/D=15 and L/D=6.

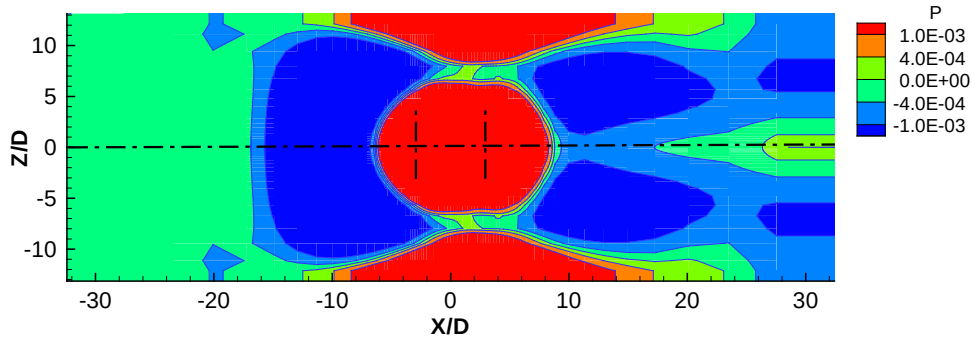

Figure 182: Pressure distribution along the field close to the ground (i.e. Y≈0) for V_j/U_0=60, H/D=15, and L/D=6 (values nondimensionalized by $1/2\rho V_{j1}^2$).

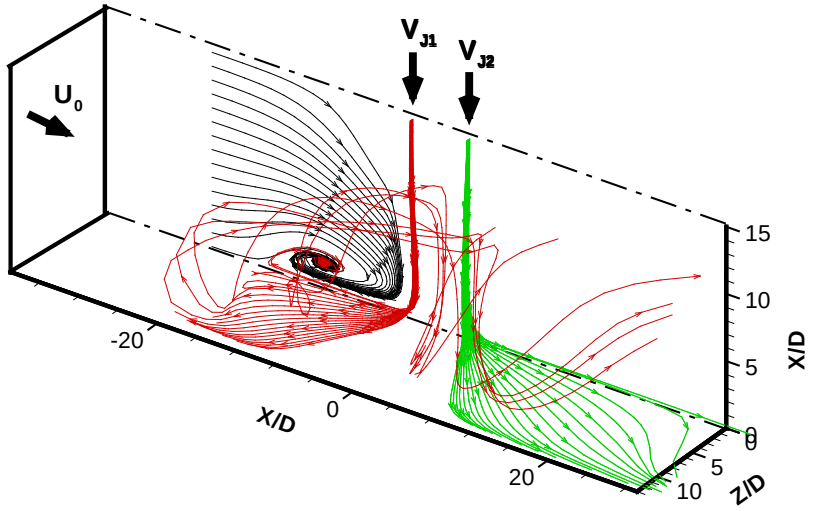

Figure 183: Tridimensional illustration of the jets flow for Re_j=43,000, V_j/U_0= 60, H/D=15 and L/D=6.

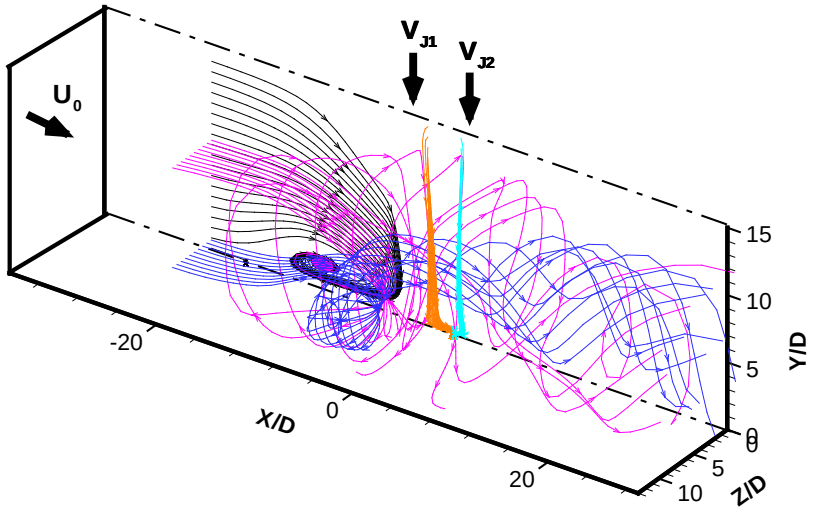

Figure 184: Tridimensional illustration of the jets and scarf vortex flow Re_j=43,000, V_j/U_0=60, H/D=15 and L/D=6.

5.3.2.3.2.2 H/D= 10

V_j/U_0= 15

The planes at X/D=0.0 and 4.9 show close to the ground (Y/D <1) the first jet radial wall jet. For X/D=9.8 it is possible to see a red area that identify a region with large positive values of the mean horizontal velocity component indicating that the second jet touched the ground, giving rise to a radial wall jet. Part of the wall jet flows directly to downstream, close to the symmetry plane.

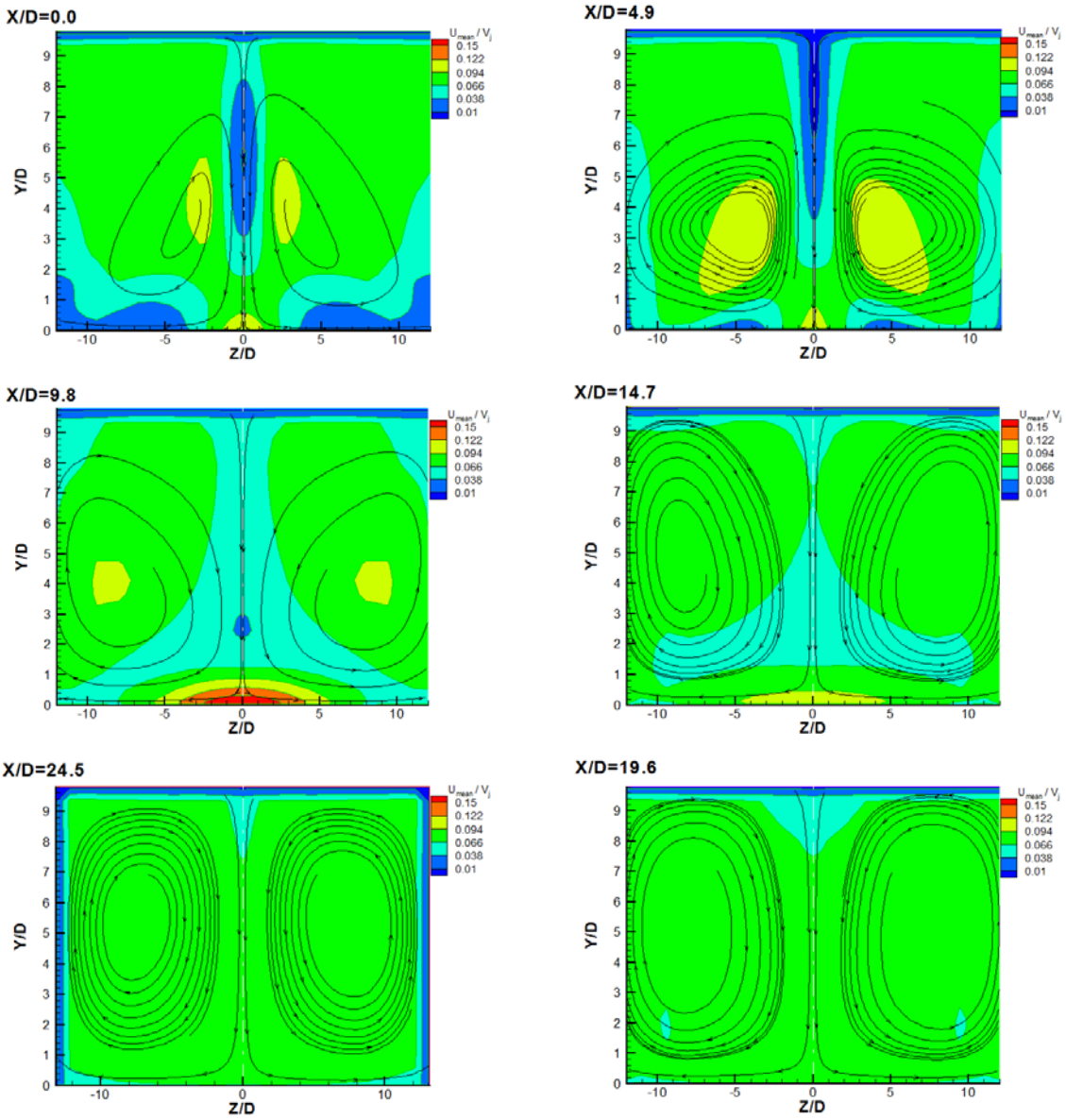

Figure 185: Mean velocity component (U_{mean}/V_j) in a vertical plane perpendicular to crossflow for Re_j=43,000, V_j/U_0= 15, H/D=10 and L/D=6.

Part of the crossflow fluid is entrained by the scarf vortex. The scarf vortex rises and it passes over the wall jets. The remaining of the crossflow fluid passes over the scarf vortex, going

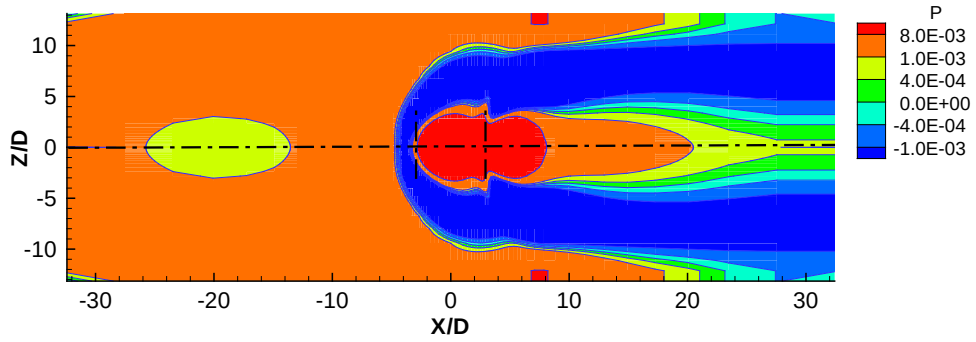

Figure 186: Pressure distribution along the field close to the ground (i.e. Y≈0) for V_j/U_0=15, H/D=10, and L/D=6 (values nondimensionalized by $1/2\rho V_{j1}^2$).

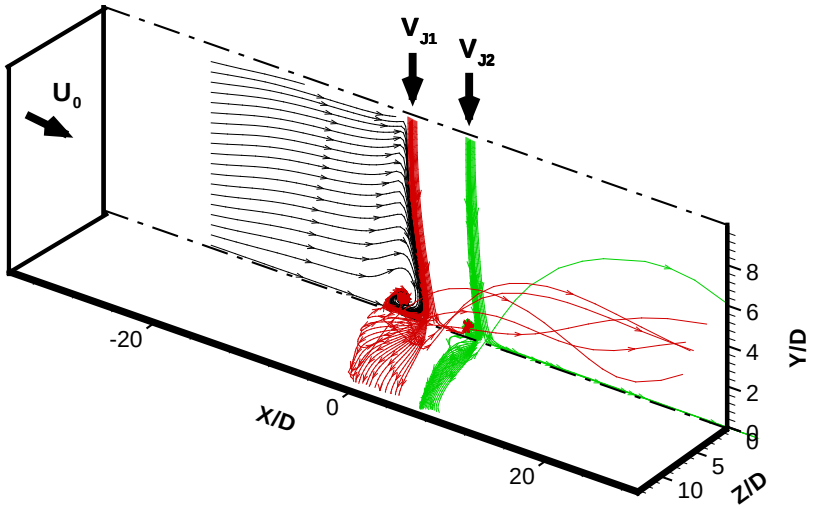

Figure 187: Tridimensional illustration of the jets flow for Re_j=43,000, V_j/U_0= 15, H/D=10 and L/D=6.

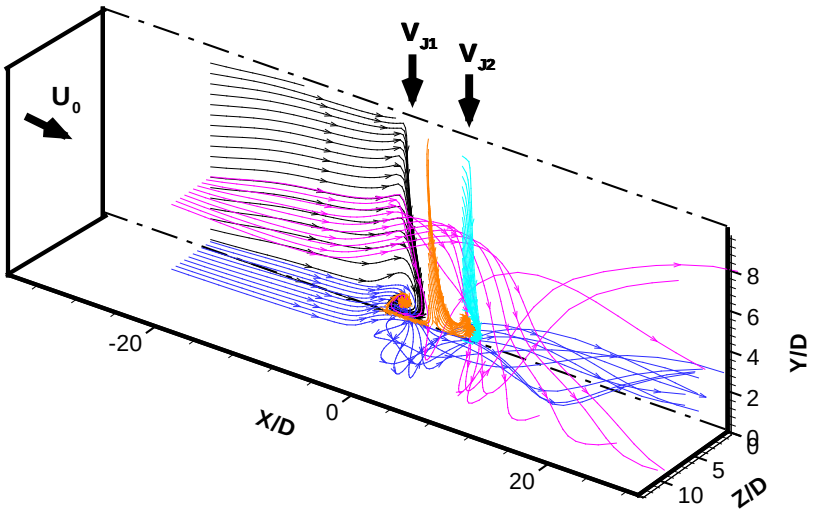

Figure 188: Tridimensional illustration of the jets and scarf vortex flow for Re_j=43,000, V_j/U_0=15, H/D=10 and L/D=6.

around the impingement jets through the region between them, and go down due to the downwards effect of the second jet flow direction.

For X/D>14.7 the entire cross section is occupied by two vortical structures rotating in opposite directions, resulting from the merge of the flows described above, flowing always downstream over the second jet radial wall jet.

V_j/U_0= 33.7

For V_j/U_0=33.7 and X/D=0 both jets touch the ground. It is also possible to see the scarf vortex development over the first jet radial wall jet. The flow pattern is quite similar to the one observed for H/D=15. In the region between the jets, when the first jet touches the ground the inner wall jet flows and rises up like an upwash flow, but it is captured by the second jet inner wall jet, and a little clockwise vortex is formed close to the second jet.

For X/D≥14.7 the entire cross section is occupied by two vortical structures rotating in opposite directions, revealing that the second jet radial wall jet and the vortical structure composed by the scarf vortex fluid and the remaining crossflow fluid merge and flow together downstream.

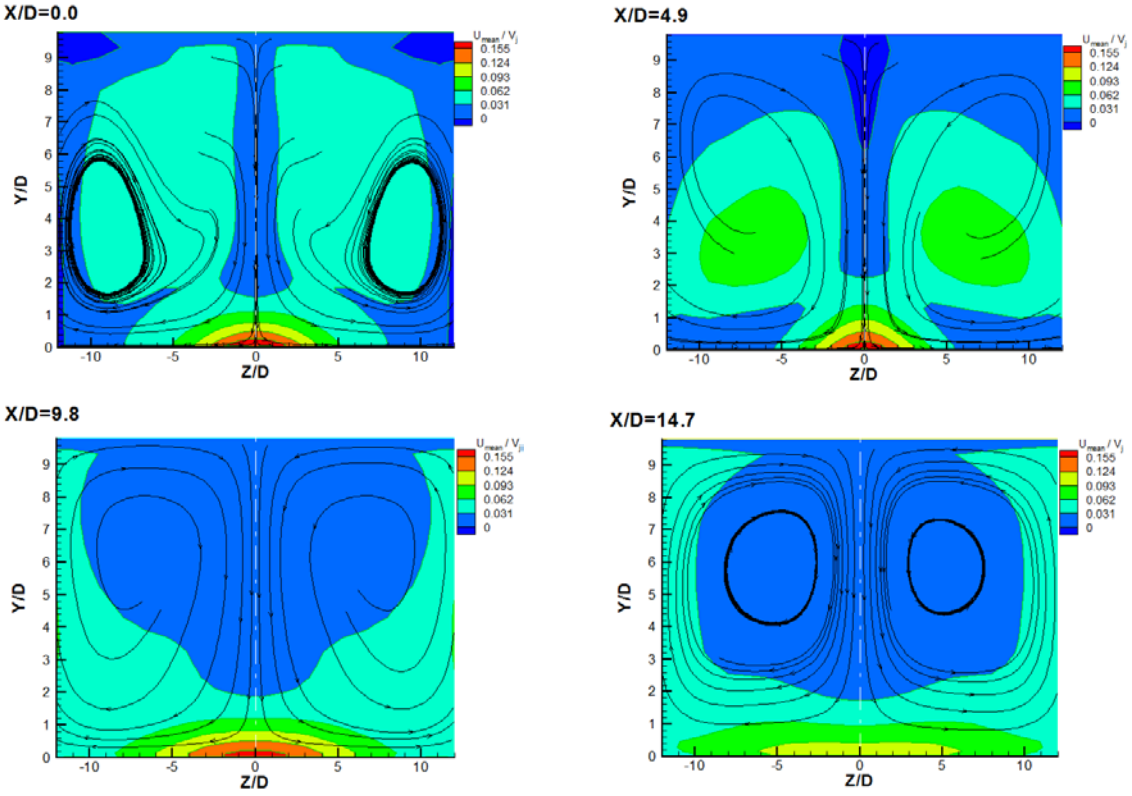

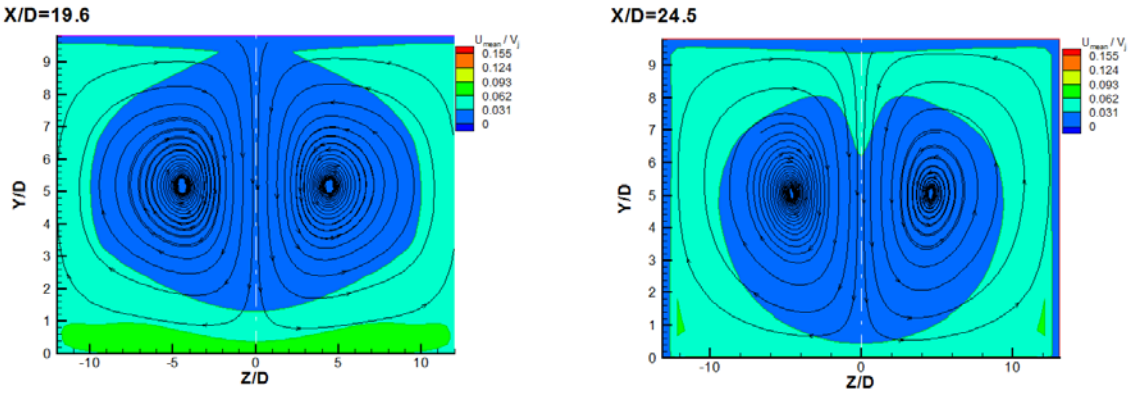

Figure 189: Mean velocity component (U_{mean}/V_j) in a vertical plane perpendicular to crossflow for Re_j=43,000, V_j/U_0= 33.7, H/D=10 and L/D=6.

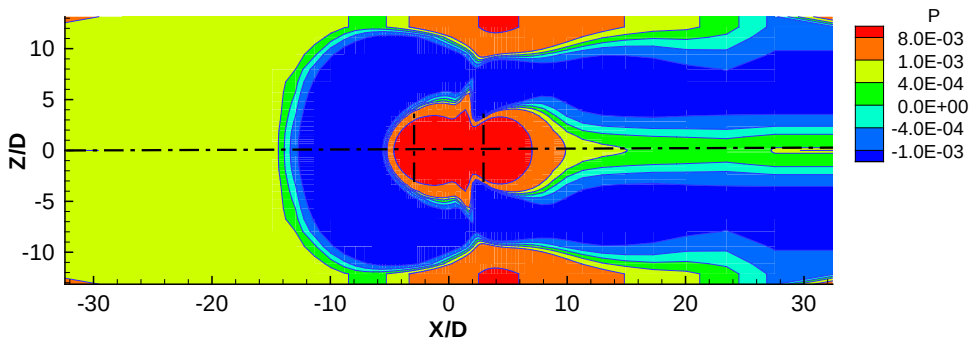

Figure 190: Pressure distribution along the field close to the ground (i.e. Y≈0) for V_j/U_0=33.7, H/D=10, and L/D=6 (values nondimensionalized by $1/2\rho V_{j1}^2$).

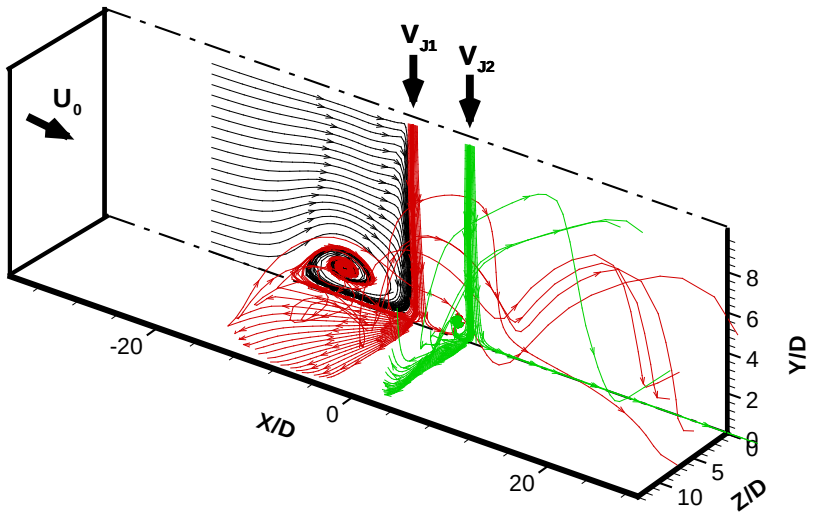

Figure 191: Tridimensional illustration of the jets flow for Re_j=43,000, V_j/U_0= 33.7, H/D=10 and L/D=6.

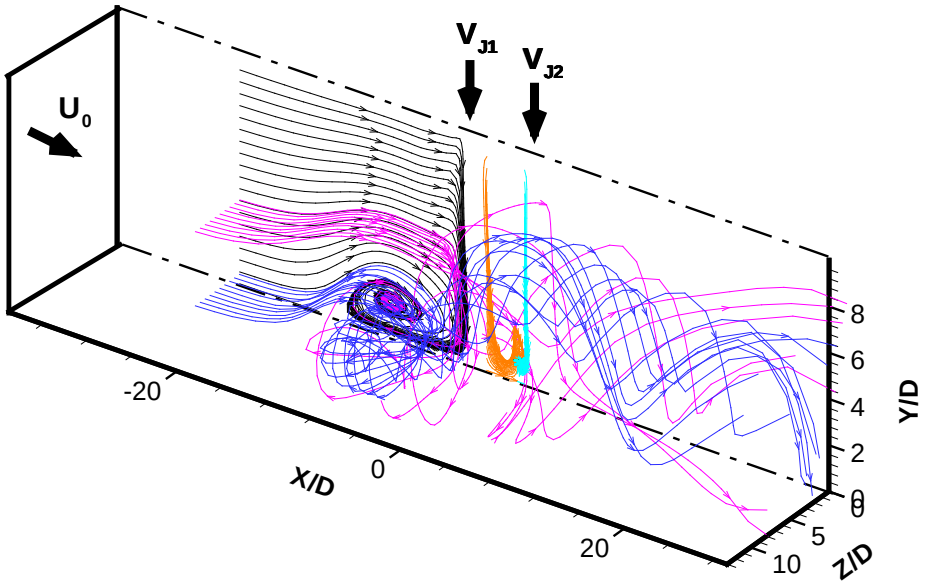

Figure 192: Tridimensional illustration of the jets and scarf vortex flow for Re_j=43,000, V_j/U_0=33.7, H/D=10 and L/D=6.

V_j/U_0= 60

Similarly, to the previous velocity ratio, for X/D=0 the first jet already touched the ground. It is also possible to see the scarf vortex development over the first jet radial wall jet (Y/D≈4 and Z/D≈2,5). The increase of the velocity ratio (meaning the decrease of the crossflow velocity) causes the scarf vortex to feel the lateral confinement earlier because the position of the ground vortex centre is located further upstream. So, compared with the previous velocity ratio the scarf vortex changes its shape and moves further upstream. In the next downstream location, the second wall jet in ground by the blue area. Part of this wall jet flows directly downstream close to the symmetry plane. In the region between the jets, when the first jet touches the ground the inner wall jet flows and rises up like an upwash flow, but it is captured by the second jet inner wall jet, and a little clockwise ground vortex is formed close to the second jet.

For X/D≥14.7 the entire cross section is occupied by two vortical structures rotating in opposite directions, revealing that the second jet radial wall jet and the vortical structure composed by the scarf vortex fluid and the remaining crossflow fluid merged and flowing together to downstream.

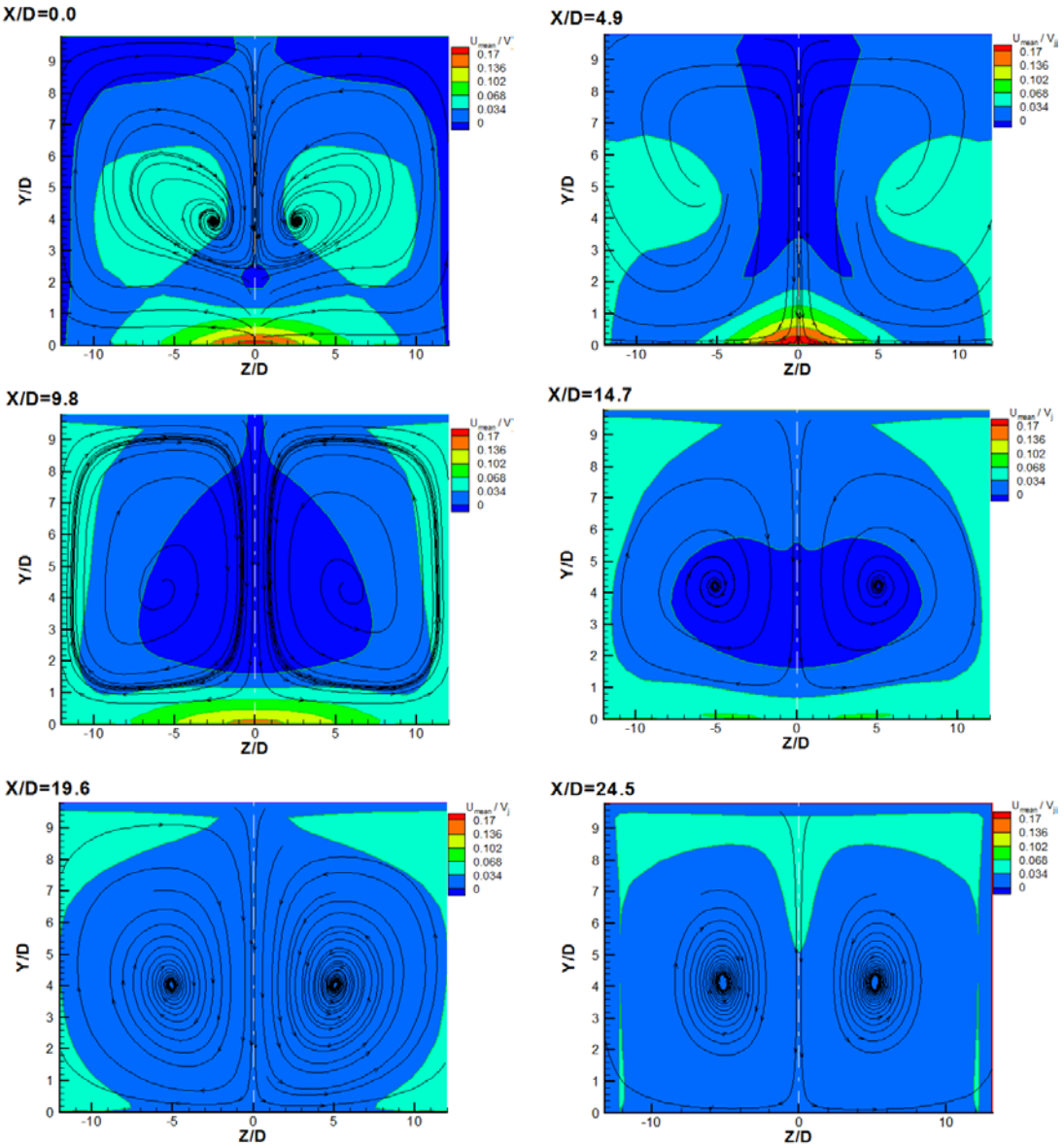

Figure 193: Mean velocity component (U_{mean}/V_j) in a vertical plane perpendicular to crossflow for Re_j=43,000, V_j/U_0= 60, H/D=10 and L/D=6.

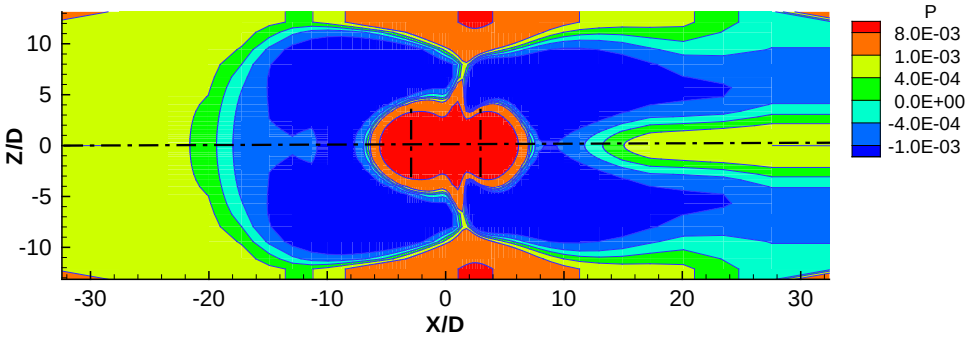

Figure 194: Pressure distribution along the field close to the ground (i.e. Y≈0) for V_j/U_0=33.7, H/D=10, and L/D=6 (values nondimensionalized by $1/2\rho V_{j1}^2$).

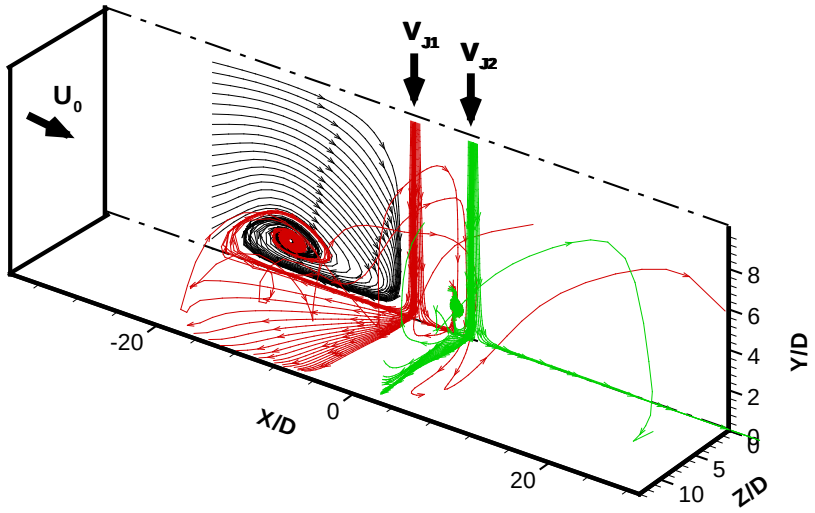

Figure 195: Tridimensional illustration of the jets flow for Re_j=43,000, V_j/U_0= 60, H/D=10 and L/D=6.

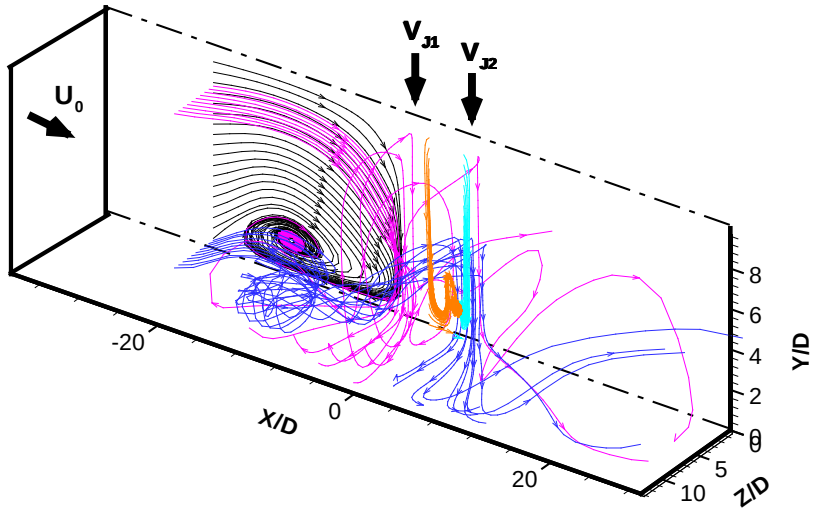

Figure 196: Tridimensional illustration of the jets and scarf vortex flow for Re_j=43,000, V_j/U_0=60, H/D=10 and L/D=6.

5.3.2.3.2.3 H/D= 5

V_j/U_0= 15

From figure 197 at X/D=0 it is possible to see that the first jet already touched the ground for V_j/U_0=15. The impingement jet is not too affected by the crossflow presence, since the jet impinges in the ground for X/D≈-4.9, revealing that for lower impingement heights the crossflow effect on the jet deflection disappears due to the increase of the jet strength. It is also possible to see the scarf vortex development over the first jet radial wall jet. The Part of the crossflow fluid that is not entrained passes over the scarf vortex, going around the impingement jets through the region between them and near X/D=4.9 goes down, due to the downwards direction of the second jet flow. Then for X/D≈12 it impacts on the ground, rising

again and flowing downstream. Due to the lateral confinement imposed the scarf vortex it rises and loses its structure, originating a vortical structure that flows downstream together with part of the radial wall jet of the upstream jet. In the next downstream location, the touch of the second jet on the ground is noticeable with the formation of a radial wall jet. Part of this wall jet flow directly downstream close to the symmetry plane. The other part when feeling the lateral confinement rises up and flows downstream always above the resulting scarf vortex flow. Both flows are associated with the negative pressure regions upstream each impinging jet (figure 198).

In the region between the jets, when the first jet touches the ground the inner wall jet flows and rises up like an upwash flow, but it is captured by the second jet inner wall jet, and a little clockwise ground vortex is formed close to the second jet (figure 199). Figure 197 represent the further downstream locations X/D=19.6 and 24.5 and show the mixture of the different flows analysed above.

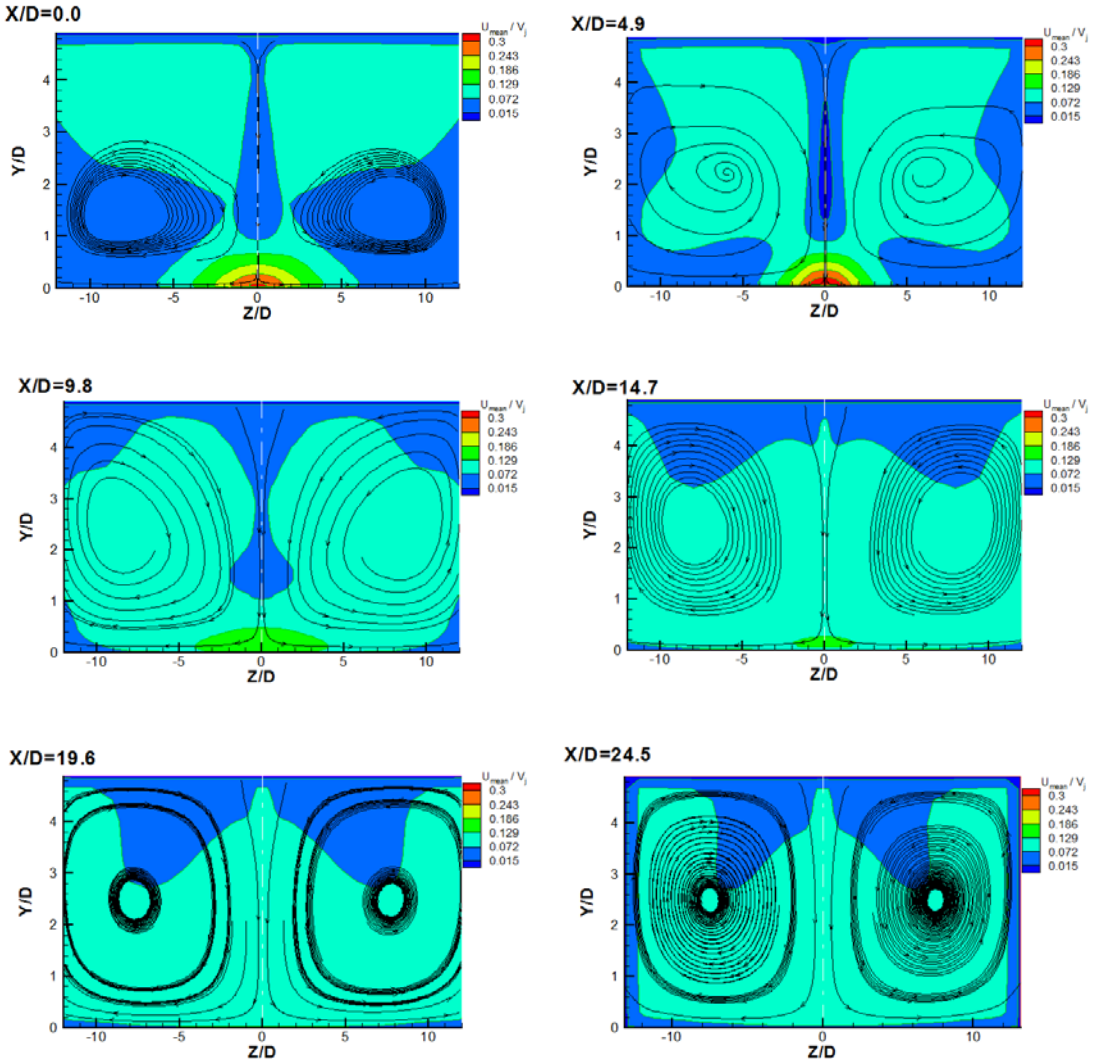

Figure 197: Mean velocity component (U_{mean}/V_j) in a vertical plane perpendicular to crossflow for Re_j=43,000, V_j/U_0= 15, H/D=5 and L/D=6.

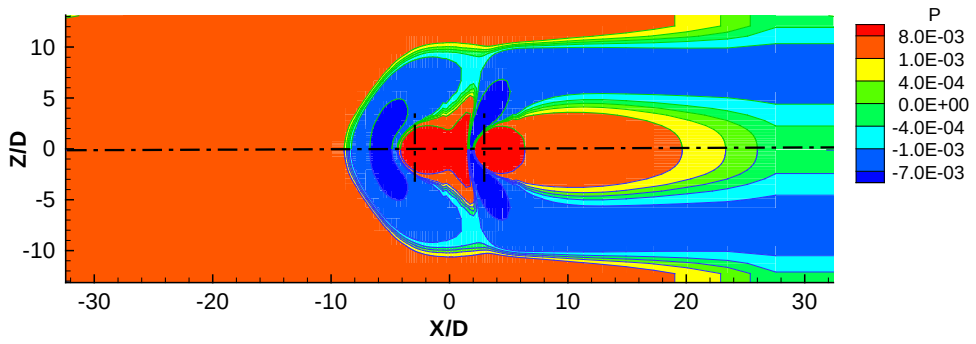

Figure 198: Pressure distribution along the field close to the ground (i.e. Y≈0) for V_j/U_0=15, H/D=5, and L/D=6 (values nondimensionalized by $1/2\rho V_{j1}^2$).

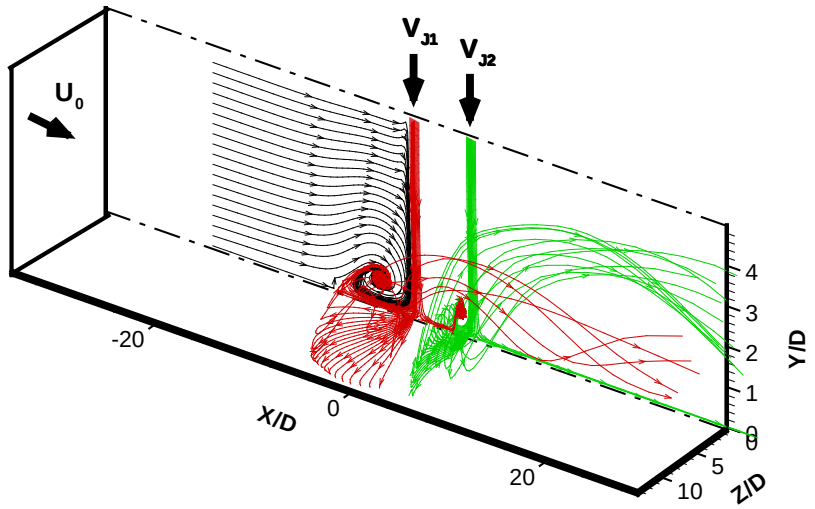

Figure 199: Tridimensional illustration of the jets flow for Re_j=43,000, V_j/U_0= 15, H/D=5 and L/D=6.

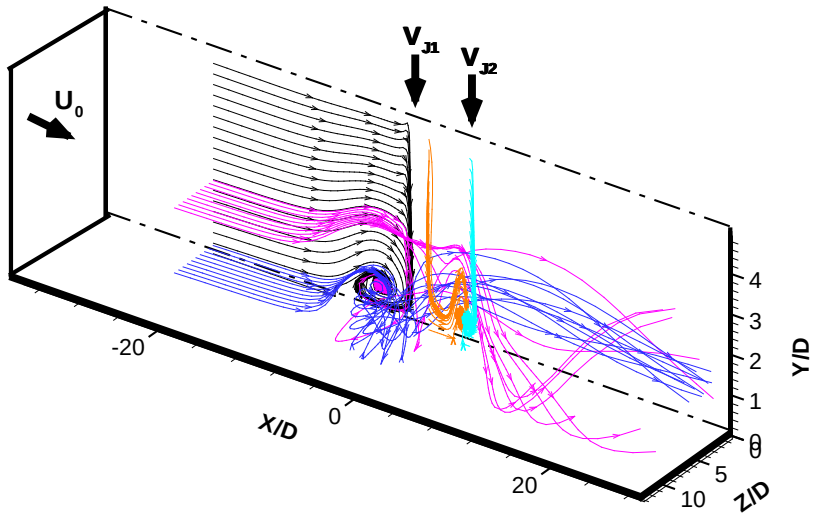

Figure 200: Tridimensional illustration of the jets and scarf vortex flow for Re_j=43,000, V_j/U_0=15, H/D=5 and L/D=6.

V_j/U_0= 33.7

For V_j/U_0=33.7 (figures 201 to 203) the flow pattern is similar to the previous one of V_j/U_0=15.

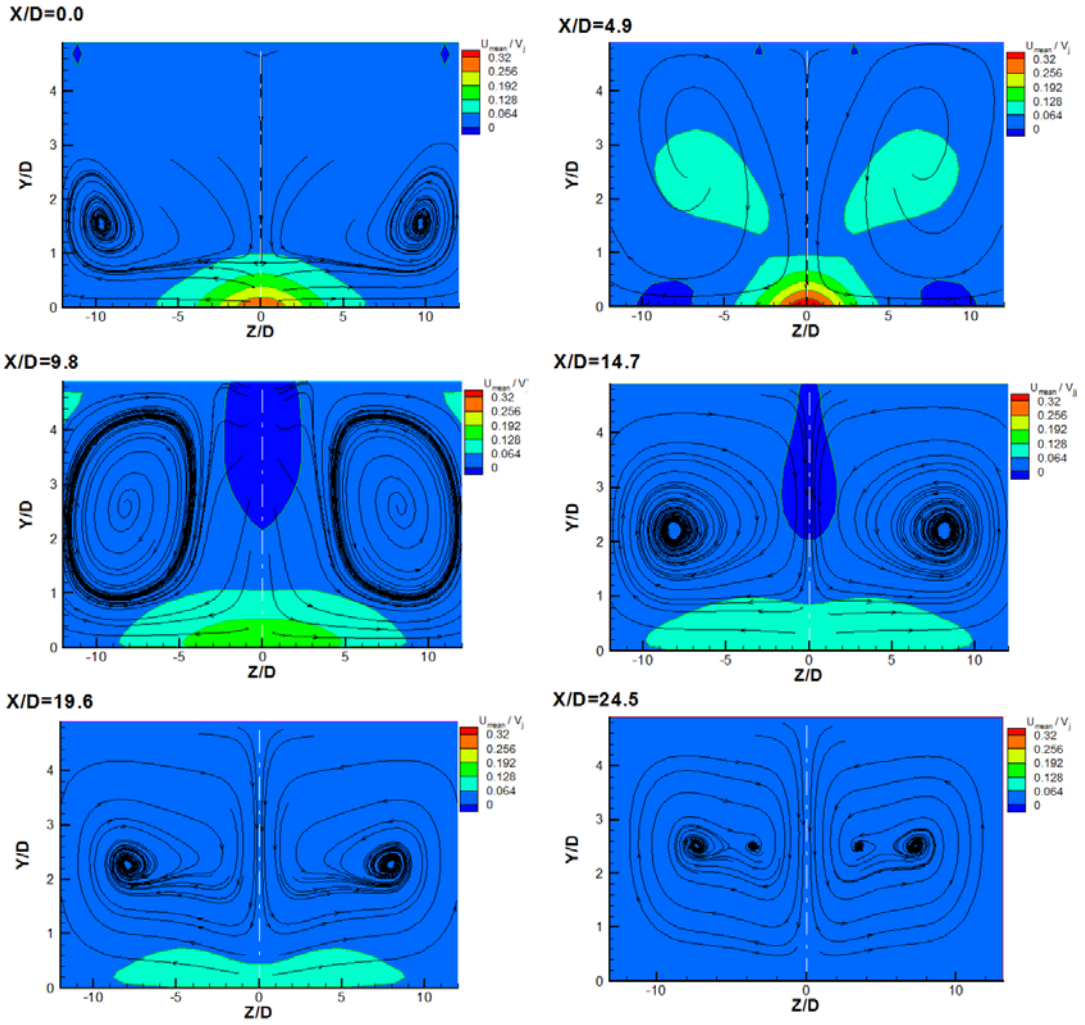

Figure 201: Mean velocity component (U_{mean}/V_j) in a vertical plane perpendicular to crossflow for Re_j=43,000, V_j/U_0= 33.7, H/D=5 and L/D=6.

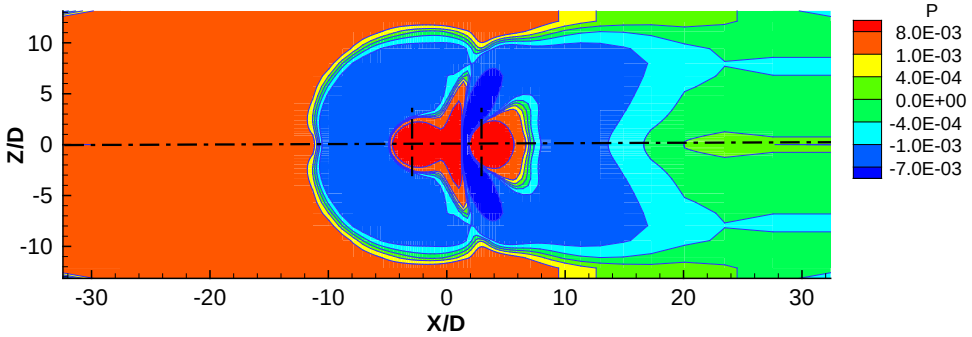

Figure 202: Pressure distribution along the field close to the ground (i.e. Y≈0) for V_j/U_0=33.7, H/D=5, and L/D=6 (values nondimensionalized by $1/2\rho V_{j1}^2$).

Nevertheless, the downstream ground vortex resulting from the second jet increases its width and affects the development of the upstream one. This effect can be confirmed in figure 202 by the negative pressure distribution.

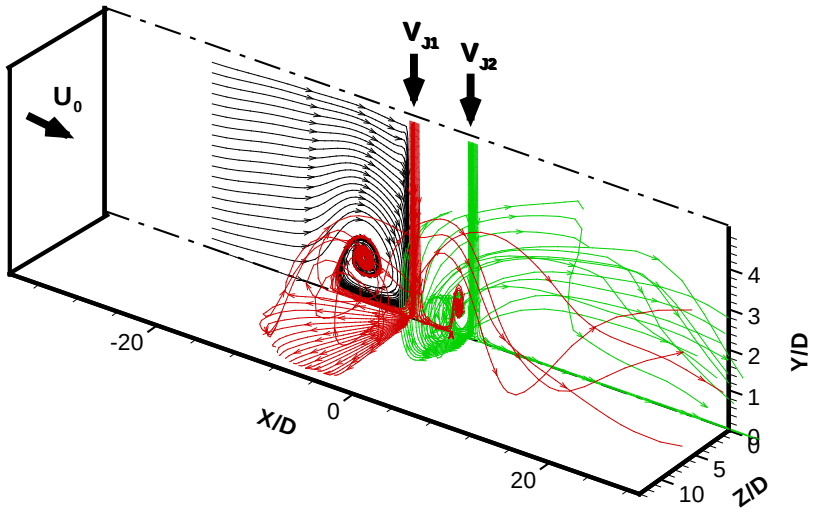

Figure 203: Tridimensional illustration of the jets flow for Re_j=43,000, V_j/U_0= 33.7, H/D=5 and L/D=6.

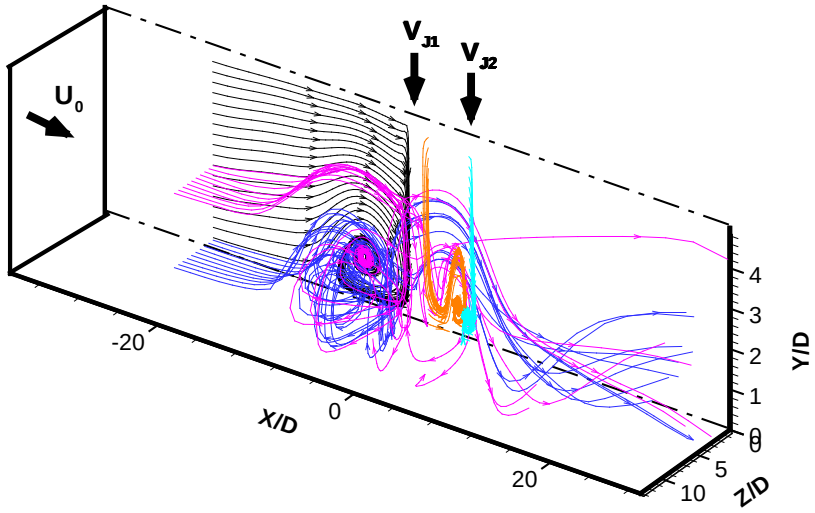

Figure 204: Tridimensional illustration of the jets and scarf vortex flow for Re_j=43,000, V_j/U_0=33.7, H/D=5 and L/D=6.

V_j/U_0= 60

For V_j/U_0=60 some changes in the flow are registered for X/D≥14.7 the entire cross section is occupied by two vortical structures rotating in opposite directions, revealing that all the different parts of the flow merged and are flowing together to downstream. Although for X/D=19.6 close to Z/D=0, it seems that a little part of the flow try to form another two vortical structures with the opposite rotation direction, but for X/D=24.5 these two little structures do not appear.

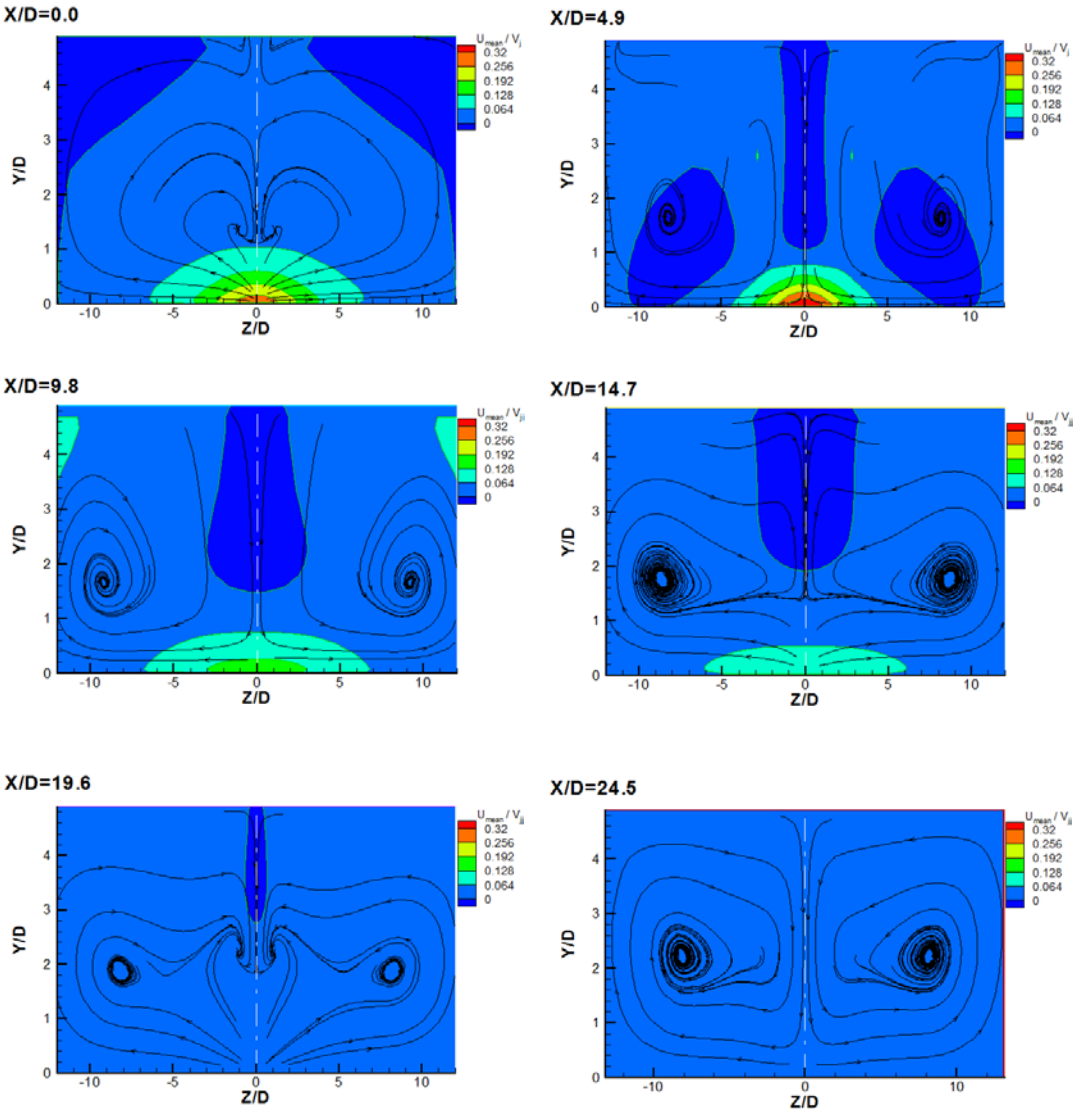

Figure 205: Mean velocity component (U_{mean}/V_j) in a vertical plane perpendicular to crossflow for Re_j=43,000, V_j/U_0= 60, H/D=5 and L/D=6.

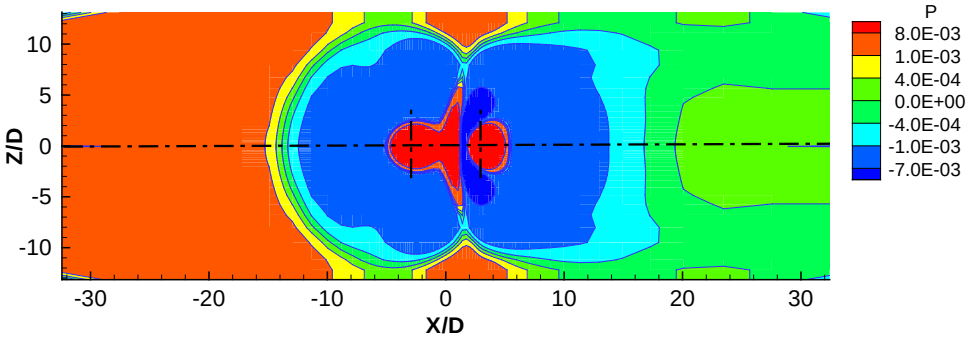

Figure 206: Pressure distribution along the field close to the ground (i.e. Y≈0) for V_j/U_0=60, H/D=5, and L/D=6 (values nondimensionalized by $1/2\rho V_{j1}^2$).

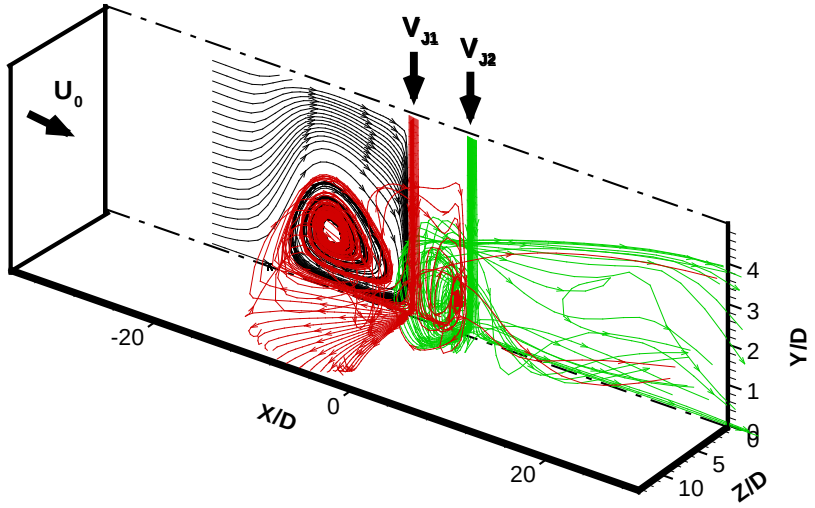

Figure 207: Tridimensional illustration of the jets flow for Re_j=43,000, V_j/U_0= 60, H/D=5 and L/D=6.

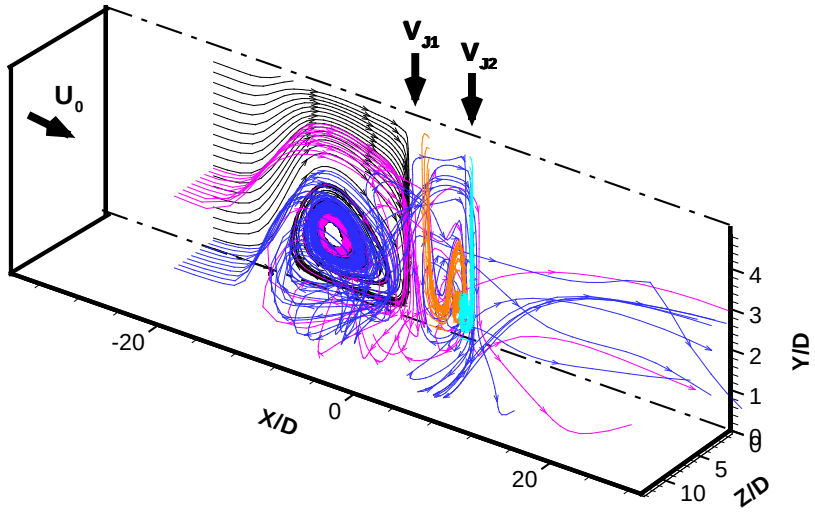

Figure 208: Tridimensional illustration of the jets and scarf vortex flow for Re_j=43,000, V_j/U_0=60, H/D=5 and L/D=6.

5.3.2.3.2.4 H/D= 3

As shown in figures 209 to 220 for H/D=3 the results are similar to those obtained for H/D=5. However, the effect of confinement is much less pronounced and the flow is more concentrated near the longitudinal vertical plane of symmetry.

V_j/U_0= 15

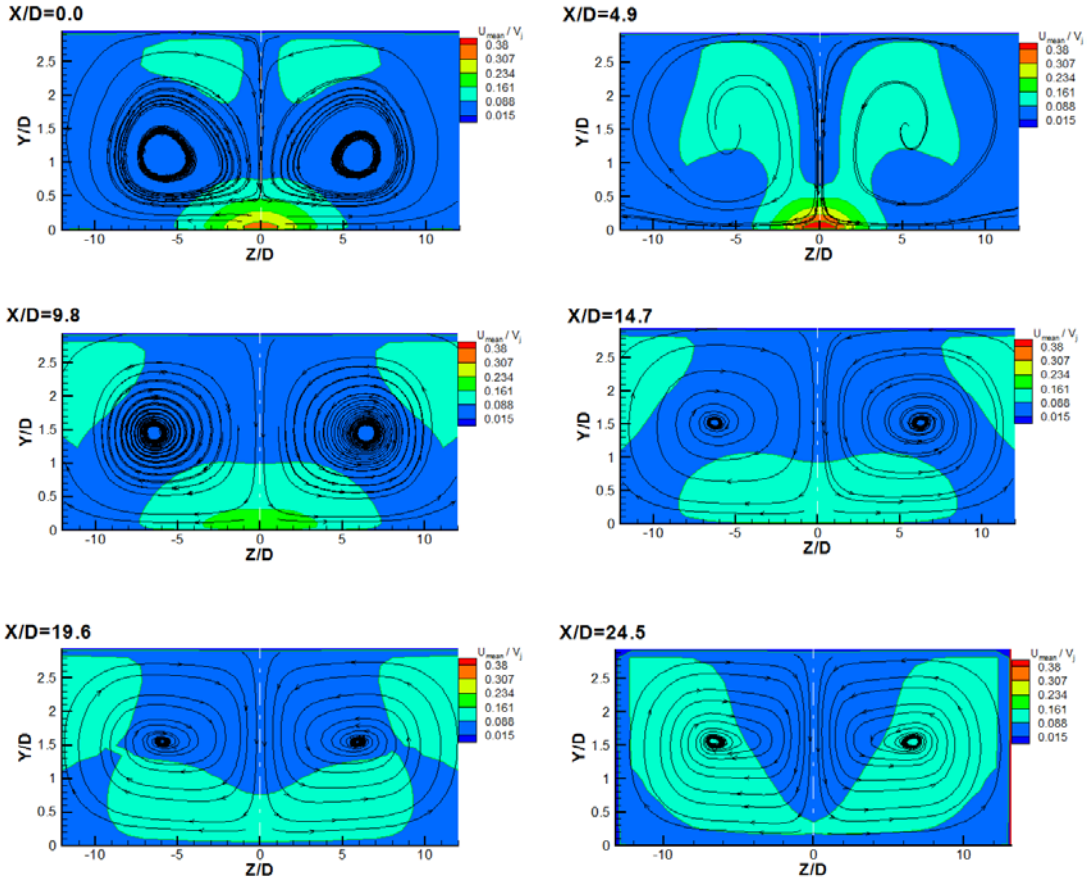

Figure 209: Mean velocity component (U_{mean}/V_j) in a vertical plane perpendicular to crossflow for Re_j=43,000, V_j/U_0= 15, H/D=3 and L/D=6.

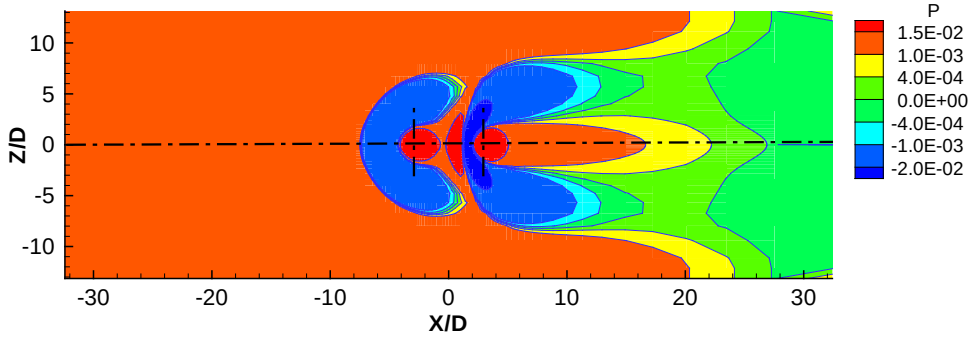

Figure 210: Pressure distribution along the field close to the ground (i.e. Y≈0) for V_j/U_0=15, H/D=3, and L/D=6 (values nondimensionalized by $1/2\rho V_{j1}^2$).

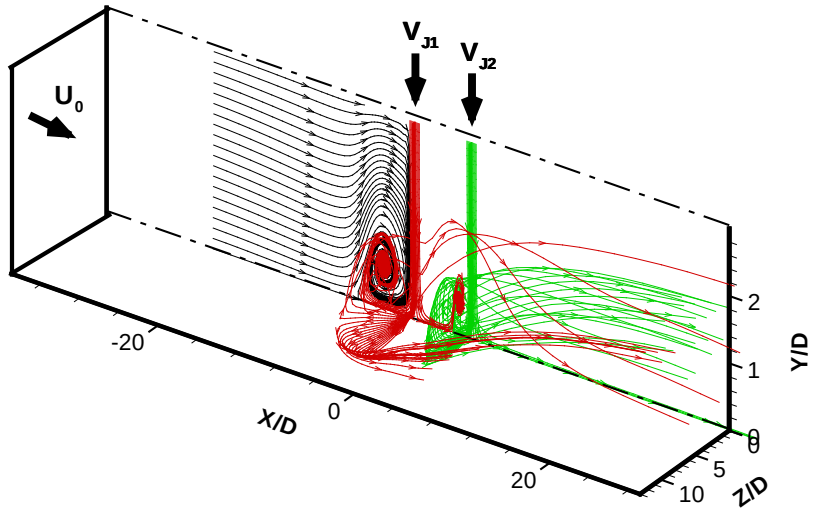

Figure 211: Tridimensional illustration of the jets flow for Re_j=43,000, V_j/U_0= 15, H/D=3 and L/D=6.

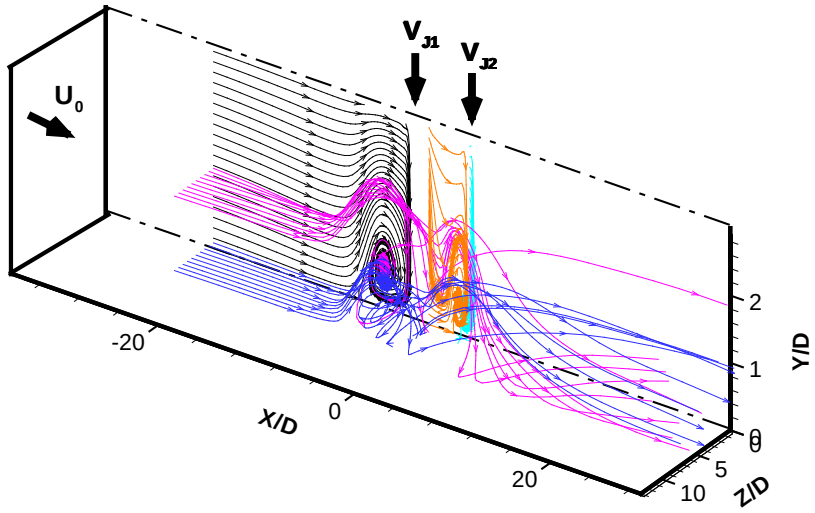

Figure 212: Tridimensional illustration of the jets and scarf vortex flow for Re_j=43,000, V_j/U_0=15, H/D=3 and L/D=6.

V_j/U_0=33.7

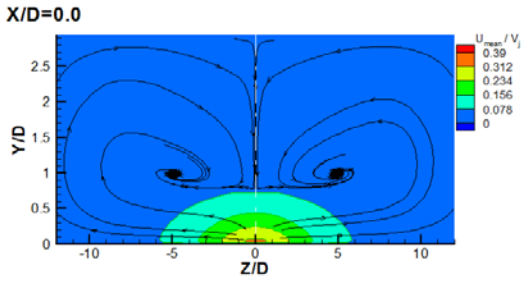

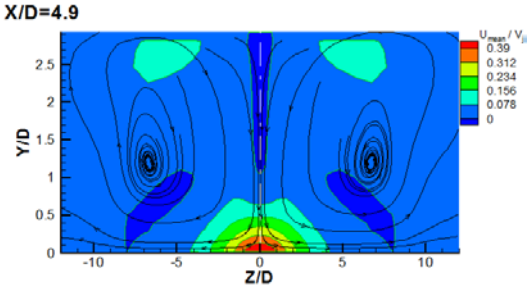

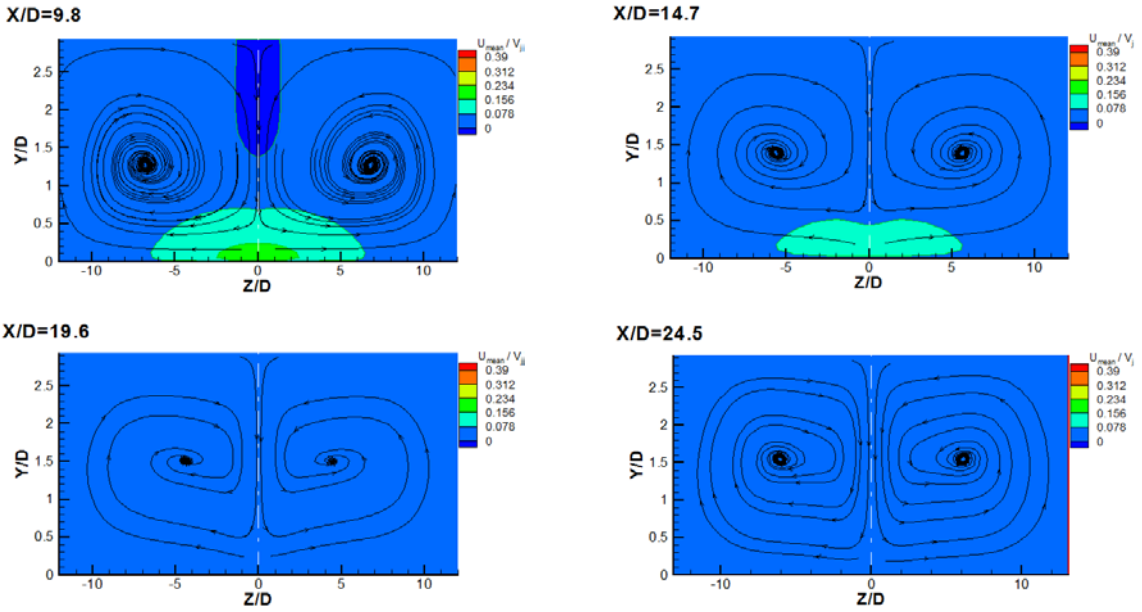

Figure 213: Mean velocity component (U_{mean}/V_j) in a vertical plane perpendicular to crossflow for Re_j=43,000, V_j/U_0= 33.7, H/D=3 and L/D=6.

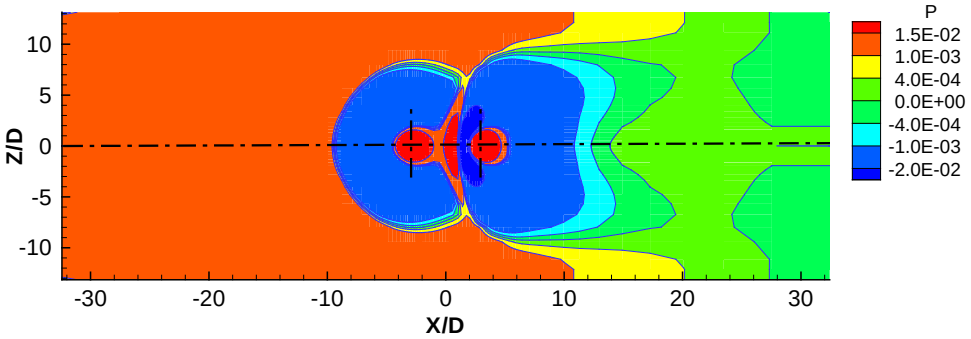

Figure 214: Pressure distribution along the field close to the ground (i.e. Y≈0) for V_j/U_0=33.7, H/D=3, and L/D=6 (values nondimensionalized by $1/2\rho V_{j1}^2$).

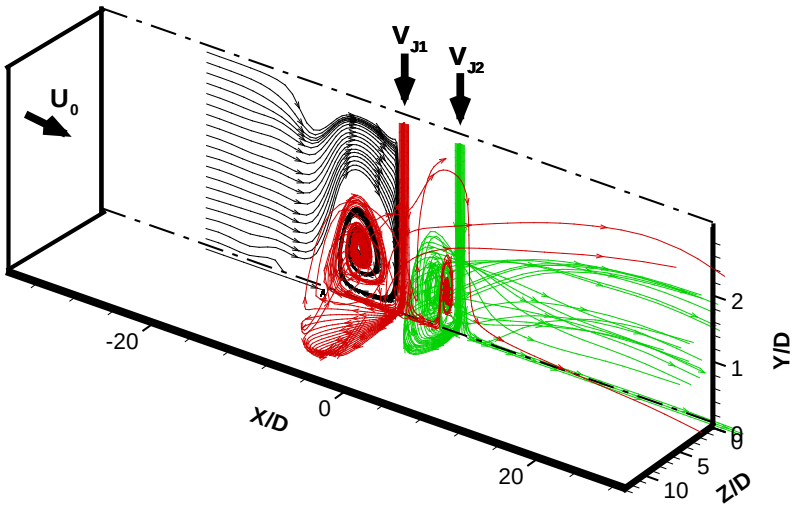

Figure 215: Tridimensional illustration of the jets flow for Re_j=43,000, V_j/U_0= 33.7, H/D=3 and L/D=6.

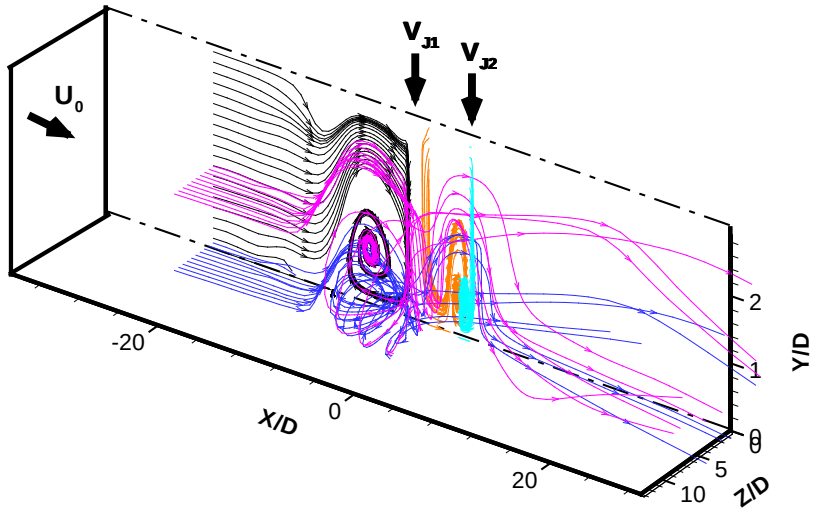

Figure 216: Tridimensional illustration of the jets and scarf vortex flow for Re_j=43,000, V_j/U_0=33.7, H/D=3 and L/D=6.

V_j/U_0=60

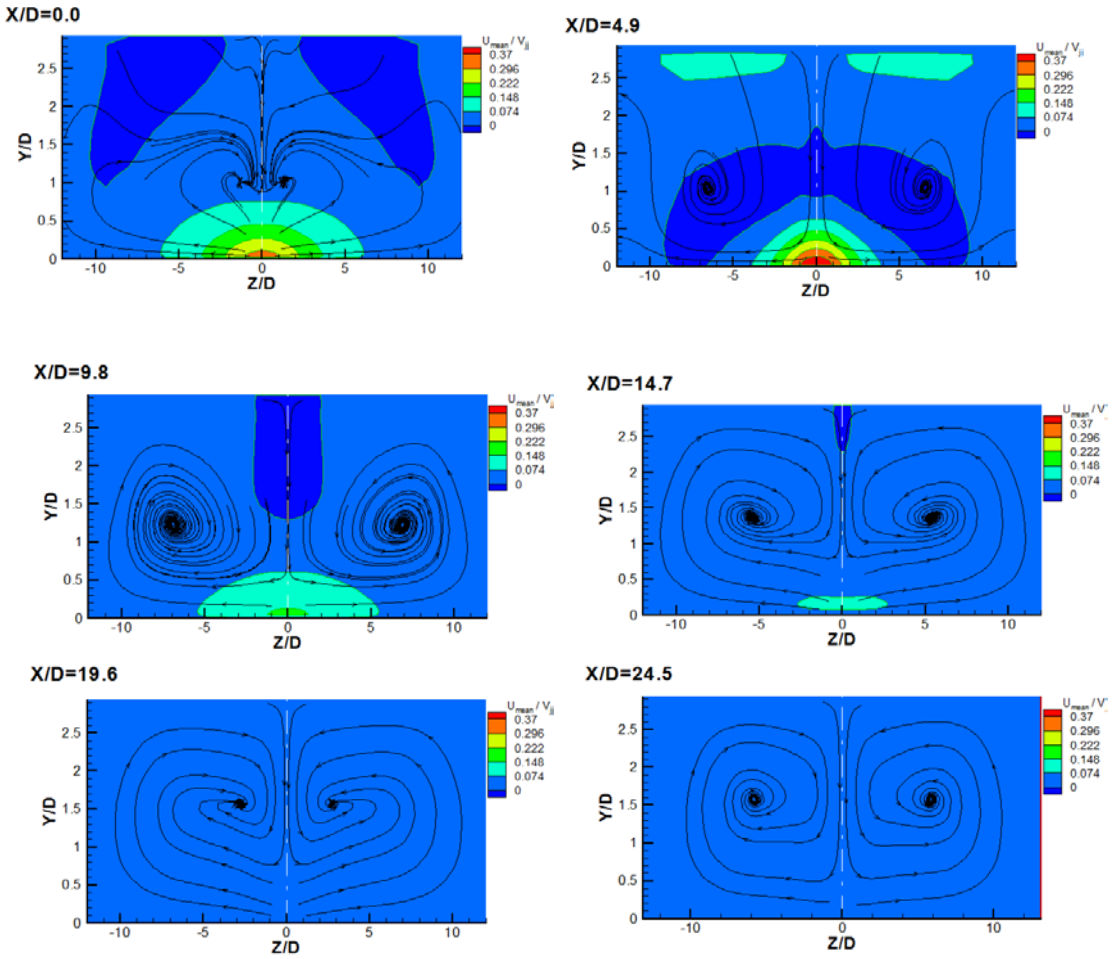

Figure 217: Mean velocity component (U_{mean}/V_j) in a vertical plane perpendicular to crossflow for Re_j=43,000, V_j/U_0= 60, H/D=3 and L/D=6.

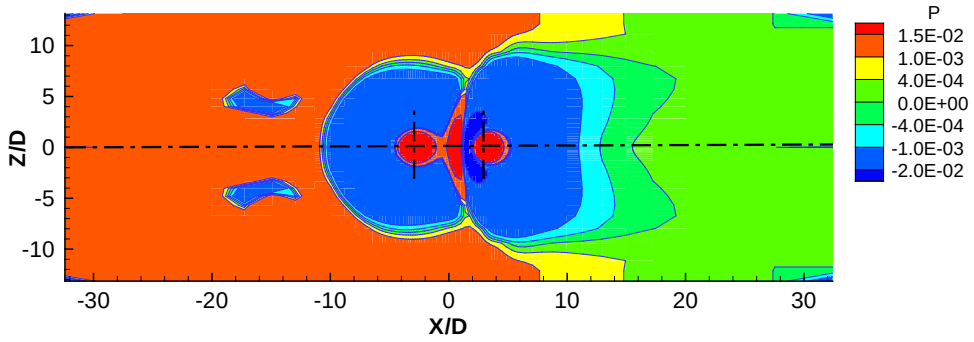

Figure 218: Pressure distribution along the field close to the ground (i.e. Y≈0) for V_j/U_0=60, H/D=3 and L/D=6.

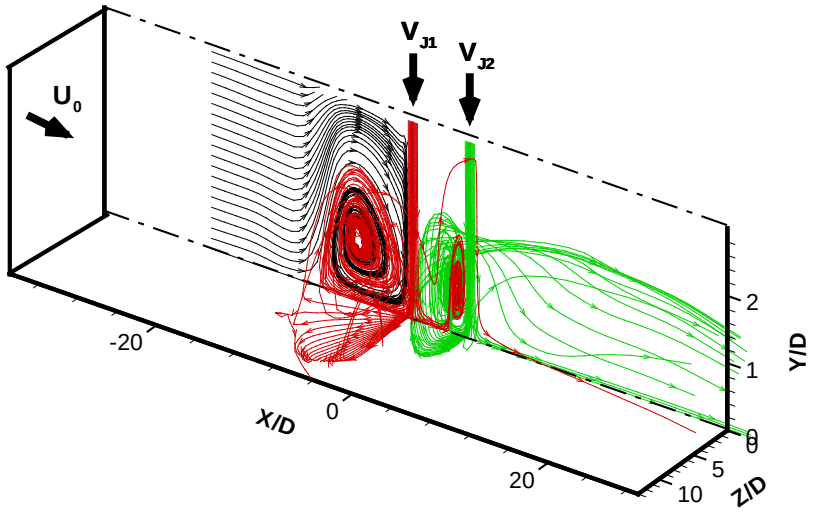

Figure 219: Tridimensional illustration of the jets flow for Re_j=43,000, V_j/U_0= 60, H/D=3 and L/D=6.

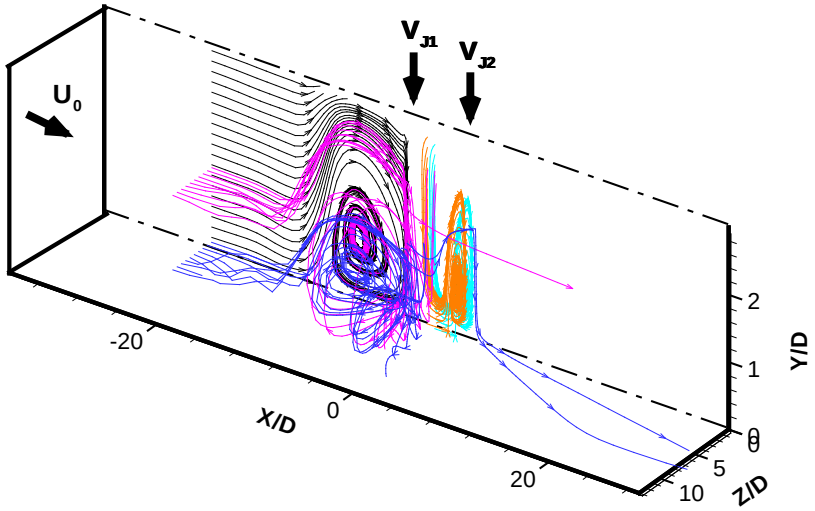

Figure 220: Tridimensional illustration of the jets and scarf vortex flow for Re_j=43,000, V_j/U_0=60, H/D=3 and L/D=6 (values nondimensionalized by $1/2\rho V_{j1}^2$).

5.3.2.3.2.5 Summary

Globally analysing all results obtained, it is possible to draw some important conclusions about the effect of the impingement height on the flowfield behaviour:

- With the decrease of the impingement height and the velocity ratio increase, the first jet deflection caused by the crossflow action is virtually annulled, even disappears for lower impingement heights. This is explained by the fact of the increase of the jet strength when it is close to the ground as the impingement height will be lower.
- Due to the lateral confinement the radial wall jets, the ground vortex becomes larger and may flow up over the wall jets.
- Only for one of the combinations of impingement height and velocity ratio (V_j/U_0=60 and H/D=3), the scarf vortex does not lose it shape, despite it feels the lateral confinement.
- For H/D≤10 is observed for all the velocity ratios considered the formation of a ground vortex in the region between the jets. The interaction of the lift jets with the ground results in the formation of a wall jet, that can be described as deflected flow turning into a high-speed flow parallel the ground plane, and can be classified into inner wall jet region (between the jets) and outer wall jet region (in the downstream and upstream direction). The collision of the resulting wall jets, normally, results in the formation of the fountain flow and a stagnation line between the two jets[121,122,123,124]. This it was part of our hypothesis when the study was started. However the results have shown much more complex flow patterns, and some have not yet been reported in the literature. When the first jet touches the ground, its inner wall jet rise up, but in the ascendant trajectory it is captured by the second jet inner wall jet. When the first jet inner wall jet interacts with the second jet inner wall jet acquires the clockwise direction of the second jet inner wall jet and a ground vortex type of flow is formed closed to the second jet. This result is a new discovery about the jets interaction behaviour.
- Analysing all the situations studied we can conclude that the crossflow does not really affects the second jet, i.e., the rear jet it is not so affected by the crossflow in terms of deflection, since it is protected by the upstream jet. Once again, it is possible to

[121] Barata J. M. M. (1993b). Fountain Flows Produced by Multijet Impingement on a Ground Plane. *Journal of Aircraft*. 30(1): 50-56.

[122] Barata, J.M.M. (1996b). Fountain Flows Produced by Multiple Impinging Jets in a Crossflow. *AIAA Journal.* 34(12): 2523-2530.

[123] Barata, J.M.M (2013). Multiple Jet/Wall/Cross-Wind Interaction Relevant to VSTOL Ground Effects. *Proceedings of the 2013 International Powered Lift Conference*, Los Angeles, California, August 12-14 2013. AIAA paper 2013-4380.

[124] Kate, R. P., Das, P., K. and Chakraborty, Suman, "An experimental investigation on the interaction of hydraulic jumps formed by two normal impinging circular liquid jets", J. Fluid Mech. (2007), vol. 590, pp. 355-380.

confirm that the downstream jet is entrained by the upstream jet and not by the crossflow itself.

5.4 Overview

This chapter analyses the numerical results that allow a clearer understanding of the flowfield under consideration in the present study. The numerical simulation was successfully made through the implementation of a numerical model that translates the present case study. Through this numerical analysis it was also possible to extend the results for velocity ratios and impingement heights beyond the limits of the experimental conditions enabling the better understanding of the flow.

The numerical results obtained in the first part of this study, allowed the observation of a new structure never reported in the literature and not observed in the experimental results. It was observed the flowfield behaviour for different velocity ratios beyond the limits of the experimental conditions, as well as, the confirmation of what the real role and contribution of the second jet in the flow. This information are very important, because improves the knowledge about this subject and allows a better understanding what happens on a VSTOL aircraft when operating in ground vicinity.

The identification of the kidney shape of the cross section in the first jet helped us to understand how the two impinging jets interact with each other and how they merge in a single flow in the downstream direction. This numerical analysis revealed that the principal role of the second jet is to reinforce the strength of the first jet by influencing the size and position of the ground vortex. This is due to how major is the second jet velocity, more strength is transmitted to the first jet. The improvement of the first jet strength is associated with enhanced flow into the vorticity structure, increasing the ground vortex size and the location of the centre of the ground vortex further upstream. If the second jet begins to lose its strength, traduced by the decrease of its velocity, the flow dragged to the inside of the ground vortex will be lower. In this case, the size of the ground vortex decreases and the location of the ground vortex centre moves to downstream.

In order to add even more knowledge and better understanding about this type of complex flow, the numerical study was extended to other impingement heights in order to observe the flow behaviour. In this second part of the numerical study, four different impingement heights are studied for several velocity ratios. Generally, the impingement jet height decrease, the crossflow effect in the first jet deflection disappears. This is explained by an increase of the jet strength when it is close to the ground since the impingement height will be lower. The ground vortex centre position is coming to upstream and the ground vortex increases (when compared with the impingement height used) with the velocity ratio escalation. Regarding the impingement height, it will decrease, as it is expected.

Taking into account studies referenced in the literature[125,126] it would be expected that with the impingement height decrease, the fountain upwash flow phenomenon would be observed in the flowfield results. However, in the region between the jets and for H/D≤10, it is observed the formation of a second ground vortex. This is the result of an interaction between the two inner walls jets, being the first inner wall jet captured by the second one, given rise to a clockwise recirculation close to the second jet. This event it is new and it has not yet been reported in the literature.

Regarding this part of study, once again is verified a conclusion already drawn about the second jet protection by the crossflow action from first jet, considering the second jet entrained by the upstream jet.

For some of the cases studied, the scarf vortex feels the lateral confinement of the computational domain, thus not representing completely a real VSTOL situation of operation. Lower impingement heights represent a real VSTOL operation situation, since the vortex scarf does not degenerate into a distorted vortical structure due to the lateral confinement.

The results presented in this chapter were partially published at Vieira *et al.* (2015)[127].

[125] Barata, J.M.M., Durão, D.F.G. (1989c). Numerical Study of Single and Multiple Impinging Jets through a Crossflow. Proceeding of the fifth International Symposium on Numerical Methods in Engineering, Vol. 2, Lausanne, Swiss, 11-15 September, 1989.

[126] Barata, J.M.M. (1989d) "Estudo Numérico e Experimental de Jactos Incidentes Sobre Placas Planas Através de um Escoamento Cruzado". PhD Thesis (in Portuguese). Universidade Técnica de Lisboa, Instituto Superior Técnico, 1989.

[127] Vieira D.F.C, Barata J.M.M, Neves F.M.S.P, Silva A.R.R. (2015). Numerical Simulation of Twin Impinging Jets in Tandem through a Crossflow. Journal of Engineering and Applied Sciences. 10(6): 123-136. ISSN: 1816-949X. DOI: 10.3923/jeasci.2015.123.136.

Chapter 6

Conclusions

This chapter presents the most important conclusions of this thesis, focusing their contribution to the study of the inline impinging jets on a flat plate through crossflow. More detailed information about this study and their conclusions were partially systematized on the final of each chapter.

6.1 Summary of the Thesis

On the first chapter it was presented a brief history about how the VSTOL aircraft idea was born, with some aircraft models that arose before the Lockheed Martin F-35 VSTOL aircraft. It was also presented the literature review of numerical and experimental studies of impinging jets on plates regarding several numbers of jets, jets configurations, jets nozzle types, with or without crossflow presence, several velocity ratios and impingement heights. Finally, the most relevant contributions obtained with earlier studies were presented and it was stated the real importance of this thesis since it is dedicated to a configuration that has not been considered so far in the published literature. Nevertheless, it is the most relevant for the simulation of the aerodynamics ground effects of the future VSTOL aircraft generation.

The second chapter presented the experimental method, describing the setup used to obtain the results. This chapter also describes briefly the Laser Doppler Anemometry principles to better understand of how the results were measured during the experimental study.

The third chapter presented the experimental results of two inline impinging jets on a flat plate through a low velocity confined crossflow for velocity ratios V_j/U_0, equals to 22.5, 33.7 and 43.8 and for an impingement height of 20.1D. The experimental analysis was made via direct photography and Laser Doppler Anemometry in order to visualize the flow and to obtain mean and turbulent velocities of the entire flowfield.

On the fourth chapter it was presented the computational method employed on the flowfield simulation of the experimental study done earlier.

It was explained how it was obtained the solution of the discretized algebraic equation system and how to obtain a higher numeric accuracy solution, through the mesh generation and numeric schemes used to the discretization of the convective terms on the transport equations. Three numerical schemes were analysed, and the QUICK scheme proved to be more accurate than the others, allowing to obtain the solution independently of the grid

dimension and minimized the false diffusion errors. Also, it was presented different boundary conditions used to reproduce integrally the experimental situation.

In the fifth chapter it was presented the numerical results and a comparison was made regarding the experimental results. Through the first part of the numerical simulation, it was possible to extend the results of this case study beyond the limits of the experimental conditions. For the same experimental velocity ratios, the numerical study corroborates the experimental results.

6.2 Discussion

6.2.1 Contribution of this Thesis

The present thesis is dedicated to the analysis of the complex flowfield of two in-line turbulent circular air jets with a low velocity crossflow impinging on a flat surface perpendicular to the geometrical jet nozzle axis. The flow configuration and the selected cases are relevant to the flow around the next generation F-35 VSTOL aircraft when operating in ground vicinity. The jets exit conditions are changed along the study to provide a better understanding of the flowfields. To complete this analysis and in order to validate the experimental results a detailed numerical study is also presented, where all the features of the experimental flow are maintained.

The numerical results extend the experimental study, revealing that the deflection of the rear jet is due to the competing influences of the wake, the shear layer, the downstream wall jet of the first jet and the crossflow. The first jet deflection and the location of the ground vortex depend on the velocity ratio between the jet exit and the crossflow as well as the impingement height used. Through the rear jet velocity change, it is possible to verify the quick deflection of the second jet, never reaching the ground directly, i.e., the downstream jet is entrained by the upstream jet and not by the crossflow itself. Through the impingement height change, it is possible to observe the absence of upwash fountain formation in the region between the impingement jets, as it was expected. In this region, it is unexpectedly observed the formation of a second ground vortex, something not yet reported in the literature.

For all the velocity ratios studied, it was shown a large penetration of the first jet, which was deflected by the crossflow. The interaction of the wall jet localized upstream of the stagnation point with the crossflow generates a recirculation zone (ground vortex) that wraps around the impinging zone like a scarf. Its centre moves closer to the first jet with the velocity ratio decrease. The rear jet seemed not so affected by the crossflow in terms of deflection for all velocity ratios because it is protected by the upstream jet. However, due to

the downstream wall jet that flows radially from the impinging point, the rear jet does not reach the ground. As consequence, no upstream wall jet or ground vortex resulting from the second (downstream) jet was detected.

From the horizontal profiles it was concluded that the jet inclination due to the crossflow action was attenuated by the velocity ratio increase. The horizontal profiles of the mean horizontal and vertical turbulent velocity, made possible quantify the turbulent diffusion process and revealed that the shear layer that is surrounding each impinging jet is a region characterized by higher velocity fluctuations. This corresponds to the higher mean velocity gradients.

The presence of the fountain upwash flow, resulting from the wall jets collision of the impinging jet flow, was not detected for any the velocity ratios studied.

The numerical work was very important because it allowed the observation of a kidney shape in the cross section of the first jet. Additionally, it was detected that the kidney shape of the cross section of the first jet was the responsible for capturing and trying to swallow the second (downstream) jet in tandem which remains almost circular. This complex phenomenon is a new one that was never reported in the literature or observed during the experimental work. Additionally, it could be understood that the real role and contribution of the second jet is to reinforce the first jet by influencing the size and location of centre of the ground vortex. Changing the rear jet (second jet) velocity, it was possible to prove that the second jet is quickly deflected, and never reaching the ground. Thus proving the accuracy of the experimental results, leading us to conclude that when the impinging jets are positioned in tandem configuration, the downstream jet is entrained by the upstream jet (first jet) and not by the crossflow itself.

The second part of the numerical study was dedicated to the jet height effect and showed a formation of a ground vortex in the region between the impingement jets. A fact that was never been reported in the literature and it is surprising at the first sight, since it was expected to be found an upwash fountain flow when the impingement jet decreases. The lateral confinement of the computational domain proved to be a problem on the simulation of a real VSTOL aircraft operation. This is due to when the scarf vortex contacts with the lateral confinement losses its shape, degenerating in a vortical structure flowing to downstream with the remaining flow.

Once again the protection of the rear jet by the first jet it is proved. The crossflow only interacts with the first jet. Indirectly, we can say that interacts with the second jet when the crossflow action causes the first jet deflection and the impingement point of the first jet is located to further downstream. The wall jet flows radially from the impingement point not allowing the rear jet to reach the ground. In this part of the study the second jet always

reached the ground, and for H/D<10 the first practically does not suffer deflection caused by the crossflow interaction.

6.2.2 Limitations of the Current Work

The main limitation of the present work is due to the fact that the F-35 aerodynamic configuration (initially JSF/ Variant B) has been changing during the beginning of the contest. So, most of the case studies were selected using the knowledge and experience related with similar issues of the previous VSTOL aircraft (Harrier – AV/8B) as well as the information obtained from some of the participants in the project that we could contact within the scope of the AIAA (American Institute of Aeronautics and Astronautics).

As already demonstrated before, most of the characteristics of impinging jets in ground effect through a crossflow are particularly dependent on the jet-to-crossflow velocity (V_j/U_0) and impinging distance to diameter of the jet (H/D) ratios.

The compressibility effects that may occur with the rear jet affect essentially the impinging jet, but the remaining of the flow (after the impact on the ground) is similar to those for the case of incompressible and isothermal conditions.

6.3 Future Work

On this thesis was been studied the flow of turbulent impingement jets on a flat surface with the presence of a low velocity crossflow. This generated a ground vortex and a complex structure resulting from the interaction between the first (kidney shape) and second (circular) jets. The present work revealed an extremely complex flow with strong induced additional secondary phenomena not reported before demanding further investigation. Some suggestions can be made for the continuation of the investigation of this type of flowfields.

From the experimental point of view it is recommend the following objectives:

- Measurements with laser anemometry regarding the horizontal and vertical velocity field on the plane of symmetry for lower impingement heights applied in this study. With special attention to the near impingement flat surface, in order to understand what will be the real consequence for the aircraft when this type of phenomenon occurs.
- Measurements with laser anemometry of the horizontal and vertical velocity field in parallel planes to the symmetry plane for the same impingement height used.
- Measurements with laser anemometry of the horizontal and vertical velocity field in parallel planes to the symmetry plane for lower impingement heights that the ones used for this study.

- Obtaining experimental measurements taking into account the objectives previously mentioned for impingement jets with different diameters.
- To do the all the experimental work but without lateral confinement.
- To the numerical work it is recommended to reproduce computationally all the suggestions done to the experimental work, in order to evaluate experimental results.

Bibliography

Abbott, W. A., White, D. R. (1989). The effect of nozzle pressure ratio on the fountain formed between two impinging jets. Royal Aerospace Establishment Technical Memorandum, P1166.

Abdel-Fattah A. (2007). Numerical and Experimental study of turbulent impinging twin-jet flow. *Experimental Thermal and Fluid Science*. **31(8)**: 1061-1072.

Adler D., Baron A. (1979). Prediction of a Three-Dimensional Circular Turbulent Jet in Crossflow. *AIAA Journal*. **17(2)**: 168-174.

Aldabbagh L. B. Y., Sezai I. (2002). Numerical simulation of three dimensional laminar multiple impinging square jets. *International Journal of Heat and Fluid Flow*. **23(4)**: 509-518.

Aldabbagh L. B. Y., Sezai I. (2002). Numerical simulation of three-dimensional laminar, square twin-jet on a flat plate, flow structure, and heat transfer. *Numerical Heat Transfer, Part A*. **41**: 835-850.

Aldabbagh L. B. Y., Mohamad A. A. (2007). Effect of jet-to-jet plate spacing in laminar array jets impinging. *Heat and Mass Transfer*. **43(3)**: 265-273.

Alvi F. S., Ladd J. A., Bower W. W. (2002). Experimental and Computational Investigation of Supersonic Impinging jets. *AIAA Journal*. **40(4)**: 599-609.

Andreopoulos J. (1983). Heat Transfer Measurements in a Heated jet Issuing into a Cross-Flow. *Physics of Fluids*. **26:**3201-3210.

Andreopoulos, J., Rodi, W. (1984). Experimental Investigation of Jets in a Crossflow. *Journal of Fluid Mechanics*. **138**: 93-127.

Baker O.J. (1980). The Turbulent Horseshoe Vortex. *Journal of Wind Engineering and Industrial Aerodynamics*. **6 (1-2)**: 9-23.

Barata, J.M.M., Durão, D.F.G., Heitor, M.V. e McGuirk, J.J. (1986a). Experimental and Numerical Study on the Aerodynamics of Jets in Ground Effect. Proceedings of the Tenth Symposium on Turbulence, Univ. Rolla-Missouri, EUA, 22-24 September, 1986.

Barata, J.M.M, Durão, D.F.G, Firmino, F.J.C. (1986b). An Investigation on Impinging Jets. Proceedings of Third International Symposium on Applications of Laser Anemometry to Fluid Mechanics, 7-9 July, 1986.

Barata, J.M.M., Durão, D.F.G., Heitor, M.V. e McGuirk, J.J. (1987). The Turbulence Characteristics of a Single Impinging Jet through a Crossflow. Proceedings of 6th Symposium on Turbulent Shear Flows, Toulouse, 7-9 September, 1987.

Barata, J.M.M., Durão, D.F.G., e Heitor, M.V. (1988a). Laser-Doppler Measurements of Multiple Impinging Jets through a Crossflow. Proceedings of 4th International Symposium on Applications of Laser Anemometry to Fluid Mechanics, Lisbon, 11-14 July, 1988.

Barata, J.M.M., Durão, D.F.G., Heitor, M.V. e McGuirk, J.J. (1988b). On the Validation of 3-D Numerical Simulations of Turbulent Impinging Jets through a Crossflow. Proceedings of AGARD Symposium on the Validation of Computational Fluid Dynamics, Lisbon, 2-5 May. AGARD CP 437, 1988, pp. 35.1-35.10.

Barata, J.M.M., Durão, D.F.G., e Heitor, M.V. (1988c). Laser-Doppler Measurements of Impinging Jets. Laser Tech. in Industry, Porto, 6-8 June, 1988. Published in SPIE vol.952, "Laser Technologies in Industry", 1988, pp.435-444, ed. O.D. Soares et all, SPIE.

Barata, J.M.M., Durão, D.F.G., e Heitor, M.V. (1989a). On the Velocity Characteristics of Impinging Jets through a Crossflow. Proceedings of 10th Brazilian Congress of Mechanical Engineering, Rio de Janeiro, Brazil, 4-8 December 1989.

Barata J. M. M., Durão D. F. G., McGuirk J. J. (1989b). Numerical Study of Single Impinging Jet through a Crossflow. *Journal of Aircraft*. **26(1)**: 1002-1008.

Barata, J.M.M., Durão, D.F.G. (1989c). Numerical Study of Single and Multiple Impinging Jets through a Crossflow. Proceeding of the fifth International Symposium on Numerical Methods in Engineering, Vol. 2, Lausanne, Swiss, 11-15 September, 1989.

Barata, J.M.M. (1989d) "Estudo Numérico e Experimental de Jactos Incidentes Sobre Placas Planas Através de um Escoamento Cruzado". PhD Thesis (in Portuguese). Universidade Técnica de Lisboa, Instituto Superior Técnico, 1989.

Barata J. M. M., Durão D. F. G., Heitor M. V. (1991a). Turbulent Energy Budgets in Impinging Zones. Proceedings of Eight Symposium on Turbulent Shear Flows, Munich, Germany, 9-11 September, 1991.

Barata J. M. M., Durão D. F. G., Heitor M. V., McGuirk J. J. (1991b). Impingement of Single and Twin Turbulent Jets through a Crossflow. *AIAA Journal*. **29(4)**: 595-602.

Barata, J.M.M., Durão, D.F.G., Heitor, M.V. (1992a). Velocity Characteristics of Multiple Impinging Jets through a Crossflow. Journal of Fluids Engineering. **114**: 231-239.

Barata, J.M.M., Durão, D.F.G., Heitor, M.V. e McGuirk, J.J. (1992b). The Turbulence Characteristics of a Single Impinging Jet through a Crossflow. Experimental Thermal and Fluid Science. **5**: 487-498.

Barata J. M. M., Durão D. F. G., Heitor M. V., McGuirk J. J. (1993a). On the analysis of an impinging jet on ground effects. *Experiments in Fluids*. **15**: 117-129.

Barata J. M. M. (1993b). Fountain Flows Produced by Multijet Impingement on a Ground Plane. *Journal of Aircraft*. **30(1)**: 50-56.

Barata, J.M.M. (1996a). Ground Vortex Formation with Twin Impinging Jets. *Proceedings of the International Powered Lift Conference*, Jupiter, Florida, 18-20 Nov., 1996. Paper SAE 962257.

Barata, J.M.M. (1996b). Fountain Flows Produced by Multiple Impinging Jets in a Crossflow. *AIAA Journal.* **34(12)**: 2523-2530.

Barata J. M. M. (1998). Jets in Ground Effect with a Crossflow. *AIAA Journal*. **36(9)**: 1737-40.

Barata J. M. M., Durão D. F. G. (2004). Laser-Doppler Measurements of Impinging Jet Flows through a Crossflow. *Experiments in Fluids*, **36**: 665-674.

Barata J. M. M., Castro P., Silvestre M. A., Durão D. F. G. (2005a). The Turbulent Characteristics of a Ground Vortex Flow. *Proceedings of the 43rd AIAA Aerospace Sciences Meeting & Exhibit*, Reno, Nevada, 10-13 January 2005. AIAA 2005-0064.

Barata J. M. M., Durão D. F. G. (2005b). Laser Doppler Measurements of a Highly Curved Flow. *AIAA Journal*. **43(12)**: 2652-2655.

Barata J. M. M., Ribeiro S. D. G., Santos P. J. C. T., Silva A. R. R. (2009a). Experimental Study of the Collision Zone of a Boundary Layer with a Wall Jet. *Proceedings of the 47th AIAA Aerospace Science Meeting Including the New Horizons Forum and Aerospace Exposition*, Orlando, Florida, 5-8 January 2009.

Barata J. M. M., Ribeiro S. D. G., Santos P. J. C. T., Silva A. R. R. (2009b). Experimental Study of a Ground Vortex. *Journal of Aircraft*. **46(4)**: 1152-1159.

Silva, A.R.R., Durão, D.F.G., Barata, J.M.M., Santos, P.J.C.T., Ribeiro, S.D.G. (2009). Laser-Doppler Analysis of the Separation Zone of a Ground Vortex. *International Review of Aerospace Engineering*. **2(3)**: 167-174.

Barata J. M. M., Durão S. D. G., Santos P. J. C. T., Silva A. R. R (2010). Turbulent Energy Budgets of a Ground Vortex Flow. *Proceedings of the 15th International Symposium on Applications of Laser Techniques to Fluid Mechanics*, Lisbon, Portugal, 05-08 July 2010.

Barata, J.M.M (2013). Multiple Jet/Wall/Cross-Wind Interaction Relevant to VSTOL Ground Effects. *Proceedings of the 2013 International Powered Lift Conference*, Los Angeles, California, August 12-14 2013. AIAA paper 2013-4380.

Barata J. M. M., Neves F. M., S. P., Vieira D. F. C., Silva A. R. R. (2014a). Experimental Study of Two Impinging Jets Aligned With a Crossflow. *Journal of Modern Physics*. **5(16)**: 1779-1788.

Barata J. M. M.,Carvalho P. S. D., Neves F. M., S. P., Vieira D. F. C., Silva A. R. R. (2014b). Laser Doppler Measurements of Twin Impinging Jets Aligned with a Crossflow. *Journal of Physical Science and Application*. **4(7)**: 403-411.

Baydar E. (1999). Confined impinging air jet at low Reynolds number. *Experimental Thermal ad Fluid Science.* **19**: 27-33.

Baydar E., Ozmen Y (2005). An Experimental and Numerical Investigation on a Confined Impinging Air Jet at High Reynolds Numbers. *Applied Thermal Engineering*. **25(2-3)**: 409-421.

Behrouzi P., McGuirk J. J. (1998). Experimental data for CFD validation of the intake ingestion process in STOVL aircraft. *Flow Turbulence and Combustion*. **64(3-4)**: 265-277.

Behrouzi P., McGuirk J. J. (1999). Computational fluid dynamics prediction of intake ingestion relevant to short take-off and vertical landing aircraft. *Proceeding of the Institution of Mechanical Engineers, Part G: Journal of Aerospace Engineering*. **213(3)**: 131-142.

Behrouzi P., McGuirk J. J. (2000). Experimental Data for CFD Validation of the Intake Ingestion Process in STOVL Aircraft. *Flow, Turbulence and Combustion*. **64**: 233-251.

Behrouzi P. (2000). Numerical Studies of Twin-Jet Impingement for STOVL Flow Application. *Journal of the Chinese Institute of Engineers*. **23(6)**: 669-676.

Bevilacqua P., Margason R., Gaharan C. (2007). A Jet Entrainment Theory for VTOL Aircraft Suckdown. *Proceedings of the 45th AIAA Aerospace Science Meeting and Exhibit*, Reno, Nevada 8-11 Jan. 2007. Paper AIAA-2007-1397.

Bradshaw, P., Love, E. M. (1959). The normal impingement of a circular air jet over a flat surface. *ARC R&M 3205*.

Bray D., Knowles K. (1992). A Review of Impinging Jets in Crossflow – Experimentation and Computation. Proceedings of the 30th Aerospace Sciences Meeting & Exhibit, Reno, NV, 6-9January 1992. Paper AIAA 92-0633.

Brizzi L. –E., Bernard A., Bousgarbiès J. –L., Dorignac E., Vullierme J. –J. (2000). Study of Several *Impinging Jets. Journal of Thermal Science*. **9(3)**: 217-

Caliskan S., Baskaya S. (2012). Velocity field and turbulence effects on heat transfer characteristics from surfaces with V-shaped ribs. International *Journal of Heat and Mass Transfer*. **55**: 6260-6277.

Calvo Garcia J., Santolaya J. L., Garcia I., Aisa L. (2012). A framework about flow measurements by LDA – PDA as a spatio-temporal average: application to data post-processing. *Measurement Science and Technology*. **23(5):** 055202.

Camussi R., Guj G., Stella A. (2002). Experimental Study of a jet in crossflow at very low Reynolds number. *Journal of Fluids Mechanical*. **454**: 113-144.

Carcasci C. (1999). An experimental investigation on air impinging jets using visualization methods. *International Journal of Thermal Science*. **38**: 808-818

Chiriac V. A., Ortega A. (2002). A numerical study of the unsteady flow and heat transferi in a transitional confined slot jet impinging on an isothermal surface. *International Journal of Heat and Mass Tranfer*. **45(6)**: 1237-1248.

Chuang S. -H., Nieh T. –J. (2000). Numerical simulations and analysis of three-dimensional turbulent impinging square twin jet flow field with no-crossflow. *International Journal for Numerical Methods in Fluids*. **33**: 475-498.

Crabb, D., Durão, D.F.G., and Whitelaw, J.H. (1981). A Round Jet Normal to a Crossflow. *Journal of Fluids Engineering*. **113:** 142-153.

Dano B. P. E., Liburdy J. A., Kanokjaruvijit K. (2005). Flow Characteristics and Heat Transfer Performances of a Semi – Confined Impinging Array of Jets: Effect of Nozzle geometry. *International Journal of Heat and Mass Transfer*. **48**: 691-701.

Dano B. P. E., Liburdy J. A. (2007). Structure detection and analysis of non-circular impinging jets in a semi-confined array configuration. *Experimental Thermal and Fluid Science*. **31**: 991-1003.

Dantec dynamics (2011). *Flowlite LDA systems*. Accessed in January 2011, in: http://faculty.ksu.edu.sa/azzeer/Documents/534%20PHYS/LN7_LDA_s.pdf.

Dennis R. F., Margason R. J. (1993). Induced Surface Pressure Distribution of a Subsonic Jet in a Crossflow. *Proceedings of the 1993 International Powered Lift Conference*, Santa Clara, CA, USA, 1-3 December 1993. AIAA 93-4861.

Dimotakis P. E. (1976). Single scattering particle laser Doppler measurements of turbulence. *Proceedings of the AGARD Conference – Applications of non-intrusive instrumentation in Fluid Flow Research*. **193**.

Duran Group (2013). Product Solutions: Laboratory glass bottles & accessories. Accessed in 24 May 2013, in: http://www.duran-group.com/en/products-solutions/laboratory-glassware.html.

Durão D. F. G., Laker J., Whitelaw J. H. (1980). Bias effect in laser Doppler anemometry. *Journal of Physics E: Scientific Instruments*. **13**: 442-445.

Durst F., Melling A., Whitelaw J.H. (1976). *Principles and Practice of Laser-Doppler Anemometry*. 2nd edition, New York, Academic Press.

El-Gabry L. A., Kaminski D. (2005). Numerical investigation of jet impingement with cross flow – Comparison of yang-shih and standard k-ε Turbulence Models. *Numerical Heat Transfer, Part A*. **47**: 441-469.

Failla G., Bishop E. H., Liburdy J. A. (1999). Enhanced jet impingement heat transfer with crossflow at low Reynolds numbers. *Journal of Electronics Manufacturing*. **9(2)**: 167-178.

Fan J., Zhang Y., Wang D. (2006). Large-scale vortical structures produced by an impinging density jet in shallow crossflow. Applied Mathematics and Mechanics. **27(3)**: 369-369.

Fan J., Zhang Y., Wang D. (2007). Large Eddy simulation of three dimensional vortical structures for an impinging transverse jet in the near region. *Journal of Hydrodynamics*. **19(3)**:314-321.

Fan J., Zhang Y., Wang D. (2009). Experimental Study on the vortex formation and entrainment characteristics for a round transverse jet in shallow water. *Journal of Hydrodynamics*, **21(3)**:386-393.

Fernandes R. L. J., Sobiesiak A., Pollard A. (1996). Opposed Round Jets Issuing Into a Small Aspect Ratio Channel Crossflow. *Experimental Thermal and Fluid Science*. **13**: 374-394.

Fernández J.A., Elicer-Cortés J.C., Valencia A., Pavageau M., Gupta S. (2007). Comparison of low-cost two-equation turbulence models for prediction flow dynamics in twin-jets devices. *International Communications in Heat and Mass Transfer*. **34(5)**: 570-578.

Fitzgerald J. A., Garimella S. V. (1998). A study of the flow field of a confined and submerged impinging jet. *International Journal of Heat Mass Transfer*. **41(8-9)**: 1025-1034.

Fleischer A. S., Kramer K., Goldstein R. J. (2001). Dynamics of vortex structure of a jet impinging on a convex surface. *Experimental Thermal and Fluid Science*. **24**: 169-175.

Geers L. F. G., Tummers M. J., Hanjalic K. (2004). Experimental Investigation of Impinging Jet Arrays. *Experiments in Fluid*. **36**: 946-958.

Gopi K., Kamran M. (2010). An experimental study of a radial wall jet formed by the normal impingement of a round synthetic jet. *European Journal of Mechanics B/Fluids*. **29(4)**: 269-277.

Guillard, F., Fritzon, R., Revstedt, J., Trägårdh, C., Aldén, M., Fuchset, L. (1998) Mixing in a confined turbulent impinging jet using planar laser-induced fluorescence. *Experiments in Fluids*. **25(2)**: 143-150.

Guoneng L., Zheng Y., Hu G., Zhang Z. (2014). Convective Heat Transfer Enhancement of a Rectangular Flat Plate by an Impinging Jet in Cross Flow. *Chinese Journal of Chemical Engineering*. **22(5)**:489–495.

Gutmark E. J., Ibrahim I. M., Murugappan S. (2008). Circular and noncircular subsonic jets in cross flow. *Physics of Fluids*. **20**: 075-110

Hassan M., Assoum H. H., Sabolik V., Vétel J., Abed-Mearim K., Garon A., Sakout A. (2012). Experimental investigation of the wall shear stress and the vortex dynamics in a circular impinging jet. *Experiments of Fluids*. **52**: 1475-1489.

Ince N. Z., Leschziner M. A. (1990). Second-moment modelling of 3D turbulent jets in cross-flow with and without impingement. *Engineering Turbulence Modelling and Measurements*. 143-155

Jenkins R.C., Hill Jr. W. G. (1977). Investigation of VTOL Upwash Flows Formed by Two Impinging Jets. *Grumman Research Dept. Rept. RE-548, Bethpage*, New York, November 1977.

Jones W. P., Launder B. E. (1972). The prediction of Laminarization with a Two-Equations Model of Turbulence. *International Journal of Heat and Mass Transfer*. **15(2)**: 301-314.

Kamotani Y., Greber I. (1974). Experiments on Confined Turbulent Jets in a Crossflow. *NASA CR-2392*.

Kanoklaruvijit K., Martinez-Botas R. F. (2005). Jet impingement on a dimpled surface with different crossflow schemes. *International Journal of Heat and Mass Transfer*. **48**: 161-170.

Kate R. P., Das P. K., Chakraborty S. (2007). An experimental investigation on the interaction of hydraulic jumps formed by two normal impinging circular liquid jets. *Journal of Fluid Mechanical*. **590**: 355-380.

Kelman J. B., Greenhalgh D. A., Whiteman M. (2006). Micro-jets in confined turbulent crossflow. *Experimental Thermal and Fluid Science*. **30**: 297-305.

Knowles K., Bray D., Bailey P. J., Curtis P. (1992). Impinging jets in crossflow. *Aeronautical Journal*. **96(952)**: 47-56.

Knowles K., Bray D. (1993). The Ground Vortex Formed by Impinging Jets in Crossflow. *Journal of Aircraft*. 30(6): 872-878.

Knowles K., Myszko M. (1994). Development of a wall jet from an impinging, round turbulent, compressible jet. *Proceedings of the 25th AIAA Fluid Dynamics Conference*, Colorado Springs, CO, USA, 20-23 June 1994. AIAA 94-2327.

Knowles K., Saddington A. J. (1996). Mutual Interference between Jets and Intakes in STOVL Aircraft. *Proccedings of the RAeS/IMechE Engine-Airframe Integration Conference*, Bristol, UK, October 1996.

Knowles, K. (1996). Computational Studies of impinging jets using k-ε Turbulence Models. *International Journal for Numerical Methods in Fluids*. **22**: 799-810.

Knowles K., Kirkman L. (1998). Inverted-profile coaxial jet flows relevant to ASTOVL applications. *The Aeronautical Journal*. **102 (1017)**: 377-384.

Knowles K., Davies T.W. (1999). Studies of Turbulent Jets Impinging on Moving Surfaces. *Proceedings of the 4th International Symposium on Engineering Turbulence Modelling and Measurements*, Ajaccio, Corsica, France, 24–26 May 1999. 783–792.

Kolar V., Takao H., Todoroki T., Savory E., Okamoto S., Toy N. (2003). Vorticity transport within twin jets in crossflow. Experimental Thermal and Fluid Science. **27**: 563-571.

Kolar V., Savory E. (2007). Dominant flow features of twin jets and plumes in crossflow. *Journal of Wind Engineering and Industrial Aerodynamics*. **95**: 1199-1215.

Koseoglu M. F., Baskaya S. (2009). Experimental and numerical investigation of natural convection effects on confined impinging jet heat transfer. *International Journal of Heat and Mass Transfer*. **52(5-6)**: 1326-1336.

Kotansky D.R. (1981). The Modelling and Prediction of Multiple VTOL Aircraft Flow Fields in Ground Effect. *AGARD CP-308*, Paper 16.

Kuhlman J. M., Cavage W. M. (1994). Jet Ground Formation by Annular Jets. *Journal of Aircraft*. **31(4)**: 794-801.

Kuhn R. E, Margason R. J, Curtis P. (2006). *Jet-induced Effects: The Aerodynamics of Jet- and Fan-powered V/STOL Aircraft in Hover and Transition.* Volume 217. Frank K. Lu, Editor-in-chief. Published by the American Institute of Aeronautics, Inc. 1801 Alexander Bell Drive, Reston, Virginia 20191-4344.

Lakhamraju R. R., Murugappan S., Coppess S., Gutmark E. (2007). Characteristics of Variable Density Jets in Cross Flow. *Proceedings of the 45th AIAA Aerospace Sciences Meeting and Exhibit*, Reno, Nevada. 08 - 11 January 2007.

Landreth C.C., Adrian R. J. (1990). Impingement of a low Reynolds number turbulent circular jet onto a flat plate at normal incidence. Experiments in Fluids. **9**: 74-84.

Langer D. C., Fleck B. A., Wilson D. J. (2010). Trajectory Measurements of a Wall Jet Impinging Onto a Forward Facing Step Entering a Cross-Flow. *Journal of Hazardous Materials*. **176**: 199-206.

Lawson N. J., Eyles J. M., Knowles K. (2002). A Study Using PIV and LDA of a Compressible STOVL Ground Vortex Flow. *Proceedings of the 2002 Biennial International Powered Lift Conference and Exhibit*, Williamsburg, Virginia, USA. 5-7 November 2002.

Lawson N. J., Eyles J. M., Knowles K. (2004). An Unsteady and Time-Averaged Study of a Ground Vortex Flow. *Proceedings of the 24th International Congress of the Aeronautical Sciences*, Yokohama, Japan, 29 August - 3 September 2004.

Lee D. H., Chung Y. S., Kim D. S. (1997). Turbulent flow and heat transfer measurements on a curved surface with a fully developed round impinging jet. *International Journal of Heat and Fluid Flow*. **18**: 160-167.

Leonard, B. P. (1979). A Stable and Accurate Convective Modeling Procedure Based on Quadratic Upstream Interpolation. *Computer Methods in Applied Mechanics and Engineering*. **19(1):**59-98.

Leschziner M. A., Ince N. Z. (1995). Computational Modeling of Three-Dimensional Impinging Jets with and without Cross-Flow Using Second-Moment Closure. *Computers & Fluids*. **24**: 811-832.

Q Li, Page G J Mcguirk J J (2007). Large-eddy simulation of twin impinging jets in cross-flow. *The Aeronautical Journal*. 195-206. Paper no. 3097.

Li G., Zheng Y., Hu G., Zhang Z. (2014). Convective Heat Transfer Enhancement of a Rectangular Flat Plate by an Impinging Jet in Cross Flow. *Chinese Journal of Chemical Engineering*. **22(5)**: 489-495.

Mehyryar R., Giovannini A. (2014). Twisted symmetry in multiple impingement jets at low Reynolds number. *International Journal of Thermal Science*. **77**: 27-37.

Meireles M. S. P. (2008/2009). *Experimental Study of twin air impinging jets*. Master Thesis on Aeronautical engineering. University of Beira Interior, Covilhã.

Melling A., Whitelaw J.H. (1975). Turbulent Flow in a Rectangular Duct. *Journal of Fluid Mechanics*. **78**: 285-315.

Miao J.-M., Wu C.-Y., Chen P.-H. (2009). Numerical Investigation of Confined Multiple-Jet Impingement Cooling Over a Flat Plate at Different Crossflow Orientations. *Numerical Heat Transfer, Part A: Applications*. **55(11)**: 1019-1050.

Nakabe K., Inaoka K., Al T., Suzuki K. (1997). Flow Visualization of Longitudinal Vortices Induced by an Inclined Impinging Jet in a Crossflow – Effective Cooling of High Temperature Gas Turbine Blades. *Energy Conversion and Management - Elsevier*, **38 (10-13)**: 1145-1153.

Nakabe K., Suzuki K., Inaoka K., Higashio A., Acton J. S., Chen W. (1998). Generation of longitudinal vortices in internal flows with an inclined impinging jet and enhancement of target plate heat transfer. International Journal of Heat and Fluid Flow. **19**: 573-581.

Nakabe K., Fornalik E., Eschenbacher J. F., Yamamoto Y., Ohta T., Suzuki K. (2001). Interactions of longitudinal vortices generated by twin inclined jets and enhancement of impingement heat transfer. International Journal of Heat and Fluid Flow. **22**: 287-292.

Nasa: National Aeronautics and Space Administration. Accessed in January 2012, in: https://www.grc.nasa.gov/www/k-12/airplane/pitot.html.

Nishino K., Samada M., Kasuya, K., Torri K. (1996). Turbulence statistics in the stagnation region of an axisymmetric impinging jet flow. *International Journal of Heat and Fluid*. **17(3)**: 193-201.

Ostheimer D., Yang Z. (2012). A CFD Study of Twin Impinging Jets in a Cross-Flow. *The open Numerical Methods Journal*. **4**: 24-34.

Ozmen Y. (2011). Confined Impinging Twin Air Jets at High Reynolds Numbers. *Experimental Thermal and Fluid Science.* **35**: 355-362.

Page G.J., McGuirk J.J (2009). Large Eddy Simulation of a complete Harrier aircraft in ground effect. *The Aeronautical Journal*. **113(1140)**: 99-106.

Panday S. A., Murman S. M., Sankaran V. (2003). Unsteady Computations of a jet in crossflow with ground effect. *Proceedings of the 33rd AIAA Fluid Dynamics Conference and Exhibit*, Orlando, Florida, 23-26 August 2003

Parsons J. A., Han J. (1998). Rotation effect on jet impingement heat transfer in smooth rectangular channels with heated target walls and radially outward crossflow. *International Journal of Heat Mass Transfer.* **41(13)**: 2059-2071

Patankar S. V., Basu D. K., Alpay S. A. (1977). Prediction of the Tree-Dimensional Velocity Field of a Deflected Turbulent Jet. *Journal of Fluids Engineering.* **99(4)**: 758-762.

Porcar R., Prenel J. –P., Diemunsch, Hamelin P. (1983). Visualizations by means of Coherent Light Sheets; Applications to Various Flows. Flow Visualization III (W. –J. Yang, ed.). 123-127.

Radhouane A., Bournot H., Mahjoub Said N., Mhiri H., Palec G. (2009). Numerical and experimental study of a double jet inclination variation on its dynamic evolution within a crossflow. *Heat and Mass Transfer*. **45(12)**: 1597-1616.

Ristic' S. (2007). Laser Doppler Anemometry and its Application in Wind Tunnels. *Scientific Technical Review*. **LVII(3-4)**: 64-76.

Rizk M. H., Menon S. (1988). Large eddy simulations of axisymmetric excitation effects on a row of impinging jets. *Physics of Fluid*. **31(7)**: 1892-1903.

Rodi W., Srivatsa S. K. (1980). A Locally Elliptic Calculation Procedure for Three – Dimensional Flows and its Application to a Jet in a Cross – Flow. *Computer Methods in an Applied Mechanics and Engineering*, **23(1)**: 67-83.

Said N. M., Stefanini J., Bournot P., Darreau S., Caminat P. (2006). Experimental Study on the Flow Characteristics of Streamwise Inclined Jet in Crossflow. Proceedings of the 13th International Symposium on Applications of Laser Techniques to Fluid Mechanics, Lisbon, Portugal, 26-29 June 2006.

Salewski M., Stankovic D., Fuchs L. (2007). Mixing in Circular and Non-circular Jets in Crossflow. *Flow, Turbulence and Combustion*. **80(2)**: 255-283.

San J., Shiao W., (2006). Effects of Jet Plate Size and Plate Spacing on the Stagnation Nusselt Number for a Confined Circular Air Jet Impinging on a Flat Surface. *International Journal of Heat and Mass Transfer*, **49**: 3477-3486.

Saddington A. J., Knowles K. (2000). Comparison of jet-induced lift loss for single and co-annular jets. *Proceedings of the 22nd Congress of international Council of the Aeronautical Sciences*, Harrogate, UK, 27 August-1 September 2000.

Saddington A. J., Knowles K., Cabrita P. M. (2008). Flow Measurements in a Short Takeoff, Vertical Landing Fountain: Parallel Jets. *Journal of Aircraft*. **45(5)**: 1736-1743.

Saddington A. J., Knowles K., Cabrita P. M. (2009). Flow measurements in a short Takeoff, Vertical Landing. *Journal of Aircraft*. **46(3)**: 874-882.

Saripalli K. R. (1983). Visualization of Multijet Impingement Flow. *AIAA Journal*. **21**: 483-484.

Saripalli K. R. (1987). Laser Doppler Velocimeter Measurements in 3D Impinging Twin-Jet Fountain Flows. *Turbulent Shear Flows*. **5:**147-168. Edited by Durst et al., Springer-Verlag, Berlin.

Savory E., Toy N., McGuirk J. J., Sakellariou N. (1990). An Experimental and Numerical Study of the Velocity Field Associated with a Jet in a Crossflow. *Elsevier Science Publishing Co*.

Schetz, J.A., Jakubowsky, A.K. and Aoyagi, K. (1984). Surface Pressures on a Flat Plate with Dual Jet Configurations. *Journal of Aircraft*. **21(7)**: 484-490.

Siclari M.J., Migdal D., Luzzi T.W. Jr., Barche J., Palcza J.L. (1976). Development of Theoretical Models of Jet-Induced Effects on V/STOL Aircraft. *Journal of Aircraft*. **13(12)**:.938-944.

Soong C. Y., Tzeng P. Y., Hsieh C. D. (1998). Numerical Investigation of flow structure and bifurcation phenomena of confined plane twin-jet flows. *Physics of Fluids*. **10(11)**: 2910-2921.

Souris N., Liakos H., Founti M., Palyvos J., Markatos N. (2002). Study of Impinging Turbulent Jet Flows Using the Isotropic Low-Reynolds Number and the Algebraic Stress Methods. *Computational Mechanics*. **28(5)**: 381-389.

Souris N., Liakos H., Founti M. (2004). Impinging jet cooling on concave surfaces. AIChE Journal. **50(8)**: 1672-1683.

Stoy, R. L., BEN – HAIM Y. (1973). Turbulent Jets in a Confined Crossflow. *Journal of Fluids Engineering*. **95(4)**: 551-556.

Syres R. I., Lewellen W. S., Parker S. F. (1986). On the Vorticity Dynamics of a Turbulent Jet in a Crossflow. *Journal of Fluid Mechanics*. **168**: 393-413.

Tchavdarov B. M. (1997). Two dimensional vortex dynamics of inviscid-viscous interaction of turbulent slot jet impingement. *International Journal of Heat and Fluid Flow*. **18**: 316-327.

Tsubokura M., Kobayashi T., Taniguchi N., Jones W. P. (2003). A numerical study on the eddy structures of impinging jets excited at the inlet. *International Journal of Heat and Fluid Flow*. **24(4)**: 500-511.

Véret C. (1985). Flow Visualization by Light Sheet. *In Flow Visualization III* (W. –J. Yang, ed.), 106-112. Hemisphere, Washington, D. C.

Vieira D. F. C. (2012). *Turbulent Structure of the Impact of a Ground Vortex Flow*. Master Thesis in Aeronautical Engineering. University of Beira Interior, Covilhã, 110 pp.

Vieira D.F.C., Silva A.R.R., Carvalho P.S.D., Neves F.M.S.P., Barata, J.M.M. (2013). Numerical and Experimental Study of Two Impinging Jets in a Row through a Crossflow. Proceedings of the 51th AIAA Aerospace Science Meeting Including the New Horizons Forum and Aerospace Exposition, Grapevine (Dallas/Ft. Worth Region), Texas, 7-10 Jan. 2013. AIAA Paper 2013-0806.

Vieira D.F.C, Durão D.F.G., Neves F.M.S.P., Silva A.R.R., Barata J.M.M. (2014). Laser Doppler Measurements of Twin Impinging Jets in Tandem through a Crossflow. *Proceeding of the 17th International Symposium on Applications of Laser Techniques to Fluid Mechanics*, Lisbon, Portugal, 07-10 July 2014.

Vieira D. F. C., Barata J. M. M, Neves F. M. S. P., Silva A. R. R. (2015). Numerical Simulation of Twin Impinging jets in Tandem through a Crossflow. *Proceedings of the 53rd AIAA Aerospace Science Meeting, Scitech 2015*, Kissimmee, Florida, 5-9 January 2015.

Vieira D.F.C, Barata J.M.M, Neves F.M.S.P, Silva A.R.R. (2015). Numerical Simulation of Twin Impinging Jets in Tandem through a Crossflow. Journal of Engineering and Applied Sciences. 10(6): 123-136. ISSN: 1816-949X. DOI: 10.3923/jeasci.2015.123.136.

Voke P., Gao S. (1998). Numerical study of heat transfer from an impinging jet. *International Journal of Heat Mass Transfer*. **41(4-5)**: 671-680.

Wae-hayee M., Tekasakul P., Eiamsa-ard S., Nuntadusit C. (2014). Effect of cross-flow velocity on flow and heat transfer characteristics of impinging jet with low jet-to-plate distance. *Journal of Mechanical Science and Technology*. **28(7)**: 2909-2917.

Wang L., Sundén B., Borg A., Abrahamsson H. (2011). Control of jet impingement heat transfer in crossflow by using a rib. *International Journal of Heat and Mass Transfer*. **54**: 4157-4166.

Webster D. R., Longmire E. K. (1997). Vortex dynamics in jets from inclined nozzles. *Physics of Fluids*. **9 (3)**: 655-666.

Wegner B., Huai Y., Sadiki A. (2004). Comparative study of turbulent mixing in jet in cross-flow configurations using LES. *International Journal of Heat and Fluid Flow*. **25(5)**: 767-775.

Wilcox D. C. (1993). Turbulence Modeling for CFD. 1º Edition. DCW Industries, Inc. 5354 Palm Drive, La Canada, California 91011.

Worth N. A, Yang Z. (2006). Simulation of an impinging jet in a crossflow using a Reynolds stress transport model. *International Journal for Numerical Methods in Fluids*. **52**:199-211.

Xiao Y., Tang H.-w., Liang D.-f., Zhang J.-d. (2011). Numerical study of hydrodynamics of multiple tandem jets in cross flow. *Journal of Hydrodynamics*. **23(6)**: 806-813.

Yan L. L., Street R. L., Ferziger J. H. (1999). Large eddy simulations of a round jet in crossflow. *Journal of Fluid Mechanics*. **379**: 71-104.

Yang YT, Shyu, CH (1998) Numerical study of multiple impinging slot jets with an inclined confinement surface. *Numerical Heat Transfer Part A-Applications*. **33(1)**: 23-27

Yang Y. –T., Hao T. –P. (1999). Numerical studies of three turbulent slot jets with and without moving surface. *Acta Mechanica*. **136(1-2)**: 17-27.

Yang Y. –T., Wang Y. –X. (2005). Three-dimensional numerical simulation of an inclined jet with crossflow. International Journal of Heat and Mass Transfer. **48(19-20)**: 4019-4027.

Yang Z. (2014). Assessment of unsteady-RANS approach against steady-RANS approach for predicting twin impinging jets in a crossflow. *Congent Engineering*. **1**:936995.

Yanta W.J., Smith R.A. (1978). Measurements of Turbulent Transport Properties with a Laser-Doppler Velocimeter. *Proceeding of the 11th Aerospace Sciences Meeting*, Washington. AIAA Paper 73-0169

Yeh Y., Cummins H. Z. (1964). Localized Fluid Flow Measurements with an He-Ne Laser Spectrometer. *Applied Physics Letters*. **4 (10)**: 176-178.

Yin Z. –q, Zhang H. –j., Lin j. –z. (2007). Experimental study on the flow field characteristics in the mixing regions of twin jets. *Journal of hydrodynamics*. **19(3)**: 309-313.

Zhang X., Ing D. N. (1994). Computational Analysis of a Single Impingement Ground Effect Lift Loss. Journal of Aircraft. 31(2): 256-262.

Zhang Z. (2010). *LDA Application Methods, Laser Doppler Anemometry Fluid Dynamics*. 1st edition, Springer-Verlag Berlin Heidelberg. e-ISBN 978-3-642-13514-9.

Zhang X., Collins M. W. (1997). Measurements of a longitudinal vortex generated by a rectangular jet in a turbulent boundary layer. *Physics of Fluids*. 9 (6): 1665-1673.

Zhang X. (2000). Turbulence measurements of an inclined rectangular jet embedded in a turbulent boundary. *International Journal of Heat and Fluid Flows*. **21**: 291-296.

Annexes

Annex 1

Papers published in Journal

Journal of Physical Science and Application 4 (7) (2014) 403-411

Laser Doppler Measurements of Twin Impinging Jets Aligned with a Crossflow

Jorge M.M. Barata[1], Pedro S.D. Carvalho[1], Fernando M.S.P. Neves[1], André R.R. Silva[1], Diana F.C. Vieira[1] and Diamantino F.G. Durão[2]

1. Departmentof Aerospace Sciences, University of Beira Interior, Covilhã 6200-001, Portugal

2. Instituto Lusíada de Investigação e Desenvolvimento, Universidade Lusíada, Lisbon 1349-001, Portugal

Received: April 25, 2014 / Accepted: June 13, 2014 / Published: July 15, 2014.

Abstract: This paper presents a detailed analysis of the complex flow beneath two impinging jets aligned with a low-velocity crossflow which is relevant for the future F-35 VSTOL configuration, and provides a quantitative picture of the main features of interest for impingement type of flows. The experiments were carried out for a Reynolds number based on the jet exit conditions of $Re_j = 4.3 \times 10^4$, an impingement height of 20.1 jet diameters and for a velocity ratio between the jet exit and the crossflow $V_R = V_j/U_o$ of 22.5. The rear jet is located at $S = 6\ D$ downstream of the first jet. The results show a large penetration of the first (upstream) jet that is deflected by the crossflow and impinges on the ground, giving rise to a ground vortex due to the collision of the radial wall and the crossflow that wraps around the impinging point like a scarf. The rear jet (located downstream) it is not so affected by the crossflow in terms of deflection, but due to the downstream wall jet that flows radially from the impinging point of the first jet it does not reach the ground. The results indicate a new flow pattern not yet reported so far, that for a VSTOL aircraft operating in ground vicinity with front wind or small forward movement may result in enhanced under pressures in the aft part of the aircraft causing a suction down force and a change of the pitching moment towards the ground.

Key words: VSTOL, ground vortex, turbulence, complex flows.

Nomenclatures

D:	Diameter of the jet
H:	Impinging height
K:	Turbulent kinetic energy
Re:	Reynolds number
S:	Spacing of the jets axis in the wind direction
U:	Horizontal velocity, $\overline{U} + u'$
V:	Vertical velocity, $\overline{V} + v'$
W:	Transverse $\overline{W} + w'$
X:	Horizontal coordinate
Y:	Vertical coordinate
Z:	Transverse coordinate

Subscripts

J:	Jet-exit value
O:	Crossflow value

Corresponding author: Jorge M.M. Barata, full professor, hab., PhD, research fields: aerodynamics, computational fluid dynamics and VSTOL. E-mail: jbarata@ubi.pt.

1. Introduction

Turbulent jets impinging on flat surfaces through a low-velocity crossflow are typical in impinging cooling applications in industry [1] as well as of the flow beneath a short/vertical take-off aircraft which is lifting off or landing with zero or small forward momentum [2]. Ground effect may occur and change the lift forces on the aircraft, cause reingestion of exhaust gases into the engine intake and raise fuselage skin temperatures. In this latter application the impingement of each downward-directed jet on the ground results in the formation of a wall jet which flows radially from the impinging point along the ground surface. The interaction of this wall jet with the free stream results in the formation of a ground vortex far upstream of the impinging jet, which has profound implications on the aircraft design. In addition the

collision of the wall jets originates a fountain upwash flow, affecting the forces and moments induced in the aircraft when operating in ground effect. Improved knowledge of impinging flows is therefore necessary to avoid these effects and to be able to model a range of jet-impingement type of applications with practical interest.

Earlier published work has been concentrated on 1, 2, and 3 jets configurations relevant to the Harrier/AV-8B aircraft [2]. In this case, when the aircraft is operating with small forward movement the configuration of interest is 2 impinging jets with the direction of the crossflow perpendicular to the line containing their centers, because each impinging jet is located on the sides of the fuselage.

If attention is concentrated on the next generation of VSTOL aircrafts (X-35/F-35/JSF-Joint Strike Fighter) then no relevant studies can be found, because the impinging jets are aligned with the crossflow, and this geometry has not been considered. In this case a vertically oriented lift fan (SDLF) generates a column of cool air that produces nearly 20,000 pounds of lifting power, along with an equivalent amount of thrust from the vectored rear exhaust (3BSM-Three Bearing Swivel Module). The lift system was successfully demonstrated during a flight testing of the X-35B during the summer of 2001. The complexity of the new VSTOL configuration together with the very stringent requirements has required an enormous amount of R&D in the last decade. On 12th May 2012 the 200th test flight of the F-35B (BF-3) measured stresses on the aircraft during supersonic maneuvers. So, most of the published work reported so far has therefore only peripheral relevance to the F35-B/JSF ground effect problem.

Ref. [3] reports a study of multijet impinging configurations producing upwash fountain flows, which are the heart of the complicated effects by VSTOL aircraft when they operate in ground proximity, but as far as twin jets are concerned only the geometry with the jets side by side was considered. This paper presents a detailed analysis of the complex flow field beneath two impinging jets aligned with a low-velocity crossflow relevant for the new F-35 VSTOL configuration, and provides a quantitative picture of the main features of interest of impingement type of flows.

The remainder of this paper is presented in four sections. Section 2 describes the experimental configuration and measurement procedure, gives details of the laser-Doppler velocimeter and provides assessments of accuracy. The arguments associated with these assessments are based on previous experiments and are presented in condensed form. Section 3 presents the experimental results obtained in the vertical plane of symmetry containing the axis of both jets and quantifies the mean and turbulent velocity characteristics of the flow. The final section summarizes the main findings and conclusions of this work.

2. Experiments

The wind tunnel facility designed and constructed for the present work is schematically shown in Fig. 1. A fan with 15 kW nominal power drives a maximum flow of 3,000 m^3/h through the boundary layer wind tunnel of 300 × 302 mm exit section. Each jet unit of 15 mm inner diameter is mounted vertically in the top of the test section with the axis contained in the vertical plane o symmetry parallel to the crossflow.

The origin of the horizontal, X, and vertical, Y, coordinates is taken at the midpoint between the centers of the jets exit. The X coordinate is positive in the direction of the wind tunnel exit and Y is positive upwards.

The present results were obtained at the vertical plane of symmetry for jet mean velocities of V_j = 36 m/s and mean crossflow velocity of U_0 = 1.6 m/s, corresponding to a velocity ratio, $V_R = V_j/U_o$ of 22.5. The rear jet is located at S = 6D downstream of the first jet (Fig. 2).

The velocity field was measured with a two-color (two-component) Laser-Doppler velocimeter (Dantec

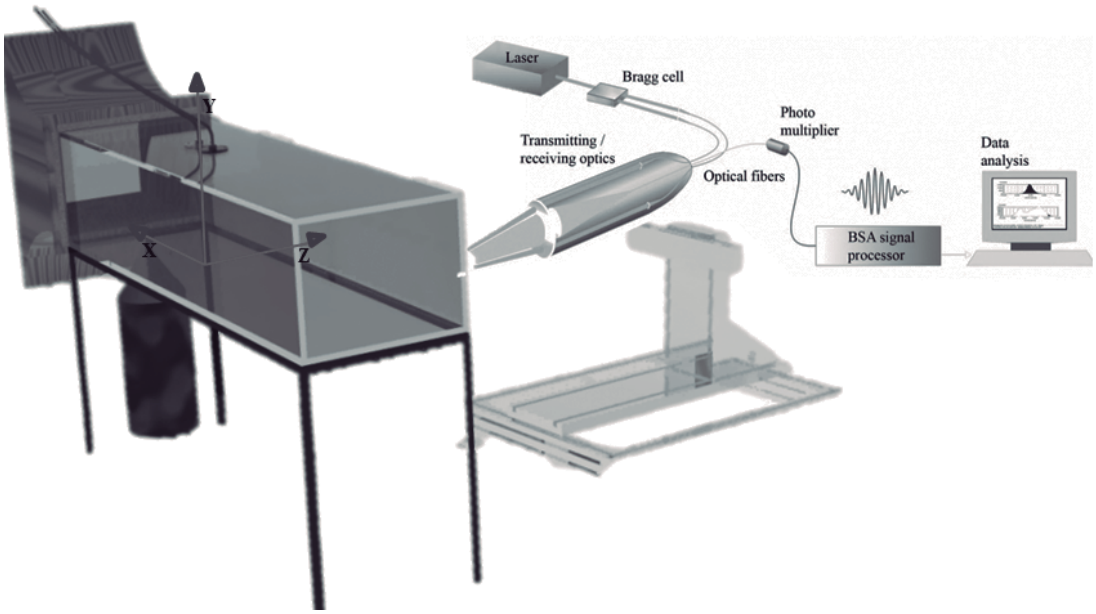

Fig. 1 Experimental set-up.

Table 1 Principal characteristics of the 2D Laser-Doppler velocimeter.

	He-Ne laser	Diode Laser
Wave length, λ (nm)	633	532
Focal length of focusing lens, f (mm)	400	400
Beam diameter at e-2 intensity (mm)	1.35	1.35
Beam spacing, s (mm)	38.87	39.13
Calculated half-angle of beam intersection, θ	2.78°	2.8°
Fringe spacing, δ_f (μm)	6.53	5.45
Velocimeter transfer constant, K (MHz/ms^{-1})	0.153	0.183

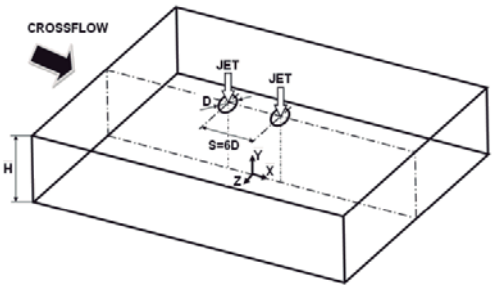

Fig. 2 Geometrical arrangement of the jets.

Flowlite 2D), which comprised a 10 mW He-Ne and a 25 mW diode-pumped frequency doubled Nd:YAG lasers, sensitivity to the flow direction provided by frequency shifting from a Bragg cell at f_0 = 40 MHz, a transmission and backward-scattered light collection focal lens of 400 mm. The half-angle between the beams was 2.8° and the calculated dimensions of the axis of the measuring ellipsoid volume at the e^{-2} intensity locations were 135 × 6.54 × 6.53 μm and 112 × 5.46 × 5.45 μm, respectively (Table 1 for details). The horizontal, *U*, and vertical *V*, mean and turbulent velocities were determined by a two-velocity channel Dantec BSA F60 processor. The seeding of the flow with glycerinparticles of 0.1-5 μm was produced by a smoke generator. The transmitting and collecting optics is mounted on a three-dimensional traversing unit, allowing the positioning of the center of the control volume within ±0.1 mm.

In order to measure the vertical components in near wall regions, the transmitting optics were inclined by half angle of beam intersection and the scattered light

was collected off-axis. Measurements could then be obtained up to 0.5 mm from the ground plate without a significant deterioration of the Doppler signals. Results obtained 20 mm above the ground plate with both the on-axis and the off-axis arrangements have shown a close agreement, within the precision of the equipment.

Errors incurred in the measurement of velocity by displacement and distortion of the measuring volume due to refraction on the duct walls and change in the refractive index were found to be negligibly small and within the accuracy of the measuring equipment. Non-turbulent Doppler broadening errors due to gradients of mean velocity across the measuring volume may affect essentially the variance of the velocity fluctuations [4], but for the present experimental conditions are of the order of $10^{-4}V_j^2$ and, therefore, sufficiently small for their effect to be neglected. The largest statistical (random) errors derived from populations of, at least, 10,000 velocity values were of 0.5% and 3%, respectively for the mean and the variance values, according to the analysis recommended by Yanta and Smith [5] for a 95% confidence interval. No corrections were made for sampling bias, but no correlations were found between Doppler frequencies and time interval between consecutive bursts even in the zones of the flow characterized by the lowest particle arrival rates, suggesting that those effects are unimportant for the present flow conditions.

Systematic errors incurred in the measurements of Reynolds shear stresses can arise from lack of accuracy in the orientation angle on the normal to the anemometer fringe pattern, and can be particularly large in the vicinity of the zones characterized by zero shear stress [6]: for the present experimental conditions the largest errors are expected to be smaller than -2.5%.

3. Results

In this chapter, experimental data obtained are presented and discussed under two headings. First, flow visualization is presented, and then mean and turbulent velocity profiles are presented and discussed for the velocity ratios V_R of 22.5.

3.1 Visualization

Flow visualization was performed using digital direct photography to guide the choice of the measurement locations and to provide a qualitative picture of the flow. The longitudinal vertical plane of symmetry was illuminated with a sheet of light. The photos were taken perpendicular to the vertical plane of symmetry. For all the flows studied, the results have shown (for each jet) a pattern similar to that of a single impinging jet. Fig. 3 identifies the flow development along the vertical plane of symmetry, i.e., $Z = 0$. Each jet has an initial potential-core jet region, where the flow characteristics are identical to those of a free jet, and near the horizontal plate the impingement region, characterized by considerable deflection of the jet. The selected picture shows the wall jet corresponding to the upstream impinging jet which is almost parallel to the ground plate and exhibits behavior similar to that of a radial wall jet where the upstream effects of interaction due to impingement are no longer important. The upstream wall jet interacts with the crossflow and forms a horseshoe vortex close to the ground plate, which wraps around both impinging jets. As a result, two streamwise counter-rotating vortices develop side-to-side and decay further downstream of each impinging zone forming a ground vortex. The nature of each ground vortex is similar to the horseshoe structure known to be generated by the deflection of a boundary layer by a solid obstacle [7], but is different from the vortex pair known to exist in a “bent-over” jet in a crossflow far from the ground [8]. No evidence of a ground vortex corresponding to the downstream impinging jet could be confirmed, which is an indication that the upstream impinging jet and its ground vortex are blocking the crossflow and provoking an alteration to the flow pattern. If the jets were positioned side by side in front of the crossflow two ground vortexes would appear as well as a fountain

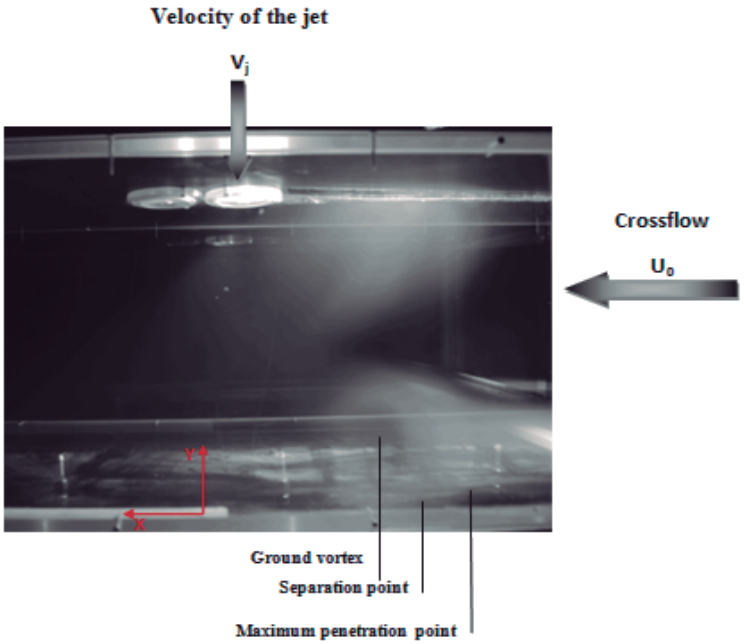

Fig. 3 Visualization of the twin jet flow in the vertical plane of symmetry for $Re_j = 4.3 \times 10^4$, $V_j/U_o = 22.5$, $H/D = 20.1$, and $S/D = 6$.

flow in the vertical plane of symmetry due to the collision of the two individual radial wall jets [9-10]. In the present case for a velocity ratio between the jet and the crossflow of $V_R = 22.5$ no fountain flow could be detected.

Analysis of Fig. 3 also suggests that the crossflow is deflected sideways by the penetration of the jet and may cause a recirculation region just downstream of the discharge, away from the ground plate, but cannot be clearly identified. These features of the flow are quantified in Figs. 4-6 through a detailed set of mean and turbulent velocity measurements obtained in the vertical plane of symmetry ($Z = 0$) for a Reynolds number based on the jet-exit conditions of 4.3×10^4, a free stream to jet velocity ratio, $V_R = V_j/U_o$ of 22.5, a jet height to jet diameter ratio, H/D, of 20.1, and a spacing between the jets in the wind direction, S/D, of 6.

3.2 Measurements

Fig. 4 shows vertical profiles of the mean horizontal velocity component, $\overline{U}$, along the vertical plane of symmetry (Z = 0).

The mean horizontal velocity profiles at X/D = -2.93, -1.47, 0 and +1.47 show negative values near the ground ($Y = 0$) that correspond to the upstream wall jet, revealing that the first impinging jet was deflected by the crossflow. The impinging point of the first jet is located at about X/D = +2.93 in a position that is vertically near the axis of the rear jet exit (X/D = +3), which is more strongly deflected due to this interference. As a consequence, the downstream wall jet of the first jet and the rear jet seems to merge rapidly in a single flow in the crossflow direction. These profiles exhibit maximum positive (downstream) values of the mean horizontal velocity component between Y = 100 mm and 150 mm that reach twice the crossflow velocity. This means that no upstream wall jet resulting from the rear jet exists, but the complete jet is deflected by the crossflow. This result is consistent with the conclusions of Ref. 4 that found for a single impinging jet flow that the ground vortex blocks the passage of the confined crossflow increasing the velocity of the crossflow that passes over. So, for this configuration the final result is that the rear jet "feels" a

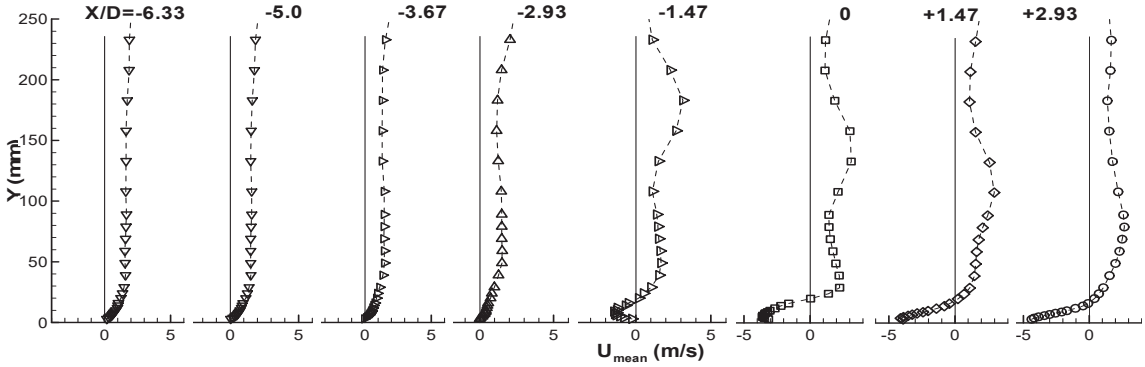

Fig. 4 Vertical profiles of the mean horizontal velocity component, $\bar{U}$, along the longitudinal (symmetry) plane crossing the center of the twin jets. $Re_j = 4.3 \times 10^4$, $V_j/U_o = 22.5$, $H/D = 20.1$, and $S/D = 6$.

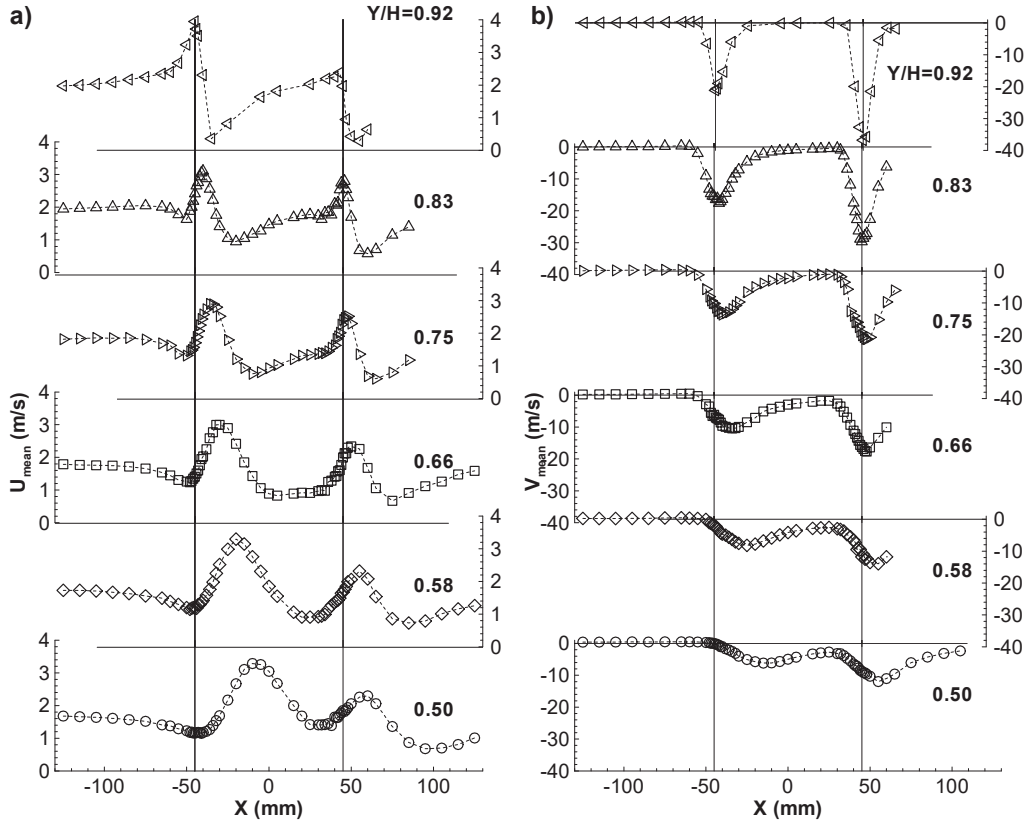

Fig. 5 Horizontal profiles of the mean velocity characteristics along the longitudinal (symmetry) plane crossing the center of the twin jets. $Re_j = 4.3 \times 10^4$, $V_j/U_o = 22.5$, $H/D = 20.1$, and $S/D = 6$. (a) Horizontal velocity, $\bar{U}$. (b) Vertical velocity, $\bar{V}$.

smaller jet-to-crossflow velocity ratio and no impingement occurs. In the practical situation of a VSTOL aircraft this may result in a different pressure distribution in the under surface of the aircraft, that with front wind or small forward movement may result in enhanced under pressures in the aft part of the aircraft causing a suction down force and a change of the pitching moment towards the ground.

Figs. 5a and 5b show horizontal profiles of horizontal, $\bar{U}$, and vertical, $\bar{V}$, mean velocity

components, quantify the development of the impinging jets and confirm the above description of the flow. The measurements, and particularly those of the vertical velocity component, do not identify a centrally located fountain rising from the ground plate without interference from the main jets, as it occurs in practical VSTOL applications [10].

This result confirms our hypothesis that the alignment of the twin jets with the crossflow would create a special flow pattern not yet reported before. The wall jet resulting from the first jet flows underneath the rear one, but the ground vortex formed upstream is only interfering away from the vertical symmetry plane.

The mean vertical velocity component is always positive from the upper wall (Y/H = 1) up to the middle of the crossflow (Y/H = 0.5), confirming the conclusions drawn from the vertical velocity profiles in the lower part of the crossflow and discussed in the previous paragraphs.

The asymmetry of the flow can be confirmed from the horizontal profiles of the mean vertical velocity component with higher peaks up to 10% of the vertical velocity in the upstream side (X < -50 mm or 3.33 D). The middle value between the maximum and the minimum of the mean horizontal velocity component or the mean vertical velocity components can be used to indicate the center of the jet, and in the upstream side it moves in the crossflow direction from -43.02 mm at Y/H = 0.92 to 10.47 mm at Y/H = 0.5 corresponding to a deflection angle of 21.9º. The downstream jet is protected from the action of the crossflow by the first

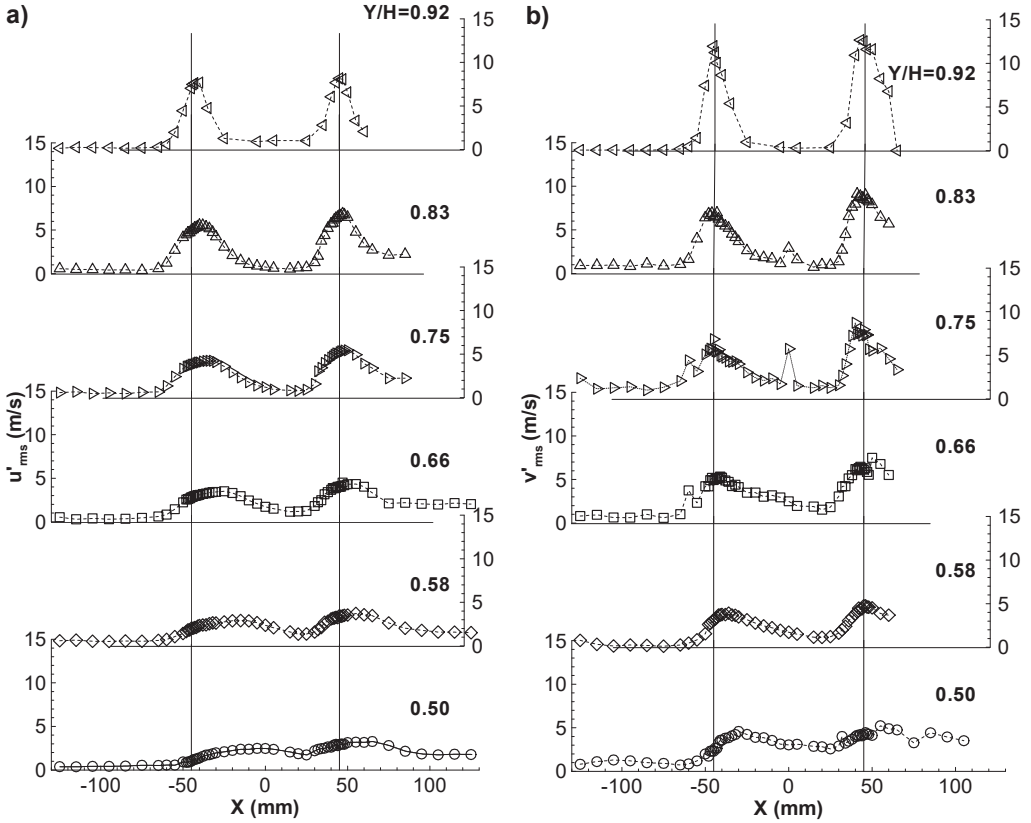

Fig. 6 Horizontal profiles of the fluctuating velocity characteristics along the longitudinal (symmetry) plane crossing the center of the twin jets. Re_j = 4.3 × 10^4, V_j/U_o = 22.5, H/D = 20.1, and S/D = 6. (a) Horizontal rms velocity, $\sqrt{\overline{u'^2}}$. (b) Vertical rms velocity, $\sqrt{\overline{v'^2}}$.

jet and as a consequence it is less deflected: the center of the jet is almost coincident with the geometrical axis of the exit, and for $Y/H = 0.5$ it is located at $X/D = +4.0$ corresponding to an inclination angle of 12.3º. However, considering the maximum of the mean vertical velocity component the calculated inclination angle is only 4.8º, which reinforces the conclusion, and the difference is probably associated with an enhanced entrainment of the rear jet due to its smaller angle with the surrounding flow.

Fig. 6 shows horizontal profiles of the normal stresses, $\overline{u'^2}$ and $\overline{v'^2}$, in a *rms* form, and show results that are somewhat surprising at first sight, because it seems that it is not possible to identify completely the shear layer surrounding the impinging jets for the highest stations ($Y/H = 0.92$ and 0.83). However, it should be noted that the diameter of the jet is only 15 mm and so the peak observed corresponds to the shear layer which exhibits similar values in the upstream and downstream sides of the jet.

The peaks in the fluctuating vertical velocity components occur in the upstream side of the first jet as expected, because in this region the higher velocity gradients occur. Other peaks were observed near $X = 0$ for the $X/H = 0.83$ and 0.75 profiles that correspond to the downstream side of the first impinging jet. For the $X/H = 0.66$ profile the peak is very weak, and for the lower profiles they cannot be pointedly identified, confirming the rapid mixing between the jets as already detected from the lower part of the flow through the vertical velocity profiles. For the second (downstream) impinging jet the shear layer surrounding the jet cannot be clearly identified. However, for the $Y/H = 0.66$ profile a small decrease in the normal vertical stress is noted near the center of the jet, but the peaks around the jet are so close that the minimum value is somewhat masked.

4. Conclusions

A laser Doppler velocimeter was used to provide information on the flowfield created by twin impinging jets aligned with a low velocity crossflow. The experiments were carried out for a Reynolds number based on the jet exit conditions of $Re_j = 4.3 \times 10^4$, an impingement height of 20.1 jet diameters and for a velocity ratio between the jet exit and the crossflow $V_R = V_j/U_o$ of 22.5. The rear jet is located at $S = 6\ D$ downstream of the first jet.

The results show a large penetration of the first (upstream) jet, which is deflected by the crossflow and impinges on the ground, giving rise to a ground vortex due to the collision of the radial wall and the crossflow that wraps around the impinging point like a scarf. The rear jet is not so affected by the crossflow in terms of deflection because it is protected by the upstream jet, but due to the downstream wall jet that flows radially from the impinging point the first jet does not reach the ground. Also, due to the confinement and the ground vortex, the crossflow is blocked and accelerates in the upper part and also contributes to an enhanced mixing of each secondary flow. As consequence, no upstream wall jet or ground vortex resulting from the second (downstream) jet was detected. The result of the rear jet impinging on the downstream wall jet resulting from the first jet had not been reported so far and requires further investigation.

The shear layers surrounding the jet cannot be clearly identified from the fluctuating velocities that do not exhibit distinct peaks in the edges, and the values in the center are also high. Nevertheless, the high levels of turbulent velocities correspond to the expected values in the upstream and downstream sides of the impinging jets.

Acknowledgments

The present work has been performed in the scope of the activities of the AeroG-Aeronautics and Astronautics Center of the Portuguese Associate Laboratory in Energy, Transport and Aeronautics.

The financial support of the FCT-Fundação para a Ciência e Tecnologia of the Portuguese Ministry of

Science under Contract No. PTDC/EME/-MFE/ 102190/2008 is gratefully acknowledged.

References

[1] W. Bernhard, S. Sebastian, Multiple jet impingement: A review, Heat Transfer Research 42 (2) (5) (2011) 101-142.

[2] J.M.M. Barata, D.F.G. Durão, J.J. McGuirk, Numerical study of single impinging jets through a crossflow, Journal of Aircraft 26 (11) (1989) 1002-1008.

[3] J.M.M. Barata, Fountain flows produced by multiple impinging jets in a crossflow, AIAA Journal 34 (12) (1996) 2523-2530.

[4] F. Durst, A. Melling, J.H. Whitelaw, Principles and Practice of Laser-Doppler Anemometry, 2nd ed., New York, Academic Press, 1981.

[5] W.J. Yanta, R.A. Smith, Measurements of turbulent transport properties with a Laser-Doppler velocimeter, in: 11th Aerospace Sciences Meeting, Washington, 1978.

[6] A. Melling, J.H. Whitelaw, Turbulent flow in a rectangular duct, J. Fluid Mechanics 78 (1975) 285-315.

[7] C.J. Baker, The turbulent horseshoe vortex, Journal of Wind Engineering and Industrial Aerodynamics 6 (1981) 9.

[8] J. Andreopoulos, W. Rodi, Experimental investigation of jets in a crossflow, Journal of Fluid Mechanics 138 (1984) 127.

[9] M.J. Siclari, D. Migdal, T.W. Luzzi, J. Barche, J.L. Palcza, Development of theoretical models of jet-induced effects on V/STOL aircraft, Journal of Aircraft 13 (12) (1976) 938-944.

[10] D.R. Kotansky, The modeling and prediction of multiple VTOL aircraft flow fields in ground effect, AGARD CP-308 (1982) 16.

Journal of Modern Physics, 2014, 5, 1779-1788
Published Online October 2014 in SciRes. http://www.scirp.org/journal/jmp
http://dx.doi.org/10.4236/jmp.2014.516175

Experimental Study of Two Impinging Jets Aligned With a Crossflow

Jorge M. M. Barata*, Fernando M. S. P. Neves, Diana F. C. Vieira, André R. R. Silva

Universidade Beira Interior, Covilhã, Portugal
Email: *jbarata@ubi.pt

Received 15 August 2014; revised 11 September 2014; accepted 2 October 2014

Abstract

Laser Doppler measurements provide information on the flowfield created by twin impinging jets aligned with a low velocity crossflow. The experiments were carried out for a Reynolds number based on the jet exit conditions of $Re_j = 4.3 \times 10^4$, an impingement height of 20.1 jet diameters and for a velocity ratio between the jet exit and the crossflow $V_R = V_j/U_o$ of 22.5, and an inter-jet spacing of S = 6D. The results show a large penetration of the first (upstream) jet that is deflected by the crossflow and impinges on the ground, giving rise to a ground vortex due to the collision of the radial wall and the crossflow that wraps around the impinging point like a scarf. The second jet (located downstream) is not so affected by the crossflow in terms of deflection, but due to the downstream wall jet that flows radially from the impinging point of the first jet it does not reach the ground. The results indicate a new flow pattern not yet reported so far, that is most relevant for a VSTOL aircraft operating in ground vicinity with front wind or small forward movement may result in enhanced under pressures in the aft part of the aircraft causing a suction down force and a change of the pitching moment towards the ground.

Keywords

Impinging Jets, Crossflow

1. Introduction

Turbulent jets impinging on flat surfaces through a low-velocity crossflow are typical in impingement cooling applications in industry, as well as of the flow beneath a short/vertical take-off aircraft which is lifting off or landing with zero or small forward momentum. Ground effect may occur and change the lift forces on the aircraft, cause reingestion of exhaust gases into the engine intake and raise fuselage skin temperatures. In this latter

*Corresponding author.

How to cite this paper: Barata, J.M.M., Neves, F.M.S.P., Vieira, D.F.C. and Silva, A.R.R. (2014) Experimental Study of Two Impinging Jets Aligned With a Crossflow. *Journal of Modern Physics*, **5**, 1779-1788.
http://dx.doi.org/10.4236/jmp.2014.516175

application the impingement of each downward-directed jet on the ground results in the formation of a wall jet which flows radially from the impinging point along the ground surface. The interaction of this wall jet with the free stream results in the formation of a ground vortex far upstream of the impinging jet, which has profound implications on the aircraft design [1] [2]. In addition the collision of the wall jets originates a fountain upwash flow, affecting the forces and moments induced in the aircraft when operating in ground effect. Improved knowledge of impinging flows is therefore necessary to avoid these effects and to be able to model a range of jet-impingement type of applications with practical interest.

This paper presents a detailed analysis of the complex flow field beneath twin jets through a low-velocity crossflow and provides a quantitative picture of the main features of interest of impingement type of flows. The results include laser-Doppler velocity measurements of flow characteristics, which are complemented by flow visualization.

Earlier detailed measurements of the flow properties of fountain upwash are scarce and have been presented essentially in the absence of a crossflow and with the use of probe techniques. The most relevant works have been reviewed by [3] and [4], and indicated high turbulence levels and spreading rates in the fountains [5] [6]. Different interpretations of the measurements were presented by [7] and [8] due to the difficulties in measuring complex flows using hot-film and pitot-probe techniques. Ref. [9] and [10] also presented flowfield and pressure data for twin-rectangular jets for small jet-to-crossflow velocity ratios (<10). Ref. [4] reports laser Doppler velocity (LDV) measurements, including those of shear stress, for axisymmetric impinging jets with S/D = 9 and 14 and H/D = 3 and 5.5, but again the existence of a crossflow was not considered. Detailed measurements of the velocity characteristics of normal impinging jets on a flat surface can be more easily found for single jet configurations for relatively large impingement heights and normally for H/D > 10, using either probe and optical techniques, as reviewed for example by [3] and [11]. Experiments on the aerodynamics of jets through a confined crossflow are much scarcer, and have only been reported for large impingement heights and for low velocity ratios between the jet and the crossflow V_j/U_o. These works have therefore only peripheral relevance to the VSTOL ground effect problem. Ref. [12]-[14] report hot-wire measurements for ratios H/D greater than 24 and for values of V_j/U_o respectively up to 1.95, 2 and 16. Ref. [15] presents results for H/D = 12 and [16] gives Pitot-tube measurements for values of H/D = 3.05 and for jet-to-crossflow velocity ratios up to 6.8. Ref. [17] reports LDV measurements, including those of shear stress, but for values of H/D = 12 and for velocity ratios up to 2.3. Only [3] provided detailed LDV measurements for a single jet configuration for a jet Reynolds number of $Re_j = 6 \times 10^4$, a velocity ratio between the jet and the crossflow of 30, 42 and 73 for the jet exit 3, 4 and 5 jet-diameters above the ground plate. The measurements include time-resolved velocity characteristics along the horizontal and vertical directions, and respective correlations, in planes parallel to the jet nozzle axis [18] [19]. Ref. [20] and [21] extended their study to multijet impinging configurations producing upwash fountain flows, which are the heart of the complicated effects by VSTOL aircraft when they operate in ground proximity, but as far as twin jets are concerned only the geometry with the jets side by side was considered. In the present work the twin jets are aligned with the crossflow, which is the geometry relevant for the next generation of VSTOL aircraft JSF (**Figure 1**).

The remainder of this paper is presented in four sections. Section 2 describes the experimental configuration and measurement procedure, gives details of the laser-Doppler velocimeter and provides assessments of accuracy. The arguments associated with these assessments are based on previous experiments and are presented in condensed form. Section 3 presents the experimental results obtained in the vertical plane of symmetry containing the axis of both jets and quantifies the mean and turbulent velocity characteristics of the flow. The final section summarizes the main findings and conclusions of this work.

2. Experimental Work

The wind tunnel facility designed and constructed for the present work is schematically shown in **Figure 2**. During all the design process, especially for the boundary layer part of the flow, were followed the recommendations of [22] for open circuit wind tunnels. A fan with 15 KW nominal power drives a maximum flow of 3000 m^3/h through the boundary layer wind tunnel of 300 × 302 mm exit section. Each jet unit of 15 mm inner diameter is mounted vertically in the top of the test section with the axis contained in the vertical plane o symmetry parallel to the crossflow.

The origin of the horizontal, X, and vertical, Y, coordinates is taken at the midpoint between the centers of the

Figure 1. Representation of the ground vortex flow phenomena adapted to the JSF F-35 Variant B.

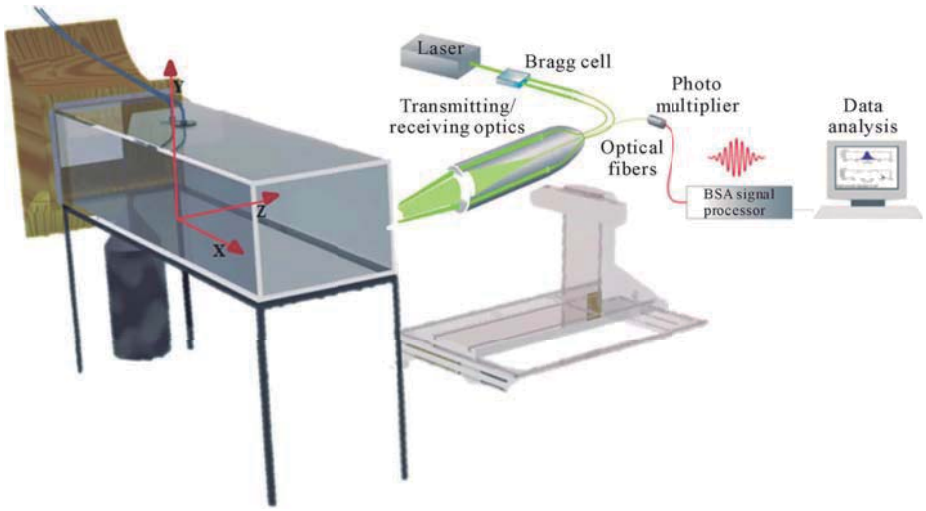

Figure 2. Experimental set-up.

jets exit. The X coordinate is positive in the direction of the wind tunnel exit and Y is positive upwards.

The present results were obtained at the vertical plane of symmetry for jet mean velocities of V_j = 36 m/s and mean crossflow velocity of U_0 = 1.6 m/s, corresponding to a velocity ratio, $V_R = V_j/U_o$ of 22.5.

The velocity field was measured with a two-color (two-component) Laser-Doppler velocimeter (DantecFlow-lite 2D), which comprised a 10 mW He-Ne and a 25 mW diode-pumped frequency doubled Nd:YAG lasers, sensibility to the flow direction provided by frequency shifting from a Bragg cell at f_0 = 40 MHz, a transmission and backward-scattered light collection focal lens of 400 mm. The half-angle between the beams was 2.8˚ and the calculated dimensions of the axis of the measuring ellipsoid volume at the e^{-2} intensity locations were 135 × 6.54 × 6.53 μm and 112 × 5.46 × 5.45 μm respectively (see **Table 1** for details). The horizontal, U, and vertical V, mean and turbulent velocities were determined by a two-velocity channel Dantec BSA F60 processor. The seeding of the flow with glycerin particles of 0.1 - 5 μm was produced by a smoke generator. The transmitting

Table 1. Principal characteristics of the 2D Laser-Doppler velocimeter.

	He-Ne Laser	Diode Laser
Wave length, λ [nm]	633	532
Focal length of focusing lens, f [mm]	400	400
Beam diameter at e-2 intensity [mm]	1.35	1.35
Beam spacing, s [mm]	38.87	39.13
Calculated half-angle of beam intersection, θ	2.78˚	2.8˚
Fringe spacing, δ_f [μm]	6.53	5.45
Velocimeter transfer constant, K [MHz/m·s^{-1}]	0.153	0.183

and collecting optics is mounted on a three-dimensional traversing unit, allowing the positioning of the center of the control volume within ±0.1 mm.

In order to measure the vertical components in near wall regions, the transmitting optics were inclined by half angle of beam intersection and the scattered light was collected off-axis. Measurements could then be obtained up to 0.5 mm from the ground plate without a significant deterioration of the Doppler signals. Results obtained 20 mm above the ground plate with both the on-axis and the off-axis arrangements have shown a close agreement, within the precision of the equipment.

Errors incurred in the measurement of velocity by displacement and distortion of the measuring volume due to refraction on the duct walls and change in the refractive index were found to be negligibly small and within the accuracy of the measuring equipment. Non-turbulent Doppler broadening errors due to gradients of mean velocity across the measuring volume may affect essentially the variance of the velocity fluctuations [23], but for the present experimental conditions are of the order of $10^{-4}V_j^2$ and, therefore, sufficiently small for their effect to be neglected. The largest statistical (random) errors derived from populations of, at least, 10,000 velocity values were of 0.5% and 3%, respectively for the mean and the variance values, according to the analysis recommended by [24] for a 95% confidence interval. No corrections were made for sampling bias, but no correlations were found between Doppler frequencies and time interval between consecutive bursts even in the zones of the flow characterized by the lowest particle arrival rates, suggesting that those effects are unimportant for the present flow conditions.

Systematic errors incurred in the measurements of Reynolds shear stresses can arise from lack of accuracy in the orientation angle on the normal to the anemometer fringe pattern, as shown in [25], and can be particularly large in the vicinity of the zones characterized by zero shear stress: for the present experimental conditions the largest errors are expected to be smaller than −2.5%.

3. Results

In this chapter, experimental data obtained will be presented and discussed under two headings. First, flow visualization is presented, and then mean and turbulent velocity profiles are presented and discussed for the velocity ratios V_R of 22.5.

3.1. Visualization

Flow visualization was performed using digital direct photography to guide the choice of the measurement locations and to provide a qualitative picture of the flow. The longitudinal vertical plane of symmetry was illuminated with a sheet of light. The photos were taken perpendicular to the vertical plane of symmetry. For all the flows studied, the results have shown (for each jet) a pattern similar to that of a single impinging jet. **Figure 3** identifies the flow development along the vertical plane of symmetry, *i.e.* $Z = 0$. Each jet has an initial potential-core jet region, where the flow characteristics are identical to those of a free jet, and near the horizontal plate the impingement region, characterized by considerable deflection of the jet. It was not possible to identify all the regions simultaneously in the same photo, neither a deflection of each jet by the crossflow. The selected picture shows the wall jet corresponding to the upstream impinging jet which is almost parallel to the ground plate and

exhibits a behavior similar to that of a radial wall jet where the upstream effects of interaction due to impingement are no longer important. The upstream wall jet interacts with the crossflow and forms a horseshoe vortex close to the ground plate, which wraps around both impinging jets. As a result, two streamwise counter-rotating vortices develop side-to-side and decay further downstream of each impinging zone forming a ground vortex. The nature of each ground vortex is similar to the horseshoe structure known to be generated by the deflection of a boundary layer by a solid obstacle [26], but is different from the vortex pair known to exist in a "bent-over" jet in a crossflow far from the ground [13]. No evidence of a ground vortex corresponding to the downstream impinging jet could be confirmed, which is an indication that the upstream impinging jet and its ground vortex are blocking the crossflow and provoking an alteration to the flow pattern. If the jets were positioned side by side in front of the crossflowtwoground vortexes would appear as well as a fountain flow in the vertical plane of symmetry due to the collision of the two individual radial wall jets [20] [27]-[29]. In the present case for a velocity ratio between the jet and the crossflow of $V_R = 22.5$ no fountain flow could be detected.

Analysis of **Figure 4** also suggests that the crossflow is deflected sideways by the penetration of the jet and may cause a recirculation region just downstream of the discharge, away from the ground plate, but cannot be clearly identified. These features of the flow are quantified in **Figures 5-7** through a detailed set of mean and turbulent velocity measurements obtained in the vertical plane of symmetry ($Z = 0$) for a Reynolds number

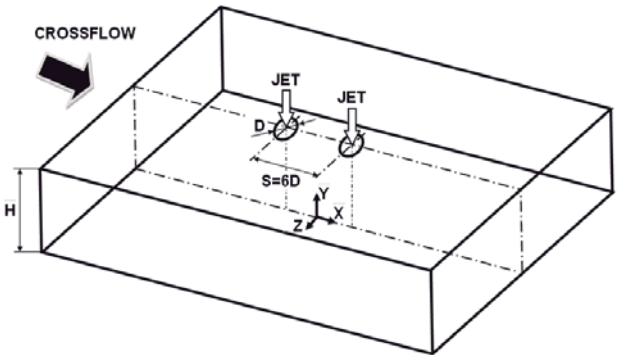

Figure 3. Geometrical arrangement of the jets.

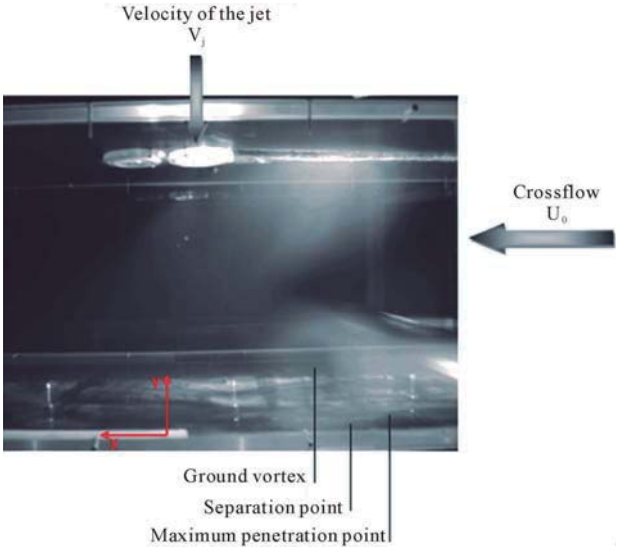

Figure 4. Visualization of the twin jet flow in the vertical plane of symmetry for $Re_j = 4.3 \times 10^4$, $V_j/U_o = 22.5$, H/D = 20.1, and S/D = 6.

based on the jet-exit conditions of 4.3×10^4, a free stream to jet velocity ratio, $V_R = V_j/U_o$ of 22.5, a jet height to jet diameter ratio, H/D, of 20.1, and a spacing between the jets, S/D, of 6.

3.2. Measurements

Figure 5(a) and **Figure 5(b)** show vertical profiles of horizontal, $\overline{U}$, and vertical, $\overline{V}$, mean velocity components along the vertical plane of symmetry ($Z = 0$).

The mean horizontal velocity profiles at X/D = −2.93, −1.47, 0 and +1.47 show negative values near the ground ($Y = 0$) that correspond to the upstream wall jet, revealing that the first impinging jet was deflected by the crossflow. The impinging point of the first jet is located at about X/D = +2.93 in a position that is vertically near the axis of the second jet exit (X/D = +3), which is more strongly deflected due to this interference. As a consequence, the downstream wall jet of the first jet and the second jet seems to merge rapidly in a single flow in the crossflow direction. These profiles exhibit maximum positive (downstream) values of the mean horizontal velocity component between $Y = 100$ mm and 150 mm that reach twice the crossflow velocity. This result can also be confirmed with the help of **Figure 5(b)** that shows only positive values (upwards) of the mean vertical velocity component just 2D downstream of the geometrical axis of the second jet (X/D = +5.0). The second jet is still detected in the profile at X/D = +2.93 by the negative (downwards) values of $\overline{V}$, but only quite near of the upper wall for $Y > 180$ mm (Y/H > 0.596). This means that no upstream wall jet resulting from the second jet exists, but the complete jet is deflected by the crossflow. This result is consistent with the conclusions of [5] that found for a single impinging jet flow that the ground vortex blocks the passage of the confined crossflow increasing the velocity of the crossflow that passes over. So, for the configuration the final result is that the second jet "views" a smaller jet-to-crossflow velocity ratio and no impingement occurs. In the practical situation of a

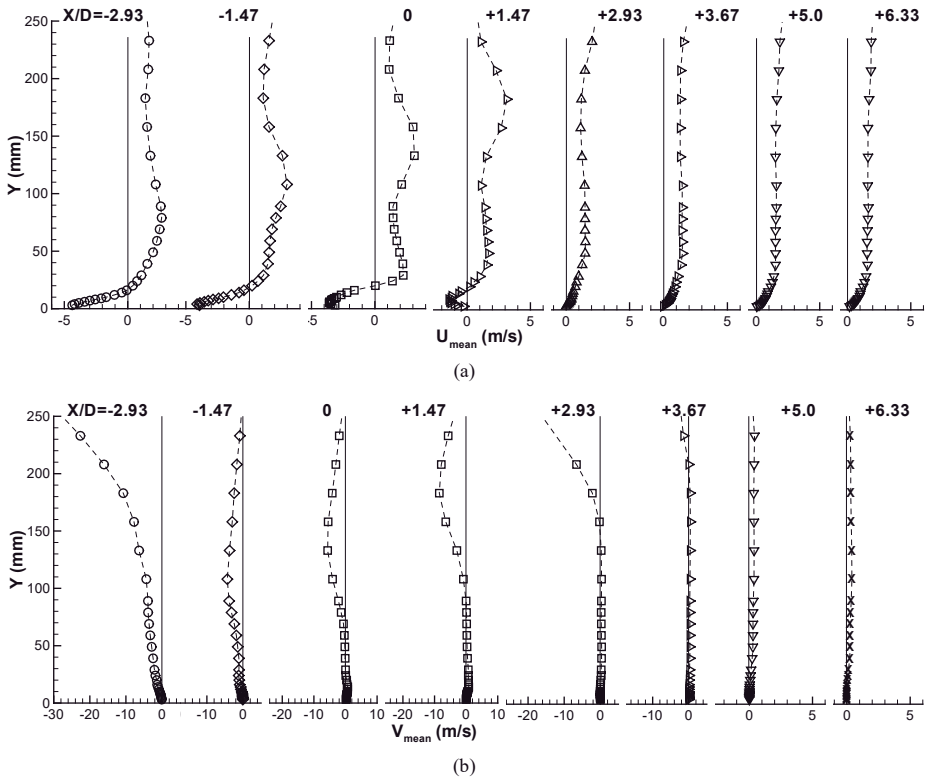

Figure 5. Vertical profiles of the mean velocity characteristics along the longitudinal (symmetry) plane crossing the center of the twin jets. $Re_j = 4.3 \times 10^4$, $V_j/U_o = 22.5$, H/D = 20.1, and S/D = 6. (a) Horizontal velocity, $\overline{U}$. (b) Vertical velocity, $\overline{V}$.

VSTOL aircraft this may result in a different pressure distribution in the under surface of the aircraft, that with front wind or small forward movement may result in enhanced under pressures in the aft part of the aircraft causing a suction down force and a change of the pitching moment towards the ground.

Figure 6(a) and **Figure 6(b)** show horizontal transversal profiles of horizontal, $\overline{U}$, and vertical, $\overline{V}$, mean velocity components, quantify the development of the impinging jets and confirm the above description of the flow. The measurements, and particularly those of the vertical velocity component, do not identify a centrally located fountain rising from the ground plate without interference from the main jets, as it occurs in practical VSTOL applications [29]. This result confirms our hypothesis that the alignment of the twin jets with the crossflow would create a special flow pattern not yet reported before. The wall jet resulting from the first jet flows underneath the second one, but the ground vortex formed upstream is only interfering away from the vertical symmetry plane.

The mean vertical velocity component is always positive from the upper wall (Y/H = 1) up to the middle of the crossflow (Y/H = 0.5), confirming the conclusions drawn from the vertical velocity profiles in the lower part of the crossflow and discussed in the previous paragraphs.

The asymmetry of the flow can be confirmed from the horizontal profiles of the mean vertical velocity component with higher peaks up to 10% of the vertical velocity in the upstream side ($X < -50$ mm or 3.33D). The middle value between the maximum and the minimum of the mean horizontal velocity component or the mean vertical velocity components can be used to indicate the center of the jet, and in the upstream side it moves in the crossflow direction from −43.02 mm at Y/H = 0.92 to 10.47 mm at Y/H = 0.5 corresponding to a deflection angle of 21.9 degrees. The downstream jet is protected from the action of the crossflow by the first jet and as a consequence it is less deflected: the center of the jet is almost coincident with the geometrical axis of the exit, and for Y/H = 0.5 it is located at X/D = +4.0 corresponding to an inclination angle of 12.3 degrees. However, considering the maximum of the mean vertical velocity component the calculated inclination angle is only 4.8 degrees which reinforces the conclusion, and the difference is probably associated with an enhanced entrainment of the second jet due to its smaller angle with the surrounding flow.

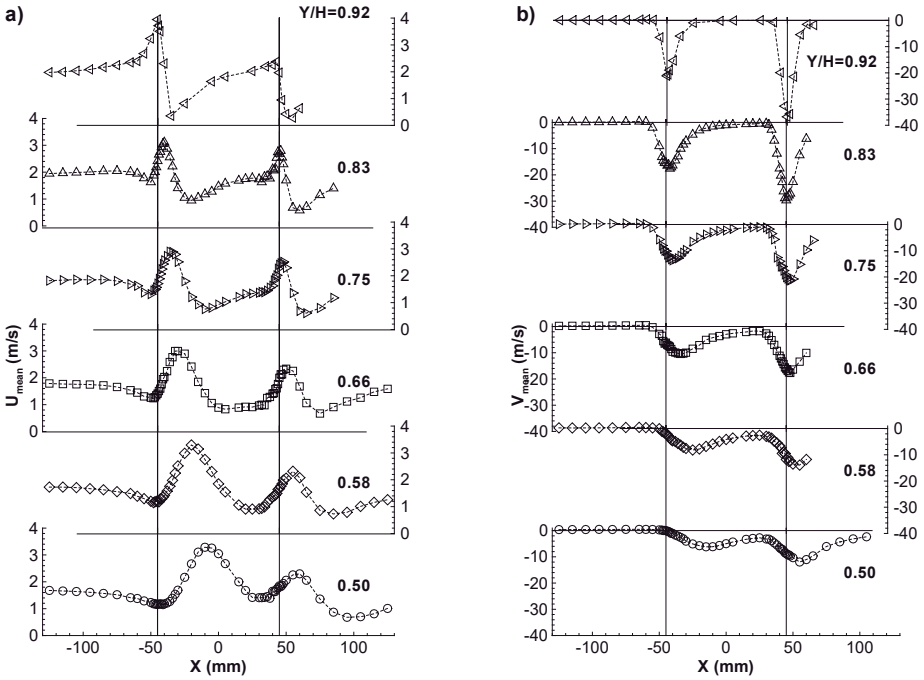

Figure 6. Horizontal profiles of the mean velocity characteristics along the longitudinal (symmetry) plane crossing the center of the twin jets. $Re_i = 4.3 \times 10^4$, $V_i/U_o = 22.5$, H/D = 20.1, and S/D = 6. (a) Horizontal velocity, $\overline{U}$. (b) Vertical velocity, $\overline{V}$.

Figure 7 shows horizontal profiles of the normal stresses, $\overline{u'^2}$ and $\overline{v'^2}$, in a *rms* form, and show results that are somewhat surprising at first sight, because it seems that it is not possible to identify completely the shear layer surrounding the impinging jets.

The peaks in the fluctuating vertical velocity components occur in the upstream side of the first jet as expected, because in this region the higher velocity gradients occur. Other peaks were observed near X = 0 for the X/H = 0.83 and 0.75 that correspond to the downstream side of the first impinging jet. For the X/H = 0.66 the peak is very weak, and for the lower profiles they cannot be pointedly identified, confirming the rapid mixing between the jets as already detected from the lower part of the flow through the vertical velocity profiles.

For the second (downstream) impinging jet the shear layer surrounding the jet cannot be clearly identified. However, for the Y/H = 0.66 profile a small decrease in the normal vertical stress is noted near the center of the jet, but the peaks around the jet are so close that the minimum value is somewhat masked.

4. Conclusions

A laser Doppler velocimeter was used to provide information on the flowfield created by twin impinging jets aligned with a low velocity crossflow. The experiments were carried out for a Reynolds number based on the jet exit conditions of $Re_j = 4.3 \times 10^4$, an impingement height of 20.1 jet diameters, a velocity ratio between the jet exit and the crossflow $V_R = V_j/U_o$ of 22.5, and an inter-jet spacing of S = 6D.

The results show a large penetration of the first (upstream) jet, which is deflected by the crossflow and impinges on the ground, giving rise to a ground vortex due to the collision of the radial wall and the crossflow that wraps around the impinging point like a scarf. This pattern is the usual for and impinging jet through a low velocity crossflow.

The second jet (located downstream) it is less affected by the crossflow in terms of deflection, because it is protected from the influence of the crossflow by the upstream jet. It does not reach the ground. It impinges on the wall jet that flows radially from the impinging point of the first jet.

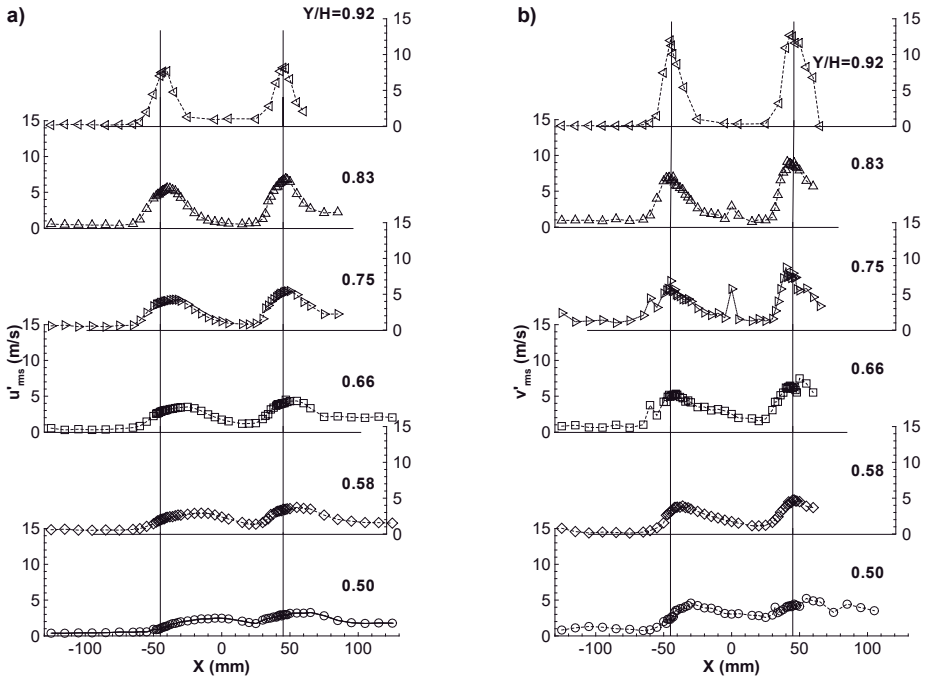

Figure 7. Horizontal profiles of the mean velocity characteristics along the longitudinal (symmetry) plane crossing the center of the twin jets. $Re_j = 4.3 \times 10^4$, $V_j/U_o = 22.5$, H/D = 20.1, and S/D = 6. (a) Horizontal rms velocity, $\sqrt{u'^2}$. (b) Vertical rms velocity, $\sqrt{v'^2}$.

Due to the confinement and the ground vortex, the crossflow is blocked and accelerates in the upper part and also contributes to an enhanced mixing of each secondary flow. As consequence, no upstream wall jet or ground vortex resulting from the second (downstream) jet was detected. The effect of the second jet impinging on the downstream wall jet resulting from the first jet had not been reported so far and requires further investigation.

The shear layers surrounding the jet cannot be clearly identified from the fluctuating velocities that do not exhibit clear peaks in the edges, and the values in the center are also high.

Acknowledgements

The financial support of FCT-Fundação para a Ciência e Tecnologia under contract PTDC/EME-MFE/102190/2008 is gratefully acknowledged.

The present work was done in the scope of the activities of LAETA-Associated Laboratory of Energy, Transports and Aeronautics.

References

[1] Barata, J.M.M., Durão, D.F.G. and McGuirk, J. (1989) *Journal of Aircraft*, **26**, 1002-1008. http://dx.doi.org/10.2514/3.45873

[2] Knowles, K., and Bray, D. (1991) The Ground Vortex Formed by Impinging Jets in Crossflow. *AIAA 29th Aerospace Sciences Meeting*, Reno, 7-10 January 1991, AIAA Paper 91-0768.

[3] Barata, J.M.M. (1989) Numerical and Experimental Study of Jets Impinging on Flat Surfaces through a Crossflow. Ph.D. Thesis, Instituto Superior Técnico, Technical Univ. of Lisbon, Lisbon. (in Portuguese)

[4] Sarippali, K.R. (1987) Laser Doppler Velocimeter Measurements in 3D Impinging Twin-Jet Fountain Flows. In: Durst, F., *et al.*, Eds., *Turbulent Shear Flows*, Vol. 5, Springer-Verlag, Berlin, 147-168. http://dx.doi.org/10.1007/978-3-642-71435-1_14

[5] Kind, R.J. and Suthanthiran, K. (1980) The Interaction of Two Opposing Plane Turbulent Wall Jets. AIAA Paper 72-0211, January.

[6] Gilbert, B.L. (1983) Detailed Turbulence Measurements in a Two Opposing Plane Turbulent Wall Jets. *AIAA 16th Fluid and Plasma Dynamics Conference*, Danvers, 12-14 July 1983, AIAA Paper 83-1678.

[7] Jenkins, R.C. and Hill Jr., W.G. (1977) Investigation of VTOL Upwash Flows Formed by Two Impinging Jets. Grumman Research Dept. Rept. RE-548, Bethpage, November.

[8] Kotansky, D.R. and Glaze, L.W. (1980) The Effects of Ground Wall-Jet Characteristics on Fountain Upwash Flow Formation and Development. Report ONR-CR212-216-1F.

[9] Kavasaoglu, M.S., Schetz, J.A. and Jakubowsky, A.K. (1989) *Journal of Aircraft*, **26**, 793-804. http://dx.doi.org/10.2514/3.45843

[10] Schetz, J.A., Jakubowsky, A.K. and Aoyagi, K. (1984) *Journal of Aircraft*, **21**, 484-490. http://dx.doi.org/10.2514/3.44997

[11] Araújo, S.R.B., Durão, D.F.G. and Firmino, F.J.G. (1981) Jets Impinging Normally and Obliquelly to a Wall. AGARD CP 308, Paper 5.

[12] Sugiyama, Y. and Usami, Y. (1979) *Bulletin of JSME*, **22**, 1736-1745. http://dx.doi.org/10.1299/jsme1958.22.1736

[13] Andreopoulos, J. and Rodi, W. (1984) *Journal of Fluid Mechanics*, **138**, 93-127. http://dx.doi.org/10.1017/S0022112084000057

[14] Shayesteh, M.V., Shabaka, I.M.N.A. and Bradshaw, P. (1985) Turbulent Structure of a Three-Dimensional Impinging Jet in a Crossflow. *AIAA 23rd Aerospace Sciences Meeting*, Reno, 14-17 January 1985, AIAA Paper 85-0044.

[15] Kamotani, Y. and Greber, I. (1974) Experiments on Confined Turbulent Jets in a Crossflow. NASA CR-2392.

[16] Stoy, R.C. and Ben-Haim, Y. (1973) *Journal of Fluids Engineering*, **95**, 551- 556.

[17] Crabb, D., Durão, D.F.G. and Whitelaw, J.H. (1981) *Journal of Fluids Engineering*, **103**, 142-153. http://dx.doi.org/10.1115/1.3240764

[18] Barata, J.M.M., Durão, D.F.G. and McGuirk, J.J. (1989) *Journal of Aircraft*, **26**, 1002-1008. http://dx.doi.org/10.2514/3.45873

[19] Barata, J.M.M., Durão, D.F.G., Heitor, M.V. and McGuirk, J.J. (1993) *Experiments in Fluids*, **15**, 117-129.

[20] Barata, J.M.M. (1996) Ground Vortex Formation with Twin Impinging Jets. *International Powered Lift Conference*, Jupiter, 18-20 November 1996, Artigo SAE 962257.

[21] Barata, J.M.M. (1996) *AIAA Journal*, **34**, 2523-2530.

[22] Metha R.D. and Bradshaw P. (1979) Design Rules for Small Low-Speed Wind Tunnels. *The Aeronautical Journal of the Royal Aeronautical Society*, November.

[23] Durst, F., Melling, A. and Whitelaw, J.H. (1981) Principles and Practice of Laser-Doppler Anemometry. 2nd Edition, Academic Press, New York.

[24] Yanta, W.J. and Smith, R.A. (1973) Measurements of Turbulent Transport Properties with a Laser-Doppler Velocimeter. 11*th Aerospace Sciences Meeting*, Washington DC, 10-12 January 1973.

[25] Melling, A. and Whitelaw, J.H. (1975) *Journal of Fluid Mechanics*, **78**, 285- 315.

[26] Baker, C.J. (1981) *Journal of Wind Engineering and Industrial Aerodynamics*, **6**, 9- 23. http://dx.doi.org/10.1016/0167-6105(80)90018-5

[27] Saripalli, K.R. (1983) *AIAA Journal*, **21**, 483-484. http://dx.doi.org/10.2514/3.8102

[28] Siclari, M.J., Migdal, D., Luzzi Jr., T.W., Barche, J. and Palcza, J.L. (1976) *Journal of Aircraft*, **13**, 938-944. http://dx.doi.org/10.2514/3.58733

[29] Kotansky, D.R. (1981) The Modelling and Prediction of Multiple VTOL Aircraft Flow Fields in Ground Effect. AGARD CP-308, Paper 16.

Nomenclature

D = diameter of the jet
H = impinging height
k = turbulent kinetic energy
Re = Reynolds number
S = distance between the jets axis
U = horizontal velocity, $\overline{U}+u'$
V = vertical velocity, $\overline{V}+v'$
W = transverse $\overline{W}+w'$
X = horizontal coordinate
Y = vertical coordinate
Z = transverse coordinate

Subscripts

j = jet-exit value
o = crossflow value

Scientific Research Publishing (SCIRP) is one of the largest Open Access journal publishers. It is currently publishing more than 200 open access, online, peer-reviewed journals covering a wide range of academic disciplines. SCIRP serves the worldwide academic communities and contributes to the progress and application of science with its publication.

Other selected journals from SCIRP are listed as below. Submit your manuscript to us via either submit@scirp.org or Online Submission Portal.

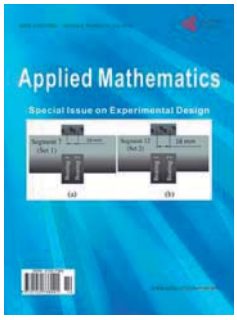

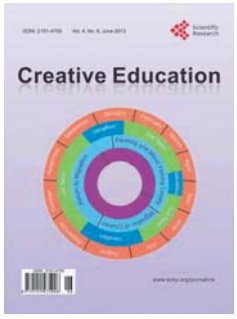

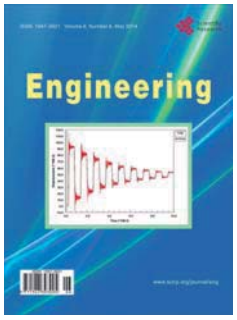

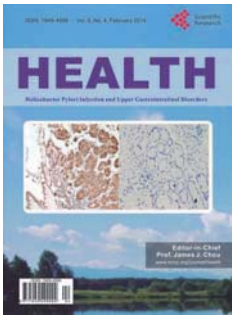

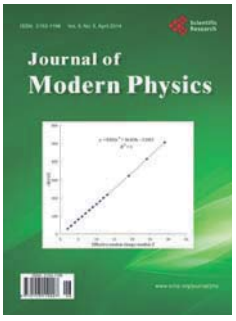

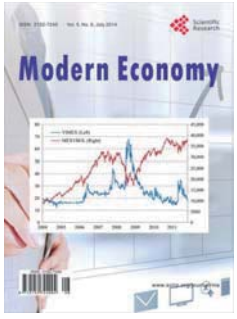

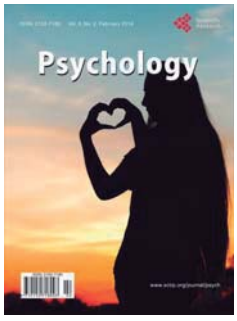

Journal of Engineering and Applied Sciences 10 (6): 123-136, 2015
ISSN: 1816-949X

Numerical Simulation of Twin Impinging Jets in Tandem Through a Crossflow

Diana F.C. Vieira, Jorge, M.M. Barata, Fernando M.S.P. Neves and Andre R.R. Silva
Universidade Beira Interior, 6200-358 Covilha, Portugal

Abstract: The flow field of ground vortex generated by twin impinging jets in tandem through a crossflow is numerically studied in detail. Numerical simulation and visualization are presented for two turbulent circular jets emerging into a low velocity cross stream, impinging after on a flat surface perpendicular to the geometrical jet nozzle axis. The numerical study is based in experimental studies done early, so all the features of the experimental flow were maintained when the numerical simulation was performed. The Reynolds number used was based on the jet exit conditions of 43.000-105.000, a jet to crossflow velocity ratio of 22.5-43.8 an impinging height of 20.1 jet diameters and an interject spacing's of S = 5D and L = 6D. The analysis of the flow was extended to regions and flow conditions for which no measurements have been obtained in last experimental studies, i.e., for velocity ratios of 7.5-60. The numerical results show that for the smallest velocity ratios the jets initially do not mix but remain together in two layers. Three different types of flow regimes were identify, therefore when VSTOL aircrafts operating in ground vicinity, only the regime with strong impingement on ground and with a formation of a ground vortex is relevant. The numerical results allowed to extend the last experimental studies and prove that the deflection of the rear jet is due to the competing influences the wake, the shear layer, the downstream wall jet of the first jet and the crossflow.

Key words: Impinging jets, crossflow, tandem, ground vortex, wake

INTRODUCTION

In external aerodynamics applications such as VSTOL aircrafts, turbulent jets impinging on flat surfaces through a low velocity crossflow are typical of the flow beneath of this type of aircraft. During its landing or near ground hovering phase, the VSTOL aircraft creates a complex three dimensional flow field between the jet streams, the airframe surface and the ground. When ground effect occurs, the lift forces on the aircraft changes cause hot gas re-ingestion into the engine intake and due to the fountain upwash and ground flows, the fuselage skin temperature rises. The unsteadiness of the flow and raise of the temperature cause several problems in the engine performance such as compressor surge or even stall and thrust reduction. In respect to the intake ingestion phenomenon, it is very complex and can be associated with the design and operational parameters such as jet configuration, head wind velocity, jet impingement height or intake configuration. In the case of the hot gas ingestion problem, there are three mechanism involved, i.e., far field ingestion, near field ingestion and ground vortex ingestion. The first mechanism is results of the forward away initially movement of the ground sheet wall jet due to the aircraft movement. This happened because the hot gases after some distance loses its momentum, rising and separating from the ground. The portion of the hot gases that separating from the ground, mixes with the surrounding air and backs again to the intake. The second mechanism, near field ingestion has a much greater impact on hot gas ingestion compared to the first because it directly affected the lift nozzle exits into the surrounding area of the intake being that when exits multiple impinging jets, its impact on the ground plane create a fan shape up wash fountain beneath the aircraft. When the fountain impinges on the underside of the fuselage, flowing from the fuselage to the intake, the engine may sucks the flow to the intake, creating severe temperature distortion to the intake, since, these gases are much hotter than those from the far field ingestion. The latter mechanism is due to the presence of a ground vortex. During a landing or hover the impingement of each downward-directed jet on the ground results in the formation of a wall jet which flows radially from the impinging point along the ground surface. The interaction of this wall jet with the free stream results in the formation of a ground vortex far upstream of the impinging jet. This flow field transports exhaust gases away from the ground and up toward the intake region. The level and intensity of the ingestion resulting from this mechanism depends critically on the forward velocity. If there are two or more adjacent jets, the resulting wall jets meet and a fan-shaped upwash or "fountain" is normally

Corresponding Author: Diana Filipa da Conceicao Vieira, Department of Aerospace Science, University of Beira Interior, 6200-358 Covilha, Portugal

formed between the jets. The fountain upwash flow depending on its strength and direction affects the forces and moments induced in the aircraft when operating in ground effect. The resulting ground vortex shape is strongly affected and the corresponding induced suckdown effect tends to be reduced by the upload produced by the fountain. In the last 30 or 40 years, this type of complex flow fields have been studied extensively but improve the knowledge are ever required because the aircraft design have been changed since its first design and some problems were solved but others were not. Earlier published work has been concentrated on 1, 2 and 3 jets configurations relevant to the AV-8B Harrier II aircraft. In this case when the aircraft operates with small forward movement the configuration of interest are two impinging jets with the direction of the crossflow perpendicular to the line containing their centers.

For the next generation of VSTOL aircrafts F-35 no relevant studies can be found because the impinging jets are aligned with the crossflow and this geometry has not yet been considered. In this case, a vertically oriented lift fan (SDLF) generates a column of cool air that produces the nearly 20,000 pounds of lifting power, along with an equivalent amount of thrust from the vectored rear exhaust (3BSM-Three Bearing Swivel Module). Figure 1 shows the position of the thrust vectoring nozzle and lift fan in the F-35 aircraft. The lift system was successfully demonstrated during a flight test of the X-35B during the Summer of 2001. The complexity of the new VSTOL configuration together with the very stringent requirements has required an enormous amount of R&D in the last decade. On 12th May 2012, the 200th test flight of the F-35B (BF-3) measurement of stresses on the aircraft during supersonic maneuvers was done. Therefore, most of the published work reported so far has only peripheral relevance to the F35-B/JSF ground effect problem.

This study aims presents results that are relevant to the future F-35 VSTOL configuration (Fig. 2), through a detailed analysis of the complex flow field beneath two impinging jets in tandem through a low velocity crossflow.

The present study is a piece of a most comprehensive experimental study on impinging jet flows in ground effect which included two different experimental installations: 2D ground vortex and wind tunnel. Here, the main focus is the extrapolation of the measurements beyond the limits of the latter experimental rig through computational simulations.

Previous detailed measurements of the flow properties for fountain up wash flow are scarce and have been presented essentially in the absence of a crossflow and with the use of probe techniques and more recently with particle image velocimetry. The most relevant works have been reviewed by Barata (1989) and Saripalli (1983) showing high turbulence levels and spreading rates in the fountains (Gilbert, 1983; Nishino *et al*., 1996). In the case (Nishino *et al*., 1996), the turbulent normal stress of the axial component made a substantial contribution to the increase in the static pressure on a region near the impingement plate being the turbulence close an axisymmetric state in the stagnation region. Saripalli (1987) reports Laser Doppler Velocity (LDV) measurements including those of shear stress for axisymmetric impinging jets with an distance between the jet axis, S/D = 9 and 14 with an impinging height, H/D of 3 and 5.5 but again the existence of a crossflow was not considered. Detailed measurements of the velocity characteristics of normal impinging jets on a flat surface (Fig. 3) can be found for single jet configurations for relatively large impingement heights and normally for H/D>10 using either probe or optical techniques as reviewed for example by Barata *et al*. (1993). Crabb *et al*. (1981) reports LDV

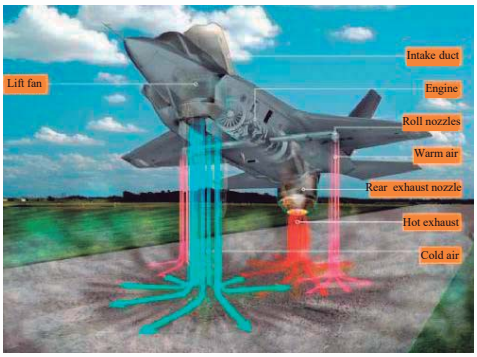

Fig. 1: F-35's thrust vectoring nozzle and lift fan

Fig. 2: F-35 VSTOL configuration

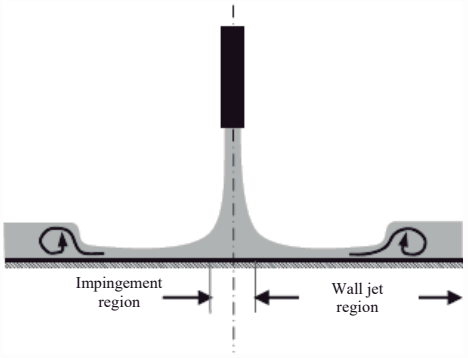

Fig. 3: Schematic of a normal impinging jet on a flat plate or ground (Kate *et al*., 2007)

measurements including shear stress measurements for values of H/D = 12 and for velocity ratios up to 2.3. Only Barata (1989) provided detailed LDV measurements for a single jet configuration for a jet with Reynolds number $Re_j = 6\times10^4$, a velocity ratio between the jet, V_j and the crossflow, U_0, $V_R = V_j/U_0$ of 30, 42 and 73 with jet exit above the ground plate 3, 4 and 5 diameters. The measurements include time-resolved velocity characteristics along the horizontal, vertical directions with respective correlations in planes parallel to the jet nozzle axis.

Barata (1996a, b) extended their study to multi jet impinging configurations producing upwash fountain flows (Fig. 4) which are the heart of the complex effects produced by VSTOL aircraft when they operate in ground proximity but as far as twin jets are concerned only the geometry with the jets side by side was considered. Experiments on the aerodynamics of jets through a confined crossflow are scarcer and have only been reported for large impingement heights and for low velocity ratios between the jet and the crossflow V_j/U_0. Therefore, these works have only peripheral relevance to the VSTOL ground effect problem with the same geometry of the F-35. Behrouzi and McGuirk (2000) studied the experimental data of the intake in a short take off and vertical landing aircraft in ground effect through laser Doppler measurements. The results confirmed that the flow pattern produced with the impingement height and velocity ratio parameters selected were typical of practically occurring re-ingestion flow fields. Researchers also did this study to obtain results as benchmark validation data for time averaged Turbulence Model based RANS CFD predictions. Kolar *et al*. (2003) reports a hot-wire anemometry measurements for two different (tandem and side by side) twin jets arrangement for values

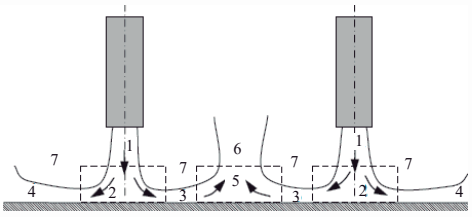

Fig. 4: Schematic of the upwash fountain flow by two impinging jets: 1: Free jet, 2: Jet impingement region, 3: Inner wall jet region, 4: Outer wall jet region, 5: Fountain formation region, 6: Fountain upwash flow and 7: Entrainment (Kate *et al*., 2007)

of V_j/U_0 to equals 8. The results show that the vorticity distribution, vortex strength, transverse penetration ability and intensity of vorticity transport were strongly dependent function of the geometrical parameters. More recently a brief survey of the recent studies of twin jets in crossflow was carried out by Kolar and Savory (2007), show that the tadem configurations have rapid mixing and great penetration into the crossflow than side by side configurations.

They also report how the transverse penetration ability and vortex strength are subject to the nozzle arrangement and they found that all cases of twin jets in crossflow lead qualitatively to the some dominant vertical structures, counter rotating vortex pair being responsible by convective entrainment. An important characteristic of two impingement jets with the presence of a crossflow are the fountain upwash flow produced by the collision of the wall jets and the entrainment of ambient air into different regions of the flow (Saripalli, 1983). Kate *et al*. (2007) studied the spreading flow due to the normal impingement of two closely spaced liquid jets. The visualization results allowed the researchers to conclude that depending on the spacing between the two jets and their relative strength, different kinds of thin film interactions are possible, resulting in a variety of flow pattern. Saddington *et al*. (2005) also studied the fountain flow for two under expanded, axisymmetric and turbulent impinging jets on a ground plane using Laser Doppler Velocimetry and Particle Image Velocimetry. It was identify the presence of a large scale structures on the fountain flow and at the stagnation region with high degree at asymmetry. Some experimental work published about impingement jet in crossflow not only quantified the flow field but also the heat transfer characteristics. Wae-Hayee *et al*. (2014) reports oil film technique for values of V_j/U_0 up to 33, 5 and 7 for an impinging jeta small jet to plate distance, H/D = 2. The results show that

the Nusselt number peak shifts downstream and increases with the increase of crossflow velocity. In order to explore the convective heat transfer of an impinging jet in a crossflow, Li *et al.* (2014) report a study where the enhancement factor was found to increase with the jet-to-crossflow mass ratio and the Reynolds number but decrease with the jet diameter. The presence of a crossflow was observed to degrade the heat transfer performance. Caliskan and Baskaya (2012) report a laser Doppler anemometry and an infrared thermal imaging study for two different impingement height, H/D = 3 and 12 for a smooth surface and a V-shaped ribs. When the jet to plate spacing was low the V-SR surface showed higher values of turbulent kinetic energy and Nusselt number, being the Nusselt number at the stagnation point decrease with the increase in H/D.

Most of the computational work published on jets with crossflow has been based on integral methods admitting assumptions simplified which are only capable of predicting global effects such as trajectories and jet cross-section shapes, for example Adler and Baron (1979) and Patankar *et al.* (1979) employed a finite-difference numerical procedure together with a two-equation Turbulence Model to predict a single jet in an unconfined crossflow and obtained good agreement with the experiments by Knowles and Bray (1991) for velocity ratios from 2-10. A similar approach was used by Jones and McGuirk (1980) to calculate the confined flow measured by Kamotani and Greber (1974). The gross features of the flow are well predicted but the calculations appear to exhibit diffusion rates larger than those consistent with measured profiles which can be attributed either to numerical or Turbulence Model errors. Grids up to 20×15×15 nodes were used but further grid refinement is essential to identify the precise source of disagreement between measurements and predictions. Knowles (1996) has shown that the standard "k-ε" Model over predicts the spreading rate of a free jet and under predicts the spreading rate of a radial wall jet. Barata *et al.* (1991) and Worth and Yang (2006) used the steady-RANS or SRANS approach but the results did not capture the turbulent structure of the fountain flow and impingement regions being the predicted turbulent quantities particularly poor. Recently, Yang (2014) reports a numerical study employing the Unsteady-RANS or URANS approach, comparing the results with (Barata *et al.*, 1991). Compared the results with the computational results with the SRANS approach by Worth and Yang (2006), the URANS approach was the one that better agreement with the experimental data. Fan *et al.* (2006) employed in their numerical studies large eddy simulation and RNG Turbulence Model. Fan *et al.* (2006) detected the formation and evolution of the steady or quasi-steady vortical structures by the interaction of an impinging jet in a confined crossflow but without reference to the instantaneous flow patterns by the RNG "k-ε" Turbulence Model. However, in this two works (Fan *et al.*, 2006) the forming and time evolution characteristics of highly 3D vertical structures are not well understood due to the limitations of the two computational methods being the mixing of the ambient crossflow fluid by the unsteady vertical structures in the near wall regions not fully exposed. Abdel-Fattah (2007) presented a comparison of experimental data and computational simulation about an impinging jet without crossflow for different impingement heights, 3<H/D<12, jet to jet spacing and jet angle, 0°<θ<20°. The results showed that the stagnation primary point moves away in the radial main flow direction with jet angle increase and become stronger with the jet to jet spacing increase. The pressure at the stagnation point located at the middle between the two jets increase with the jet angle but decrease with the Reynolds number. The increase of the impingement height decreases the intensity of the re-circulation zone in the middle of the jets and the jet spreading. An identical numerical study was reported by Yang and Shyu (1998) but the main focus of the study was the study of heat characteristics with the modification of the jet angle. The increase of the jet angle showed a downstream move of the maximum local nusselt number and the maximum pressure. When compared with the Reynolds number, the jet angle proved to have a more significant effect on the recirculation zone. Miao *et al.* (2009) report a numerical study with different crossflow orientations and jet to surface spacing. The study revealed that the flow exit crossflow e orientation affected significantly the developing jet flow fields and the Nusselt number. Aldabbagh and Sezai (2002a, b) and Aldabbagh and Mohamad (2006) studied the flowfield and the heat transfer for square array impinging jets for different impingement height where the local Nusselt number reduces with the increase of the H/D but the number of jets combined not affected the heat characteristics.

MATERIALS AND METHODS

Flow configuration: The experiments were performed on a wind tunnel facility designed and constructed for the present work with an exit section of 300×402 mm that is schematically shown in Fig. 5. The test section was made of Perspex allowing the passage of laser beams. During all the design process special consideration was taken for the boundary layer in which the recommendations by

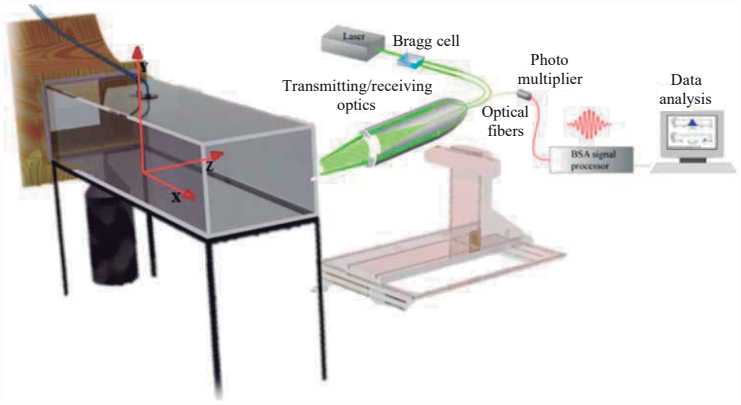

Fig. 5: Experimental set-up

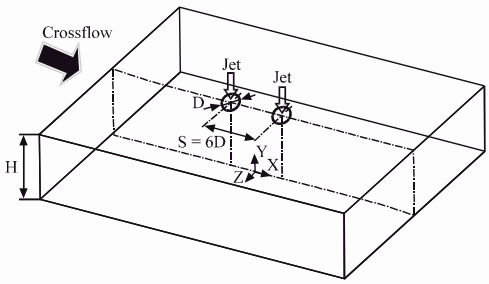

Fig. 6: Geometrical arrangement of the jets

Durst *et al.* (1976) for open circuit wind tunnels was followed. A fan with 15 kW nominal power drives a maximum flow of 3000 m^3/h through the boundary layer wind tunnel exit section.

In the present study each jet unit of 15 mm of inner diameter is mounted vertically in the top of the test section 20.1D above the ground plane with the axis contained in the vertical plane of symmetry parallel to the crossflow as showed schematically in Fig. 6.

The origin of the horizontal, X and vertical, Y, coordinates is taken at the midpoint between the centers of the jets exit. The X coordinate is positive in the direction of the wind tunnel exit and Y is positive upwards. The present results were obtained at the vertical plane of symmetry for jet mean velocity of $V_j = 36$ msec, a jet Reynolds number of $Re_j = 4.3\times10^4$ and mean crossflow velocities of $U_o = 0.8$ msec, corresponding to a velocity ratio, $V_R = V_j/U_o = 43.8$.

Visualization technique: Flow visualization was performed using digital direct photography to guide the choice of the measurement locations and to provide a qualitative picture of the flow.

The longitudinal plane of symmetry was illuminated with a sheet of light. This sheet was used to illuminate any cross section that has been seeded with seeding particles. The laser light reflected from the seeding particles but dark images was observed where there was an absence of seeding particles. The photos were taken perpendicular to the vertical plane of symmetry.

Computational method: This study presents a numerical analysis based on the experimental data presented by Vieira *et al.* (2013). The objective of the numerical simulation is to compare the numerical predictions with the experimental data in order to quantify the performance of the computational model and to extend the analysis of the flow.

Mathematical model: The mathematical model used in the numerical simulation is based on the solution of the continuity and momentum equations. A Reynolds-Averaged Navier Stokes (RANS) formulation was adopted with the "k-ε" Turbulence Model to represent the turbulent stresses. The governing equations are written in a similar form:

$$\frac{\partial}{\partial x}(\rho u\phi)+\frac{1}{r}\frac{\partial}{\partial r}(r\rho v\phi)=\frac{\partial}{\partial x}\left(\Gamma_\phi\frac{\partial\phi}{\partial x}\right)+\frac{1}{r}\frac{\partial}{\partial r}\left(r\Gamma_\phi\frac{\partial\phi}{\partial r}\right)+S_\phi \quad (1)$$

where, the property ϕ represents the velocity, turbulent kinetic energy or dissipation while S_ϕ and Γ_ϕ assume different values related with ϕ as described in Table 1. The turbulent diffusion terms are approximated by two equations from "k-ε" Turbulent Model where the Reynolds tension is related with shear tension:

Table 1: Differential equations coefficients

Φ	Γ_Φ	S_Φ
1	0	0
U	μ_T	$-\frac{\partial p}{\partial x}+\frac{\partial}{\partial x}\left(\mu_T\frac{\partial U}{\partial x}\right)+\frac{1}{r}\frac{\partial}{\partial r}\left(r\mu_T\frac{\partial V}{\partial x}\right)$
V	μ_T	$-\frac{\partial p}{\partial r}+\frac{\partial}{\partial x}\left(\mu_T\frac{\partial U}{\partial r}\right)+\frac{1}{r}\frac{\partial}{\partial r}\left(r\mu_T\frac{\partial V}{\partial r}\right)-2\mu_T\frac{V}{r^2}$
k	μ_T/σ_k	$\Phi-\rho\varepsilon$
ϵ	μ_T/σ_k	$C_{\varepsilon 1}\Phi\frac{\varepsilon}{k}-C_{\varepsilon 2}\rho\frac{\varepsilon^2}{k}$

Γ_ϕ: Transport coefficient; ε: Turbulent kinetic energy dissipation; μ_T: Turbulent viscosity; ρ: Density; σ_k, σ_ε: Turbulent prandtl/schmidt numbers; ϕ: Variable in general conservation equation; Φ: Turbulent kinetic energy production term; j: Jet-exit value; o: Crossflow value

Table 2: Turbulent Model constants

C_μ	C_1	C_2	σ_k	σ_E
0.09	1.44	1.92	1.0	1.3

$$\rho\overline{u'_i u'_j} = -\mu_T\left(\frac{\partial U_i}{\partial x_j}+\frac{\partial U_j}{\partial x_{ij}}\right)+\frac{2}{3}\delta_{ij}\rho k \qquad (2)$$

where, μ_T represent turbulent viscosity derivative from the Turbulent Model expressed by:

$$\Phi = \mu_T\left\{2\left[\left(\frac{\partial U}{\partial x}\right)^2+\left(\frac{\partial V}{\partial r}\right)^2+\left(\frac{V}{r}\right)^2\right]+\left[\frac{\partial U}{\partial r}+\frac{\partial V}{\partial x}\right]^2\right\} \qquad (3)$$

Where:

k = Turbulent kinetic energy
r = Radius of cylindrical coordinates
S_Φ = Source term
U = Horizontal velocity, $\bar{U}+u'$ ($U_{mean}+u'$)
V = Vertical velocity, $\bar{V}+v'$ ($V_{mean}+v'$)
W = Transverse $\bar{W}+w'$ ($W_{mean}+w'$)
X = Horizontal coordinate
Y = Vertical coordinate
Z = Transverse coordinate

The computational domain (Fig. 7) corresponds to the experimental conditions and has 201 mm of transversal length, remaining constant the following measurements as followed: 1080 mm of longitudinal length, 402 mm of height where the inner diameter of the jets D is 15 mm, the spacing between jets are S = 6D and the height of impact, H is 20.1 D. The Turbulent Model constants allow good results for several types of flows and are summarized in Table 2. To reduce the computational costs and to reduce the time simulation of the flow, we only simulation half of the test section.

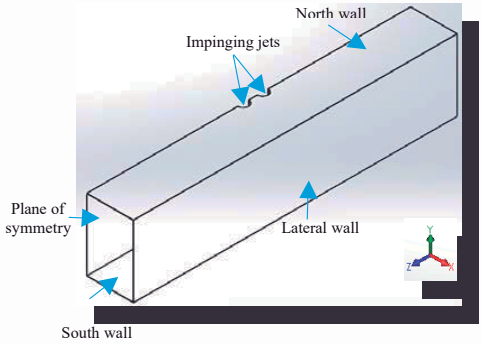

Fig. 7: Computational domain used in the numerical simulation

RESULTS AND DISCUSSION

The results presented and discussed in this section are to the flow visualization for the velocity ratio V_R of 43.8.

Visualization results: For the flow studied, the result has shown a pattern similar to that of a single impinging jet. Figure 8 identifies the flow development along the vertical plane of symmetry, i.e., Z = 0. Each jet has an initial potential-core jet region where the flow characteristics are identical to those of a free jet and near the horizontal plate the impingement region, characterized by considerable deflection of the first jet. Analysing Fig. 8, it is clear that for this velocity ratio the deflection of the first jet is small. In the case of the rear jet deflection, we can verify that it is quite small compared with the first jet deflection because the first jet protects the rear jetof the influence of the crossflow and there was not impact of the rear jet on the ground for the lower velocity ratio. However, it is notorious a drop (Fig. 8c) in the rear jet potential core region that it has not been reported in literature. The horseshoe vortex resulting from the interaction of the upstream wall jet with the crossflow could not be clearly identified for this velocity ratio. The nature of each ground vortex is similar to the horseshoe structure known to be generated by the deflection of aboundary layer by a solid obstacle but is different from the vortex pair known to exist in a "bent-over" jet in a crossflow far from the ground. Figure 8e shows that the crossflow is deflected sideways by the penetration of the jet and may cause a recirculation region just downstream of the discharge, away from the ground plate but cannot be clearly identified. Also, it is possible see a little ground vortex and the wall jet corresponding to the upstream impinging jet which is almost parallel the ground plate and

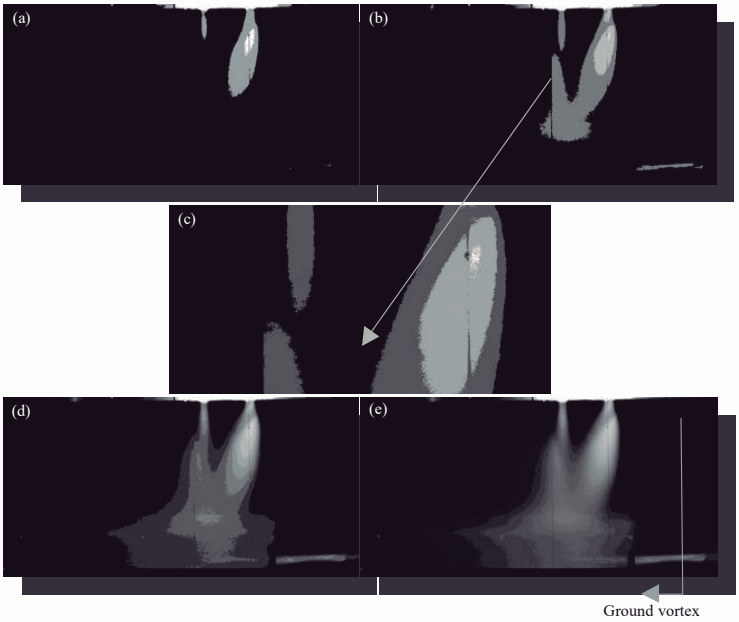

Fig. 8: a-e) Visualization of the twin jet flow in the vertical plane of symmetry in different phases of the flow development for $Re_j = 4.3\times10^4$, H/D = 20.1 and S/D = 6

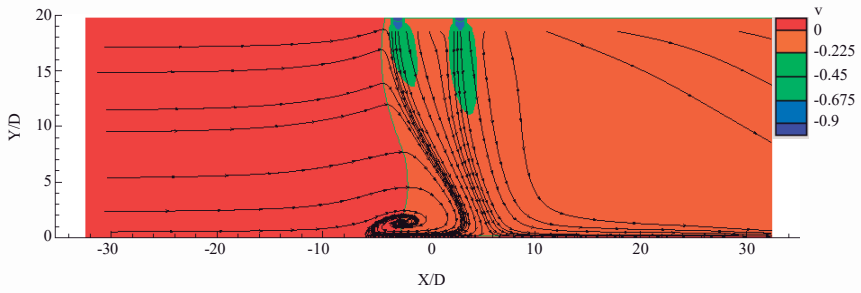

Fig. 9: Calculated stream traces and mean vertical velocity component distribution along the vertical plane of symmetry (i.e., Z = 0). $V_j/U_0 = 22.5$, $Re_j = 43{,}000$, H/D = 20.1 and L/D = 6

exhibit a behaviour similar to that of a radial wall jet where the upstream effects of interaction due to impingement are no longer important. The upstream wall jet interacts with the crossflow and forms a horseshoe vortex close to the ground plate which wraps mostly around the first impinging jet. As a result, two stream wise counter-rotating vortices develop side-to-side and decay further downstream of each impinging zone forming a ground vortex. If the jets were positioned side by side in front of the crossflow two ground vortexes would appear as well as a fountain flow in the vertical plane of symmetry due to the collision of the two individual radial wall jets (Barata, 1996a, b; Saripalli, 1987). No evidence of a ground vortex corresponding to the downstream impinging jet could be confirmed which is an indication that the upstream impinging jet and its ground vortex are blocking the crossflow and provoking an alteration to the flow pattern. Also in the present study no fountain flow was detected.

Numerical results: This study presents a numerical study to extend the analysis of the flow to regions and flow conditions for which no measurements have been obtained. The numerical method is based on the solution

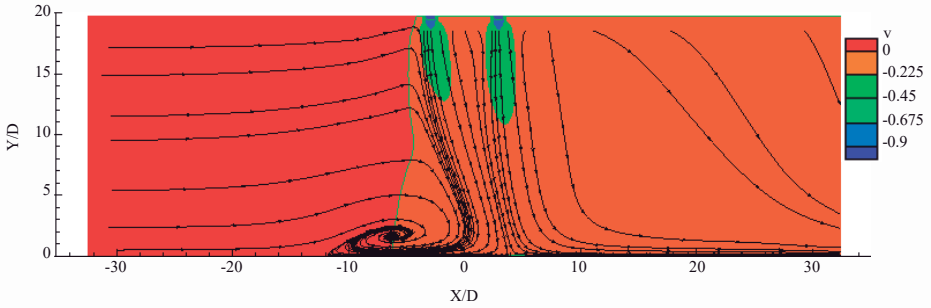

Fig. 10: Calculated stream traces and mean vertical velocity component distribution along the vertical plane of symmetry (i.e., Z = 0). V_j/U_0 = 33.7, Re_j = 43,000, H/D = 20.1 and L/D = 6

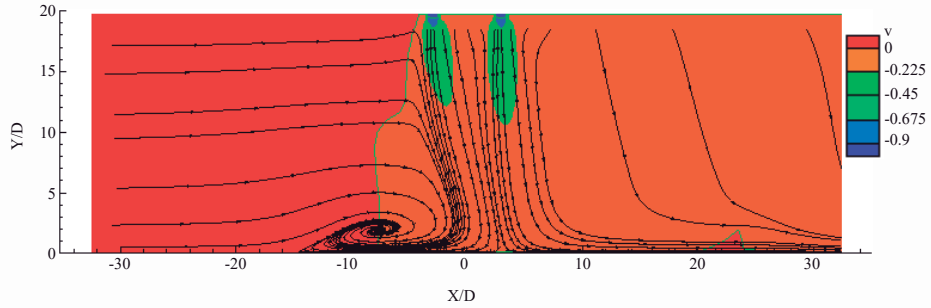

Fig. 11: Calculated stream traces and mean vertical velocity component distribution along the vertical plane of symmetry (i.e., Z = 0). V_j/U_0 = 43.8, Re_j = 43,000, H/D = 20.1 and L/D = 6

of the conservation laws for mass and momentum which is a modified version of the method described else where (Barata *et al*., 1989).

Figure 9-11 show the mean vertical velocity component (V_{mean}) distribution along the vertical plane of symmetry (i.e., Z = 0) together with calculated stream traces. For all velocity ratios the collision of the upstream wall jet with the crossflow is clearly registered. Meanwhile, the ground vortex is also identified for all velocity ratios but its centre change with the velocity ratio applied because the increase of the velocity ratio corresponds to a decrease in crossflow velocity. Comparing this result with that obtained experimentally (Vieira *et al*., 2013, 2014) we can confirm that the deflection sensed by the first jet experimentally is greater than the jet deflection felt numerically thus leading for example for V_j/U_0 = 33.7, the centre of the ground vortex is located close to X/D = -4 in the experimental case, whereas for the numerical case it is located close to X/D = -7. As far as the downstream jet (rear jet) is concerned the predictions confirmed the experimental results (Vieira *et al*., 2013, 2014) and its complete deflection by the crossflow was calculated for all the velocity ratios considered with no impingement directly on the wall. Figure 12 shows in more detail the central zone between the two jets with white stream traces that begin near the top wall. The results show that even for the smallest velocity ratios of V_j/U_0 = 7.5 and 15 the jets do not mix but remain together in two layers. As a consequence for V_j/U_0 = 15 the downstream jet does not reach directly the ground but it impinges on the wall jet resulting from the first jet which is moving downstream. For the two higher velocity ratios the ground vortex is always present but its size and location changes. It moves upstream with V_j/U_0 because increasing the velocity ratio in volves decreasing the relative influence of the crossflow velocity. Barata (2013a, b) identified three different types of flow regimes but for a V/STOL aircraft operating in ground vicinity the regime with strong impingement on the ground and a ground vortex is the most relevant. However in transition from hover to horizontal flight the other regimes are also important.

One major issue in the present flow configuration is the possible deflection of the rear jet by the first jet

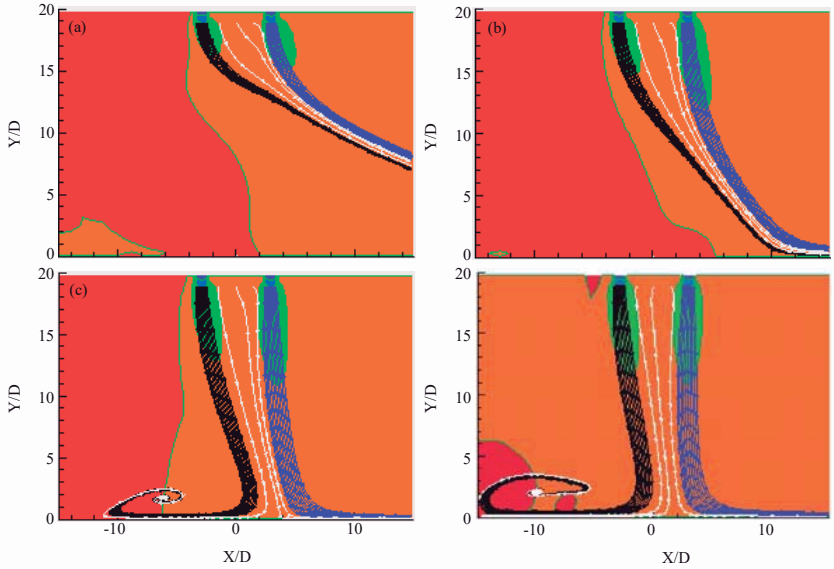

Fig. 12: Details of the calculated stream traces and mean vertical velocity component distribution along the vertical plane of symmetry (i.e., Z = 0). $Re_j = 4.3\times10^4$, H/D = 20.1 and L/D = 6: a) $V_j/U_0 = 7.5$; b) $V_j/U_0 = 15.0$; c) $V_j/U_0 = 33.7$ and d) $V_j/U_0 = 60.0$

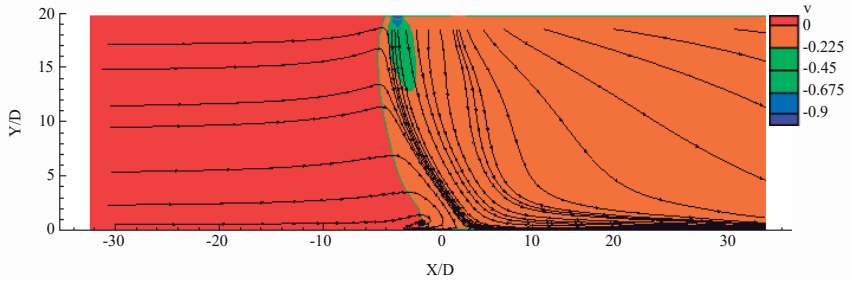

Fig. 13: Calculated stream traces and mean vertical velocity component distribution along the vertical plane of symmetry, Z = 0. $Re_j = 43{,}000$, H/D = 20.1, L/D = 6, $V_{j2} = 5.4$ m sec^{-1}

without occurring impact on the ground. Another possibility (not yet demonstrated) is the impact of the second jet with the first deflected jet or its downstream wall (depending on the velocity ratio).

Any of the figure presented above it is sufficiently conclusive about these hypothesis nor about the blending of the two structures further downstream. In order to better understand this type of flow and in particular that happened with the rear jet and downstream of the impinging jets, a meticulous numerical study simulation was performed for $V_j/U_0 = 22.5$ by varying the velocity of the second jet, V_{j2} from 5.4 m sec^{-1} up to 36 m sec^{-1}. The velocity of the first jet was kept constant to preserve the location of the centre of the ground vortex.

Despite being varied the second jet velocity from 5.4, up to 36 m sec^{-1}, it was only possible to view significant changes on the flow to $V_{j2} \leq 13.5$ m sec^{-1}. Figure 13 and 14 show the results for V_{j2} = 5.4 and 13.5 m sec^{-1}, respectively.

Both figures show that lowering the velocity of the second jet in relation to the first jet, the wall jet of the second jet is always above the wall jet formed by the interaction of the first jet with the crossflow, heading the flow to downstream. The location of the ground vortex is practically not affected by this change in the second jet velocity, confirming that the second jet does not contribute to the occurrence of this structure.

In order to investigate the possible existence of a kidney shape of the crossection of the jets and their

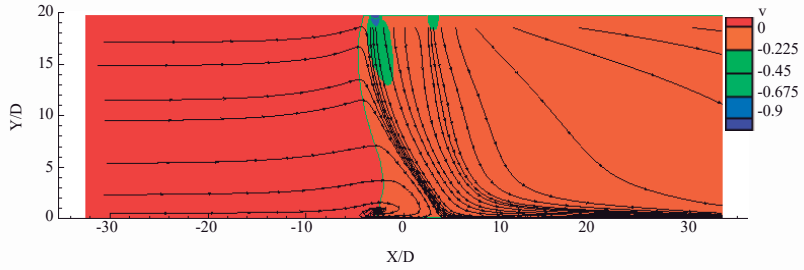

Fig. 14: Calculated stream traces and mean vertical velocity component distribution along the vertical plane of symmetry, Z = 0. Re_j = 43,000, H/D = 20.1, L/D = 6, V_{j2}= 13.5 m sec^{-1}

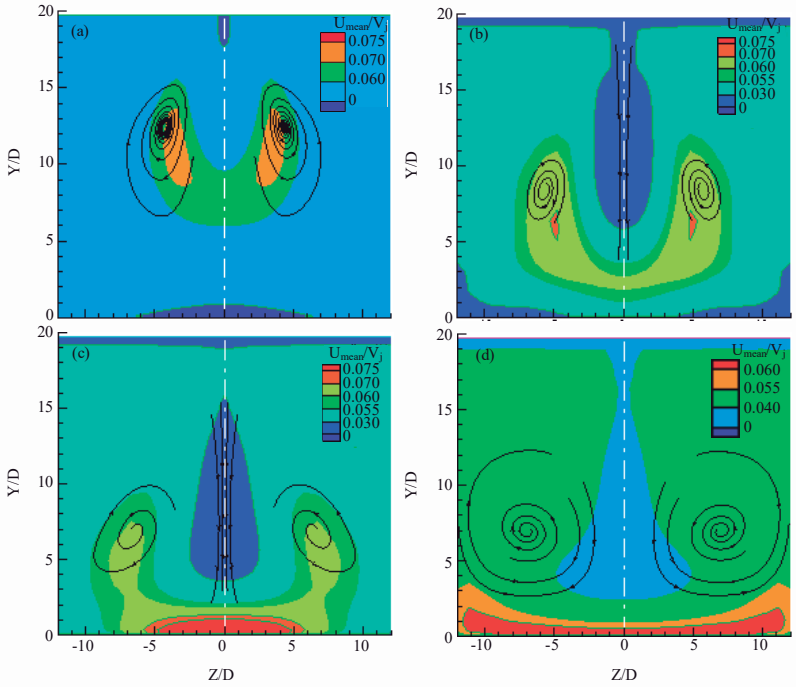

Fig. 15: Mean velocity component (U_{mean}/V_{j1}) in a vertical plane perpendicular to crossflow (Re_{j1} = 43,000, V_{j2} = 5.4 m sec^{-1}, Re_{j2} = 5,339, H/D = 20.1, L/D = 6): a) X/D = 0.0; b) X/D = 4.9; c) X/D = 9.8 and d) X/D = 19.6

mutual interactions, isolines of the velocity component U_{mean} were obtained in vertical planes perpendicular to the crossflow for X/D = 0.0, 4.9, 9.8 and 19.6. Figure 15 and 16 show the results for V_{j2} = 5.4 and V_{j2}= 13.5 m sec^{-1}, respectively. For X/D = 0, i.e. in the middle between the axis of the jets exit, the kidney shape can be clearly identified for the first jet (the second jet it is not yet visible because its exit is further downstream).

For X/D = 4.9, the second jet can be identified by the dark blue area corresponding to velocities larger than 0.03 V_{j1} that reveals the slight deflection of the second jet inside the wake of the first impinging jet. The kidney shape of the cross section of the first jet is still present but it is widening rapidly due to the additional influence of the second imping jet. It should be pointed out that the impinging jet and first jet do not mix and are separated by lower values of the velocity component in the crossflow direction (light blue). Additionally, no stream traces from the second jet are captured by the deflected upstream jet, revealing that a complete mixing between the two jets has not yet occurred. However, from this location downstream (in the crossflow direction) the second impinging jet will

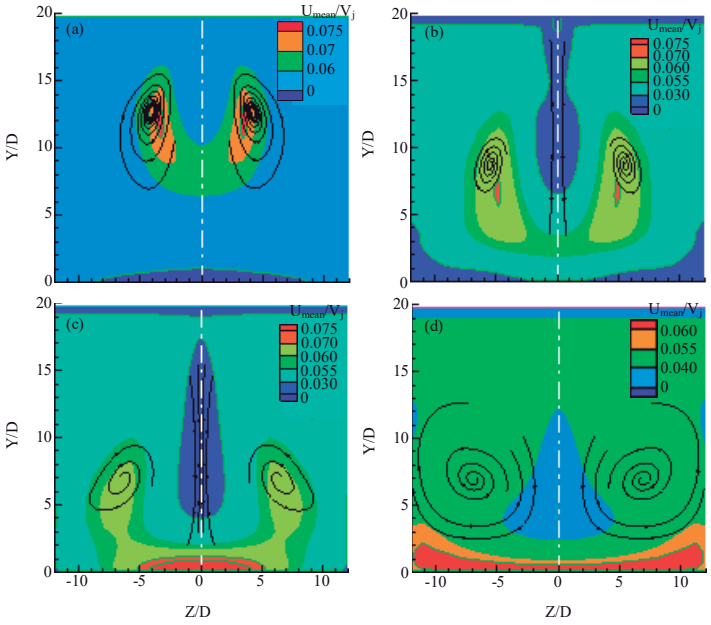

Fig. 16: Mean velocity component (U_{mean}/V_{j1}) in a vertical plane perpendicular to crossflow (Re_{j1} = 43,000, V_{j2} = 13.5 m sec^{-1}, Re_{j2} = 16,125, H/D = 20.1, L/D = 6): a) X/D = 0.0; b) X/D = 4.9; c) X/D = 9.8 and d) X/D = 19.6

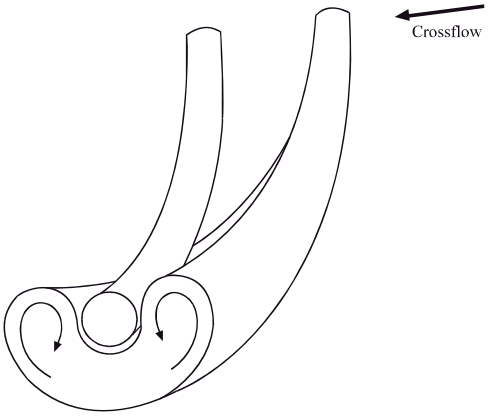

Fig. 17: Illustration of the kidney shape of the cross section of the first jet before reaching the ground and the second (downstream) jet interaction

suffer two opposing effects: first the fact that is developing in the wake of the first impinging jet will contribute to its less deflection and secondly since it is impinging in a flow moving in the crossflow direction with a higher velocity it will be forced to deflect. This novel flow configuration that occurs before the first jet reaching the ground is schematically shown in Fig. 17. So, the final behaviour of the second jet can be described as the flow of a jet through a zero or small upstream crossflow (corresponding to the wake of the first jet) impinging on a horizontal jet with a kidney cross section flowing in the crossflow direction with a higher velocity. In the next downstream location, at X/D = 9.8, the red area identifies a region with relatively large positive values of the velocity component U_{mean} (in the crossflow direction) which is an indication that the first jet touched the ground. The rear jet impacts on this wall jet (resulting from the first jet) and is quickly deflected but does not reach the ground. For X/D = 19.6, the entire cross section is occupied by two vortical structures rotating in opposite directions, revealing that the two parallel jets flowing in the crossflow direction finally merge.

CONCLUSION

The flow field created by ground vortex generated by twin impinging jets in tadem through a crossflow is studied in detail. Flow visualization and numerical simulation are presented for two turbulent circular jets impinging on a flat surface perpendicular to the geometrical nozzle axis, through a low velocity crossflow. The numerical simulation were performed

for Reynolds based on the jet exit conditions of 43,000-105,000, a jet-to-crossflow velocity ratio between 15 and 60 being the focus of the study the velocity ratio used in experimental research (Vieira *et al*., 2013, 2014) for an impinging height of 20.1 diameters (the same used in experimental work) and with an interjet spacing of S = 6D (the same used in experimental work).

The results show a large penetration of the first (upstream) jet which is deflected by the crossflow and impinges on the ground giving rise to a ground vortex due to the collision of the radial wall and the crossflow that wraps around the impinging point like a scarf. The first jet deflection and the location of the ground vortex depend on the velocity ratioused. For higher velocity ratios the deflection of the first jet is smaller and closer to the first jet is located the centre of the ground vortex. The rear jet it is not so affected by the crossflow in terms of deflection for all velocity ratios because it is protected by the upstream jet but due to the downstream wall jet that flows radially from the impinging point the first jet does not reach the ground. Also due to the confinement and the ground vortex, the crossflow is blocked and accelerates in the upper part and also contributes to an enhanced mixing of each secondary flow. As consequence, no upstream wall jet or ground vortex resulting from the second (downstream) jet was detected. The effect of the rear jet impinging on the downstream wall jet resulting from the first jet had not been reported so far and requires further investigation.

In case of the numerical analysis beyond the rig experimental limits there sults show that for the two lowest velocity ratios, the jets do not mix remaining in two layers together and therefore, it is not detected the presence of ground vortex. For V_j/U_0 = 33.7 and 60 the ground vortex is completely present and it moves with the increase of V_j/U_0.

As far as the downstream jet (rear jet) is concerned the predictions confirmed the experimental results obtain by Vieira *et al*. (2013) and its complete deflection by the crossflow was calculated for all the velocity ratios considered with no impingement directly on the wall. By changing the rear jet velocity and extracting perpendicular planes to the jets flow was possible to prove that the second jet is deflected quickly, never reaching the ground thus proving the accuracy of the experimental results, leading us to conclude that impinging jet in tandem configuration, the downstream jet is entrained by the upstream jet and not by the crossflow itself. In the future, this issue should be further investigated in order to understand what the real consequence for the air craft when this type of phenomenon occurs.

ACKNOWLEDGEMENTS

The assistance of Ms. Ines Carvalho with some illustrations of the flow field is gratefully acknowledged. The present research was done in the scope of the activities of LAETA-Associated Laboratory of Energy, Transports and Aeronautics and funded by FCT-Fundacao para a Ciencia e Tecnologia through contract PTDC/EME-MFE/102190/2008 and grant SFRH/BD/86434/2012.

REFERENCES

Abdel-Fattah, A., 2007. Numerical and experimental study of turbulent impinging twin-jet flow. Exp. Therm. Fluid Sci., 31: 1061-1072.

Adler, D. and A. Baron, 1979. Prediction of a three-dimensional circular turbulent jet in crossflow. AIAA J., 17: 168-174.

Aldabbagh, L.B.Y. and A.A. Mohamad, 2006. Effect of jet-to-plate spacing in laminar array jets impinging. Heat Mass Trans., 43: 265-273.

Aldabbagh, L.B.Y. and I. Sezai, 2002a. Numerical simulation of three-dimensional laminar multiple impinging square jets. Int. J. Heat Fluid Flow, 23: 509-518.

Aldabbagh, L.B.Y. and I. Sezai, 2002b. Numerical simulation of three-dimensional laminar, square twin-jet impingement on a flat plate, flow structure and heat transfer. Numeric. Heat Trans. Part A: Applic.: Int. J. Comput. Methodol., 41: 835-850.

Barata, J.M.M., 1989. Numerical and experimental study of jets impinging on flat surfaces through a crossflow. Ph.D. Thesis, Technical University of Lisbon, Lisbon, Portugal.

Barata, J.M.M., 1996a. Fountain flows produced by multiple impinging jets in a crossflow. AIAA J., 34: 2523-2530.

Barata, J.M.M., 1996b. Ground vortex formation with twin impinging jets. Proceedings of the International Powered Lift Conference, November 18-20, 1996, Jupiter, Florida.

Barata, J.M.M., 2013a. Multiple jet/wall/cross-wind interaction relevant to VSTOL ground effects. Proceedings of the International Powered Lift Conference, August 12-14, 2013, Los Angeles, California.

Barata, J.M.M., 2013b. Twin impinging jets aligned with a crossflow. Proceedings of the 49th AIAA/ASME/SAE/ASEE Joint Propulsion Conference and Exhibit, July 15-17, 2013, San Jose, California.

Barata, J.M.M., D.F.G. Durao and J.J. McGuirk, 1989. Numerical study of single impinging jets through a crossflow. J. Aircraft, 26: 1002-1008.

Barata, J.M.M., D.F.G. Durao and J.J. McGuirk, 1991. Impingement of single and twin turbulent jets through a crossflow. AIAA J., 29: 595-602.

Barata, J.M.M., D.F.G. Durao, M.V. Heitor and J.J. McGuirk, 1993. On the analysis of an impinging jet on ground effects. Exp. Fluids, 15: 117-129.

Behrouzi, P. and J.J. McGuirk, 2000. Experimental data for CFD validation of the intake ingestion process in STOVL aircraft. Flow Turbulence Combustion, 64: 265-277.

Caliskan, S. and S. Baskaya, 2012. Velocity field and turbulence effects on heat transfer characteristics from surfaces with V-Shaped ribs. Int. J. Heat Mass Trans., 55: 6260-6277.

Crabb, D., D.F.G. Durao and J.H. Whitelaw, 1981. A round jet normal to a crossflow. J. Fluids Eng., 113: 142-153.

Durst, F., A. Melling and J.H. Whitelaw, 1976. Principles and Practice of Laser-Doppler Anemometry. 2nd Edn., Academic Press, New York, USA., ISBN-13: 9780122252501, Pages: 405.

Fan, J.Y., D.Z. Wang and Y. Zhang, 2006. Large-scale vortical structures produced by an impinging density jet in shallow crossflow. Applied Math. Mech., 27: 363-369.

Gilbert, B.L., 1983. Detailed turbulence measurements in a two opposing plane turbulent wall jets. Proceedings of the AIAA 16th Fluid and Plasma Dynamics Conference, July 12-14, 1983, Danvers, MA.

Jones, W.P. and J.J. McGuirk, 1980. Computation of a Round Turbulent Jet Discharging into a Confined Crossflow. In: Turbulent Shear Flows 2: Selected Papers from the Second International Symposium on Turbulent Shear Flows, Imperial College London, July 2-4, 1979, Bradbury, L.J.S. (Ed.). Springer Verlag, Heidelberg, German, ISBN-13: 9783540100676, pp: 223-245.

Kamotani, Y. and I. Greber, 1974. Experiments on confined turbulent jets in cross flow. Technical Report, NASA-CR-2392; NAS 1.26:2392, Washington, DC., USA., March 1974.

Kate, R.P., P.K. Das and S. Chakraborty, 2007. An experimental investigation on the interaction of hydraulic jumps formed by two normal impinging circular liquid jets. J. Fluid Mech., 590: 355-380.

Knowles, K. and D. Bray, 1991. The ground vortex formed by impinging jets in crossflow. Proceedings of the AIAA 29th Aerospace Sciences Metting, January 7-10, 1991, Reno, NV.

Knowles, K., 1996. Computational studies of impinging jets using k-ε Turbulence Models. Int. J. Numer. Meth. Fluids, 22: 799-810.

Kolar, V. and E. Savory, 2007. Dominant flow features of twin jets and plumes in crossflow. J. Wind Eng. Ind. Aerodynamics, 95: 1199-1215.

Kolar, V., H. Takao, T. Todoroki, E. Savory, S. Okamoto and N. Toy, 2003. Vorticity transport within twin jets in crossflow. Exp. Therm. Fluid Sci., 27: 563-571.

Li, G., Y. Zheng, G. Hu and Z. Zhang, 2014. Convective heat transfer enhancement of a rectangular flat plate by an impinging jet in cross flow. Chin. J. Chem. Eng., 22: 489-495.

Miao, J.M., C.Y. Wu and P.H. Chen, 2009. Numerical investigation of confined multiple-jet impingement cooling over a flat plate at different crossflow orientations. Numer. Heat Transfer Part A: Applic., 55: 1019-1050.

Nishino, K., M. Samada, K. Kasuya and K. Torii, 1996. Turbulence statistics in the stagnation region of an axisymmetric impinging jet flow. Int. J. Heat Fluid, 17: 193-201.

Patankar, S.V., D.K. Basu and S.A. Alpay, 1979. Prediction of the three-dimensional velocity field of a deflected turbulent jet. J. Fluids Eng., 99: 758-762.

Saddington, A.J., P.M. Cabrita and K. Knowles, 2005. Large-scale instabilities in a STOVL upwash fountain. Proceedings of the 6th International Symposium on Engineering Turbulence Moddelling and Measurements, May 23-25, 2005, Cagliari, Italy.

Saripalli, K.R., 1983. Visualization of multijet impingement flow. AIAA J., 21: 483-484.

Saripalli, K.R., 1987. Laser Doppler Velocimeter Measurements in 3-D Impinging Twin-Jet Fountain Flows. In: Turbulent Shear Flows 5: Selected Papers from the Fifth International Symposium on Turbulent Shear Flows, Cornell University, Ithaca, New York, USA, August 7-9, 1985, Durst, F., B.E. Launder, J.L. Lumley, F.W. Schmidt and J.H. Whitelaw (Eds.). Springer-Verlag, Berlin, Germany, ISBN-13: 978-3-642-71435-1, pp: 147-168.

Vieira, D.F.C., A.R.R. Silva, P. Carvalho, F. Neves and J.M.M. Barata, 2013. Numerical and experimental study of two impinging jets in a row through a crossflow. Proceedings of the AIAA 51th Aerospace Science Meeting Including the New Horizons Forum and Aerospace Exposition, January 7-10, 2013, Texas.

Vieira, D.F.C., D.F.G. Durao, F.M.S.P. Neves, A.R.R. Silva and J.M.M. Barata, 2014. Laser doppler measurements of twin impinging jets in taderm through a crossflow. Proceedings of the 17th International Symposium on Applications of Laser Techniques to Fluid Mechanics Lisbon, July 7-10, 2014, Portugal.

Wae-Hayee, M., P. Tekasakul, S. Eiamsa-Ard and C. Nuntadusit, 2014. Effect of cross-flow velocity on flow and heat transfer characteristics of impinging jet with low jet-to-plate distance. J. Mech. Sci. Technol., 28: 2909-2917.

Worth, N.A. and Z. Yang, 2006. Simulation of an impinging jet in a crossflow using a Reynolds stress transport model. Int. J. Numer. Meth., 52: 199-211.

Yang, Y.T. and C.H. Shyu, 1998. Numerical study of multiple impinging slot jets with an inclined confinement surface. Numer. Heat Transfer Part A: Applic., 33: 23-27.

Yang, Z., 2014. Assessment of unsteady-RANS approach against steady-RANS approach for predicting twin impinging jets in a cross-flow. Congent Eng., Vol. 1. 10.1080/23311916.2014.936995.

Annex 2

Papers published in Conferences

AIAA 2012-1219

Twin Impinging Jets Through a Crossflow

J.M.M. Barata , F.M.S.P. Neves , D.F.C. Vieira , A.R.R. Silva
Universidade da Beira Interior
Covilhã, Portugal

50th AIAA Aerospace Sciences Meeting including the New Horizons Forum and Aerospace Exposition

9-12 January 2012/ Gaylord Opryland Resort & Convention Center, Nashville, Tennessee

Twin Impinging Jets Through a Crossflow

J.M.M. Barata[1], F.M.S.P. Neves[2], D.F.C. Vieira[3], André R.R. Silva[4]
Universidade Beira Interior, Covilhã, 6200-358, Portugal

Laser Doppler measurements provide information on the flowfield created by twin impinging jets aligned with a low velocity crossflow. The experiments were carried out for a Reynolds number based on the jet exit conditions of Re_j=4.3x10^4, an impingement height of 20.1 jet diameters and for a velocity ratio between the jet exit and the crossflow $V_R=V_j/U_o$ of 22.5, and an interjet spacing of S=6D. The results show a large penetration of the first (upstream) jet that is deflected by the crossflow and impinges on the ground, giving rise to a ground vortex due to the collision of the radial wall and the crossflow that wraps around the impinging point like a scarf. The second jet (located downstream) it is not so affected by the crossflow in terms of deflection, but due to the downstream wall jet that flows radially from the impinging point of the first jet it does not reach the ground. The results indicate a new flow pattern not yet reported so far, that for a VSTOL aircraft operating in ground vicinity with front wind or small forward movement may result in enhanced under pressures in the aft part of the aircraft causing a suction down force and a change of the pitching moment towards the ground.

Nomenclature

D	=	diameter of the jet
H	=	impinging height
k	=	turbulent kinetic energy
Re	=	Reynolds number
S	=	distance between the jets axis
U	=	horizontal velocity, $\overline{U} + u'$
V	=	vertical velocity, $\overline{V} + v'$
W	=	transverse $\overline{W} + w'$
X	=	horizontal coordinate
Y	=	vertical coordinate
Z	=	transverse coordinate
Subscripts		
j	=	jet-exit value
o	=	crossflow value

I. Introduction

TURBULENT jets impinging on flat surfaces through a low-velocity crossflow are typical in impingement cooling applications in industry, as well as of the flow beneath a short/vertical take-off aircraft which is lifting off or landing with zero or small forward momentum. Ground effect may occur and change the lift forces on the aircraft, cause reingestion of exhaust gases into the engine intake and raise fuselage skin temperatures. In this latter application the impingement of each downward-directed jet on the ground results in the formation of a wall jet which flows radially from the impinging point along the ground surface. The interaction of this wall jet with the free stream results in the formation of a ground vortex far upstream of the impinging jet, which has profound implications on the aircraft design[1,2]. In addition the collision of the wall jets originates a fountain upwash flow, affecting the forces and moments induced in the aircraft when operating in ground effect. Improved knowledge of

[1] Full Professor, Aerospace Sciences Department, Associate Fellow of AIAA. Corresponding author.
[2] Ph. D. Student, Aerospace Sciences Department, Student Member of AIAA.
[3] M.Eng. Student, Aerospace Sciences Department.
[4] Assistant Professor, Aerospace Sciences Department, Member of AIAA.

impinging flows is therefore necessary to avoid these effects and to be able to model a range of jet-impingement type of applications with practical interest.

This paper presents a detailed analysis of the complex flow field beneath twin jets through a low-velocity crossflow and provides a quantitative picture of the main features of interest of impingement type of flows. The results include laser-Doppler velocity measurements of flow characteristics, which are complemented by flow visualization.

Earlier detailed measurements of the flow properties of fountain upwash are scarce and have been presented essentially in the absence of a crossflow and with the use of probe techniques. The most relevant works have been reviewed Refs. 3 and 4, and indicated high turbulence levels and spreading rates in the fountains (e.g. Refs. 5 and 6). Different interpretations of the measurements presented due to the difficulties in measuring complex flows using hot-film and pitot-probe techniques[7,8]. Refs. 9 and 10 also presented flowfield and pressure data for twin-rectangular jets for small jet-to-crossflow velocity ratios (<10). Ref. 4 reports laser Doppler velocity (LDV) measurements, including those of shear stress, for axisymmetric impinging jets with S/D=9 and 14 and H/D=3 and 5.5, but again the existence of a crossflow was not considered. Detailed measurements of the velocity characteristics of normal impinging jets on a flat surface can be more easily found for single jet configurations for relatively large impingement heights and normally for H/D>10, using either probe and optical techniques, as reviewed for example by Ref. 3 and 11. Experiments on the aerodynamics of jets through a confined crossflow are much scarcer, and have only been reported for large impingement heights and for low velocity ratios between the jet and the crossflow V_j/U_o. These works have therefore only peripheral relevance to the VSTOL ground effect problem. Refs. 12-14 report hot-wire measurements for ratios H/D greater than 24 and for values of V_j/U_o respectively up to 1.95, 2 and 16. Ref. 15 presents results for H/D=12 and Ref. 16 gives pitot-tube measurements for values of H/D=3.05 and for jet-to-crossflow velocity ratios up to 6.8. Ref. 17 reports LDV measurements, including those of shear stress, but for values of H/D=12 and for velocity ratios up to 2.3. Only Ref. 3 provided detailed LDV measurements for a single jet configuration for a jet Reynolds number of Rej=$6x10^4$, a velocity ratio between the jet and the crossflow of 30, 42 and 73 for the jet exit 3, 4 and 5 jet-diameters above the ground plate. The measurements include time-resolved velocity characteristics along the horizontal and vertical directions, and respective correlations, in planes parallel to the jet nozzle axis[18,19]. Refs. 20 and 21 extended their study to multijet impinging configurations producing upwash fountain flows, which are the heart of the complicated effects by VSTOL aircraft when they operate in ground proximity, but as far as twin jets are concerned only the geometry with the jets side by side was considered. In the present work the twin jets are aligned with the crossflow, which is the geometry relevant for the next generation of VSTOL aircraft JSF (Fig. 1).

Figure 1. Representation of the ground vortex flow phenomena adapted to the JSF F-35 Variant B.

The remainder of this paper is presented in four sections. Section II describes the experimental configuration and measurement procedure, gives details of the laser-Doppler velocimeter and provides assessments of accuracy. The arguments associated with these assessments are based on previous experiments and are presented in condensed form. Section III presents the experimental results obtained in the vertical plane of symmetry containing the axis of both jets and quantifies the mean and turbulent velocity characteristics of the flow. The final section summarizes the main findings and conclusions of this work

II. Experimental Method

The wind tunnel facility designed and constructed for the present work is schematically shown in Fig. 2. During all the design process, especially for the boundary layer part of the flow, were followed the recommendations of Ref. 22 for open circuit wind tunnels. A fan with 15KW nominal power drives a maximum flow of 3000m^3/h through the boundary layer wind tunnel of 300x302mm exit section. Each jet unit of 15mm inner diameter is mounted vertically in the top of the test section with the axis contained in the vertical plane o symmetry parallel to the crossflow.

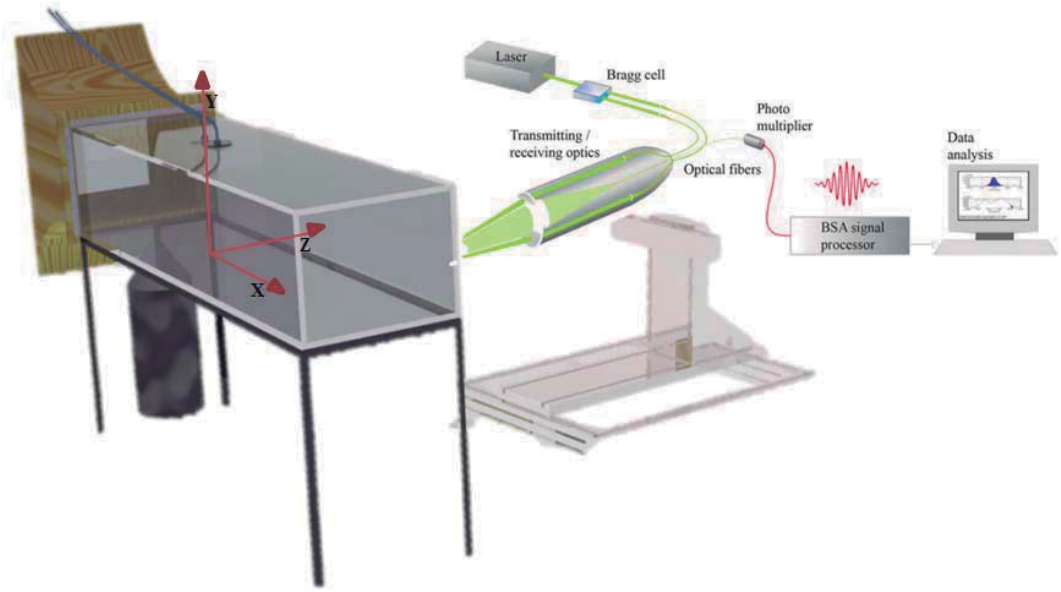

Figure 2. Experimental set-up.

The origin of the horizontal, *X*, and vertical, *Y*, coordinates is taken at the midpoint between the centers of the jets exit. The *X* coordinate is positive in the direction of the wind tunnel exit and *Y* is positive upwards.

The present results were obtained at the vertical plane of symmetry for jet mean velocities of V_j=36m/s and mean crossflow velocity of U_0=1.6m/s, corresponding to a velocity ratio, $V_R=V_j/U_o$ of 22.5.

The velocity field was measured with a two-color (two-component) Laser-Doppler velocimeter (Dantec Flowlite 2D), which comprised a 10mW He-Ne and a 25mW diode-pumped frequency doubled Nd:YAG lasers, sensivity to the flow direction provided by frequency shifting from a Bragg cell at f_0=40MHz, a transmission and backward-scattered light collection focal lens of 400mm. The half-angle between the beams was 2.8° and the calculated dimensions of the axis of the measuring ellipsoid volume at the e^{-2} intensity locations were 135x6.54x6.53µm and 112x5.46x5.45µm respectively (see Table 1 for details). The horizontal, *U*, and vertical *V*, mean and turbulent velocities were determined by a two-velocity channel Dantec BSA F60 processor. The seeding of the flow with glycerin particles of 0.1-5µm was produced by a smoke generator. The transmitting and collecting optics is mounted on a three-dimensional transversing unit, allowing the positioning of the centre of the control volume within ±0.1mm.

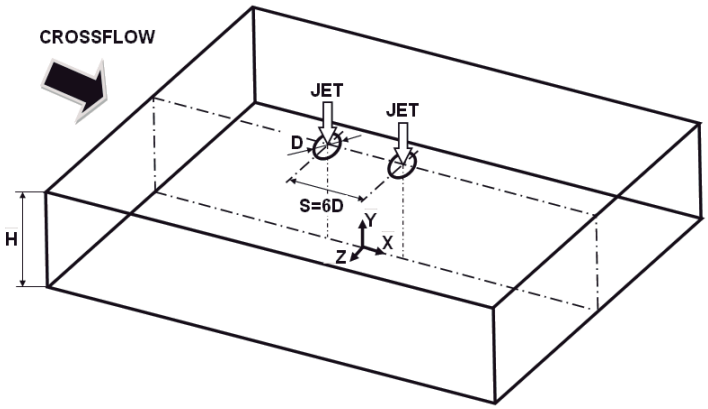

Fig. 3 Geometrical arrangement of the jets

In order to measure the vertical components in near wall regions, the transmitting optics were inclined by half angle of beam intersection and the scattered light was collected off-axis. Measurements could then be obtained up to 0.5mm from the ground plate without a significant deterioration of the Doppler signals. Results obtained 20mm above the ground plate with both the on-axis and the off-axis arrangements have shown a close agreement, within the precision of the equipment.

Errors incurred in the measurement of velocity by displacement and distortion of the measuring volume due to refraction on the duct walls and change in the refractive index were found to be negligibly small and within the accuracy of the measuring equipment. Non-turbulent Doppler broadening errors due to gradients of mean velocity across the measuring volume may affect essentially the variance of the velocity fluctuations[23], but for the present experimental conditions are of the order of $10^{-4}V_j^2$ and, therefore, sufficiently small for their effect to be neglected. The largest statistical (random) errors derived from populations of, at least, 10000 velocity values were of 0.5 and 3%, respectively for the mean and the variance values, according to the analysis recommended by Ref. 24 for a 95% confidence interval. No corrections were made for sampling bias, but no correlations were found between Doppler frequencies and time interval between consecutive bursts even in the zones of the flow characterized by the lowest particle arrival rates, suggesting that those effects are unimportant for the present flow conditions.

Table 1. Principal characteristics of the 2D Laser-Doppler velocimeter.

	He-Ne laser	Diode Laser
- Wave length, λ [nm]	633	532
- Focal length of focusing lens, f [mm]	400	400
- Beam diameter at e-2 intensity [mm]	1.35	1.35
- Beam spacing, s [mm]	38.87	39.13
- Calculated half-angle of beam intersection, θ	2.78^o	2.8^o
- Fringe spacing, δ_f [μm]	6.53	5.45
- Velocimeter transfer constant, K [MHz/ms^{-1}]	0.153	0.183

Systematic errors incurred in the measurements of Reynolds shear stresses can arise from lack of accuracy in the orientation angle on the normal to the anemometer fringe pattern, as shown by Ref. 25, and can be particularly large in the vicinity of the zones characterized by zero shear stress: for the present experimental conditions the largest errors are expected to be smaller than -2.5%.

III. Results

In this chapter, experimental data obtained will be presented and discussed under two headings. First, flow visualization is presented, and then mean and turbulent velocity profiles are presented and discussed for the velocity ratios V_R of 22.5.

A. Visualization

Flow visualization was performed using digital direct photography to guide the choice of the measurement locations and to provide a qualitative picture of the flow. The longitudinal vertical plane of symmetry was illuminated with a sheet of light. The photos were taken perpendicular to the vertical plane of symmetry. For all the flows studied, the results have shown (for each jet) a pattern similar to that of a single impinging jet. Fig. 4 identifies the flow development along the vertical plane of symmetry, i.e. Z=0. Each jet has an initial potential-core jet region, where the flow characteristics are identical to those of a free jet, and near the horizontal plate the impingement region, characterized by considerable deflection of the jet. It was not possible to identify all the regions simultaneously in the same photo, neither a deflection of each jet by the crossflow. The selected picture shows the wall jet corresponding to the upstream impinging jet which is almost parallel to the ground plate and exhibits a behavior similar to that of a radial wall jet where the upstream effects of interaction due to impingement are no longer important. The upstream wall jet interacts with the crossflow and forms a horseshoe vortex close to the ground plate, which wraps around both impinging jets. As a result, two streamwise counter-rotating vortices develop side-to-side and decay further downstream of each impinging zone forming a ground vortex. The nature of each ground vortex is similar to the horseshoe structure known to be generated by the deflection of a boundary layer by a solid obstacle[26], but is different from the vortex pair known to exist in a "bent-over" jet in a crossflow far from the ground[27]. No evidence of a ground vortex corresponding to the downstream impinging jet could be confirmed,

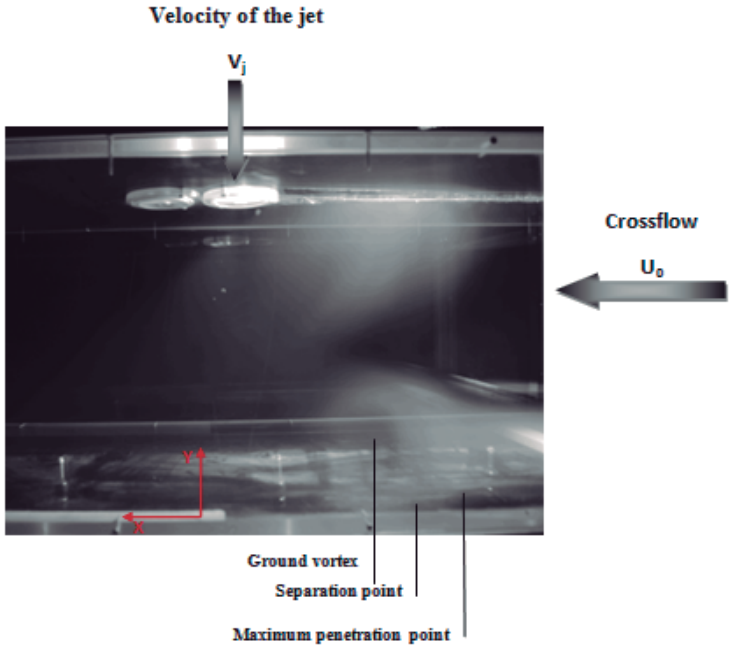

Fig. 4 Visualization of the twin jet flow in the vertical plane of symmetry for Re_j=4.3x10^4, V_j/U_o=22.5, H/D=20.1, and S/D=6.

which is an indication that the upstream impinging jet and its ground vortex are blocking the crossflow and provoking an alteration to the flow pattern. If the jets were positioned side by side in front of the crossflow two ground vortexes would appear as well as a fountain flow in the vertical plane of symmetry due to the collision of the two individual radial wall jets (e.g., Refs. 20, 27-29). In the present case for a velocity ratio between the jet and the crossflow of V_R = 22.5 no fountain flow could be detected.

Analysis of Fig. 4 also suggests that the crossflow is deflected sideways by the penetration of the jet and may cause a recirculation region just downstream of the discharge, away from the ground plate, but cannot be clearly identified. These features of the flow are quantified in figures 5 to 7 through a detailed set of mean and turbulent velocity measurements obtained in the vertical plane of symmetry (Z=0) for a Reynolds number based on the jet-exit conditions of $4.3x10^4$, a free stream to jet velocity ratio, V_R=V_j/U_o of 22.5, a jet height to jet diameter ratio, H/D, of 20.1, and a spacing between the jets, S/D, of 6.

B. Measurements

Figures 5(a) and (b) show vertical profiles of horizontal, $\overline{U}$, and vertical, $\overline{V}$, mean velocity components along the vertical plane of symmetry (Z=0).

The mean horizontal velocity profiles at X/D=-2.93, -1.47, 0 and +1.47 show negative values near the ground (*Y*=0) that correspond to the upstream wall jet, revealing that the first impinging jet was deflected by the crossflow. The impinging point of the first jet is located at about X/D=+2.93 in a position that is vertically near the axis of the second jet exit (X/D=+3), which is more strongly deflected due to this interference. As a consequence, the downstream wall jet of the first jet and the second jet seems to merge rapidly in a single flow in the crossflow direction. These profiles exhibit maximum positive (downstream) values of the mean horizontal velocity component between *Y*=100mm and 150mm that reach twice the crossflow velocity. This result can also be confirmed with the help of Fig. 5b that shows only positive values (upwards) of the mean vertical velocity component just 2D downstream of the geometrical axis of the second jet (X/D=+5.0) . The second jet is still detected in the profile at X/D=+2.93 by the negative (downwards) values of $\overline{V}$, but only quite near of the upper wall for Y>180mm (Y/H>0.596). This means that no upstream wall jet resulting from the second jet exists, but the complete jet is deflected by the crossflow. This result is consistent with the conclusions of Ref. 5 that found for a single impinging jet flow that the ground vortex blocks the passage of the confined crossflow increasing the velocity of the crossflow that passes over. So, for the configuration the final result is that the second jet "views" a smaller jet-to-crossflow velocity ratio and no impingement occurs. In the practical situation of a VSTOL aircraft this may result in a different pressure distribution in the under surface of the aircraft, that with front wind or small forward movement may result in enhanced under pressures in the aft part of the aircraft causing a suction down force and a change of the pitching moment towards the ground.

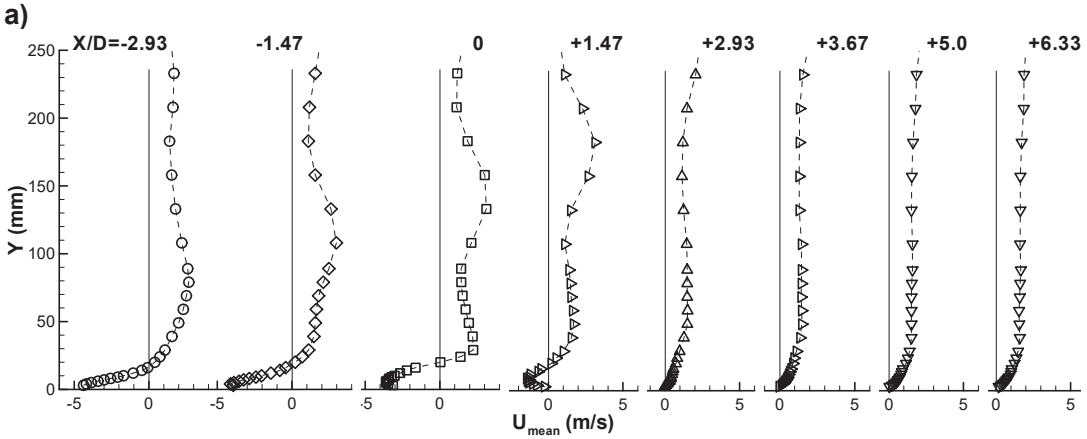

Figure 5. Vertical profiles of the mean velocity characteristics along the longitudinal (symmetry) plane crossing the center of the twin jets. Re_j=$4.3x10^4$, V_j/U_o=22.5, H/D=20.1, and S/D=6. (a) Horizontal velocity, $\overline{U}$. (b) Vertical velocity, $\overline{V}$.

b)

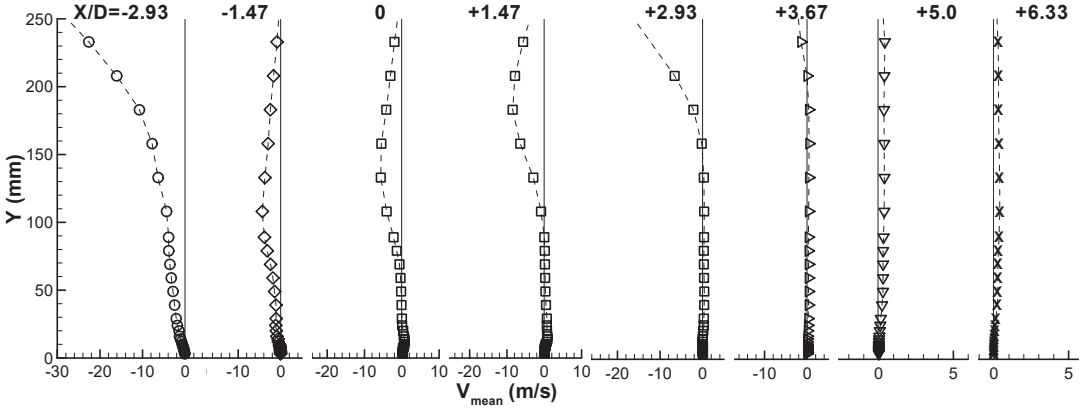

Figure 5 (cont'd). Vertical profiles of the mean velocity characteristics along the longitudinal (symmetry) plane crossing the center of the twin jets. Re_j=4.3x10^4, V_j/U_o=22.5, H/D=20.1, and S/D=6. (a) Horizontal velocity, $\overline{U}$. (b) Vertical velocity, $\overline{V}$.

Figures 6 (a) and (b) show horizontal transversal profiles of horizontal, $\overline{U}$, and vertical, $\overline{V}$, mean velocity components, quantify the development of the impinging jets and confirm the above description of the flow. The measurements, and particularly those of the vertical velocity component, do not identify a centrally located fountain rising from the ground plate without interference from the main jets, as it occurs in practical VSTOL applications[29]. This result confirms our hypothesis that the alignment of the twin jets with the crossflow would create a special flow pattern not yet reported before. The wall jet resulting from the first jet flows underneath the second one, but the ground vortex formed upstream is only interfering away from the vertical symmetry plane.

The mean vertical velocity component is always positive from the upper wall (Y/H=1) up to the middle of the crossflow (Y/H=0.5), confirming the conclusions drawn from the vertical velocity profiles in the lower part of the crossflow and discussed in the previous paragraphs.

The asymmetry of the flow can be confirmed from the horizontal profiles of the mean vertical velocity component with higher peaks up to 10% of the vertical velocity in the upstream side (X<-50mm or 3.33D). The middle value between the maximum and the minimum of the mean horizontal velocity component or the mean vertical velocity components can be used to indicate the center of the jet, and in the upstream side it moves in the crossflow direction from -43.02mm at *Y/H*=0.92 to 10.47mm at *Y/H*=0.5 corresponding to a deflection angle of 21.9 degrees. The downstream jet is protected from the action of the crossflow by the first jet and as a consequence it is less deflected: the center of the jet is almost coincident with the geometrical axis of the exit, and for *Y/H*=0.5 it is located at *X/D*=+4.0 corresponding to an inclination angle of 12.3 degrees. However, considering the maximum of the mean vertical velocity component the calculated inclination angle is only 4.8 degrees which reinforces the conclusion, and the difference is probably associated with an enhanced entrainment of the second jet due to its smaller angle with the surrounding flow.

Figure 7 shows horizontal profiles of the normal stresses, $\overline{u'^2}$ and $\overline{v'^2}$, in a *rms* form, and show results that are somewhat surprising at first sight, because it seems that it is not possible to identify completely the shear layer surrounding the impinging jets.

The peaks in the fluctuating vertical velocity components occur in the upstream side of the first jet as expected, because in this region the higher velocity gradients occur. Other peaks were observed near *X*=0 for the *X/H*=0.83 and 0.75 hat correspond to the downstream side of the first impinging jet. For the *X/H*=0.66 the peak is very weak, and for the lower profiles they cannot be pointedly identified, confirming the rapid mixing between the jets as already detected from the lower part of the flow through the vertical velocity profiles.

For the second (downstream) impinging jet the shear layer surrounding the jet cannot be clearly identified. However, for the *Y/H*=0.66 profile a small decrease in the normal vertical stress is noted near the center of the jet, but the peaks around the jet are so close that the minimum value is somewhat masked.

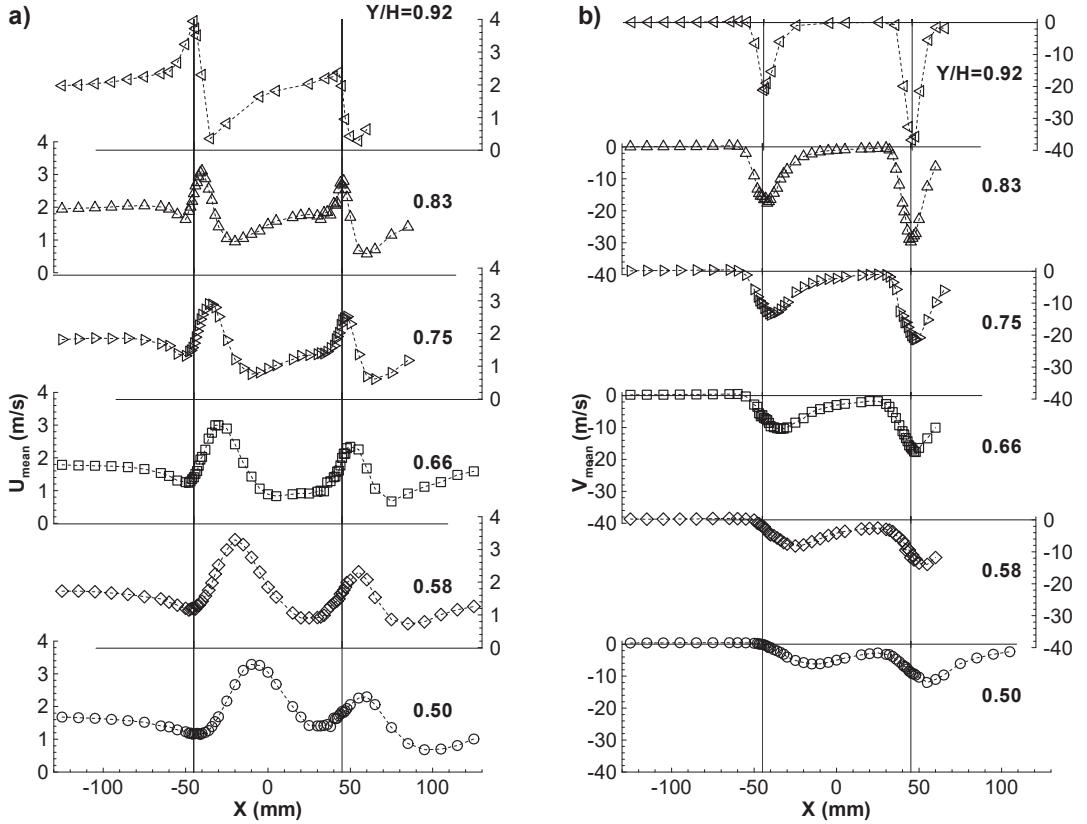

Figure 6: Horizontal profiles of the mean velocity characteristics along the longitudinal (symmetry) plane crossing the center of the twin jets. Re_j=4.3x10^4, V_j/U_o=22.5, H/D=20.1, and S/D=6. (a) Horizontal velocity, $\overline{U}$. (b) Vertical velocity, $\overline{V}$.

IV. Conclusion

A laser Doppler velocimeter was used to provide information on the flowfield created by twin impinging jets aligned with a low velocity crossflow. The experiments were carried out for a Reynolds number based on the jet exit conditions of Re_j=4.3x10^4, an impingement height of 20.1 jet diameters and for a velocity ratio between the jet exit and the crossflow $V_R=V_j/U_o$ of 22.5, and an interjet spacing was S=6D

The results show a large penetration of the first (upstream) jet, which is deflected by the crossflow and impinges on the ground, giving rise to a ground vortex due to the collision of the radial wall and the crossflow that wraps around the impinging point like a scarf. The second jet (located downstream) it is not so affected by the crossflow in terms of deflection because it is protected by the upstream jet, but due to the downstream wall jet that flows radially from the impinging point the first jet does not reach the ground . Also, due to the confinement and the ground vortex, the crossflow is blocked and accelerates in the upper part and also contributes to an enhanced mixing of each secondary flow. As consequence, no upstream wall jet or ground vortex resulting from the second (downstream) jet

was detected. The result of the second jet impinging on the downstream wall jet resulting from the first jet had not been reported so far and requires further investigation.

The shear layers surrounding the jet cannot be clearly identified from the fluctuating velocities that do not exhibit clear peaks in the edges, and the values in the center are also high.

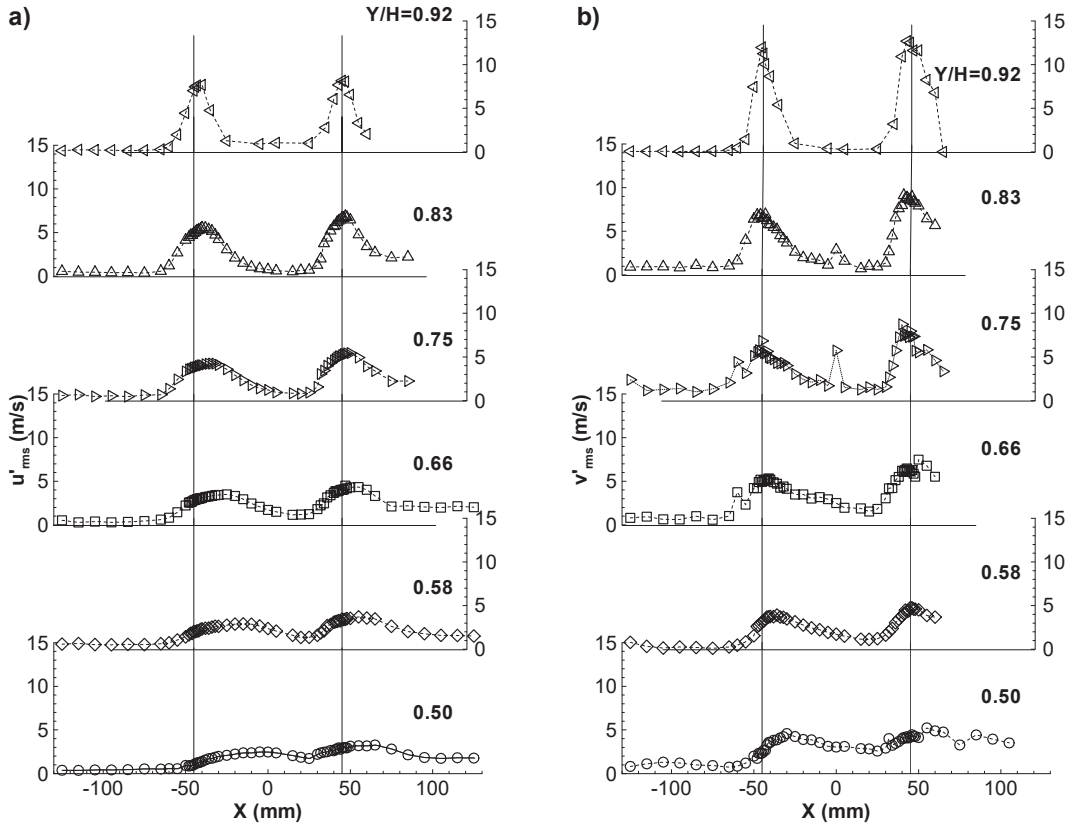

Figure 7: Horizontal profiles of the mean velocity characteristics along the longitudinal (symmetry) plane crossing the center of the twin jets. Re_j=4.3x10^4, V_j/U_o=22.5, H/D=20.1, and S/D=6. (a) Horizontal rms velocity, $\sqrt{u'^2}$. (b) Vertical rms velocity, $\sqrt{v'^2}$.

Acknowledgments

The financial support of FCT-Fundação para a Ciência e Tecnologia under contract PTDC/EME-MFE/102190/2008 is gratefully acknowledged.

The present work was done in the scope of the activities of LAETA-Associated Laboratory of Energy, Transports and Aeronautics/UBI-AEROG.

References

[1]Barata, J.M.M., Durão, D.F.G., and McGuirk, J.J., "Numerical Study of Single Impinging Jets Through a Crossflow", *Journal of Aircraft,*Vol.26, No.11, 1989, pp. 1002-1008.

[2]Knowles, K., and Bray, D., "The Ground Vortex Formed by Impinging Jets in Crossflow", AIAA 29th Aerospace Sciences Metting, AIAA Paper 91-0768, Reno, NV, Jan. 7-10, 1991.

[3]Barata, J.M.M., "Numerical and Experimental Study of Jets Impinging on Flat Surfaces Through a Crossflow", Ph.D. Thesis (in Portuguese), Instituto Superior Técnico, Technical Univ. of Lisbon, Lisbon, Portugal, 1989.
[4]Sarippali, K.R., "Laser Doppler Velocimeter Measuremnts in 3D Impinging Twin-Jet Fountain Flows", *Turbulent Shear Flows,* Vol.5, edited by Durst et al., Springer-Verlag, Berlin, 1987, pp. 147-168.
[5]Kind, R.J., and Suthanthiran, K., "The Interaction of Two Opposing Plane Turbulent Wall Jets", AIAA Paper 72-0211, Jan., 1980.
[6]Gilbert, B.L., "Detailed Turbulence Measurements in a Two Opposing Plane Turbulent Wall Jets", AIAA 16th Fluid and Plasma Dynamics Conf., AIAA Paper 83-1678, Danvers, MA, July 12-14, 1983.
[7]Jenkins, R.C., and Hill, W.G., Jr., "Investigation of VTOL Upwash Flows Formed by Two Impinging Jets", Grumman Research Dept. Rept. RE-548, Bethpage, NY, Nov., 1977.
[8]Kotansky, D.R., and Glaze, L.W., "The Effects of Ground Wall-Jet Characteristics on Fountain Upwash Flow Formation and Development", Rept. ONR-CR212-216-1F, 1980.
[9]Kavasaoglu, M.S., Schetz, J.A., and Jakubowsky, A.K., "Rectangular Jets in a Crossflow", *Journal of Aircraft,* Vol.26, No. 9, 1989, pp. 793-804.
[10]Schetz, J.A., Jakubowsky, A.K. and Aoyagi, K., "Surface Pressures on a Flat Plate With Dual Jet Configurations", *Journal of Aircraft*, Vol.21, No.7, 1984, pp. 484-490.
[11]Araújo, S.R.B., Durão, D.F.G., and Firmino, F.J.G., "Jets Impinging Normally and Obliquelly to a Wall", AGARD CP 308, paper 5.
[12]Sugiyama Y., and Usami, Y., "Experiments on the Flow in and Around Jets Directed Normal to a Crossflow", *Bulletin JSME*, No.22, 1979, pp. 1736-1745.
[13]Andreopoulos, J., and Rodi, W., "Experimental Investigation of Jets in a Crossflow", *J. Fluid Mech.*, Vol.138, 1984, pp.93-127.
[14]Shayesteh, M.V. Shabaka, I.M.N.A., and Bradshaw, P., "Turbulent Structure of a Three-Dimensional Impinging Jet in a Crossflow", AIAA 23rd Aerospace Sciences Meeting, AIAA Paper 85-0044, Reno, NV, Jan. 14-17, 1985.
[15]Kamotani, Y., and Greber, I., "Experiments on Confined Turbulent Jets in a Crossflow", NASA CR-2392, 1974.
[16]Stoy, R.C., and Ben-Haim, Y., "Turbulent Jets in a Confined Crossflow", *J. Fluids Engng.*, No.95, 1973, pp.551-556.
[17]Crabb, D., Durão, D.F.G., and Whitelaw, J.H., "A Round Jet Normal to a Crossflow", *J. Fluids Engng.,*Vol.113, 1981, pp. 142-153.
[18]Barata, J.M.M., Durão, D.F.G., and McGuirk, J.J., "Numerical Study of Single Impinging Jets Through a Crossflow", *J. of Aircraft*, Vol.26, No.11, 1989, pp.1002-1008.
[19]Barata, J.M.M., Durão, D.F.G., Heitor, M.V., and McGuirk, J.J., "On the Analysis of an Impinging Jet on Ground Effects", *Experiments in Fluids*, No.15, 1993, pp.117-129.
[20]Barata, J.M.M., "Ground Vortex Formation With Twin Impinging Jets". Artigo SAE 962257, International Powered Lift Conference, Jupiter, Florida, 18-20 Novembro, 1996.
[21]Barata, J.M.M., "Fountain Flows Produced by Multiple Impinging Jets in a Crossflow". *AIAA Journal*, Vol. 34, No.12, Dez. 1996, pp. 2523-2530 e *AIAA Journal on Disc*, Vol. 2, No.1, 1996.
[22]Durst, F., Melling, A., and Whitelaw, J.H., "*Principles and Practice of Laser-Doppler Anemometry*", 2nd ed., New York, Academic Press.
[23]Yanta, W.J. and Smith, R.A., "Measurements of Turbulent Transport Properties with a Laser-Doppler Velocimeter", 11th Aerospace Sciences Meeting, AIAA Paper 73-0169, Washington, 1978.
[24]Melling, A., and Whitelaw, J.H., "Turbulent Flow in a Rectangular Duct", *J. Fluid Mechanics*, Vol. 78, 1975, pp.285-315.
[25]Baker, O.J., "The Turbulent Horseshoe Vortex", *J. Wind Engineering and Industrial Aerodynamics*, Vol. 6, 1981, pp. 9.
[26]Andreopoulos, J. and Rodi, W., "Experimental Investigation of Jets in a Crossflow", *J. Fluid Mechanics*, Vol. 138, 1984, pp. 127.
[27]Saripalli, K.R., "Visualization of Multijet Impingement Flow", *AIAA Journal*, Vol. 21, 1983, pp. 483-484.
[28]Siclari, M.J., Migdal, D., Luzzi, T.W., Jr., Barche, J., and Palcza, J.L., "Development of Theoretical Models of Jet-Induced Effects on V/STOL Aircraft", *Journal of Aircraft*, Vol. 13, No. 12, 1976, pp.938-944.
[29]Kotansky, D.R., " The Modelling and Prediction of Multiple VTOL Aircraft Flow Fields in Ground Effect", AGARD CP-308, Paper 16.

Laser Doppler Measurements of Twin Impinging Jets Aligned With a Crossflow

Jorge M. M. Barata[1,*], Pedro S. D. Carvalho[1], Diamantino F. G. Durão[2], Fernando M. S. P. Neves[1], André R. R. Silva[1], Diana F. C. Vieira[1]

1: Aerospace Sciences Department, Universidade Beira Interior, Covilhã, 6200-358, Portugal
2: Universidade Lusíada, Lisbon, Portugal
*Corresponding author: jbarata@ubi.pt

Abstract This paper presents a detailed analysis of the complex flow beneath two impinging jets aligned with a low-velocity crossflow which is relevant for the future F-35 VSTOL configuration, and provides a quantitative picture of the main features of interest for impingement type of flows. The experiments were carried out for a Reynolds number based on the jet exit conditions of Re_j=4.3x10^4, an impingement height of 20.1 jet diameters and for a velocity ratio between the jet exit and the crossflow V_R=V_j/U_o of 22.5. The rear jet is located at S=6D downstream of the first jet. The results show a large penetration of the first (upstream) jet that is deflected by the crossflow and impinges on the ground, giving rise to a ground vortex due to the collision of the radial wall and the crossflow that wraps around the impinging point like a scarf. The rear jet (located downstream) it is not so affected by the crossflow in terms of deflection, but due to the downstream wall jet that flows radially from the impinging point of the first jet it does not reach the ground. The results indicate a new flow pattern not yet reported so far, that for a VSTOL aircraft operating in ground vicinity with front wind or small forward movement may result in enhanced under pressures in the aft part of the aircraft causing a suction down force and a change of the pitching moment towards the ground.

Nomenclature

D	=	diameter of the jet
H	=	impinging height
k	=	turbulent kinetic energy
Re	=	Reynolds number
S	=	spacing of the jets axis in the wind direction
U	=	horizontal velocity, $\overline{U} + u'$
V	=	vertical velocity, $\overline{V} + v'$
W	=	transverse $\overline{W} + w'$
X	=	horizontal coordinate
Y	=	vertical coordinate
Z	=	transverse coordinate
Subscripts		
j	=	jet-exit value
o	=	crossflow value

1. Introduction

Turbulent jets impinging on flat surfaces through a low-velocity crossflow are typical in impinging cooling applications in industry[1] as well as of the flow beneath a short/vertical take-off aircraft which is

lifting off or landing with zero or small forward momentum[2,3]. Ground effect may occur and change the lift forces on the aircraft, cause reingestion of exhaust gases into the engine intake and raise fuselage skin temperatures. In this latter application the impingement of each downward-directed jet on the ground results in the formation of a wall jet which flows radially from the impinging point along the ground surface. The interaction of this wall jet with the free stream results in the formation of a ground vortex far upstream of the impinging jet, which has profound implications on the aircraft design. In addition the collision of the wall jets originates a fountain upwash flow, affecting the forces and moments induced in the aircraft when operating in ground effect. Improved knowledge of impinging flows is therefore necessary to avoid these effects and to be able to model a range of jet-impingement type of applications with practical interest.

Earlier published work has been concentrated on 1, 2, and 3 jets configurations relevant to the Harrier / AV-8B aircraft (e.g. Ref. 2 and 3). In this case when the aircraft is operating with small forward movement the configuration of interest is 2 impinging jets with the direction of the crossflow perpendicular to the line containing their centres, because each impinging jet is located on the sides of the fuselage.

If attention is concentrated on the next generation of VSTOL aircrafts (X-35/F-35/JSF-Joint Strike Fighter) then no relevant studies can be found, because the impinging jets are aligned with the crossflow, and this geometry has not been considered. In this case a vertically oriented lift fan (SDLF) generates a column of cool air that produces nearly 20,000 pounds of lifting power, along with an equivalent amount of thrust from the vectored rear exhaust (3BSM-Three Bearing Swivel Module). The lift system was successfully demonstrated during a flight testing of the X-35B during the summer of 2001. The complexity of the new VSTOL configuration together with the very stringent requirements has required an enormous amount of R&D in the last decade. On 12th May 2012 the 200th test flight of the F-35B (BF-3) measured stresses on the aircraft during supersonic maneuvres. So, most of the published work reported so far has therefore only peripheral relevance to the F35-B/JSF ground effect problem.

Ref. 4 reports a study of multijet impinging configurations producing upwash fountain flows, which are the heart of the complicated effects by VSTOL aircraft when they operate in ground proximity, but as far as twin jets are concerned only the geometry with the jets side by side was considered. This paper presents a detailed analysis of the complex flow field beneath 2 impinging jets aligned with low-velocity crossflow relevant for the new F-35 VSTOL configuration, and provides a quantitative picture of the main features of interest of impingement type of flows.

The remainder of this paper is presented in four sections. Section II describes the experimental configuration and measurement procedure, gives details of the laser-Doppler velocimeter and provides assessments of accuracy. The arguments associated with these assessments are based on previous experiments and are presented in condensed form. Section III presents the experimental results obtained in the vertical plane of symmetry containing the axis of both jets and quantifies the mean and turbulent velocity characteristics of the flow. The final section summarizes the main findings and conclusions of this work

2. Experimental Method

The wind tunnel facility designed and constructed for the present work is schematically shown in Fig. 1. A fan with 15kW nominal power drives a maximum flow of 3000m^3/h through the boundary layer wind tunnel of 300x302mm exit section. Each jet unit of 15mm inner diameter is mounted vertically in the top of the test section with the axis contained in the vertical plane o symmetry parallel to the crossflow.

The origin of the horizontal, X, and vertical, Y, coordinates is taken at the midpoint between the centres of the jets exit. The X coordinate is positive in the direction of the wind tunnel exit and Y is positive upwards.

The present results were obtained at the vertical plane of symmetry for jet mean velocities of V_j=36m/s and mean crossflow velocity of U_0=1.6m/s, corresponding to a velocity ratio, $V_R=V_j/U_o$ of 22.5. The rear jet is located at S=6D downstream of the first jet (see Fig. 2).

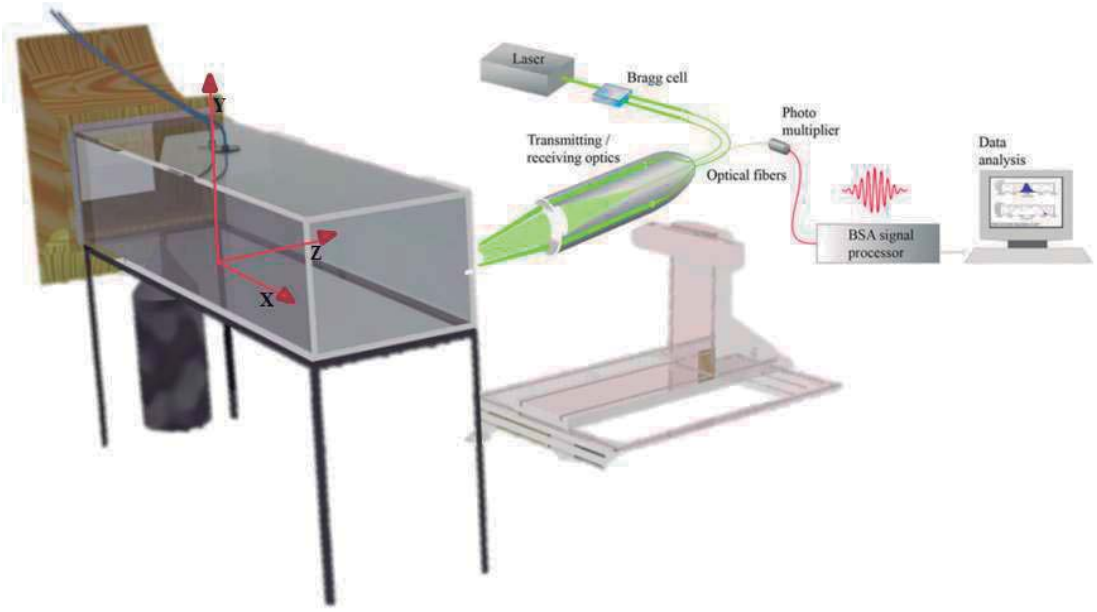

Figure 1. Experimental set-up.

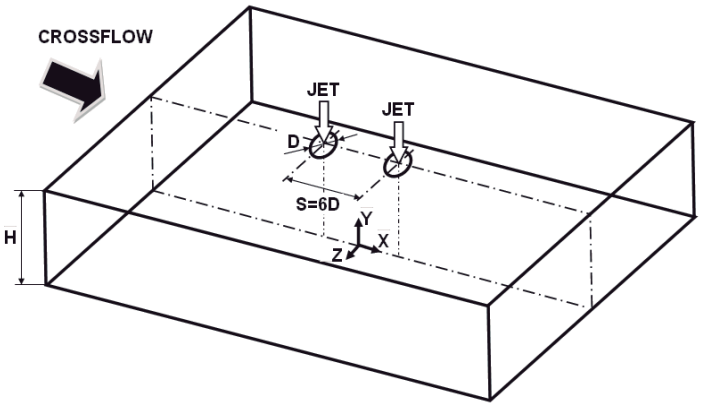

Figure 2. Geometrical arrangement of the jets.

The velocity field was measured with a two-colour (two-component) Laser-Doppler velocimeter (Dantec Flowlite 2D), which comprised a 10mW He-Ne and a 25mW diode-pumped frequency doubled Nd:YAG lasers, sensivity to the flow direction provided by frequency shifting from a Bragg cell at f_0=40MHz, a transmission and backward-scattered light collection focal lens of 400mm. The half-angle between the beams was 2.8° and the calculated dimensions of the axis of the measuring ellipsoid volume at the e^{-2} intensity locations were 135x6.54x6.53µm and 112x5.46x5.45µm respectively (see Table 1 for details). The horizontal, *U*, and vertical *V*, mean and turbulent velocities were determined by a two-velocity channel Dantec BSA F60 processor. The seeding of the flow with glycerine particles of 0.1-5µm was produced by a smoke generator. The transmitting and collecting optics is mounted on a three-

dimensional transversing unit, allowing the positioning of the centre of the control volume within ±0.1mm.
In order to measure the vertical components in near wall regions, the transmitting optics were inclined by half angle of beam intersection and the scattered light was collected off-axis. Measurements could then be obtained up to 0.5mm from the ground plate without a significant deterioration of the Doppler signals. Results obtained 20mm above the ground plate with both the on-axis and the off-axis arrangements have shown a close agreement, within the precision of the equipment.
Errors incurred in the measurement of velocity by displacement and distortion of the measuring volume due to refraction on the duct walls and change in the refractive index were found to be negligibly small and within the accuracy of the measuring equipment. Non-turbulent Doppler broadening errors due to gradients of mean velocity across the measuring volume may affect essentially the variance of the velocity fluctuations[5], but for the present experimental conditions are of the order of $10^{-4}V_j^2$ and, therefore, sufficiently small for their effect to be neglected. The largest statistical (random) errors derived from populations of, at least, 10000 velocity values were of 0.5 and 3%, respectively for the mean and the variance values, according to the analysis recommended by Ref. 6 for a 95% confidence interval. No corrections were made for sampling bias, but no correlations were found between Doppler frequencies and time interval between consecutive bursts even in the zones of the flow characterized by the lowest particle arrival rates, suggesting that those effects are unimportant for the present flow conditions.

Table 1. Principal characteristics of the 2D Laser-Doppler velocimeter.

	He-Ne laser	Diode Laser
- Wave length, λ [nm]	633	532
- Focal length of focusing lens, f [mm]	400	400
- Beam diameter at e-2 intensity [mm]	1.35	1.35
- Beam spacing, s [mm]	38.87	39.13
- Calculated half-angle of beam intersection, θ	2.78°	2.8°
- Fringe spacing, δ_f [μm]	6.53	5.45
- Velocimeter transfer constant, K [MHz/ms^{-1}]	0.153	0.183

Systematic errors incurred in the measurements of Reynolds shear stresses can arise from lack of accuracy in the orientation angle on the normal to the anemometer fringe pattern, as shown by Ref. 7, and can be particularly large in the vicinity of the zones characterized by zero shear stress: for the present experimental conditions the largest errors are expected to be smaller than -2.5%.

3. Results

In this chapter, experimental data obtained will be presented and discussed under two headings. First, flow visualization is presented, and then mean and turbulent velocity profiles are presented and discussed for the velocity ratios V_R of 22.5.

A. Visualization

Flow visualization was performed using digital direct photography to guide the choice of the measurement locations and to provide a qualitative picture of the flow. The longitudinal vertical plane of

symmetry was illuminated with a sheet of light. The photos were taken perpendicular to the vertical plane of symmetry. For all the flows studied, the results have shown (for each jet) a pattern similar to that of a single impinging jet. Fig. 3 identifies the flow development along the vertical plane of symmetry, i.e. Z=0. Each jet has an initial potential-core jet region, where the flow characteristics are identical to those of a free jet, and near the horizontal plate the impingement region, characterized by considerable deflection of the jet. It was not possible to identify all the regions simultaneously in the same photo, neither a deflection of each jet by the crossflow. The selected picture shows the wall jet corresponding to the upstream impinging jet which is almost parallel to the ground plate and exhibits behaviour similar to that of a radial wall jet where the upstream effects of interaction due to impingement are no longer important. The upstream wall jet interacts with the crossflow and forms a horseshoe vortex close to the ground plate, which wraps around both impinging jets. As a result, two streamwise counter-rotating vortices develop side-to-side and decay further downstream of each impinging zone forming a ground vortex. The nature of each ground vortex is similar to the horseshoe structure known to be generated by the deflection of a boundary layer by a solid obstacle[8], but is different from the vortex pair known to exist in a "bent-over" jet in a crossflow far from the ground[9]. No evidence of a ground vortex corresponding to the downstream impinging jet could be confirmed, which is an indication that the upstream impinging jet and its ground vortex are blocking the crossflow and provoking an alteration to the flow pattern. If the jets were positioned side by side in front of the crossflow two ground vortexes would appear as well as a fountain flow in the vertical plane of symmetry due to the collision of the two individual radial wall jets (e.g., Refs. 10-11). In the present case for a velocity ratio between the jet and the crossflow of $V_R = 22.5$ no fountain flow could be detected.

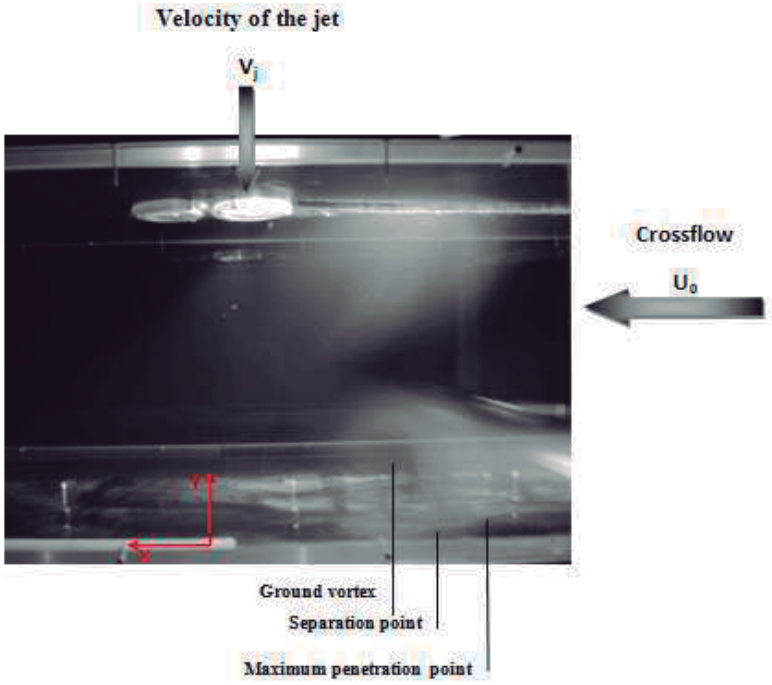

Figure 3. Visualization of the twin jet flow in the vertical plane of symmetry for Re_j=4.3x10^4, V_j/U_o=22.5, H/D=20.1, and S/D=6.

Analysis of Fig. 3 also suggests that the crossflow is deflected sideways by the penetration of the jet and may cause a recirculation region just downstream of the discharge, away from the ground plate, but cannot be clearly identified. These features of the flow are quantified in figures 4 to 6 through a detailed set of mean and turbulent velocity measurements obtained in the vertical plane of symmetry (Z=0) for a

Reynolds number based on the jet-exit conditions of $4.3x10^4$, a free stream to jet velocity ratio, $V_R=V_j/U_o$ of 22.5, a jet height to jet diameter ratio, H/D, of 20.1, and a spacing between the jets in the wind direction, S/D, of 6.

B. Measurements

Figure 4 shows vertical profiles of the mean horizontal velocity component, $\overline{U}$, along the vertical plane of symmetry (Z=0).

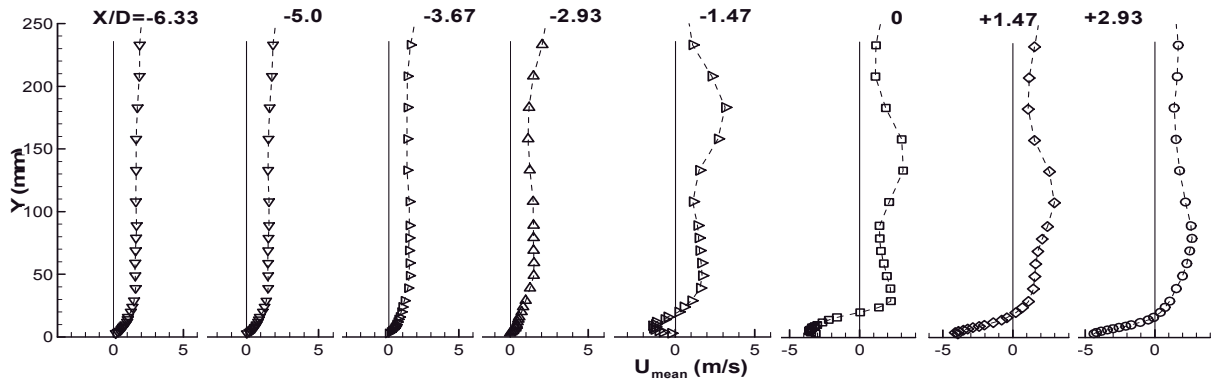

Figure 4. Vertical profiles of the mean horizontal velocity component, $\overline{U}$, along the longitudinal (symmetry) plane crossing the center of the twin jets. $Re_j=4.3x10^4$, $V_j/U_o=22.5$, H/D=20.1, and S/D=6.

The mean horizontal velocity profiles at X/D=-2.93, -1.47, 0 and +1.47 show negative values near the ground (Y=0) that correspond to the upstream wall jet, revealing that the first impinging jet was deflected by the crossflow. The impinging point of the first jet is located at about X/D=+2.93 in a position that is vertically near the axis of the rear jet exit (X/D=+3), which is more strongly deflected due to this interference. As a consequence, the downstream wall jet of the first jet and the rear jet seems to merge rapidly in a single flow in the crossflow direction. These profiles exhibit maximum positive (downstream) values of the mean horizontal velocity component between Y=100mm and 150mm that reach twice the crossflow velocity. This means that no upstream wall jet resulting from the rear jet exists, but the complete jet is deflected by the crossflow. This result is consistent with the conclusions of Ref. 4 that found for a single impinging jet flow that the ground vortex blocks the passage of the confined crossflow increasing the velocity of the crossflow that passes over. So, for this configuration the final result is that the rear jet "feels" a smaller jet-to-crossflow velocity ratio and no impingement occurs. In the practical situation of a VSTOL aircraft this may result in a different pressure distribution in the under surface of the aircraft, that with front wind or small forward movement may result in enhanced under pressures in the aft part of the aircraft causing a suction down force and a change of the pitching moment towards the ground.

Figures 5 (a) and (b) show horizontal profiles of horizontal, $\overline{U}$, and vertical, $\overline{V}$, mean velocity components, quantify the development of the impinging jets and confirm the above description of the flow. The measurements, and particularly those of the vertical velocity component, do not identify a centrally located fountain rising from the ground plate without interference from the main jets, as it occurs in practical VSTOL applications[11].

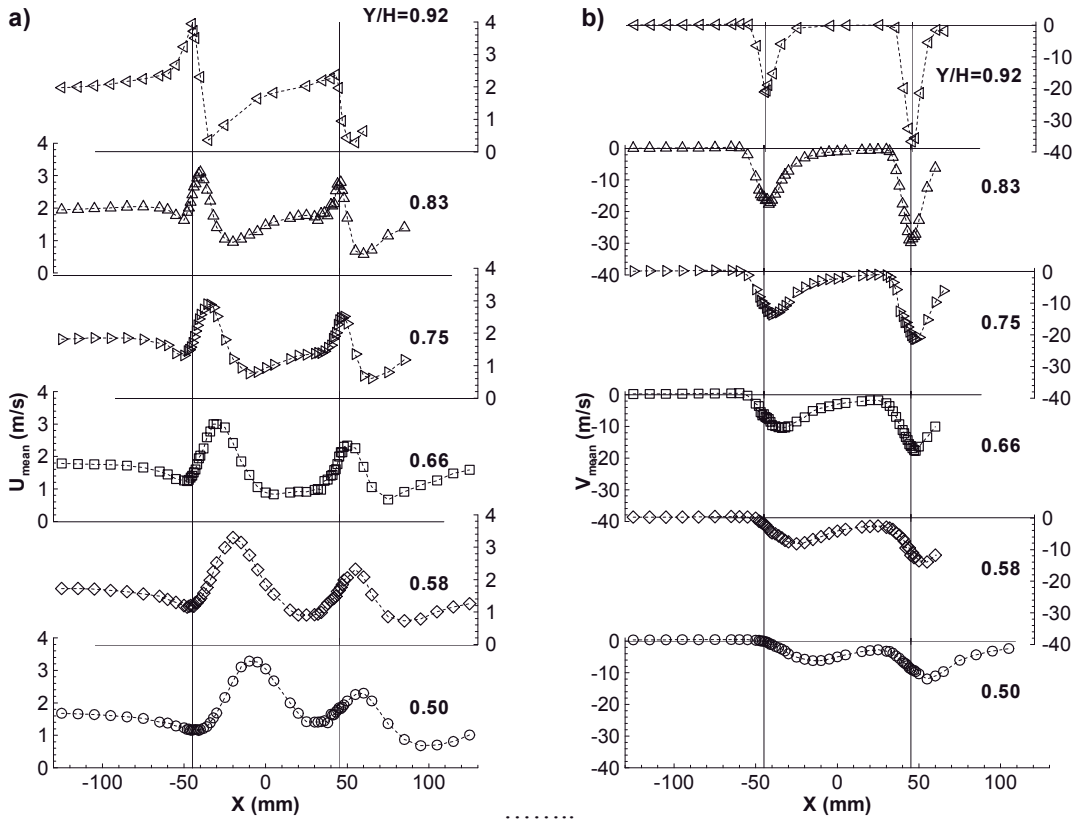

Figure 5. Horizontal profiles of the mean velocity characteristics along the longitudinal (symmetry) plane crossing the center of the twin jets. Re_j=4.3x10^4, V_j/U_o=22.5, H/D=20.1, and S/D=6. (a) Horizontal velocity, $\overline{U}$. (b) Vertical velocity, $\overline{V}$.

This result confirms our hypothesis that the alignment of the twin jets with the crossflow would create a special flow pattern not yet reported before. The wall jet resulting from the first jet flows underneath the rear one, but the ground vortex formed upstream is only interfering away from the vertical symmetry plane.

The mean vertical velocity component is always positive from the upper wall (Y/H=1) up to the middle of the crossflow (Y/H=0.5), confirming the conclusions drawn from the vertical velocity profiles in the lower part of the crossflow and discussed in the previous paragraphs.

The asymmetry of the flow can be confirmed from the horizontal profiles of the mean vertical velocity component with higher peaks up to 10% of the vertical velocity in the upstream side (X<-50mm or 3.33D). The middle value between the maximum and the minimum of the mean horizontal velocity component or the mean vertical velocity components can be used to indicate the centre of the jet, and in the upstream side it moves in the crossflow direction from -43.02mm at *Y/H*=0.92 to 10.47mm at *Y/H*=0.5 corresponding to a deflection angle of 21.9 degrees. The downstream jet is protected from the action of the crossflow by the first jet and as a consequence it is less deflected: the centre of the jet is almost coincident with the geometrical axis of the exit, and for *Y/H*=0.5 it is located at *X/D*=+4.0 corresponding to an inclination angle of 12.3 degrees. However, considering the maximum of the mean vertical velocity component the calculated inclination angle is only 4.8 degrees which reinforces the conclusion, and the difference is probably associated with an enhanced entrainment of the rear jet due to its smaller angle with the surrounding flow.

Figure 6 shows horizontal profiles of the normal stresses, $\overline{u'^2}$ and $\overline{v'^2}$, in a *rms* form, and show results that are somewhat surprising at first sight, because it seems that it is not possible to identify completely the shear layer surrounding the impinging jets.

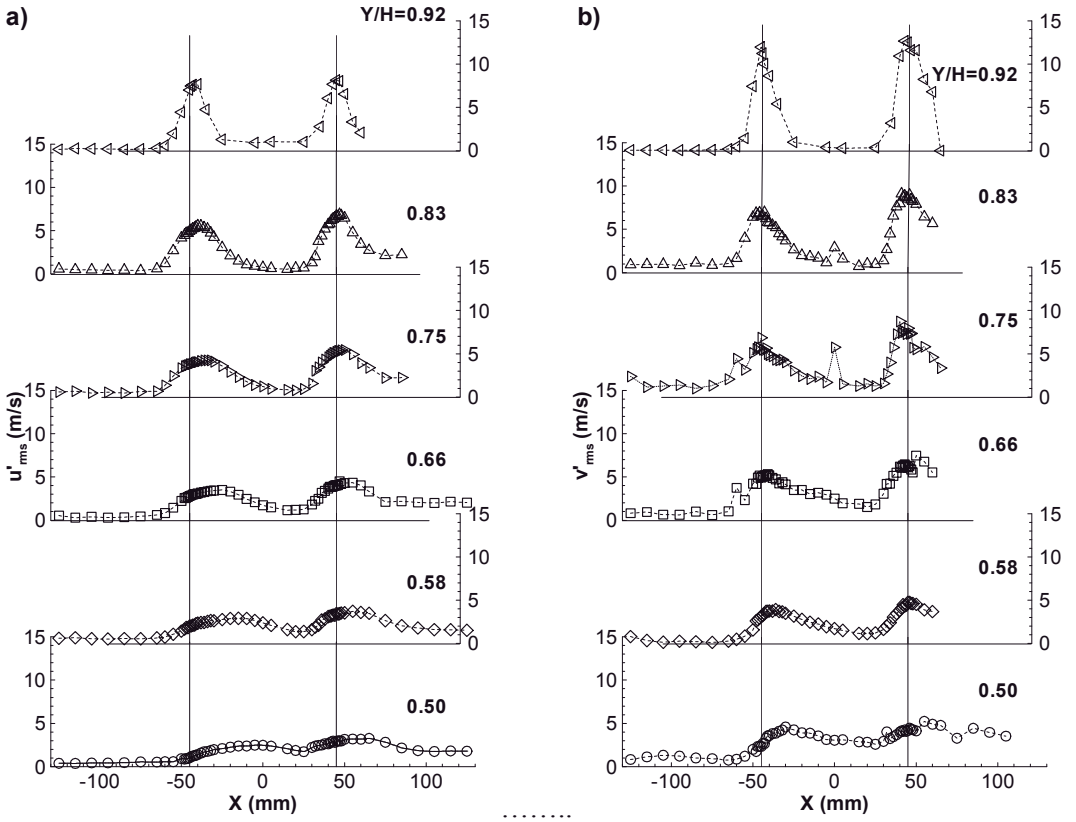

Figure 6. Horizontal profiles of the mean velocity characteristics along the longitudinal (symmetry) plane crossing the center of the twin jets. Re_j=4.3x10^4, V_j/U_∞=22.5, H/D=20.1, and S/D=6. (a) Horizontal rms velocity, $\sqrt{u'^2}$. (b) Vertical rms velocity, $\sqrt{v'^2}$.

The peaks in the fluctuating vertical velocity components occur in the upstream side of the first jet as expected, because in this region the higher velocity gradients occur. Other peaks were observed near *X*=0 for the *X/H*=0.83 and 0.75 profiles that correspond to the downstream side of the first impinging jet. For the *X/H*=0.66 profile the peak is very weak, and for the lower profiles they cannot be pointedly identified, confirming the rapid mixing between the jets as already detected from the lower part of the flow through the vertical velocity profiles.

For the second (downstream) impinging jet the shear layer surrounding the jet cannot be clearly identified. However, for the *Y/H*=0.66 profile a small decrease in the normal vertical stress is noted near the centre of the jet, but the peaks around the jet are so close that the minimum value is somewhat masked.

4. Conclusions

A laser Doppler velocimeter was used to provide information on the flowfield created by twin impinging jets aligned with a low velocity crossflow. The experiments were carried out for a Reynolds number

based on the jet exit conditions of Re_j=4.3x10^4, an impingement height of 20.1 jet diameters and for a velocity ratio between the jet exit and the crossflow V_R=V_j/U_o of 22.5. The rear jet is located at S=6D downstream of the first jet.
The results show a large penetration of the first (upstream) jet, which is deflected by the crossflow and impinges on the ground, giving rise to a ground vortex due to the collision of the radial wall and the crossflow that wraps around the impinging point like a scarf. The rear jet it is not so affected by the crossflow in terms of deflection because it is protected by the upstream jet, but due to the downstream wall jet that flows radially from the impinging point the first jet does not reach the ground . Also, due to the confinement and the ground vortex, the crossflow is blocked and accelerates in the upper part and also contributes to an enhanced mixing of each secondary flow. As consequence, no upstream wall jet or ground vortex resulting from the second (downstream) jet was detected. The result of the rear jet impinging on the downstream wall jet resulting from the first jet had not been reported so far and requires further investigation.
The shear layers surrounding the jet cannot be clearly identified from the fluctuating velocities that do not exhibit clear peaks in the edges, and the values in the centre are also high.

Acknowledgments

The financial support of FCT-Fundação para a Ciência e Tecnologia under contract PTDC/EME-MFE/102190/2008 is gratefully acknowledged.
The present work was done in the scope of the activities of LAETA-Associated Laboratory of Energy, Transports and Aeronautics/AEROG.

References

[1]Bernhard, W., and Sebastian, S., "Multiple Jet Impingement – A Review", *Heat Transfer Research*, Vol. 42, Issue 2, Special Issue 5, 2011, pp. 101-142.
[2]Barata, J.M.M., Durão, D.F.G., and McGuirk, J.J., "Numerical Study of Single Impinging Jets Through a Crossflow", *Journal of Aircraft,*Vol.26, No.11, 1989, pp. 1002-1008.
[3]Knowles, K., and Bray, D., "The Ground Vortex Formed by Impinging Jets in Crossflow", AIAA 29th Aerospace Sciences Meeting, AIAA Paper 91-0768, Reno, NV, Jan. 7-10, 1991.
[4]Barata, J.M.M., "Fountain Flows Produced by Multiple Impinging Jets in a Crossflow". *AIAA Journal*, Vol. 34, No.12, Dez. 1996, pp. 2523-2530 e *AIAA Journal on Disc*, Vol. 2, No.1, 1996.
[5]Durst, F., Melling, A., and Whitelaw, J.H., "*Principles and Practice of Laser-Doppler Anemometry*", 2nd ed., New York, Academic Press.
[6]Yanta, W.J. and Smith, R.A., "Measurements of Turbulent Transport Properties with a Laser-Doppler Velocimeter", 11th Aerospace Sciences Meeting, AIAA Paper 73-0169, Washington, 1978.
[7]Melling, A., and Whitelaw, J.H., "Turbulent Flow in a Rectangular Duct", *J. Fluid Mechanics*, Vol. 78, 1975, pp.285-315.
[8]Baker, O.J., "The Turbulent Horseshoe Vortex", *J. Wind Engineering and Industrial Aerodynamics*, Vol. 6, 1981, pp. 9.
[9]Andreopoulos, J. and Rodi, W., "Experimental Investigation of Jets in a Crossflow", *J. Fluid Mechanics*, Vol. 138, 1984, pp. 127.
[10]Siclari, M.J., Migdal, D., Luzzi, T.W., Jr., Barche, J., and Palcza, J.L., "Development of Theoretical Models of Jet-Induced Effects on V/STOL Aircraft", *Journal of Aircraft*, Vol. 13, No. 12, 1976, pp.938-944.
[11]Kotansky, D.R., " The Modelling and Prediction of Multiple VTOL Aircraft Flow Fields in Ground Effect", AGARD CP-308, Paper 16.

Numerical and Experimental Study of Two Impinging Jets in a Row through a Crossflow

Diana. F.C. Vieira[1], André. R.R. Silva[2], Fernando. M.S.P. Neves[3], Pedro D.S. Carvalho[4], Jorge. M.M. Barata[5]
Universidade Beira Interior, Covilhã, 6200-358, Portugal

An experimental and numerical study is carried out to investigate the flowfield created by twin impinging jets aligned with a low velocity crossflow. The mean velocity, velocity fluctuation and visualization in the impingement region were obtained for a Reynolds number based on the jet exit conditions of Re_j=4.3x10^4, an impingement height of 20.1 diameter and for a velocity ratios between the jet exit and the crossflow $V_R=V_j/U_o$ of 22.5, 33.7 and 43.8 with interject spacing, S of 6D. The experimental results show a large penetration of the first (upstream) impinging jet, giving rise to a ground vortex due to the collision of the radial wall jet and the crossflow that wraps around the impinging point like a scarf. The second jet (located downstream) it is not so affected by the crossflow in terms of deflection, but it does not reach the ground due to the downstream wall jet that flows radially from the impinging point of the first jet along the ground. The results indicate a new flow pattern not yet reported so far, in which a VSTOL aircraft operating in ground vicinity with front wind or small forward movement may result in enhanced negative pressures in the underside of the aircraft causing a pitching moment and a suction down force towards the ground. To extend the experimental results, the flow was also numerically simulated using a Reynolds Averaged Navier-Stokes formulation with the "k-ε" turbulence model.

Nomenclature

C_μ, C_1, C_2 = turbulent model constants
D = diameter of the jet
H = impinging height
k = turbulent kinetic energy
r = radius of cylindrical coordinates
Re = Reynolds number
S = distance between the jets axis
S_ϕ = source term
U = horizontal velocity, $\overline{U} + u'$ (U_{mean}+u')
V = vertical velocity, $\overline{V} + v'$ (V_{mean}+v')
V_R = velocity ratio, V_j/U_o
W = transverse $\overline{W} + w'$ (W_{mean}+w')
X = horizontal coordinate
Y = vertical coordinate
Z = transverse coordinate

Greek symbols

Γ_ϕ = transport coefficient
ε = turbulent kinetic energy dissipation
μ_T = turbulent viscosity
ρ = density
σ_k, σ_ε = turbulent Prandtl/Schmidt numbers
ϕ = variable in general conservation equation
Φ = turbulent kinetic energy production term

---

[1] Ph. D. Student, Aerospace Sciences Department, Student Member of AIAA.
[2] Assistant Professor, Aerospace Sciences Department, Member of AIAA.
[3] Researcher, Aerospace Sciences Department, Member of AIAA.
[4] M.Eng., Aerospace Sciences Department.
[5] Full Professor, Aerospace Sciences Department, Associate Fellow of AIAA. Corresponding author.

Subscripts
j = jet-exit value
o = crossflow value

I. Introduction

TURBULENT jets impinging on flat surfaces through a low-velocity crossflow has application in equipment cooling , pollution dispersion as well as the flow beneath a short/vertical take-off aircraft which take of or lands with zero or small forward movement. Ground effect due to the interaction between jets and impact surface may lead to a change in lift forces of the aircraft causing reingestion of exhaust gases into the engine intake and raise fuselage skin temperatures. In this latter application the impingement of each downward-directed jet on the ground results in the formation of wall jets which expand radially from the impinging point along the ground surface. The interaction of this wall jet with the free stream results in the formation of a ground vortex far upstream of the impinging jet which has profound implications on the aircraft performance[1, 2]. In addition the collision of the wall jets originates a fountain upwash flow affecting the forces and momentum induced in the aircraft when operating near ground. Improve knowledge of this king of flow is necessary to avoid these effects and allowing the modeling of a range of jet-impingement type of applications with practical interest.
Earlier published work has been concentrated on 1, 2, and 3 jets configurations relevant to the AV-8B Harrier II aircraft. In this case when the aircraft operates with small forward movement the configuration of interest are two impinging jets with the direction of the crossflow perpendicular to the line containing their centers.
For the next generation of VSTOL aircrafts F-35 no relevant studies can be found, because the impinging jets are aligned with the crossflow and this geometry has not yet been considered. In this case a vertically oriented lift fan (SDLF) generates a column of cool air that produces the nearly 20,000 pounds of lifting power, along with an equivalent amount of thrust from the vectored rear exhaust (3BSM-Three Bearing Swivel Module). Figure 1 shows the position of the thrust vectoring nozzle and lift fan in the F-35 aircraft.

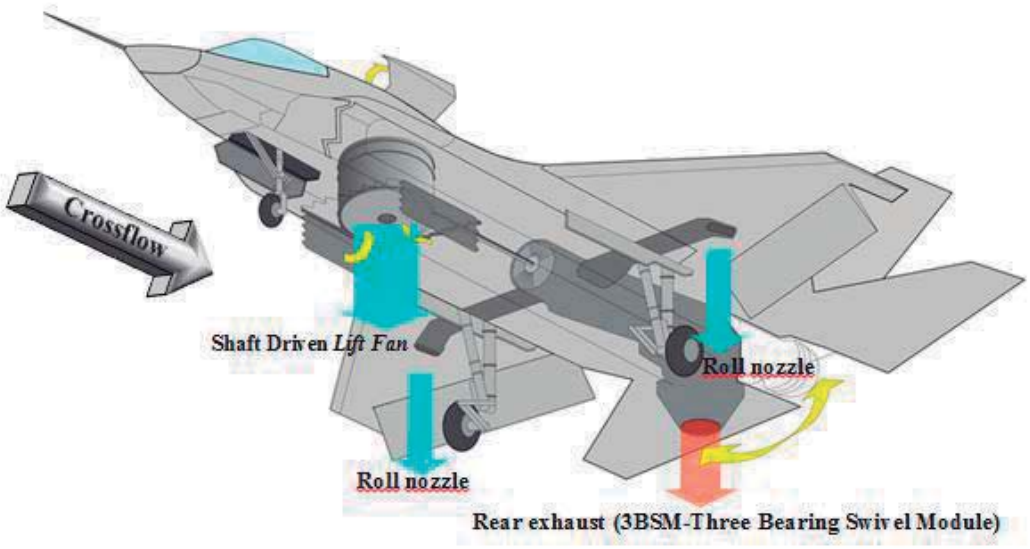

Figure 1: F-35's thrust vectoring nozzle and lift fan

The lift system was successfully demonstrated during a flight test of the X-35B during the summer of 2001. The complexity of the new VSTOL configuration together with the very stringent requirements has required an enormous amount of R&D in the last decade. On 12th May 2012 the 200th test flight of the F-35B (BF-3) measurement of stresses on the aircraft during supersonic maneuvers was done. Therefore most of the published work reported so far has only peripheral relevance to the F35-B/JSF ground effect problem.
This paper presents a detailed analysis (experimental and numerical) of the complex flow field beneath 2 impinging jets aligned with a low-velocity crossflow relevant for the F-35 with VSTOL configuration, also providing a quantitative picture of the main features of interest for this type of flow.

Previous detailed measurements of the flow properties for fountain upwash flow are scarce and have been presented essentially in the absence of a crossflow and with the use of probe techniques. The most relevant

works have been reviewed by Refs. 3 and 4, showing high turbulence levels and spreading rates in the fountains (e.g. Refs. 5 and 6). Different interpretations of the measurements exist due to the difficulties in measuring complex flows using hot-film and pitot-probe techniques[7,8]. Refs. 9 and 10 also shows flowfields and pressure data for twin-rectangular jets for small jet-to-crossflow velocity ratios (<10). Ref. 4 reports laser Doppler velocity (LDV) measurements, including those of shear stress, for axisymmetric impinging jets with *S/D*=9 and 14 with an impinging height, *H/D*, of 3 and 5.5, but again the existence of a crossflow was not considered. Detailed measurements of the velocity characteristics of normal impinging jets on a flat surface can be found for single jet configurations for relatively large impingement heights and normally for *H/D*>10, using either probe or optical techniques, as reviewed for example by Ref. 3 and 11. Experiments on the aerodynamics of jets through a confined crossflow are scarcer and have only been reported for large impingement heights and for low velocity ratios between the jet and the crossflow V_j/U_o. Therefore these works have only peripheral relevance to the VSTOL ground effect problem with the same geometry of the F-35. Refs. 12-14 report hot-wire measurements for height ratios, *H/D*, greater than 24 and for values of V_j/U_o up to 1.95, 2 and 16. Ref. 15 presents results for *H/D*=12 and Ref. 16 gives pitot-tube measurements for values of *H/D*=3.05 and for jet-to-crossflow velocity ratios up to 6.8. Ref. 17 reports LDV measurements including shear stress measurements for values of *H/D*=12 and for velocity ratios up to 2.3. Only Ref. 3 provided detailed LDV measurements for a single jet configuration for a jet with Reynolds number Re_j=6x10^4, a velocity ratio between the jet and the crossflow of 30, 42 and 73 with jet exit above the ground plate 3, 4 and 5 diameters. The measurements include time-resolved velocity characteristics along the horizontal, vertical directions with respective correlations in planes parallel to the jet nozzle axis[18,19]. Refs. 20 and 21 extended their study to multijet impinging configurations producing upwash fountain flows which are the heart of the complex effects produced by VSTOL aircraft when they operate in ground proximity, but as far as twin jets are concerned only the geometry with the jets side by side was considered.

Most of the computational work published on jets with crossflow has been based on integral methods admitting assumptions simplified, which are only capable of predicting global effects such as trajectories and jet cross-section shapes, for example Refs. 16 and 22. Ref. 24 employed a finite-difference numerical procedure together with a two-equation turbulence model to predict a single jet in an unconfined crossflow, and obtained good agreement with the experiments of Ref. 26 for velocity ratios from 2 to 10. A similar approach was used by Ref. 28 to calculate the confined flow measured by Ref. 15. The gross features of the flow are well predicted but the calculations appear to exhibit diffusion rates larger than those consistent with measured profiles, which can be attributed either to numerical or turbulence model errors. Grids up to 20 x 15 x 15 nodes were used, but further grid refinement is essential to identify the precise source of disagreement between measurements and predictions. Ref. 29 presented predictions of the flow measured by Ref. 25 using a three-dimensional finite-difference scheme together with the "k- ε" turbulence model and has showed the importance in prescribing the correct boundary conditions at the jet discharge. Making use of a similar procedure, Ref. 32 have shown that the primary characteristics of impinging flows are computed with reasonable accuracy, although specific aspects related with the strong curvature and anisotropy of impingement zones are dependent on accurate modeling of turbulent shear stresses which are not well predicted. Ref. 33 has shown that the standard "k-ε" model over predicts the spreading rate of a free jet and under predicts the spreading rate of a radial wall jet. More recently, Ref. 34 presented a comparison of experimental data and computational simulation to develop a jet entrainment theory for the prediction of lift loss.

The present paper presents a detailed analysis of the complex flow field beneath 2 impinging jets aligned with a low-velocity crossflow relevant for the future F-35 VSTOL configuration, and provides a quantitative picture of the main features of interest for impingement type of flows. This paper has four sections in which section II describes the experimental configuration and procedure, given details of the laser-Doppler velocimeter and assessments of accuracy. The arguments associated with these assessments are based on previous experiments data which are presented in condensed form. Section III presents the experimental results obtained in the vertical plane of symmetry containing the axis of both jets and quantifies the mean and turbulent velocity characteristics of the flow. The numerical results are discussed in Sect. IV on the basis of numerical visualization of the three-dimensional flow. The last section summarizes the main findings and conclusions of this work.

II. Experimental Method

A. Flow Configuration

The experiments were performed on a wind tunnel facility designed and constructed for the present work, with an exit section of 300x402 mm that is schematically shown in Fig. 2. The test section was made of Perspex allowing the passage of laser beams. During all the design process special consideration was taken for the boundary layer in which the recommendations of Ref. 23 for open circuit wind tunnels was followed. A fan with 15KW nominal power drives a maximum flow of 3000m^3/h through the boundary layer wind tunnel exit section.

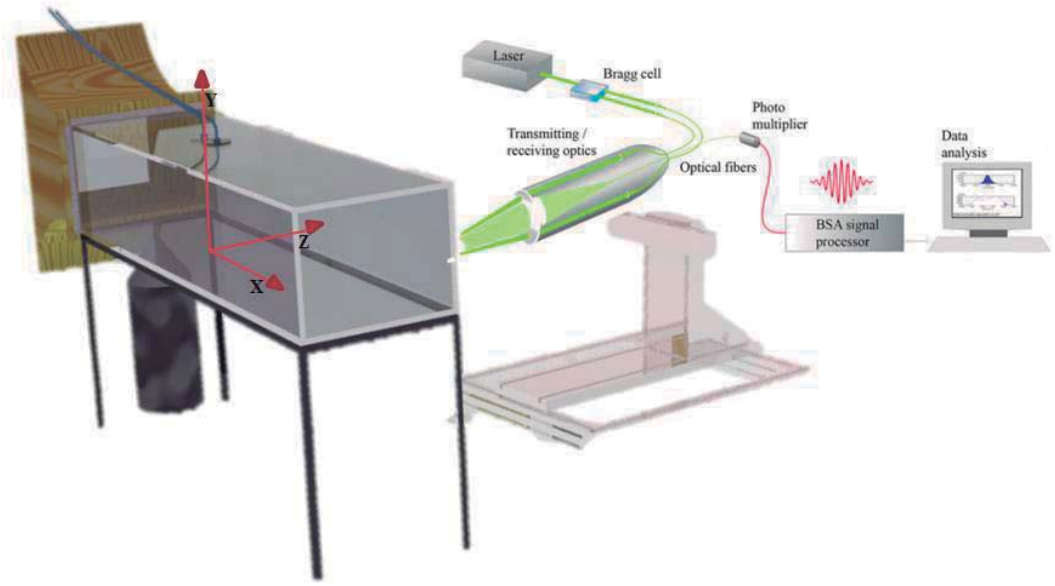

Figure 2: Experimental set-up

In the present study each jet unit of 15mm of inner diameter is mounted vertically in the top of the test section 20.1*D* above the ground plane with the axis contained in the vertical plane of symmetry parallel to the crossflow as showed schematically in Fig. 3.

The origin of the horizontal, *X*, and vertical, *Y*, coordinates is taken at the midpoint between the centers of the jets exit. The *X* coordinate is positive in the direction of the wind tunnel exit and *Y* is positive upwards.

The present results were obtained at the vertical plane of symmetry for jet mean velocity of V_j = 36m/s, a jet Reynolds number of $Re_j = 4.3\text{x}10^4$ and mean crossflow velocities of 0.8 m/s < U_o< 1.6m/s, corresponding to a velocities ratio, $22.5 < V_R = V_j/U_o < 43.8$.

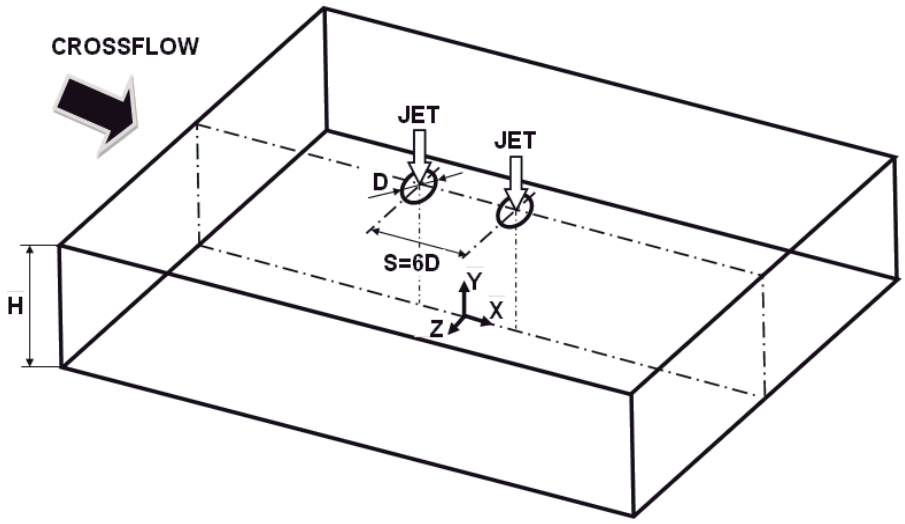

Figure 3: Geometrical arrangement of the jets

B. Experimental technique and accuracy

The velocity field was measured with a two-color (two-component) Laser-Doppler velocimeter (Dantec Flowlite 2D), which comprised a 10mW He-Ne and a 25mW diode-pumped frequency doubled Nd:YAG lasers, sensitivity to the flow direction provided by frequency shifting from a Bragg cell at f_0=40MHz, a transmission and backward-scattered light collection focal lens of 400mm. The half-angle between the beams was 2.8° and the calculated dimensions of the axis of the measuring ellipsoid volume at the e^{-2} intensity locations were 135x6.54x6.53μm and 112x5.46x5.45μm respectively (see Table 1 for details). The horizontal, $\overline{U}$ and vertical $\overline{V}$, mean and turbulent velocities were determined by a two-velocity channel Dantec BSA F60 processor. The seeding of the flow with glycerin particles of 0.1-5μm was produced by a smoke generator. The transmitting and collecting optics is mounted on a three-dimensional traversing unit, allowing the positioning of the center of the control volume within ±0.1mm.

In order to measure the vertical components in near wall regions, the transmitting optics were inclined by half angle of beam intersection and the scattered light was collected off-axis. Measurements could then be obtained up to 0.5mm from the ground plate without a significant deterioration of the Doppler signals. Results obtained 20mm above the ground plate with both the on-axis and the off-axis arrangements have shown a close agreement, within the precision of the equipment.

Table 1. Principal characteristics of the 2D Laser-Doppler velocimeter.

	He-Ne laser	Diode Laser
- Wave length, λ [nm]	633	532
- Focal length of focusing lens, f [mm]	400	400
- Beam diameter at e-2 intensity [mm]	1.35	1.35
- Beam spacing, s [mm]	38.87	39.13
- Calculated half-angle of beam intersection, θ	2.78°	2.8°
- Fringe spacing, δ_f [μm]	6.53	5.45
- Velocimeter transfer constant, K [MHz/ms^{-1}]	0.153	0.183

Systematic errors incurred in the measurements of Reynolds shear stresses can arise from lack of accuracy in the orientation angle on the normal to the anemometer fringe pattern, as shown by Ref. 31, and can be particularly large in the vicinity of the zones characterized by zero shear stress: for the present experimental conditions the largest errors are expected to be smaller than −2.5%.

III. Results

The results presented and discussed in this section include flow visualization for the velocity ratio V_R of 22.5 and detailed mean and turbulent velocity profiles for the velocity ratios V_R of 22.5, 33.7 and 43.8.

A. Visualization

Flow visualization was performed using digital direct photography to guide the choice of the measurement locations and to provide a qualitative picture of the flow. The longitudinal plane of symmetry was illuminated with a sheet of light. The photos were taken perpendicular to the vertical plane of symmetry. For all the flows studied, the results have shown (for each jet) a pattern similar to that of a single impinging jet. Figure 4 identifies the flow development along the vertical plane of symmetry, i.e. $Z = 0$. Each jet has an initial potential-core jet region, where the flow characteristics are identical to those of a free jet, and near the horizontal plate is present an impingement region, characterized by considerable deflection of the jet.

It was not possible to identify all the regions simultaneously in the same photo, neither a deflection of each jet by the crossflow. The selected picture shows the wall jet corresponding to the upstream impinging jet which is almost parallel to the ground plate and exhibits behavior similar to that of a radial wall jet where the upstream effects of interaction due to impingement are no longer important. The upstream wall jet interacts with the crossflow and forms a horseshoe vortex close to the ground plate, which wraps around both impinging jets. As a result, two streamwise counter-rotating vortices develop side-to-side and decay further downstream of each impinging zone forming a ground vortex. The nature of each ground vortex is similar to the horseshoe structure known to be generated by the deflection of a boundary layer by a solid obstacle[35], but is different from the

vortex pair known to exist in a "bent-over" jet in a crossflow far from the ground[36]. No evidence of a ground vortex corresponding to the downstream impinging jet could be confirmed, which is an indication that the upstream impinging jet and its ground vortex are blocking the crossflow and provoking an alteration to the flow pattern. If the jets were positioned side by side in front of the crossflow two ground vortexes would appear as well as a fountain flow in the vertical plane of symmetry due to the collision of the two individual radial wall jets (e.g., Refs. 20, 36-38). In the present case for a velocity ratio between the jet and the crossflow of V_R = 22.5 no fountain flow could be detected.

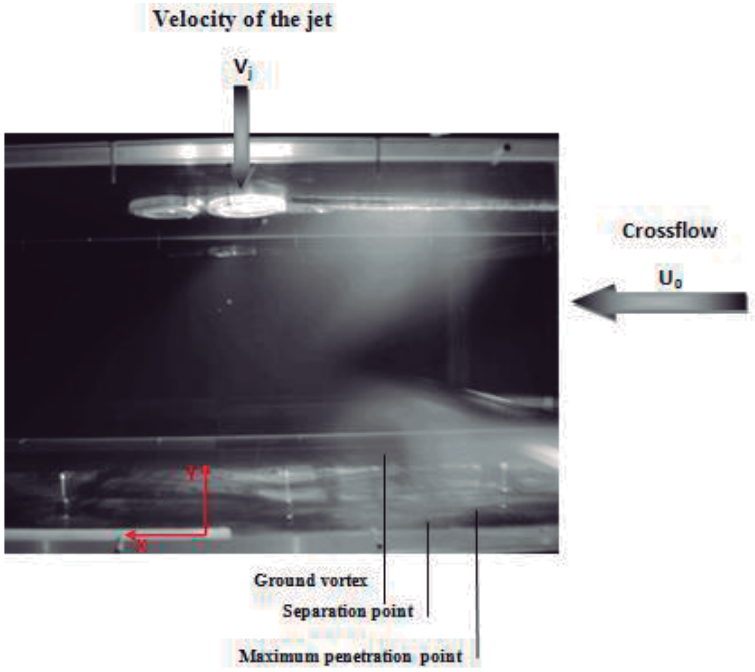

Figure 4: Visualization of the twin jet flow in the vertical plane of symmetry for Re_j = 4.3x10^4, V_j/U_o = 22.5, H/D = 20.1 and S/D = 6.

Analysis of Fig. 4 also suggests that the crossflow is deflected sideways by the penetration of the jet and may cause a recirculation region just downstream of the discharge, away from the ground plate, but cannot be clearly identified. These features of the flow are quantified in figures 2, 3 and 4 through a detailed set of mean and turbulent velocity measurements obtained in the vertical plane of symmetry (Z=0) for a Reynolds number based on the jet-exit conditions of 4.3x10^4, a free stream to jet velocity ratios, $V_R = V_j / U_o$ of 22.5, 33.7 and 43.8, a jet height to jet diameter ratio, H/D, of 20.1, and a spacing between the jets, S/D, of 6.

B. Measurements

Figures 5 and 7 show the vertical profiles of the horizontal, $\overline{U}$ and vertical, $\overline{V}$, mean velocity components along the vertical plane of symmetry (Z=0) for all the velocity ratios studied.

The results indicate that for the lower velocity ratio, the profiles corresponding to X/D = −6.33, −5.0 and −3.67 exhibit high velocity gradients in the region of 0 mm < Y <30 mm, and for Y > 30mm the horizontal velocity is substantially uniform. For the other two velocity ratios the corresponding profiles present negative values of mean horizontal velocity in the region Y < 30mm, evidence of presence of the flow recirculation. The experimental results have been fed to a plotting routine to calculate pathlines at selected locations, and the results shown in Fig. 6 confirmed this hypothesis.

The profile at X/D = −2.93 exposes the location of the first impinging jet. This profile and those further upstream exhibit negative values close to the ground, indicating the presence of a wall jet, revealing that the first jet was deflected by the crossflow. Figure 6a) indicates that the impinging point of the first jet is located at X/D= +2.93 vertically near the axis of the rear jet exit nozzle. As a consequence, the downstream wall jet of the first jet and the rear jet seems to merge rapidly in a single flow structure in the crossflow direction.

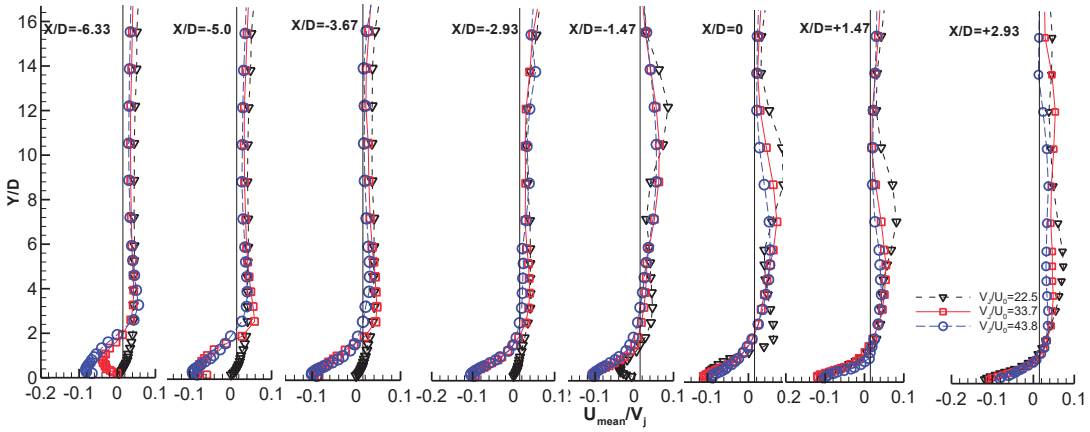

Figure 5: Vertical profiles of the mean horizontal velocity component, $\overline{U}/V_j$ (U_{mean}/V_j), along the longitudinal (symmetry) plane crossing the center of the twin jets. (Re_j = 4.3x10^4, H/D = 20.1, and S/D = 6).

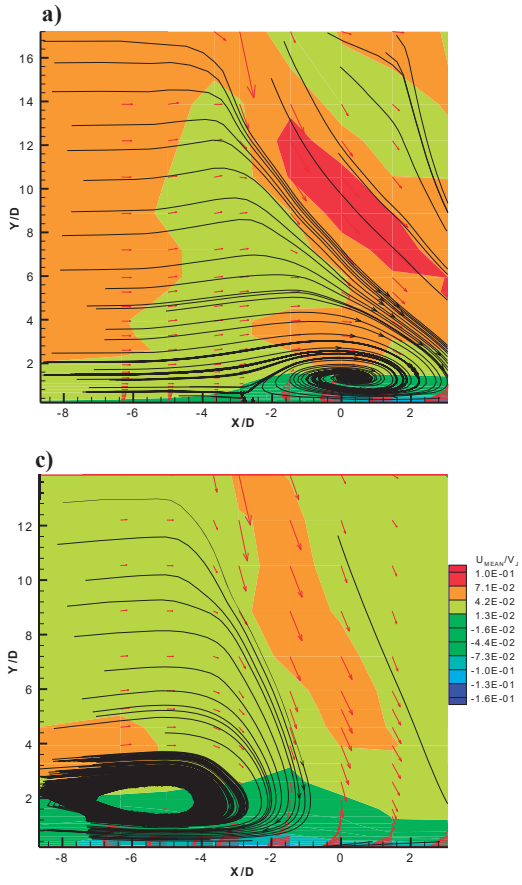

Figure 6: Mean vertical velocity field corresponding to the measured vertical profiles: a) V_j / U_o = 22.5; b) V_j / U_o = 33.7; c) V_j / U_o = 43.8.

The effect of the velocity ratio on the deflection of the upstream jet can be inferred from Figure 5 that reveals that the deflection of the jet decreases when the velocity ratio increases. This result is accompanied by the corresponding change of the impinging point location for each velocity ratio, from $X/D = 0$ for $V_j / U_o = 33.7$ and $X/D = -1.47$ for $V_j / U_o = 43.8$. Far away from the ground the positive values of the horizontal velocity component reach twice the value of the crossflow velocity, suggesting that no upstream wall jet resulting from the rear jet exists, but the complete jet is deflected by the crossflow. This result is consistent with the conclusion of Ref 21 that found for a single impinging jet that the ground vortex blocks the passage of the confined crossflow increasing the velocity of the crossflow. This is a most relevant result because a different pressure distribution in the under surface of a VSTOL aircraft may occur when it operates near ground with front wind or small forward movement, and may result in under pressures causing a suction down force and changing the pitching moment.

Figure 7 shows vertical profiles for mean vertical velocity component, $\overline{V}$ along the vertical plane of symmetry (Z=0).

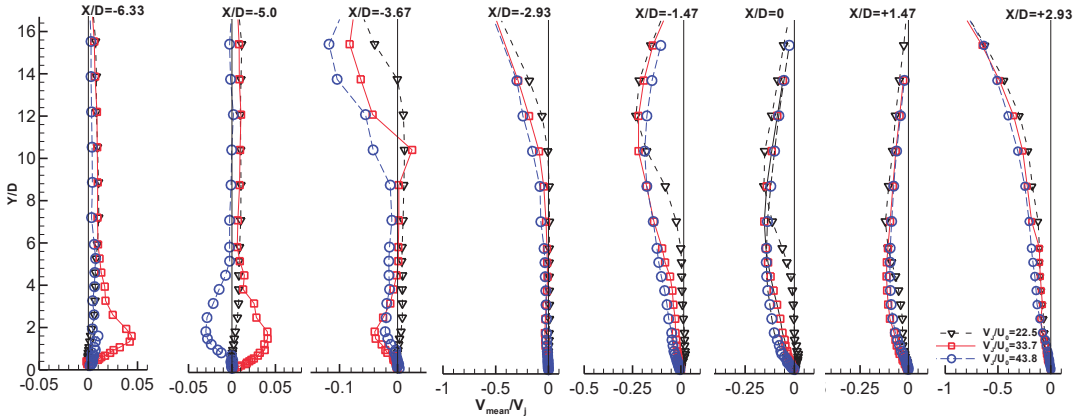

Figure 7: Vertical profiles of the mean horizontal velocity component, $\overline{V}/V_j$ (V_{mean}/V_j), along the longitudinal (symmetry) plane crossing the center of the twin jets. (Re_j=4.3x10^4, H/D=20.1, and S/D=6).

The first profile at $X/D = -6.33$ shows positive values of the mean vertical velocity component for all the velocity ratios studied, and for $V_j/U_0 = 33.7$ there is an increase at 0mm < Y < 30mm, which is not identified for the other velocity ratios. The next profile shows a large influence of the velocity ratio on the vertical velocity component. For an intermediate velocity ratio only positive values of the mean vertical velocity exist, with the largest values at 0mm < Y < 60mm due to a slight acceleration of the flow which passes over the ground vortex. For a higher velocity ratio ($V_j /U_o = 43.8$), the profile at the same location shows negative values of the mean vertical velocity, that correspond to locations inside the ground vortex.

The first jet is clearly identified at $X/D = -2.93$ for all the velocity ratios, through the negative values of vertical velocity close to the top wall, namely for $Y/D > 12$. For $X/D = -1.47$ and 0 the presence of the first jet it is also noticeable, by the negative values of the vertical velocity, which are more pronounced at $V_j /U_o = 33.7$ and 43.8. Finally the second jet it is identified in the profile at $X/D = 2.93$, that shows values of the mean vertical velocity component greater than those shown in the first jet. This means that there is no wall jet localized upstream of the rear jet, as mentioned before in the analysis of the mean horizontal velocity profiles, the rear jet is completely deflected by the crossflow.

Figures 8 (a) and (b) show horizontal profiles of the horizontal, $\overline{U}$ and vertical, $\overline{V}$ mean velocity components for all the velocity ratios studied, and quantify the development of the impinging jets and confirm the above description of the flow. In addition, this profile allows that the center of the first jet is moving in the crossflow direction. For $V_j /U_o = 22.5$ the center of the first jet moves from $X/D = -2.87$ at Y/D =18.6 to $X/D = +0.7$ at Y/D= +10.0, corresponding to a deflection angle of 21.9º.

For the higher velocity ratios, the jet deflection is smaller, corresponding to an angle of 14.42º for V_j /U_o = 33.7 and 12.66º for $V_j /U_o = 43.8$.

The rear jet is less deflected than the first jet due to the alignment with the first jet and the corresponding wake. In this case, the center of the rear jet is nearly coincident with the geometrical axis of the exit, and for

V_j/U_o = 22.5 and 33.7 it is located in X/D = +4 for Y/D = 10.0, corresponding to a deflection angle of 12.3º. For the other velocity ratio (V_j/U_o = 43.8), the deflection observed is slightly smaller, of the order of 8.2º.

The horizontal profiles of the mean vertical velocity component exhibit only positive values from the top wall (Y/D = 20.1) to the middle of the impinging height (Y/D = 10.0) for all the velocity ratios studied. This confirms the conclusions drawn from the vertical velocity profiles and discussed above.

The asymmetry of the flow can be confirmed from the horizontal profiles of the mean vertical velocity component with higher peaks up to 10% of the vertical velocity in the upstream side (X/D < 3.33). Also it is also possible to ascertain that for all the velocity ratios the horizontal profiles are very similar, showing only a small difference near the center of the jets for the mean vertical velocity. However, based on the maximum of the mean vertical velocity component the deflection angle of the rear jet is only 4.8º approximately for all the velocity ratios. Thus, this result confirms the initial hypothesis that the alignment of the jets with the crossflow would create a special flow pattern. The wall jet resulting from the first jet flows under the rear jet, and the upstream ground vortex is only interacting with the rear jet induced flow away from the vertical plane of symmetry.

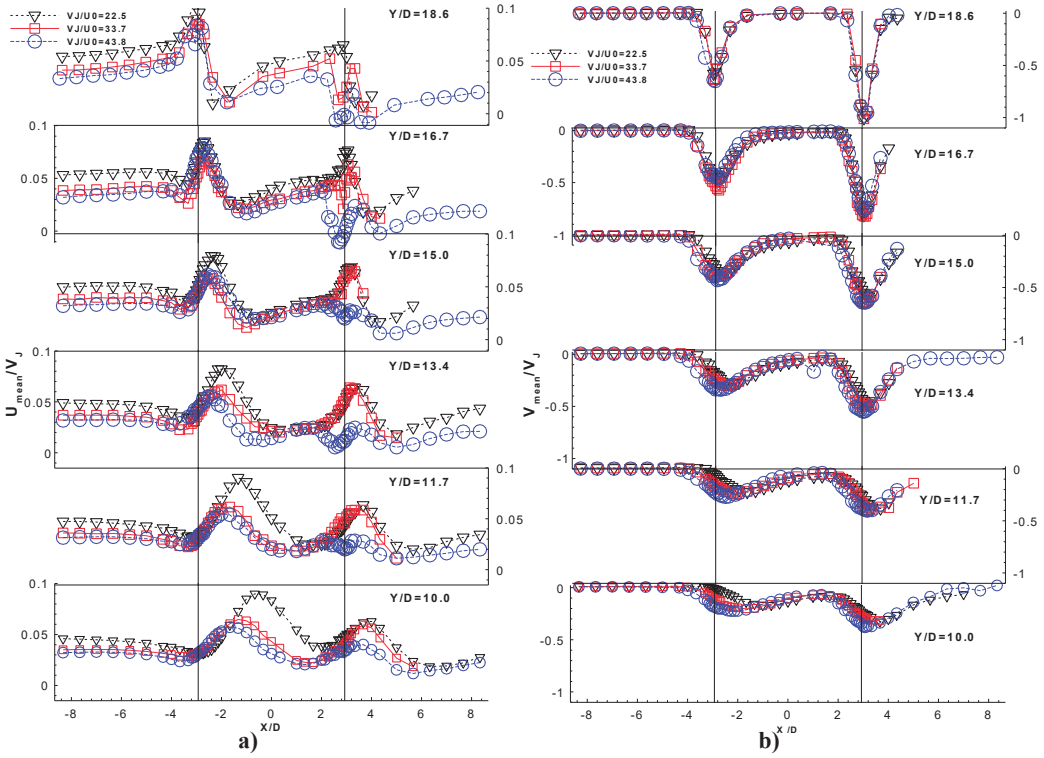

Figure 8: Horizontal profiles of the mean velocity characteristics along the longitudinal (symmetry) plane crossing the center of the twin jets: (a) Horizontal velocity, (b) Vertical velocity. (Re_j = 4.3x10^4, H/D = 20.1, and S/D = 6).

Figure 9 shows horizontal profiles of the rms values of the normal stresses, $\overline{u'^2}$ and $\overline{v'^2}$, and quantifies the effect of the velocity ratio. The profiles show results that are somewhat surprising at first sight, because it seems that it is not possible to identify completely the shear layer surrounding the impinging jets.

The horizontal profiles of the normal stresses show small peaks in the in the upstream side of the first jet (X/D < 3) for all the velocity ratios. In the downstream side of the first impinging jet others peaks are observed, mainly in the region close to X/D = 0 in Y/D = 16.7 and 15.0, which are more evident for the lower velocity ratio. For Y/D = 13.4 and 12.7, the peaks are practically unrecognizable for V_j/U_o = 22.5 and 33.7, but for the highest velocity ratio this peaks are very clear, with a maximum value of u_{rms}/V_j^2 = 0.015 at Y/D = 13.4. Downstream of the rear jet the shear layer surrounding the jet cannot be clearly identified for the lower velocity ratio. For the other velocity ratios the three profiles under the downstream jet exit of the impinging jets show some enhanced values localized downstream of the rear jet, that need further investigation.

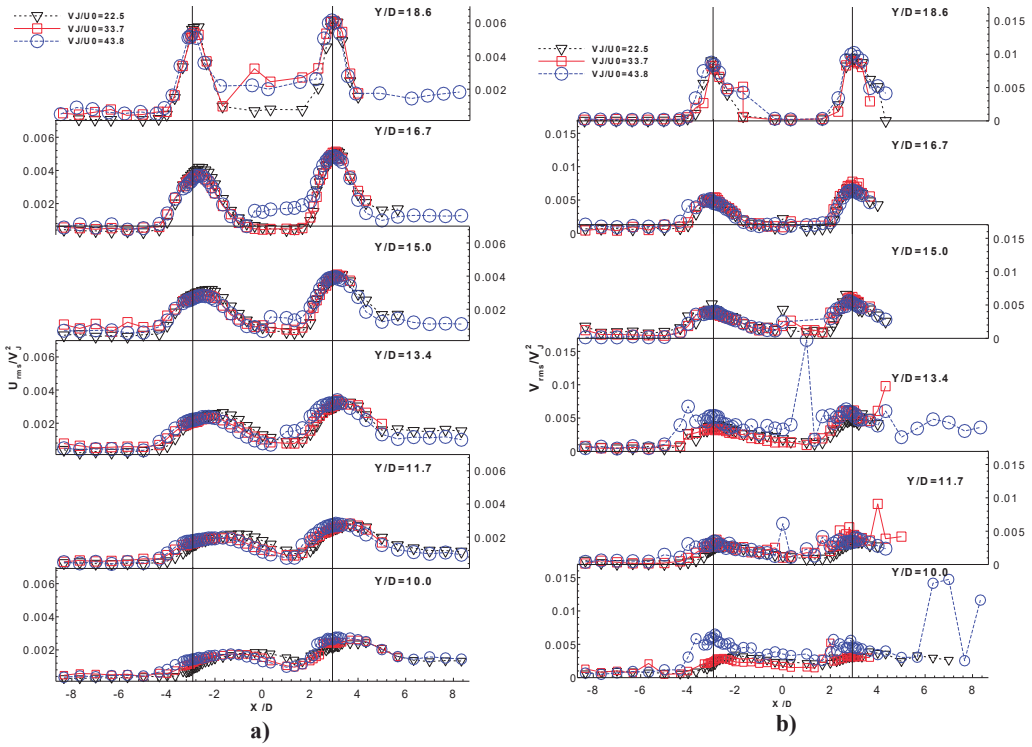

Figure 9: Horizontal profiles of the mean velocity characteristics along the longitudinal (symmetry) plane crossing the center of the twin jets: (a) Horizontal rms velocity, (b) Vertical rms velocity. (Re_j = 4.3x10^4, H/D = 20.1, and S/D = 6).

IV. Numerical Results

This section presents a numerical analysis based on the experimental data presented above. The objective of the numerical simulation is to compare the numerical predictions with the experimental data in order to quantify the performance of the computational model and to extend the analysis of the flow.

A. Mathematical Model

The mathematical model used in the numerical simulation is based on the solution of the continuity and momentum equations. A Reynolds-Averaged Navier Stokes (RANS) formulation was adopted with the "k-ε" turbulence model to represent the turbulent stresses.

The governing equations are written in a similar form:

$$\frac{\partial}{\partial x}(\rho u\phi) + \frac{1}{r}\frac{\partial}{\partial r}(r\rho v\phi) = \frac{\partial}{\partial x}\left(\Gamma_\phi \frac{\partial \phi}{\partial x}\right) + \frac{1}{r}\frac{\partial}{\partial r}\left(r\Gamma_\phi \frac{\partial \phi}{\partial r}\right) + S_\phi \qquad (1)$$

Where the property ϕ represents the velocity, turbulent kinetic energy or dissipation while S_ϕ and Γ_ϕ assume different values related with ϕ as described in table 2.

The turbulent diffusion terms are approximated by two equations from "k-ε" turbulent model where the Reynolds tension is related with shear tension:

$$\rho\overline{u'_\iota u'_J} = -\mu_T\left(\frac{\partial U_i}{\partial x_j} + \frac{\partial U_j}{\partial x_{ij}}\right) + \frac{2}{3}\delta_{ij}\rho k \qquad (2)$$

Where μ_T represent turbulent viscosity derivative from the turbulent model expressed by:

$$\Phi = \mu_T\left\{2\left[\left(\frac{\partial U}{\partial x}\right)^2 + \left(\frac{\partial V}{\partial r}\right)^2 + \left(\frac{V}{r}\right)^2\right] + \left[\frac{\partial U}{\partial r} + \frac{\partial V}{\partial x}\right]^2\right\} \qquad (3)$$

Table 2. Differential equations coefficients.

ϕ	Γ_ϕ	S_ϕ
1	0	0
U	μ_T	$-\frac{\partial p}{\partial x}+\frac{\partial}{\partial x}\left(\mu_T\frac{\partial U}{\partial x}\right)+\frac{1}{r}\frac{\partial}{\partial r}\left(r\mu_T\frac{\partial V}{\partial x}\right)$
V	μ_T	$-\frac{\partial p}{\partial r}+\frac{\partial}{\partial x}\left(\mu_T\frac{\partial U}{\partial r}\right)+\frac{1}{r}\frac{\partial}{\partial r}\left(r\mu_T\frac{\partial V}{\partial r}\right)-2\mu_T\frac{V}{r^2}$
k	μ_T/σ_k	$\Phi-\rho\varepsilon$
ε	μ_T/σ_ε	$C_{\varepsilon 1}\Phi\frac{\varepsilon}{k}-C_{\varepsilon 2}\rho\frac{\varepsilon^2}{k}$

The turbulent model constants allow good results for several types of flows and are summarized in the following table:

Table 3. Turbulent model constants**.**

C_μ	C_1	C_2	σ_k	σ_E
0.09	1.44	1.92	1.0	1.3

The computational domain corresponds to the experimental conditions and has 201 mm of transversal length, remaining constant the following measurements as followed: 1080 mm of longitudinal length, 402 mm of height where the inner diameter of the jets D is 15 mm, the spacing between jets are $S = 6D$ and the height of impact, H is 20.1 D.

B. Discussion

Figure 10 presents the numerical results for three velocity ratios, V_j/U_o of 22.5 33.7 and 43.8. For the smallest velocity ratio ($V_j/U_o = 22.5$) the impinging jet is considerably deflected by the crossflow before it reaches the ground, and no upstream wall jet is formed. The predictions show that the impact of the impinging jet on the ground occurs for $X/D > 20$ while the experiments indicate a stagnation line corresponding to the impact further upstream at $X/D = 4$. So, the computational method fails to predict the ground vortex which is located at $X/D = 0$ for this velocity ratio (see Fig. 6). Increasing the velocity ratio to $V_j/U_o = 33.7$ (case b) a small upwards structure corresponding to the ground vortex flow can now be identified with its center located near $X/D = 0$. However, the deflection of the impinging jet is still underpredicted with the impact occurring at $X/D = +5$ while the experimental location is $X/D = +1$. This deviation is also confirmed by the location of the center of the ground vortex which is $X/D = -4.5$ while the predicted value is $X/D = +1$. For $V_j/U_o = 43.8$ the predicted characteristics of the impinging zone and ground vortex are closer to the experimental values, but the deflection is still overpredicted. The predicted and experimental location of the center of the ground vortex are $X/D = -4$ and -5 respectively.

As far as the downstream jet (rear jet) is concerned the predictions confirmed the experimental results, and its complete deflection by the crossflow was calculated for all the velocity ratios considered with no impingement directly on the wall.

Figure 11 represents a section of the computational flow for the higher velocity ratio of 43.8. The colored areas limited by isolines represent the dimensionless mean horizontal velocity in the plane of symmetry. The wall jet and the ground vortex upstream the first jet near the ground can be identified by the negative values of the mean horizontal velocity component and the first pathline. The complete deflection of the second jet is also noticed by the pathline, and no interaction with the ground vortex resulting from the upstream jet can be detected.

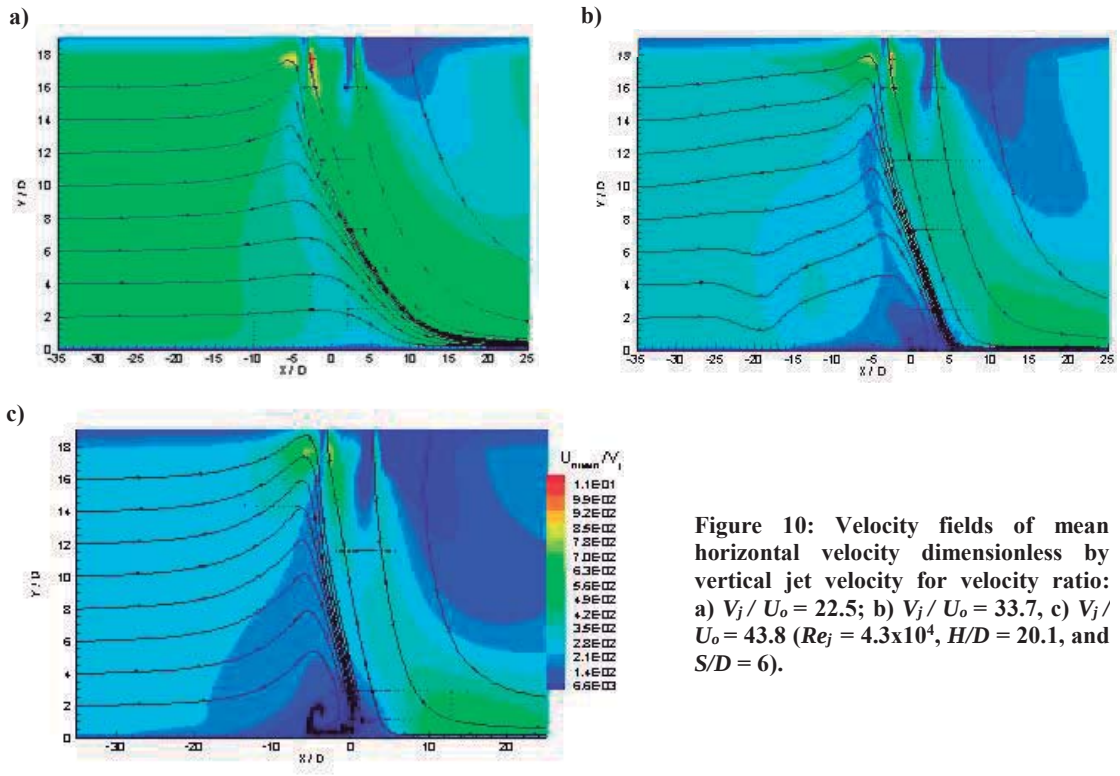

Figure 10: Velocity fields of mean horizontal velocity dimensionless by vertical jet velocity for velocity ratio: a) $V_j / U_o = 22.5$; b) $V_j / U_o = 33.7$, c) $V_j / U_o = 43.8$ ($Re_j = 4.3 \times 10^4$, $H/D = 20.1$, and $S/D = 6$).

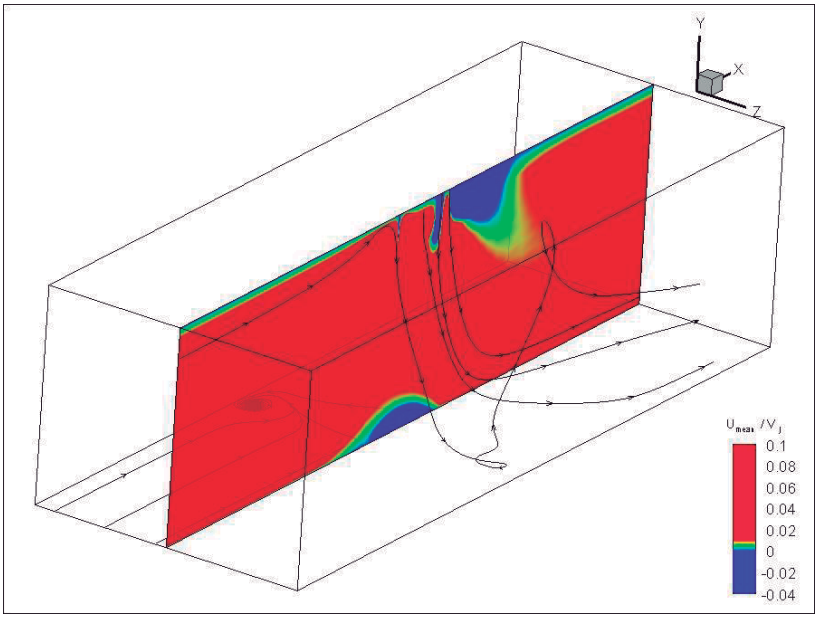

Figure 11: Mean horizontal velocity component and numerical flow visualization (pathline) for $V_j/U_o = 43.8$, $Re_j = 4.3 \times 10^4$, $H/D = 20.1$, and $S/D = 6$.

Figure 12 shows a zoom of the ground vortex region. This figure shows clearly that the part of the crossflow which is not captured by the ground vortex is strongly deflected upwards passing over it. This phenomenon is associated with a flow acceleration, and due to the confinement may be responsible for the "suckdown" effect.

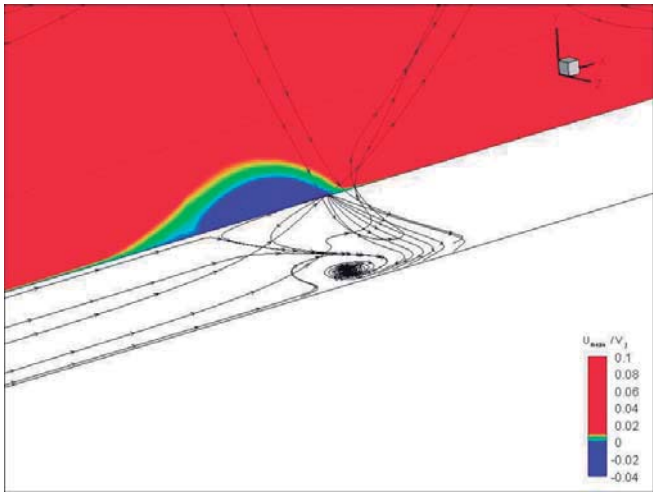

Figure 12: Detail of the ground vortex flow corresponding to Fig.11 (V_j / U_o = 43.8, Re_j = 4.3x10^4, H/D = 20.1, and S/D = 6).

V. Conclusion

A Laser Doppler Velocimeter was used to provide information on the flowfield created by twin impinging jets aligned with a low velocity crossflow. The experiment was carried out for a Reynolds number based on the jet exit conditions of Re_j=4.3x10^4 with an impingement height of 20.1 jet diameters and for a velocities ratio between the jet exit and the crossflow, V_R= V_j/U_o of 22.5, 33.7 and 43.8 with and an interjet spacing of S=6D. The results show a large penetration of the first (upstream) jet, which is deflected by the crossflow and impinges on the ground giving rise to a ground vortex due to the collision of the radial wall and the crossflow that wraps around the impinging point like a scarf. The first jet deflection and the location of the ground vortex depend on the velocity ratio used. For high velocities ratios the deflection of the first jet is smaller and closer to the first jet is located the center of the ground vortex. The rear jet it is not so affected by the crossflow in terms of deflection for all velocities ratio because it is protected by the upstream jet, but due to the downstream wall jet that flows radially from the impinging point the first jet does not reach the ground. Also due to the confinement and the ground vortex, the crossflow is blocked and accelerates in the upper part and also contributes to an enhanced mixing of each secondary flow. As consequence, no upstream wall jet or ground vortex resulting from the second (downstream) jet was detected. The effect of the rear jet impinging on the downstream wall jet resulting from the first jet had not been reported so far and requires further investigation.

A numerical analysis based on the experimental data was performed for three velocity ratios, ratios, V_j /U_o of 22.5 33.7 and 43.8. It was found that the deflection of the first impinging jet is overpredicted. The ground vortex was detected for the higher velocity ratios (V_j /U_o = 33.7 and 43.8) in agreement with the experimental data, although the size of the ground vortex was under estimated. As far as the downstream jet (rear jet) is concerned the predictions confirmed the experimental results, and its complete deflection by the crossflow was calculated for all the velocity ratios considered with no impingement directly on the wall.

Acknowledgments

The financial support of FCT-Fundação para a Ciência e Tecnologia under contract PTDC/EME-MFE/102190/2008 is gratefully acknowledged.

The present work was done in the scope of the activities of LAETA-Associated Laboratory of Energy, Transports and Aeronautics.

References

[1]Barata, J.M.M., Durão, D.F.G., and McGuirk, J.J., "Numerical Study of Single Impinging Jets Through a Crossflow", *Journal of Aircraft,*Vol.26, No.11, 1989, pp. 1002-1008.

[2]Knowles, K., and Bray, D., "The Ground Vortex Formed by Impinging Jets in Crossflow", AIAA 29th Aerospace Sciences Metting, AIAA Paper 91-0768, Reno, NV, Jan. 7-10, 1991.

[3]Barata, J.M.M., "Numerical and Experimental Study of Jets Impinging on Flat Surfaces Through a Crossflow", Ph.D. Thesis (in Portuguese), Instituto Superior Técnico, Technical Univ. of Lisbon, Lisbon, Portugal, 1989.

[4]Sarippali, K.R., "Laser Doppler Velocimeter Measuremnts in 3D Impinging Twin-Jet Fountain Flows", *Turbulent Shear Flows,* Vol.5, edited by Durst et al., Springer-Verlag, Berlin, 1987, pp. 147-168.

[5]Kind, R.J., and Suthanthiran, K., "The Interaction of Two Opposing Plane Turbulent Wall Jets", AIAA Paper 72-0211, Jan., 1980.

[6]Gilbert, B.L., "Detailed Turbulence Measurements in a Two Opposing Plane Turbulent Wall Jets", AIAA 16th Fluid and Plasma Dynamics Conf., AIAA Paper 83-1678, Danvers, MA, Jul. 12-14, 1983.

[7]Jenkins, R.C., and Hill, W.G., Jr., "Investigation of VTOL Upwash Flows Formed by Two Impinging Jets", Grumman Research Dept. Rept. RE-548, Bethpage, NY, Nov., 1977.

[8]Kotansky, D.R., and Glaze, L.W., "The Effects of Ground Wall-Jet Characteristics on Fountain Upwash Flow Formation and Development", Rept. ONR-CR212-216-1F, 1980.

[9]Kavasaoglu, M.S., Schetz, J.A., and Jakubowsky, A.K., "Rectangular Jets in a Crossflow", *Journal of Aircraft,* Vol.26, No. 9, 1989, pp. 793-804.

[10]Schetz, J.A., Jakubowsky, A.K. and Aoyagi, K., "Surface Pressures on a Flat Plate With Dual Jet Configurations", *Journal of Aircraft*, Vol.21, No.7, 1984, pp. 484-490.

[11]Araújo, S.R.B., Durão, D.F.G., and Firmino, F.J.G., "Jets Impinging Normally and Obliquelly to a Wall", AGARD CP 308, paper 5.

[12]Sugiyama Y., and Usami, Y., "Experiments on the Flow in and Around Jets Directed Normal to a Crossflow", *Bulletin JSME*, No.22, 1979, pp. 1736-1745.

[13]Andreopoulos, J., and Rodi, W., "Experimental Investigation of Jets in a Crossflow", *J. Fluid Mech.*, Vol.138, 1984, pp.93-127.

[14]Shayesteh, M.V. Shabaka, I.M.N.A., and Bradshaw, P., "Turbulent Structure of a Three-Dimensional Impinging Jet in a Crossflow", AIAA 23rd Aerospace Sciences Meeting, AIAA Paper 85-0044, Reno, NV, Jan. 14-17, 1985.

[15]Kamotani, Y., and Greber, I., "Experiments on Confined Turbulent Jets in a Crossflow", NASA CR-2392, 1974.

[16]Stoy, R.C., and Ben-Haim, Y., "Turbulent Jets in a Confined Crossflow", *J. Fluids Engng.*, No.95, 1973, pp.551-556.

[17]Crabb, D., Durão, D.F.G., and Whitelaw, J.H., "A Round Jet Normal to a Crossflow", *J. Fluids Engng.,*Vol.113, 1981, pp. 142-153.

[18]Barata, J.M.M., Durão, D.F.G., and McGuirk, J.J., "Numerical Study of Single Impinging Jets Through a Crossflow", *J. of Aircraft*, Vol.26, No.11, 1989, pp.1002-1008.

[19]Barata, J.M.M., Durão, D.F.G., Heitor, M.V., and McGuirk, J.J., "On the Analysis of an Impinging Jet on Ground Effects", *Experiments in Fluids*, No.15, 1993, pp.117-129.

[20]Barata, J.M.M., "Ground Vortex Formation with Twin Impinging Jets". Artigo SAE 962257, International Powered Lift Conference, Jupiter, Florida, 18-20 Nov., 1996.

[21]Barata, J.M.M., "Fountain Flows Produced by Multiple Impinging Jets in a Crossflow". *AIAA Journal*, Vol. 34, No.12, Dez. 1996, pp. 2523-2530 e *AIAA Journal on Disc*, Vol. 2, No.1, 1996.

[22]Adler, D.; Baron, A "Prediction of a three-dimensional circular turbulent jet in crossflow" *AIAA Journal, No.* 17, 1979, pp.168-174

[23]Durst, F., Melling, A., and Whitelaw, J.H., "*Principles and Practice of Laser-Doppler Anemometry*", 2nd ed., New York, Academic Press.

[24]Patankar, S. V., Basu, D. K. and Alpay, S. A "Prediction of the three-dimensional velocity field of a deflected jet" *J. Fluids Engng*., Vol. 99, 1979, pp. 758-762

[25] Sugiyama, Y. and Usami, Y. "Experiments on the flow in and around jets directed normal to a crossflow", Bulletin JSME, 1979, Vol. 22, pp. 1736-1745.

[26]Keffer, J. F. and Baines, W. D. "The round turbulent jet in a cross-wind", *J. Fluid Mech*., Vol. 15, 1963,pp. 481-496

[27]Yanta, W.J. and Smith, R.A., "Measurements of Turbulent Transport Properties with a Laser-Doppler Velocimeter", 11th Aerospace Sciences Meeting, AIAA Paper 73-0169, Washington, 1978.

[28]Jones, W. P. and McGuirk, J. J. ”Computation of a round turbulent jet discharging into a confined crossflow”, In: *"Turbulent Shear Flows-2",~* Bradbury et al., Springer Verlag, 1980, pp.223-245
[29]Demuren, A. O.”Numerical calculations of steady three-dimensional turbulent jets in crossflow” Comp. Meth. In Appl. Mech. and Engng. 1983, Vol. 37, pp. 309-328.
[30]Melling, A., and Whitelaw, J.H., “Turbulent Flow in a Rectangular Duct”, *J. Fluid Mechanics*, Vol. 78, 1975, pp.285-315.
[31]Baker, O.J., “The Turbulent Horseshoe Vortex”, *J. Wind Engineering and Industrial Aerodynamics*, Vol. 6, 1981, pp. 9.
[32] Childs, R. E. and Nixon, D. “Simulation of impinging turbulent jets”, paper AIAA-85-0047, presented at the AIAA 23rd Aerospace Science Meeting, Jan. 14- 17, 1985, Reno, Nevada.
[33] K. Knowles, “Computational Studies of impinging jets using k-ε Turbulence Models”, International Journal for Numerical Methods in Fluids, 1996, Vol. 22, pp. 799-810.
[34] Paul Bevilacqua, Richard Margason and Charles Gaharan, “A Jet Entrainment Theory for VTOL Aircraft Suckdown”, paper AIAA-2007-1397, 45th AIAA Aerospace Science Meeting and Exhibit, 8-11 Jan. 2007, Reno, Nevada.
[35]Andreopoulos, J. and Rodi, W., “Experimental Investigation of Jets in a Crossflow”, *J. Fluid Mechanics*, Vol. 138, 1984, pp. 127.
[36]Saripalli, K.R., “Visualization of Multijet Impingement Flow”, *AIAA Journal*, Vol. 21, 1983, pp. 483-484.
[37]Siclari, M.J., Migdal, D., Luzzi, T.W., Jr., Barche, J., and Palcza, J.L., “Development of Theoretical Models of Jet-Induced Effects on V/STOL Aircraft”, *Journal of Aircraft*, Vol. 13, No. 12, 1976, pp.938-944.
[38]Kotansky, D.R., “ The Modelling and Prediction of Multiple VTOL Aircraft Flow Fields in Ground Effect”, AGARD CP-308, Paper 16.

Laser Doppler Measurements of Twin Impinging Jets in Tandem through a Crossflow

Diana F. C. Vieira[1*], Diamantino F. G. Durão[2], Fernando M. S. P. Neves[1], André R. R. Silva[1], Jorge M. M. Barata[1]

1: Aerospace Science Department, Universidade da Beira Interior, Covilhã, 6200-358, Portugal
2: Universidade Lusíada, Lisboa, 1349-001, Portugal
* Correspondent author: dianavieir@gmail.com

Abstract Laser Doppler measurements provide information on the flow field created by twin impinging jets in tandem through a crossflow. The present experiments were carried out for a Reynolds number based on the jet exit conditions of Re_j=4.3x10^4, an impingement height of 20.1 jet diameters and mean crossflow velocities of 0.8 m/s < U_0 < 1.6 m/s, corresponding to velocity ratios, V_R= V_j/U_0, from 22.5 to 43.8, and an interject spacing of S=6D. The results show a large penetration of the first (upstream) jet that is deflected by the crossflow and impinges on the ground, giving rise to a ground vortex due to the collision of the radial wall and the crossflow that wraps around the impinging point like a scarf. The rear jet (located downstream) is completely deflected by the crossflow, and no wall jet is localized upstream of the rear jet. The experimental results confirm the initial hypothesis that the alignment of the jets with the crossflow would create a special flow pattern. To complete the experimental work, the investigation continued for velocity beyond the limits of the experimental rig through computational simulations. The numerical results show that for the smallest velocity ratios the jets initially do not mix, but remain together in two layers. Three different types of flow regimes were identified, but for a V/STOL aircraft operating in ground vicinity the regime associated with strong impingement on the ground and a ground vortex is the most relevant. In both experimental and numerical cases the first jet deflection and the location of the ground vortex depend on the velocity ratio used. Finally, the numerical results allowed to extend the experimental results, and to prove that the deflection of the rear jet is due to the competing influences the wake, shear layer and downstream wall jet of the first jet and the crossflow.

Nomenclature

C_μ, C_1, C_2 = turbulent model constants
D = diameter of the jet
H = impinging height
k = turbulent kinetic energy
r = radius of cylindrical coordinates
Re = Reynolds number
S = distance between the jets axis
S_φ = source term
U = horizontal velocity, $\overline{U} + u'$ (U_{mean}+u′)
V = vertical velocity, $\overline{V} + v'$ (V_{mean}+v′)
V_R = velocity ratio, V_j/U_o
W = transverse $\overline{W} + w'$ (W_{mean}+w′)
X = horizontal coordinate
Y = vertical coordinate
Z = transverse coordinate

Greek symbols

Γ_φ = transport coefficient
ε = turbulent kinetic energy dissipation
μ_T = turbulent viscosity

ρ = density
σ_k, σ_ε = turbulent Prandtl/Schmidt numbers
φ = variable in general conservation equation
Φ = turbulent kinetic energy production term
Subscripts
j = jet-exit value
o = crossflow value

1. Introduction

Turbulent jets impinging on flat surfaces through a low-velocity crossflow are typical of the flow beneath a short/vertical take-off aircraft which is lifting off or landing with zero or small forward momentum. Ground effect may occur and change the lift forces on the aircraft, cause reingestion of exhaust gases into the engine intake and raise fuselage skin temperatures. During a landing or hover the impingement of each downward-directed jet on the ground results in the formation of a wall jet which flows radially from the impinging point along the ground surface. The interaction of this wall jet with the free stream results in the formation of a ground vortex far upstream of the impinging jet, which has serious implications on the aircraft design. If there are two or more adjacent jets, the resulting wall jets meet, and a fan-shaped upwash, or "fountain", is normally formed between the jets. The fountain upwash flow depending on its strength and direction affects the forces and moments induced in the aircraft when operating in ground effect. The resulting ground vortex shape is strongly affected and the corresponding induced suckdown effect tends to be reduced by the upload produced by the fountain. Therefore, improved knowledge of impinging jet flows are required to control these effects and to be able to model a range of jet-impingement types of applications with practical interest. Earlier published work has been concentrated on 1, 2, and 3 jets configurations relevant to the Harrier / AV-8B aircraft. In this case when the aircraft is operating with small forward movement the configuration of interest are 2 impinging jets with the direction of the crossflow perpendicular to the line containing their centres. If the attention is concentrated on the next generation of VSTOL aircrafts (X-35/F-35/JSF-Joint Strike Fighter) then no relevant studies can be found, because the impinging jets are aligned with the crossflow, and this geometry has not been considered.

In this case a vertically oriented lift fan (SDLF) generates a column of cool air that produces the nearly 20,000 pounds of lifting power, along with an equivalent amount of thrust from the vectored rear exhaust (3BSM-Three Bearing Swivel Module). The lift system of the X-35B was successfully demonstrated during a flight testing in the summer of 2001. The complexity of the new VSTOL configuration together with the very stringent requirements has required an enormous amount of R&D in the last decade. So, most of the published work reported so far has therefore only peripheral relevance to the F35-B/JSF ground effect problem.

A recent papers (Ref. 15 and 16) reports experimental and numerical study of multijet impinging jet configuration or fountain upwash flows, which are the centre of the complicated effects by V/STOL aircrafts when they operate in ground vicinity, being the most studied geometry that presents jets arranged side by side. Thus, and so represent more realistically what happens in the future F-35 VSTOL configuration (Fig.1), this paper presents a detailed analysis of the complex flow field beneath two impinging jets aligned with a low velocity crossflow, and provides a quantitative and a qualitative picture of the main features of interest for impinging types of flows. The measurements were extended to regions where the measurements were difficult to obtain by numerical simulations, and the effect of the velocity. Additionally, a study of the effect of the velocity ratio between the jet exit and the crossflow, $V_R = V_J/U_0$, was also performed numerically.

The remainder of this paper is presented in four sections. Section II describes the experimental configuration and measurement procedure, gives details of the laser-Doppler velocimeter and provides assessments of accuracy. The arguments associated with these assessments are based on previous experiments and are presented in condensed form. Section III presents the experimental results obtained in the vertical plane of symmetry containing the axis of both jets and quantifies the mean and turbulent velocity characteristics of the flow. The numerical results are discussed in Sect. IV on the basis of numerical visualization of the three-dimensional flow. The last section summarizes the main findings and conclusions of this work.

Fig. 1 Representation of the ground vortex flow phenomena adapted to the JSF F-35 Variant B.

2. Experimental method

The wind tunnel facility designed and constructed for the present work is schematically shown in Fig. 2. During all the design process, especially for the boundary layer part of the flow, were followed the recommendations of Ref. 20 for open circuit wind tunnels. A fan with 15KW nominal power drives a maximum flow of 3000m^3/h through the boundary layer wind tunnel of 300x302mm exit section. Each jet unit of 15mm inner diameter is mounted vertically in the top of the test section with the axis contained in the vertical plane o symmetry parallel to the crossflow.
The origin of the horizontal, X, and vertical, Y, coordinates is taken at the midpoint between the centres of the jets exit (Fig. 3). The X coordinate is positive in the direction of the wind tunnel exit and Y is positive upwards.
The present results were obtained at the vertical plane of symmetry for jet mean velocities of V_j=36m/s and mean crossflow velocities of 0.8 m/s<U_0<1.6m/s, corresponding to a velocity ratios, 22.5<V_R=V_j/U_o <43.8.
The velocity field was measured with a two-colour (two-component) Laser-Doppler velocimeter (Dantec Flowlite 2D), which comprised a 10mW He-Ne and a 25mW diode-pumped frequency doubled Nd:YAG lasers, sensitivity to the flow direction provided by frequency shifting from a

Bragg cell at f_0=40MHz, a transmission and backward-scattered light collection focal lens of 400mm. The half-angle between the beams was 2.8° and the calculated dimensions of the axis of the measuring ellipsoid volume at the e^{-2} intensity locations were 135x6.54x6.53μm and 112x5.46x5.45μm respectively (see Table 1 for details). The horizontal, $\overline{U}$ and vertical $\overline{V}$, mean and turbulent velocities were determined by a two-velocity channel Dantec BSA F60 processor. The seeding of the flow with glycerine particles of 0.1-5μm was produced by a smoke generator. The transmitting and collecting optics is mounted on a three-dimensional traversing unit, allowing the positioning of the centre of the control volume within ±0.1mm.

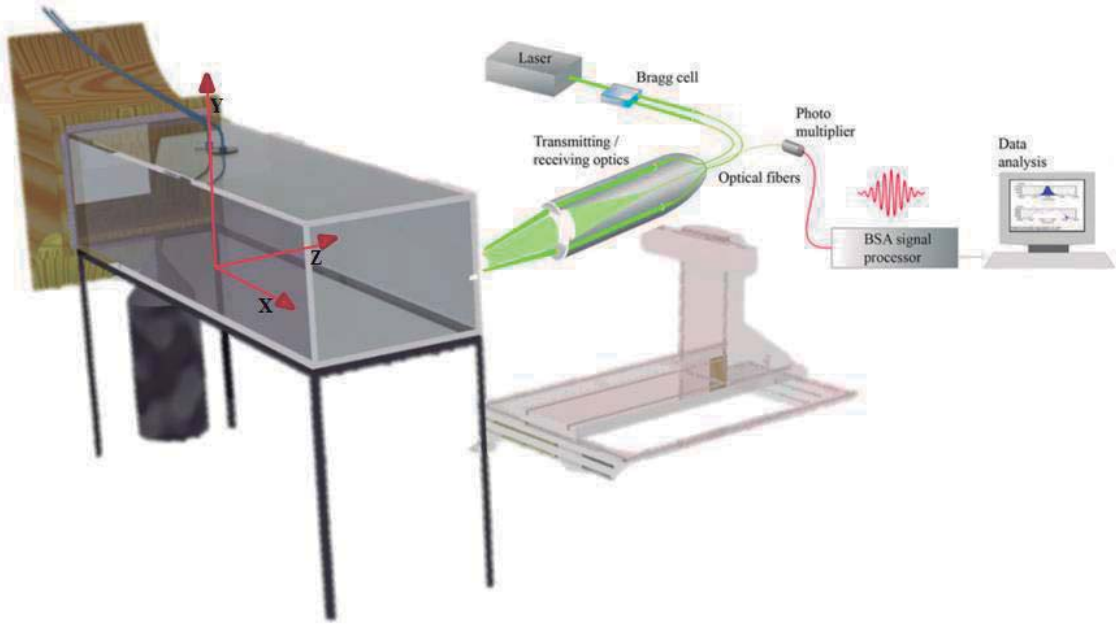

Fig 2 Experimental set-up.

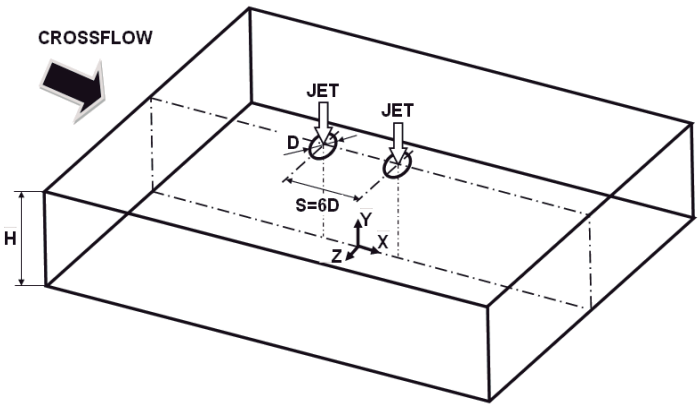

Fig 3 Geometrical arrangement of the jets

Table 1 Principal characteristics of the 2D Laser-Doppler velocimeter.

	He-Ne laser	Diode Laser
- Wave length, λ [nm]	633	532
- Focal length of focusing lens, f [mm]	400	400
- Beam diameter at e-2 intensity [mm]	1.35	1.35
- Beam spacing, s [mm]	38.87	39.13
-Calculated half-angle of beam intersection, θ	2.78º	2.8º
- Fringe spacing, δ_f [μm]	6.53	5.45
-Velocimeter transfer constant, K [MHz/ms^{-1}]	0.153	0.183

In order to measure the vertical components in near wall regions, the transmitting optics were inclined by half angle of beam intersection and the scattered light was collected off-axis. Measurements could then be obtained up to 0.5mm from the ground plate without a significant deterioration of the Doppler signals. Results obtained 20mm above the ground plate with both the on-axis and the off-axis arrangements have shown a close agreement, within the precision of the equipment.

Errors incurred in the measurement of velocity by displacement and distortion of the measuring volume due to refraction on the duct walls and change in the refractive index were found to be negligibly small and within the accuracy of the measuring equipment. Non-turbulent Doppler broadening errors due to gradients of mean velocity across the measuring volume may affect essentially the variance of the velocity fluctuations[21], but for the present experimental conditions are of the order of $10^{-4}V_j^2$ and, therefore, sufficiently small for their effect to be neglected. The largest statistical (random) errors derived from populations of, at least, 10000 velocity values were of 0.5 and 3%, respectively for the mean and the variance values, according to the analysis recommended by Ref. 32 for a 95% confidence interval. No corrections were made for sampling bias, but no correlations were found between Doppler frequencies and time interval between consecutive bursts even in the zones of the flow characterized by the lowest particle arrival rates, suggesting that those effects are unimportant for the present flow conditions. Systematic errors incurred in the measurements of Reynolds shear stresses can arise from lack of accuracy in the orientation angle on the normal to the anemometer fringe pattern, as shown by Ref. 5, and can be particularly large in the vicinity of the zones characterized by zero shear stress: for the present experimental conditions the largest errors are expected to be smaller than -2.5%.

3. Results

In this chapter, experimental data obtained will be presented and discussed under three headings. First, flow visualization is presented, then mean and turbulent velocity profiles are presented and discussed for the velocity ratios $22.5 < V_R < 43.8$ and to finish this chapter will be presented the computational results for velocity ratios beyond the limits of the experimental rig.

A. **Visualization**

Flow visualization was performed using digital direct photography to guide the choice of the measurement locations and to provide a qualitative picture of the flow. The longitudinal vertical

plane of symmetry was illuminated with a sheet of light. The photos were taken perpendicular to the vertical plane of symmetry. For all the flows studied, the results have shown a pattern similar to that of a single impinging jet. Fig. 4 identifies the flow development along the vertical plane of symmetry, i.e. Z=0. Each jet has an initial potential-core jet region, where the flow characteristics are identical to those of a free jet, and near the horizontal plate the impingement region, characterized by considerable deflection of the first jet. Analysing the fig. 3, it is clear that for the higher velocity ratios the deflection of the first jet is smaller. For all velocity ratios the deflection of the rear jet is very small compared with the first jet deflection because the first jet protects the rear jet of the influence of the crossflow, and there was not impact of the rear jet on the ground for the lower velocity ratio. However, for the two higher velocity ratios is notorious a drop in the rear jet potential core region that it has not been reported in literature. The horseshoe vortex resulting from the interaction of the upstream wall jet with the crossflow could not be identified for all the velocity ratios. The nature of each ground vortex is similar to the horseshoe structure known to be generated by the deflection of a boundary layer by a solid obstacle[2], but is different from the vortex pair known to exist in a "bent-over" jet in a crossflow far from the ground[37]. It was not possible to identify the ground vortex corresponding to the upstream impinging jet for the smallest velocity ratios. In case of the higher velocity ratio, the Fig.3c) shows that the crossflow is deflected sideways by the penetration of the jet and may cause a recirculation region just downstream of the discharge, away from the ground plate, but cannot be clearly identified. Also, it is possible see a little ground vortex and the wall jet corresponding to the upstream impinging jet which is almost parallel the ground plate and exhibit a behaviour similar to that of a radial wall jet where the upstream effects of interaction due to impingement are no longer important. The upstream wall jet interacts with the crossflow and forms a horseshoe vortex close to the ground plate, which wraps mostly around the first impinging jet. As a result, two streamwise counter-rotating vortices develop side-to-side and decay further downstream of each impinging zone forming a ground

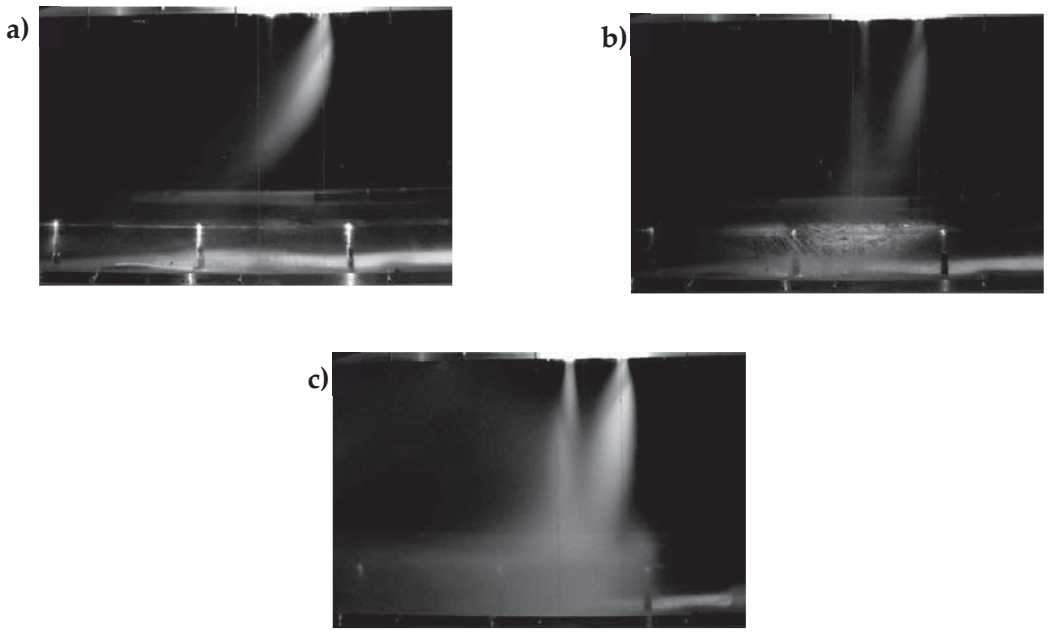

Fig 4 Visualization of the twin jet flow in the vertical plane of symmetry for Re_j=4.3x10^4, H/D=20.1, and S/D=6: a) V_j/U_0=22.5, b) V_j/U_0= 33.7, and c) V_j/U_0=43.8.

vortex. If the jets were positioned side by side in front of the crossflow two ground vortexes would appear as well as a fountain flow in the vertical plane of symmetry due to the collision of the two individual radial wall jets (e.g., Refs. 10, 31, 35, 37). No evidence of a ground vortex corresponding to the downstream impinging jet could be confirmed, which is an indication that the upstream impinging jet and its ground vortex are blocking the crossflow and provoking an alteration to the flow pattern. Also, in the present study no fountain flow was detected for all velocity ratios considered. All these features of the flow are quantified in the next figures through a detailed set of experimental and numerical results obtained in the vertical plane of symmetry (Z=0) for a Reynolds number based on the jet-exit conditions of 4.3×10^4, a free stream to jet velocity ratios, $22.5<V_R=V_j/U_o<43.8$, a jet height to jet diameter ratio, H/D, of 20.1, and a spacing between the jets, S/D, of 6.

B. Measurements

Figure 5 shows vertical profiles of the mean horizontal velocity component, $\overline{U}$, along the vertical plane of symmetry (Z=0).

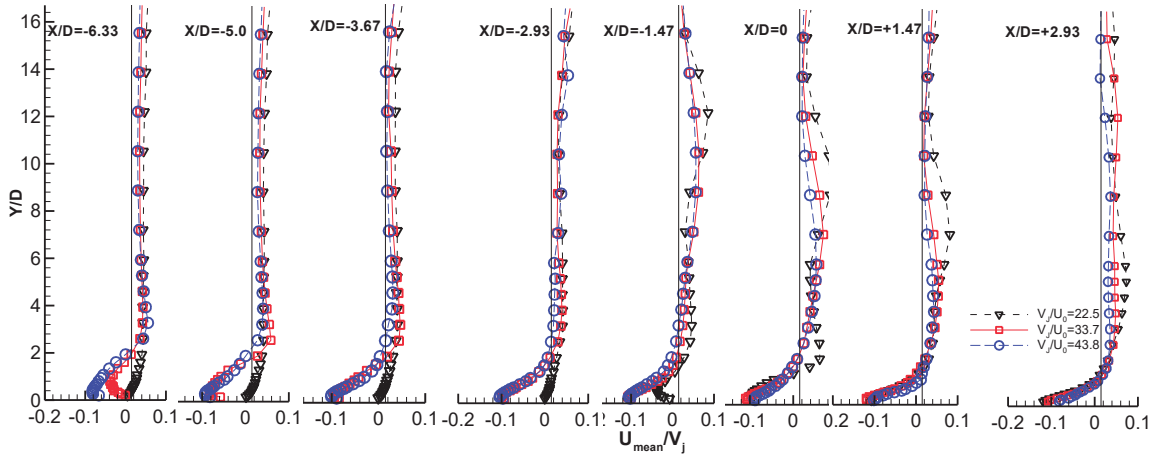

Fig 5 Vertical profiles of the mean horizontal velocity component, $\overline{U}/V_j$ (U_{mean}/V_j), along the longitudinal (symmetry) plane crossing the centre of the two jets. ($Re_j = 4.3\times10^4$, H/D = 20.1, and S/D = 6).

The results indicate that for the lower velocity ratio, the profiles corresponding to $X/D = -6.33$, -5.0 and -3.67 exhibit high velocity gradients in the region of 0 mm < Y <30 mm, and for Y > 30mm the horizontal velocity is substantially uniform. For the other two velocity ratios the corresponding profiles present negative values of mean horizontal velocity in the region Y < 30mm, evidence of presence of the flow recirculation. The profile at $X/D = -2.93$ exposes the location of the first impinging jet. This profile and those further upstream exhibit negative values close to the ground, indicating the presence of a wall jet, revealing that the first jet was deflected by the crossflow.

Figure 6 shows vertical profiles for mean vertical velocity component, $\overline{V}$ along the vertical plane of symmetry (Z=0). The first profile at $X/D = -6.33$ shows positive values of the mean vertical velocity component for all the velocity ratios studied, and for $V_j/U_0 = 33.7$ there is an increase at 0mm < Y < 30mm, which is not identified for the other velocity ratios. The next profile shows a large influence of the velocity ratio on the vertical velocity component. For an intermediate velocity ratio only positive values of the mean vertical velocity exist, with the largest values at

0mm < *Y* < 60mm due to a slight acceleration of the flow which passes over the ground vortex. For a higher velocity ratio (V_j/U_o = 43.8), the profile at the same location shows negative values of the mean vertical velocity, that correspond to locations inside the ground vortex.

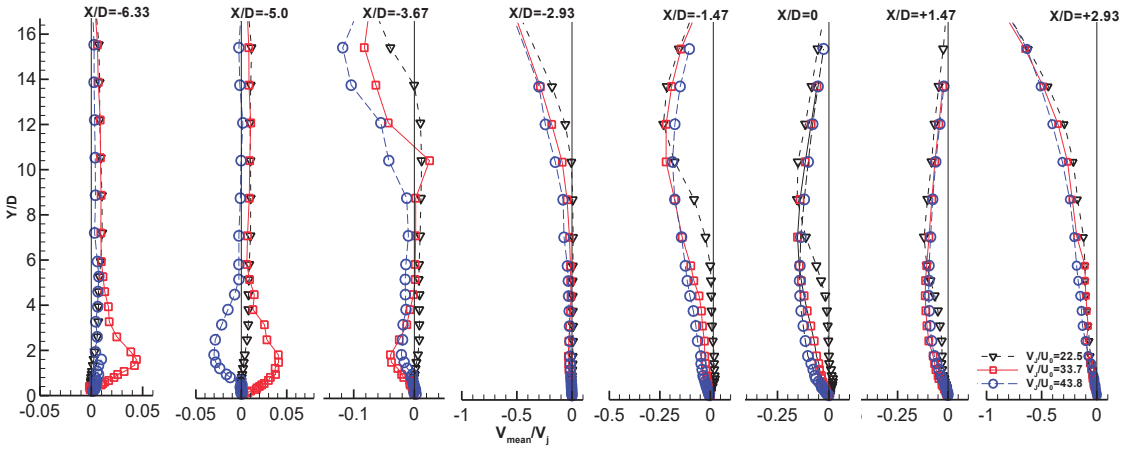

Fig. 6 Vertical profiles of the mean horizontal velocity component, $\overline{V}/V_j$ (V_{mean}/V_j), along the longitudinal (symmetry) plane crossing the centre of the twin jets. (Re_j=4.3x10⁴, H/D=20.1, and S/D=6).

The first jet is clearly identified at *X/D* = −2.93 for all the velocity ratios, through the negative values of vertical velocity close to the top wall, namely for *Y/D* > 12. For *X/D*= −1.47 and 0 the presence of the first jet it is also noticeable, by the negative values of the vertical velocity, which are more pronounced at V_j/U_o = 33.7 and 43.8. Finally the second jet it is identified in the profile at *X/D* = 2.93, that shows values of the mean vertical velocity component greater than those shown in the first jet. This means that there is no wall jet localized upstream of the rear jet, as mentioned before in the analysis of the mean horizontal velocity profiles, the rear jet is completely deflected by the crossflow.

Figures 7 (a) and (b) show horizontal profiles of the horizontal, $\overline{U}$ and vertical, $\overline{V}$ mean velocity components for all the velocity ratios studied, quantify the development of the impinging jets, and confirm the above description of the flow. In addition, these profiles show that the centre of the first jet is moving in the crossflow direction. For V_j/U_o = 22.5 the centre of the first jet moves from *X/D* = −2.87 at *Y/D* =18.6 to *X/D* = +0.7 at *Y/D*= +10.0, corresponding to a deflection angle of 21.9º. For the higher velocity ratios, the jet deflection is smaller, corresponding to an angle of 14.42º for V_j/U_o = 33.7 and 12.66º for V_j/U_o = 43.8. The rear jet is less deflected than the first jet due to the alignment with the first jet and the corresponding wake. In this case, the centre of the rear jet is nearly coincident with the geometrical axis of the exit, and for V_j/U_o = 22.5 and 33.7 it is located in *X/D* = +4 for *Y/D* = 10.0, corresponding to a deflection angle of 12.3º. For the other velocity ratio (V_j/U_o = 43.8), the deflection observed is slightly smaller, of the order of 8.2º. The horizontal profiles of the mean vertical velocity component exhibit only positive values from the top wall (*Y/D* = 20.1) to the middle of the impinging height (*Y/D* = 10.0) for all the velocity ratios studied. This confirms the conclusions drawn from the vertical velocity profiles and discussed above.

The asymmetry of the flow can be confirmed from the horizontal profiles of the mean vertical velocity component with higher peaks up to 10% of the vertical velocity in the upstream side (*X/D*

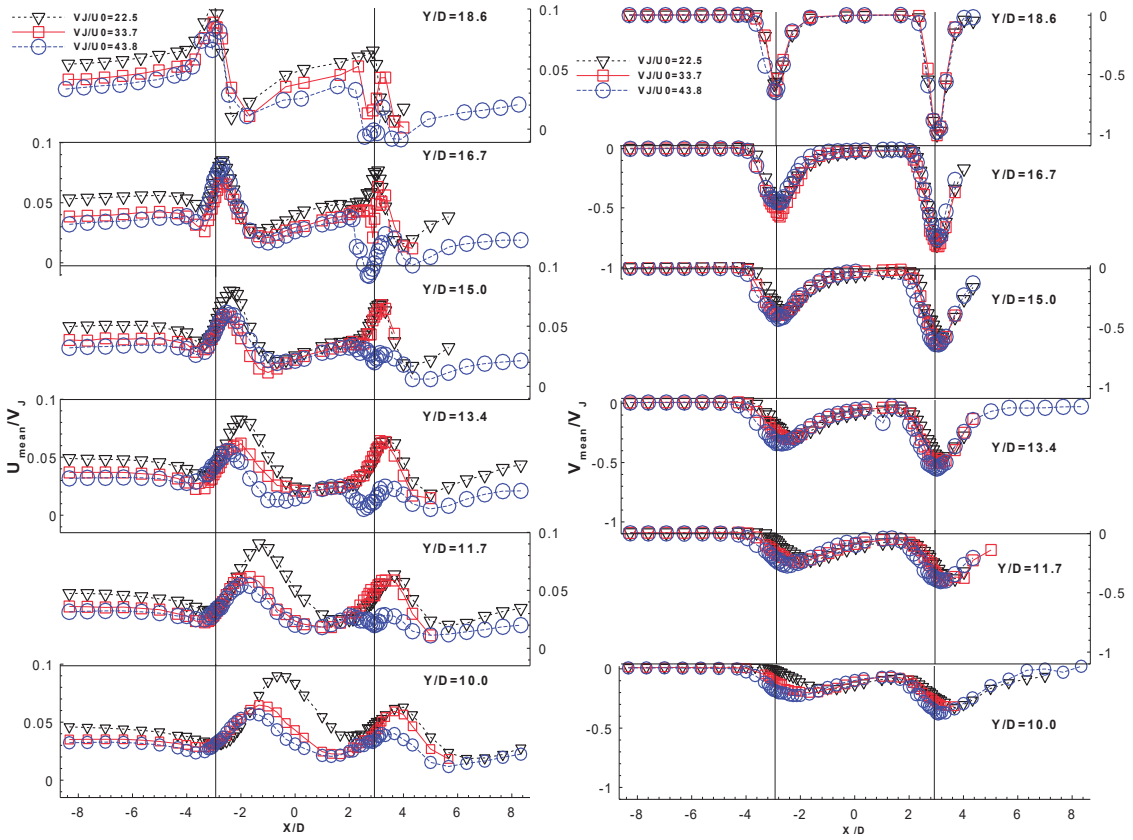

Fig 7 Horizontal profiles of the mean velocity characteristics along the longitudinal (symmetry) plane crossing the center of the twin jets: (a) Horizontal velocity, (b) Vertical velocity. (Re_j = 4.3x10⁴, H/D = 20.1, and S/D = 6).

< 3.33). Also it is also possible to ascertain that for all the velocity ratios the horizontal profiles are very similar, showing only a small difference near the centre of the jets for the mean vertical velocity. However, based on the maximum of the mean vertical velocity component the deflection angle of the rear jet is only 4.8º approximately for all the velocity ratios. Thus, this result confirms the initial hypothesis that the alignment of the jets with the crossflow would create a special flow pattern. The wall jet resulting from the first jet flows under the rear jet, and the upstream ground vortex is only interacting with the rear jet induced flow away from the vertical plane of symmetry. Figure 8 shows horizontal profiles of the rms values of the normal stresses, $\overline{u'^2}$ and $\overline{v'^2}$, and quantifies the effect of the velocity ratio. The profiles show results that are somewhat surprising at first sight, because it seems that it is not possible to identify completely the shear layer surrounding the impinging jets.

The horizontal profiles of the normal stresses show small peaks in the in the upstream side of the first jet (X/D < 3) for all the velocity ratios. In the downstream side of the first impinging jet others peaks are observed, mainly in the region close to X/D = 0 in Y/D = 16.7 and 15.0, which are more evident for the lower velocity ratio. For Y/D = 13.4 and 12.7, the peaks are practically unrecognizable for V_j/U_o = 22.5 and 33.7, but for the highest velocity ratio this peaks are very clear, with a maximum value of u_{rms}/V_j^2 = 0.015 at Y/D = 13.4. Downstream of the rear jet the shear layer

surrounding the jet cannot be clearly identified for the lower velocity ratio. For the other velocity ratios the three profiles under the downstream jet exit of the impinging jets show some enhanced values localized downstream of the rear jet, that need further investigation.

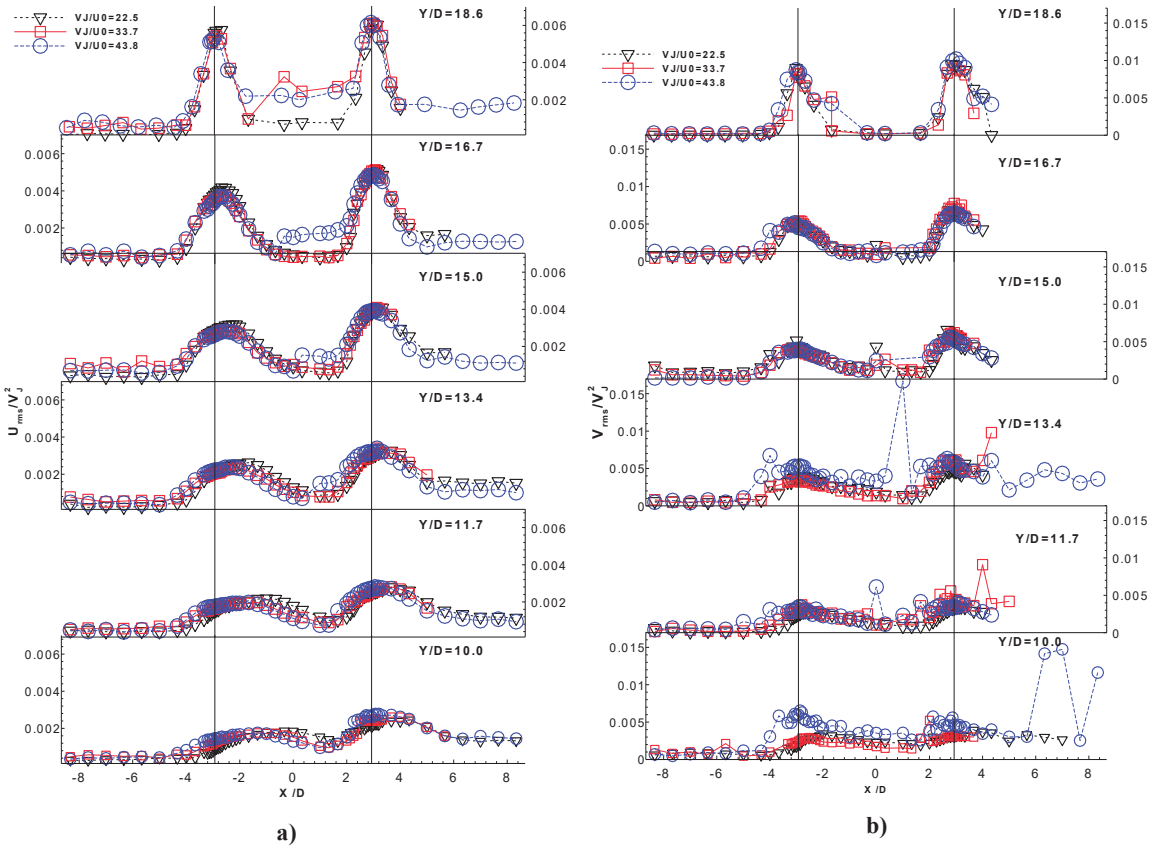

Fig 8 Horizontal profiles of the mean velocity characteristics along the longitudinal (symmetry) plane crossing the centre of the twin jets: (a) Horizontal rms velocity, (b) Vertical rms velocity. (Re_j = 4.3x10^4, H/D = 20.1, and S/D = 6).

4. Discussion

This section presents a numerical study to extend the analysis of the flow to regions and flow conditions for which no measurements have been obtained. The numerical method is based on the solution of the conservation laws for mass and momentum which is a modified version of the method described elsewhere (see Ref. 6 for details).

Figure 9 shows the mean vertical velocity component (V_{mean}) distribution along the vertical plane of symmetry (i.e. Z=0) together with calculated streamtraces. For this velocity ratio the collision of the upstream wall jet with the crossflow is clearly registered and the ground vortex is identified with its centre at X/D= -8. Comparing this result with that obtained experimentally we can confirm that the deflection sensed by the first jet experimentally is greater than the jet deflection felt numerically, thus leading to the centre of the ground vortex is located close to X / D = -4. As far as the downstream jet (rear jet) is concerned the predictions confirmed the experimental results, and its complete deflection by the crossflow was calculated for all the velocity ratios considered with no impingement directly on the wall.

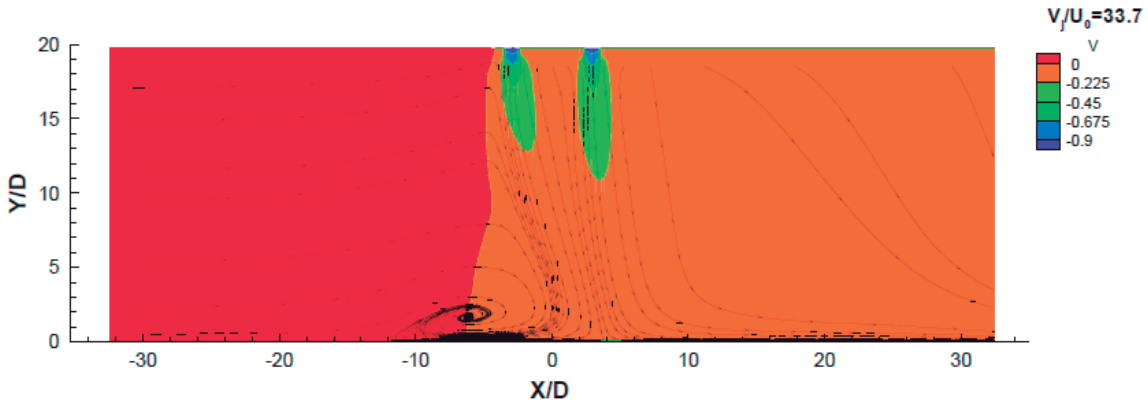

Fig. 9 Calculated stream traces and mean vertical velocity component distribution along the vertical plane of symmetry (i.e. Z=0). Re_j=43,000, H/D=20.1, and L/D=6).

Figure 10 shows in more detail the central zone between the two jets with white streamtraces that begin near the top wall. The results show that even for the smallest velocity ratios of V_j/U_0=7.5 and 15 the jets do not mix, but remain together in two layers. As a consequence, for V_j/U_0=15 the downstream jet does not reach directly the ground, but it impinges on the wall jet resulting from the first jet which is moving downstream. For the two higher velocity ratios the ground vortex is always present, but its size and location changes. It moves upstream with V_j/U_0, because increasing the velocity ratio involves decreasing the relative influence of the crossflow velocity. Ref. 16 identified three different types of flow regimes, but for a V/STOL aircraft operating in ground

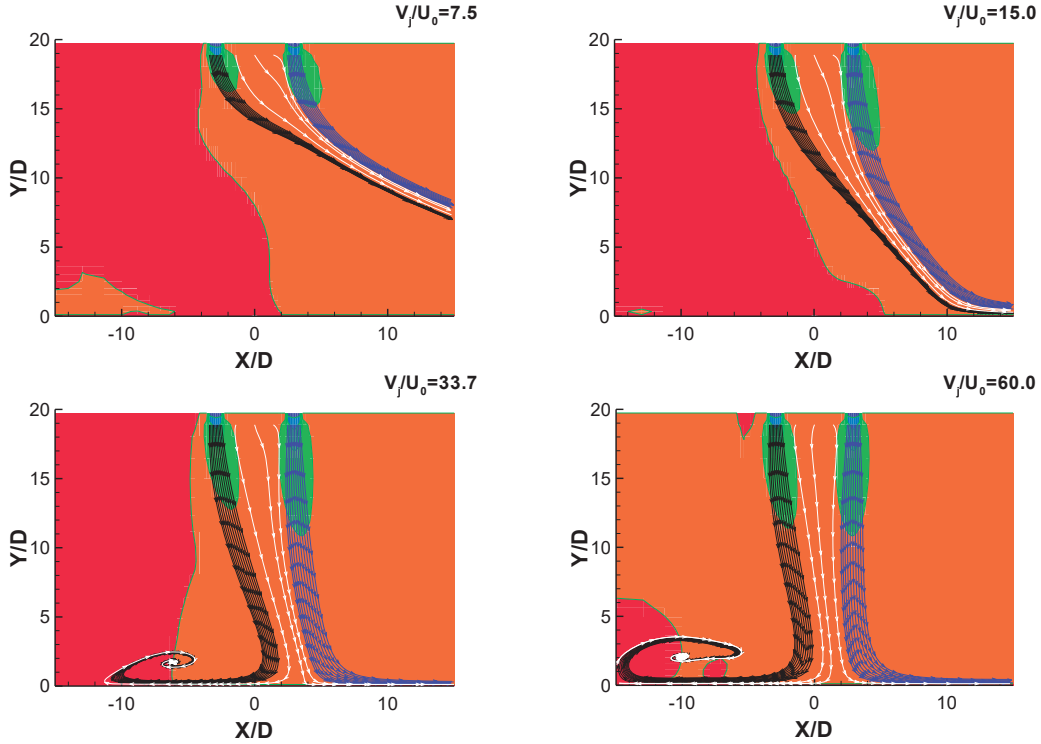

Fig. 10 Details of the calculated stream traces and mean vertical velocity component distribution along the vertical plane of symmetry (i.e. Z=0). Re_j=4.3x10^4, H/D=20.1, and L/D=6.

vicinity the regime with strong impingement on the ground and a ground vortex is the most relevant. However, in transition from hover to horizontal flight the other regimes are also important.

One major issue in the present flow configuration is the possible deflection of the rear jet by the first jet without occurring impact on the ground. Another possibility (not yet demonstrated) is the impact of the second jet with the first deflected jet or its downstream wall (depending on the velocity ratio). Figure 9 it is not sufficiently conclusive about these hypothesis, nor about the blending of the two structures further downstream. In order to better understand this type of flow, and in particular that happened with the second jet and downstream, a detailed numerical study simulation was performed by varying the velocity of the second jet, V_{j2}, from, 5.4 m/s up to 36 m/s. The velocity of the first jet was kept constant to preserve the location of the centre of the ground vortex. Figures 11 and 12 show the results for V_{j2} = 5.4 m/s and 13.5 m/s, respectively. Both figures show that lowering the velocity of the second jet in relation to the first jet, the wall jet of the second jet is always above the wall jet formed by the interaction of the first jet with the crossflow, heading the flow to downstream. The location of the ground vortex is practically not affected by this change in the second jet velocity, confirming that the second jet does not contribute to the occurrence of this structure.

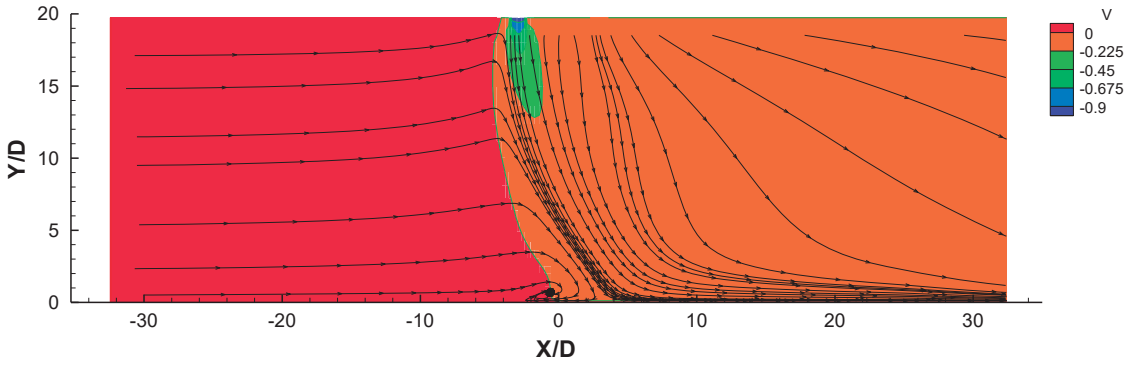

Fig. 11 Calculated stream traces and mean vertical velocity component distribution along the vertical plane of symmetry, Z=0. (Re_j=43,000, H/D=20.1, L/D=6, V_{j2}= 5.4 m/s).

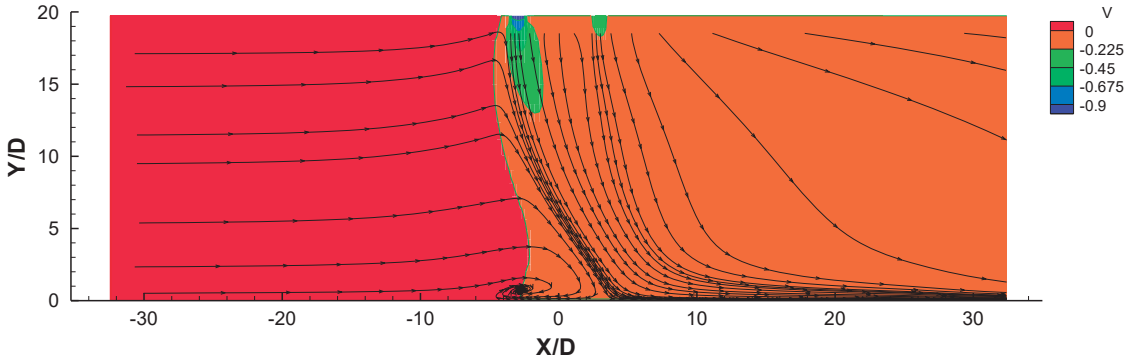

Fig. 12 Calculated stream traces and mean vertical velocity component distribution along the vertical plane of symmetry, Z=0. (Re_j=43,000, H/D=20.1, L/D=6, V_{j2}= 13.5 m/s).

In

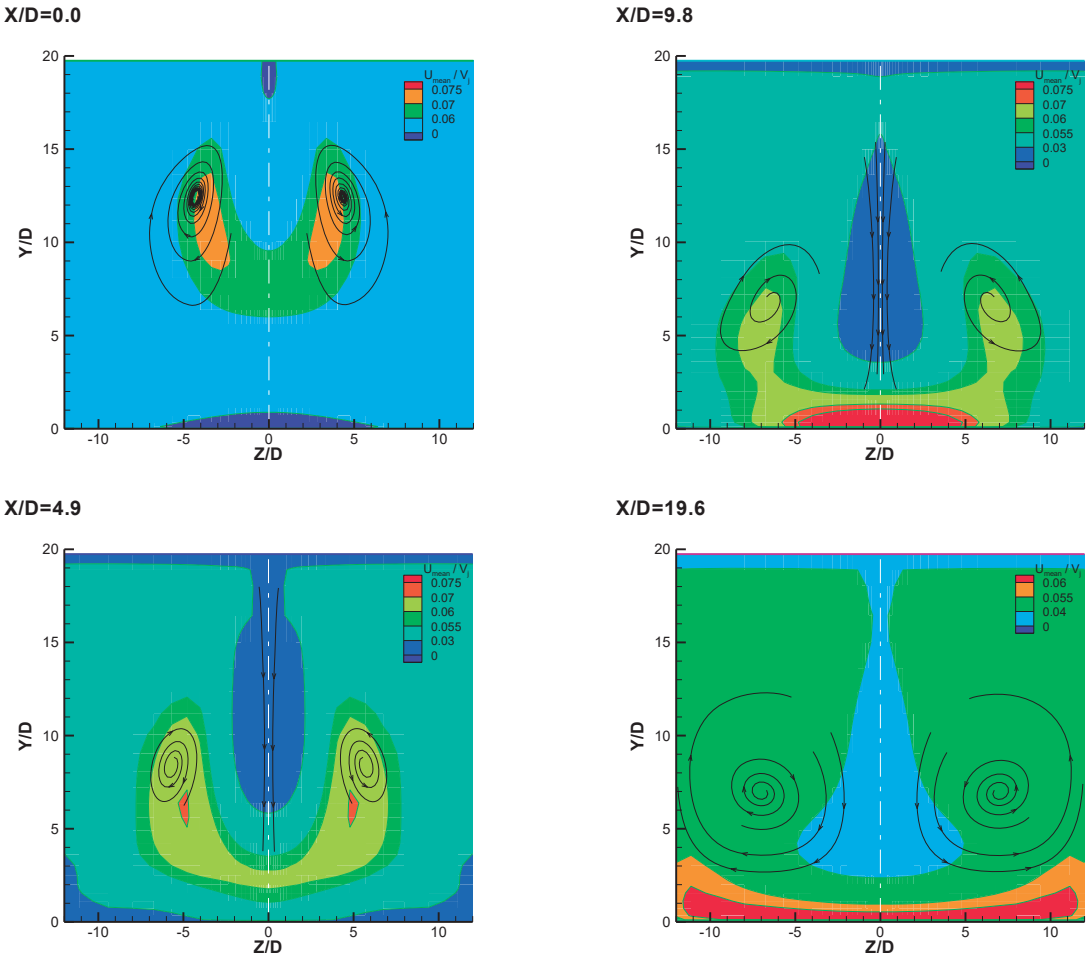

Fig.13 Mean velocity component (Umean/V_{j1}) in a vertical plane perpendicular to crossflow. (Re_{j1}=43,000, V_{j2} = 5.4 m/s, Re_{j2}=5,339, H/D=20.1, L/D=6).

In order to investigate the possible existence of a kidney shape of the crossection of the jets, and their mutual interactions, isolines of the velocity component U_{mean} were obtained in vertical planes perpendicular to the crossflow for X / D = 0.0, 4.9, 9.8 and 19.6. Figures 13 and 14 show the results for V_{j2} = 5.4 m / s and V_{j2} = 13.5 m/s, respectively. For X / D = 0, i.e. in the middle between the axis of the jets exit, the kidney shape can be clearly identified for the first jet (the second jet it is not yet visible, because its exit is further downstream).

For X / D = 4.9, the second jet can be identified by the dark blue area corresponding to velocities larger than $0.03V_{j1}$, that reveals the slight deflection of the second jet inside the wake of the first impinging jet. The kidney shape of the cross section of the first jet is still present, but it is widening rapidly due to the additional influence of the second imping jet. It should be pointed out that the impinging jet and first jet do not mix and are separated by lower values of the velocity component in the crossflow direction (light blue). Additionally, no streamtraces from the second jet are captured by the deflected upstream jet, revealing that a complete mixing between the two jets has not yet occurred.

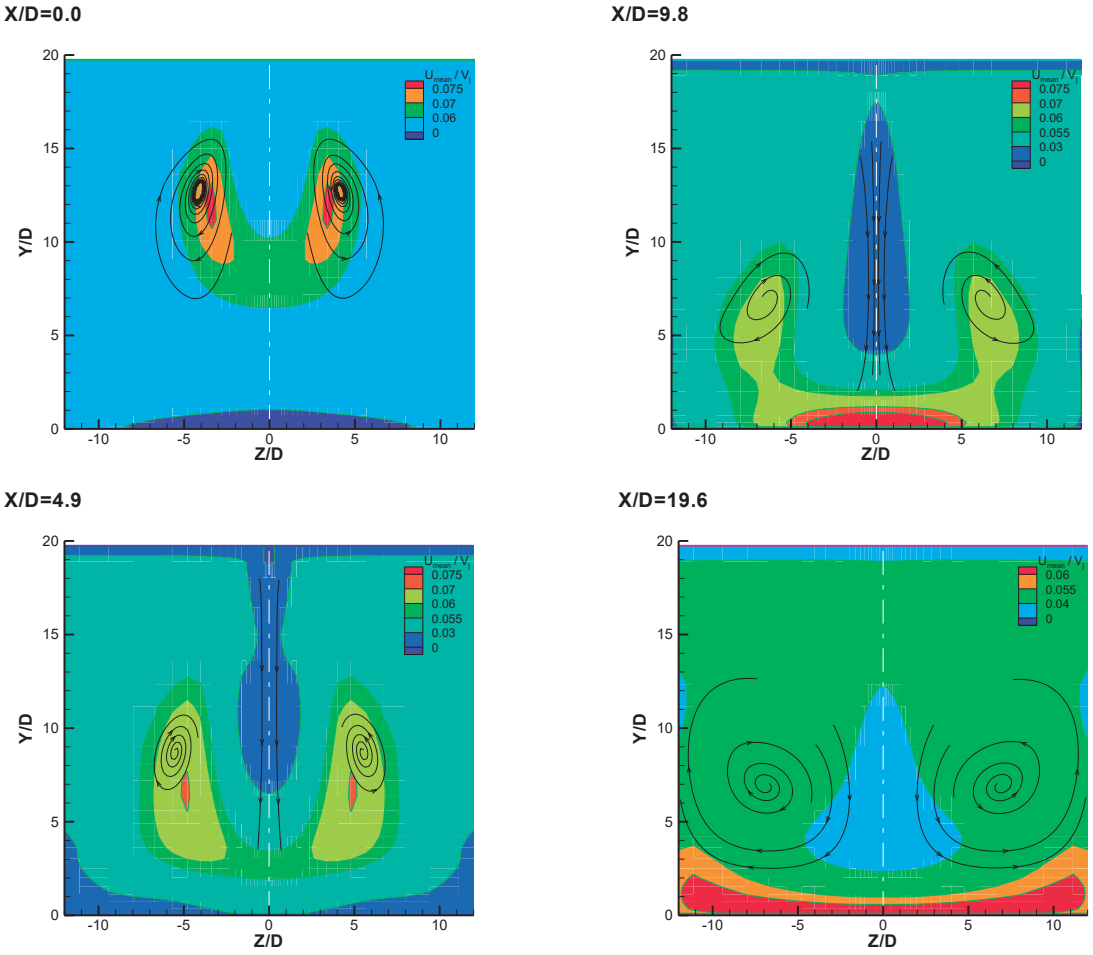

Fig. 14 Mean velocity component (U_{mean}/V_{j1}) in a vertical plane perpendicular to crossflow. (Re_{j1}=43,000, V_{j2} = 13.5 m/s, Re_{j2}=16,125, H/D=20.1, L/D=6).

However, from this location downstream (in the crossflow direction) the second impinging jet will suffer two opposing effects: first the fact that is developing in the wake of the first impinging jet will contribute to its less deflection, and secondly since it is impinging in a flow moving in the crossflow direction with a higher velocity it will be forced to deflect. This novel flow configuration that occurs before the first jet reaching the ground is schematically shown in Fig. 15. So, the final behaviour of the second jet can be described as the flow of a jet through a zero or small upstream crossflow (corresponding to the wake of the first jet) impinging on a horizontal jet with a kidney cross section flowing in the crossflow direction with a higher velocity.

In the next downstream location, at X/D = 9.8, the red area identifies a region with relatively large positive values of the velocity component U_{mean} (in the crossflow direction), which is an indication that the first jet touched the ground. The rear jet impacts on this wall jet (resulting from the first jet), and is quickly deflected, but does not reach the ground.

For X/D = 19.6, the entire cross section is occupied by two vortical structures rotating in opposite directions, revealing that the two parallel jets flowing in the crossflow direction finally merge.

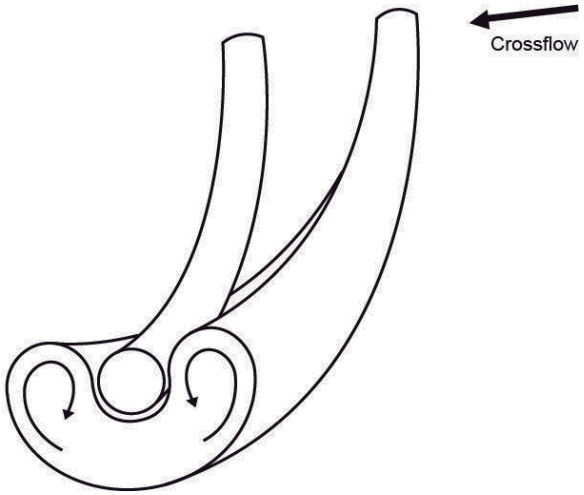

Fig. 15 Illustration of the kidney shape of the cross section of the first jet before reaching the ground and the second (downstream) jet interaction.

5. Conclusions

A Laser Doppler Velocimeter was used to provide information on the flow field created by twin impinging jets in tandem through a crossflow and, then, impinging on a flat surface perpendicular to the geometrical jet-nozzle axis. The experiments was carried out for a Reynolds number based on the jet exit conditions of Re_j=4.3x10^4 with an impingement height of 20.1 jet diameters and for a velocities ratio between the jet exit and the crossflow, $V_R = V_j/U_o$ of 22.5, 33.7 and 43.8 with and an interject spacing of S=6D. To complete the investigation were also performed numerical simulations for velocity ratios beyond the rig experimental limits.

The results show a large penetration of the first (upstream) jet, which is deflected by the crossflow and impinges on the ground giving rise to a ground vortex due to the collision of the radial wall and the crossflow that wraps around the impinging point like a scarf. The first jet deflection and the location of the ground vortex depend on the velocity ratio used. For higher velocity ratios the deflection of the first jet is smaller and closer to the first jet is located the centre of the ground vortex. The rear jet it is not so affected by the crossflow in terms of deflection for all velocity ratios because it is protected by the upstream jet, but due to the downstream wall jet that flows radially from the impinging point the rear jet does not reach the ground. Also due to the confinement and the ground vortex, the crossflow is blocked and accelerates in the upper part and also contributes to an enhanced mixing of each secondary flow. As consequence, no upstream wall jet or ground vortex resulting from the second (downstream) jet was detected. The effect of the rear jet impinging on the downstream wall jet resulting from the first jet had not been reported so far and requires further investigation.

In case of the numerical analysis, the results show that for the two lowest velocity ratios, the jets do not mix remaining in two layers together, and therefore, it is not detected the presence of ground vortex. For V_j/U_0 = 33.7 and 60 the ground vortex is completely present, and it moves with the increase of V_j/U_0. Compared the experimental results with the numerical results for V_j/U_0= 33.7, we can conclude that the deflection of the first jet in the numerical case is lower than that recorded for the experimental case, implying therefore a different location from the centre of the vortex ground.

As far as the downstream jet (rear jet) is concerned the predictions confirmed the experimental results, and its complete deflection by the crossflow was calculated for all the velocity ratios considered with no impingement directly on the wall. By changing the rear jet velocity and extracting perpendicular planes to the jets flow was possible to prove that the second jet is deflected quickly, never reaching the ground, thus proving the accuracy of the experimental results, leading us to conclude that impinging jet in tandem configuration, the downstream jet is entrained by the upstream jet and not by the crossflow itself. In the future, this issue should be further investigated in order to understand what the real consequence for the aircraft when this type of phenomenon occurs.

Acknowledgments

The assistance of Ms. Inês Carvalho with some illustrations of the flow field is gratefully acknowledged.
The present work was done in the scope of the activities of LAETA-Associated Laboratory of Energy, Transports and Aeronautics, and funded by FCT-Fundação para a Ciência e Tecnologia through contract PTDC/EME-MFE/102190/2008 and grant SFRH/BD/86434/2012.

References

[1]Adler, D.; Baron, A "Prediction of a three-dimensional circular turbulent jet in crossflow" *AIAA Journal, No.* 17, 1979, pp.168-174
[2]Andreopoulos, J., and Rodi, W., "Experimental Investigation of Jets in a Crossflow", *J. Fluid Mech.*, Vol.138, 1984, pp.93-127.
[3]Andreopoulos, J. and Rodi, W., "Experimental Investigation of Jets in a Crossflow", *J. Fluid Mechanics*, Vol. 138, 1984, pp. 127.
[4]Araújo, S.R.B., Durão, D.F.G., and Firmino, F.J.G., "Jets Impinging normally and obliquely to a Wall", AGARD CP 308, paper 5.
[5]Baker, O.J., "The Turbulent Horseshoe Vortex", *J. Wind Engineering and Industrial Aerodynamics*, Vol. 6, 1981, pp. 9.
[6]Barata, J.M.M., Durão, D.F.G., and McGuirk, J.J., "Numerical Study of Single Impinging Jets Through a Crossflow", *Journal of Aircraft,* Vol.26, No.11, 1989, pp. 1002-1008.
[7]Barata, J.M.M., "Numerical and Experimental Study of Jets Impinging on Flat Surfaces Through a Crossflow", Ph.D. Thesis (in Portuguese), Instituto Superior Técnico, Technical Univ. of Lisbon, Lisbon, Portugal, 1989.
[8]Barata, J.M.M., Durão, D.F.G., and McGuirk, J.J., "Numerical Study of Single Impinging Jets Through a Crossflow", *J. of Aircraft*, Vol.26, No.11, 1989, pp.1002-1008.
[9]Barata, J.M.M., Durão, D.F.G., Heitor, M.V., and McGuirk, J.J., "On the Analysis of an Impinging Jet on Ground Effects", *Experiments in Fluids*, No.15, 1993, pp.117-129.
[10]Barata, J.M.M., "Ground Vortex Formation with Twin Impinging Jets". SAE paper 962257, International Powered Lift Conference, Jupiter, Florida, 18-20 Nov., 1996.
[11]Barata, J.M.M., "Fountain Flows Produced by Multiple Impinging Jets in a Crossflow". *AIAA Journal*, Vol. 34, No.12, December 1996, pp. 2523-2530 e *AIAA Journal on Disc*, Vol. 2, No.1, 1996.
[12]Bevilacqua, P., Margason, R., and Gaharan, C., "A Jet Entrainment Theory for VTOL Aircraft Suckdown", paper AIAA-2007-1397, 45th AIAA Aerospace Science Meeting and Exhibit, 8-11 Jan. 2007, Reno, Nevada.
[13]Barata , J.M.M., Carvalho, P.S.D., Durão, D.F.G., Neves, F.M.S.P., Silva, A.R.R., and Vieira, D.F.C., "Laser Doppler Measurements of Twin Impinging Jets Aligned With a Crossflow", July 2012, 16th

Int Symp on Applications of Laser Techniques to Fluid Mechanics Lisbon, Portugal, 09-12 July, 2012.

[14]Barata, J.M.M., Neves, F.M.S.P., Vieira, D.F.C., and Silva, A.R.R., "Twin Impinging Jets Through a Crossflow", 50th AIAA Aerospace Sciences Meeting including the New Horizons Forum and Aerospace Exposition, 9-12 January 2012/ Gaylord Opryland Resort & Convention Center, Nashville, Tennessee.

[15]Barata, J.M.M, "Multiple Jet/Wall/Cross-Wind Interaction Relevant to VSTOL Ground Effects", AIAA paper 2013-4380, 2013 International Powered Lift Conference, Los Angeles, California, August 12-14, 2013.

[16]Barata, J.M.M., "Twin Impinging Jets Aligned With a Crossflow". AIAA paper 2013-3600, 49th AIAA/ASME/SAE/ ASEE Joint Propulsion Conference and Exhibit, San Jose, California, 15-17 July, 2013.

[17]Childs, R. E. and Nixon, D. "Simulation of impinging turbulent jets", paper AIAA-85-0047, presented at the AIAA 23rd Aerospace Science Meeting, Jan. 14- 17, 1985, Reno, Nevada.

[18]Crabb, D., Durão, D.F.G., and Whitelaw, J.H., "A Round Jet Normal to a Crossflow", *J. Fluids Engng.*, Vol.113, 1981, pp. 142-153.

[19]Demuren, A. O. "Numerical calculations of steady three-dimensional turbulent jets in crossflow" Comp. Meth. In Appl. Mech. and Engng. 1983, Vol. 37, pp. 309-328.

[20]Durst, F., Melling, A., and Whitelaw, J.H., "*Principles and Practice of Laser-Doppler Anemometry*", 2nd ed., New York, Academic Press.

[21]Gilbert, B.L., "Detailed Turbulence Measurements in a Two Opposing Plane Turbulent Wall Jets", AIAA 16th Fluid and Plasma Dynamics Conf., AIAA Paper 83-1678, Danvers, MA, Jul. 12-14, 1983.

[22]Jenkins, R.C., and Hill, W.G., Jr., "Investigation of VTOL Upwash Flows Formed by Two Impinging Jets", Grumman Research Dept. Rept. RE-548, Bethpage, NY, Nov., 1977.

[23]Jones, W. P. and McGuirk, J. J. "Computation of a round turbulent jet discharging into a confined crossflow", In: *"Turbulent Shear Flows-2",~* Bradbury et al., Springer Verlag, 1980, pp.223-245.

[24]Kamotani, Y., and Greber, I., "Experiments on Confined Turbulent Jets in a Crossflow", NASA CR-2392, 1974.

[25]Kavasaoglu, M.S., Schetz, J.A., and Jakubowsky, A.K., "Rectangular Jets in a Crossflow", *Journal of Aircraft,* Vol.26, No. 9, 1989, pp. 793-804.

[26]Keffer, J. F. and Baines, W. D. "The round turbulent jet in a cross-wind", *J. Fluid Mech.*, Vol. 15, 1963, pp. 481-496

[27]Kind, R.J., and Suthanthiran, K., "The Interaction of Two Opposing Plane Turbulent Wall Jets", AIAA Paper 72-0211, Jan., 1980.

[28]Knowles, K., and Bray, D., "The Ground Vortex Formed by Impinging Jets in Crossflow", AIAA 29th Aerospace Sciences Meeting, AIAA Paper 91-0768, Reno, NV, Jan. 7-10, 1991.

[29]K. Knowles, "Computational Studies of impinging jets using k-ε Turbulence Models", International Journal for Numerical Methods in Fluids, 1996, Vol. 22, pp. 799-810.

[30]Kotansky, D.R., and Glaze, L.W., "The Effects of Ground Wall-Jet Characteristics on Fountain Upwash Flow Formation and Development", Rept. ONR-CR212-216-1F, 1980.

[31]Kotansky, D.R., "The Modelling and Prediction of Multiple VTOL Aircraft Flow Fields in Ground Effect", AGARD CP-308, Paper 16.

[32]Melling, A., and Whitelaw, J.H., "Turbulent Flow in a Rectangular Duct", *J. Fluid Mechanics*, Vol. 78, 1975, pp.285-315.

[33]Patankar, S. V., Basu, D. K. and Alpay, S. A "Prediction of the three-dimensional velocity field of a deflected jet" *J. Fluids Engng.*, Vol. 99, 1979, pp. 758-762

[34]Sarippali, K.R., "Laser Doppler Velocimeter Measurements in 3D Impinging Twin-Jet Fountain Flows", *Turbulent Shear Flows,* Vol.5, edited by Durst et al., Springer-Verlag, Berlin, 1987, pp. 147-168.
[35]Saripalli, K.R., "Visualization of Multijet Impingement Flow", *AIAA Journal*, Vol. 21, 1983, pp. 483-484.
[36]Schetz, J.A., Jakubowsky, A.K. and Aoyagi, K., "Surface Pressures on a Flat Plate with Dual Jet Configurations", *Journal of Aircraft*, Vol.21, No.7, 1984, pp. 484-490.
[37]Siclari, M.J., Migdal, D., Luzzi, T.W., Jr., Barche, J., and Palcza, J.L., "Development of Theoretical Models of Jet-Induced Effects on V/STOL Aircraft", *Journal of Aircraft*, Vol. 13, No. 12, 1976, pp.938-944.
[38]Shayesteh, M.V. Shabaka, I.M.N.A., and Bradshaw, P., "Turbulent Structure of a Three-Dimensional Impinging Jet in a Crossflow", AIAA 23rd Aerospace Sciences Meeting, AIAA Paper 85-0044, Reno, NV, Jan. 14-17, 1985.
[39]Stoy, R.C., and Ben-Haim, Y., "Turbulent Jets in a Confined Crossflow", *J. Fluids Engng.*, No.95, 1973, pp.551-556.
[40]Sugiyama Y., and Usami, Y., "Experiments on the Flow in and Around Jets Directed Normal to a Crossflow", *Bulletin JSME*, No.22, 1979, pp. 1736-1745.
[41]Sugiyama, Y. and Usami, Y. "Experiments on the flow in and around jets directed normal to a crossflow", Bulletin JSME, 1979, Vol. 22, pp. 1736-1745.
[42]Vieira, D.F.C., Silva, A.R.R., Carvalho, P.S.D., Neves, F.M.S.P. and Barata, J.M.M. " Numerical and Experimental Study of Two Impinging Jets in a Row through a Crossflow", AIAA Paper 2013-0806, 51th AIAA Aerospace Science Meeting Including the New Horizons Forum and Aerospace Exposition, Grapevine (Dallas/Ft. Worth Region), Texas, 7-10 Jan., 2013.
[43]Yanta, W.J. and Smith, R.A., "Measurements of Turbulent Transport Properties with a Laser-Doppler Velocimeter", 11th Aerospace Sciences Meeting, AIAA Paper 73-0169, Washington, 1978.

Numerical Simulation of Twin Impinging jets in Tandem through a Crossflow

Diana. F.C. Vieira[1], Jorge. M.M. Barata [2], Fernando. M.S.P. Neves[3], André. R.R. Silva[4]
Universidade Beira Interior, Covilhã, 6200-358, Portugal

The flow field of ground vortex generated by twin impinging jets in tandem through a crossflow is numerically studied in detail. Numerical simulation and visualization are presented for two turbulent circular jets emerging into a low velocity cross stream, impinging after on a flat surface perpendicular to the geometrical jet nozzle axis. The numerical study is based in experimental studies done early, so all the features of the experimental flow were maintained when the numerical simulation was performed. The Reynolds number used was based on the jet exit conditions of 43,000 to 105,000, a jet to crossflow velocity ratio of 22.5 to 43.8, an impinging height of 20.1 jet diameters and an interject spacing's of S=5D and L=6D. The analysis of the flow was extended to regions and flow conditions for which no measurements have been obtained in last experimental studies, i.e., for velocity ratios of 15 to 90. The numerical results show that for the smallest velocity ratios the jets initially do not mix, but remain together in two layers. Three different types of flow regimes were identify, therefore when VSTOL aircrafts operating in ground vicinity, only the regime with strong impingement on ground and with a formation of a ground vortex is relevant. The numerical results allowed to extend the last experimental studies, and prove that the deflection of the rear jet is due to the competing influences the wake, the shear layer, the downstream wall jet of the first jet and the crossflow.

Nomenclature

C_μ, C_1, C_2 = turbulent model constants
D = diameter of the jet
H = impinging height
k = turbulent kinetic energy
r = radius of cylindrical coordinates
Re = Reynolds number
S = distance between the jets axis
S_ϕ = source term
U = horizontal velocity, $\overline{U} + u'$ (U_{mean}+u')
V = vertical velocity, $\overline{V} + v'$ (V_{mean}+v')
V_R = velocity ratio, V_j/U_o
W = transverse $\overline{W} + w'$ (W_{mean}+w')
X = horizontal coordinate
Y = vertical coordinate
Z = transverse coordinate

Greek symbols

Γ_ϕ = transport coefficient
ε = turbulent kinetic energy dissipation
μ_T = turbulent viscosity
ρ = density
σ_k, σ_ε = turbulent Prandtl/Schmidt numbers

[1] Ph. D. Student, Aerospace Sciences Department, Student Member of AIAA. Corresponding author.
[2] Full Professor, Aerospace Sciences Department, Associate Fellow of AIAA.
[3]PostDoc Student, Aerospace Sciences Department, Member of AIAA.
[4] Assistant Professor, Aerospace Sciences Department, Member of AIAA

ϕ = variable in general conservation equation
Φ = turbulent kinetic energy production term
j = jet-exit value
o = crossflow value

I. Introduction

In external aerodynamics applications, such as, VSTOL aircrafts, turbulent jets impinging on flat surfaces through a low velocity crossflow are typical of the flow beneath of this type of aircraft. During its landing or near ground hovering phase, the VSTOL aircraft creates a complex three dimensional flow field between the jet streams, the airframe surface and the ground. When ground effect occurs, the lift forces on the aircraft changes, cause hot gas re-ingestion into the engine intake and due to the fountain upwash and ground flows, the fuselage skin temperature rises. The unsteadiness of the flow and raise of the temperature cause several problems in the engine performance, such as, compressor surge or even stall and thrust reduction. In respect to the intake ingestion phenomenon, it is very complex and can be associated with the design and operational parameters, such as, jet configuration, head wind velocity, jet impingement height or intake configuration. In the case of the hot gas ingestion problem, there are three mechanism involved, i.e., far field ingestion, near field ingestion and ground vortex ingestion. The first mechanism is results of the forward away initially movement of the ground sheet wall jet due to the aircraft movement. This happened because the hot gases after some distance loses its momentum, rising and separating from the ground. The portion of the hot gases that separating from the ground, mixes with the surrounding air and backs again to the intake. The second mechanism, near field ingestion, has a much greater impact on hot gas ingestion compared to the first, because it directly affected the lift nozzle exits into the surrounding area of the intake, being that when exits multiple impinging jets, its impact on the ground plane create a fan shape up wash fountain beneath the aircraft. When the fountain impinges on the underside of the fuselage, flowing from the fuselage to the intake, the engine may sucks the flow to the intake, creating severe temperature distortion to the intake, since, these gases are much hotter than those from the far field ingestion. The latter mechanism is due to the presence of a ground vortex. During a landing or hover the impingement of each downward-directed jet on the ground results in the formation of a wall jet which flows radially from the impinging point along the ground surface. The interaction of this wall jet with the free stream results in the formation of a ground vortex far upstream of the impinging jet. This flow field transports exhaust gases away from the ground and up toward the intake region. The level and intensity of the ingestion resulting from this mechanism depends critically on the forward velocity. If there are two or more adjacent jets, the resulting wall jets meet, and a fan-shaped upwash, or "fountain", is normally formed between the jets. The fountain upwash flow depending on its strength and direction affects the forces and moments induced in the aircraft when operating in ground effect. The resulting ground vortex shape is strongly affected and the corresponding induced suckdown effect tends to be reduced by the upload produced by the fountain. In the last thirty or forty years, this type of complex flow fields have been studied extensively, but improve the knowledge are ever required because the aircraft design have been changed since its first design, and some problems were solved but others were not.

Earlier published work has been concentrated on 1, 2, and 3 jets configurations relevant to the AV-8B Harrier II aircraft. In this case when the aircraft operates with small forward movement the configuration of interest are two impinging jets with the direction of the crossflow perpendicular to the line containing their centers.

For the next generation of VSTOL aircrafts F-35 no relevant studies can be found, because the impinging jets are aligned with the crossflow and this geometry has not yet been considered. In this case a vertically oriented lift fan (SDLF) generates a column of cool air that produces the nearly 20,000 pounds of lifting power, along with an equivalent amount of thrust from the vectored rear exhaust (3BSM-Three Bearing Swivel Module). Figure 1 shows the position of the thrust vectoring nozzle and lift fan in the F-35 aircraft. The lift system was successfully demonstrated during a flight test of the X-35B during the summer of 2001. The complexity of the new VSTOL configuration together with the very stringent requirements has required an enormous amount of R&D in the last decade. On 12th May 2012 the 200th test flight of the F-35B (BF-3) measurement of stresses on the aircraft during supersonic maneuvers was done. Therefore most of the published work reported so far has only peripheral relevance to the F35-B/JSF ground effect problem.

This paper aims presents results that are relevant to the future F-35 VSTOL configuration (Figure 1), through a detailed analysis of the complex flow field beneath two impinging jets in tandem through a low velocity crossflow. The present study is a piece of a most comprehensive experimental study on impinging jet flows in ground effect, which included two different experimental installations: 2-D ground vortex, and wind tunnel. Here, the main focus is the extrapolation of the measurements beyond the limits of the latter experimental rig through computational simulations.

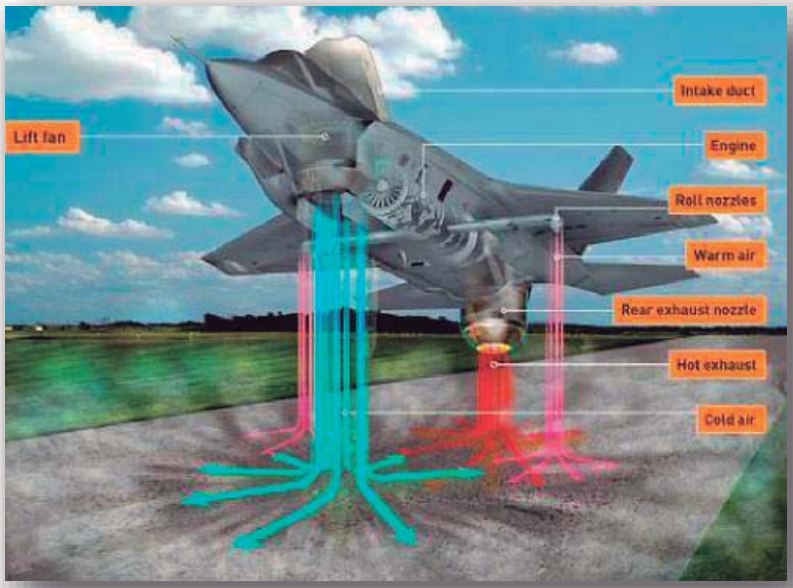

Figure 1: F-35's thrust vectoring nozzle and lift fan

Previous detailed measurements of the flow properties for fountain upwash flow are scarce and have been presented essentially in the absence of a crossflow and with the use of probe techniques. The most relevant works have been reviewed by Refs. 6 and 34, showing high turbulence levels and spreading rates in the fountains (e.g. Refs. 19 and 25). Different interpretations of the measurements exist due to the difficulties in measuring complex flows using hot-film and pitot-probe techniques[20, 28]. Refs. 23 and 35 also shows flow fields and pressure data for twin-rectangular jets for small jet-to-crossflow velocity ratios (<10). Ref. 34 reports laser Doppler velocity (LDV) measurements, including those of shear stress, for axisymmetric impinging jets with S/D=9 and 14 with an impinging height, H/D, of 3 and 5.5, but again the existence of a crossflow was not considered. Detailed measurements of the velocity characteristics of normal impinging jets on a flat surface can be found for single jet configurations for relatively large impingement heights and normally for H/D>10, using either probe or optical techniques, as reviewed for example by Ref. 3 and 8. Experiments on the aerodynamics of jets through a confined crossflow are scarcer and have only been reported for large impingement heights and for low velocity ratios between the jet and the crossflow V_j/U_o. Therefore these works have only peripheral relevance to the VSTOL ground effect problem with the same geometry of the F-35. Refs. 2, 36 and 39 report hot-wire measurements for height ratios, H/D, greater than 24 and for values of V_j/U_o up to 1.95, 2 and 16. Ref. 22 presents results for H/D=12 and Ref. 38 gives pitot-tube measurements for values of H/D=3.05 and for jet-to-crossflow velocity ratios up to 6.8. Ref. 16 reports LDV measurements including shear stress measurements for values of H/D=12 and for velocity ratios up to 2.3. Only Ref. 6 provided detailed LDV measurements for a single jet configuration for a jet with Reynolds number Re_j=6x10^4, a velocity ratio between the jet and the crossflow of 30, 42 and 73 with jet exit above the ground plate 3, 4 and 5 diameters. The measurements include time-resolved velocity characteristics along the horizontal, vertical directions with respective correlations in planes parallel to the jet nozzle axis[7, 8]. Refs. 9 and 10 extended their study to multi jet impinging configurations producing upwash fountain flows which are the heart of the complex effects produced by VSTOL aircraft when they operate in ground proximity, but as far as twin jets are concerned only the geometry with the jets side by side was considered.

Most of the computational work published on jets with crossflow has been based on integral methods admitting assumptions simplified, which are only capable of predicting global effects such as trajectories and jet cross-section shapes, for example Refs. 1 and 38. Ref. 31 employed a finite-difference numerical procedure together with a two-equation turbulence model to predict a single jet in an unconfined crossflow, and obtained good agreement with the experiments of Ref. 26 for velocity ratios from 2 to 10. A similar approach was used by Ref. 21 to calculate the confined flow measured by Ref. 12. The gross features of the flow are well predicted but the calculations appear to exhibit diffusion rates larger than those consistent

with measured profiles, which can be attributed either to numerical or turbulence model errors. Grids up to 20 x 15 x 15 nodes were used, but further grid refinement is essential to identify the precise source of disagreement between measurements and predictions. Ref. 17 presented predictions of the flow measured by Ref. 39 using a three-dimensional finite-difference scheme together with the "k- ε" turbulence model and has showed the importance in prescribing the correct boundary conditions at the jet discharge. Making use of a similar procedure, Ref. 15 have shown that the primary characteristics of impinging flows are computed with reasonable accuracy, although specific aspects related with the strong curvature and anisotropy of impingement zones are dependent on accurate modeling of turbulent shear stresses which are not well predicted. Ref. 27 has shown that the standard "k-ε" model over predicts the spreading rate of a free jet and under predicts the spreading rate of a radial wall jet. More recently, Ref. 32 presented a comparison of experimental data and computational simulation to develop a jet entrainment theory for the prediction of lift loss. This paper has four sections in which section II describes the experimental configuration and procedure, given details of the laser-Doppler velocimeter and assessments of accuracy. The arguments associated with these assessments are based on previous experiments data which are presented in condensed form. Section III presents the experimental results obtained in the visualization on the vertical plane of symmetry containing the axis of both. The numerical results are discussed in Sect. IV on the basis of numerical visualization of the three-dimensional flow. The last section summarizes the main findings and conclusions of this work.

II. Experimental Method

A. Flow Configuration

The experiments were performed on a wind tunnel facility designed and constructed for the present work, with an exit section of 300x402 mm that is schematically shown in Fig. 2. The test section was made of Perspex allowing the passage of laser beams. During all the design process special consideration was taken for the boundary layer in which the recommendations of Ref. 23 for open circuit wind tunnels was followed. A fan with 15KW nominal power drives a maximum flow of 3000m^3/h through the boundary layer wind tunnel exit section.

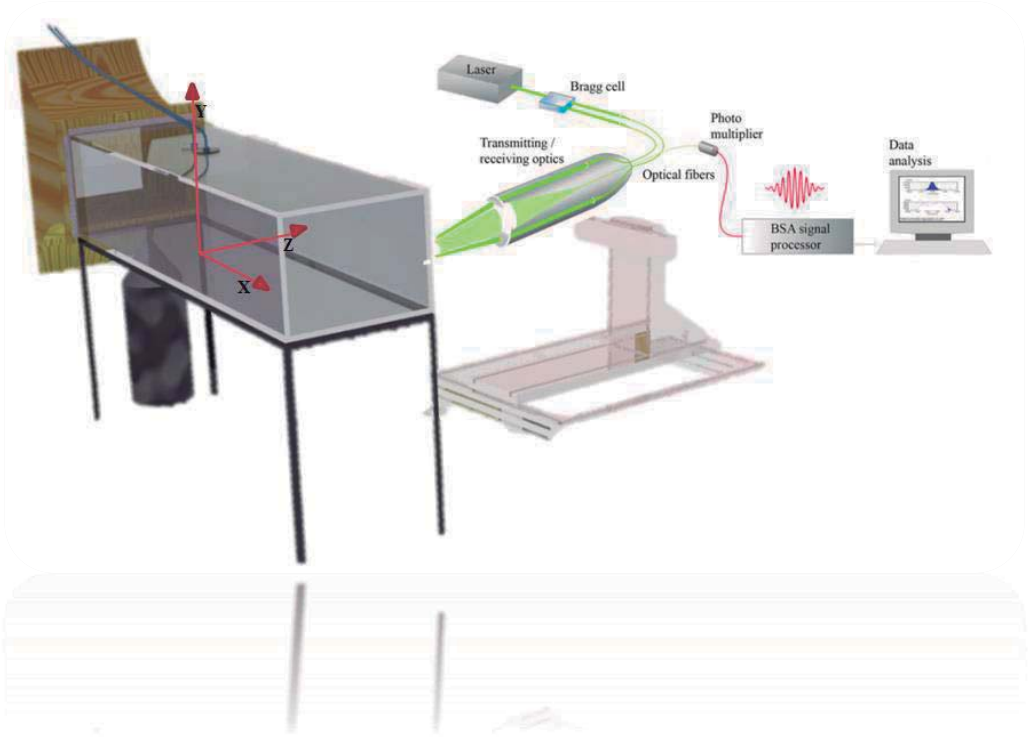

Figure 2: Experimental set-up

In the present study each jet unit of 15mm of inner diameter is mounted vertically in the top of the test section 20.1*D* above the ground plane with the axis contained in the vertical plane of symmetry parallel to the crossflow as showed schematically in Fig. 3.

The origin of the horizontal, *X*, and vertical, *Y*, coordinates is taken at the midpoint between the centers of the jets exit. The *X* coordinate is positive in the direction of the wind tunnel exit and *Y* is positive upwards.

The present results were obtained at the vertical plane of symmetry for jet mean velocity of V_j = 36m/s, a jet Reynolds number of Re_j = 4.3x10^4 and mean crossflow velocities of U_o=0.8m/s, corresponding to a velocity ratio, $V_R = V_j/U_o$ = 43.8.

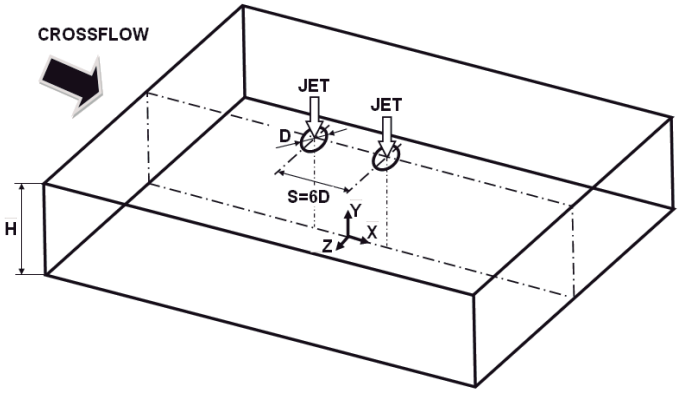

Figure 3: Geometrical arrangement of the jets

B. Visualization Technique

Flow visualization was performed using digital direct photography to guide the choice of the measurement locations and to provide a qualitative picture of the flow. The longitudinal plane of symmetry was illuminated with a sheet of light. This sheet was used to illuminate any cross section that has been seeded with seeding particles. The laser light reflected from the seeding particles, but dark images was observed where there was an absence of seeding particles. The photos were taken perpendicular to the vertical plane of symmetry.

III. Results

The results presented and discussed in this section are to the flow visualization for the velocity ratio V_R of 43.8.

A. Visualization

For the flow studied, the result has shown a pattern similar to that of a single impinging jet. Fig. 4 identifies the flow development along the vertical plane of symmetry, i.e. Z=0. Each jet has an initial potential-core jet region, where the flow characteristics are identical to those of a free jet, and near the horizontal plate the impingement region, characterized by considerable deflection of the first jet. Analysing the fig. 4, it is clear that for this velocity ratio the deflection of the first jet is small. In the case of the rear jet deflection, we can verify that it is quite small compared with the first jet deflection because the first jet protects the rear jet of the influence of the crossflow, and there was not impact of the rear jet on the ground for the lower velocity ratio. However, it is notorious a drop (figure 4 c)) in the rear jet potential core region that it has not been reported in literature. The horseshoe vortex resulting from the interaction of the upstream wall jet with the crossflow could not be clearly identified for this velocity ratio. The nature of each ground vortex is similar to the horseshoe structure known to be generated by the deflection of a boundary layer by a solid obstacle[2], but is different from the vortex pair known to exist in a “bent-over” jet in a crossflow far from the ground[37]. The Figure 4 e) shows that the crossflow is deflected sideways by the penetration of the jet and may cause a recirculation region just downstream of the discharge, away from the ground plate, but cannot be clearly identified. Also, it is possible see a little ground vortex and the wall jet corresponding to the upstream impinging jet which is almost parallel the ground plate and exhibit a behaviour similar to that of a radial wall jet where the upstream effects of interaction due to impingement are no longer important. The upstream wall jet interacts with the crossflow and forms a horseshoe vortex close to the ground plate, which wraps mostly around the first impinging jet. As a result, two streamwise counter-rotating vortices

develop side-to-side and decay further downstream of each impinging zone forming a ground vortex. If the jets were positioned side by side in front of the crossflow two ground vortexes would appear as well as a fountain flow in the vertical plane of symmetry due to the collision of the two individual radial wall jets

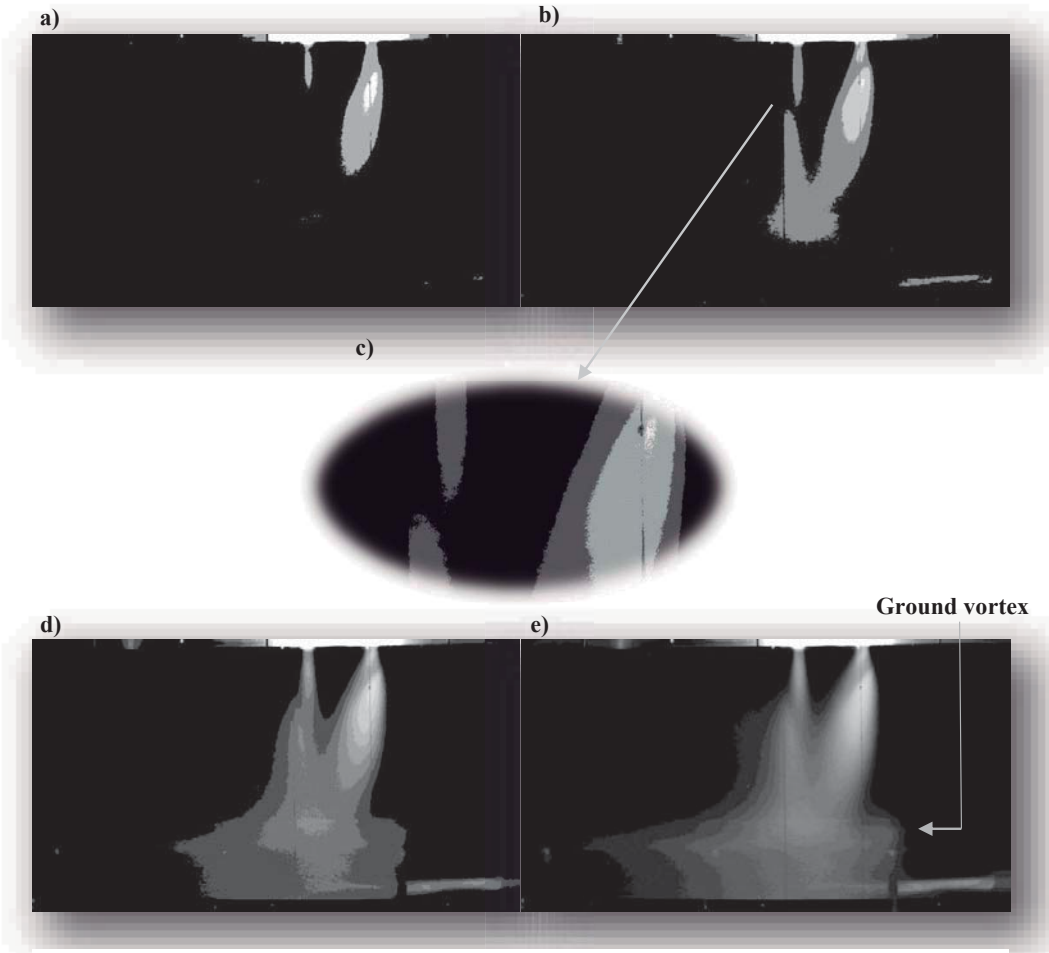

Figure 4: Visualization of the twin jet flow in the vertical plane of symmetry in different phases of the flow development for Re_j=4.3x10^4, H/D=20.1, and S/D=6.

(e.g., Refs. 9, 29, 34, 37). No evidence of a ground vortex corresponding to the downstream impinging jet could be confirmed, which is an indication that the upstream impinging jet and its ground vortex are blocking the crossflow and provoking an alteration to the flow pattern. Also, in the present study no fountain flow was detected.

IV. Numerical Results

This section presents a numerical analysis based on the experimental data presented by Ref.42. The objective of the numerical simulation is to compare the numerical predictions with the experimental data in order to quantify the performance of the computational model and to extend the analysis of the flow.

A. Mathematical Model

The mathematical model used in the numerical simulation is based on the solution of the continuity and momentum equations. A Reynolds-Averaged Navier Stokes (RANS) formulation was adopted with the "*k*-*ε*" turbulence model to represent the turbulent stresses.

The governing equations are written in a similar form:

$$\frac{\partial}{\partial x}(\rho u\phi)+\frac{1}{r}\frac{\partial}{\partial r}(r\rho v\phi)=\frac{\partial}{\partial x}\left(\Gamma_\phi\frac{\partial\phi}{\partial x}\right)+\frac{1}{r}\frac{\partial}{\partial r}\left(r\Gamma_\phi\frac{\partial\phi}{\partial r}\right)+S_\phi \quad (1)$$

Where the property ϕ represents the velocity, turbulent kinetic energy or dissipation while S_ϕ and Γ_ϕ assume different values related with ϕ as described in table 2.

The turbulent diffusion terms are approximated by two equations from "*k*-ε" turbulent model where the Reynolds tension is related with shear tension:

$$\rho\overline{u'_\iota u'_J}=-\mu_T\left(\frac{\partial U_i}{\partial x_j}+\frac{\partial U_j}{\partial x_{ij}}\right)+\frac{2}{3}\delta_{ij}\rho k \quad (2)$$

Where μ_T represent turbulent viscosity derivative from the turbulent model expressed by:

$$\Phi=\mu_T\left\{2\left[\left(\frac{\partial U}{\partial x}\right)^2+\left(\frac{\partial V}{\partial r}\right)^2+\left(\frac{V}{r}\right)^2\right]+\left[\frac{\partial U}{\partial r}+\frac{\partial V}{\partial x}\right]^2\right\} \quad (3)$$

Table 2. Differential equations coefficients.

ϕ	Γ_ϕ	S_ϕ
1	0	0
U	μ_T	$-\frac{\partial p}{\partial x}+\frac{\partial}{\partial x}\left(\mu_T\frac{\partial U}{\partial x}\right)+\frac{1}{r}\frac{\partial}{\partial r}\left(r\mu_T\frac{\partial V}{\partial x}\right)$
V	μ_T	$-\frac{\partial p}{\partial r}+\frac{\partial}{\partial x}\left(\mu_T\frac{\partial U}{\partial r}\right)+\frac{1}{r}\frac{\partial}{\partial r}\left(r\mu_T\frac{\partial V}{\partial r}\right)-2\mu_T\frac{V}{r^2}$
k	μ_T/σ_k	$\Phi-\rho\varepsilon$
ε	μ_T/σ_ε	$C_{\varepsilon 1}\Phi\frac{\varepsilon}{k}-C_{\varepsilon 2}\rho\frac{\varepsilon^2}{k}$

The turbulent model constants allow good results for several types of flows and are summarized in the following table:

Table 3. Turbulent model constants**.**

C_μ	C_1	C_2	σ_k	σ_E
0.09	1.44	1.92	1.0	1.3

The computational domain corresponds to the experimental conditions and has 201 mm of transversal length, remaining constant the following measurements as followed: 1080 mm of longitudinal length, 402 mm of height where the inner diameter of the jets *D* is 15 mm, the spacing between jets are *S* = 6*D* and the height of impact, *H* is 20.1 *D*.

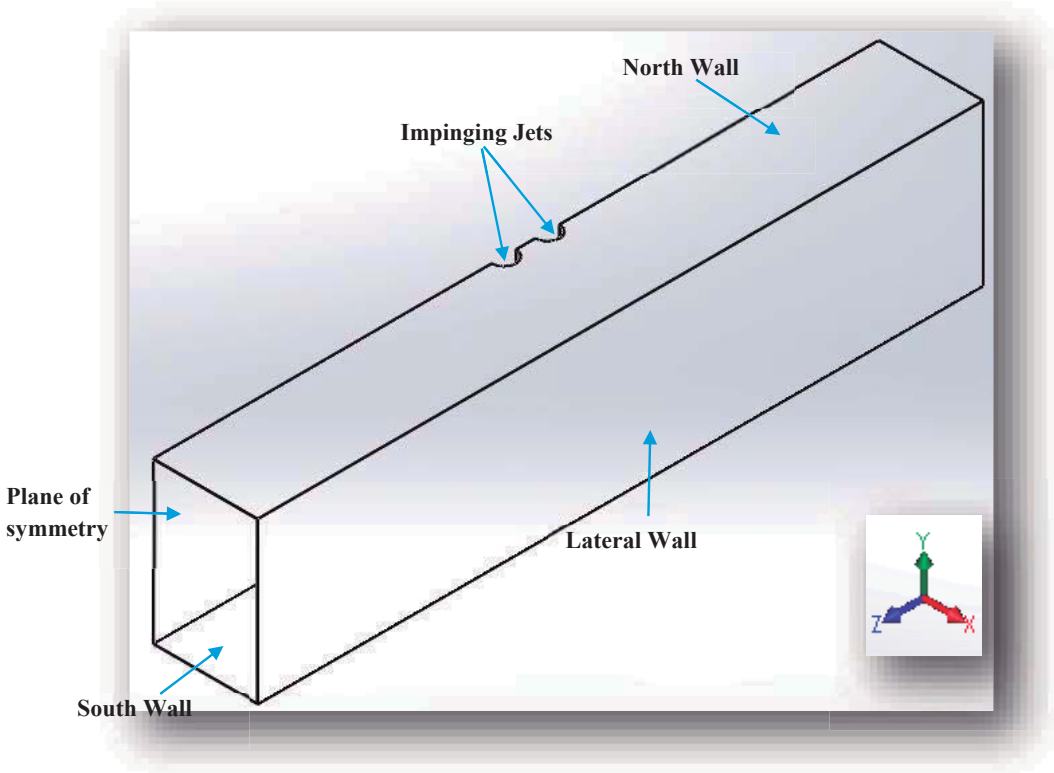

Figure 5: Computational domain used in the numerical simulation

To reduce the computational costs and to reduce the time simulation of the flow, we only simulation half of the test section.

B. Discussion

This section presents a numerical study to extend the analysis of the flow to regions and flow conditions for which no measurements have been obtained. The numerical method is based on the solution of the conservation laws for mass and momentum which is a modified version of the method described elsewhere (see Ref. 7 for details).

Figures 6 to 8 show the mean vertical velocity component (V_{mean}) distribution along the vertical plane of symmetry (i.e. Z=0) together with calculated streamtraces. For all velocity ratios the collision of the upstream wall jet with the crossflow is clearly registered. Meanwhile, the ground vortex is also identified for all velocity ratios, but its centre change with the velocity ratio applied, because the increase of the velocity ratio corresponds to a decrease in crossflow velocity. Comparing this result with that obtained experimentally (Ref. 42 and 43) we can confirm that the deflection sensed by the first jet experimentally is greater than the jet deflection felt numerically, thus leading for example for V_j/U_0=33.7, the centre of the ground vortex is located close to X / D = -4 in the experimental case, whereas for the numerical case it is located close to X/D=-7. As far as the downstream jet (rear jet) is concerned the predictions confirmed the experimental results (Ref. 42 and 43), and its complete deflection by the crossflow was calculated for all the velocity ratios considered with no impingement directly on the wall.

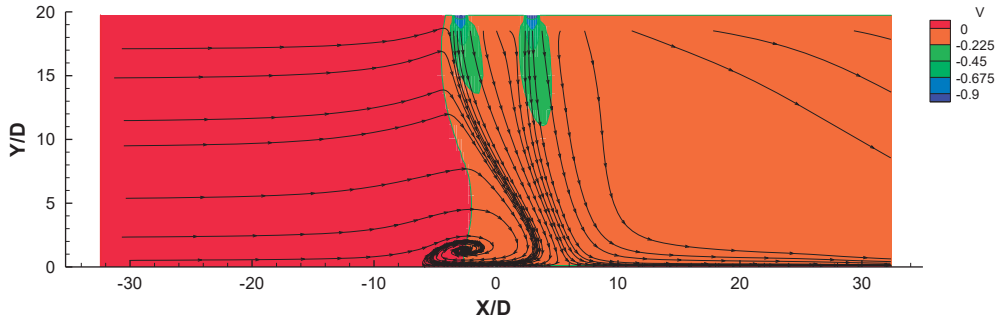

Figure 6: Calculated stream traces and mean vertical velocity component distribution along the vertical plane of symmetry (i.e. Z=0). V_j/U_0=22.5, Re_j=43,000, H/D=20.1, and L/D=6).

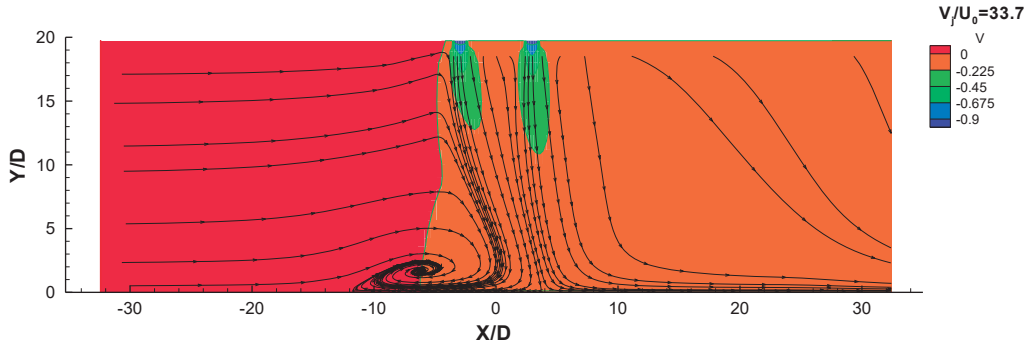

Figure 7: Calculated stream traces and mean vertical velocity component distribution along the vertical plane of symmetry (i.e. Z=0). Vj/U0=33.7, Re_j=43,000, H/D=20.1, and L/D=6).

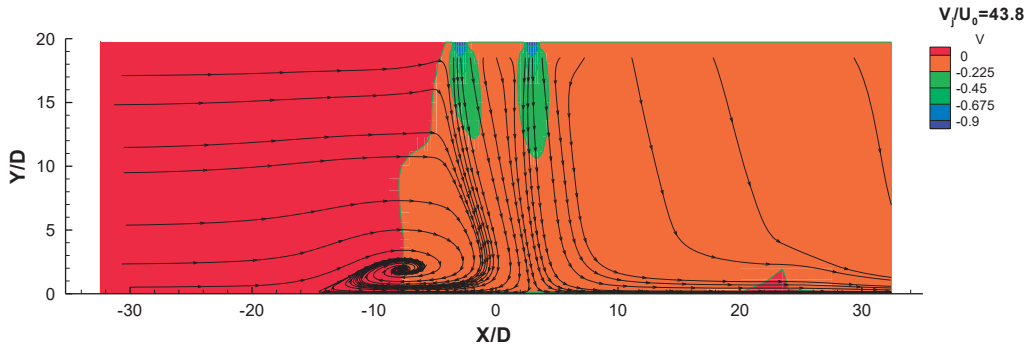

Figure 8 :Calculated stream traces and mean vertical velocity component distribution along the vertical plane of symmetry (i.e. Z=0). Vj/U0=43.8, Re_j=43,000, H/D=20.1, and L/D=6).

Figure 9 shows in more detail the central zone between the two jets with white streamtraces that begin near the top wall. The results show that even for the smallest velocity ratios of V_j/U_0=7.5 and 15 the jets do not mix, but remain together in two layers. As a consequence, for V_j/U_0=15 the downstream jet does not reach directly the ground, but it impinges on the wall jet resulting from the first jet which is moving downstream. For the two higher velocity ratios the ground vortex is always present, but its size and location

changes. It moves upstream with V_j/U_0, because increasing the velocity ratio involves decreasing the relative influence of the crossflow velocity. Ref. 12 identified three different types of flow regimes, but for a V/STOL aircraft operating in ground vicinity the regime with strong impingement on the ground and a ground vortex is the most relevant. However, in transition from hover to horizontal flight the other regimes are also important.

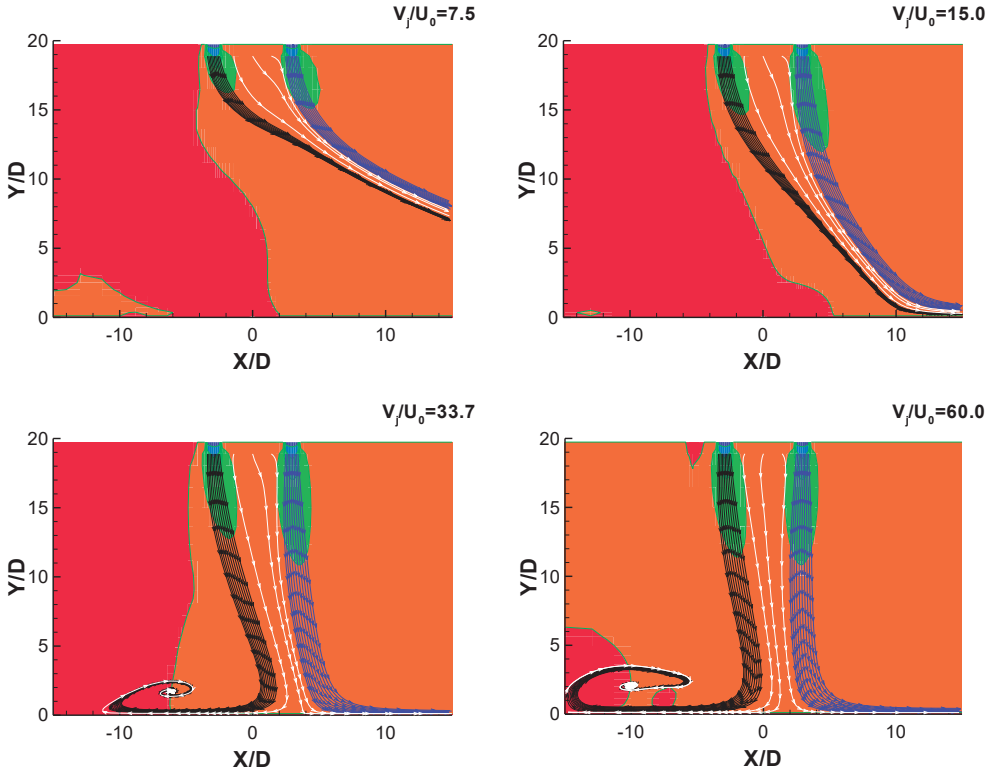

Figure 9 :Details of the calculated stream traces and mean vertical velocity component distribution along the vertical plane of symmetry (i.e. Z=0). Re_j=4.3x10^4, H/D=20.1, and L/D=6.

One major issue in the present flow configuration is the possible deflection of the rear jet by the first jet without occurring impact on the ground. Another possibility (not yet demonstrated) is the impact of the second jet with the first deflected jet or its downstream wall (depending on the velocity ratio). Any of the figure presented above it is sufficiently conclusive about these hypothesis, nor about the blending of the two structures further downstream. In order to better understand this type of flow, and in particular that happened with the rear jet and downstream of the impinging jets, a meticulous numerical study simulation was performed for V_j/U_0=22.5 by varying the velocity of the second jet, $V_{j\,2}$, from, 5.4 m/s up to 36 m/s. The velocity of the first jet was kept constant to preserve the location of the centre of the ground vortex. Despite being varied the second jet velocity from 5.4, up to 36 m/s, it was only possible to view significant changes on the flow to $V_{j\,2} \leq$ 13.5 m/s. Figures 10 and 11 show the results for $V_{j\,2}$ = 5.4 m/s and 13.5 m/s, respectively.

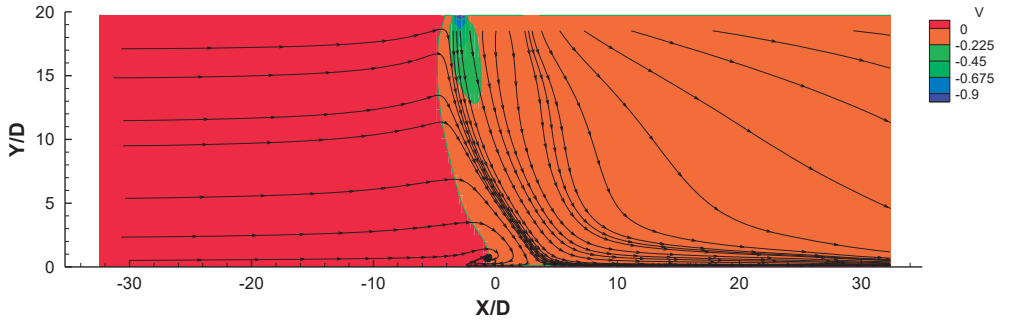

Figure 10 :Calculated stream traces and mean vertical velocity component distribution along the vertical plane of symmetry, Z=0. (Rej=43,000, H/D=20.1, L/D=6, Vj2= 5.4 m/s).

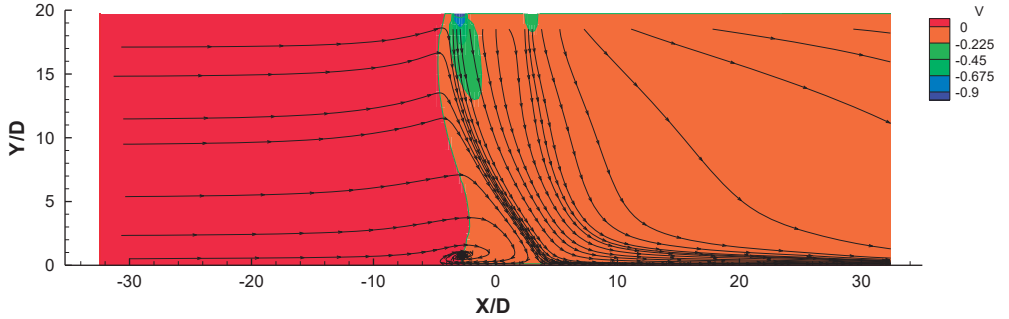

Figure 11 :Calculated stream traces and mean vertical velocity component distribution along the vertical plane of symmetry, Z=0. (Rej=43,000, H/D=20.1, L/D=6, Vj2= 13.5 m/s).

Both figures show that lowering the velocity of the second jet in relation to the first jet, the wall jet of the second jet is always above the wall jet formed by the interaction of the first jet with the crossflow, heading the flow to downstream. The location of the ground vortex is practically not affected by this change in the second jet velocity, confirming that the second jet does not contribute to the occurrence of this structure.

In order to investigate the possible existence of a kidney shape of the crossection of the jets, and their mutual interactions, isolines of the velocity component U_{mean} were obtained in vertical planes perpendicular to the crossflow for X / D = 0.0, 4.9, 9.8 and 19.6. Figures 12 and 13 show the results for $V_{j\,2}$ = 5.4 m / s and $V_{j\,2}$ = 13.5 m/s, respectively. For X / D = 0, i.e. in the middle between the axis of the jets exit, the kidney shape can be clearly identified for the first jet (the second jet it is not yet visible, because its exit is further downstream).

For X / D = 4.9, the second jet can be identified by the dark blue area corresponding to velocities larger than $0.03V_{j\,1}$, that reveals the slight deflection of the second jet inside the wake of the first impinging jet. The kidney shape of the cross section of the first jet is still present, but it is widening rapidly due to the additional influence of the second imping jet. It should be pointed out that the impinging jet and first jet do not mix and are separated by lower values of the velocity component in the crossflow direction (light blue). Additionally, no streamtraces from the second jet are captured by the deflected upstream jet, revealing that a complete mixing between the two jets has not yet occurred.

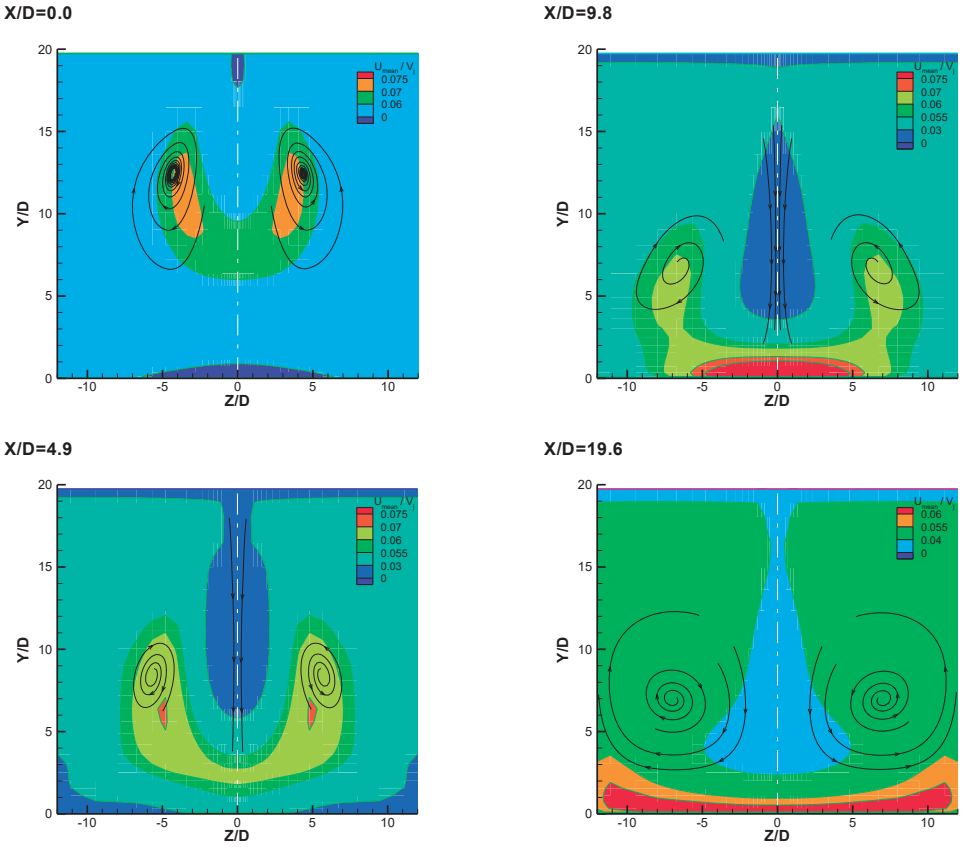

Figure 12 :Mean velocity component (U_{mean}/V_{j1}) in a vertical plane perpendicular to crossflow. (Re_{j1}=43,000, V_{j2} = 5.4 m/s, Re_{j2} =5,339, H/D=20.1, L/D=6).

However, from this location downstream (in the crossflow direction) the second impinging jet will suffer two opposing effects: first the fact that is developing in the wake of the first impinging jet will contribute to its less deflection, and secondly since it is impinging in a flow moving in the crossflow direction with a higher velocity it will be forced to deflect. This novel flow configuration that occurs before the first jet reaching the ground is schematically shown in Fig. 15. So, the final behaviour of the second jet can be described as the flow of a jet through a zero or small upstream crossflow (corresponding to the wake of the first jet) impinging on a horizontal jet with a kidney cross section flowing in the crossflow direction with a higher velocity.

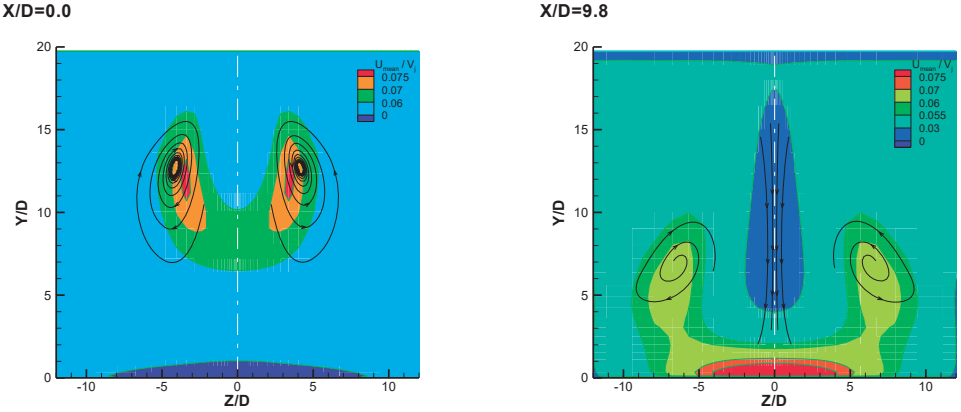

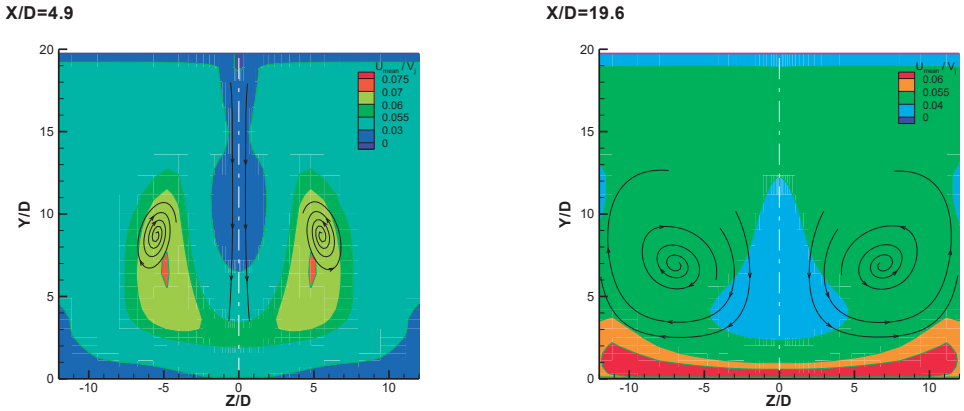

Figure 13 :Mean velocity component (U_{mean}/Vj1) in a vertical plane perpendicular to crossflow. (Re_{j1}=43,000, V_{j2} = 13.5 m/s, Re_{j2} =16,125, H/D=20.1, L/D=6).

In the next downstream location, at X/D = 9.8, the red area identifies a region with relatively large positive values of the velocity component U_{mean} (in the crossflow direction), which is an indication that the first jet touched the ground. The rear jet impacts on this wall jet (resulting from the first jet), and is quickly deflected, but does not reach the ground.
For X/D = 19.6, the entire cross section is occupied by two vortical structures rotating in opposite directions, revealing that the two parallel jets flowing in the crossflow direction finally merge.

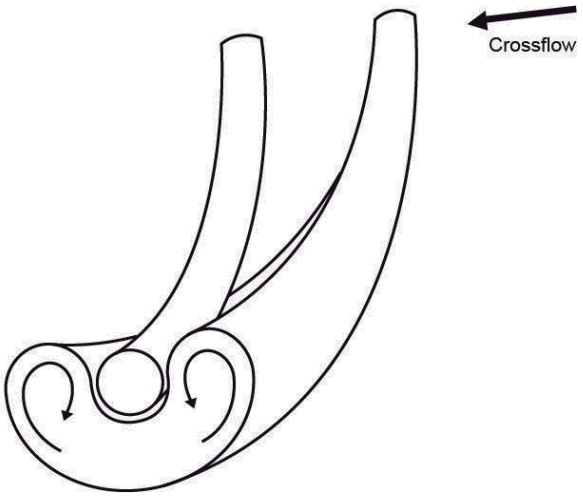

Figure 14: Illustration of the kidney shape of the cross section of the first jet before reaching the ground and the second (downstream) jet interaction.

V. Conclusion

The flowfield created by ground vortex generated by twin impinging jets in tadem through a crossflow is studied in detail. Flow visualization and numerical simulation are presented for two turbulent circular jets

impinging on a flat surface perpendicular to the geometrical nozzle axis, through a low velocity crossflow. The numerical simulation were performed for Reynolds based on the jet exit conditions of 43,000 to 105,000, a jet-to-crossflow velocity ratio between 15 and 60, being the focus of the study the velocity ratio used in experimental work (Ref. 42 and 43), for an impinging height of 20.1 diameters (the same used in experimental work), and with an interjet spacing of S=6D (the same used in experimental work).

The results show a large penetration of the first (upstream) jet, which is deflected by the crossflow and impinges on the ground giving rise to a ground vortex due to the collision of the radial wall and the crossflow that wraps around the impinging point like a scarf. The first jet deflection and the location of the ground vortex depend on the velocity ratio used. For higher velocity ratios the deflection of the first jet is smaller and closer to the first jet is located the centre of the ground vortex. The rear jet it is not so affected by the crossflow in terms of deflection for all velocity ratios because it is protected by the upstream jet, but due to the downstream wall jet that flows radially from the impinging point the first jet does not reach the ground. Also due to the confinement and the ground vortex, the crossflow is blocked and accelerates in the upper part and also contributes to an enhanced mixing of each secondary flow. As consequence, no upstream wall jet or ground vortex resulting from the second (downstream) jet was detected. The effect of the rear jet impinging on the downstream wall jet resulting from the first jet had not been reported so far and requires further investigation.

In case of the numerical analysis beyond the rig experimental limits, the results show that for the two lowest velocity ratios, the jets do not mix remaining in two layers together, and therefore, it is not detected the presence of ground vortex. For $V_j/U_0 = 33.7$ and 60 the ground vortex is completely present, and it moves with the increase of V_j/U_0.

As far as the downstream jet (rear jet) is concerned the predictions confirmed the experimental results obtain by Ref. 42, and its complete deflection by the crossflow was calculated for all the velocity ratios considered with no impingement directly on the wall. By changing the rear jet velocity and extracting perpendicular planes to the jets flow was possible to prove that the second jet is deflected quickly, never reaching the ground, thus proving the accuracy of the experimental results, leading us to conclude that impinging jet in tandem configuration, the downstream jet is entrained by the upstream jet and not by the crossflow itself. In the future, this issue should be further investigated in order to understand what the real consequence for the aircraft when this type of phenomenon occurs.

Acknowledgments

The assistance of Ms. Inês Carvalho with some illustrations of the flow field is gratefully acknowledged.
The present work was done in the scope of the activities of LAETA-Associated Laboratory of Energy, Transports and Aeronautics, and funded by FCT-Fundação para a Ciência e Tecnologia through contract PTDC/EME-MFE/102190/2008 and grant SFRH/BD/86434/2012

References

[1]Adler, D.; Baron, A "Prediction of a three-dimensional circular turbulent jet in crossflow" *AIAA Journal, No.* 17, 1979, pp.168-174

[2]Andreopoulos, J. and Rodi, W., "Experimental Investigation of Jets in a Crossflow", *J. Fluid Mechanics*, Vol. 138, 1984, pp. 127.

[3]Araújo, S.R.B., Durão, D.F.G., and Firmino, F.J.G., "Jets Impinging Normally and Obliquely to a Wall", AGARD CP 308, paper 5.

[4]Baker, O.J., "The Turbulent Horseshoe Vortex", *J. Wind Engineering and Industrial Aerodynamics*, Vol. 6, 1981, pp. 9.

[5]Barata, J.M.M., Durão, D.F.G., and McGuirk, J.J., "Numerical Study of Single Impinging Jets Through a Crossflow", *Journal of Aircraft,* Vol.26, No.11, 1989, pp. 1002-1008.

[6]Barata, J.M.M., "Numerical and Experimental Study of Jets Impinging on Flat Surfaces Through a Crossflow", Ph.D. Thesis (in Portuguese), Instituto Superior Técnico, Technical Univ. of Lisbon, Lisbon, Portugal, 1989.

[7]Barata, J.M.M., Durão, D.F.G., and McGuirk, J.J., "Numerical Study of Single Impinging Jets through a Crossflow", *J. of Aircraft*, Vol.26, No.11, 1989, pp.1002-1008.

[8]Barata, J.M.M., Durão, D.F.G., Heitor, M.V., and McGuirk, J.J., "On the Analysis of an Impinging Jet on Ground Effects", *Experiments in Fluids*, No.15, 1993, pp.117-129.

[9]Barata, J.M.M., "Ground Vortex Formation with Twin Impinging Jets". Paper SAE 962257, International Powered Lift Conference, Jupiter, Florida, 18-20 Nov., 1996.

[10]Barata, J.M.M., "Fountain Flows Produced by Multiple Impinging Jets in a Crossflow". *AIAA Journal*, Vol. 34, No.12, Dez. 1996, pp. 2523-2530 e *AIAA Journal on Disc*, Vol. 2, No.1, 1996.

[11]Barata , J.M.M., Carvalho, P.S.D., Durão, D.F.G., Neves, F.M.S.P., Silva, A.R.R., and Vieira, D.F.C., "Laser Doppler Measurements of Twin Impinging Jets Aligned With a Crossflow", July 2012, 16th Int Symp on Applications of Laser Techniques to Fluid Mechanics Lisbon, Portugal, 09-12 July, 2012.

[12]Barata, J.M.M., Neves, F.M.S.P., Vieira, D.F.C., and Silva, A.R.R., "Twin Impinging Jets Through a Crossflow", 50th AIAA Aerospace Sciences Meeting including the New Horizons Forum and Aerospace Exposition, 9-12 January 2012/ Gaylord Opryland Resort & Convention Centre, Nashville, Tennessee.

[13]Barata, J.M.M, "Multiple Jet/Wall/Cross-Wind Interaction Relevant to VSTOL Ground Effects", AIAA paper 2013-4380, 2013 International Powered Lift Conference, Los Angeles, California, August 12-14, 2013.

[14]Barata, J.M.M., "Twin Impinging Jets Aligned With a Crossflow". AIAA paper 2013-3600, 49th AIAA/ASME/SAE/ ASEE Joint Propulsion Conference and Exhibit, San Jose, California, 15-17 July, 2013.

[15]Childs, R. E. and Nixon, D. "Simulation of impinging turbulent jets", paper AIAA-85-0047, presented at the AIAA 23rd Aerospace Science Meeting, Jan. 14- 17, 1985, Reno, Nevada.

[16]Crabb, D., Durão, D.F.G., and Whitelaw, J.H., "A Round Jet Normal to a Crossflow", *J. Fluids Engng.* Vol.113, 1981, pp. 142-153.

[17]Demuren, A. O."Numerical calculations of steady three-dimensional turbulent jets in crossflow" Comp. Meth. In Appl. Mech. and Engng. 1983, Vol. 37, pp. 309-328.

[18]Durst, F., Melling, A., and Whitelaw, J.H., "*Principles and Practice of Laser-Doppler Anemometry*", 2nd ed., New York, Academic Press.

[19]Gilbert, B.L., "Detailed Turbulence Measurements in a Two Opposing Plane Turbulent Wall Jets", AIAA 16th Fluid and Plasma Dynamics Conf., AIAA Paper 83-1678, Danvers, MA, Jul. 12-14, 1983.

[20]Jenkins, R.C., and Hill, W.G., Jr., "Investigation of VTOL Upwash Flows Formed by Two Impinging Jets", Grumman Research Dept. Rept. RE-548, Bethpage, NY, Nov., 1977.

[21]Jones, W. P. and McGuirk, J. J. "Computation of a round turbulent jet discharging into a confined crossflow", In: *"Turbulent Shear Flows-2",*~ Bradbury et al., Springer Verlag, 1980, pp.223-245

[22]Kamotani, Y., and Greber, I., "Experiments on Confined Turbulent Jets in a Crossflow", NASA CR-2392, 1974.

[23]Kavasaoglu, M.S., Schetz, J.A., and Jakubowsky, A.K., "Rectangular Jets in a Crossflow", *Journal of Aircraft,* Vol.26, No. 9, 1989, pp. 793-804.

[24]Keffer, J. F. and Baines, W. D. "The round turbulent jet in a cross-wind", *J. Fluid Mech*., Vol. 15, 1963, pp. 481-496

[25]Kind, R.J., and Suthanthiran, K., "The Interaction of Two Opposing Plane Turbulent Wall Jets", AIAA Paper 72-0211, Jan., 1980.

[26]Knowles, K., and Bray, D., "The Ground Vortex Formed by Impinging Jets in Crossflow", AIAA 29th Aerospace Sciences Metting, AIAA Paper 91-0768, Reno, NV, Jan. 7-10, 1991.

[27]K. Knowles, "Computational Studies of impinging jets using k-ε Turbulence Models", International Journal for Numerical Methods in Fluids, 1996, Vol. 22, pp. 799-810.

[28]Kotansky, D.R., and Glaze, L.W., "The Effects of Ground Wall-Jet Characteristics on Fountain Upwash Flow Formation and Development", Rept. ONR-CR212-216-1F, 1980.

[29]Kotansky, D.R., "The Modelling and Prediction of Multiple VTOL Aircraft Flow Fields in Ground Effect", AGARD CP-308, Paper 16.

[30]Melling, A., and Whitelaw, J.H., "Turbulent Flow in a Rectangular Duct", *J. Fluid Mechanics*, Vol. 78, 1975, pp.285-315.

[31]Patankar, S. V., Basu, D. K. and Alpay, S. A "Prediction of the three-dimensional velocity field of a deflected jet" *J. Fluids Engng*., Vol. 99, 1979, pp. 758-762

[32]Paul Bevilacqua, Richard Margason and Charles Gaharan, "A Jet Entrainment Theory for VTOL Aircraft Suckdown", paper AIAA-2007-1397, 45th AIAA Aerospace Science Meeting and Exhibit, 8-11 Jan. 2007, Reno, Nevada.

[33]Saripalli, K.R., "Visualization of Multijet Impingement Flow", *AIAA Journal*, Vol. 21, 1983, pp. 483-484.

[34]Sarippali, K.R., "Laser Doppler Velocimeter Measuremnts in 3D Impinging Twin-Jet Fountain Flows", *Turbulent Shear Flows,* Vol.5, edited by Durst et al., Springer-Verlag, Berlin, 1987, pp. 147-168.

[35]Schetz, J.A., Jakubowsky, A.K. and Aoyagi, K., "Surface Pressures on a Flat Plate with Dual Jet Configurations", *Journal of Aircraft*, Vol.21, No.7, 1984, pp. 484-490.

[36]Shayesteh, M.V. Shabaka, I.M.N.A., and Bradshaw, P., "Turbulent Structure of a Three-Dimensional Impinging Jet in a Crossflow", AIAA 23rd Aerospace Sciences Meeting, AIAA Paper 85-0044, Reno, NV, Jan. 14-17, 1985.

[37]Siclari, M.J., Migdal, D., Luzzi, T.W., Jr., Barche, J., and Palcza, J.L., "Development of Theoretical Models of Jet-Induced Effects on V/STOL Aircraft", *Journal of Aircraft*, Vol. 13, No. 12, 1976, pp.938-944.

[38]Stoy, R.C., and Ben-Haim, Y., "Turbulent Jets in a Confined Crossflow", *J. Fluids Engng.*, No.95, 1973, pp.551-556.

[39]Sugiyama Y., and Usami, Y., "Experiments on the Flow in and Around Jets Directed Normal to a Crossflow", *Bulletin JSME*, No.22, 1979, pp. 1736-1745.

[40]Sugiyama, Y. and Usami, Y. "Experiments on the flow in and around jets directed normal to a crossflow", Bulletin JSME, 1979, Vol. 22, pp. 1736-1745.

[41]Yanta, W.J. and Smith, R.A., "Measurements of Turbulent Transport Properties with a Laser-Doppler Velocimeter", 11th Aerospace Sciences Meeting, AIAA Paper 73-0169, Washington, 1978.

[42]Vieira, D.F.C., Silva, A.R.R., Carvalho, P.S.D., Neves, F.M.S.P. and Barata, J.M.M. " Numerical and Experimental Study of Two Impinging Jets in a Row through a Crossflow", AIAA Paper 2013-0806, 51th AIAA Aerospace Science Meeting Including the New Horizons Forum and Aerospace Exposition, Grapevine (Dallas/Ft. Worth Region), Texas, 7-10 Jan., 2013.

[43]Vieira, D.F.C, Durão, D.F.G., Neves, F.M.S.P., Silva, A.R.R., Barata J.M.M., and., "Laser Doppler Measurements of Twin Impinging Jets in Tadem through a Crossflow", July 2014, 17th Int Symp on Applications of Laser Techniques to Fluid Mechanics Lisbon, Portugal, 07-10 July, 2014.

STUDY OF TWIN IMPINGING JETS/CROSSFLOW INTERACTION RELEVANT TO F-35 VSTOL GROUND EFFECTS

Diana Vieira[a*], Jorge Barata[a], André Silva[a]
a) AEROG, Aerospace Sciences Department, Universidade Beira Interior, Calçada Fonte do Lameiro, 6200-358, Covilhã, Portugal

* e-mail: dianavieir@gmal.com

Key words: VSTOL, ground effect, impinging jets through a crossflow

Abstract. *An experimental and numerical study is carried out to investigate the flowfield of a ground vortex generated by twin impinging jets in tandem through a crossflow. Experimental measurements and the numerical simulation are presented for two turbulent circular jets emerging into a low velocity cross stream, impinging after on a flat surface perpendicular to the geometrical jet nozzle axis. The mean velocity, velocity fluctuation and visualization in the impingement region were obtained for a Reynolds number based on the jet exit conditions of $Re_j=4.3x10^4$, an impingement height of 20.1 diameter and for a velocity ratios between the jet exit and the crossflow $22.5<V_R=V_j/U_o<43.8$ with interject spacing, S of 6D. The numerical study is based in experimental studies, so all the features of the experimental flow were maintained when the numerical simulation was performed. The Reynolds number used was based on the jet exit conditions of 43,000 to 105,000, a jet to crossflow velocity ratio of 22.5 to 43.8, an impinging height of 20.1 jet diameters and an interject spacing's of S=5D and L=6D. The analysis of the flow was extended to regions and flow conditions for which no measurements have been obtained in experimental study, i.e., for velocity ratios of 7.5 to 90. The numerical results allowed to extend the experimental study, and prove that the deflection of the rear jet is due to the competing influences the wake, the shear layer, the downstream wall jet of the first jet and the crossflow. To the velocities ratio beyond the limits of the experimental conditions the numerical results show that for the smallest velocity ratios the jets initially do not mix, but remain together in two layers. Also, it is possible identify three different types of flow regimes, therefore to the case of study, when VSTOL aircrafts operating in ground vicinity, only the regime with strong impingement on ground and with a formation of a ground vortex is relevant.*

1 HEADLINE

In external aerodynamics applications, such as, VSTOL aircrafts, turbulent jets impinging on flat surfaces through a low velocity crossflow are typical of the flow beneath of this type of aircraft. During its landing or near ground hovering phase, the VSTOL aircraft creates a complex three dimensional flow field between the jet streams, the airframe surface and the ground. When ground effect occurs (Figure 1), the lift forces on the aircraft changes, cause hot gas re-ingestion into the engine intake and due to the fountain up wash and ground flows, the fuselage skin temperature rises. The unsteadiness of the

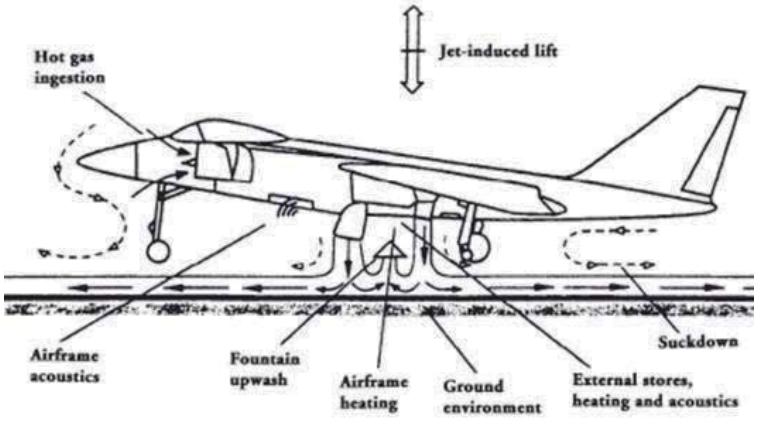

Figure 1: Hovering environment for jet-powered V/STOL aircraft [30]

flow and raise of the temperature cause several problems in the engine performance, such as, compressor surge or even stall and thrust reduction. In respect to the intake ingestion phenomenon, it is very complex and can be associated with the design and operational parameters, such as, jet configuration, head wind velocity, jet impingement height or intake configuration. The flow mechanisms leading to hot gas ingestion can be broken into three categories: far field, crossflow and near field (Figure 2). The first mechanism is results of the forward away initially movement of the ground sheet wall jet due to the aircraft movement. This happened because the hot gases after some distance loses its momentum, rising and separating from the ground. The portion of the hot gases that separating from the ground, mixes with the surrounding air and backs again to the intake. The second mechanism is due as a consequence of the instability of the jet and the fountain flows. The entrainment action into the flow leads to discrete vortices which can detach from the main jet The latter mechanism, near field ingestion is usually the most serious and occurs when fountain flows find their ways to the aircraft inlet, being that when exits multiple impinging jets, its impact on the ground plane create a fan shape up wash fountain beneath the aircraft. When the fountain impinges on the underside of the fuselage, flowing from the fuselage to the intake, the engine may sucks the flow to the intake, creating severe temperature distortion to the intake, since, these gases are much hotter than those from the far field ingestion.. If there are two or more adjacent jets, the resulting wall jets meet, and a fan-shaped up wash, or "fountain", is normally formed between the jets. The fountain up wash flow depending on its strength and direction affects the forces and moments induced in the aircraft when operating in ground effect. The resulting ground vortex shape is strongly affected and the corresponding induced suckdown effect tends to be reduced by the upload produced by the fountain. In the last thirty or forty years, this type of complex flow fields have been studied extensively, but improve the knowledge are ever required because the aircraft design have been changed since its first design, and some problems were solved but others were not. For the next generation of VSTOL aircrafts F-35 no relevant studies can be found, because the impinging jets are aligned with the crossflow and this geometry has not yet been

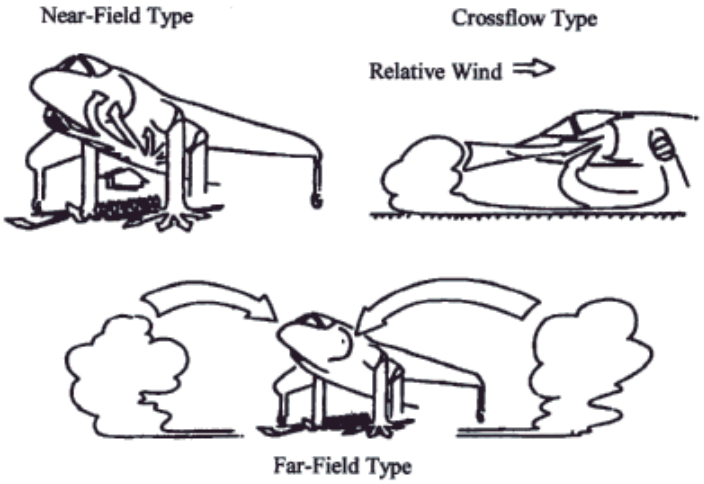

Figure 2: Flowfields that can lead to hot gas ingestion

considered. In this case a vertically oriented lift fan (SDLF) generates a column of cool air that produces the nearly 20,000 pounds of lifting power, along with an equivalent amount of thrust from the vectored rear exhaust (3BSM-Three Bearing Swivel Module). Fig. 2 shows the position of the thrust vectoring nozzle and lift fan in the F-35 aircraft. The lift system was successfully demonstrated during a flight test of the X-35B during the summer of 2001. The complexity of the new VSTOL configuration together with the very stringent requirements has required an enormous amount of R&D in the last decade. This paper aims presents results that are relevant to the future F-35 VSTOL configuration (Figure 3), through a detailed analysis of the complex flow field beneath two impinging jets in tandem through a low velocity crossflow.

The present study is a piece of a most comprehensive experimental and numerical study on impinging jet flows in ground effect, which included two different experimental installations: 2-D ground vortex, and wind tunnel, and numerically the extrapolation of the measurements beyond the limits of experimental rig through computational simulations.

Previous detailed measurements of the flow properties for fountain up wash flow are scarce and have been presented essentially in the absence of a crossflow and with the use of probe techniques and more recently with Particle image velocimetry. The most relevant works have been reviewed by Refs. [6] and [34], showing high turbulence levels and spreading rates in the fountains (e.g. Refs. [22] and [31]). In the case of Ref. [31] the turbulent normal stress of the axial component made a substantial contribution to the increase in the static pressure on a region near the impingement plate,

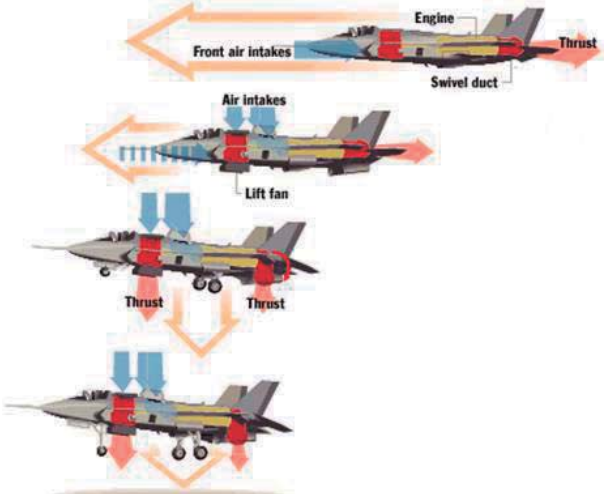

Figure 3: Position of the thrust vectoring nozzle and lift fan

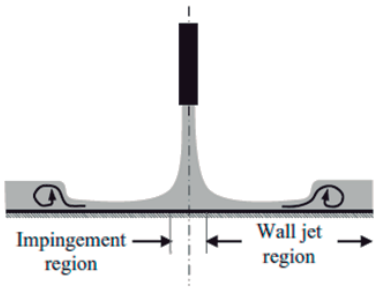

Figure 4: Schematic of a normal impinging jet on a flat plate or ground [25]

being the turbulence close an axisymmetric state in the stagnation region. Ref [35] reports laser Doppler velocity (LDV) measurements, including those of shear stress, for axisymmetric impinging jets with an distance between the jet axis, S/D=9 and 14 with an impinging height, H/D, of 3 and 5.5, but again the existence of a crossflow was not considered. Detailed measurements of the velocity characteristics of normal impinging jets on a flat surface (Figure. 4) can be found for single jet configurations for relatively large impingement heights and normally for H/D>10, using either probe or optical techniques, as reviewed for example by. Refs. [4] and [10]. Ref. [18] reports LDV measurements including shear stress measurements for values of H/D=12 and for velocity ratios up to 2.3. Only Ref. [6] provided detailed LDV measurements for a single jet configuration for a jet with Reynolds number Rej=6x104, a velocity ratio between the jet, V_j and the crossflow, U_0, $V_R=V_j/U_0$ of 30, 42 and 73 with jet exit above the ground plate 3, 4 and 5 diameters. Refs. [11-12] extended their study to multi jet impinging configurations producing up wash fountain flows (Figure.5) which are the heart of the complex effects produced by VSTOL aircraft when they operate in ground proximity, but as far as twin jets are concerned only the geometry with the jets side by side was considered. Experiments on the aerodynamics of jets through a confined crossflow are scarcer and have only been reported for large impingement heights and for low velocity ratios between the jet and the crossflow V_j/U_0. Therefore these works have only peripheral relevance to the VSTOL ground effect problem with the same geometry of the F-35. Ref. [17] studied the experimental data of the intake in a short take off and vertical landing aircraft in ground effect through laser Doppler measurements. The results confirmed that the flow pattern produced with the impingement height and velocity ratio parameters selected were typical of practically occurring re-ingestion flow fields. The authors also did this study to obtain results as benchmark validation data for time averaged turbulence model based RANS CFD predictions. Ref. [28] reports a hot-wire anemometry measurements for two different twin jets arrangement for values of V_j/U_0 to equals 8. The results show that the vorticity distribution, vortex strength, transverse penetration ability and intensity of vorticity transport were strongly dependent function of the geometrical parameters. More recently a brief survey of the recent studies of twin jets in crossflow was carried out by Ref. [29], show that the tadem configurations have rapid mixing and great penetration into the crossflow than side by side configurations. They also report how the transverse penetration ability and vortex strength are subject to the nozzle arrangement, and they found that all cases of twin jets in crossflow lead qualitatively to the some dominant vertical structures, counter rotating vortex pair, being responsible by convective entrainment. An important characteristic of two impingement jets with the presence of a crossflow are the fountain up wash flow produced by the collision of the wall jets and the

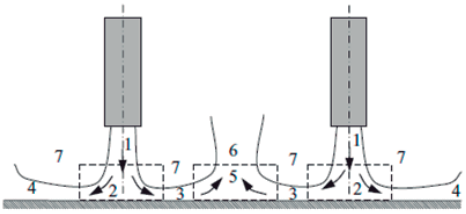

Figure 5: Schematic of the upwash fountain flow by two impinging jets: 1. Free jet, 2. Jet impingement region, 3. Ineer wall jet region, 4. Outer wall jet region, 5. Fountain formation region, 6. Fountain upwash flow, 7. Entrainment [25]

entrainment of ambient air into different regions of the flow Refs. [34] and [25] studied the spreading flow due to the normal impingement of two closely spaced liquid jets. The visualization results allowed the authors to conclude that depending on the spacing between the two jets and their relative strength, different kinds of thin film interactions are possible, resulting in a variety of flow pattern. Ref. [33] also studied the fountain flow for two under expanded, axisymmetric and turbulent impinging jets on a ground plane using LDV and PIV. It was identify the presence of a large scale structures on the fountain flow and at the stagnation region with high degree at asymmetry.

Most of the computational work published on jets with crossflow has been based on integral methods admitting assumptions simplified, which are only capable of predicting global effects such as trajectories and jet cross-section shapes, for example Refs. [2] and [32] employed a finite-difference numerical procedure together with a two-equation turbulence model to predict a single jet in an unconfined crossflow, and obtained good agreement with the experiments of Ref. [26] for velocity ratios from 2 to 10. A similar approach was used by Ref. [23] to calculate the confined flow measured by Ref. [24]. The gross features of the flow are well predicted but the calculations appear to exhibit diffusion rates larger than those consistent with measured profiles, which can be attributed either to numerical or turbulence model errors. Ref. [27] has shown that the standard "k-ε" model over predicts the spreading rate of a free jet and under predicts the spreading rate of a radial wall jet. Refs. [9] and [38] used the Steady-RANS or SRANS approach but the results did not capture the turbulent structure of the fountain flow and impingement regions, being the predicted turbulent quantities particularly poor. Recently Ref. [39] reports a numerical study employing the Unsteady-RANS or URANS approach, comparing the results with Ref. [9]. Compared the results with the SRANS approach results of the Ref. [38], the URANS approach was the one that better agreement with the experimental data. Refs. [20-21] employed in their numerical studies LES and RNG turbulence model. Ref. [20] detected the formation and evolution of the steady or quasi-steady vortical structures by the interaction of an impinging jet in a confined crossflow but without reference to the instantaneous flow patterns by the RNG "k-ε" turbulence model. However, in this two works (Refs. [20-21]) the forming and time evolution characteristics of highly 3-D vertical structures are not well understood due to the limitations of the two computational methods, being the mixing of the ambient crossflow fluid by the unsteady vertical structures in the near wall regions not fully exposed. Ref. [1] presented a comparison of experimental data and computational simulation about an impinging jet without crossflow for different impingement heights, $3<H/D<12$, S/D and $0º<\theta jet<20º$. The results showed that the stagnation primary point moves away in the radial main flow direction with jet angle increase and become stronger with the jet to jet spacing increase. The pressure at the stagnation point located at the middle between the two jets increase with the jet angle and decrease with the Re. The increase of the H/D decreases the intensity of the re-circulation zone in the middle of the jets and the jet spreading.

This paper has four sections in which section II describes the experimental configuration and procedure. Section III presents the experimental results obtained in the vertical plane of symmetry containing the axis of both jets and quantifies the mean velocity characteristics of the flow. The numerical results are discussed in Sect. IV on the basis of numerical visualization of the three-dimensional flow. The last section summarizes the main findings and conclusions of this work.

2 EXPERIMENTAL METHOD

The experiments were performed on a wind tunnel facility designed and constructed for the present work, with an exit section of 300x402 mm that is schematically shown in Figure 6. The test section was made of Perspex allowing the passage of laser beams. During all the design process special consideration was taken for the boundary layer in which the recommendations of Ref. [19] for open circuit wind tunnels was followed. A fan with 15KW nominal power drives a maximum flow of 3000m^3/h through the boundary layer wind tunnel exit section. In the present study each jet unit of D_{inner}=15mm is mounted vertically in the top of the test section 20.1D above the ground as showed schematically in Figure 7. The origin of the horizontal, X, and vertical, Y, coordinates is taken at the midpoint between the centers of the jets exit. The X coordinate is positive in the direction of the wind tunnel exit and Y is positive upwards. The present results were obtained at the vertical plane of symmetry for jet mean velocity of V_j = 36m/s, a jet Reynolds number of $Re_j = 4.3x10^4$ and mean crossflow velocities of 1.6 m/s<U_0<0.8m/s, corresponding to a velocity ratio, 22.5<V_R=V_j/U_0<43.8.

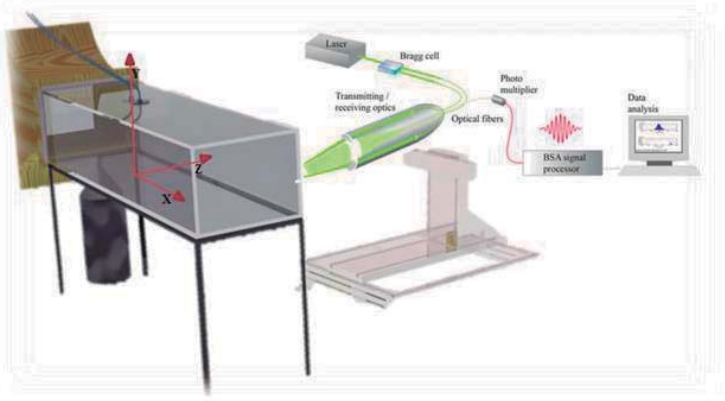

Figure 6: Experimental set-up

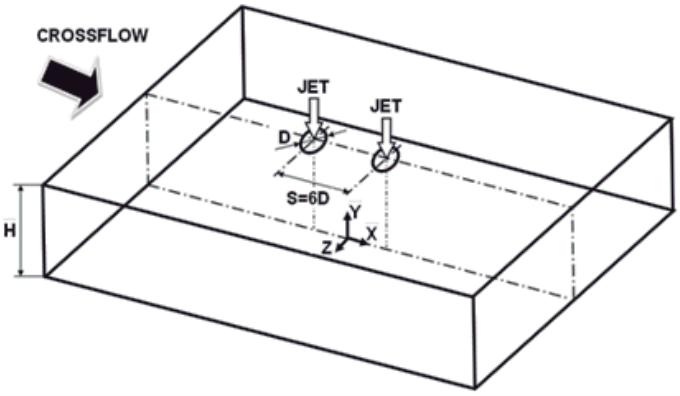

Figure 7: Geometrical arrangement of the jets

3 Results

3.1 Visualization

For the flow studied, the result has shown a pattern similar to that of a single impinging jet. Figure 8 identifies the flow development along the vertical plane of symmetry, i.e. Z=0. Each jet has an initial potential-core jet region, where the flow characteristics are identical to those of a free jet, and near the horizontal plate the impingement region, characterized by considerable deflection of the first jet. Analysing the Figure 8, it is clear that for this velocity ratio the deflection of the first jet is small. In the case of the rear jet deflection, we can verify that it is quite small compared with the first jet deflection because the first jet protects the rear jet of the influence of the crossflow, and there was not impact of the rear jet on the ground for the lower velocity ratio. However, it is notorious a drop (Figure 8 c)) in the rear jet potential core region that it has not been reported in literature.

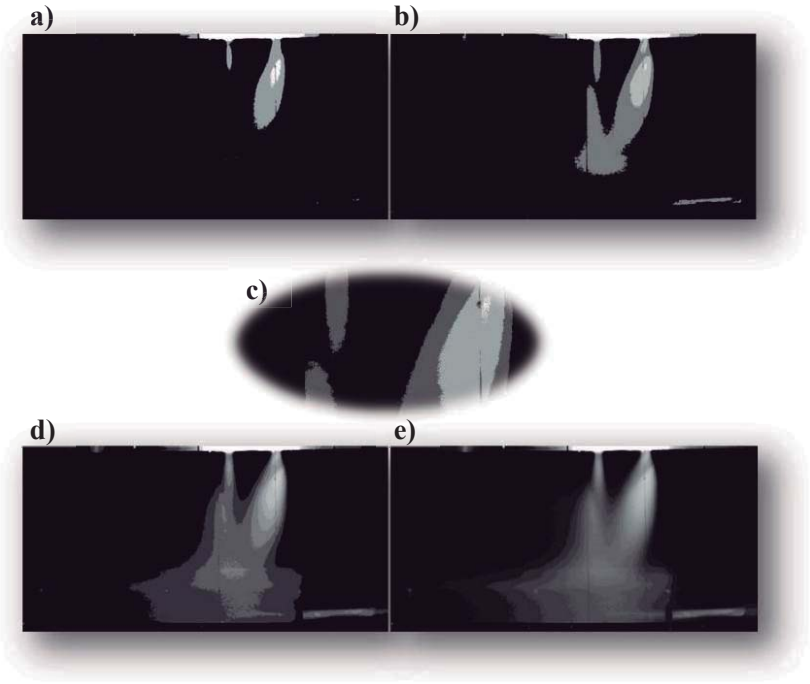

Figure 8: Visualization of the twin jet flow in the vertical plane of symmetry in different phases of the flow development for Re_j=4.3x104, H/D=20.1, and S/D=6.

The horseshoe vortex resulting from the interaction of the upstream wall jet with the crossflow could not be clearly identified for this velocity ratio. The nature of each ground vortex is similar to the horseshoe structure known to be generated by the deflection of a boundary layer by a solid obstacle, but is different from the vortex pair known to exist in a “bent-over” jet in a crossflow far from the ground. The Figure 8 e) shows that the crossflow is deflected sideways by the penetration of the jet and may cause a recirculation region just downstream of the discharge, away from the ground plate, but cannot be clearly identified. Also, it is possible see a little ground vortex and the wall jet corresponding to the upstream impinging jet which is almost parallel the ground plate and exhibit a behaviour similar to that of a radial wall jet where the upstream effects of

interaction due to impingement are no longer important. The upstream wall jet interacts with the crossflow and forms a horseshoe vortex close to the ground plate, which wraps mostly around the first impinging jet. No evidence of a ground vortex corresponding to the downstream impinging jet could be confirmed, which is an indication that the upstream impinging jet and its ground vortex are blocking the crossflow and provoking an alteration to the flow pattern. Also, in the present study no fountain flow was detected.

3.2 Measurments

Figure 9 shows vertical profiles for mean vertical velocity component along the vertical plane of symmetry (Z=0). The first profile at X/D=−6.33 shows positive values of the mean vertical velocity component for all the velocity ratios studied, and for $V_j/U_0 = 33.7$ there is an increase at Y <30mm, which is not identified for the other velocity ratios. The next profile shows a large influence of the velocity ratio on the vertical velocity component. For an intermediate velocity ratio only positive values of the mean vertical velocity exist, with the largest values Y <60mm due to a slight acceleration of the flow which passes over the ground vortex. For a higher velocity ratio, the profile at the same location shows negative values of the mean vertical velocity that correspond to a location inside the ground vortex.

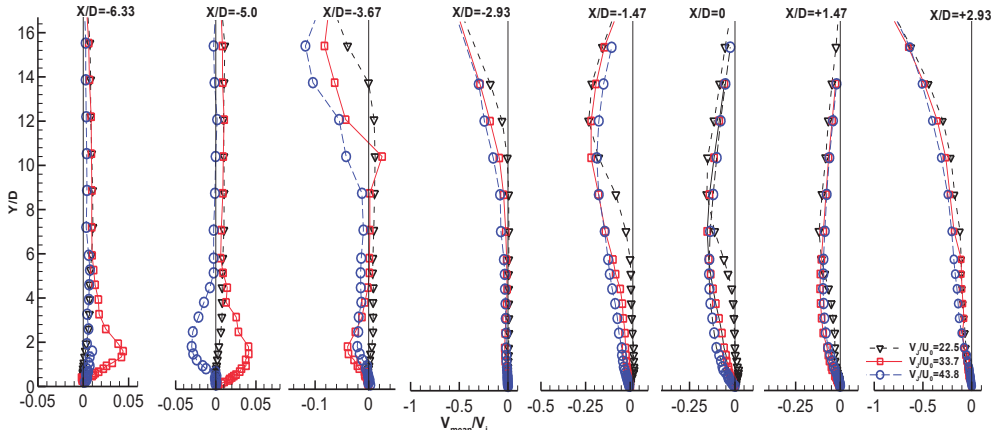

Figure 9: Vertical profiles of the mean horizontal velocity component, V_{mean}/V_j, along the longitudinal (symmetry) plane crossing the center of the twin jets. (Re_j=4.3x10^4, H/D=20.1, and S/D=6).

The first jet is clearly identified at X/D=−2.93 for all the velocity ratios, through the negative values of V_{mean} close to the top wall. For X/D=−1.47 and 0 the presence of the first jet it is also noticeable, by the negative values of the V_{mean}, which are more pronounced at $V_j/U_0 = 33.7$ and 43.8. Finally the second jet it is identified in last profile that shows values of the V_{mean} greater than those shown in the first jet. This means that there is no wall jet localized upstream of the rear jet, being the rear jet completely deflected by the crossflow.

Figures 10 (a) and (b) show horizontal profiles of the horizontal and vertical mean velocity components for all the velocity ratios studied, quantifying the flow, and confirming the above description of the flow. The results show that the centre of the first jet is moving in the crossflow direction for all the velocities ratio. For $V_j/Uo = 22.5$ the deflection angle is 21.9º, while for the higher velocity ratios, the jet deflection is smaller (14.42º for $V_j/U_0 = 33.7$ and 12.66º for $V_j/U_0 = 43.8$). The rear jet is less deflected than the first jet due to the alignment with the first jet and the corresponding wake. In this case,

the centre of the rear jet is nearly coincident with the geometrical axis of the exit, and for Vj /U_0 = 22.5 and 33.7 the deflection angle is 12.3º, while for V_j /U_0 = 43.8 is only 8.2º. The horizontal profiles of V_{mean} exhibit only positive values from the top wall (Y/D = 20.1) to the middle of the impinging height (Y/D = 10.0) for all the velocity ratios studied. This confirms the conclusions drawn from the vertical velocity profiles and discussed above. The asymmetry of the flow can be confirmed from the horizontal profiles of V_{mean} with higher peaks up to 10% of the vertical velocity in the upstream side (X/D < 3.33). Also it is also possible to ascertain that for all the velocity ratios the horizontal profiles are very similar, showing only a small difference near the centre of the jets for V_{mean}. However, based on the maximum of V_{mean} the deflection angle of the rear jet is only 4.8º approximately for all the velocity ratios. Thus, this result confirms the initial hypothesis that the alignment of the jets with the crossflow would create a special flow pattern. The wall jet resulting from the first jet flows under the rear jet, and the upstream ground vortex is only interacting with the rear jet induced flow away from the vertical plane of symmetry.

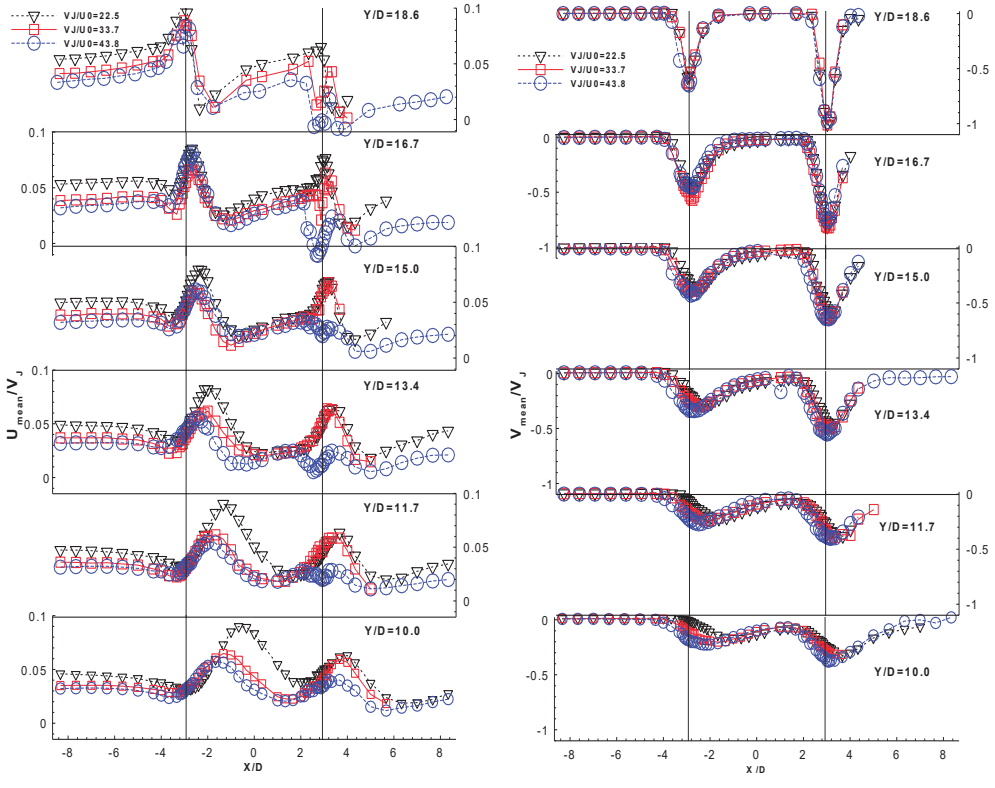

Figure 10**:** Horizontal profiles of the mean velocity characteristics along the longitudinal (symmetry) plane crossing the center of the twin jets: (a) Horizontal velocity, (b) Vertical velocity. (Re_j = 4.3x10^4, H/D = 20.1, and S/D = 6).

Figure 11 shows horizontal profiles of the rms values of the normal stresses, $\overline{u'^2}$ and $\overline{v'^2}$, and quantifies the effect of the velocity ratio. The profiles show results that are somewhat surprising at first sight, because it seems that it is not possible to identify completely the shear layer surrounding the impinging jets. The horizontal profiles of the normal stresses

show small peaks in the in the upstream side of the first jet ($X/D < 3$) for all the velocity ratios. In the downstream side of the first impinging jet others peaks are observed, mainly in the region close to $X/D = 0$ in $Y/D = 16.7$ and 15.0, which are more evident for the lower velocity ratio. For $Y/D = 13.4$ and 12.7, the peaks are practically unrecognizable for $V_j/U_o = 22.5$ and 33.7, but for the highest velocity ratio this peaks are very clear, with a maximum value of $u_{rms}/V_j^2 = 0.015$ at $Y/D = 13.4$. Downstream of the rear jet the shear layer surrounding the jet cannot be clearly identified for the lower velocity ratio. For the other velocity ratios the three profiles under the downstream jet exit of the impinging jets show some enhanced values localized downstream of the rear jet, that need further investigation.

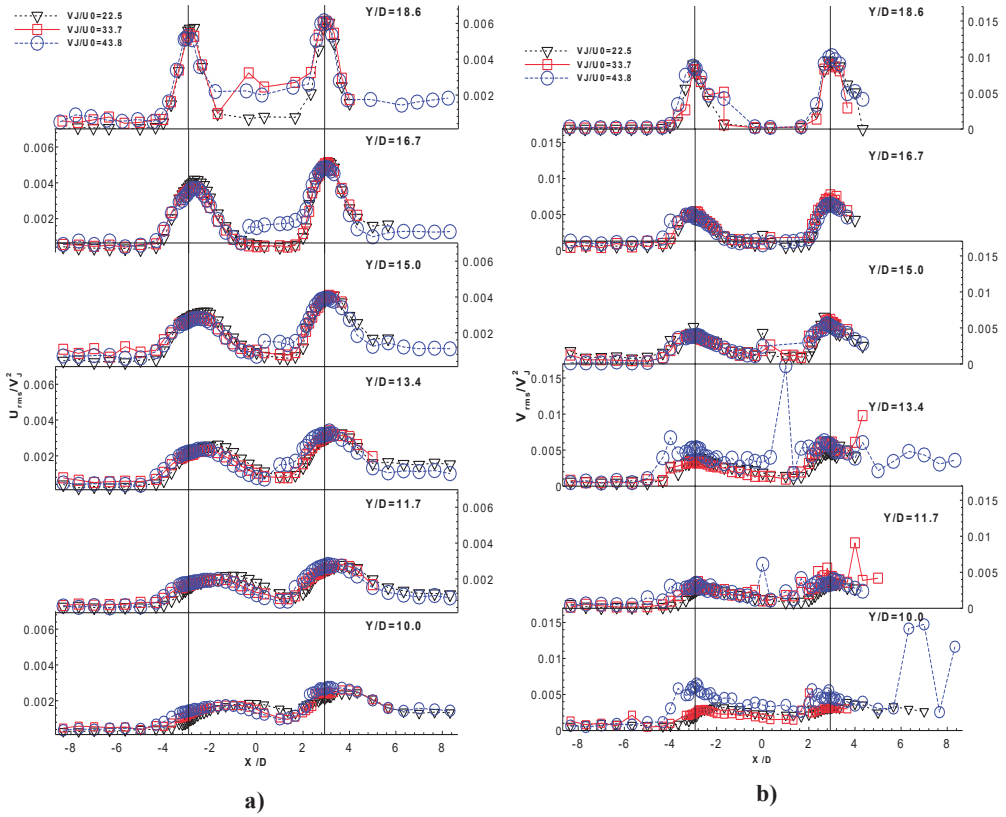

Figure 11: Horizontal profiles of the mean velocity characteristics along the longitudinal (symmetry) plane crossing the center of the twin jets: (a) Horizontal rms velocity, $\overline{u'^2}$,(b) Vertical rms velocity, $\overline{v'^2}$ ($Re_j = 4.3\text{x}10^4$, $H/D = 20.1$, and $S/D = 6$).

4 DISCUSSION

This section presents a numerical study to extend the analysis of the flow to regions and flow conditions for which no measurements have been obtained. The numerical method is based on the solution of the conservation laws for mass and momentum which is a modified version of the method described elsewhere (see Ref. [6]). Figures 12 to 14 show V_{mean} distribution along the vertical plane of symmetry (i.e. Z=0) together with calculated streamtraces. For all velocity ratios the collision of the upstream wall jet with the crossflow is clearly registered. Meanwhile, the ground vortex is also identified for all velocity ratios, but its centre change with the velocity ratio applied, because the increase

of V_j/U_0 corresponds to a decrease in U_0. Comparing this result with that obtained experimentally we can confirm that the deflection sensed by the first jet experimentally is greater than the jet deflection felt numerically. As far as the downstream jet is concerned the predictions confirmed the experimental results, and its complete deflection by the crossflow was calculated for all the velocity ratios considered with no impingement directly on the wall.

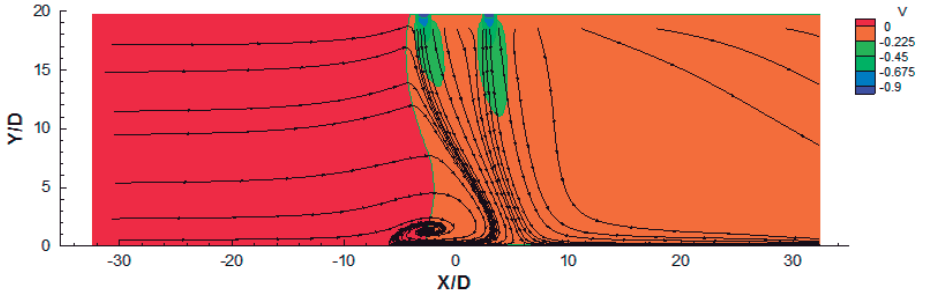

Figure 12: Calculated stream traces and mean vertical velocity component distribution along the vertical plane of symmetry (i.e. Z=0). V_j/U_0=22.5, Re_j=43,000, H/D=20.1, and L/D=6).

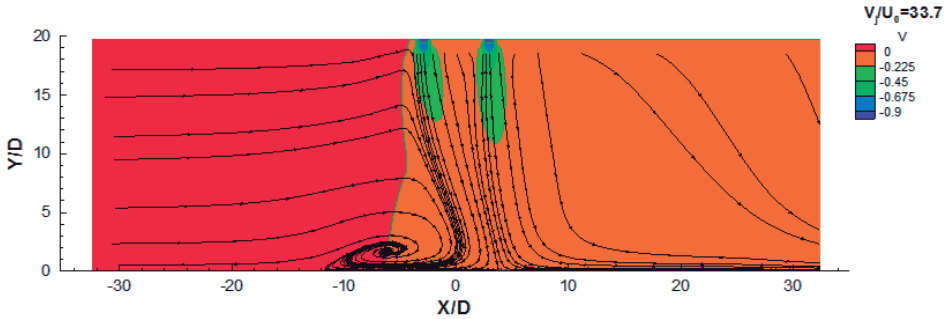

Figure 13: Calculated stream traces and mean vertical velocity component distribution along the vertical plane of symmetry (i.e. Z=0). V_j/U_0=33.7, Re_j=43,000, H/D=20.1, and L/D=6).

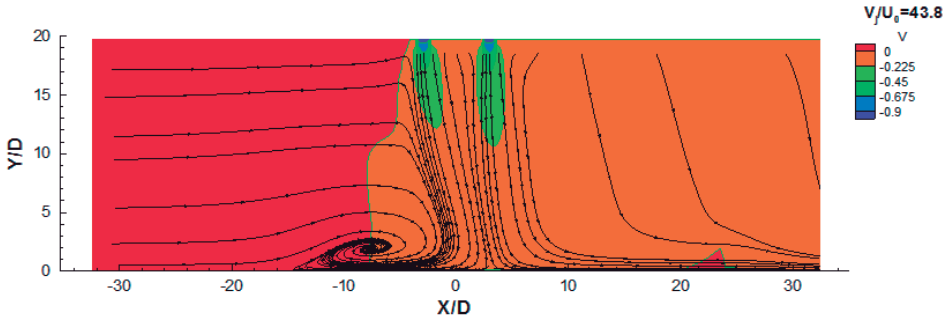

Figure 14: Calculated stream traces and mean vertical velocity component distribution along the vertical plane of symmetry (i.e. Z=0). Vj/U0=43.8, Rej=43,000, H/D=20.1, and L/D=6).

Fig. 15 shows in more detail the central zone between the two jets with white streamtraces that begin near the top wall. The results show that even for the smallest velocity ratios of V_j/U_0=7.5 and 15 the jets do not mix, but remain together in two layers. As a consequence, for V_j/U_0=15 the downstream jet does not reach directly the ground, but it impinges on the first jet wall jet is moving downstream. Here, we can identified two different flow

regimes. The first is characterized by the absence of jets impact and ground vortex formation. The second also is characterized by the absence of ground vortex formation but one of the jets impacts on the ground. This two regimes are important in transition from hover to horizontal flight, where the freestream deflects the jets flow, and the jets flow alters the freestream flow with profound effects on the lift and moments experienced by the aircraft. For the two higher velocity ratios the ground vortex is always present, but its size and location changes. It moves upstream with V_j/U_0, because increasing V_j/U_0 involves decreasing the relative influence of U_0. Here, we can identify another flow regime, being this the most important for a V/STOL aircraft operating in ground vicinity because is characterized by a strong jets impingement on the ground with a formation of a ground vortex. However the other regimes are also important.

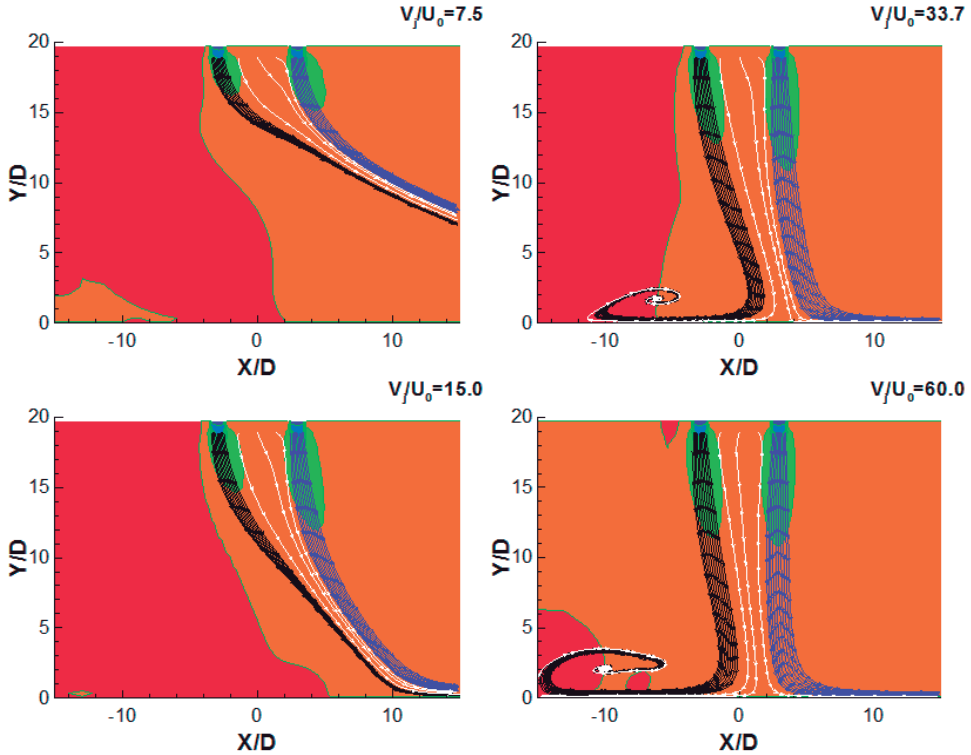

Figure 15: Details of the calculated stream traces and mean vertical velocity component distribution along the vertical plane of symmetry (i.e. Z=0). Rej=4.3x104, H/D=20.1, and L/D=6

One major issue in the present flow configuration is the possible deflection of the rear jet by the first jet without occurring impact on the ground. Another possibility, not yet demonstrated, is the impact of the second jet with the first deflected jet or its downstream wall (depending on the velocity ratio).

Any of the figure presented above it is sufficiently conclusive about these hypothesis, nor about the blending of the two structures further downstream. In order to better understand this type of flow, and in particular that happened with the rear jet and downstream of the impinging jets, a meticulous numerical study simulation was performed for V_j/U_0=22.5 by varying the velocity of the second jet, V_{j2} , from, 5.4 m/s up to 36 m/s (Figures 16-17).

The velocity of the first jet was kept constant to preserve the location of the centre of the ground vortex. Despite being varied the second jet velocity from 5.4, up to 36 m/s, it was only possible to view significant changes on the flow to $V_{j2} \leq 13.5$ m/s. Both figures show that lowering the velocity of the second jet in relation to the first jet, the wall jet of the second jet is always above the wall jet formed by the interaction of the first jet with the crossflow, heading the flow to downstream. The location of the ground vortex is practically not affected by this change in the second jet velocity, confirming that the second jet does not contribute to the occurrence of this structure

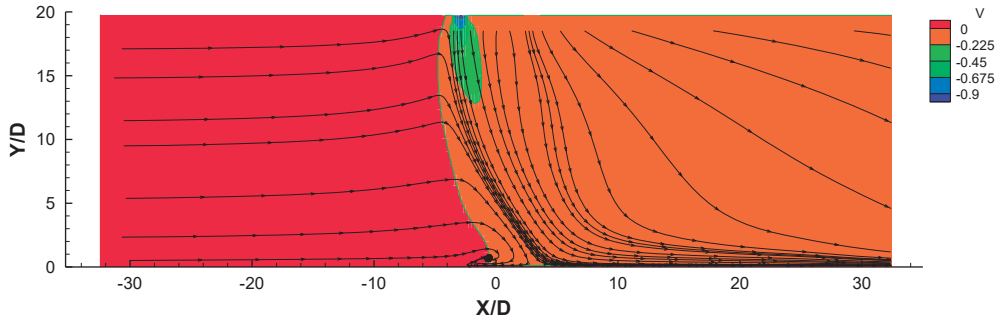

Figure 16: Calculated stream traces and mean vertical velocity component distribution along the vertical plane of symmetry, Z=0. (Re_j=43,000, H/D=20.1, L/D=6, V_{j2}= 5.4 m/s).

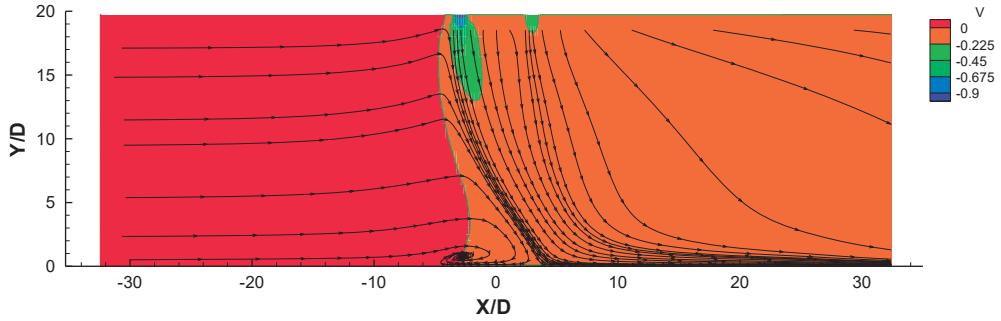

Figure 17: Calculated stream traces and mean vertical velocity component distribution along the vertical plane of symmetry, Z=0. (Re_j=43,000, H/D=20.1, L/D=6, V_{j2}= 13.5 m/s).

In order to investigate the possible existence of a kidney shape of the cross section of the jets, and their mutual interactions, isolines of the velocity component U_{mean} were obtained in vertical planes perpendicular to the crossflow for different values of X/D. Figure 16 show the results for V_{j2} = 5.4 m / s. For X/D =0, i.e. in the middle between the axis of the jets exit, the kidney shape can be clearly identified for the first jet (the second jet it is not yet visible, because its exit is further downstream). For X/D =4.9, the second jet can be identified by the dark blue area, that reveals the slight deflection of the second jet inside the wake of the first impinging jet. The kidney shape of the cross section of the first jet is still present, but it is widening rapidly due to the additional influence of the second imping jet. It should be pointed out that the impinging jet and first jet do not mix and are separated by lower values of the velocity component in the crossflow direction (light blue). Additionally, no streamtraces from the second jet are captured by the deflected upstream jet, revealing that a complete mixing between the two jets has not yet occurred. However,

from this location downstream (in the crossflow direction) the second impinging jet will suffer two opposing effects: first the fact that is developing in the wake of the first impinging jet will contribute to its less deflection, and secondly since it is impinging in a flow moving in the crossflow direction with a higher velocity it will be forced to deflect. This novel flow configuration that occurs before the first jet reaching the ground is schematically shown in Fig. 17. So, the final behaviour of the second jet can be described as the flow of a jet through a zero or small upstream crossflow, corresponding to the wake of the first jet, impinging on a horizontal jet with a kidney cross section flowing in the crossflow direction with a higher velocity. In the next downstream location, at X/D=9.8, the red area identifies a region with relatively large positive values of the velocity component U_{mean} (in the crossflow direction), which is an indication that the first jet touched the ground. The rear jet impacts on this wall jet (resulting from the first jet), and is quickly deflected, but does not reach the ground. For X/D=19.6, the entire cross section is occupied by two vortical structures rotating in opposite directions, revealing that the two parallel jets flowing in the crossflow direction finally merge.

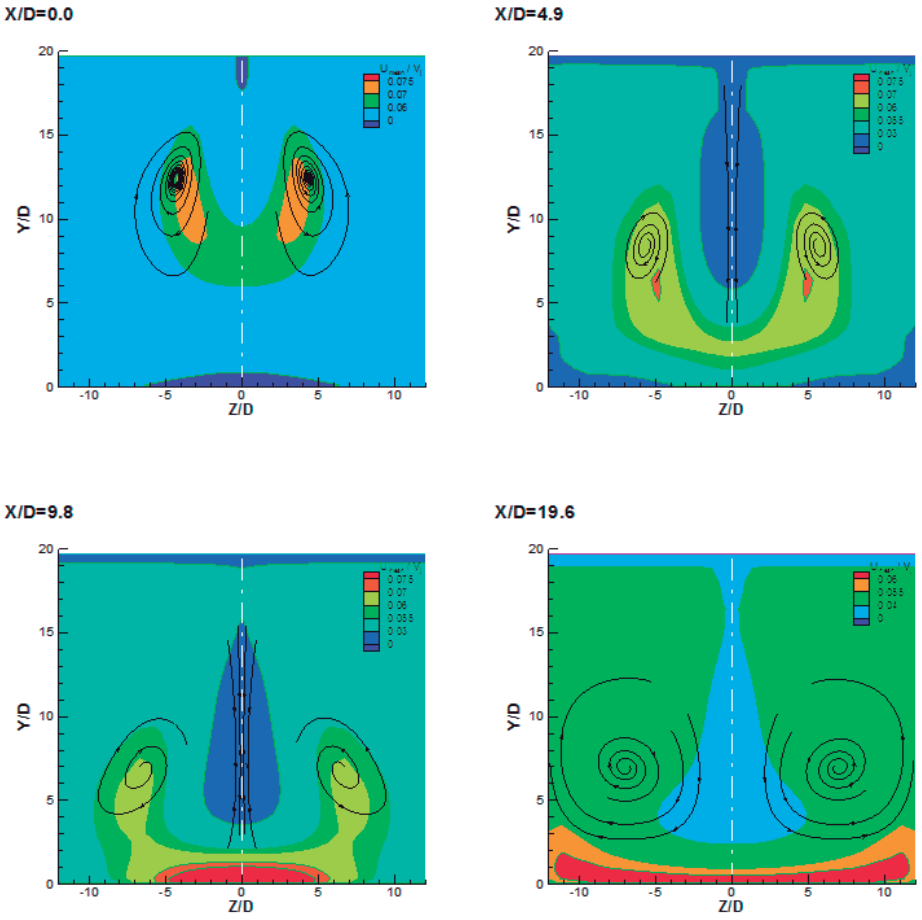

Figure 16: Mean velocity component (U_{mean}/V_{j1}) in a vertical plane perpendicular to crossflow. (Re_{j1}=43,000, V_{j2} = 5.4 m/s, Re_{j2} =5,339, H/D=20.1, L/D=6).

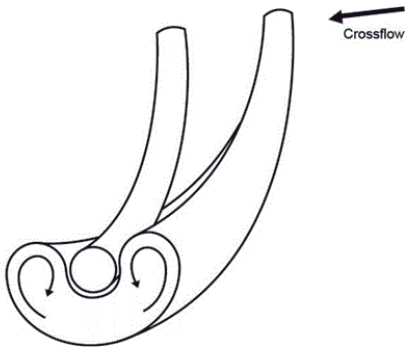

Figure 17: Illustration of the kidney shape of the cross section of the first jet before reaching the ground and the second (downstream) jet interaction.

5 CONCLUSIONS

The flow field created by ground vortex generated by twin impinging jets in tadem through a crossflow is studied in detail. Flow visualization, experimental measurements and numerical simulation are presented for two turbulent circular jets impinging on a flat surface perpendicular to the geometrical nozzle axis, through a low velocity crossflow. The experiments was carried out for a Reynolds number based on the jet exit conditions of $Re_j=4.3x10^4$ with H/D=20.1 and for VR= V_j/U_0 of 22.5, 33.7 and 43.8 and with an interject spacing of S=6D. To complete the investigation were also performed numerical simulations for velocity ratios beyond the rig experimental limits.

The results show a large penetration of the first (upstream) jet, which is deflected by the crossflow and impinges on the ground giving rise to a ground vortex due to the collision of the radial wall and the crossflow that wraps around the impinging point like a scarf. The first jet deflection and the location of the ground vortex depend on the velocity ratio used. For higher velocity ratios the deflection of the first jet is smaller and closer to the first jet is located the centre of the ground vortex. The rear jet it is not so affected by the crossflow in terms of deflection for all velocity ratios because it is protected by the upstream jet, but due to the downstream wall jet that flows radially from the impinging point the rear jet does not reach the ground. Also due to the confinement and the ground vortex, the crossflow is blocked and accelerates in the upper part and also contributes to an enhanced mixing of each secondary flow. As consequence, no upstream wall jet or ground vortex resulting from the second (downstream) jet was detected. The effect of the rear jet impinging on the downstream wall jet resulting from the first jet had not been reported so far and requires further investigation.

In case of the numerical analysis, the results show that for the two lowest velocity ratios, the jets do not mix remaining in two layers together, and therefore, it is not detected the presence of ground vortex. For highest velocities ratio the ground vortex is completely present, and it moves with the increase of V_j/U_0. Compared the experimental results with the numerical results, we can conclude that the deflection of the first jet in the numerical case is lower than that recorded for the experimental case, implying therefore a different location from the centre of the vortex ground. As far as the downstream jet is concerned the predictions confirmed the experimental results, and its complete deflection by the crossflow was calculated for all the velocity ratios considered with no impingement directly on the wall. By changing the rear jet velocity and extracting perpendicular planes to the jets flow was possible to prove that the second jet is deflected quickly, never reaching the ground, thus proving the accuracy of the experimental results, leading us to conclude that impinging jet in tandem configuration, the downstream jet is entrained by

the upstream jet and not by the crossflow itself. In the future, this issue should be further investigated in order to understand what the real consequence for the aircraft when this type of phenomenon occurs.

ACKNOWLEDGEMENTS

The assistance of Ms. Inês Carvalho with some illustrations of the flow field is gratefully acknowledged.
The present work was done in the scope of the activities of LAETA-Associated Laboratory of Energy, Transports and Aeronautics, and funded by FCT-Fundação para a Ciência e Tecnologia through contract PTDC/EME-MFE/102190/2008 and grant SFRH/BD/86434/2012

REFERENCES

[1] A. Abdel-Fattah, "Numerical and Experimental study of turbulent impinging twin-jet flow", Experimental Thermal and Fluid Science, 31(2007), pp. 1061-1072.
[2] Adler, D.; Baron, A "Prediction of a three-dimensional circular turbulent jet in crossflow" AIAA Journal, No. 17, 1979, pp.168-174
[3] Andreopoulos, J. and Rodi, W., "Experimental Investigation of Jets in a Crossflow", J. Fluid Mechanics, Vol. 138, 1984, pp. 127.
[4] Araújo, S.R.B., Durão, D.F.G., and Firmino, F.J.G., "Jets Impinging Normally and Obliquely to a Wall", AGARD CP 308, paper 5.
[5] Baker, O.J., "The Turbulent Horseshoe Vortex", J. Wind Engineering and Industrial Aerodynamics, Vol. 6, 1981, pp. 9.
[6] Barata, J.M.M., Durão, D.F.G., and McGuirk, J.J., "Numerical Study of Single Impinging Jets Through a Crossflow", Journal of Aircraft, Vol.26, No.11, 1989a, pp. 1002-1008.
[7] Barata, J.M.M., "Numerical and Experimental Study of Jets Impinging on Flat Surfaces Through a Crossflow", Ph.D. Thesis (in Portuguese), Instituto Superior Técnico, Technical Univ. of Lisbon, Lisbon, Portugal, 1989b.
[8] Barata, J.M.M., Durão, D.F.G., and McGuirk, J.J., "Numerical Study of Single Impinging Jets through a Crossflow", J. of Aircraft, Vol.26, No.11, 1989, pp.1002-1008.
[9] Barata, J.M.M., Durão, D.F.G., and McGuirk, J.J., "Impingement of single and twin turbulent jets through a cross-flow", AIAA Journal, Vol.29, No.4, 1991, pp.595-602.
[10] Barata, J.M.M., Durão, D.F.G., Heitor, M.V., and McGuirk, J.J., "On the Analysis of an Impinging Jet on Ground Effects", Experiments in Fluids, No.15, 1993, pp.117-129.
[11] Barata, J.M.M., "Ground Vortex Formation with Twin Impinging Jets". Paper SAE 962257, International Powered Lift Conference, Jupiter, Florida, 18-20 Nov., 1996.

[12] Barata, J.M.M., "Fountain Flows Produced by Multiple Impinging Jets in a Crossflow". AIAA Journal, Vol. 34, No.12, Dez. 1996, pp. 2523-2530 e AIAA Journal on Disc, Vol. 2, No.1, 1996.
[13] Barata , J.M.M., Carvalho, P.S.D., Durão, D.F.G., Neves, F.M.S.P., Silva, A.R.R., and Vieira, D.F.C., "Laser Doppler Measurements of Twin Impinging Jets Aligned With a Crossflow", July 2012, 16th Int Symp on Applications of Laser Techniques to Fluid Mechanics Lisbon, Portugal, 09-12 July, 2012.
[14] Barata, J.M.M., Neves, F.M.S.P., Vieira, D.F.C., and Silva, A.R.R., "Twin Impinging Jets Through a Crossflow", 50th AIAA Aerospace Sciences Meeting including the New Horizons Forum and Aerospace Exposition, 9-12 January 2012/ Gaylord Opryland Resort & Convention Centre, Nashville, Tennessee.
[15] Barata, J.M.M., "Twin Impinging Jets Aligned With a Crossflow". AIAA paper 2013-3600, 49th AIAA/ASME/SAE/ ASEE Joint Propulsion Conference and Exhibit, San Jose, California, 15-17 July, 2013a.
[16] Barata, J.M.M, "Multiple Jet/Wall/Cross-Wind Interaction Relevant to VSTOL Ground Effects", AIAA paper 2013-4380, 2013 International Powered Lift Conference, Los Angeles, California, August 12-14, 2013b.
[17] Behrouzi, P, McGuirk, JJ. "Experimental data for CFD validation of the intake ingestion process in STOVL aircraft, Flow Turbulence and Combustion, Vol. 64, No. 3-4, pp. 265-277, 1998.
[18] Crabb, D., Durão, D.F.G., and Whitelaw, J.H., "A Round Jet Normal to a Crossflow", J. Fluids Engng. Vol.113, 1981, pp. 142-153.
[19] Durst, F., Melling, A., and Whitelaw, J.H., "Principles and Practice of Laser-Doppler Anemometry", 2nd ed., New York, Academic Press.
[20] Fan, Jing-yu, Wang Dao-zeng, Zhang Yan, "Large-Scale vortical structures produced by an impinging density jet in shallow crossflow", Applied Mathematics and Mechanics, 2006, 27(3) 363-369.
[21] Fan, Jing-yu, Zhang Yan, Wang Dao-zeng, "Large Eddy simulation of three dimensional vortical structures for an impinging transverse jet in the near region", Journal of Hydrodynamics, 2007, 19(3):314-321
[22] Gilbert, B.L., "Detailed Turbulence Measurements in a Two Opposing Plane Turbulent Wall Jets", AIAA 16th Fluid and Plasma Dynamics Conf., AIAA Paper 83-1678, Danvers, MA, Jul. 12-14, 1983.
[23] Jones, W. P. and McGuirk, J. J. "Computation of a round turbulent jet discharging into a confined crossflow", In: "Turbulent Shear Flows-2",~ Bradbury et al., Springer Verlag, 1980, pp.223-245
[24] Kamotani, Y., and Greber, I., "Experiments on Confined Turbulent Jets in a Crossflow", NASA CR-2392, 1974.
[25] Kate, R. P., P. K. Das, Suman Chakraborty, "An experimental investigation on the interaction of hydraulic jumps formed by two normal impinging circular liquid jets", Journal of Fluid Mechanical, (2007), vol. 590, pp. 355-380.
[26] Knowles, K., and Bray, D., "The Ground Vortex Formed by Impinging Jets in Crossflow", AIAA 29th Aerospace Sciences Metting, AIAA Paper 91-0768, Reno, NV, Jan. 7-10, 1991.
[27] Knowles, K., "Computational Studies of impinging jets using k-ε Turbulence Models", International Journal for Numerical Methods in Fluids, 1996, Vol. 22, pp. 799-810.

[28] Kolár, V., H. Takao, T. Todoroki, E. Savory, S. Okamoto, N. Toy, "Vorticity transport within twin jets in crossflow", Experimental Thermal and Fluid Science, No. 27 (2003), pp. 563-571
[29] Kolár, V., E. Savory, "Dominant flow features of twin jets and plumes in crossflow", Journal of wind Engineering and Industrial Aerodynamics, 95(2007), pp. 199-1215.
[30] Kuhn R., Margason R., Curtis P., Jet Induced Effects: The Aerodynamics of jet and Fan Powered V/STOL Aircraft in Hover and Transition, AIAA book, Volume 217.
[31] Nishino, K., Samada, M., Kasuya, K., et al., "Turbulence statistics in the stagnation region of na axisymmetric impinging jet flow, International Journal of Heat and Fluid, vol.17, No.3, 193-201, 1996.
[32] Patankar, S. V., Basu, D. K. and Alpay, S. A "Prediction of the three-dimensional velocity field of a deflected jet" J. Fluids Engng., Vol. 99, 1979, pp. 758-762.
[33] Saddington, AJ, Cabrita, PM, Knowles, K, "Large-scale instabilities in a STOVL upwash fountain", 6th International Symposium on Engineering Turbulence Moddelling and Measurements, Cagliari, Italy, May 23-25, 2005.
[34] Saripalli, K.R., "Visualization of Multijet Impingement Flow", AIAA Journal, Vol. 21, 1983, pp. 483-484.
[35] Sarippali, K.R., "Laser Doppler Velocimeter Measuremnts in 3D Impinging Twin-Jet Fountain Flows", Turbulent Shear Flows, Vol.5, edited by Durst et al., Springer-Verlag, Berlin, 1987, pp. 147-168.
[36] Vieira, D.F.C., Silva, A.R.R., Carvalho, P.S.D., Neves, F.M.S.P. and Barata, J.M.M. " Numerical and Experimental Study of Two Impinging Jets in a Row through a Crossflow", AIAA Paper 2013-0806, 51th AIAA Aerospace Science Meeting Including the New Horizons Forum and Aerospace Exposition, Grapevine (Dallas/Ft. Worth Region), Texas, 7-10 Jan., 2013.
[37] Vieira, D.F.C, Durão, D.F.G., Neves, F.M.S.P., Silva, A.R.R., Barata J.M.M., and., "Laser Doppler Measurements of Twin Impinging Jets in Tadem through a Crossflow", July 2014, 17th Int Symp on Applications of Laser Techniques to Fluid Mechanics Lisbon, Portugal, 07-10 July, 2014.
[38] Worth, N., Yang, Z., "Simulation of an impinging jet in a crossflow using a Reynolds stress transport model", International Journal for Numerical Methods, 52(2006), pp. 199-211.
[39] Yang, Zhiying, "Assessment of unsteady-RANS approach against steady-RANS approach for predicting twin impinging jets in a crossflow, Congent Engineering (2014), 1:936995
[40] Yanta, W.J. and Smith, R.A., "Measurements of Turbulent Transport Properties with a Laser-Doppler Velocimeter", 11th Aerospace Sciences Meeting, AIAA Paper 73-0169, Washington, 1978.Numbered according to order of appearance in the main text.

CEM 2016 – Mechanical Engineering Conference
Porto, Portugal, 1-3 June 2016
LAETA - Associated Laboratory for Energy, Transports and Aeronautics

NOZZLE IMPINGEMENT HEIGHT INFLUENCE ON THE TWIN IMPINGEMENT JETS IN TANDEM THROUGH A CROSSFLOW

Vieira, Diana[1]; Barata, Jorge[2]; Silva, André[3]

[1] University of Beira Interior, Department of Aerospace Science, Portugal, dianavieir@gmail.com
[2] University of Beira Interior, Department of Aerospace Science, Portugal, jbarata@ubi.pt
[3] University of Beira Interior, Department of Aerospace Science, Portugal, andre@ubi.pt

KEYWORDS: *Impinging Jets, Computational Fluid Dynamics, Impingement height*

ABSTRACT: The complex flow field generated by the impact of twin impinging jets in tandem through a low velocity crossflow was numerically studied. The Reynolds number based on the jet exit conditions was 43,000, the jet-to-crossflow velocity ratio from 7.5 to 90, and an interject spacing of 6 diameters of the jet. The impingement heights used were 3 to 15. The mathematical model used is based on the solution of the continuity and momentum equations. A RANS formulation was adopted with the *"k-ε"* turbulent model to represent the turbulent stresses. The numerical results showed the influence of the impingement height on the ground vortex location, size and interaction with the surrounding flow, but new aspects of this type of flows were found for the present case of a tandem configuration. In the region between the jets the usual fountain upwash flow does not occur, but a second small ground vortex was detected for H/D≤10, due to the interaction between the wall jets of each impinging jet. To our knowledge this is a new phenomenon that is being reported in the literature for the very first time.

1 INTRODUCTION

Turbulent jets impinging on flat surfaces through a low velocity crossflow are typical of the flow beneath of VSTOL aircrafts. During its operation there are different stages during the flight, with its own flow characteristics and with different kind of problems associated: the hover phase, the transition to forward flight phase and the forward flight operation. The hover phase is the most complex phase during the flight and can be further divided into two more phases because the flowfield associated in each phase are completely different. So, the hover phase can be subdivided into out-of-ground-operation and hover in the vicinity of the ground. During its landing or near ground hovering phase, the VSTOL aircraft creates a complex three dimensional flow field between the jet streams, the airframe surface and the ground. When ground effect occurs, the lift forces on the aircraft changes, cause hot gas re-ingestion into the engine intake and due to the fountain upwash and ground flows, the fuselage skin temperature rises. The unsteadiness of the flow and raise of the temperature cause several problems in the engine performance, such as, compressor surge or even stall and thrust reduction. In respect to the intake ingestion phenomenon, it is very complex and can be associated with the design and operational parameters, such as, jet configuration, head wind velocity, jet impingement height or intake configuration. In the case of the hot gas ingestion problem, there are three mechanism involved, i.e., far field

ingestion, near field ingestion and ground vortex ingestion. During a landing or hover the impingement of each downward-directed jet on the ground results in the formation of a wall jet which flows radially from the impinging point along the ground surface. The interaction of this wall jet with the free stream results in the formation of a ground vortex far upstream of the impinging jet. This flow field transports exhaust gases away from the ground and up toward the intake region. The level and intensity of the ingestion resulting from this mechanism depends critically on the forward velocity. If there are two or more adjacent jets, the resulting wall jets meet, and a fan-shaped upwash, or "fountain", is normally formed between the jets (Fig. 1).

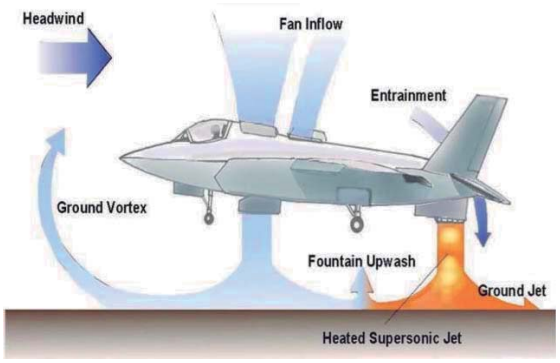

Figure 1. STOVL aircraft ground effect aerodynamics.

The fountain upwash flow depending on its strength and direction affects the forces and moments induced in the aircraft when operating in ground effect. The resulting ground vortex shape is strongly affected and the corresponding induced suckdown effect tends to be reduced by the upload produced by the fountain. The improvements of the knowledge are ever required because the aircraft design has been changed since its first design, and some problems still persists. In this case when the aircraft operates with small forward movement the configuration of interest are two impinging jets with the direction of the crossflow perpendicular to the line containing their centres For the next generation of VSTOL aircrafts F-35 no relevant studies can be found, because the impinging jets are aligned with the crossflow and this geometry has not yet been considered. This paper aims to present a detailed analysis of the complex flow field beneath two impinging jets in tandem through a low velocity crossflow for different impingement heights relevant to the future F-35 VSTOL configuration (Fig. 1). This is also a continuation of the numerical and experimental studies done early on side-by-side impinging jets or tandem impinging jets (Barata, 2013 and Vieira et al., 2015). Here, the main focus is to study how the impingement height affects the flowfield behaviour and to find out if a fountain upwash flow is formed, which could not be observed for the previous experimental and numerical studies for an higher impingement height of H/D=20.1.

Experiments on the aerodynamics of jets through a crossflow have mostly been reported for large impingement heights and for low velocity ratios between the jet and the crossflow V_j/U_0. Therefore these works have only peripheral relevance to the VSTOL F-35 ground effect problem. Until the early 80's most of the computational work published on jets with crossflow had been based on integral methods admitting simplified assumptions, which are only capable of predicting global effects such as trajectories and jet cross-section shapes. Only Adler and Baron (1979), Patankar *et al*. (1977), and Jones and McGuirk (1980) employed computational finite-difference numerical procedures together with a two-equation turbulence model to predict a single jet in an unconfined crossflow, and obtained some agreement with the experiments of other authors. In the late 80's and 90's new developments emerged fostered by the need of improving the Harrier / AV-8B and several research took place especially funded by the UK and US. Barata (2013) presents a comprehensive bibliographic review of that era and also introduces the new age (of the JSF-Joint Strike Fighter) and the relevant investigation including the aspects of the fountain upwash flows that emerge from multi-jet impingement.

In the present paper special attention is devoted to the flow between each impinging jet, which normally would give rise to an upwash flow and to the details of the present in tandem configuration. Previous detailed measurements of the flow properties for fountain upwash flow are scarce and have been presented essentially in the absence of a crossflow. The most relevant works have been reviewed by Barata *et al.* (1989a) and Saripalli (1983), showing high turbulence levels and spreading rates in the fountains (e.g. Gilbert (1983) and Nishino *et al*. (1996)). Barata (1996a) and Barata (1996b) extended their study to multi jet impinging configurations producing upwash fountain flows (Fig.2) which are the heart of the complex effects produced by VSTOL aircraft when they operate in ground proximity, but as far as twin jets are concerned only the geometry with the jets side by side was considered.

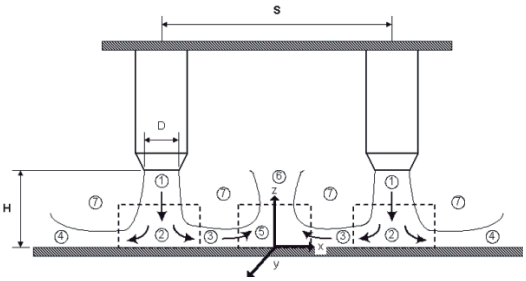

Figure 2. Schematic of the upwash fountain flow by two impinging jets: 1. Free jet, 2. Jet impingement region, 3. Inner wall jet region, 4. Outer wall jet region, 5. Fountain formation region, 6. Fountain upwash flow, 7. Entrainment. Saddington (2005)

2 METHODOLOGY

2.1 Mathematical Model

This section presents a numerical analysis based on the experimental data presented by Barata *et al.* (2014) and Vieira *et al.* (2015). The mathematical model used in the numerical simulation is based on the solution of the continuity and momentum equations. A Reynolds-Averaged Navier Stokes (RANS) formulation was adopted with the "*k-ε*" turbulence model described by Launder and Spalding (1974), to represent the turbulent stresses. The governing equations used are described in detail by Vieira *et al.* (2015).

2.2 Boundary conditions

The computational domain has six boundaries where dependent values are specified (Fig. 3). At the inlet boundary uniform profiles of all dependent variables are specified from the experimental conditions. At the outflow boundary the gradients of the dependent variables in the axial direction are set to zero. On the symmetry plane the normal velocity disappears and the normal derivate of the other variables are zero. Ate the solid walls the wall function method used by Launder and Spalding (1974) is used to prescribe the boundary conditions for the velocity and turbulence quantities. At the jet exit boundary the mass flow rates and the momentum are the same than those in the experimental study. The computational domain corresponds to the experimental conditions that are detailed by Barata (2013) and Barata *et al.* (2014).

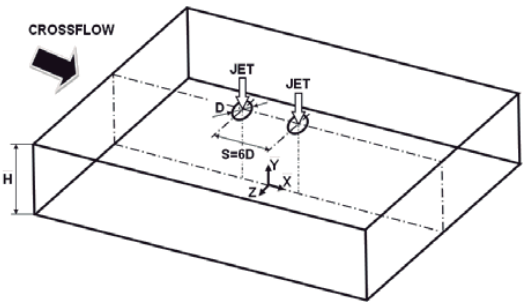

Figure 3. Computational domain.

3 RESULTS AND DISCUSSION

The numerical predictions presented in this section are compared with experimental and numerical results of Vieira *et al.* (2015) and Barata (2013) obtained at the central plane of symmetry for two impingement jets of 15 mm jet exit diameter and 20.1 jet diameters above the ground. The Reynolds number is Re_j= 43,000 for a jet exit mean velocity of V_j =36 m/s and a crossflow velocity 0.4 m/s $\leq U_0 \leq$ 4.8 m/s, corresponding a range of velocity ratios

between 7.5 and 90. The present numerical results were obtained for 4 different impingement heights of H/D=3, 5, 10, and 15, all of them lower than the one used in the numerical and experimental studies of Vieira *et al.* (2015). The results were predicted using the QUICK scheme to evaluate the convection terms of the transport equations and a grid of 26x71x26 nodes. The grid spacing was non uniform in order to concentrate the nodes, due to its refinement in area of greater interest for the study, i.e., near the jets and close to the impingement region where the gradients are steepest. The results discussed here are a small sample of a more complete set obtained for seven different velocity ratios (V_j/U_0= 7.5, 15, 22.5, 33.7, 43.8, 60 and 90) and for four different impingement heights. The flowfield results obtained for H/D= 15 were found similar to those obtained by Vieira *et al.* (2015) for H/D=20.1. However, significant changes on the flowfield behaviour were registered for H/D<10. To illustrate and discuss this changes in the flowfield two different cases for H/D=5 with V_j/U_0= 15 and 60 were chosen.

Fig. 4 shows the mean vertical velocity component in the vertical plane of symmetry (Z=0) for V_j/U_0= 15 and H/D=5. The streamtraces show the formation of a ground vortex, both downstream of the first impinging jet and the region between the two impinging jets. The first (upstream) jet impinges on the ground with a considerably high strength and almost no deflection can be observed. This is a different result from what was observed before for higher impinging heights (e.g. H/D=20.1) with the two impinging jets remaining together in two layers and flowing downstream, as a result of the impingement of the second jet on the wall jet of the first jet. A small recirculation in the region between the two impingement jets is also registered which has not yet reported before in the permanent literature. The interaction of the impinging jets with the ground results in the formation of a wall jet, that can be described as a deflected flow turning into a high-speed flow parallel to the ground plane (inner wall jet region and

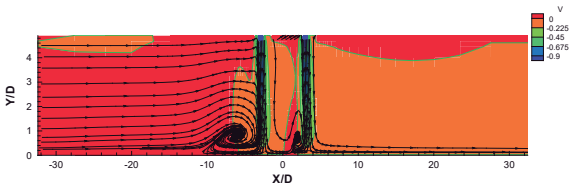

Figure 4. Predicted mean vertical velocity component distribution along the vertical plane of symmetry (i.e. Z=0) for V_j/U_0=15, Re_j=43,000, H/D=5, and L/D=6.

outer wall jet region). In the collision of the encountering inner wall jets, one from each jet, the inner wall jet from the first jet is captured by the inner wall jet of the second jet, resulting in the formation of a recirculation similar to a ground vortex, but with no direct influence of the crossflow. For the present impingement height and velocity ratio combinations no fountain flow can be observed.

Part of the crossflow fluid is not entrained by the scarf vortex, and is deflected upwards passing over it and going around the impingement jets through the region between them. At X/D=4.9 it goes down, due to the interaction with the second jet flow. Then, for X/D≈12 it reaches the minimum height, rising again and flowing downstream. This particular part of the flow is associated with the negative pressure regions as shown in figure 5. In the region between the jets, when the first jet touches the ground the inner wall jet flows and rises up like an upwash flow, but it is captured by the second jet inner wall jet, and a little clockwise ground vortex is formed close to the second jet (fig. 6 and 7).

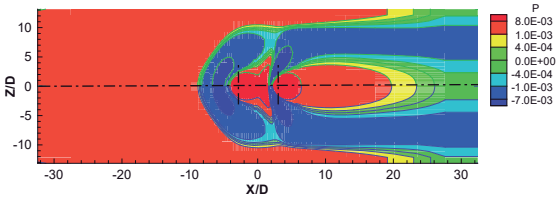

Figure 5. Pressure distribution along the field close to the ground (i.e. Y≈0) for V_j/U_0=15, H/D=5, and L/D=6 (values nondimensionalized by $\mathbf{1/2\rho V_{j1}^2}$).

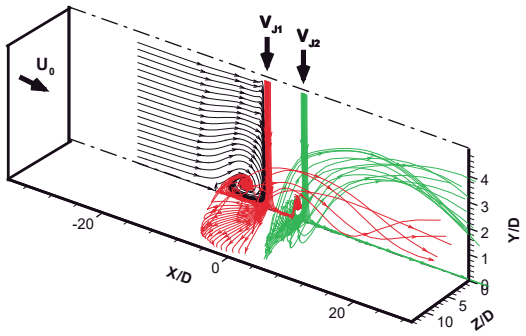

Figure 6. Tridimensional illustration of the jets flow for Re_j=43,000, V_j/U_0= 15, H/D=5 and L/D=6.

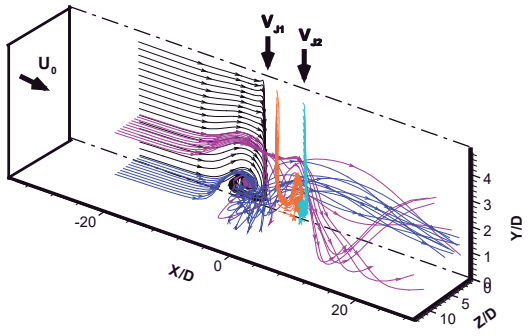

Figure 9. Tridimensional illustration of the jets flow for Rej=43,000, V_j/U_0= 60, H/D=5 and L/D=6.

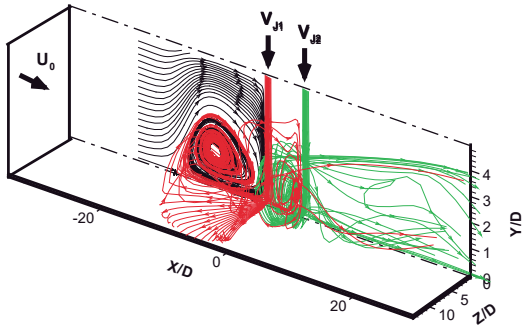

Figure 7. Tridimensional illustration of the jets and scarf vortex flow for Rej=43,000, V_j/U_0=15, H/D=5 and L/D=6.

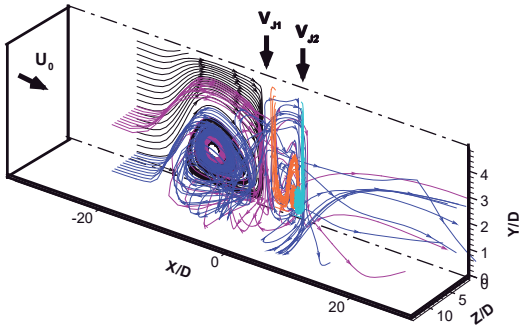

Figure 10. Tridimensional illustration of the jets and scarf vortex flow for Rej=43,000, V_j/U_0=60, H/D=5 and L/D=6.

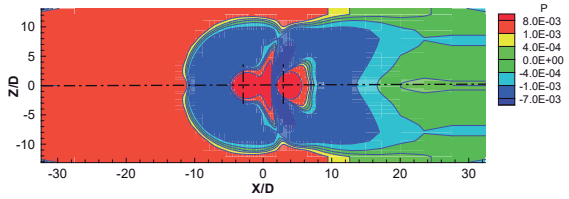

Figure 8. Pressure distribution along the field close to the ground (i.e. Y≈0) for V_j/U_0=60, H/D=5, and L/D=6 (values nondimensionalized by $1/2\rho V_{j1}^2$).

For V_j/U_0= 60 the flow pattern is apparently similar (figs. 9 and 10), but the relatively weaker influence of the crossflow allows the transversal (Z) component of the velocity (W) to assume a more important role as far the wall jets are concerned. So, the negative pressure regions in the ground plane are much wider when the velocity ratio between the jet and crossflow increases from 15 to 60 (fig. 13). The direct relation between the surface underpressure (blue zone) and the ground vortex is now almost imperceptible for this velocity ratio. The negative pressure zone is now much wider and is concentrated near the impinging zones, and they do not continue to the downstream exit of the control volume at X/D=24 as for the case of V_j/U_0=15. Additionally, it should be noticed that the height of the upstream ground vortex increased from 1D to 2.5D, occupying almost 50% of the impingement height (H=5D). Also the maximum penetration point (Barata and Durão, 2005) moved further upstream from X/D=-10 for V_j/U_0=15 to X/D=-17 for V_j/U_0=60.

4 CONCLUSIONS

The numerical simulation of the effect of the impinging distance and jet-to-crossflow velocity ratio was successfully made for twin

impinging jets in tandem through a low velocity crossflow.

Special attention was devoted to the flow between each impinging jet, which normally would give rise to an upwash flow and to the details of the present in tandem configuration.

With this numerical analysis it was possible to extend the results for velocity ratios and impingement heights beyond the limits of the experimental conditions enabling the better understanding of the flow.

To illustrate and discuss the particular aspects of the present flow for short jet impingement and tandem configuration two different cases for H/D=5 with Vj/U_0= 15 and 60 were chosen.

The present paper shows that the deflection of the first (upstream) jet almost disappears when the impingement height decreases from H/D=15 to 5.

A small recirculation in the region between the two impinging jets in tandem was detected which has not yet reported before in the permanent literature.

For the present impingement height and velocity ratio combinations no fountain flow can be observed.

This zone around the ground vortexes is associated with the negative pressure regions.

The height of the upstream ground vortex increases considerably (from 1D to 2.5D) when the impingement height H is reduced from 15 to 5D. For H/D=5, the maximum penetration point moves further upstream from X/D=-10 for V_j/U_0=15 to X/D=-17 for V_j/U_0=60.

5 AKNOWLEDGEMENTS

The present work was done in the scope of the activities of LAETA-Associated Laboratory of Energy, Transports and Aeronautics, and funded by FCT-Fundação para a Ciência e Tecnologia through grant SFRH/BD/86434/ 2012.

6 REFERENCES

Adler, D., Baron, A. Prediction of a three-dimensional circular turbulent jet in crossflow. *AIAA Journal,* (1979); 17: 168-174.

Barata J.M.M., Durão D.F.G., McGuirk J.J. Numerical Study of Single Impinging Jets through a Crossflow. *Journal of Aircraft.* (1989); 26(11): 1002-1008.

Barata J.M.M. Ground Vortex Formation With Twin Impinging Jets. *Proceedings of the International Powered Lift* Conference. Jupiter, FL, 18-20 November. 1996a. SAE Paper 962257.

Barata J.M.M. Fountain Flows Produced by Multiple Impinging Jets in a Crossflow. *AIAA Journal*. (1996b); 34(12): 2523-2530 and *AIAA Journal on Disc*, **2(1).**

Barata J.M.M. Multiple Jet/Wall/Cross-Wind Inter-action Relevant to VSTOL Ground Effects. *Proceedings of the International Powered Lift Conference*, Los Angeles, California, August 12-14 2013. AIAA paper 2013-4380. (2013).

Barata J.M.M., Carvalho P.S.D., Durão D.F.G., Neves F.M.S.P., Silva A.R.R., Vieira D.F.C. Laser Doppler Measurements of Twin Impinging Jets Aligned With a Crossflow. *Journal of Physical Science and Application*. (2014); 4 (7): 403-411.

Gilbert B.L. Detailed Turbulence Measurements in a Two Opposing Plane Turbulent Wall Jets. Proceedings of the 16th AIAA Fluid and Plasma Dynamics Conference, Danvers, MA, Jul. 12-14 1983; AIAA Paper 83-1678.

Jones W. P., McGuirk J. J. Computation of a round turbulent jet discharging into a confined crossflow. In: *"Turbulent Shear Flows-2", Ed.* Bradbury et al., Springer Verlag. 1980; 223-245.

Launder B. E., Spalding D. B. The Numerical Computation of Turbulent Flows. Computer Methods in Applied Mechanics and Engineering. 1974; 3: 269-289.

Nishino K., Samada M., Kasuya, K., Torri K. Turbulence statistics in the stagnation region of an axisymmetric impinging jet flow. *International Journal of Heat and Fluid*. 1996; 17(3): 193-201.

Patankar S. V., Basu D. K., Alpay S. A. Prediction of the Tree-Dimensional Velocity Field of a Deflected Turbulent Jet. *Journal of Fluids Engineering*. 1977; 99(4): 758-762.

Saripalli K. R. Visualization of Multijet Impingement Flow. *AIAA Journal*. 1983; 21: 483-484.

Vieira D. F. C., Barata J. M. M, Neves F. M. S. P, Silva S. R. R. Numerical Simulation of Twin Impinging Jets in Tandem Through a Crossflow. Journal of Engineering and Applied Sciences. 2015; 10 (6): 123-136.

Annex 3

Papers accepted to Conferences

Aerodynamics of a Powered Lift F35-B Aircraft in Ground Effect

Barata, J.M.M.[1*], Cerdeira, A.T.S.[1], Durão, D.F.G.[2], Neves, F.M.S.P.[1], Silva, A.R. R.[1], Vieira, D.F.C.[1]
1: Aerospace Science Department, Universidade da Beira Interior, Covilhã, 6201-001, Portugal
2: Universidade Lusíada, Lisboa, 1349-001, Portugal
* Correspondent author: jbarata@ubi.pt

Keywords: Impinging Jets, Ground Vortex, Fountain Upwash Flow

ABSTRACT

The complex flow field generated by the impact of twin impinging jets in tandem through a low velocity crossflow was experimental and numerically studied to represent aerodynamically the powered lift of the F35-B aircraft when it operate with ground effect. A wind-tunnel investigation has been conducted in the AeroG V/STOL tunnel with a vectored-thrust F35-B fighter configuration to the pressure measurement on the body and on the wing in the transition-speed range The Reynolds number based on the jet exit conditions was 43,000, the jet-to-crossflow velocity ratio from 15 to 33.7, and an inter-jet spacing of S=6Dmean, where Dmean = $(D_1+D_2)/2$. The impingement height used was 3 diameters. The mathematical model used is based on the solution of the continuity and momentum equations. A RANS formulation was adopted with the "k-ε" turbulent model to represent the turbulent stresses. The experimental results were used to make a more complete analysis of the flow field using a computational method, and revealed that the deflection of the rear jet is due to the competing influences the wake, the shear layer, the downstream wall jet of the first jet and the crossflow. The numerical results showed the influence of the impingement height on the ground vortex location, size and interaction with the surrounding flow, but new aspects of this type of flows were found for the present case of a tandem configuration. In the region between the jets the usual fountain upwash flow does not occur, but a second small ground vortex was detected, due to the interaction between the wall jets of each impinging jet. To our knowledge this is a new phenomenon that is being reported in the literature for the very first time. These studies have shown a complex flow field with regions of strong curvature and vigorous velocity variations that may be associated with important negative pressures which are of major importance for a V/STOL aircraft in ground vicinity.

1. Introduction

Turbulent jets impinging on flat surfaces through a low velocity crossflow are typical of the flow beneath of VSTOL aircrafts. When a VSTOL aircraft operates there are three different stages during the flight, being all different, with its own flow characteristics and with different kind of problems associated. A VSTOL flight comprises the hover phase, the transition to forward flight phase and the forward flight operation. The hover phase is the most complex phase during the flight and can be further divided into two more phases because the flowfield associated in each

phase are completely different. So, the hover phase can be subdivided into out-of-ground-operation and hover in the vicinity of the ground. During its landing or near ground hovering phase, the VSTOL aircraft creates a complex three dimensional flow field between the jet streams, the airframe surface and the ground. When ground effect occurs, the lift forces on the aircraft changes, cause hot gas re-ingestion into the engine intake and due to the fountain upwash and ground flows, the fuselage skin temperature rises. The unsteadiness of the flow and raise of the temperature cause several problems in the engine performance, such as, compressor surge or even stall and thrust reduction. In respect to the intake ingestion phenomenon, it is very complex and can be associated with the design and operational parameters, such as, jet configuration, head wind velocity, jet impingement height or intake configuration. In the case of the hot gas ingestion problem, there are three mechanism involved, i.e., far field ingestion, near field ingestion and ground vortex ingestion. The first mechanism is results of the forward away initially movement of the ground sheet wall jet due to the aircraft movement. This happened because the hot gases after some distance lose its momentum, rising and separating from the ground. The portion of the hot gases that separating from the ground, mixes with the surrounding air and backs again to the intake. The second mechanism, near field ingestion, has a much greater impact on hot gas ingestion compared to the first, because it directly affected the lift nozzle exits into the surrounding area of the intake, being that when exits multiple impinging jets, its impact on the ground plane create a fan shape up wash fountain beneath the aircraft. When the fountain impinges on the underside of the fuselage, flowing from the fuselage to the intake, the engine may sucks the flow to the intake, creating severe temperature distortion to the intake, since, these gases are much hotter than those from the far field ingestion. The latter mechanism is due to the presence of a ground vortex. During a landing or hover the impingement of each downward-directed jet on the ground results in the formation of a wall jet which flows radially from the impinging point along the ground surface. The interaction of this wall jet with the free stream results in the formation of a ground vortex far upstream of the impinging jet. This flow field transports exhaust gases away from the ground and up toward the intake region. The level and intensity of the ingestion resulting from this mechanism depends critically on the forward velocity. If there are two or more adjacent jets, the resulting wall jets meet, and a fan-shaped upwash, or “fountain”, is normally formed between the jets. The fountain upwash flow depending on its strength and direction affects the forces and moments induced in the aircraft when operating in ground effect. The resulting ground vortex shape is strongly affected and the corresponding induced suckdown effect tends to be reduced by the upload produced by the fountain.

The improvements of the knowledge are ever required because the aircraft design has been

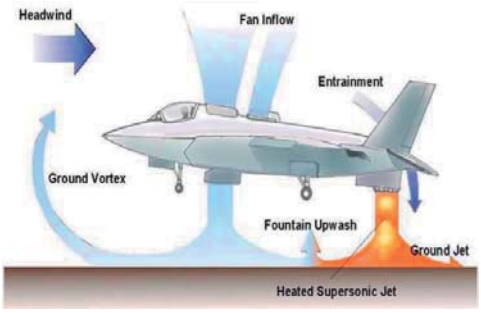

Fig. 1: STOVL aircraft ground effect aerodynamics

changed since its first design, and some problems still persists. One of them is the negative pressure coefficient region on the lower surface of the wing and on the bottom of the fuselage induced by the vectored-thrust jet. The region is larger and the pressure coefficients are more negative for the front vectored-thrust nozzles than for the rear vectored-thrust nozzles. The jet exhaust also induces a region of negative pressure coefficients on the bottom of the fuselage. The induced pressure effects are larger at the larger velocity ratios and at the location nearest to the jet. For the next generation of VSTOL aircrafts F-35 no relevant studies can be found, because the impinging jets are aligned with the crossflow and this geometry has not yet been considered.

This paper aims to present an experimental and numerical work of the pressure measurement on the body and on the wing of the vectored-thrust F35-B fighter configuration in the transition-speed range. The numerical work is also extended to a detailed analysis of the three dimensional flowfield for different velocity ratios. Both experimental and numerical are continuation of the numerical and experimental studies done early on side-by-side impinging jets or tandem impinging jets (Barata (2013) and Vieira et al. (2015)).

Experiments on the aerodynamics of jets through a crossflow have mostly been reported for large impingement heights, for low velocity ratios between the jet and the crossflow V_j/U_0 and the focus of the most studies are the velocity distribution on the flow field. In this Therefore these works have only peripheral relevance to the VSTOL F-35 ground effect problem, being the pressure distribution an important parameter to analyse this phenomenon. Until the early 80's most of the computational work published on jets with crossflow had been based on integral methods admitting simplified assumptions, which are only capable of predicting global effects such as trajectories and jet cross-section shapes. In the late 80's and 90's new developments emerged fostered by the need of improving the Harrier / AV-8B and several research took place especially funded by the UK and US. Barata (2013) presents a comprehensive bibliographic review of that era and also introduces the new age (of the JSF-Joint Strike Fighter) and the

relevant investigation including the aspects of the fountain upwash flows that emerge from multi-jet impingement.

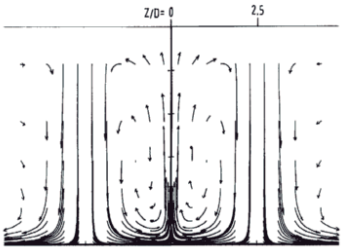

Fig. 2: Fountain upwash flow formation in the middle of the impingement jets

In the present paper part of the attention is devoted to the flow between each impinging jet, which normally would give rise to an upwash flow and to the details of the present in tandem configuration. Previous detailed measurements of the flow properties for fountain upwash flow are scarce and have been presented essentially in the absence of a crossflow. The most relevant works have been reviewed by Barata et al. (1989a) and Saripalli (1983), showing high turbulence levels and spreading rates in the fountains (e.g. Gilbert (1983) and Nishino et al. (1996)). Barata (1996a) and Barata (1996b) extended their study to multi jet impinging configurations for twin impingement jets, producing upwash fountain flows (Fig.2) which are the heart of the complex effects produced by VSTOL aircraft when they operate in ground proximity. Therefore, studies with the impingement jets aligned with the crossflow are scare in the literature, but of great importance to understand the complexity involved in this type of flowfield.
The remainder of this paper is presented in four sections. Section II describes the experimental and numerical methodology. Section III presents the experimental and numerical results and discussion. The last section summarizes the main findings and conclusions of this work.

2. Methodology

Experimental Method

The AeroG V/STOL tunnel facility designed and constructed for the present work is schematically shown in Fig. 3. During all the design process, especially for the boundary layer part of the flow, were followed the recommendations for open circuit wind tunnels[7]. A fan with 15KW nominal power drives a maximum flow of 3000m^3/h through the boundary layer wind tunnel of 300x302mm exit section.

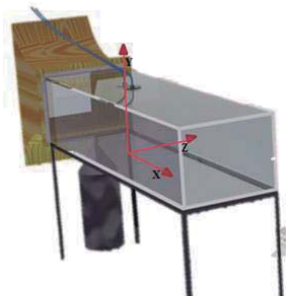

Fig. 3: Wind tunnel and test section

The test section used is an adaptation of the one used in previous experimental works for an impingement height equals to 20.1D (Barata et al. (2014)). The present experimental work is dedicated to the pressure measurement on the body and on the wing of the vectored-thrust F35-B fighter configuration in the transition-speed range for a low impingement height.

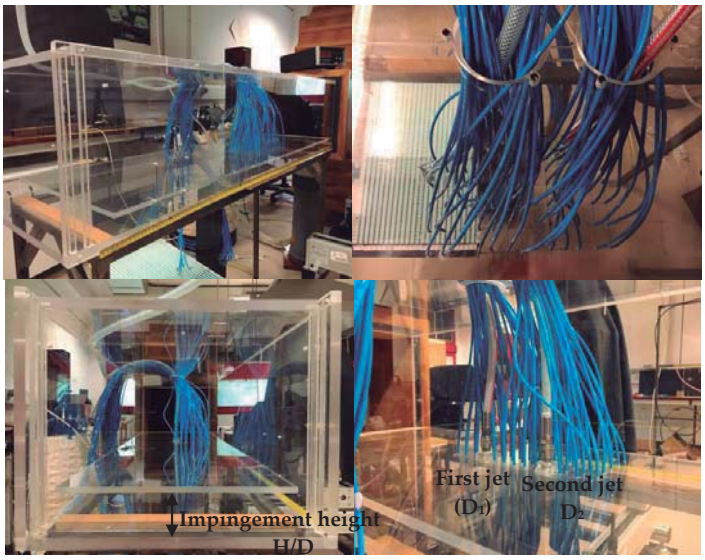

Fig. 4: Test section with pressure measurement system installed

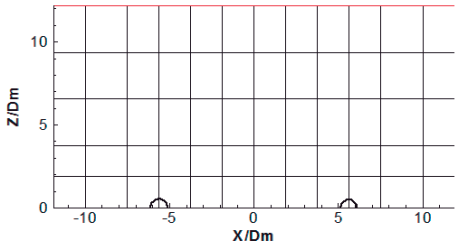

Fig. 5: Mesh created on the plate to the pressure measurement

Therefore, it is design a plate with the same length and width of the teste section with 76 pressure taps with 1 mm inner diameter and 2 nozzles that represents the impingement jets (Fig. 4). The mesh created with the pressure taps on the plate is showed in Fig. 5, corresponding to each of the nodes of the mesh to the location of a pressure tapping.

Each jet unit have a different diameter, where the front/first jet (D_1) has 11 mm inner diameter and the rear/second jet (D_2) has 10.35 mm inner diameter, and both are mounted vertically in the

plate with the axis contained in the vertical plane o symmetry parallel to the crossflow. The inter-jet spacing used is S=11.5Dmean, where $D_{mean} = (D_1+D_2)/2$ and the impingement height used is 3 diameters.

The origin of the horizontal, X, and vertical, Y, coordinates is taken at the midpoint between the centres of the jets exit (Fig. 3). The X coordinate is positive in the direction of the wind tunnel exit and Y is positive upwards.

The present results were obtained at each location for jet mean velocities of V_j=36m/s and mean crossflow velocities of 1.06 m/s<U_0<2.4 m/s, corresponding to a velocity ratios, 15<$V_R=V_j/U_0$ <33.7. These velocity ratios are used in order to continue and complete the experimental study begun by Barata et al. (2014).

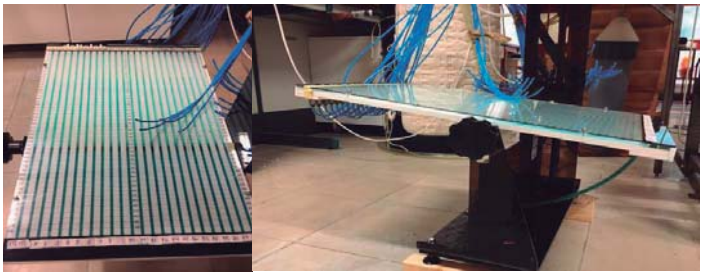

Fig. 6: Pressure gauge used in experiments

The pressure measurements were done through a pressure gauge with 22 pressure taps (Fig. 6). The pressure gauge was inclined about 7 degrees with the horizontal plane in order to obtain more accuracy in the results.

Numerical Method

Mathematical Model

In order to better understand if the experimental results realistically portray the situation under study, a numerical simulation was performed for the same conditions presented experimentally.

Governing differential equations

This section presents a numerical analysis based on the experimental data presented by Barata et al. (2014) and Vieira et al. (2015). The mathematical model used in the numerical simulation is

based on the solution of the continuity and momentum equations. A Reynolds-Averaged Navier Stokes (RANS) formulation was adopted with the "*k-ε*" turbulence model described by Launder and Spalding (1974), to represent the turbulent stresses.
The governing equations are written in a similar form:

$$\frac{\partial}{\partial x}(\rho u\phi)+\frac{1}{r}\frac{\partial}{\partial r}(r\rho v\phi)=\frac{\partial}{\partial x}\left(\Gamma_\phi\frac{\partial\phi}{\partial x}\right)+\frac{1}{r}\frac{\partial}{\partial r}\left(r\Gamma_\phi\frac{\partial\phi}{\partial r}\right)+S_\phi \quad (1)$$

Where the property ϕ represents the velocity, turbulent kinetic energy or dissipation while Sϕ and Γϕ assume different values related with ϕ as described in table 1.

ϕ	Γ_ϕ	S_ϕ
1	0	0
U	μ_T	$-\frac{\partial p}{\partial x}+\frac{\partial}{\partial x}\left(\mu_T\frac{\partial U}{\partial x}\right)+\frac{1}{r}\frac{\partial}{\partial r}\left(r\mu_T\frac{\partial V}{\partial x}\right)$
V	μ_T	$-\frac{\partial p}{\partial r}+\frac{\partial}{\partial x}\left(\mu_T\frac{\partial U}{\partial r}\right)+\frac{1}{r}\frac{\partial}{\partial r}\left(r\mu_T\frac{\partial V}{\partial r}\right)-2\mu_T\frac{V}{r^2}$
k	μ_T/σ_k	$\Phi-\rho\varepsilon$
ε	μ_T/σ_k	$C_{\varepsilon 1}\Phi\frac{\varepsilon}{k}-C_{\varepsilon 2}\rho\frac{\varepsilon^2}{k}$

Table 1: Differential equation coefficients

The turbulent diffusion terms are approximated by two equations from "*k-ε*" turbulent model where the Reynolds tension is related with shear tension:

$$\rho\overline{u'_i u'_j}=-\mu_T\left(\frac{\partial U_i}{\partial x_j}+\frac{\partial U_j}{\partial x_{ij}}\right)+\frac{2}{3}\delta_{ij}\rho k \quad (2)$$

Where μ_T represent turbulent viscosity derivative from the turbulent model expressed by:

$$\Phi=\mu_T\left\{2\left[\left(\frac{\partial U}{\partial x}\right)^2+\left(\frac{\partial V}{\partial r}\right)^2+\left(\frac{V}{r}\right)^2\right]+\left[\frac{\partial U}{\partial r}+\frac{\partial V}{\partial x}\right]^2\right\} \quad (3)$$

The turbulence model constants which are used are those indicated by Launder and Spalding (1974):

C_μ	C_1	C_2	σ_k	σ_E
0.09	1.44	1.92	1.0	1.3

Table 2: Turbulent model constants

The solutions of the governing equations were obtained using a finite difference method. This method that uses the discretized algebraic equations deduced from the exact differential equations which they represent. The discretized equations are obtained integrating the flow equations on the control volume defined by the domain discretization.

Solution Procedure

The solution procedure is based on the SIMPLE algorithm widely used by several references (e.g. Patankar et al. (1977)). This algorithm it used to staggered grid arrangement and correct procedure to solve the problem of obtaining a pressure field such that the solution of the momentum equations satisfies the continuity equation.

Boundary conditions

The computational domain has six boundaries where dependent values are specified (Fig. 7). At the inlet boundary uniform profiles of all dependent variables are specified from the experimental conditions. At the outflow boundary the gradients of the dependent variables in the axial direction are set to zero. On the symmetry plane the normal velocity disappears and the normal derivate of the other variables are zero. Ate the solid walls the wall function method used by Launder and Spalding (1974) is used to prescribe the boundary conditions for the velocity and turbulence quantities. At the jet exit boundary the mass flow rates and the momentum are the same than those in the experimental study. The computational domain corresponds to the experimental conditions that are detailed by Barata (2013) and Barata et al. (2014).

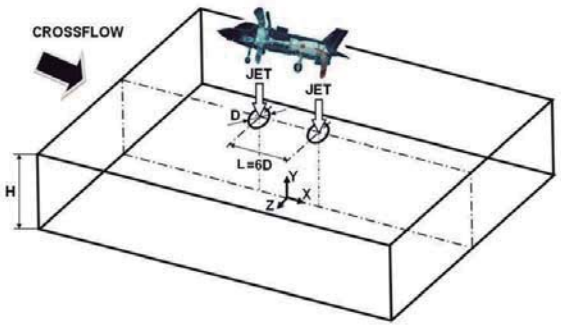

Fig. 7: Computational domain

3. Results and Discussion

In this section, experimental and numerical data obtained will be presented and discussed for the velocity ratios 15 <V_R < 33.7 and an impingement height, H/D, equals to 3. Figures 8 to 13 show the pressure measurements obtained experimental and numerically.

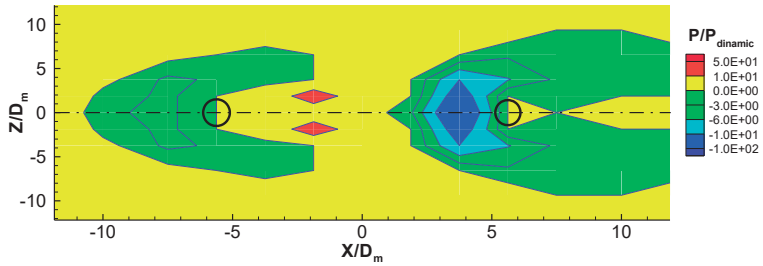

Fig. 8: Experimental pressure distribution along the bottom of the fuselage and wing (i.e. Y≈3) for V_j/U_0=15, H/D_m=3, and L/D_m=11.5 (values non dimensionalized by $1/2\rho V_j^2$)

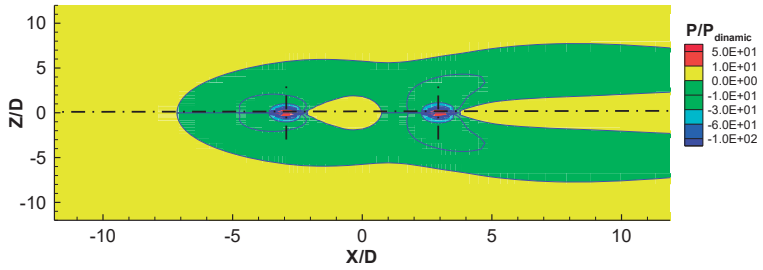

Fig. 9: Numerical pressure distribution along the bottom of the fuselage and wing (i.e. Y≈3) for V_j/U_0=15, H/D=3, and L/D=6 (values non dimensionalized by $1/2\rho V_j^2$)

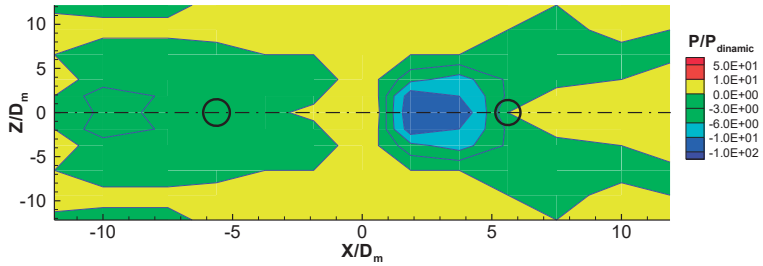

Fig. 10: Experimental pressure distribution along the bottom of the fuselage and wing (i.e. Y≈3) for V_j/U_0=22.5, H/D_m=3, and L/D_m=11.5 (values non dimensionalized by $1/2\rho V_j^2$)

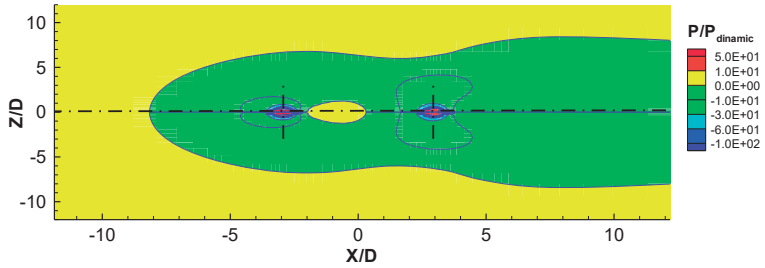

Fig. 11: Numerical pressure distribution along the bottom of the fuselage and wing (i.e. Y≈3) for V_j/U_0=22.5, H/D=3, and L/D=6 (values non dimensionalized by $1/2\rho V_j^2$)

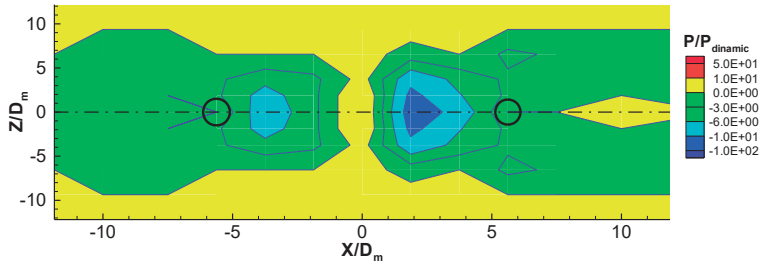

Fig. 12: Experimental pressure distribution along the bottom of the fuselage and wing (i.e. Y≈3) for V_j/U_0=33.7, H/D_m=3, and L/D_m=11.5 (values non dimensionalized by $1/2\rho V_j^2$)

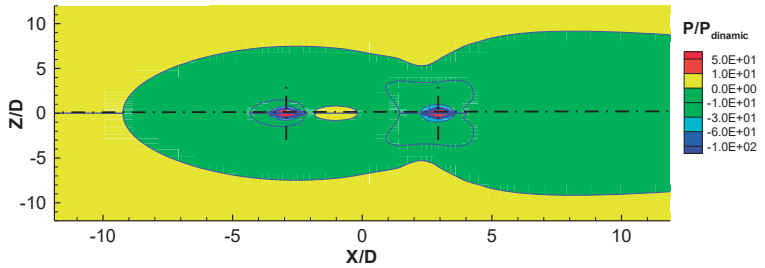

Fig. 13: Numerical pressure distribution along the bottom of the fuselage and wing (i.e. Y≈3) for V_j/U_0=33.7, H/D=3, and L/D=6 (values non dimensionalized by $1/2\rho V_j^2$)

The impingement jet location is identified in the experimental figure through a circle, while in the numerical figures is identified by the intersection of the vertical line with the symmetry plane (Z/D=0).

Comparing the experimental results to the ones obtained numerically, it is evident that the experimental mesh used needed more points especially in the region between the impingement jets, $-5.62<X/D_m<5.62$, to increase the results resolution. Analyzing the results for all the velocity ratios studied, on the impingement jets location a red area is presented correspondent to a regions of high static pressure, due to the large positive values of the horizontal velocity

component. The cold coloured regions around the impingement jet location on the numerical results correspond to low pressures and are associated with the core of the ground vortexes. As it expected the location nearest to the jets are the region with larger induced pressure effects. These large negative pressure coefficients induced a suction region around the impingement location, corresponding to the phenomenon of the hot gas re-ingestion into the engine intake that causes several problems in the engine performance due to the unsteadiness of the flow and raise of the temperature.

Through the figures 14 to 15 (obtained numerically) it is observed that for a lower impingement height the formation of a ground vortex in the region between the jets. Taking into account studies referenced in the literature, it would be expected that for lower impingement height, the fountain upwash flow phenomenon was observed in the flowfield results. Instead of this, in the region between the jets, it is observed the formation of a second ground vortex that results of the

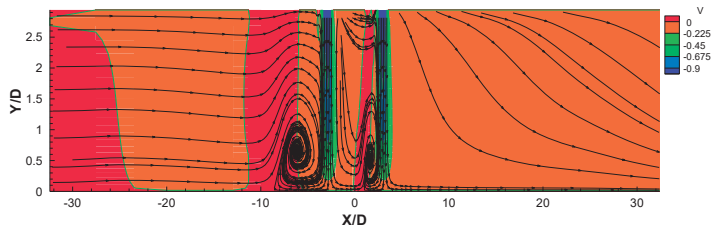

Fig. 14: Predicted mean vertical velocity component distribution along the vertical plane of symmetry (i.e. Z=0) for V_j/U_0=15, Re_j=43,000, H/D=3 and L/D=6

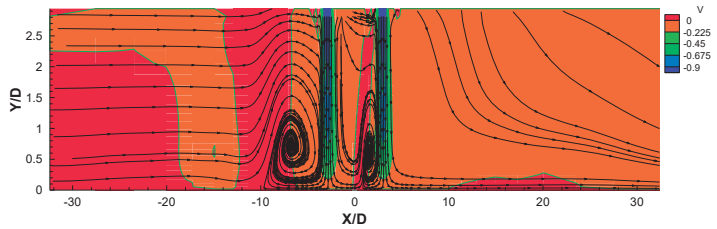

Fig. 15: Predicted mean vertical velocity component distribution along the vertical plane of symmetry (i.e. Z=0) for V_j/U_0=22.5, Re_j=43,000, H/D=3 and L/D=6

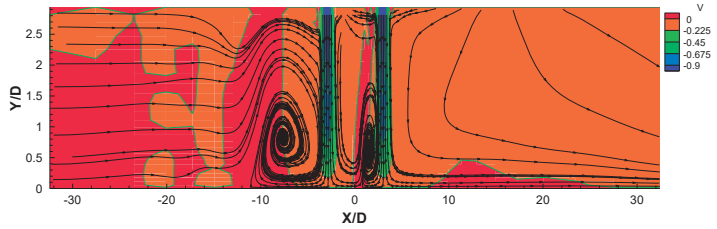

Fig. 16: Predicted mean vertical velocity component distribution along the vertical plane of symmetry (i.e. Z=0) for V_j/U_0=33.7, Re_j=43,000, H/D=3 and L/D=6

interaction of the first jet inner wall jet with the second inner wall jet that captured it and given rise to a clockwise recirculation close to the second jet. This result it is new and it has not yet reported in the literature. The ground vortex centre position is coming to upstream and the ground vortex becomes increasingly with the velocity ratio increase, as it is expected, traduced in an increased on the induced pressure effect. When compared this results with the ones obtained by Barata et al (2014), it is verified that for lower H/D the first jet practically does not suffer deflection caused by the crossflow interaction, due to the increase of the jet strength when it is close to the ground as the impingement height will be lower, and protects the rear jet of the crossflow influence. So, the rear jet is entrained by the upstream jet and not by the crossflow itself.

For all the velocity ratios, when the upstream ground vortex feels the presence of the ground vortex formed between the impingement jets, it becomes wider and closer to the lateral walls (identified by the green area). In the experimental results (fig. 8, 10 and 12) the development of the ground vortex in the region between the jets is not clearly identified due to the low number of pressure taps in this location. While the impingement jets location do not have any pressure tap, it is not possible to see the same pressure distribution that the one exposed numerically, being the results presented in this regions results of the interpolation made by the Tecplot. This interpolation assumed zero pressure in the location between the jets, breaking the upstream ground vortex flow, something that is merely an error evidenced by the results obtained numerically.

4. Conclusions

An experimental study and numerical study were done to provide information to the pressure measurement on the body and on the wing of the vectored-thrust F35-B fighter configuration in the transition-speed range. The experiments was carried out for a Reynolds number based on the jet exit conditions of $Re_j=4.3x10^4$ with an impingement height of 3 jet diameters and for a velocities ratio between the jet exit and the crossflow, $V_R= V_j/U_0$ of 15, 22.5 and 33.7 with and an interject spacing of $S=11.5D_m$. The jet exit conditions and velocity ratios were chosen in order to complete the experimental study initiated by Barata et al. (2014). To complete the investigation and compared the experimental results were also performed a numerical simulation for the same impingement height and velocity ratios.

Through the numerical results it is showed the formation of a ground vortex in the region between the impingement jets, a fact that has not been reported in the literature and it is surprising at the first sight, because it was expected to find an upwash fountain flow for lower

impingement heights. This structure results of the interaction of the first jet inner wall jet with the second inner wall jet that captured it and given rise to a clockwise recirculation close to the second jet. From the numerical results another important conclusion can be taken about the real role and contribution of the second jet, being this responsible for the first jet reinforce, influencing the size and location of the ground vortexes centres.

Comparing the experimental results obtained for the pressure measurements with the ones obtained numerically, it can be conclude that the experimental results do not have enough resolution in the region impingement jets region and in the region between them. In a general way the pressure distribution results agree with the expected for the situation on study, the aircraft hovering in the vicinity of the ground. The region where the vectored-thrust jets impinge presents the high static pressure, due to the large positive values of the horizontal velocity component, while the location nearest of them exhibit the larger negative pressure coefficients, being one of the causes for the hot gas re-ingestion into the engine intake phenomenon.

Acknowledgments

The present work was done in the scope of the activities of LAETA-Associated Laboratory of Energy, Transports and Aeronautics, and funded by FCT-Fundação para a Ciência e Tecnologia through contract PTDC/EME-MFE/102190/2008 and grant SFRH/BD/86434/2012.

References

[1]Adler, D., Baron, A. Prediction of a three-dimensional circular turbulent jet in crossflow. AIAA Journal, (1979); 17: 168-174.

[2]Barata J.M.M., Durão D.F.G., McGuirk J.J. Numerical Study of Single Impinging Jets through a Crossflow. Journal of Aircraft. (1989); 26(11): 1002-1008.

[3]Barata J.M.M. Ground Vortex Formation With Twin Impinging Jets. Proceedings of the International Powered Lift Conference. Jupiter, FL, 18-20 November. 1996a. SAE Paper 962257.

[4]Barata J.M.M. Fountain Flows Produced by Multiple Impinging Jets in a Crossflow. AIAA Journal. (1996b); 34(12): 2523-2530 and AIAA Journal on Disc, 2(1).

[5]Barata J.M.M. Multiple Jet/Wall/Cross-Wind Inter-action Relevant to VSTOL Ground Effects. Proceedings of the International Powered Lift Conference, Los Angeles, California, August 12-14 2013. AIAA paper 2013-4380. (2013).

[6]Barata J.M.M., Carvalho P.S.D., Durão D.F.G., Neves F.M.S.P., Silva A.R.R., Vieira D.F.C. Laser Doppler Measurements of Twin Impinging Jets Aligned With a Crossflow. Journal of Physical Science and Application. (2014); 4 (7): 403-411.

[7]Durst, F., Melling, A., and Whitelaw, J.H., "Principles and Practice of Laser-Doppler Anemometry", 2nd ed., New York, Academic Press.

[8]Gilbert B.L. Detailed Turbulence Measurements in a Two Opposing Plane Turbulent Wall Jets. Proceedings of the 16th AIAA Fluid and Plasma Dynamics Conference, Danvers, MA, Jul. 12-14 1983; AIAA Paper 83-1678.

[9]Jones W. P., McGuirk J. J. Computation of a round turbulent jet discharging into a confined crossflow. In: "Turbulent Shear Flows-2", Ed. Bradbury et al., Springer Verlag. 1980; 223-245.

[10]Knowles, K., and Bray, D., "The Ground Vortex Formed by Impinging Jets in Crossflow", AIAA 29th Aerospace Sciences Meeting, AIAA Paper 91-0768, Reno, NV, Jan. 7-10, 1991.

[11]K. Knowles, "Computational Studies of impinging jets using k-ε Turbulence Models", International Journal for Numerical Methods in Fluids, 1996, Vol. 22, pp. 799-810.

[12]Launder B. E., Spalding D. B. The Numerical Computation of Turbulent Flows. Computer Methods in Applied Mechanics and Engineering. 1974; 3: 269-289.

[13]Nishino K., Samada M., Kasuya, K., Torri K. Turbulence statistics in the stagnation region of an axisymmetric impinging jet flow. International Journal of Heat and Fluid. 1996; 17(3): 193-201.

[14]Patankar S. V., Basu D. K., Alpay S. A. Prediction of the Tree-Dimensional Velocity Field of a Deflected Turbulent Jet. Journal of Fluids Engineering. 1977; 99(4): 758-762.

[15]Saripalli K. R. Visualization of Multijet Impingement Flow. AIAA Journal. 1983; 21: 483-484.

[16]Sarippali, K.R., "Laser Doppler Velocimeter Measurements in 3D Impinging Twin-Jet Fountain Flows", Turbulent Shear Flows, Vol.5, edited by Durst et al., Springer-Verlag, Berlin, 1987, pp. 147-168.

[17]Vieira D. F. C., Barata J. M. M, Neves F. M. S. P, Silva S. R. R. Numerical Simulation of Twin Impinging Jets in Tandem Through a Crossflow. Journal of Engineering and Applied Sciences. 2015; 10 (6): 123-136.

AIAA 2017-1663

Effect of the Impinging Height of Twin Jets in Tandem Through a Crossflow

Jorge M.M. Barata, André R.R. Silva, Diana F.C. Vieira
Universidade da Beira Interior
Covilhã, Portugal

55th AIAA Aerospace Sciences Meeting

9-13 January 2017, Grapevine, TX

Effect of the Impinging Height of Twin Jets in Tandem Through a Crossflow

Jorge M. M. Barata[1], André R. R. Silva[2] and Diana F. C. Vieira[3]
Universidade da Beira Interior, Covilhã, 6200-358, Portugal

The complex flow field generated by the impact of twin impinging jets in tandem through a low velocity crossflow was numerically studied. The Reynolds number based on the jet exit conditions was 43,000, the jet-to-crossflow velocity ratio from 7.5 to 90, and an interject spacing of 6 diameters of the jet. The impingement heights used were 3 to 15. The mathematical model used is based on the solution of the continuity and momentum equations. A RANS formulation was adopted with the "k-ε" turbulent model to represent the turbulent stresses. The numerical results showed the influence of the impingement height on the ground vortex location, size and interaction with the surrounding flow, but new aspects of this type of flows were found for the present case of a tandem configuration. In the region between the jets the usual fountain upwash flow does not occur, but a second small ground vortex was detected for H/D≤10, due to the interaction between the wall jets of each impinging jet. To our knowledge this is a new phenomenon that is being reported in the literature for the very first time.

I. Nomenclature

D	=	diameter of the jet
H	=	impinging height
k	=	turbulent kinetic energy
P	=	Pressure
Re	=	Reynolds number
S	=	distance between the jets axis
U	=	horizontal velocity (in the crossflow direction)
V	=	vertical velocity
V_R	=	velocity ratio, V_j/U_o
W	=	transverse velocity
X	=	horizontal coordinate (in the crossflow direction)
Y	=	vertical coordinate
Z	=	transverse coordinate
Subscripts		
j	=	jet exit value
j1	=	upstream jet exit value
j2	=	rear jet exit value
0	=	crossflow value
Greek symbols		
ε	=	turbulent kinetic energy dissipation
μ_T	=	turbulent viscosity

II. INTRODUCTION

TURBULENT jets impinging on flat surfaces through a low velocity crossflow are typical of the flow beneath of VSTOL aircrafts. When a VSTOL aircraft operates there are three different stages during the flight, being all

[1] Full Professor, Aerospace Sciences Department, Associate Fellow of AIAA, Corresponding author.
[2] Assistant Professor, Aerospace Sciences Department, Senior Member of AIAA.
[3] Ph. D. Student, Aerospace Sciences Department, Student Member of AIAA.

different, with its own flow characteristics and with different kind of problems associated. A VSTOL flight comprises the hover phase, the transition to forward flight phase and the forward flight operation. The hover phase is the most complex phase during the flight and can be further divided into two more phases because the flowfield associated in each phase are completely different. So, the hover phase can be subdivided into out-of-ground-operation and hover in the vicinity of the ground. During its landing or near ground hovering phase, the VSTOL aircraft creates a complex three dimensional flow field between the jet streams, the airframe surface and the ground. When ground effect occurs, the lift forces on the aircraft changes, cause hot gas re-ingestion into the engine intake and due to the fountain upwash and ground flows, the fuselage skin temperature rises. The unsteadiness of the flow and raise of the temperature cause several problems in the engine performance, such as, compressor surge or even stall and thrust reduction. In respect to the intake ingestion phenomenon, it is very complex and can be associated with the design and operational parameters, such as, jet configuration, head wind velocity, jet impingement height or intake configuration. In the case of the hot gas ingestion problem, there are three mechanism involved, i.e., far field ingestion, near field ingestion and ground vortex ingestion. During a landing or hover the impingement of each downward-directed jet on the ground results in the formation of a wall jet which flows radially from the impinging point along the ground surface. The interaction of this wall jet with the free stream results in the formation of a ground vortex far upstream of the impinging jet. This flow field transports exhaust gases away from the ground and upwards to the intake region. The level and intensity of the ingestion resulting from this mechanism depends critically on the forward velocity. If there are two or more adjacent jets, the resulting wall jets meet, and a fan-shaped upwash, or "fountain", is normally formed between the jets (Fig. 1).

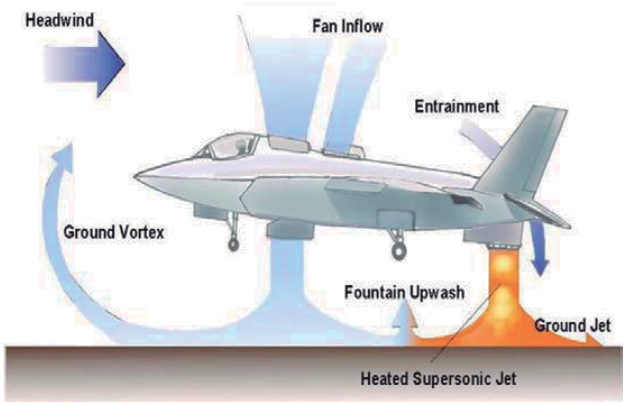

Figure 1. STOVL aircraft ground effect aerodynamics.

The fountain upwash flow affects the forces and moments induced in the aircraft when operating in ground effect, depending on its strength and direction. The resulting ground vortex shape is strongly affected and the corresponding induced suckdown effect tends to be reduced by the upwards force produced by the fountain. The improvements of the knowledge of this flow are even more required because the aircraft design has been changed since its first design, and some problems still persists. In this case when the aircraft operates with small forward movement the configuration of interest are two impinging jets with the direction of the crossflow perpendicular to the line containing their centers For the next generation of VSTOL aircrafts F-35 no relevant studies can be found, because the impinging jets are aligned with the crossflow and this geometry has not yet been considered. This paper aims presents results that are relevant to the future F-35 VSTOL configuration (Fig. 2), through a detailed analysis of the complex flow field beneath two impinging jets in tandem through a low velocity crossflow for different impingement heights. It is also a continuation of the numerical and experimental studies done previously[1,2].

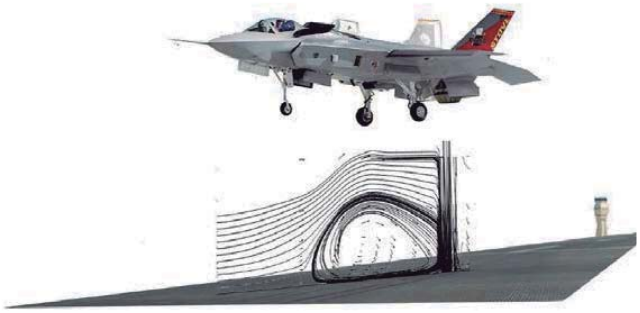

Figure 2. F-35 VSTOL configuration

Here, the main focus is the comprehension how the impingement height affects the flowfield and to find out if there is formation of the fountain upwash flow, something that has not happened for the experimental and numerical impingement height of H/D=20.1 that was used in the previous studies. Detailed measurements of the flow

properties for fountain upwash flow are scarce and have been presented essentially in the absence of a crossflow and with the use of probe techniques and more recently with Particle image velocimetry. The most relevant works have been reviewed by Ref. 3 and 4, showing high turbulence levels and spreading rates in the fountains[5,6]. Ref. 7 and 8 extended their study to multi jet impinging configurations producing upwash fountain flows (Fig.3) which are the heart of the complex effects produced by VSTOL aircraft when they operate in ground proximity, but as far as twin jets are concerned only the geometry with the jets side by side was considered. Experiments on the aerodynamics of jets through a confined crossflow are scarcer and have only been reported for large impingement heights and for low velocity ratios between the jet and the crossflow V_j/U_0. Therefore these works have only peripheral relevance to the VSTOL ground effect problem with the same geometry of the F-35.

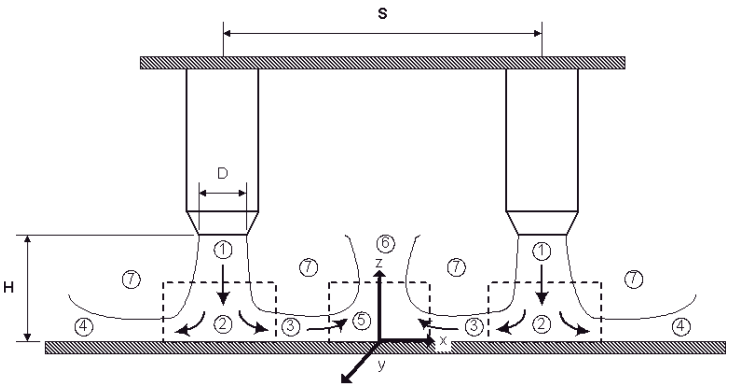

Figure 3. Schematic of the upwash fountain flow by two impinging jets: 1. Free jet, 2. Jet impingement region, 3. Inner wall jet region, 4. Outer wall jet region, 5. Fountain formation

Most of the computational work published on jets with crossflow has been based on integral methods admitting assumptions simplified, which are only capable of predicting global effects such as trajectories and jet cross-section shapes (for example Ref. 9 and 10). Ref. 11 employed a finite-difference numerical procedure together with a two-equation turbulence model to predict a single jet in an unconfined crossflow, and obtained good agreement with the experiments of Ref 12 and 13 for velocity ratios from 2 to 10. A similar approach was used by Ref. 14 to calculate the confined flow measured by Ref. 15. The gross features of the flow are well predicted but the calculations appear to exhibit diffusion rates larger than those consistent with measured profiles, which can be attributed either to numerical or turbulence model errors. Grids up to 20 x 15 x 15 nodes were used, but further grid refinement is essential to identify the precise source of disagreement between measurements and predictions. Ref. 16 has shown that the standard "k-ε" model over predicts the spreading rate of a free jet and under predicts the spreading rate of a radial wall jet. Ref. 17 and 18 used the Steady-RANS or SRANS approach but the results did not capture the turbulent structure of the fountain flow and impingement regions, being the predicted turbulent quantities particularly poor. Ref. 19 reports a numerical study employing the Unsteady-RANS or URANS approach, comparing the results with the measurements of Ref. 17, revealing that the URANS approach was the one that gives a better agreement with the experimental data. Ref. 20 presented a comparison of experimental data and computational simulation of an impinging jet without crossflow for different impingement heights, $3<H/D<12$, jet-to-jet spacing and jet angles of $0^o<\theta<20^o$. The results showed that the primary stagnation point moves away in the radial flow direction with jet angle increase and become stronger with the jet to jet spacing increase. The pressure at the stagnation point located at the middle between the two jets increases with the jet angle and decreases with the Reynolds number. The increase of the impingement height decreases the intensity of the re-circulation zone in the middle of the jets and the jet spreading. Ref. 21 reports a numerical study with different crossflow orientations and jet to surface spacing. The study revealed that the flow exit crossflow e orientation affected significantly the developing jet flow fields and the Nusselt number. Ref. 22 to 24 studied the flowfield and the heat transfer for square array impinging jets and for different impingement heights; the local Nusselt number decreases with H/D, but the number of jets combinations did not affect the heat transport characteristics.

III. METHODOLOGY

A. Mathematical Model

This section presents a numerical analysis based on the experimental data presented by Ref. 1 and 25. The mathematical model used in the numerical simulation is based on the solution of the continuity and momentum equations. A Reynolds-Averaged Navier Stokes (RANS) formulation was adopted with the "k-ε" turbulence model

described by Ref. 26, to represent the turbulent stresses. The governing equations used are described in detail in Ref. 1.

B. Boundary conditions

The computational domain has six boundaries where dependent values are specified (Fig. 4). At the inlet boundary uniform profiles of all dependent variables are specified from the experimental conditions. At the outflow boundary the gradients of the dependent variables in the axial direction are set to zero. On the symmetry plane the normal velocity disappears and the normal derivate of the other variables are zero. Ate the solid walls the wall function method used by Ref. 26 is used to prescribe the boundary conditions for the velocity and turbulence quantities. The jet exit boundary is characterized by a right angle and the mass flow rates and the momentum of the jet are the same that the ones used in the experimental study. Also the kept exit boundary conditions are the same use in the experiments. The computational domain corresponds to the experimental conditions that are detailed by Ref. 2 and 25.

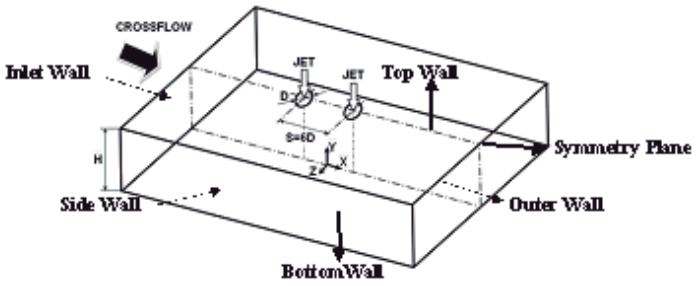

Figure 4. Computational domain

IV. RESULTS AND DISCUSSION

The numerical predictions presented in this section are compared with experimental and numerical results of Ref. 1 and 2 obtained at the central plane of symmetry for two impingement jets of 15 mm jet exit diameter and 20.1 jet diameters above the ground. The Reynolds number is Rej= 43,000 for a jet exit mean velocity of Vj =36 m/s and a crossflow velocity 0.4 m/s ≤U0≤ 4.8 m/s, corresponding a range of velocity ratios between 7.5 and 90. The present numerical results were obtained for 4 different impingement heights of H/D=3, 5, 10, and 15, all of them lower than the one used in the numerical and experimental studies of Ref. 1. The results were predicted using the QUICK scheme to evaluate the convection terms of the transport equations and a grid of 26x71x26 nodes. The grid spacing was non uniform in order to concentrate the nodes, due to its refinement in area of greater interest for the study, i.e., near the jets and close to the impingement region where the gradients are steepest. The results discussed here are a small sample of a more complete set obtained for seven different velocity ratios (Vj/U0= 7.5, 15, 22.5, 33.7, 43.8, 60 and 90) and for four different impingement heights. The flowfield results obtained for H/D= 15 were found similar to those obtained by Ref. 24 for H/D=20.1. However, significant changes on the flowfield behavior were registered for H/D<10. To illustrate and discuss this changes in the flowfield two different cases for H/D=5 with Vj/U0= 15 and 60 were chosen.

Fig. 4 shows the mean vertical velocity component in the vertical plane of symmetry (Z=0) for Vj/U0= 15 and H/D=5. The streamtraces show the formation of a ground vortex, both downstream of the first impinging jet and the region between the two impinging jets. The first (upstream) jet impinges on the ground with a considerably high

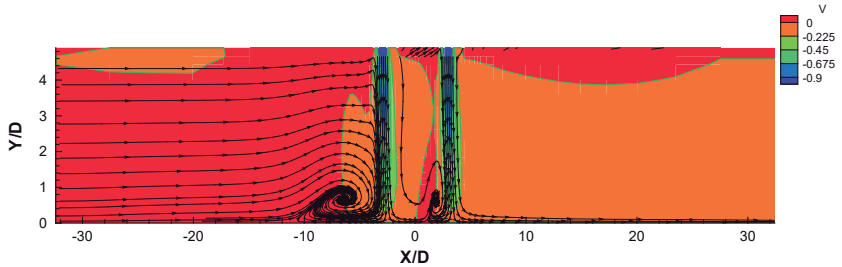

Figure 4. Predicted mean vertical velocity component distribution along the vertical plane of symmetry (i.e. Z=0) for V_j/U_0=15, Re_j=43,000, H/D=5, and L/D=6.

strength and almost no deflection can be observed. This is a different result from what was observed before for higher impinging heights (e.g. H/D=20.1) with the two impinging jets remaining together in two layers and flowing downstream, as a result of the impingement of the second jet on the wall jet of the first jet. A small recirculation in the region between the two impingement jets is also registered which has not yet reported before in the permanent literature. The interaction of the impinging jets with the ground results in the formation of a wall jet, that can be described as a deflected flow turning into a high-speed flow parallel to the ground plane (inner wall jet region and outer wall jet region). In the collision of the encountering inner wall jets, one from each jet, the inner wall jet from the first jet is captured by the inner wall jet of the second jet, resulting in the formation of a recirculation similar to a ground vortex, but with no direct influence of the crossflow. For the present impingement height and velocity ratio combinations no fountain flow can be observed.

Part of the crossflow fluid is not entrained by the scarf vortex, and is deflected upwards passing over it and going around the impingement jets through the region between them. At X/D=4.9 it goes down, due to the interaction with the second jet flow. Then, for X/D≈12 it reaches the minimum height, rising again and flowing downstream. This particular part of the flow is associated with the negative pressure regions as shown in Fig. 5. In the region between the jets, when the first jet touches the ground the inner wall jet flows and rises up like an upwash flow, but it is captured by the second jet inner wall jet, and a little clockwise ground vortex is formed close to the second jet (Figs. 6 and 7).

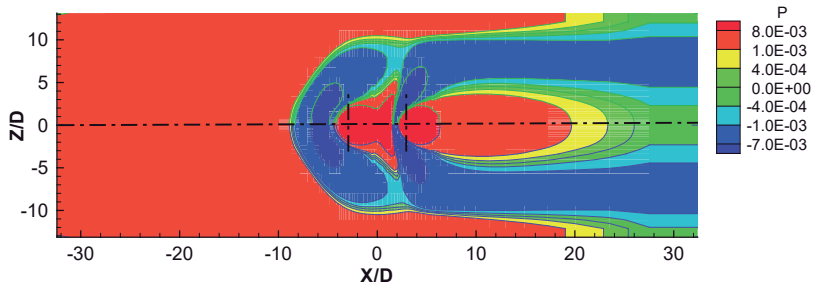

Figure 5. Pressure distribution along the field close to the ground (i.e. Y≈0) for V_j/U_0=15, H/D=5, and L/D=6 (values nondimensionalized by $1/2\rho V_{j1}^2$).

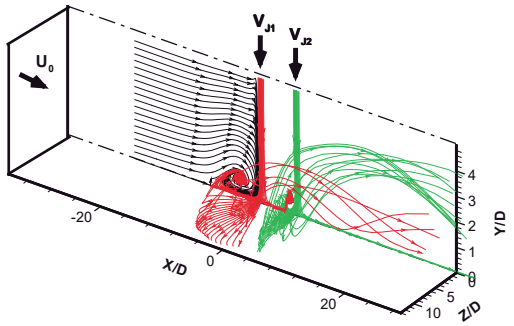

Figure 6. Tridimensional illustration of the jets flow for Re_j=43,000, V_j/U_0= 15, H/D=5 and L/D=6.

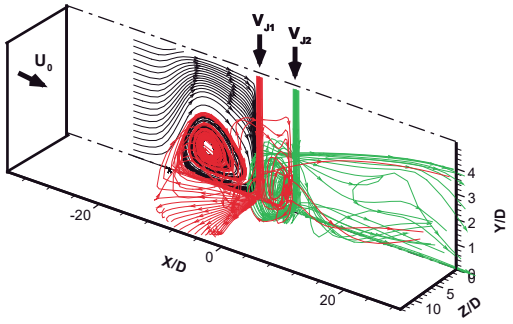

Figure 7. Tridimensional illustration of the jets and scarf vortex flow for Rej=43,000, V_j/U_0=15, H/D=5 and L/D=6.

For V_j/U_0= 60 the flow pattern is apparently similar (Figs. 8 to 10), but the relatively weaker influence of the crossflow allows the transversal (Z) component of the velocity (W) to assume a more important role as far the wall jets are concerned. So, the negative pressure regions in the ground plane are much wider when the velocity ratio between the jet and crossflow increases from 15 to 60 (Fig. 8). The direct relation between the surface underpressure (blue zone) and the ground vortex is now almost imperceptible for this velocity ratio. The negative pressure zone is

now much wider and is concentrated near the impinging zones, and they do not continue to the downstream exit of the control volume at X/D=24 as for the case of V_j/U_0=15. Additionally, it should be noticed that the height of the upstream ground vortex increased from 1D to 2.5D, occupying almost 50% of the impingement height (H=5D). Also the maximum penetration point[26] moved further upstream from X/D=-10 for V_j/U_0=15 to X/D=-17 for V_j/U_0=60.

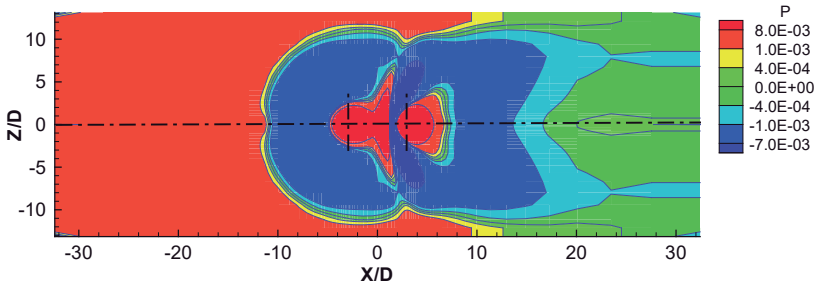

Figure 8. Pressure distribution along the field close to the ground (i.e. Y≈0) for V_j/U_0=60, H/D=5, and L/D=6 (values nondimensionalized by $1/2\rho V_{j1}^2$).

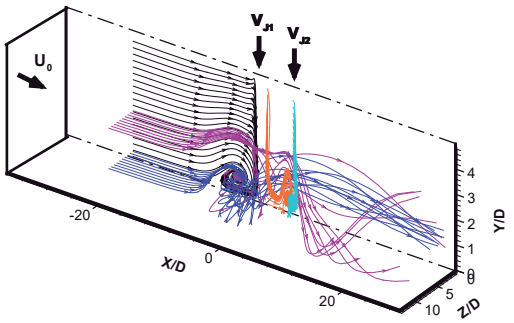

Figure 9. Tridimensional illustration of the jets flow for Rej=43,000, V_j/U_0= 60, H/D=5 and L/D=6.

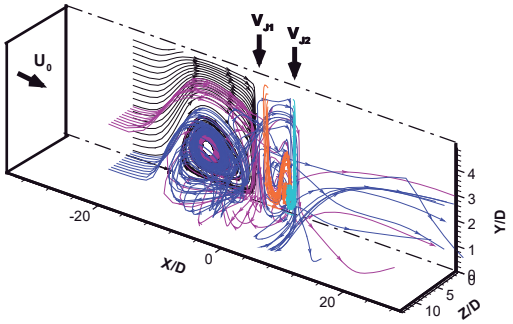

Figure 10. Tridimensional illustration of the jets and scarf vortex flow for Rej=43,000, V_j/U_0=60, H/D=5 and L/D=6.

V. CONCLUSIONS

A numerical study of the flow field generated by twin impinging jets in tandem through a low velocity crossflow was performed to extend the experimental results for velocity ratios and impingement heights beyond the limits of the experimental rig enabling a better understanding of the flow. A large number of impingement heights / jet-to-crosflow velocity ratios combinations were studied. In general, decreasing the impingement height reduces the crossflow effect in the first jet deflection, but the rear jet is much less affected. The ground vortex center position moves upstream and the ground vortex becomes larger when the velocity ratio increases or the impingement height decreases. No fountain upwash flow was observed in the present study. Instead of this, in the region between the jets and for H/D≤10, it is observed the formation of a second ground vortex that results from the interaction of the first jet inner wall jet with the second inner wall jet that captured it and given rise to a clockwise recirculation close to the second jet. To our knowledge his result it is new and it has not yet reported in the literature.

VI. REFERENCES

[1]Vieira D. F. C., Barata J. M. M, Neves F. M. S. P, Silva S. R. R. "Numerical Simulation of Twin Impinging Jets in Tandem Through a Crossflow", *Journal of Engineering and Applied Sciences*, Vol. 10, No. 6, 2015, pp. 123-136.

[2]Barata J.M.M. “Multiple Jet/Wall/Cross-Wind Interaction Relevant to VSTOL Ground Effects”, *Proceedings of the International Powered Lift Conference*, Los Angeles, California, August 12-14 2013, AIAA paper 2013-4380.

[3]Barata J.M.M., Durão D.F.G., McGuirk J.J. “Numerical Study of Single Impinging Jets through a Crossflow”, *Journal of Aircraft*, Vol. 26, No. 11, 1989, pp. 1002-1008.

[4]Saripalli K. R. “Visualization of Multijet Impingement Flow”, *AIAA Journal*, Vol. 21, 1983, pp. 483-484.

[5]Gilbert B.L. “Detailed Turbulence Measurements in a Two Opposing Plane Turbulent Wall Jets”, *Proceedings of the 16th AIAA Fluid and Plasma Dynamics Confenrence*, Danvers, MA, Jul. 12-14 1983, AIAA Paper 83-1678.

[6]Nishino K., Samada M., Kasuya, K., Torri K. “Turbulence statistics in the stagnation region of an axisymmetric impinging jet flow”, *International Journal of Heat and Fluid*, Vol. 17, No. 3, 1996, pp. 193-201.

[7]Barata J.M.M. “Ground Vortex Formation with Twin Impinging Jets”, *Proceedings of the International Powered Lift Conference*, Jupiter, Florida, 18-20 November 1996, Paper SAE 962257.

[8]Barata J.M.M. “Fountain Flows Produced by Multiple Impinging Jets in a Crossflow”, *AIAA Journal*, Vol. 34, No. 12, 1996, pp. 2523-2530 and AIAA Journal on Disc, Vol. 2, No. 1.

[9]Stoy, R. C. and Ben-Haim, Y. “Turbulent Jets in a Confined Crossflow”, *J. Fluids Engng.*, Vol. 95, 1973, pp. 551-556.

[10]Adler, D., Baron, A. “Prediction of a three-dimensional circular turbulent jet in crossflow”, *AIAA Journal*, Vol. 17, 1979, pp. 168-174.

[11]Patankar S. V., Basu D. K., Alpay S. A. “Prediction of the Tree-Dimensional Velocity Field of a Deflected Turbulent Jet”, *Journal of Fluids Engineering*, Vol. 99, No. 4, pp. 758-762.

[12]Keffer, J. F., Baines, W. D. “The Round Jet in a Crosswind”, *J. Fluid Mech.*, Vol. 15, 1963, pp.481-496.

[13]Ramsey, J. W., Goldstein, R.J. “Interaction of a Heated Jet With a Deflecting Stream”, 1972, NASA CR 72613.

[14]Jones W. P., McGuirk J. J. “Computation of a round turbulent jet discharging into a confined crossflow”. In: "*Turbulent Shear Flows-2*", Bradbury et al., Springer Verlag, 1980, pp. 223-245.

[15]Kamotani Y., Greber I. “Experiments on Confined Turbulent Jets in a Crossflow”, NASA CR-2392, 1974.

[16]Knowles, K. “Computational Studies of impinging jets using k-ε Turbulence Models”, *International Journal for Numerical Methods in Fluids*, Vol. 22, 1996, pp. 799-810.

[17]Barata J.M.M., Durão D.F.G., McGuirk J.J. “Impingement of single and twin turbulent jets through a cross-flow”, *AIAA Journal*, Vol. 29, No. 4, 1991, pp. 595-602.

[18]Worth N. A, Yang Z. “Simulation of an impinging jet in a crossflow using a Reynolds stress transport model”, *International Journal for Numerical Methods in Fluids*, Vol. 52, 2006, pp. 199-211.

[19]Yang Z. “Assessment of unsteady-RANS approach against steady-RANS approach for predicting twin impinging jets in a crossflow”, *Congent Engineering*, Vol. 1, 2014, 936995.

[20]Abdel-Fattah A. “Numerical and Experimental study of turbulent impinging twin-jet flow”, *Experimental Thermal and Fluid Science*, Vol. 31, No. 8, 2007, pp. 1061-1072.

[21]Miao Jr-Ming, Chen-Yuan Wu, Ping-Hei Chen, “Numerical Investigation of Confined Multiple-Jet Impingement Cooling Over a Flat Plate at Different Crossflow Orientations”, *Numerical Heat Transfer, Part A: Applications*, Vol. 55, No. 11, 2009, pp. 1019-1050.

[22]Aldabbagh L.B.Y, Sezai I. “Numerical simulation of three-dimensional laminar, square twin-jet impingement on a flat plate, flow structure, and heat transfer”, *Numerical Heat transfer, Part A: Applications: An International Journal of Computation and Methodology*, Vol. 41, No. 8, 2002, pp. 835-850.

[23]Aldabbagh L.B.Y, Sezai I. “Numerical simulation of three-dimensional multiple impinging-square jets”, *International Journal of Heat and Fluid Flow*, Vol. 23, No. 4, 2002b, pp. 509-518.

[24]Aldabbagh L. B. Y., Mohamad A. A. “Effect of jet-to-jet plate spacing in laminar array jets impinging”, *Heat and Mass Transfer*, Vol. 43, No. 3, 2006, pp. 265-273.

[25]Barata J.M.M., Carvalho P.S.D., Durão D.F.G., Neves F.M.S.P., Silva A.R.R., Vieira D.F.C. “Laser Doppler Measurements of Twin Impinging Jets Aligned With a Crossflow", *Journal of Physical Science and Application*, Vol. 4, No. 7, 2014, pp. 403-411.

[26]Launder B. E., Spalding D. B. “The Numerical Computation of Turbulent Flows”, *Computer Methods in Applied Mechanics and Engineering*, Vol. 3, 1974, pp. 269-289.